Influence of the molecular structure of biofuels on combustion in a compression ignition engine

University College London

(UCL)

Department of Mechanical Engineering

Alessandro Schönborn

Submitted in partial fulfilment of the of the requirements for the degree of

Doctor of Philosophy

July 2009

I, Alessandro Schönborn confirm that the work presented in this thesis is my own. Where information has been derived from other sources, I confirm that this has been indicated in the thesis.

Dated:

Abstract

This thesis presents an experimental study on the influence of the molecular structure of potential biofuels on combustion in a compression ignition engine. The molecular structure of a fuel is amongst the most fundamental parameter controlling its physical and chemical characteristics, and is thus critical to the combustion process within an engine. The approach employed in this work was to study the combustion of several individual molecules in a series of experiments whilst varying a single feature of the molecular structure at a time. This yielded information about how a particular structural feature of a molecule affects the combustion process. During the course of this project, a special fuel injection system was developed, which allowed the injection of small fuel samples into the engine at high pressure. This allowed tests to be carried out on purposely synthesised fuel samples that were only obtainable in small quantities. Detailed studies on the combustion of fatty alkyl esters (commonly termed biodiesel), acetals, ethers and alcohols were conducted. The combustion chamber pressure of the engine, the energy release of combustion, the engine efficiency, the exhaust gas composition and the emission of particulate matter were measured and analysed. It was observed that in the diffusion combustion of biofuels, the emission of nitrogen oxides from the engine depend primarily on the ignition delay of the fuel, which governs the combustion stoichiometry and peak cylinder pressures and temperatures within the combustion chamber, and secondly on the adiabatic flame temperature of the biofuels. It was found that the number of double bonds present in biofuel molecules correlated with the amount of particulate mass emitted from the engine. It was further observed that oxygenated biofuels such as fatty acid alkyl esters, acetals, ethers and alcohols produced much lower levels of particulate mass from their combustion than petroleum-derived diesel fuel. The emission of particulates depended on the fuel oxygen content, as well as on the boiling point of the fuel. Combustion experiments conducted in homogeneous charge compression ignition combustion demonstrated that ethers of low molecular mass could be amongst the most-suited liquid fuel molecules for this type of combustion method.

Acknowledgements

I am immensely grateful to my supervisor Prof. Nicos Ladommatos for the invaluable support, trust, ideas and knowledge I have benefited from throughout the course of this project. Without his help, this work would not have been possible.

Thanks are also due to Dr. Pavlos Aleiferis for moral support as second supervisor.

I much thank Dr. John Williams, Dr. Robert Allan and Dr. John Rogerson at BP for funding, support and invaluable intellectual contributions to this project. Thanks are also due to Dr. Robert Allan for including my name on his BP patent application. Permission to publish the academic work was very much appreciated, and was of great importance.

I am very grateful to Prof. Choongsik Bae for the design of the DME fuel system, his support and intellectual contribution to the DME work. I would like to thank Dr. Balachandran for calibration of the port-fuel injection system. I thank Mr. Nnamso Akpanudoh and Dr. George Manos for their uncomplicated and kind help with the TGA analyses. Thanks to Dr. Jinwook Lee for the collaborative work on particulates. I thank Steven Santa for his work on the inductive engine TDC sensor. Thanks to Prof. Hua Zhao and Dr. Lyn McWilliam for making the MOUDI available to UCL. Thanks are also due to Dr. Robert Bulpett, Dr. Alan Reynolds and Mrs. Nita Verma for help with the SEM and XPS analyses of the particulate samples. Thanks to Dr. Steve Firth for help with the TEM imaging. Thanks to Mr. Kevin Reeves for help with the FTIR analyses. Thanks to Dr. David Wood for synthesis of the fuel samples and for information about the synthesis processes. Thanks also to all those at the UCL mechanical engineering department who have taught me over the years and made it possible for me to start this project.

A very particular gratitude is due to all the members of the UCL IC-engines group. Without the continuous help and moral support received, it would have been impossible to carry-out this work. Firstly, thanks to Dr. Alan W. P. Todd for his orderly ways, humour, and introducing me to the IC-engines group. Thanks to Dr. (to be) Zane van Romunde for north London barbecues; to Dr. (to be) José Serras-Pereira for explaining the meaning of ‘true’ efficiency to me; to Dr. (to be) Rishin Patel for his ‘bottle-dance’, the trip to China and immense help over the years; to Dr. (to be) John Malcolm for getting impatient at lunch time and being there when I lost control of my face; to Captain (already) Martino Rosati for receptions at Anatola resort and teaching the IC-engines group the ways of the blacksmith; to Dr. (to be) Andreas Birgel for his voluntary teaching activities at the UCL library in what a turbo-diesel engine should really sound like; to Dr. (to be) Priyesh Patel for fighting bears with bear hands and giving the IC-engines group street-cred; to Dr. (to be) Paul Hellier for maintaining that the world can be saved and taking Test-cell 1 to the next level. Thanks are also due to Garry Jones for sponsoring the IC-engines group with legendary tea-break biscuits and for his technical expertise.

I am infinitely grateful to my friends and family for their support.

To

Marco, Claudia, Carmen & Frank

Table of contents

List of figures

List of tables

Nomenclature

Symbols

a	number of C atoms in one fuel molecule
A_{bore}	cylinder bore area
b	number of H atoms in one fuel molecule
c	number of O atoms in one fuel molecule
c_p	specific heat capacity at constant pressure
c_v	specific heat capacity at constant volume
d	number of N atoms in one fuel molecule
D_{bore}	cylinder bore diameter
e	molar coefficient of air
g	molar coefficient of CO_2 in the exhaust gas
h	molar coefficient of CO in the exhaust gas
j	molar coefficient of O_2 in the exhaust gas
k	molar coefficient of N_2 in the exhaust gas
l	molar coefficient of NO in the exhaust gas
l_{con}	connecting rod length
m	molar coefficient of NO_2 in the exhaust gas
M	absolute mass of pollutant molecules emitted per engine cycle
m’	mass of pollutant molecules emitted per net indicated energy output
N_{air}	absolute number of moles of fresh air ingested by the engine per cycle
$N_{pollutant}$	absolute number of moles of pollutant emitted by the engine per cycle
p	combustion chamber pressure
p_{inj}	fuel injection pressure
Q_{ch}	apparent gross heat release rate
Q_{ht}	heat transfer rate to the combustion chamber walls
Q_{net}	apparent net heat release rate
R	specific gas constant for air
Ř	universal gas constant
r_{crank}	crank radius
s	molar coefficient of CH_4 in the exhaust gas
t	molar coefficient of H_2 in the exhaust gas
T_{ad}	adiabatic flame temperature
V	combustion chamber volume
V_{clear}	combustion chamber clearance volume
V_d	combustion chamber swept volume

W_i	net indicated displacement work per engine cycle
γ	ratio of specific heats
η	indicated thermal efficiency of the engine
θ	crank angle
μ	molar coefficient of N_2 in the intake air
π	molar coefficient of H_2O in the intake air
σ	instantaneous piston stroke
υ	molar coefficient of O_2 in the intake air
φ	molar coefficient of injected fuel
ω	molar coefficient of CO_2 in the intake air
Φ	fuel-air equivalence ratio
Φ_c	critical sooting fuel-air equivalence ratio

Abbreviations

2-EHN	2-ethylhexyl nitrate
ABE	acetone-butanol-ethanol
ADC	analogue to digital converter
ASI	after start of injection
ATDC	after top-dead-centre
BDC	bottom-dead-centre
BTDC	before top-dead-centre
CA	crank angle
CDM	crank-degree marker
CN	cetane number
DEE	diethyl ether
deg	degrees
DI	direct-injection
DIPE	diisopropyl ether
DME	dimethyl ether
EGDME	ethylene glycol dimethyl ether
EGR	exhaust gas recirculation
FID	flame-ionisation detector
HCCI	homogeneous-charge compression-ignition
HEPA	high-efficiency particulate air
HTHR	high-temperature heat release
IBE	isopropanol-butanol-ethanol
ID	ignition-delay

IDI	indirect-injection
IMEP	indicated mean-effective pressure
JME	jatropha-oil methyl ester
LII	laser-induced incandescence
LTHR	low-temperature heat release
MOUDI	micro-orifice uniform distribution impactor
MTBE	methyl-tert butyl ether
NB	natural biodiesel fuel consisting of a mixture of several fatty acid alkyl esters
NDIR	non-dispersive infrared
NOx	nitrogen oxides (NO & NO_2)
PAH	polyaromatic hydrocarbons
PID	proportional integral derivative
PLIF	planar laser-induced fluorescence
PM	particulate mass
PME	palm-oil methyl ester
PWM	pulse-width modulation
RME	rapeseed methyl ester
SEM	scanning electron microscope
SMFAE	single-molecule fatty acid ester
TDC	top-dead-centre
TEGDME	tri-ethylene glycol dimethylether
TEM	transmission electron microscope
TGA	thermo-gravimetric analysis
UHC	unburned hydrocarbons
ULVFS	ultra low-volume fuel-injection system
XPS	x-ray photoelectron spectroscopy

Chapter 1. The concept of biofuels as a sustainable source of energy

Automotive road transport was responsible for emitting 10% of the world's total greenhouse gas emissions in the year 2004 and is today one of the main contributors to climate change (Baumert, et al., 2005). The combustion of fossil fuels releases carbon in the form of carbon dioxide into the atmosphere, which had previously been stored as hydrocarbon deposits in the ground. This process has led to an increase in atmospheric carbon dioxide levels from ~280 ppm in the year 1850 to over 370 ppm in the year 2006. It is thought that the level of atmospheric carbon dioxide will exceed 560ppm before the end of the 21st century (Solomon, et al., 2007). Such an increase in atmospheric carbon dioxide levels is expected to cause disruptions to the global climate. This is because carbon dioxide has a high absorption efficiency of infrared radiation, and is thus capable of absorbing a high proportion of the infrared energy that is re-emitted towards space from the earth as a result of sunlight falling onto the earth's surface. An increase in atmospheric levels of carbon dioxide, thus results in a larger fraction of the re-emitted infrared radiation being absorbed by the atmosphere and being diverted back to the earth. This process, generally termed the 'greenhouse effect' is thought to be the main contributor to increasing temperatures in the earth's atmosphere. The combustion process in automotive engines is responsible for the emission of significant amounts of carbon dioxide and other gases with similarly high infrared absorption efficiencies (unburned hydrocarbons, carbon monoxide and nitric oxides) to the earth's atmosphere. Pollutant emissions such as nitric oxides, carbon monoxide, unburned hydrocarbons and particulate matter furthermore have direct detrimental effects on public health and the environment.

As of now, compression ignition engines represent the most energy efficient commercially available source of energy for automotive road vehicles (Stone, 1999; Heywood, 1988). They offer the capability to be fuelled by a wide range of renewable fuels as well as being compatible with currently available fossil fuels and a mix of the two. Electric powertrains drawing their energy from fuel cells or batteries could potentially provide higher conversion efficiencies in the future, but it is necessary for sustainable and efficient sources of primary energy for these powertrains to become available. Until then, renewable fuels for internal combustion engines can allow for a transition to sustainable powertrains to be made, especially because they can be used to gradually displace the use of conventional automotive fuels such as petrol and diesel fuel, and because they may be used to pave the way for a production and distribution infrastructure of renewable fuels and relevant intermediate products, which may later also be used for fuel-cell vehicles (e.g. hydrogen, methanol).

It was the aim of this project to identify and develop sustainable diesel fuels that can be produced without the emission of additional carbon dioxide to the atmosphere when considering the life cycle of the fuel, which comprises the fuel production, processing and its combustion. The project was

also aimed at improving the combustion in Diesel engines by use of these fuels, in order to reduce the emission of pollutants that have detrimental effects on public health or the environment, as well as improving the efficiency, performance and reliability of the engine where possible. To this end, an attempt was made to improve the understanding of chemical and physical combustion mechanisms which govern the compression ignition combustion of potential sustainable fuels.

Plants naturally bind carbon from atmospheric carbon dioxide in their biomass through photosynthesis during their growth by assembling organic molecules from water and atmospheric carbon dioxide. The energy used to promote this endothermic reaction is supplied by solar energy in the form of sunlight. This process releases oxygen to the atmosphere. The biomass which is thereby synthesised in the form of organic molecules stores the solar energy added during the photosynthesis process as chemical energy. If these organic molecules are oxidised using atmospheric oxygen, the stored solar energy is released during this reaction, and the carbon dioxide which was used to synthesise the organic molecules is returned to the atmosphere. Since this process involves a closed carbon cycle, biomass represents a potential feedstock for the production of carbon dioxide neutral fuels. Biomass is limited in its availability though, and needs to be used efficiently.

In order to be able to develop biomass fuels which are conducive to reliable and efficient combustion processes in compression ignition engines, it is necessary to gain an improved understanding of the combustion mechanisms involved with such fuels. The molecular composition of the fuel is amongst the most fundamental parameters to affect the combustion process in compression ignition engines. The molecular composition affects both the physical properties of the fuel such as viscosity and volatility, which are fundamental to the preparation of the fuel and air charge, as well as the chemical characteristics of the fuel, which govern the combustion reactions in terms of the start and duration of combustion and its energy release rates. All of these properties of the fuel are fundamental to the thermal efficiency and performance of an engine, as well as to the amount of pollutants emitted.

Biodiesel is the only biofuel currently used for compression ignition engines. Biodiesel was developed in the 1930's, mainly for use as fuel in tropical regions, but never went into large scale production at that time due to petroleum diesel fuel becoming cheaper and more readily available throughout the world. Biodiesel was virtually forgotten about in the midst of the 20th century, until the oil crises of 1973 and 1978 renewed interest in it, and several experimental studies using fatty acid alcohol esters as fuels for diesel engines were published in 1980 and in the following years. The first time the word 'biodiesel' was mentioned in a publication appears to be in the paper of Wang (1989). Although biodiesel has received fluctuating attention over the years, it has firmly established itself as a biofuel for modern diesel engines in the last decade. In the countries of the European Union (EU) it reached a market share of 1.5% of the total automotive diesel fuel sale in terms of energy content in the year 2005 (European Biodiesel Board, 2006). All car manufacturers allow the use of 5% biodiesel mixed with conventional diesel fuel in their vehicles, while some (Citroën,

Peugeot) allow the use of 30% biodiesel and others (VW, Scania) even allow the use of pure biodiesel on many of their models. It is estimated that the maximum potential for biodiesel in geographic Europe (EU-30) is a replacement of 6.5% of the total automotive road fuel consumption in Europe of the year 2004 (Vogel, et al., 2004). Commercial biodiesel generally reduces the total emission of carbon dioxide by about 60-80% with respect to conventional fossil diesel fuel (European Parliament and Council of the European Union, 2009). This advantage can be further improved if the production methods of biodiesel are optimised, and more efficient use of the biomass is made (Janulis, 2004). It has been shown by several researchers that the replacement of conventional fossil Diesel fuel by biodiesel significantly reduces the emission of particulate matter, carbon monoxide and unburned hydrocarbons from Diesel engines, but also results in a small increase of nitrogen oxide (NO_x) emissions (Pischinger, et al., 1982; Mittelbach, et al., 1985; Graboski & McCormick 1998; United States Environmental Protection Agency, 2002).

Agriculturally, biodiesel production is currently dependent on the cultivation of oil crops or animal fat as a feedstock. Animal fat is usually only used for the production of biodiesel when surplus animal fat is available as a by-product of meat or dairy farming, since animals are not usually held for use as biodiesel. In the case of vegetable oil, crops are today purposely grown to be processed as biodiesel. The cultivation of oil-crops can be a relatively inefficient and land-intensive way of producing biofuels, since only a small proportion of the crop is used for fuel production. It is important that use is made of the remaining crop when oil-crops are grown to make better use of the benefits which biofuels potentially offer in terms of atmospheric greenhouse gas emissions.

Synthetic biofuels which may be produced in the future could have significant advantages over current biofuels such as biodiesel. A promising possibility is to produce oxygenated biofuel molecules with ether or acetal chemical structure via the intermediate synthesis of short chained alcohols. The alcohols can be obtained through the direct fermentation of cellulosic material from plants, or through gasification and subsequent catalysis of synthesis gas obtained from biomass. These synthetic molecules promise to offer significant advantages in terms of their efficiency of production from biomass with respect to biodiesel fuel, because they make use of the whole plant rather than just the oil crop. They also offer the opportunity of controlling their molecular structure more closely via their production process. This gives the important advantage that their combustion characteristics may be tailored quite significantly towards the requirements of the engine. From an agricultural point of view, such synthetic fuels offer the opportunity that a high flexibility in the choice of crop can be maintained, because the biomass required to produce these fuels may consist of cellulose rather than plant-oils, which is a more common biomass material amongst plants. The crops grown for these types of synthetic biofuels may thus include various energy crops as well as forestry, agricultural and domestic waste products. If purposely grown crops are necessary, these may be chosen more freely according to the local climatic and agrological conditions, thus limiting the environmental impact which the biomass feedstock production has. In the future it may also be

possible to develop plants that can grow under semi-arid conditions and on land that is unsuitable for the cultivation of food crops.

When developing processes for the production of synthetic biofuels for compression ignition engines, it is necessary to understand the effects which molecules have individually and in combinations upon the combustion process. The approach developed during the course of this project was to study several individual molecules in a series experiments while varying a single feature of the molecular structure at a time. This can yield information about how a particular structure in the molecule affects the combustion process. The research presented herein is a fundamental study upon the effect of individual molecular structure of traditional and potential synthetic biofuel molecules upon the diesel combustion process. The project may be divided into three main parts: The first part examines the influence of the molecular structure of biodiesel molecules, while the second and third part of the work is dedicated to applying this methodology to potential future synthetic biofuels from two different production methods respectively.

1.1. Historical development biofuels for Diesel engines from the point of view of their molecular structure

The use of biofuels for Diesel engines can be traced back as far as the year 1900 when a diesel engine exhibited at the World Fair in Paris was run on pure, untreated peanut oil in a public demonstration (Diesel, 1912). Since these early records, the chemical composition of biofuels has undergone significant developments under the influence of technical, economical, political and environmental factors, several of which are still of central importance to current and future developments in this field. This first chapter focuses on the technical considerations affecting the combustion of biofuels in a diesel engine, and how these have led to historical changes in the molecular structure of biofuels for diesel engines.

The first traceable use of plant oil as a fuel in the year 1900 occurred only eight years after the theoretical invention and patenting of the diesel engine in 1892 and no more than three years after the first practical diesel engine was actually constructed in Augsburg in 1897 (Diesel, 1892, 1893 a, 1893 b, 1912, 1913). Fats such as plant or animal oils consist of triester molecules of fatty acids and glycerol. These are typically very large molecules of high molecular mass. Figure 1.1 below shows a typical example of a palm oil molecule as that used by Chavanne (1937). It has the sum formula $C_{53}H_{94}O_6$, and a molecular mass of 827.31 g/mol. This first successful demonstration of plant oil used as diesel engine fuel in 1900 occurred upon the request of the French government, and was aimed at demonstrating the diesel engine's suitability for use in African countries, where peanut oil could be produced locally (Diesel, 1912). The demonstration engine had been constructed for use

with mineral diesel fuel oil, but was operated smoothly on peanut oil without any technical modifications. During the decades following this demonstration, it was recognised that certain typical properties of vegetable oil can be detrimental to an efficient combustion process in a diesel engine (Mathot, 1921). The high viscosity of vegetable oil leads to poor atomisation of the fuel spray, and the low volatility of vegetable oils can lead to difficulties in fuel vaporisation within the combustion chamber. This leads to slow and incomplete combustion of the fuel and can be conducive to the formation of high amounts of exhaust gas pollutants and carbonaceous deposits in the combustion chamber.

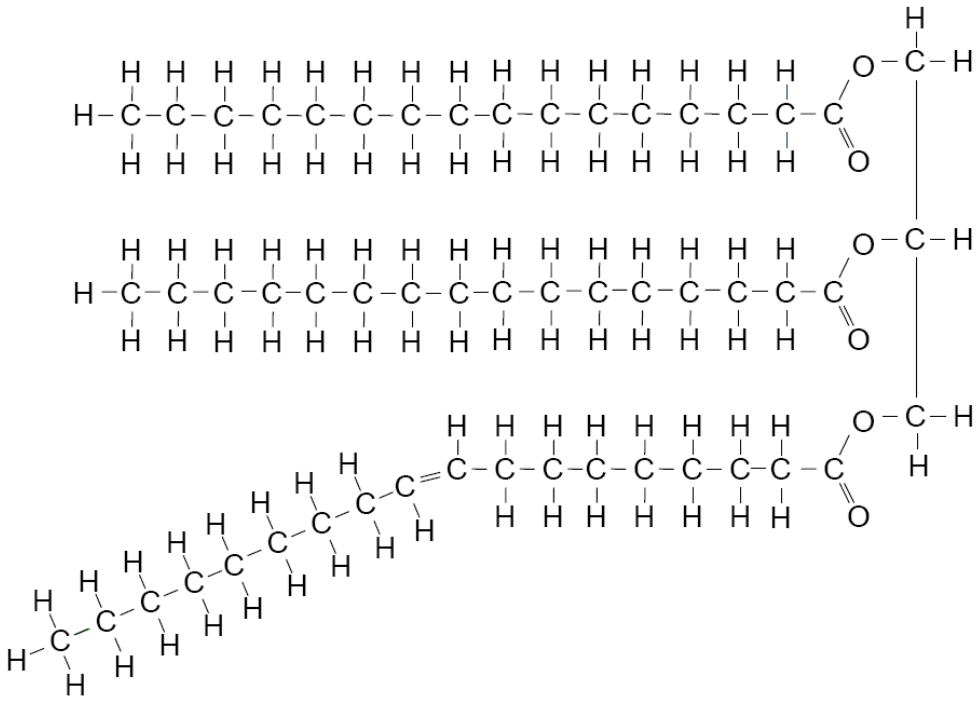

Figure 1.1 – Example of palm oil molecule. Adapted from Chavanne (1937).

The first documented attempts of changing the molecular structure of organic oils for their use as fuels in compression ignition engines involved thermally cracking and distilling plant or animal oils into lighter hydrocarbon fractions (Kobayashi, 1921[a], 1921[b]; Kobayashi & Yamaguchi, 1921). Despite its successful implementation in practice, the inherent problem with this production method is that it is relatively inefficient, because it usually involves wasting part of the raw vegetable oil, and because the process requires a significant amount of energy input.

Several years later, Walton (1938) postulated that 'to get the utmost value from vegetable oils as fuel it is academically necessary to split off the triglycerides and to run on the residual fatty acid. Practical experiments have not yet been carried out with this; the problems are likely to be much more difficult when using free fatty acids than when using the oils straight from the crushing mill. It is obvious that the glycerides have no fuel value and in addition are likely, if anything, to cause an excess of carbon in comparison with gas oil.' Walton's idea of separating the fatty acids from the

glycerol, points in the direction of a process which is today widely used in the production of biodiesel. He was aware that separating the fatty acids from the glycerol would reduce the fuels viscosity and improve volatility, but yet he was not sure what to do with either the fatty acids or the glycerol.

One year earlier, Charles Georges Chavanne (1937) filed a patent for the 'alcoholysis' or transesterification of vegetable oils for the production of a heavy motor fuel. The original patent from 1937 states (translated from the French): 'Vegetable oils, which have often been tried for their use as heavy motor fuel in the tropical regions - in which they are produced- exhibit, in this respect some unfavourable properties, which can be cited as: their acidity, their ease of solidification, their high viscosity, and their absence of good volatility. The subject of the present invention is the transformation of vegetable oils into a fuel of nearly zero acidity, which doesn't solidify [even] at the lowest temperatures known to occur at moderate altitudes in the tropical regions, which is of a fluidity hardly inferior to that of heavy petroleum fuels at their working temperatures, that is of remarkable volatility, and which is able to completely vaporise in a narrow temperature interval without leaving any appreciable residue'. The issues of viscosity, volatility, ease of solidification, the formation of deposits during combustion and to a less well-known extent the acidity of the fuel, which represent the most significant problems in using untreated vegetable oil directly as engine fuel, were addressed by the development of biodiesel fuel described in this patent. The patent (Chavanne, 1937) and a later publication (Chavanne, 1943) describe the chemical process of transesterification to detach the fatty acids of vegetable oil from each other and their common glycerol moiety, which holds the fatty acid chains together. In this reaction the fatty acids are attached to short monohydric alcohols instead, while the glycerol is removed from the fuel as a by-product.

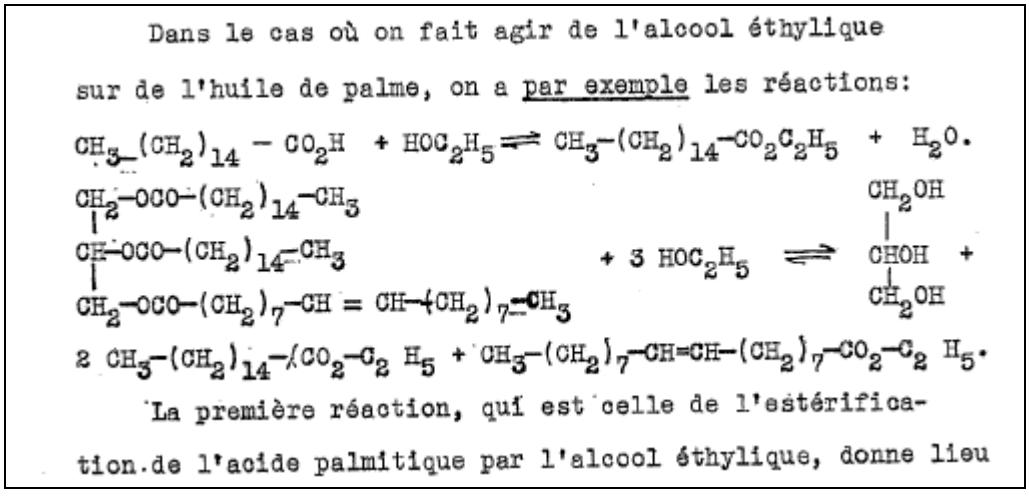

Dans le cas où on fait agir de l'alcool éthylique sur de l'huile de palme, on a par exemple les réactions:

$$CH_3-(CH_2)_{14}-CO_2H + HOC_2H_5 \rightleftharpoons CH_3-(CH_2)_{14}-CO_2C_2H_5 + H_2O.$$

$$\begin{array}{l} CH_2-OCO-(CH_2)_{14}-CH_3 \\ | \\ CH-OCO-(CH_2)_{14}-CH_3 \\ | \\ CH_2-OCO-(CH_2)_7-CH=CH-(CH_2)_7-CH_3 \end{array} + 3\ HOC_2H_5 \rightleftharpoons \begin{array}{l} CH_2OH \\ | \\ CHOH \\ | \\ CH_2OH \end{array} +$$

$$2\ CH_3-(CH_2)_{14}-CO_2-C_2H_5 + CH_3-(CH_2)_7-CH=CH-(CH_2)_7-CO_2-C_2H_5.$$

La première réaction, qui est celle de l'estérification de l'acide palmitique par l'alcool éthylique, donne lieu

Figure 1.2 – Transesterification reaction used to produce biodiesel fuel from vegetable oil and a mono-alkyl alcohol taken from the original Patent (Chavanne, 1937)

The products of this reaction are biodiesel molecules which consist in monoesters of fatty acids and monohydric alcohols (see Figure 1.3).

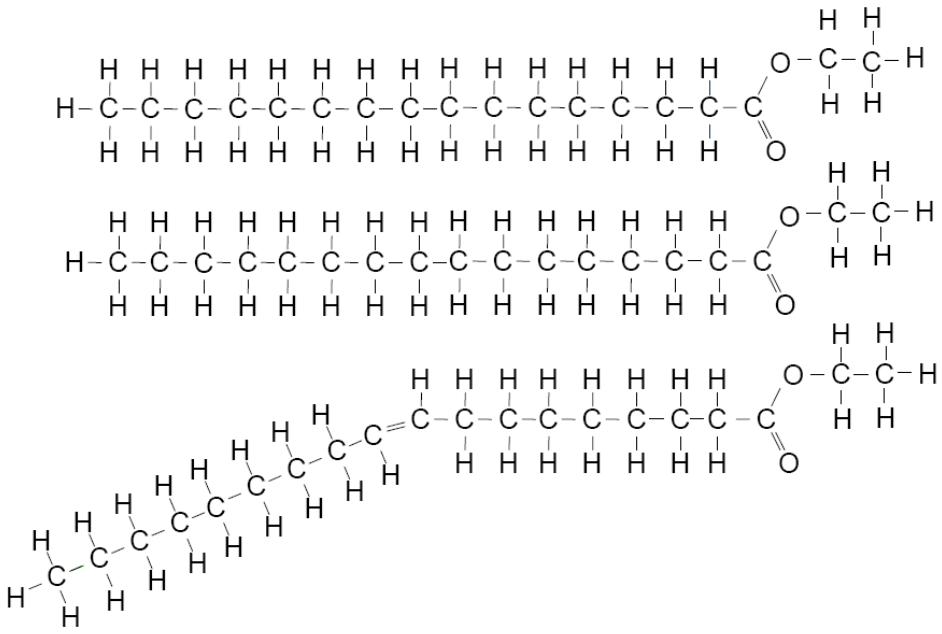

Figure 1.3 – Biodiesel molecules formed from the reaction of ethyl alcohol with the palm oil molecule in Figure 1.1.

An extensive research project followed this invention, in which large quantities of biodiesel were produced from Congolese palm oil and ethanol, and tested in laboratory and road tests in Belgium. The palm oil was to be produced from oil palms, and the ethanol from manioc or sugarcane in Congo (van den Abeele, 1942) where the resulting biodiesel fuel was intended to be utilised as a diesel engine fuel. Engine test bed and vehicle experiments revealed significant differences of the biodiesel fuel with respect to raw palm oil tested in previous studies, as well as with respect to mineral diesel fuel oil. For instance, a public passenger service which operated between the cities of Brussels and Leuven in Belgium fuelled a bus with biodiesel of palm oil for over 20,000 kilometres in 1938, and its operation was compared with a bus of identical built operating on conventional diesel fuel during the same period. The only technical difference between the two engines was that the limit of volumetrically measured fuel injection quantity per cycle was raised for the bus operating on biodiesel, so that both engines could achieve the same maximum output power due to the lower calorific value that biodiesel has on a volumetric basis. It was found that the cold-start ability of the bus operating on biodiesel was significantly better as the records which the bus-drivers made each morning showed. This was confirmed by recording indicator diagrams and carrying out cetane number measurements in an engine laboratory, which showed that the ignition delay of the fuel was significantly reduced (Figure 1.4).

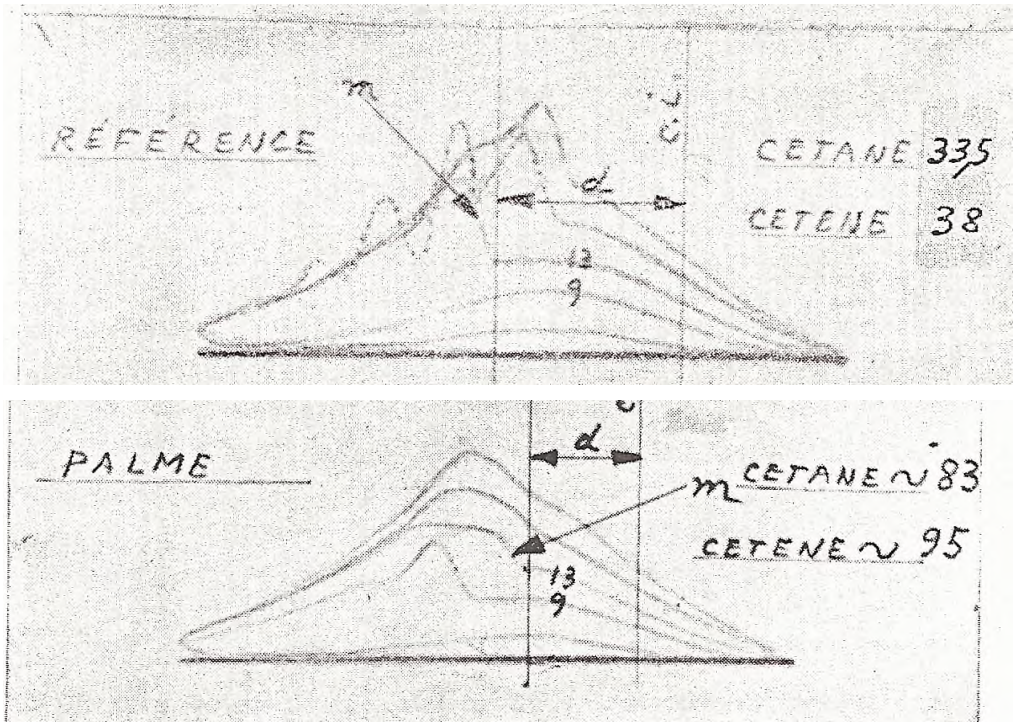

Figure 1.4 - Indicator diagrams for the same diesel engine operating on reference fossil diesel fuel (top) and Palm-oil ethyl ester biodiesel fuel (bottom), van den Abeele (1942).

Opacity measurements carried out on an engine test bed showed that the smoke output was lower for the biodiesel than for mineral diesel fuel if the same liquid volume of fuel was injected per cycle. If the fuel quantity of the biodiesel was increased however, to yield the same engine power output as delivered by the mineral diesel oil, the smoke output of both fuels was found to be comparable. This is an indication that the atomisation and combustion problems reported previously for untreated vegetable oil (Mathot, 1921) had been solved by changing the molecular structure from triacylglycerols (triesters of three fatty acids with glycerol, also referred to as triglycerides) to fatty acid ethyl esters.

After the road test on the buses had been completed, both bus engines were taken apart and inspected, and it was found that the engine which had been operated on biodiesel showed substantially less combustion deposits, than the engine operated on fossil diesel fuel oil (Figure 1.5). This gave further indication that the atomisation and combustion problems reported for untreated vegetable oils had been solved by changing the molecular structure from triacylglycerols to fatty acid ethyl esters.

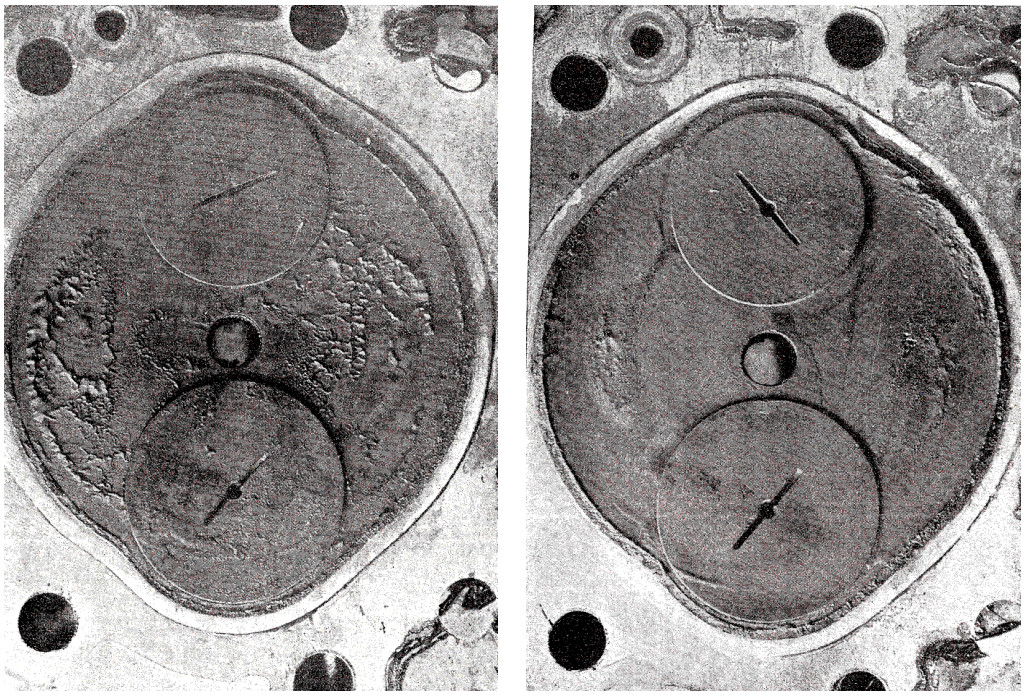

Figure 1.5 – Combustion chamber deposits in two diesel engines of the same model after being operated on fossil diesel fuel (left hand side) and palm-oil biodiesel fuel (right-hand-side) over 20,000 km in a passenger bus, van den Abeele (1942).

The development of biodiesel fuel meant that the molecular structure of plant-oils used for combustion in diesel engines could be changed from large triacylglycerols molecules to monoester molecules. This was observed to resolve several operational problems associated with triester molecules, and allowed improving the combustion process as well as engine exhaust emissions, the engine cold-start performance and its mechanical durability.

1.2. Current and future biofuel developments for diesel engines

Biodiesel is currently the only commercially available biofuel for diesel engines. Its potential in replacing fossil automotive fuels, and thereby reducing the overall emission of greenhouse gases is however, very limited if it is to be produced from land-grown crops. It is estimated that the maximum land-production potential for biodiesel within geographic Europe (EU-30) is a replacement of 6.5% of the total European automotive road fuel consumption of the year 2004 (Vogel, et al., 2004). This is based on the assumption that 17% of the European arable land can be used for the production of biodiesel, which in turn is based on the assumption that 15-20% of European land is currently left fallow with regards to avoiding food over-production under the European common agricultural policy. It is thought that commercial biodiesel generally reduces the total emission of carbon dioxide by about 60-80% with respect to conventional fossil diesel fuel

(European Parliament and Council of the European Union, 2009). If the hypothetical maximum replacement of 6.5% of all automotive road fuel could be achieved, this would result in a maximum reduction of 3.9-5.2% of CO_2 emissions linked to road transport through the implementation of biodiesel as fuel. Whilst this does indeed represent a net benefit that could be achieved in Europe without displacing the production of food crops or the need for new agricultural land, biodiesel will not solve the problem of greenhouse gas emissions from automotive road transport at current rates of fuel consumption. Part of the reason for this low reduction potential of greenhouse gases from biodiesel is that oil plants grown for the production of biodiesel make relatively inefficient use of the land and agricultural resources. Further to this, only a small portion of the plant (the oil seed or oil fruit) is used for the production of biodiesel fuel. Due to the limited production potential of biodiesel from arable land, there exists a need for diversification and more efficient use of production resources.

The production of biodiesel from aquatic microphyte organisms or micro-algae such as bacillariophyceae and chlorophyceae which produce high yields of plant oils through their metabolism, could offer some advantages over the production of biodiesel from terrestrial plants. Microphyte organisms could either be grown on land in open ponds (Sheehan, et al., 1998), or in lakes (Umakantha, 1974) and could conceivably even be grown at sea. The potential plant-oil yield per surface area for algae is estimated to be more than 35 times that of rapeseed, and approximately 10 times that of oil palms (Waltz, 2009), the latter of which has the highest known plant-oil yield for a terrestrial plant. Like many other plants, aquatic microphytes offer not only the possibility of producing triacylglycerols (commonly used as the source of fatty acids for the production of biodiesel), but also of the second ingredient necessary for the production of biodiesel molecules, i.e. monohydric alcohols (Leigh-Haag, 2007). The monohydric alcohols can be readily produced by fermentation of the starch content of the algae. Thus there exists, even for the production of biodiesel, some significant scope for improvement of its production capabilities. Biodiesel from aquatic microphytes is expected to provide a highly flexible product yield, in terms of the types of biodiesel molecules produced, due to the wide variety of different algal strains available, and the possibility of genetically engineering the metabolic pathways that control fatty acid production (Service, 2008). In view of this flexibility, research on the combustion characteristics of individual biodiesel molecules as has been carried out during the course of this project (see Chapter 5) would be expected to gain increasing significance.

Another way of making more efficient use of land is the production of synthetic biofuels from lignocellulosic biomass. Lignocellulose is one of the most common structural materials of land plants, and does thus not need to be purposely grown. It could be extracted sustainably in from existing forests or reforested areas, as long as the nutrients removed via this process are sustainably restituated to the land they are extracted from. This could be done for example using fertilisation from waste products of the fuel production. Lignocellulose is also present in many agricultural waste products stemming from food production, and could lend itself to the production of biofuels. The production of such synthetic biofuels derived from lignocellulosic materials, has the advantage that any portion of the crop can be used for fuel production, not just the oil or starch seeds used in

biodiesel production, and thus a high flexibility in the choice of crop type is maintained. This means that crops can be chosen more freely according to the local climatic and agrological conditions, thus limiting the environmental impact of the biomass feedstock production. From the point of view of combustion, the production of synthetic biofuels offers the opportunity that the combustion characteristics of the fuel molecules may be tailored to a larger extent according to the requirements of the combustion system.

Two general pathways of synthetic biofuel production from lignocellulosic biomass were explored during the course of this project. The first one consisted in the bio-metabolic decomposition of lignocellulose which could either lead directly to the fuel molecules, or yield intermediate compounds that could be used for the synthesis of the fuel molecules. The second production pathway consisted in the thermo-chemical decomposition of the lignocellulose into synthesis gas, from which fuel molecules could be produced using catalysed reactions. Both production methods shall be discussed in further detail in Chapter 2.

1.3. The potential benefits of biofuels and problems linked to their production

The principle of using biofuels as a source of sustainable renewable energy relies on the closed loop which the life cycle of biomass can take. Biomass is produced through the growth of plants in the form of organic molecules from water and carbon dioxide via an endothermic reaction driven by sunlight. Oxygen is released during this process in its gaseous molecular form. To complete the life cycle, the decomposition of biomass into its original constituents, i.e. water and carbon dioxide, occurs via its oxidation using atmospheric oxygen and under the release of its stored chemical energy. This second step offers the possibility to be conducted artificially for a portion of the biomass, whereby the chemical energy of the biomass may be used to drive a heat engine. Within this model of thought, the use of biomass as a fuel represents a form of energy that is sustainable for as long as sunlight is supplied to the system and its heat can be disposed of at an equilibrated rate.

In the real-life application of biomass fuels, a number of practical problems exist that reach beyond the above described system of thought.

The world has a growing population which must be fed from the world’s limited agricultural resources. The production of biofuels from arable land, on a scale sufficient to meet a significant portion of the worlds growing demands for energy, would be expected to cause fierce competition for land. At best, this would induce strong rise in the price of food and biofuel production but at worst would prove unsolvable. The potential for biofuel production in this way is thus limited. Proof of an increase in the cost of food was felt as soon as large scale production of biofuels commenced

(Martin, 2008). The high food prices were also observed to be a source of political unrest and conflict (Bone, 2008).

In addition to humanitarian issues, the fundamental principles on which biofuels production is based, i.e. the advantage which biofuels have over fossil energy resources in terms of avoiding the emission of greenhouse gases, have also been questioned.

Firstly, this concerns the way in which biofuel production technology is applied. Analysis of greenhouse gas emissions have shown that under certain conditions the production of biofuels can result in an increase of greenhouse gas emissions in comparison to using fossil fuel. For example the production of corn ethanol that uses fossil coal to sustain the production process has been estimated to result in a 3% increase of greenhouse gases with respect to using fossil petroleum (Wang, 2007). It is apparent that in this case, biofuel technology is not used for the reduction of greenhouse gases, but rather to the end of political energy independence, and does thus not need to be discussed further to this end.

Secondly, the above described principle of greenhouse gas neutrality of biofuels based on their life-cycle is valid only for a steady-state model of the biomass life cycle. Although the benefits of this principle are true to apply in their steady-state model, and are thus valid for an infinitesimally long application of biofuels, the transient effect of the introduction of biofuels could have severe disadvantages in terms of greenhouse gas emissions in the short-term. Research has demonstrated that if the life-cycle analysis of greenhouse gas emissions is expanded to incorporate the transient changes in land-use due to biofuel production, biofuel production could severely aggravate the emission of greenhouse gases over the coming decades, and century (Searchinger, 2008). This is because the transformation of forests, grasslands and swamps into arable land suitable for the production of certain biofuels, releases large amounts of carbon dioxide into the atmosphere due to the decomposition of biomass sequestered in the soil and plants. If the production of biofuels was to facilitate and fund the reforestation of targeted areas by increasing the demand for lignocellulose from managed forests, this could have beneficial transient effects in terms of greenhouse gas emissions. This aspect emphasises the advantage of biofuels that can be made from a common biomass material such as lignocellulose which can be extracted from forested areas, over biofuels that require the development of agricultural land, and highlights the necessity for sound concepts of biofuel production.

1.4. Aim and objectives of the project and structure of the thesis

The aim of this project was to experimentally study the influence which the molecular structure of biofuels has on their combustion in a diesel engine. This was done using a purposely developed single cylinder research engine which was instrumented to allow detailed analysis of the combustion events. The engine used a specially developed fuel injection system that allowed the electrically controlled injection of small quantities of pure samples of purposely synthesised biofuel molecules, under high pressures. In particular, the objectives may be described as follows:

- To design, construct and commission a new experimental test engine in a new laboratory at University College London, which included the development of engine instrumentation, fuel injection system, data acquisition system and methods for analytically processing the experimental data.
- To study the effects of changes in the molecular structure of fatty acid alkyl esters have on the diesel combustion process in terms of combustion chamber pressure, heat release rates and pollutant emission.
- To investigate the suitability of all of the previously mentioned types of fuel molecules for lean homogeneous charge compression ignition (HCCI) combustion processes in terms of charge preparation, pressure history, heat release rates and pollutant emission.

The text is divided into nine Chapters, which may be summarised individually as follows:

The present Chapter 1 consists of an introduction to the subject intended to place the experiments into context. After providing background information on the reasons for the work, the chapter gives an account of the historical background and an overview of modern perspectives on current and future developments in the field, as well as providing evidence of potential problems linked to this research area.

Chapter 2 is a review of technical literature on the subject. The initial section provides a discussion of the fundamental phenomena occurring in diesel combustion relevant to the experimental work. The later sections of this chapter are a review of literature examining past work on the effect which the molecular structure of biofuel molecules has on the combustion process in a diesel engine.

Chapter 3 provides a description of the experimental apparatus used in the experiments. This comprises the research engine and its instrumentation for the measurements of pressure, fuel and air flow-rates, inlet and exhaust gas concentrations and particulate measurements.

Chapter 4 gives a description of the mathematical analysis applied to the experimental data and the assumptions made. The mathematical analysis concerns the cylinder pressure and heat release analyses, IMEP and global temperature calculations, and a model for the analysis of the combustion stoichiometry.

Chapter 5 describes the experiments focussing on diesel combustion of fatty acid alkyl esters (biodiesel), which are produced from the transesterification of vegetable oils with monohydric alcohols.

Chapter 6 describes the experiments carried out on the diesel combustion of acetal molecules, a biofuel produced from cellulose via biological decomposition.

Chapter 7 describes the experiments carried out on the diesel combustion of various synthetic biofuel molecules that could be produced from cellulosic biomass, using thermochemical decomposition of the biomass into synthesis gas.

Chapter 8 is dedicated to the experimental application of the three types of biofuels used in chapters 5-7 to homogeneous charge compression ignition (HCCI) combustion. The chapter discusses the experimental results achieved with each type of fuel, and their suitability for HCCI combustion, as well as looking into how the individual molecular structure of the fuels affects this type of combustion process.

Chapter 9 summarises the of this research work whilst outlining its main conclusions. It provides an account of the novel aspects of this research, gives details of a patent and of academic publications written during the course of this project as well as providing recommendations for future work.

Chapter 2. A review of the literature on the combustion of biofuels in compression ignition engines

2.1. Definition and fundamental principles of diesel combustion

The fundamental principle of diesel combustion is an isothermal combustion process, which is achieved by the progressive introduction of an autoigniting fuel into an expanding air charge, at such a rate that the expansion of the air and the heat created by the combustion process balance, thereby achieving a constant temperature expansion process (Diesel, 1893).

Rudolf Diesel developed the idea of the diesel engine on the basis of this thermodynamic principle, in pursuit of an engine that would be able to practically achieve the ideal Carnot cycle with air as the main working fluid. One of the four processes of which the Carnot cycle famously consists, is the isothermal heat reception process, which lay at the core of this invention. In his book 'Die Entstehung des Dieselmotors' (The development of the diesel engine), he notes: 'When my honoured teacher, Professor Linde explained at the Polytechnic University of Munich in 1878 to his audience that the steam-engine only converts 6-10% of the available heat of the fuel into effective work, and then went on to explain the Carnot cycle, he demonstrated that for the isothermal change of state of a gas, the entire heat supplied to the gas is converted into effective work. I noted on the side of my notebook: 'Study if it is not possible, to practically realise the isotherm'. It was then that I set myself the task. It wasn't yet an invention, not even the idea for it. The desire to realise the ideal Carnot cycle determined my existence from then on. I left school, went into practice, had to establish my standing in life. The thought was continuously on my mind.'

The original patent for the diesel engine (Diesel, 1892) describes the isothermal combustion process as follows: '…Subsequently a finely dispersed fuel is gradually introduced from outside into the compressed air, and ignites itself because the mass of air has been heated way above the temperature necessary for ignition of the fuel. Simultaneously to the gradual introduction of the fuel, occurs an expansion of the air mass, which is controlled in such a manner that the cooling of the air charge due to its expansion is exactly counterbalanced by the heat generated through the combustion of the individual particles being introduced. In this fashion, the combustion does not result in an increase of temperature, but exclusively in the production of useful work…'

The fundamental idea was to build an internal combustion engine capable of achieving the ideal Carnot cycle using an ideal gas as working fluid. The ideal Carnot cycle for an ideal gas consists of four distinct processes: Isothermal compression at low temperature, isentropic compression, isothermal expansion at high temperature and isentropic expansion. Isentropic compression and expansion would be realised by simple adiabatic compression or expansion of the gas. The isothermal compression was to be achieved by the gradual injection of liquid water into the cylinder, wherein a constant temperature was achieved through vaporisation of this water. The isothermal expansion was to be achieved using the above described concept of isothermal combustion.
Diesel stated that in order to make this engine independent of a supply of water, the cycle could be altered in such a way, that the isothermal compression process was omitted. As a result, the air at the end of the isentropic expansion process would be hotter and at higher pressure than it was in its initial state. A replacement for the heat rejection process would thus be necessary to close the cycle. The proposed solution was an overexpansion of the gases to atmospheric pressure, followed by isobaric cooling of the gases back to their initial state. This alteration of the ideal Carnot cycle resulted in the cycle which he patented in 1892 using his mechanism of isothermal combustion. This original definition of the thermodynamic cycle upon which a diesel engine was to operate, is thus described by the thermodynamic processes shown in Figure 2.1 (P-V, T-V, P-T and η).
The efficiency of this original isothermal heat addition diesel cycle may be expressed as a function of the compression ratio r and the cut-off ratio r_c (Equation 2.1), which was derived by the author upon thermodynamic analysis of the cycle. The cut-off ratios herein defined as the ratio of the volume after combustion (3) over the volume before combustion (2). The detailed derivations of these analyses are presented in Appendix A.

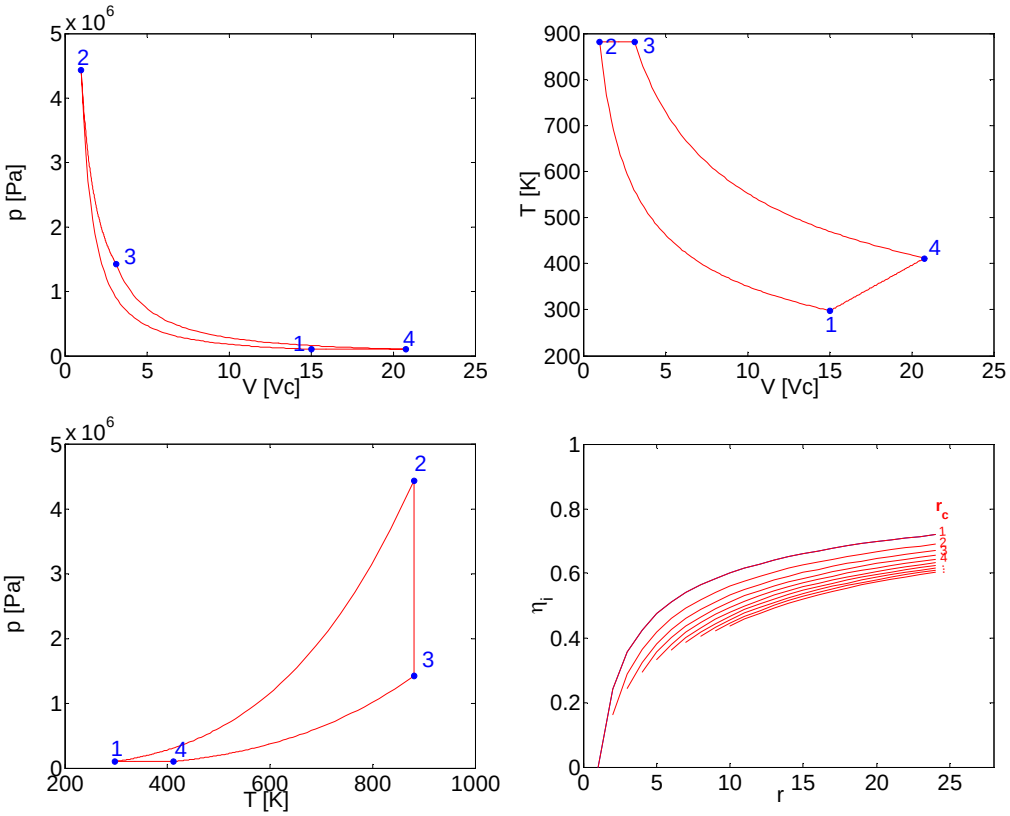

Figure 2.1 - Original over-expanded thermodynamic cycle with isothermal heat-addition according to Diesel (1892).

$$\eta_{Diesel1892} = 1 - \frac{\gamma}{\gamma - 1} \frac{1}{\ln(r_c)} \left[\left(\frac{r_c}{r^{\gamma}} \right)^{\frac{\gamma - 1}{\gamma}} - r^{1-\gamma} \right]$$

Equation 2.1

The term ‘diesel combustion’ shall in the following be used to describe a diffusion combustion process achieved through the compression ignition of a fuel within the combustion chamber of an internal combustion engine and shall not apply strictly to the process of isothermal combustion.

2.2. The influence of the diesel combustion process on the thermal efficiency of the engine

The indicated fuel conversion efficiency of an engine is strongly influenced by the way in which the diesel combustion process takes place. The principle mechanism by which the combustion process exerts its influence on engine efficiency is the way in which the heat is released to the cylinder gases and its surroundings. The concept of heat release rate of combustion is thus of central importance to this discussion.

Firstly, the effect of the heat release rate on the ideal cycle, and its efficiency shall be examined. Consider to this end an engine with a compression ratio of 15:1, equal to that of the research engine, supplied with air at atmospheric pressure and temperature as its working fluid. Consider, with all other conditions being equal, an isochoric, an isobaric and an isothermal combustion process, each resulting in an ideal cycle with the same indicated mean effective pressure per cycle. Figure 2.2 shows calculated diagrams of such ideal cycles.

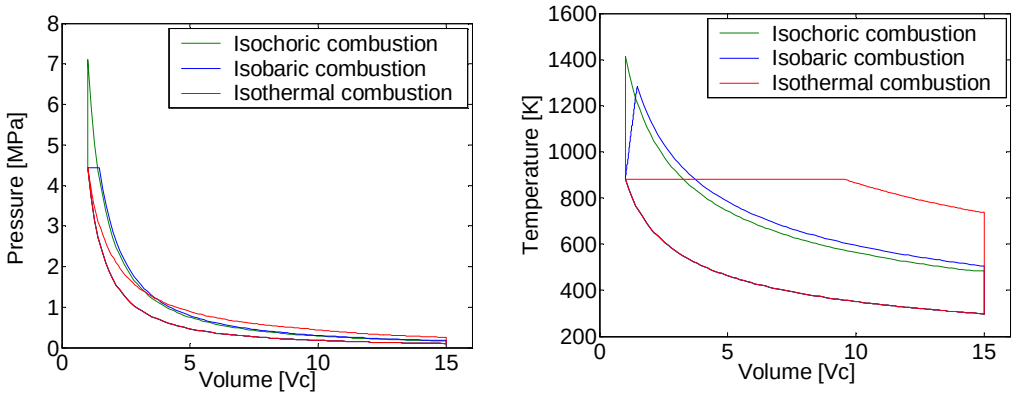

Figure 2.2 - Indicator diagram and temperature diagram

It can be seen in Figure 2.2, that the duration of the combustion is shortest for the isochoric combustion, longer for the isobaric combustion and longest for the isothermal combustion. It is further visible, that the highest combustion temperatures are reached during the isochoric cycle, followed by the isobaric cycle, and that the lowest temperatures are reached during the isothermal cycle. The exhaust gas temperatures are organised in the opposite order, indicating that the heat rejected during the exhaust process is highest for the isothermal process and lowest for the isochoric process.

Thermodynamic analysis under the assumption of ideal gas behaviour, allows the calculation of the ideal thermodynamic efficiencies achieved by each of these cycles, leading to the following expressions:

$$\eta_{isochoric} = 1 - \frac{1}{r^{\gamma-1}}$$

Equation 2.2 (Çengel and Boles, 1998)

$$\eta_{isobaric} = 1 - \frac{1}{r^{\gamma-1}}\left[\frac{r_c^{\gamma} - 1}{\gamma(r_c - 1)}\right]$$

Equation 2.3 (Çengel and Boles, 1998)

$$\eta_{isothermal} = 1 - \frac{1}{\gamma - 1}\cdot\frac{1}{\ln(r_c)}\left[\left(\frac{r_c}{r}\right)^{\gamma-1} - r^{1-\gamma}\right]$$

Equation 2.4 (See Appendix A for derivation)

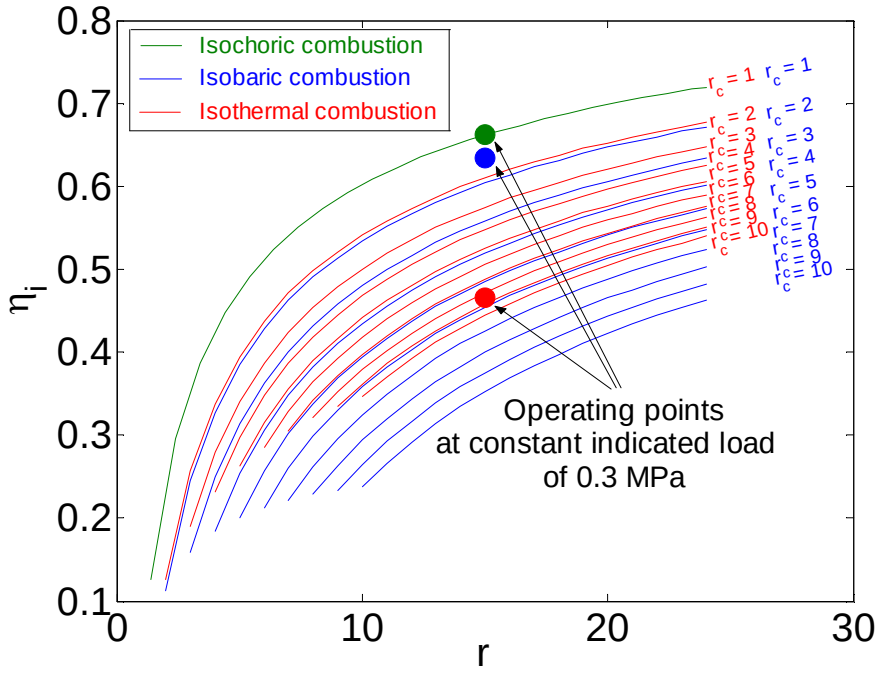

Figure 2.3 - Ideal cycle efficiencies as function of compression ratio and cut-off ratio for isochoric, isobaric and isothermal cycles

Figure 2.3 indicates the cycle efficiencies of the three types of cycles operated at the same indicated mean effective pressure (0.3 MPa) as those in Figure 2.2.

Figure 2.3 demonstrates that for a cycle with the same indicated mean effective pressure, the isochoric combustion process provides the most efficient cycle, but is closely followed by the isobaric combustion, and finally by the isothermal combustion process. The calculations were performed for a compression ratio of 15:1, for an indicated mean effective pressure of 0.3 MPa in all cases. In order to achieve a cycle with high fuel-conversion efficiency, the combustion process should shape the gas cycle in such a fashion, that it becomes as close as possible to the isochoric

cycle. Figure 2.2 shows that the isochoric cycle has the highest mean temperature of heat reception and lowest temperature of heat rejection, which provides the highest thermodynamic conversion efficiency.

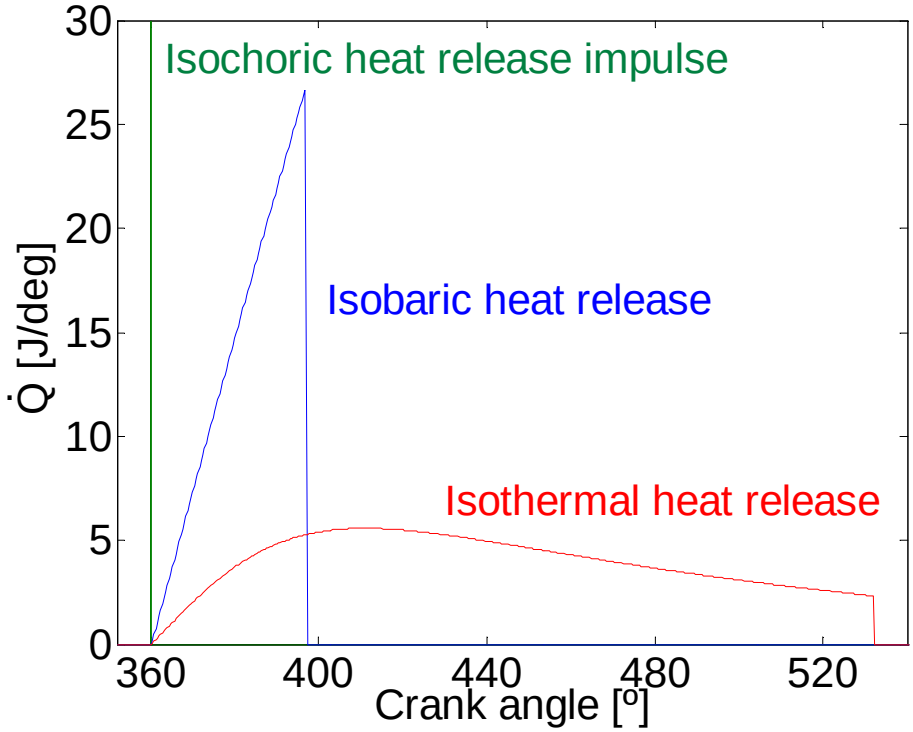

Figure 2.4 - Theoretical heat release rates on a crank-angle basis

The theoretical heat release rate necessary to achieve these three ideal gas cycles, may be calculated. For an accurate temporal representation of the combustion process this calculation is performed on a crank-angle basis, which is linearly correlated with time, rather than on a cylinder-volume basis, because the change in volume per time unit is non linear. Crank angle may thus be translated directly into time, as a linear function of engine speed. The calculation of heat release rates were performed under the assumption that the engine geometry is equal to that of the research engine (i.e. stroke 86 mm, bore 86 mm, connecting rod length 160 mm, geometric compression ratio 15:1). The theoretical heat release rates necessary to achieve the three ideal cycles previously discussed are shown in Figure 2.4. It is visible from these theoretical considerations that in order to achieve the highest ideal cycle efficiency for the engine, the diesel combustion process should be as similar as possible to an isochoric heat-release impulse. Slower combustion processes, such as those leading to isobaric and isothermal combustion, lead to progressively lower ideal cycle efficiencies of the engine.

These theoretical considerations are entirely based on an ideal cycle approach to the combustion process. In practice, the engine efficiency is influenced by further factors, which are more complex in their nature. Firstly, heat losses from the working fluid to the combustion chamber walls are significantly dependent on the combustion process. Heat losses depend not only on the peak global gas temperatures within the cylinder, but on the detailed temperature distribution within it, as well as

factors influencing the radiative and convective heat transfer from flames, such as soot luminescence and turbulence. Secondly, losses of combustion chamber mass can occur through gas leakage, and represent a further important factor influencing engine efficiency. Leakage of combustion chamber gases occurs predominantly past the piston rings, where it is usually referred-to as blow-by, and to a lesser extent past the intake and exhaust valves, especially if these are damaged or coated in combustion product deposits. Heat and mass losses from the combustion chamber are strongly dependent on the combustion chamber pressure history and the mechanical construction tolerances of the engine. Heat and mass losses from the combustion chamber are highest under conditions of high temperature and pressures of the combustion chamber gases. With reference to the pressure and temperature histories for different engine cycles shown in Figure 2.2 it can be deduced that such losses are thus most pronounced under conditions at which the ideal cycle efficiency of the engine is highest. This results in a trade-off between ideal cycle efficiency, and practical heat and mass losses from the combustion chamber. The ideal cycle efficiency is a theoretical measure of efficiency, whilst the practical heat and mass losses depend in detail on the design, manufacturing tolerances and wear of the engine.

2.3. A phenomenological model of diesel combustion

Diesel combustion is largely a diffusion controlled combustion process achieved through the gradual introduction of a compression-ignited fuel into the combustion chamber of a reciprocating internal combustion engine. The fundamental processes occurring therein shall be described in an approximately chronological sequence in a conceptual model.

In preparation of the combustion process, a charge of air is compressed in a polytropic process within the cylinder of the engine by movement of the piston until it reaches a temperature that is significantly higher than the ignition temperature of the fuel. Towards the end of the compression stroke of the piston, fuel is injected into the combustion chamber at high velocity through a small injector orifice. The jet of fuel soon entrains air and atomises into ligaments of fuel and smaller droplets which penetrate the combustion chamber in the form of a spray. The droplets can become progressively smaller due to secondary atomisation. Vaporisation of the fuel takes place alongside this atomisation process from the liquid fuel droplets and forms fuel vapour which starts mixing with the surrounding air. This mixing process with air occurs primarily at the fringes of the spray, and exposes the fuel and air to each other under high pressure and temperature conditions. This initiates chemical reactions between the different molecules which, after a period of ignition delay determined by their chemical kinetics, results in the ignition and combustion of the fuel and air mixture in areas of the combustion chamber in which the stoichiometric conditions permit this process to occur. This initial combustion occurs in areas in which the fuel has premixed with air prior to ignition and shall be referred to as the premixed combustion phase. This early combustion process is usually accompanied by a sudden and rapid release of heat, as shown in Figure 2.5, due to the combustion of much of the fuel that had premixed to within flammability limits during the

ignition delay period. Ignition of the fuel usually occurs around TDC of the piston, after which the cylinder charge starts expanding again. After the initial premixed combustion phase, the combustion proceeds, as the mixing of fuel with air allows more of the fuel to reach the dilution with air necessary for combustion. This process forms the second main phase of heat release during the diesel combustion process and shall be referred to as the mixing-controlled combustion phase. The heat release during this second phase of combustion is limited by the rate at which the fuel can mix with the surrounding air, i.e., the rates of reaction between the fuel and the air are much faster than the rates at which the fuel mixes with the air. This combustion process occurs in the form of a diffusion flame, and usually continues over a longer period of time than the premixed combustion phase. It is typically accompanied by lower heat release rates, limited by the mixing process of fuel with air. Eventually, the diesel combustion process ends with the late combustion phase occurring after fuel injection has ceased, in which the consumption of most of the remaining fuel, soot, products of rich combustion and dissociated combustion products occurs as the expansion of the cylinder charge proceeds and the gases cool down.

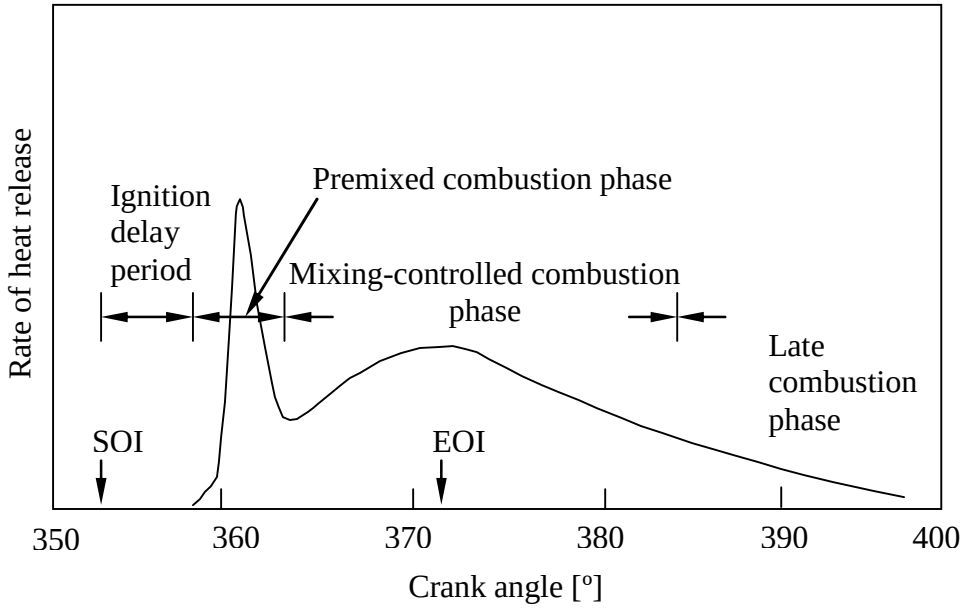

Figure 2.5 - Typical DI engine heat-release-rate diagram identifying different diesel combustion phases. Adapted from Heywood (1988, p.506).

The ignition delay commences with the start of fuel injection (SOI), and ceases with the first detectable heat release of combustion (see Figure 2.5). The premixed combustion phase begins with this first detectable heat release, and typically occurs whilst fuel injection is proceeding and typically ends before the end of fuel injection (EOI) has occurred. The beginning of the mixing-controlled combustion phase is usually marked by a trough in the heat release rate. The end of fuel injection usually introduces the decay of the heat release rate during the mixing-controlled combustion phase. A more detailed discussion of the processes has been written by Heywood (1988, pp.503-506).

2.4. Flame structure, stoichiometry and temperature of diesel combustion

The diesel combustion process has been delineated in significant detail by various researchers in terms of its flame structure, combustion stoichiometry and flame temperature, on the basis of experimental work employing optical diagnostics. A conceptual model of diesel combustion arising from such optical experiments is relevant to the discussion of pollutant formation with regards to the effects which different fuels have on the heat release patterns and formation of pollutants. This model shall thus be discussed on the basis of recent literature on the subject.

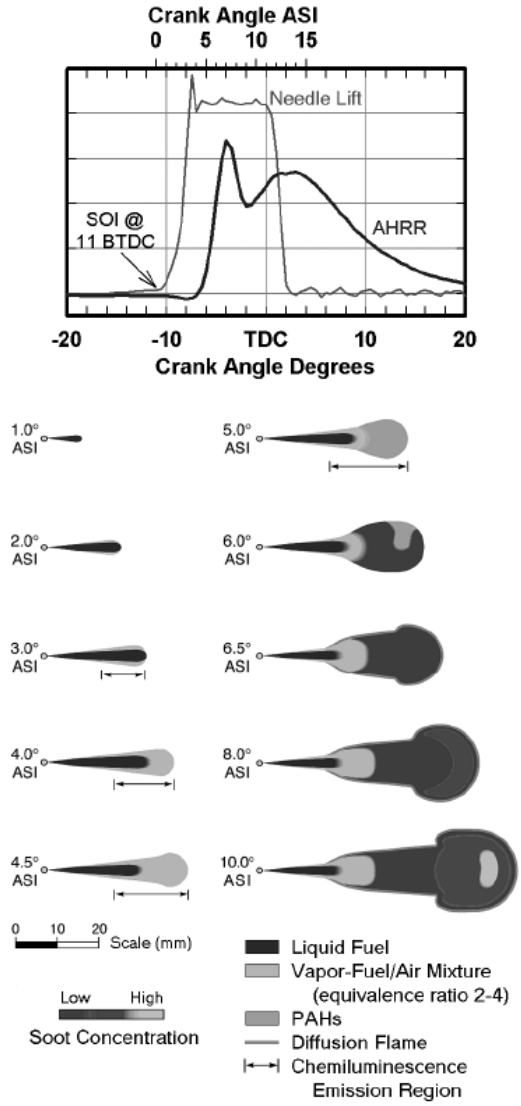

Figure 2.6 - Temporal sequence of how DI diesel combustion evolves from the start of injection through the premixed combustion phase and into the mixing-controlled combustion phase. (Dec, 1997)

Consider the spatial and temporal development of diesel combustion flames during its four combustion phases previously presented in Figure 2.5. A diagram of injection timing, combustion heat release alongside a sequence of flame development is shown in Figure 2.6, as presented by Dec (1997).

The diesel combustion process commences with the onset of fuel injection, which starts at 11º CA BTDC, and lasts until 2.0º CA ATDC, as indicated by the injector needle lift at the top of Figure 2.6. The liquid fuel leaves the injector nozzle and progressively penetrates the combustion chamber gases as shown in the first three images representing the initial 3.0º CA after the start of injection (ASI). The fuel undergoes atomisation and droplet formation as it entrains surrounding hot air into the fuel spray. The hot air transfers heat to the fuel, thereby increasing its temperature and supporting vaporisation leading to the formation of a layer at the periphery of the spray, in which fuel vapour mixes considerably with air. The fuel-air stoichiometry in this layer is fuel rich, of the order of Φ=2 to Φ=4 equivalence ratio. This is shown in the image depicting 3.0º CA ASI as part of Figure 2.6.

As the fuel vapour starts mixing with air under these high temperature conditions of up to 750 K, the chemical reactions between fuel molecules and the oxygen within the air begin to occur, which mark the start of the chemical ignition delay period. The chemical kinetic mechanisms initiated through this process, govern the chemical ignition delay, after which autoignition occurs. Autoignition of the fuel is usually marked by a measurable increase in combustion chamber pressure, and occurs through an excess of thermal energy released by the ongoing chemical reactions compared to thermal energy absorbed by these reactions (Glassman & Yetter, 2008). In optical diagnostics, natural chemiluminescence of the fuel spray has been used as an indicator of the onset of combustion (Dec & Espey, 1995). The experiments reported by Dec and Espey (1995) showed that chemiluminescence occurs at a time of 3.0º to 5.0º CA ASI, and that it occurs first within the previously described peripheral layer of the fuel spray consisting of fuel vapour and air (see Figure 2.6). This chemiluminescence is first detected on the lateral sections of the fuel spray at around 3.5º CA ASI, and later encompasses the downstream end of the spray at around 5.0º CA ASI. The ignition of this downstream portion of the fuel spray induces the premixed combustion phase (Dec & Espey, 1998). The heat release spike during the premixed combustion phase is cause by the partial oxidation of this premixed and fuel-rich part of the spray. Dec (1997) reports that the mixture strength in this region typically lies between Φ=2 and Φ=4, but later investigations showed, that under conditions of very long ignition delay the mixture strength may reach conditions of Φ=1.25 to Φ=1.7 (Musculus, 2004). In this region of rich combustion, the fuel molecules are thought to break down into smaller hydrocarbon species and radicals after which some may polymerise into polyaromatic hydrocarbons (PAH), believed to be precursors of soot formation. The presence of PAH was detected using planar laser induced fluorescence (PLIF). As the oxidation of this premixed fuel air mixture proceeds, a thin diffusion flame starts to develop around the edges of this pre-mixed burn region at about 6.0º CA ASI. In this diffusion flame, the products of the incomplete oxidation occurring in the fuel-rich pre-mixed combustion zone, proceed to mixing with the surrounding air, and undergo further oxidation in the presence of sufficient oxygen (Figure 2.6). Laser induced

incandescence (LII) images (Dec, 1997) have shown that during this time, the regions in which the premixed combustion is under way, become inoculated with very small soot particles appearing in irregular patterns, believed to have formed from PAH. At 6.5 º CA ASI this inoculation occurs throughout the entire premixed burn region and leads to the growth of larger soot particles towards the periphery of the premixed combustion zone. The presence of these larger particles has been detected by means of elastic (Rayleigh) scattering of laser light (Dec, 1997). The appearance of these larger particles at the jet periphery suggests that the soot particles undergo growth within the rich premixed flame as they move towards its edges. At the same point in time (6.5 º CA ASI), the thin diffusion flame which had begun developing around 6.0º CA ASI increases in breadth, and forms a fully-developed diffusion flame which encompassed the whole of the downstream region of the spray. It extends upstream towards the origin of the jet up as far as the flame lift-off point which is located slightly upstream of the furthest extent of liquid fuel droplets within the spray (see 6.5 º CA ASI, Figure 2.6). At this most up-stream position within the diesel jet at which combustion occurs, the jet undergoes a sudden increase in diameter. This is caused by strong air entrainment into the jet, and due to the expansion of the gases within the jet, as a result of their increasing temperature. At the most downstream end of the burning jet, large scale turbulence causes the edges of the jet to become rugged and form a jet-plume region, in which fuel vapour, burned gases and air mix with one another in a diffusion flame of larger-scale turbulence. This is defined by the downstream jet plume appearing at the downstream end of the diesel jet for 6.5º CA ASI, 8.0º ASI and 10.0º CA ASI (Figure 2.6). It is in this downstream region of the jet, that the largest soot particles have been detected (Dec, 1997). During the advanced stages of diesel jet development ranging from 6.5º CA ASI to 10.0º CA ASI, the last remnants of air are consumed within the pre-mixed downstream regions of jet, as this steadily increases in size. As the diesel combustion process begins its transition into its mixing-controlled combustion phase, the premixed burn region disappears from the downstream end of the spray and shifts to a region further upstream, located just after the lift-off point. This can be seen in the image depicting the diesel jet at 10.0º CA ASI in Figure 2.6. This final model of the diesel jet in its mixing-controlled combustion mode is shown in more detail in Figure 2.7.

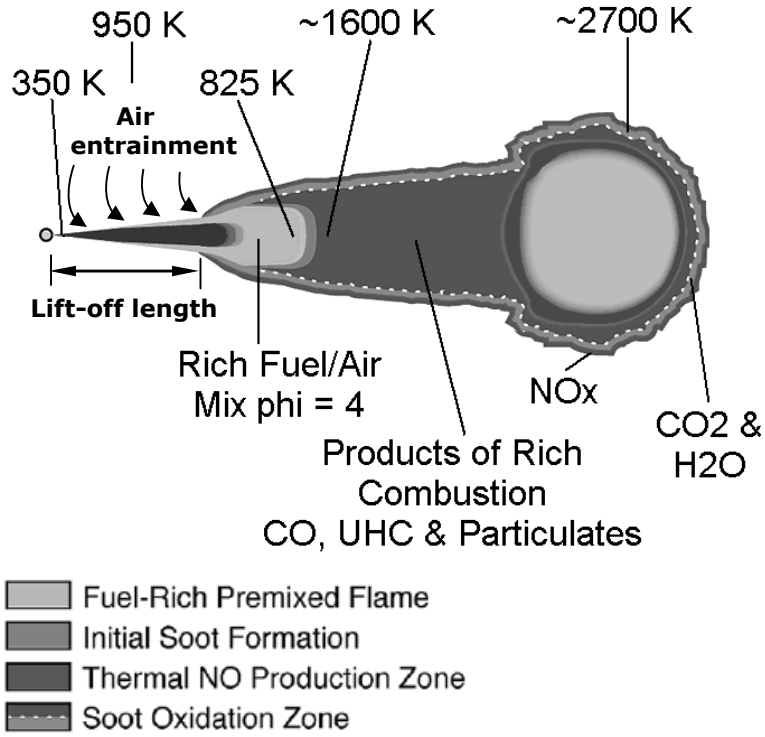

Figure 2.7 - Schematic of quasi-steady burning jet from laser measurements. Adapted from Dec (1997) and Flynn et al. (1999)

An important implication of this combustion model is that even during the later mixing-controlled stages of combustion, the fuel undergoes a two-stage oxidation process. The fuel undergoes oxidation firstly in a rich pre-mixed oxidation process at equivalence ratios between Φ=2 and Φ=4 in the regions situated immediately downstream of the lift-off length of the jet, before undergoing further oxidation in the presence of sufficient amounts of air within the diffusion flame located throughout the periphery, but most prominently at the downstream end of the combusting jet.

2.5. The influence of the diesel combustion process on pollutant formation and emission

The phenomenological description of diesel combustion in terms of flame structure, stoichiometry and gas temperatures (sections 2.3 and 2.4) has suggested that the way in which the combustion process takes place may be critical to the processes by which the formation of pollutants occurs. The following sections provide a brief literature review on pollutant formation mechanisms.

2.5.1. NO_x formation

The formation of nitric oxide (NO) and nitrogen dioxide (NO_2) in diesel combustion may be defined by five principal reaction mechanisms.

The first and most important mechanism for the formation of NO is the 'thermal' or 'Zeldovich' mechanism (Zeldovich, 1947) in which atmospheric nitrogen (N_2) is oxidised with atmospheric oxygen (O_2) at high temperatures in an endothermic reaction. This reaction principally takes place at elevated temperatures in excess of 1800 K, and its rate increases significantly with higher temperatures mostly due to its requirement for a high activation energy (Turns, 1996). The reaction rates of thermal NO formation under diesel engine conditions are slow in comparison to the hydrocarbon combustion reactions, and thus tend to take place not only within the flame front of combustion, but to a large extent in the post flame gases, if the temperatures in these gases are permitting. Thermal NO formation can take place over a wide range of equivalence ratios, but in combustion is most pronounced for gases of near stoichiometric mixture strengths, predominantly due to the high flame temperatures present under such conditions (Heywood, et al., 1971). The original Zeldovich mechanism consisting of two reaction equations is usually augmented by the hydroxyl radical reaction introduced by Lavoie et al. (1970) to form the extended Zeldovich mechanism.
The reaction equations of the extended Zeldovich mechanism may be written as:

$$O + N_2 \leftrightarrow NO + N$$

Equation 2.5

$$N + O_2 \leftrightarrow NO + O$$

Equation 2.6

$$N + OH \leftrightarrow NO + H$$

Equation 2.7

The rate of initial NO formation may be expressed in terms of O_2 and N_2 concentrations as:

$$\frac{d[NO]}{dt} = \frac{6 \cdot 10^{16}}{T^{1/2}} \exp\left(\frac{-69090}{T}\right)[O_2]_e^{1/2}[N_2]_e \quad \text{mol/cm}^3\text{·s}$$

Equation 2.8

The exponential term of Equation 2.8 shows that the formation rate of NO via the extended Zeldovich mechanism is strongly dependent on temperature. High temperatures as well as high oxygen concentrations result in a high rate of NO formation. In diesel combustion, the rate of NO formation is of principal importance to the final concentration of NO in the exhaust gases, because the overall rate of formation of NO is usually slow in comparison to the time scale of the fuel oxidation process (Miller & Bowman, 1989), and slow in comparison to the changes in combustion chamber conditions (Heywood, 1988). This means that the concentration of NO within the combustion chamber gases is largely controlled by the kinetic rate of formation, rather than by its equilibrium concentration. The rate of decomposition of NO via the extended Zeldovich mechanism is similarly slow in comparison to changes in the combustion chamber gases, so that during the cooling process occurring during the late stages of combustion, NO is not allowed to return to its equilibrium concentration and the NO chemistry is 'frozen' before significant NO decomposition can occur.

The second mechanism of NO formation in diesel combustion is that involving its 'prompt' formation, via the mechanism advanced by Fenimore (1971). This mechanism relies on the formation of cyano (HCN, CN) compounds such as hydrogen cyanide (HCN) from the reaction of fuel hydrocarbon radicals (e.g. CH, CH_2, C_2, C_2H and C) with molecular nitrogen (N_2) as intermediate species for the formation of NO. This 'prompt' NO formation mechanism is significantly faster than the 'thermal' or 'Zeldovich' mechanism, and becomes particularly important under fuel rich combustion conditions under which large concentrations of hydrocarbon radicals are produced (Miller & Bowman, 1989). Although the fuel rich combustion under which this mechanism typically occurs takes place at relatively low combustion temperatures due to incomplete heat release resulting from only partial oxidation of the fuel, the propensity of the prompt mechanism of forming NO significantly improves with rising temperature. Thus, an increase in the temperature of combustion, with all other conditions being equal, results in an increase in the amount of prompt NO formation. The following equations describe the reactions which initiate the prompt NO reaction mechanism, by the formation of cyano compounds such as HCN from CH fuel hydrocarbon radicals (Turns, 1996, p.145):

$$CH + N_2 \rightarrow HCN + N$$

Equation 2.9

$$C + N_2 \rightarrow CN + N$$

Equation 2.10

Up to an equivalence ratio of Φ=1.2, the HCN is primarily converted into NO via the chain reactions detailed below (Miller & Bowman, 1989). This second step completes the 'prompt' NO formation process:

$$HCN + O \rightarrow NCO + H$$

Equation 2.11

$$NCO + H \rightarrow NH + CO$$

Equation 2.12

$$NH + H \rightarrow N + H_2$$

Equation 2.13

$$N + OH \rightarrow NO + H$$

Equation 2.14

The third mechanism discussed herein by which the formation of NO may occur in diesel combustion is the 'fuel-bound' NO mechanism. Combustion experiments carried out in a laboratory oil furnace (Martin & Berkau, 1971) have demonstrated that the addition of small amounts of nitrogen to hydrocarbon fuels can have a strong influence on the NO exhaust gas concentration of hydrocarbon flames. In such cases, NO is produced from nitrogen that was originally present in the fuel and occurs via intermediate compounds such as NH_3, NH_2, NH, HCN or CN (Glassman & Yetter, 2008). Their conversion process into fuel-bound NO occurs via similar reactions as those representing the second step of the 'prompt' NO formation mechanism (Equation 2.11 - Equation 2.13). The reactions of the fuel-bound NO mechanism occur very fast, at rates comparable to those of the main combustion reactions. By definition, the fuel-bound NO mechanism is restricted to combustion processes in which the fuel contains significant amounts of nitrogen. This is the case for diesel fuels containing high concentrations of nitrates as ignition improving additives, such as those discussed in the experiments of Chapters 5-7 of this text.

A fourth mechanism for the formation of NO is the N_2O-intermediate mechanism, in which NO is formed via the intermediate compound of nitrous oxide (N_2O). This mechanism is believed to be particularly important in lean combustion at equivalence ratios below Φ<0.8 and low temperatures (Turns, 1996, p.145). Such conditions are encountered in the lean homogeneous charge compression ignition experiments described in Chapter 8. The reaction equation of the N_2O-intermediate mechanism may be written as:

$$O + N_2 + M \rightarrow N_2O + M$$

Equation 2.15

$$H + N_2O \rightarrow NO + NH$$

Equation 2.16

$$O + N_2O \rightarrow NO + NO$$

Equation 2.17

A fifth mechanism relevant to the formation of nitrogen oxides in diesel combustion is the conversion of nitrogen oxide (NO) into nitrogen dioxide (NO_2), and its decomposition back into nitrogen oxide (NO). NO_2 may be formed from nitric oxide (NO) in the flame-front and post-flame gases of diesel combustion via the following chemical reaction:

$$NO + HO_2 \rightarrow NO_2 + OH$$

Equation 2.18

Where the HO_2 radical is previously formed via the following reaction:

$$H + O_2 + M \rightarrow HO_2 + M$$

Equation 2.19

The so created NO_2 may subsequently be converted back into NO according to the following chemical reactions:

$$NO_2 + O \rightarrow NO + O_2$$

Equation 2.20

$$NO_2 + H \rightarrow NO + OH$$

Equation 2.21

Chemical equilibrium considerations suggest that the concentration of NO_2 formed should be negligible compared to the concentration of NO (Heywood, 1988). Yet diesel engine experiments show that NO_2 may account for 10-30% of exhaust gas nitrogen oxide concentrations (Hilliard & Wheeler, 1979). It has been postulated that these high proportions of NO_2 are formed through quenching of the hot reaction gases, which cause the NO_2 to evade its decomposition back into NO. This explanation agrees with the observation that high NO_2 concentration in the exhaust gas occurs particularly for combustion conditions conducive to quenching of the hot gases with colder combustion chamber gases (Hilliard & Wheeler, 1979). The concentrations of NO and NO_2 are usually grouped into the general species of nitrogen oxides (NO_x).

The formation of NO_x in the diesel combustion process is thought to occur primarily via the five NO_x formation mechanisms described so far, and has been the subject of extensive research in practical engine studies. Attempts have been made to delineate the precise conditions under which NO_x is formed, and to understand the spatial and temporal distribution of NO_x formation in diesel combustion.

Theoretical considerations and experimental measurements of reaction rates suggest that the formation of NO_x in diesel combustion occurs predominantly for gases of near stoichiometric mixture strength via the thermal NO mechanism. In-cylinder sampling of gases from the combustion occurring inside a direct-injection diesel engine showed (Aoyagi, et al., 1980) that only small

quantities of NO are formed during the initial premixed combustion phase. The gas concentrations indicated that peak NO concentrations within the combustion chamber are reached significantly after the end of fuel injection. This suggests that the formation of NO occurs primarily in the later mixing-controlled diffusion flames of the diesel combustion process which form at near stoichiometric conditions, and in the hot burned gases. These results have been confirmed by optical planar laser-induced fluorescence (PLIF) measurements of NO carried out by Dec and Canaan (1998), who detected NO formation in the diffusion flames, but not within the premixed combustion flames. Espey et al (1994, 1997) and Flynn et al. (1999), used planar laser-induced Rayleigh scattering images (PLIR) to show that the mixture strength in the premixed flames of diesel combustion are too fuel rich and thus too cool to support large amounts of NO formation, and that the conditions found in the diffusion flame are those expected to be conducive to significant amounts of NO formation. The PLIF NO detection experiments carried out by Dec and Canaan (1998) confirmed this by revealing the spatial distribution of NO formation within the flames. The authors reported that NO production was not detected within the initial premixed flames, but commenced around the periphery of the jet, just after the diffusion flames have formed. It was observed that NO formation was confined to the periphery of the jet throughout the entire mixing-controlled combustion phase, and that NO formation continued in the hot post-combustion gases, after the apparent heat release of combustion had ceased. The authors reported that under their experimental conditions, about a third of all NO production was detected in the hot post-combustion gases after the end of the apparent heat-release rate. Musculus (2004) later reported from optical experiments using natural luminosity images in conjunction with the spray air entrainment correlation presented by Naber and Siebers (1996), that under conditions of exceptionally long ignition delay, some of the premixed combustion become lean enough (Φ=1.25 to Φ=1.7) to support limited amounts of nitric oxide formation. Despite these findings, Musculus (2004) concluded that even under these leaner premixed combustion conditions, the diffusion flames and their respective post-combustion gases would be expected to remain the main contributors to NO_x formation.

Extensive research has been conducted on the effect which the relative amounts of heat released during the premixed combustion and mixing-controlled diffusion combustion has on the formation of NO_x. The relative amounts of heat released during the premixed and mixing-controlled combustion are to a large extent governed by the ignition delay of the fuel jet. A longer ignition delay will typically result in a larger proportion of heat release occurring in premixed combustion mode, whilst a shorter ignition delay will typically result in a larger proportion of heat release occurring in mixing-controlled diffusion combustion mode. Factors which shorten the ignition delay are typically higher charge-gas and fuel temperatures, higher chemical reactivity of the fuel and air (e.g. higher cetane number and higher oxygen content respectively), and higher engine loads and speeds. A comprehensive analysis of the factors affecting ignition delay has been carried out by Wong and Steere (1982). Experiments on NO_x formation in which the proportions of premixed combustion and mixing-controlled combustion were varied, have shown that increasing the proportion of heat released during the initial rapid premixed combustion phase (premixed burn fraction) with respect to heat released in the later mixing-controlled combustion phase (mixing-

controlled burn fraction) results in an increase in NO_x concentration in the engine exhaust gas (Ladommatos et al, 1996[a]; Cheng et al. 2006).

In view of the experiments described previously (Aoyagi, et al., 1980; Dec & Canaan, 1998), from which it was concluded that NO forms primarily within the diffusion flames and hot post-flame gases of the later mixing controlled combustion phase, it seems paradoxical that an increase in premixed burn fraction results in an increase in NO_x formation under typical diesel engine conditions. Although this phenomenon is still not fully understood, three fundamental processes which could explain this trend can be described as follows:

The first and most fundamental explanation for the increase in NO formation with premixed burn fraction is that if a larger proportion of heat is released during the rapid premixed combustion phase, higher peak temperatures will be reached within the combusting gases. This is because the heat release during the premixed combustion phase occurs at a higher rate than that of the mixing-controlled combustion phase, leading to a shorter combustion event closer to piston-TDC, which causes the gas cycle of the engine to resemble more one which involves isochoric combustion rather than isobaric or isothermal combustion (see Figure 2.2). Figure 2.2 illustrates that an isochoric combustion process involves higher global gas temperatures than the longer isobaric or isothermal combustion processes. Ladommatos et al. (1996[a]) demonstrated that a good correlation exists between the peak global cylinder gas temperatures recorded during the diesel cycle, and the fraction of fuel burned during the premixed combustion phase. Higher gas temperatures are conducive to higher amounts of thermal NO_x formation via the extended Zeldovich mechanism, and to a lesser extent via the prompt NO mechanism. Such higher temperatures caused by a higher fraction of heat release in premixed combustion influence the later stages of the premixed combustion phase, as well as the subsequently occurring diffusion flames, in which NO_x is predominantly believed to be formed. If the peak temperatures occur earlier during the engine cycle, the time period over which conditions are conducive to NO formation may be prolonged, which would be expected to increase NO concentration in the gases. This is especially important with regards to NO formation being strongly limited by its formation rates and the available time for formation. It has been shown that the sequence in which specific portions of the cylinder gases are initially compressed by the mechanical compression of the piston, subsequently combusted and eventually further compressed by the combustion of other portions of cylinder gases is critical to calculating the peak temperatures reached within the combustion chamber gases, and consequently to the formation of NO_x (Musculus, 2004).

It has been questioned whether the calculation of adiabatic temperatures alone can explain the full extent of the observed increase in NO_x concentration (Musculus, 2004), leading to further investigations about the relation between the fraction of heat released during the premixed combustion phase and NO_x formation. A second theory regarding the correlation between premixed burn fraction and NO_x emission has been developed, which concerns changes in the radiative heat transfer from soot within the diffusion flames. A higher premixed burn fraction of the fuel is usually caused by a longer ignition delay of the fuel. A longer ignition delay reflects itself in longer lift-off lengths of the flames, which in turn are known to cause increased air-entrainment into the burning

fuel spray (Siebers, 1999). It is thought that additional air entrainment may lower the flame soot-loading. A lower flame soot-loading has been hypothesised to cause higher flame temperatures, because less heat may be dissipated from the flames via soot-radiative heat transfer (Musculus 2004; Cheng, et al., 2006). Such higher flame temperatures are believed to be a potential reason for higher NO_x emissions from diesel combustion events with a higher premixed burn fraction due to increased thermal NO_x formation via the Zeldovich mechanism. Mueller et al. (2009) demonstrated for the first time in a practical engine study that changes in soot radiative heat transfer results in measurable differences of NO_x emissions for the same type of fuel. The experiments examined the effects of doping a fuel with a polyaromatic fuel additive (phenantrene) which was used to generate higher amounts of soot radiation from its flames during combustion. The experiments showed that doping the fuel with phenantrene resulted in an increase in spatially integrated natural luminosity of the flame, which was indicative of an increase in soot radiative heat transfer, and resulted in a reduction of NO_x emissions.

A third theory advanced by Musculus (2004) has suggested that the peak combustion temperatures may be higher for combustion processes involving a higher degree of premixed combustion, due to less time being available for dilution of the combustion gases with cooler bulk cylinder gases which had not directly taken part in combustion. This may be of particular relevance to NO_x formation in post flame gases. Though it is fundamentally conceivable that a higher degree of premixed combustion may delay or reduce the mixing process of combustion gases with cooler gases which did not directly partake in the combustion process, no clear evidence for this phenomenon has yet been presented.

Several fundamental engine operating parameters other than the premixed burn fraction are also known to influence the formation of NO_x during the diesel combustion process, namely the fuel injection timing, global cylinder gas equivalence ratio, degree of exhaust gas recirculation, intake air temperature, injection pressure, engine speed and compression ratio

It has been extensively documented that for typical diesel engine operating conditions, an advance in fuel injection timing results in an increase in NO_x emissions (Pischinger & Cartellieri, 1972; Kamimoto & Kobayashi, 1991; Stone, 1999; Musculus, 2004). This can be attributed to the occurrence of higher peak combustion temperatures under such conditions, which are due to a higher proportion of heat release having occurred by the time at which the combustion chamber gases are subjected to their peak geometric compression through the piston, which occurs when the piston is located in the vicinity of TDC.

It has also been shown that the global equivalence ratio of diesel combustion, which is correlated with engine load, has a significant effect on NO_x emissions. Engine experiments have shown that the total amount of NO_x formation increases with engine load (Voiculescu & Borman, 1978; Pischinger & Cartellieri, 1972; Kamimoto & Kobayashi, 1991). Dec and Canaan (1998) reported further that although the total NO_x emission increases with engine load, the fuel-specific emission of NO_x is typically reduced as the engine load is increased. The authors attribute this to a retardation of the mid-point of the combustion process, which causes combustion to occur later during the engine cycle where diffusion flame temperatures are lower, and less time for NO_x formation is available

before the charge is cooled. At low engine loads most of the heat release occurs around TDC, where diffusion flame temperatures are higher, and more time is available for NO_x formation before cooling of the gases occurs, thus resulting in a higher load-specific formation of NO_x.

A further factor influencing the formation of NO_x is the amount of exhaust gas recirculation (EGR) during the engine cycle. Engine experiments carried out by Ladommatos et al. (2000) have shown that the progressive introduction of recirculated exhaust gases substantially decrease the formation of NO_x formed during the combustion process. The authors carried out a meticulous experimental study of the individual effects which EGR has on NO_x formation in the diesel combustion process. It was concluded that the reduction in NO_x formation through EGR can mainly be attributed to a reduction in adiabatic flame temperatures and thus thermal NO_x formation, owing to a dilution of the oxidiser content (O_2) in the air. The reduction of the air oxygen content forces a given quantity of fuel to react with a larger amount of (oxygen depleted) air and thus causes the heat released by the fuel to be absorbed by a larger total mass of gases. The adiabatic flame temperature of this diluted combustion is thus lower than that of undiluted combustion in oxygen-rich air. Other effects of recirculated exhaust gas, such changes in the specific heat capacity of the reacting gases or the chemical effect of CO_2 and H_2O in the NO formation mechanism, were reported to play a subordinated role in reducing the formation of NO_x through EGR.

Solbrig and Litzinger (1990) performed a systematic study of inlet air temperature on NO_x emissions. It was reported that an optimal inlet air temperature exists, to either side of which NO_x emissions tend to increase. At temperatures below the optimal operating point, the NO_x emission appears to be primarily controlled by the ignition delay, which changes the amount of premixed burn fraction of the combustion process. Air intake temperatures below the optimal operating point result in greater amounts of heat released during the premixed combustion phase, which in turn increases the emission of NO_x via the mechanisms described above with regard to the premixed burn fraction. At intake air temperatures above the optimal intake air temperature, the ignition delay is already so short that it only results in modest changes of the premixed burn fraction. At such conditions, a further increase in intake air temperature tends to result primarily in an increase of the diffusion flame temperatures, and thus higher NO_x formation by increasing the rates of formation of NO_x via the Zeldovich mechanism. Musculus (2004) carried out a similar study in an optical engine with a simulated compression ratio of 16:1 from which it was concluded that an intake air temperature of 24 ºC yielded the lowest NO_x emissions in comparison with higher or lower intake air temperatures.

A further factor influencing the amount of NO formation during the diesel combustion process is the injection pressure. Pierpont and Reitz (1995) and Mallamo et al. (2005) carried out experiments in a direct injection diesel engine with electronically controlled injection, in which the exhaust gas concentration of NO_x was measured for engine operation at various injection pressures. The authors reported that an increase in the fuel injection pressure resulted in an increase in premixed burn fraction and thereby in an increase in NO_x emissions.

Voiculescu and Borman (1978) reported experiments investigating the effects of engine speed on NO_x emissions. The experiments of showed that a small decrease in total NO_x emission was observed as the engine speed was increased, which may be attributed to shorter residence times of

the post flame gases at higher temperatures, due to later phasing of ignition within the crank-angle domain, and faster expansion of the cylinder gas charge during the expansion stroke.

The effect of compression ratio on NO_x emissions from a diesel engine have been reported by Mallamo et al. (2005), who observed that for the same injection timing, a decrease in geometric compression ratio from 19:1 to 17.5:1 resulted in an increase in NO_x emissions. The authors attributed this change primarily to a longer ignition delay and higher premixed burn fraction incurred by the combustion at lower compression ratio.

2.5.2. Particulate formation

Diesel fuel particulates may consist of several components: Carbonaceous material formed by the decomposition and polymerisation or by the pyrolysis of organic molecules during the combustion process, liquid organic molecules resulting from the condensation of unburned or partially organic molecules, and an aqueous solution consisting mainly of condensed water but may contain significant amounts of sulphuric acid, if sulphur was brought into the combustion environment by the fuel, or other sources. These three types of particulate matter may emerge as separate particles, but are typically found in combination with each other within a single particle.

The first component, carbonaceous soot, consists predominantly of carbon atoms and a smaller proportion of hydrogen atoms, with a ratio of hydrogen to carbon atoms of approximately 0.1 (Palmer & Cullis, 1965, p.205; Smith, 1981). On its atomic scale, soot consists of arrays of face-centred platelets of carbon atoms often referred-to as ‘platelets’ (Lipkea, et al., 1978).

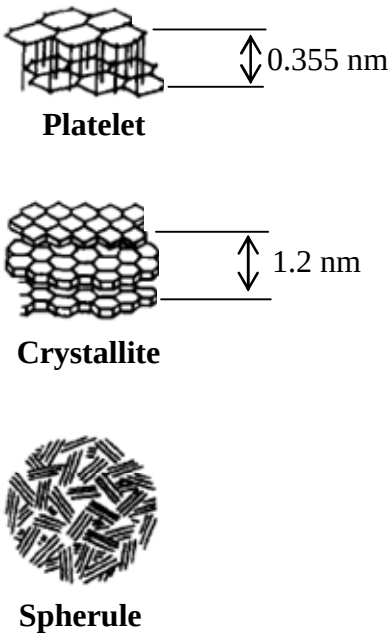

Figure 2.8 - Structure of primary particles of carbonaceous soot. Adapted from Lipkea et al. (1978)

These platelets are arranged in stacked groups of 2-5 platelets forming a larger structure called crystallite. The interlayer spacing between the platelets has been reported to be approximately 3.44 nm (Palmer & Cullis, 1965) or 3.55 nm (Smith, 1981). The crystallites are arranged in patterns of varying degrees of order, forming soot spherules which typically consist of 10^3 crystallites (Howard, et al., 1973; Mantell, 1968). The order and relative orientation of crystallites with respect to each other depends in detail on the pathway of formation of the soot as well as the type of fuel (vander Wal, 2005). The density of soot has been reported to lie around 1840 kg/m^3 (Choi, et al., 1994).
Soot formation may occur through homogeneous vapour-phase reactions of organic molecules, or through liquid-phase pyrolysis of the fuel, both occurring in the presence of only small amounts of oxygen. The general process of soot formation may be described as follows:

If the fuel is non-aromatic in nature, the process of soot-formation begins with the partial decomposition and subsequent cyclisation of the molecule to create an aromatic ring (Glassman & Yetter, 2008). This process may be achieved more directly through the dehydrogenation of aromatic fuel molecules, should they be present. This ring-structure is believed to be adjoined by alkyl, alkene and alkine groups through reactions and to grow into a polynuclear aromatic hydrocarbon (PAH) structure. These PAH and other unsaturated organic molecules are often referred to as soot precursor molecules. Simultaneously to this polymerisation process, occurs the oxidative decomposition of these soot precursor molecules. The rates of polymerisation and decomposition depend in detail on the combustion environment, as well as on the presence of chemical species that support the formation and oxidation processes of such molecules. The PAH may eventually grow larger, and into carbonaceous structures which may at this point be considered particle nuclei. Such particle nuclei still contain high amounts of hydrogen, which is progressively lost, as the nuclei spend more time under the high-temperature conditions of the combustion environment. The nuclei grow further in mass through the addition and dehydrogenation of further organic molecules and by agglomeration with other particle nuclei. Upon further dehydrogenation, these structures develop into particles of carbonaceous soot, as described previously.

In the diesel combustion process, carbonaceous soot forms under conditions of high temperatures (1000-2800 K) and pressures (5-10 MPa). The combustion process involves premixed as well as diffusion flames, for which the soot formation process is slightly different.
In premixed flames, soot and its precursor molecules are exposed to attack from oxidative molecules, which can induce their decomposition. In ideal diffusion flames, in which soot inception occurs in the fuel rich side of the flame front, the lack of sufficient oxygen in the soot inception zones located on the fuel-rich side of the flame front prevents oxidation of the soot, unless the soot is later allowed to travel through the flame front or brought into contact with excess amounts of oxygen at sufficiently high temperatures.

The presence of oxygen aids the polymerisation, but also the oxidation of soot precursor molecules. In premixed flames, an increase in oxygen concentration leads to a reduction in the amount of soot

produced due to a stronger increase in the rates of oxidation than formation of soot. A critical equivalence ratio Φ exists below which the formation of soot from a premixed flame may even be avoided entirely (Glassman & Yetter, 2008). This critical sooting equivalence ratio Φ_C depends in detail on the environmental conditions as well as on the type of fuel.
In diffusion flames, the effect of oxygen is slightly more intricate. Diffusion flame experiments have shown (Hura & Glassman, 1988) that if oxygen is gradually added to the fuel supply of a partially premixed diffusion flame, the initial effect occurring at low-levels of oxygen concentration ($\Phi \rightarrow \infty$) is an increase in the soot concentration within the flame. This is explained by the increased formation of radicals in the flame which cause an increase in the rate of polymerisation of soot precursors which is more pronounced than the increase in the rate of oxidation of the soot precursors due to increased oxygen levels. As the concentration of oxygen is increased further, the rate of oxidation of soot precursors increases more significantly than that of the rate of polymerisation, so that after its initial increase, a reduction in the soot concentration is observed. Under increasingly high contents of oxygen in the fuel supply stream, the diffusion flame eventually becomes more and more similar to a premixed flame (Glassman & Yetter, 2008).

Temperature has an important effect on soot formation and oxidation. Milliken (1962) showed through experiments under pre-mixed flame conditions, that the higher the temperature of an ethene flame is, the lower the amount of soot emitted from it is. This was explained by the way in which the rates of formation and oxidation of soot precursors respond to temperature. As the temperature of the flame is increased, the rate of formation of soot precursor molecules, and their rate of oxidation, are both increased. The rate of oxidation however, increases more rapidly with temperature than the rate of formation of soot precursor molecules, so that an increase in combustion temperature leads to a net decrease in soot formation from the flame.

In ideal diffusion flames, in which no oxidative attack on soot and its precursors can occur (as those created in counter-flow diffusion burners (Glassman & Yetter, 2008)), the effect of temperature on soot formation is different. Under such conditions, temperature only increases the rate of formation of soot but cannot increase the rate of oxidation of soot, due to its absence. Thus, an increase in temperature simply leads to an increase in soot formation.

The effect of temperature on soot formation in diffusion flames can be more intricate under conditions in which the reactants and products may travel through regions of differing stoichiometries and temperatures. In a non-ideal diffusion flame, in which the soot is allowed to travel through the flame front, soot is formed on the fuel-rich side of the flame front in the absence of sufficient oxygen, but it may subsequently pass through the flame front, and later mix with excess air in the wake of the flame. Diffusion flame experiments carried out by Kent and Wagner (1985) have shown that incipient soot particle formation occurs for temperatures around and above 1650 K, whilst the oxidation of particles and their precursors ceases for temperatures below 1300 K. The implications of these observations are that in order to prevent soot formation entirely, the

temperatures within the flame zone must be kept below the region of 1650 K. Under conditions in which this is not possible, and soot formation is still to be avoided, it is necessary that the soot oxidation zone, situated to the lean oxidiser side of the flame zone, must be at a temperature superior to 1300 K, so that the previously created soot may subsequently be oxidised in this region. Either option will eventually lead to soot-less exhaust gases, but this example emphasises the importance which soot oxidation plays in avoiding soot emissions from flames. Soot oxidation may occur at high temperatures in the lean gases of a diffusion flame typical of a diesel engine, and presents an important mechanism by which soot emissions may be reduced or avoided.

The effect of pressure and specific volume on the formation of soot is less well defined, and effects of pressure can manifest themselves in variations of diffusivity and in flame structure (Glassman & Yetter, 2008). Considerations of equilibrium conditions with regards to the principle of Le Chatelier (Turns, 1996) show, that due to the reduction in volume and pressure associated the with formation of soot, higher pressures and lower specific volumes would tend to increase the equilibrium concentration of soot within a flame.

It has been reported that the molecular structure of the fuel plays an important role in the propensity of flames to produce soot. Practical experiments carried out under controlled temperature conditions have been carried out for premixed and diffusion flames. The results have allowed broadly classifying groups of hydrocarbons according to their sooting propensity, which may be summarised by the following order of chemical substances (Glassman & Yetter, 2008):

Aromatics > Alkynes > Alkenes > Alkanes

In order to understand the formation of soot in the partially premixed and partially diffusion flame conditions in a highly turbulent and unsteady environment that occur in diesel combustion, an important number of experimental studies have been conducted in engines. The most fundamental operating parameters to affect particulate formation in a diesel engine are: Premixed burn fraction, injection timing, engine equivalence ratio and load, engine speed, fuel injection pressure, EGR and fuel oxygen content.

The effect of premixed burn fraction on smoke emissions in a diesel engine has been studied by Ladommatos et al. 1996[a]. In these experiments, the premixed burn fraction of the combustion process was altered by altering the ignition delay through the addition of varying quantities of an ignition improving additive (2-ethylhexyl nitrate) to the diesel fuel. The experiments showed that a progressive increase in smoke emissions was observed as the premixed burn fraction was reduced (Figure 2.9).

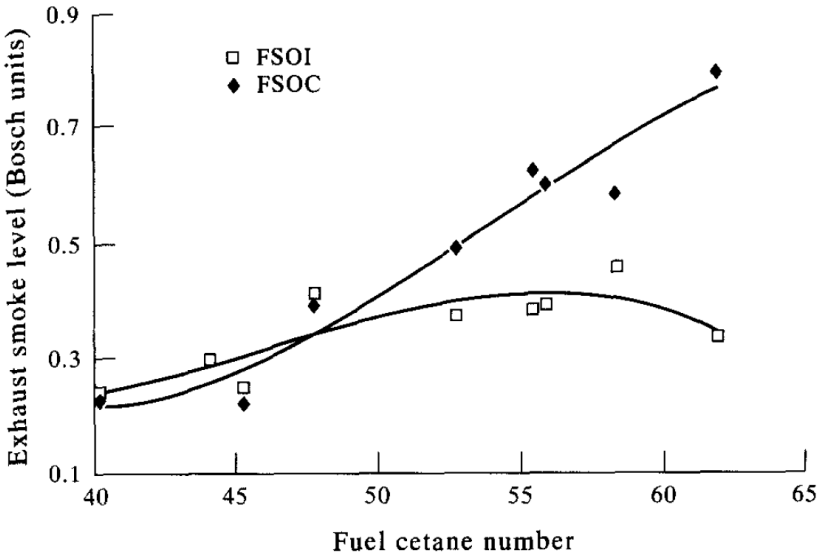

Figure 2.9 – Effect of fuel cetane number on smoke emissions. Ladommatos et al. 1996[a].

There are two main explanations for the observed trend: Firstly, the higher premixed burn fraction was induced by a longer ignition delay, which manifests itself in longer lift-off lengths of the flames. Longer lift-off lengths of the flames are known to cause increased air-entrainment (Siebers, 1999) into the burning fuel spray and have been shown to lower the flame soot-loading (Siebers, et al., 2002). Musculus (2004) showed that the peak luminosity from hot soot radiation in a diesel engine decreases dramatically as the premixed burn fraction was increased as a result of increased air entrainment into the diesel jet. Secondly, a higher premixed burn fraction resulted in higher peak combustion temperatures for many of the experiments, which in turn are likely to contribute to a higher amount of soot oxidation occurring in the post-flame gases of the combustion process (Musculus, 2004).

The effect of injection timing on particulate formation from the diesel combustion process has been documented in various experimental studies. An advance in fuel injection timing has been reported to result in a decrease in smoke emissions (Pischinger & Cartellieri, 1972; Kamimoto & Kobayashi, 1991). An advance in injection timing of the fuel is thought to increase the amount of soot formed during the combustion process, since much of the combustion occurs at higher temperatures and pressures. But since an advance in injection timing results in an advance of the combustion process, more time is later available for soot oxidation at sufficiently high temperatures during the later stages of the combustion process and in the post-combustion gases in which the soot is burned-out in the presence of sufficient oxygen. Time availability for soot oxidation has been reported to be the dominant factor in this trade-off, leading to a net reduction in exhaust gas soot emissions for earlier injection timings (Tree & Svensson, 2007). It has further been reported that for a given piston bowl and injector geometry, dramatic effects of changes in the injection timing on particulate emissions can be observed, if the changes in injection timing result in liquid fuel impingement on the piston.

The global equivalence ratio, which is correlated with the engine load, has also been observed to have a significant effect on the overall formation soot. It has been reported in experimental studies that the amount of smoke formation increases with increasing equivalence ratio, and with increasing

engine load (Pischinger and Cartellieri 1972, Kamimoto & Kobayashi 1991). This can be explained by the increased amount of fuel which is burned at higher equivalence ratio and higher load, all of which is able to contribute to soot formation, as well as by the overall reduced oxygen availability in the combustion chamber.

A further effect on particulate emissions is that of engine speed. Yu and Shahed (1981) showed that a minor increase in total particulate is observed as the engine speed is increased. This may be attributed to shorter residence times of the soot-loaded post-flame gases at high temperatures, as a result of more rapid expansion and increased turbulence of the cylinder gases. Lower residence times of the soot at high temperatures in the lean post-flame gases would be expected to reduce the oxidation of soot, and thus in an increase of soot emissions through the exhaust gases.

The formation of particulates during the diesel combustion process is strongly affected by injection pressure. Pierpont and Reitz (1995) carried out experiments in a direct injection diesel engine with electronically controlled injection, in which the total particulate emission of the engine was measured for engine operation at various injection pressures. The authors reported that an increase in the fuel injection pressure resulted in a strong decrease in particulate emissions, which could be attributed to improved air entrainment into the fuel spray (Siebers, 1999), an increase in premixed burn fraction and improved oxidation of soot and its precursors.

Exhaust gas recirculation (EGR) of the engine has also been reported to have a strong effect on particulate emissions of the engine. Ladommatos et al. (2000) have shown that the progressive introduction of recirculated exhaust gases substantially increases the formation of particulate emissions from the combustion process. The authors observed that the depletion of the oxygen concentration in the combustion chamber gases through the introduction of EGR was the main contributing mechanism by which soot emission was increased. A reduction in oxygen concentration would be expected to substantially reduce the oxidation rates of soot and its precursor molecules.

The fuel oxygen content has been reported to have a strong effect on soot formation in the diesel combustion process. Flynn et al. (1999) reported that as the fuel oxygen content is increased within a binary mixture of normal heptane and methanol, analytical models predict that the percentage of fuel carbon atoms involved in the formation of soot precursors is reduced, and even reaches a value of near zero for a fuel oxygen content in excess of 25% fuel mass. Miyamoto et al. (1998) reported similar results from engine experiments in which the fuel oxygen content was progressively increased through the addition of four different oxygenated compounds into diesel fuel.

The sizes of diesel exhaust particulate matter can vary greatly, and has been found to range from diameters of around 5 nm to such of diameters in excess of 10 μm (Kittelson, 1998). Measurements of the size distributions of exhaust gas particles have been carried out using a variety of experimental techniques (Amann & Siegla, 1981). These include the counting of particle number and measurements of particle size from photomicrographs (Medalia & Heckmann 1969), measurement of particle mass from different sizes using inertial impactors (Vuk, et al., 1976) and electrical aerosol analysers (Dolan, et al., 1975; Khatri, et al., 1978; Kittelson, et al., 1978). Kittelson (1998) reports that the size distribution of exhaust gas particles is trimodal, and that each mode is log-normal in form. The three modes of particle emissions are: nucleation mode particles

(5-50 nm diameter), accumulation mode particles (100-300 nm diameter) and the coarse mode particles (2-10 μm diameter) as shown in Figure 2.10.

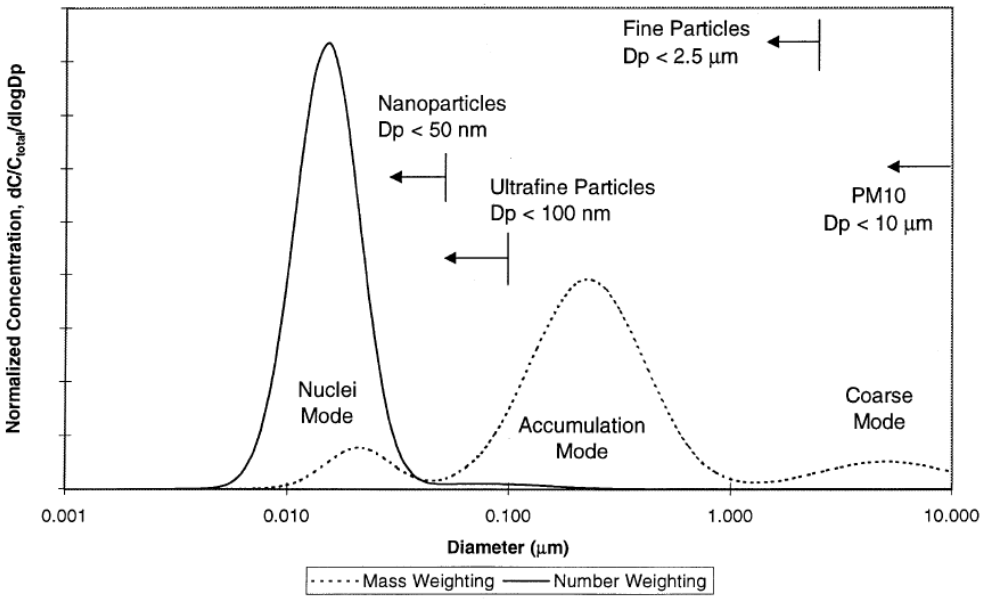

Figure 2.10 - Typical particulate size distribution of exhaust gas particulate matter. Kittelson (1998).

Figure 2.10 shows that the particle number is concentrated mostly in the nucleation mode particles (> 90%), which only contains about 1-20% of total particle mass, and that most of the particle mass is concentrated in the accumulation mode, which contains about 60-94% of total particle mass. The coarse mode contains about 5-20% of total particle mass.

The morphology and chemical composition of the individual modes of particles is believed to be significantly different for each of the size distribution modes. The accumulation mode particles consist predominantly of clusters of carbonaceous soot particles described at the start of this section.

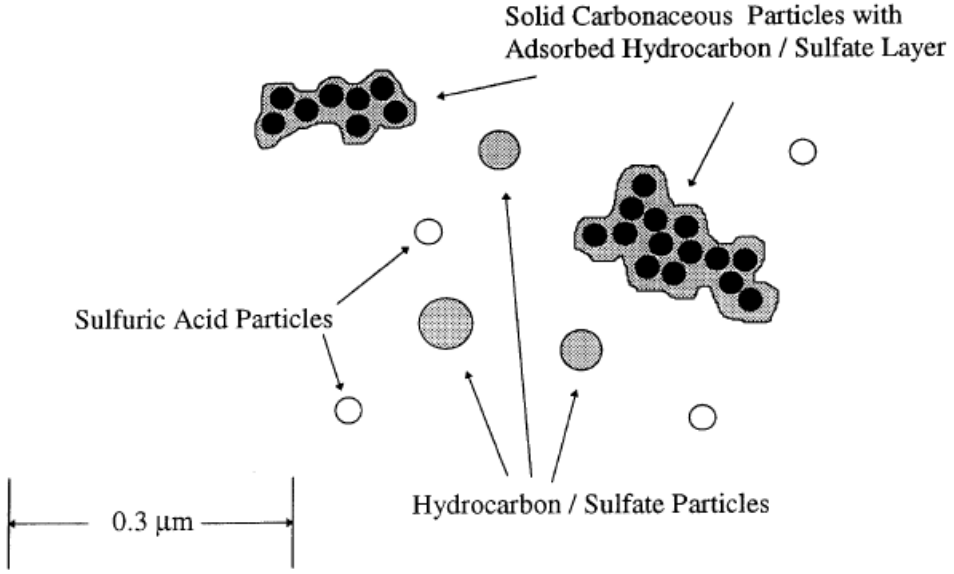

Figure 2.11 - Morphology and composition of different particle size modes. Kittelson (1998).

The coarse particle mode is thought to consist of agglomerations of accumulation mode particles which have been deposited on the surfaces of the combustion chamber and the exhaust system, and which are re-entrained into the gas exchange processes as clusters at a later point. The small nucleation mode particles are believed to consist primarily of condensed-phase hydrocarbon, sulphate and sulphuric acid particles (Kittelson, 1998), as well as water droplets if the exhaust gas mixture is brought below its dew point (see Figure 2.11).

Dolan et al. (1975) reported that the mean diameter of the accumulation mode particles was observed to increase at higher loads, and that the mean diameter of the nucleation mode particles was observed to increase at lower loads. The increase in diameter of the accumulation size particles can be explained by an increase in the soot-particle growth processes outlined earlier in this Chapter, due to a prolonged combustion process at higher loads. It could be hypothesised that the increase in nucleation mode particles at lower loads may be attributed to an increase in condensation occurring, due to the lower exhaust gas temperatures.

The hydrocarbons involved in the formation of condensed phase particulate matter are likely to have high boiling points, and to derive from the least volatile fractions of the injected fuel and the engine lubricating oil (Amann & Siegla, 1981). Mayer et al. (1980) sought to quantify the contribution of the engine lubrication to particulate formation in a series of experiments in which the engine lubricating oil was marked with a radioactive tracer. It was observed that 1.5-25% of the particulate mass could be attributed to the engine lubricating oil, whilst the remaining 75-98.5% of particulate mass originated from the injected diesel fuel oil. Mayer et al. (1980) reported that the contribution of engine oil within the particulate matter increased progressively with engine speed. The engine lubricating oil contribution to the particulate matter was observed to be present in the form of hydrocarbons rather than carbonaceous soot, indicating that the engine lubrication oil did not significantly partake in the combustion process.

The mechanism by which the formation of nucleation mode particles occurs is still not well understood (Tobias, et al., 2001; Kirchner, et al., 2009). In an experimental study Tobias et al. (2001) showed that the nucleation mode particles consist mostly of hydrocarbons from the injected fuel or the engine lubrication oil and that sulphuric acid was present at a concentration of a few percent. As a formation mechanism, the authors advanced the nucleation of sulphuric acid and water, followed by subsequent particle growth through condensation of hydrocarbons. Similar conclusions were drawn by Schneider et al. (2005). Sakurai et al. carried out studies on the volatility (2003[a]) and on the chemical composition (2003[b]) of nucleation mode particles using fuels with very low sulphur contents below 1 ppm. Thermal desorption particle beam mass spectrometric analysis of the particles indicated that in excess of 95 % by mass of the nucleation mode particles consisted of unburned engine lubricating oil. The authors concluded in both studies that some of the particles may contain a non-volatile core in addition to the hydrocarbons, which may consist of carbonaceous soot, metal oxides or low-volatility organic compounds, which may provide the initial point of nucleation for the droplets. Kirchner et al. (2009) conducted an analysis in which nucleation mode particle were visualised using transmission electron microscopy before and after entering a thermal denuder oven capable of eliminating volatile fractions from the particles. Although their analysis

showed that under most engine operating conditions, the nucleation mode particles disappeared completely when being thermally treated in the thermal denuder, the authors also noted that under certain engine operating conditions (cold start idle), remains of nucleation particles were visible after they had been treated in the thermal denuder. This suggests that in this case the particles did not solely consist of volatile hydrocarbons, water and sulphuric acid but comprised non-volatile components. Small solid components may provide the droplets with an initial nucleation surface on which condensation may take place under conditions of mild supersaturation of the vapours in air (Houghton, 1959).

2.5.3. UHC emission

The emission of hydrocarbons from the diesel combustion process shall herein be defined as organic vapours leaving the combustion chamber in the vapour phase as part of the engine exhaust gas. Hydrocarbons suspended in the exhaust gases in the form of droplets; or those absorbed onto particulates of carbonaceous soot, shall be considered to be particulate matter, and are discussed separately in section 2.5.2.

The principle source of organic vapours within the exhaust gases is the incomplete combustion of the injected fuel, and to a minor extent the vaporisation of engine lubricating oil within the combustion chamber. Overall, the extent of the problem of hydrocarbon emissions from diesel engines is relatively mild in comparison with other pollutants such as nitrogen oxides and particulate matter. This is because the combustion efficiency of diesel engines is typically exceeds 98%, and the amount of fuel emitted in the form of unburned hydrocarbons usually consists of less than 1% of the injected fuel (Heywood, 1988). This can mainly be attributed to the overall lean operation of diesel engines, and to the high combustion efficiency which diffusion flames typically have, in which the majority of the fuel is oxidised in diesel combustion.

Firstly the emission of hydrocarbons from unburned fuel shall be discussed. Consider the diesel combustion process described in section (2.3 and 2.4). There exist three mechanisms by which the fuel may escape full oxidation during this process: The first mechanism is that of lean premixed combustion in which fuel escapes full oxidation through low combustion efficiency or absence of combustion by forming overly lean mixtures with air before ignition can occur. As fuel is injected into the combustion chamber, it undergoes an ignition delay, governed by the physical and chemical processes occurring within the fuel jet. The fuel vaporises and mixes with the surrounding air. If parts of this vapour are allowed to form a lean mixture with air ($\Phi<1$) before ignition occurs, this vapour will not undergo combustion under diffusion flame conditions, but under lean premixed conditions, and may even fail to undergo oxidation if the mixture is excessively lean ($\Phi<<1$). If the mixture is strong enough to undergo lean premixed combustion, parts of the fuel will be oxidised. However, since the adiabatic flame temperature of this lean mixture is significantly lower than that of a stoichiometric mixture, and the combustion process occurs on a shorter time scale, its combustion efficiency is significantly lower than that of a diffusion flame, and a larger proportion of

unburned or partially burned fuel will result. If the mixture is excessively lean, the fuel vapour may fail to undergo auto-ignition or to support flame propagation from other flame regions, and may result in the presence of considerable amounts of unburned fuel vapour. Although some of the unburned organic vapours may still be oxidised during the later stages of combustion by mixing with hot gases that had richer stoichiometry, a substantial amount of this fuel vapour may contribute to the emission of hydrocarbons in the exhaust gas.

This mechanism occurs predominantly if a large proportion of the combustion occurs under premixed conditions, such as for combustion with a long ignition delay and at light engine load, in which the premixed burn fraction presents a substantial proportion of the total energy release. It has been shown in engine experiments under which the start of injection or the start of combustion were held constant (Ladommatos 1996[a]), that the ignition quality of the fuel expressed as fuel cetane number, shows good correlation with the emission of UHC (Figure 2.12). The fuel cetane number is correlated with the ignition delay of the fuel and the fraction of fuel burned under premixed conditions.

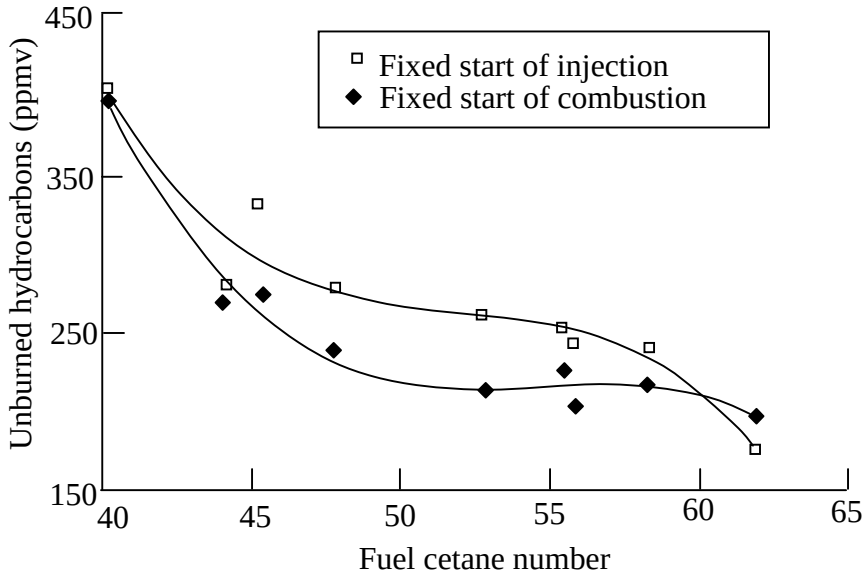

Figure 2.12 - Exhaust gas concentration of unburned hydrocarbons as a function of fuel cetane number under conditions of fixed start of injection (FSOI) and fixed start of combustion (FSOC), Ladommatos et al. (1996[a])

The second mechanism by which fuel may escape the combustion process is by the formation of excessively rich mixtures (Φ>1) which fail to mix to within fully combustible stoichiometry before the combustion process in extinguished. This can occur in the central areas of the fuel spray in which rich pockets of fuel in air, can fail to mix to within fully combustible stoichiometry before the temperatures drops to levels that are unsupportive of combustion during the late expansion stroke and exhaust process. Such conditions predominantly occur under high engine load conditions in which the injection is carried long into the expansion stroke, and the capabilities of fuel-air mixing in the combustion chamber are reaching their limits. It may also be caused by large droplet being

formed towards the end of the fuel injection process, as the injector needle begins to throttle the fuel flow, or by fuel evaporating from the injector nozzles after injection has terminated. Under most diesel operating conditions, the UHC exhaust emission mechanism due to excessively rich mixtures is of significantly less importance than that occurring due to the formation of excessively lean mixtures (Heywood, 1988).

A third mechanism of hydrocarbon emissions from diesel engines is that of flame quenching or fuel impingement on the combustion chamber walls. Heywood (1988) reports that the oil and coolant temperatures (which correlated with combustion chamber wall temperatures) of a DI diesel engine have an effect on the UHC exhaust emissions, even for operation at constant ignition delay. This suggests that wall-quenching of the diesel flames may play a role in the emission of exhaust UHC. The work of Siebers (1999) has shown that it may be possible even under modern engine operating conditions for liquid fuel to reach the combustion chamber walls in small light-duty direct-injection diesel engines. Fuel impinging on the combustion chamber walls may fail to combust due to late or incomplete vaporisation and mixing with, and may thus provide a mechanism for UHC exhaust emissions.

Another, though less significant source of unburned hydrocarbon emissions is the engine lubricating oil. Engine lubricating oil may access the combustion chamber gases either through vaporisation off the cylinder wall, or in the form of small droplets formed due to the rapid movement of the piston. The engine oil may evade combustion either in the form of a lean vapour, as well as in the form of an rich vapours stemming from evaporating oil droplets via the same principal mechanisms described above for the fuel. Such uncombusted engine oil in the form of vapours may contribute to UHC emissions through the exhaust gas.

2.5.4. CO formation

In combustion, carbon monoxide represents a product of incomplete oxidation of carbon, which typically derives from the decomposition of fuel hydrocarbons. It is thought that the formation of carbon monoxide may occur through three principal mechanisms.

Firstly, the formation of CO may occur as a combustion product for the combustion of fuel-air mixtures of rich equivalence ratios ($\Phi>1$). The absence of sufficient oxygen for full oxidation of all carbon atoms to CO_2 can result in the formation of CO as a stable combustion product (Turns, 1996, pp.488-489). In diesel combustion, which takes place at overall lean equivalence ratios, this may occur within localised fuel-rich pockets of gases that fail to undergo adequate mixing with air. This mechanism is similar to that described in section 2.5.3 regarding the incomplete oxidation of UHC in fuel-rich zones. Due to the globally lean operation ($\Phi<1$) of diesel combustion, and the turbulent nature of the air motion within the cylinder, most of the fuel vapours typically undergo sufficient mixing at high temperatures for oxidation of CO to occur.

Secondly, the formation of CO may occur as a result of dissociation of CO_2 at high temperatures. Dissociative CO is usually decomposed to CO_2 if the mixture is cooled down at a sufficiently slow rate to allow low near-equilibrium concentrations of CO to be reached (Turns, 1996). However, due

to the strongly inhomogeneous character of the turbulent diffusion flames present in diesel combustion, rapid dilution of combustion gases with cooler lean mixtures and rapid heat-transfer occurring at combustion chamber walls, may not leave sufficient time for dissociative CO to be oxidised to CO_2. Such quenching prevents CO from reaching its equilibrium concentration during the cooling process, and may be responsible for its emission as exhaust gas pollutant (Delichatsios, 1972).

Thirdly, the formation of CO may occur as an intermediate product during the combustion reactions of fuel-air mixtures. If the combustion reactions may not be completed as a result of an interruption of the oxidation process, CO formed as an intermediate species of fuel oxidation may survive the combustion process. This is typically the case if the reacting mixture of gases is quenched through turbulent mixing with cooler combustion chamber gases or through rapid heat transfer at the combustion chamber walls.

Despite these three mechanisms potentially all contributing to the formation of CO, the overall CO concentration in the exhaust gas of diesel engines are typically low in comparison with other pollutant species, such as NO_x, and typically represents a less significant problem.

2.6. Homogeneous charge compression ignition (HCCI) combustion

The preceding discussion has indicated that the formation of NO_x and particulate matter in the diesel combustion process present the most severe problem of pollutant emission in diesel engines. The formation of NO_x has been reported to occur predominantly above temperatures of 1800 K, whilst the formation of particulate matter occurs predominantly at high equivalent ratios (Φ>1), and commences at temperatures above 1650 K. It is known that by reducing the occurrence of high temperatures, the formation of NO_x can be reduced, and even completely suppressed (Kamimoto & Bae, 1988), whilst the absence of fuel-rich gases beyond a certain stoichiometry and temperature limit, suppresses the formation of soot during combustion (Kamimoto & Bae, 1988). It has thus been proposed to operate compression ignition engines on the combustion heat of a lean, homogeneous mixture of fuel and air (Onishi, et al., 1979; Najt & Foster, 1983; Thring, 1989). The ignition and combustion of homogeneous mixtures of hydrocarbons and air may be achieved through elevated temperatures, which have been shown to result in a multistage ignition process of the hydrocarbon and air mixture, depending on the temperature and pressure (Griffiths, 1971). The necessary ignition temperature in the engine is to be achieved through mechanical compression of the premixed charge of fuel and air (Najt & Foster 1983). A recent discussion of the combustion process in reciprocating engines has been reported by Dec (2009).

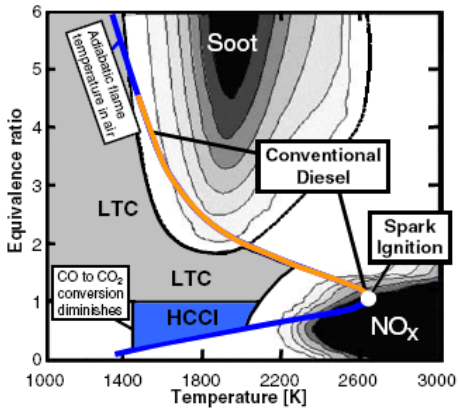

Figure 2.13 - Map of NOx and particulate matter formation as function of equivalence ratio and temperature. Adapted from Dec (2009).

The heat release of the combustion process may occur in a single or in two-stages of heat release, depending on the fuel chemistry (Dec, 2009) and on the chemical reactions and intermediate species via which the combustion occurs (Glassman & Yetter, 2008). Alkane fuels of higher molecular mass than methane and ethane, exhibit a progressively increasing tendency for a two stage ignition process and two distinct phases of heat release (Benson, 1960, p.480; Glassman & Yetter, 2008, p.103). This is because for such fuels, two distinct temperature bands exist, in which rapid oxidation of the fuel occurs, which are divided by a temperature band in which oxidation progresses slowly, and may be endothermic. The magnitude of temperatures at which these bands of rapid and slow oxidation processes occur depend on the kinetic rates of reaction of the chemical mechanisms that dominate each temperature region. The experimentally recorded single-stage and two-stage HCCI combustion of different hydrocarbon fuels in an engine are represented in Figure 2.14 in terms of temperatures and corresponding heat release rates (Hwang, et al., 2008).

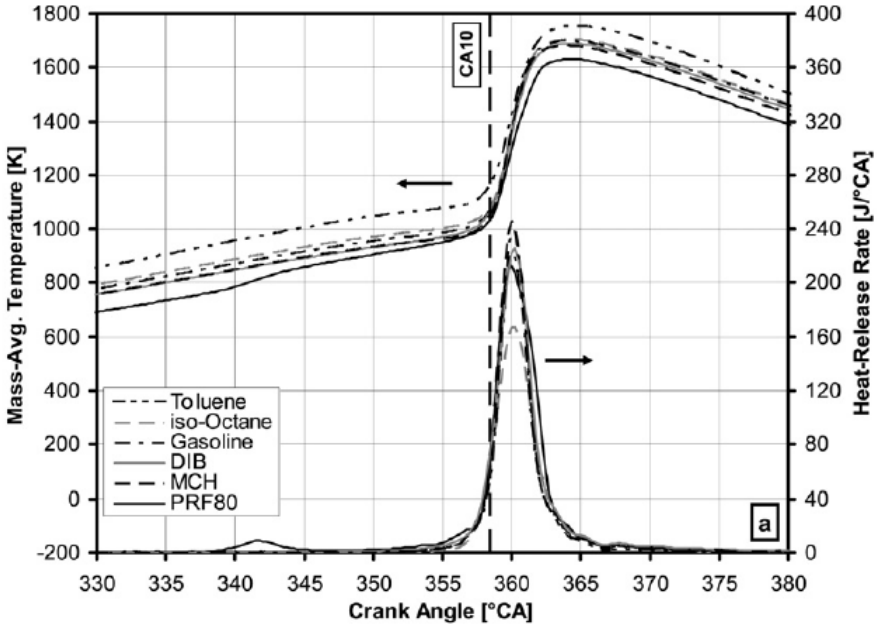

Figure 2.14 - Heat release and temperature diagram of HCCI combustion for different fuels. Hwang et al. (2008).

A variety of practical problems arise from the nature of HCCI combustion for which solutions need to be found, before HCCI combustion becomes viable for automotive applications.

A salient problem is the control of the ignition of the fuel air mixture under varying operating conditions, such as engine load, speed, and operational temperatures. Ignition of the fuel needs to be assured through the supply of sufficiently high temperatures over a sufficiently long period of time to allow the combustion process to take place. In order to achieve good engine efficiency, a further requirement is that the ignition process is timed at a point within the engine cycle that most of the heat release of the combustion occurs whilst the piston is situated in the vicinity of TDC. The point at which ignition occurs within the engine cycle is a function of equivalence ratio, temperature, pressure and composition of the cylinder charge, as well as engine speed. Since engine speed and equivalence ratio of the charge are dictated to a large extent by the instantaneous power requirement of the engine, charge pressure, temperature and composition must be modulated in order to control the time of ignition. Machrafi et al. (2008) demonstrated that an increase in compression ratio, and thus combustion chamber pressure and temperature, an increase in charge intake temperature and an increase in equivalence ratio all resulted in an advance of ignition timing. Szybist and Bunting (2005) reported that an increase in engine speed resulted in a marginally later phasing of the high temperature combustion within the engine cycle, and that a decrease in fuel cetane number resulted in a significant retardation of the combustion process. Lü et al. (2005) and Shi et al. (2006) showed that EGR can be used effectively to retard the start of combustion. Another prominent problem is that of charge preparation in HCCI combustion, especially when using fuels of low-volatility such as diesel fuel. Various methods exist to overcome this problem, such as adapted injection system and charge heating for improved evaporation (Dec, 2009), or the use of fuels with high volatility (Shudo & Ono, 2002). Further important limitations of HCCI combustion are the low combustion efficiency of the engine experienced at low loads resulting in a high loss of UHC through the exhaust gasses, and knock-limitations at high load operation (Dec, 2009).

2.7. Literature on the influence of the molecular structure of fatty acid alkyl ester (biodiesel) molecules produced from plant oils and alcohols via transesterification

The molecular structure of biodiesel was well known since its invention, where it had been formulated in the synthesis process using the example of palmitic acid ethyl ester in Chavanne's patent of 1937. The use of vegetable oils as raw material for the synthesis of a fuel inherently implies that the product will consist of esters of many different fatty acids. Chavanne recognised this in his patent and stressed that various types of monohydric alcohols can be employed for its synthesis (e.g. methanol or ethanol), yielding different molecular structures of the fatty acid alcohol esters. As a result of this variability in chemical structure of biodiesel molecules, it was not long

before experimental research was conducted to understand the detailed influence of the various fatty acid alcohol esters on the combustion process of biodiesel.

2.7.1. Influence of the molecular structure of biodiesel on auto-ignition behaviour

The first methodical study which examined the behaviour of individual fatty acid alcohol esters of various molecular structures appears to be the work of Duport (1946). Duport determined the autoignition temperatures of several fatty acid ethyl esters present in vegetable oils, and compared these with untreated vegetable oils, several alcohols including glycerol, as well as petroleum-derived diesel and spark-ignition engine fuels. His experiments were limited by the technical instruments at his disposition. He noted in his report: 'The study of these two characteristics of fuels [i.e. low ignition temperature and short ignition delay] is usually carried out on an experimental diesel C.F.R.[…] engine of the A.S.T.M. in France.' … 'As we do not dispose of a C.F.R engine, we would have had to address ourselves to an external party, which given the large number of experiments to be carried out, would have been unpractical. We thus thought that it would already be interesting to proceed by our own means to obtain comparative results for the minimum auto-ignition temperature of the products we wanted to study.'

In his experiments, Duport determined the lowest temperature at which the vapours of the fuels in question would undergo spontaneous auto-ignition. The experiments consisted of introducing a given quantity of fuel into a glass flask which was immersed in a tin or lead bath, depending on the temperature at which the particular experiment was carried out. The time taken for the fuel vapours to undergo auto-ignition was measured at several different temperatures. This allowed the author to plot curves of time taken for autoignition against temperature, and to establish the minimum autoignition temperature required for each fuel type. His investigation comprised a mixture of raw fatty acids of palm oil as well as several monohydric alcohol esters of this mixture. Several important conclusions can be drawn from his findings which are presented in Figure 2.15:

Duport (1946) observed that all monohydric alcohol esters of fatty acids of palm oil had shorter ignition times and lower minimum auto-ignition temperatures than their raw fatty acids. He observed that butyl esters of palm oil had shorter ignition times and lower minimum auto-ignition temperatures than ethyl esters of palm oil. Ethyl esters of palm oil had, in turn, shorter ignition times and lower minimum auto-ignition temperatures than methyl esters. This data indicated that the chain length of the alcohol on a fatty acid alcohol ester improves the ignition quality of the fuel molecules. Duport also showed that using iso-pentyl alcohol ($C_5H_{12}O$) for the esterification process of fatty acids of palm oil resulted in a product with slightly lower ignition quality than using butyl alcohol ($C_4H_{10}O$). This finding - although it is not explicitly discussed by the author in the text - indicates that branching of the alcohol-chain in the molecule reduces ignition quality of the fuel. It appears that by adding a side-chain consisting of a single carbon atom to the alcohol part of the molecule, a slight reduction in the ignition quality of the fatty acid alcohol ester is obtained, despite its increased

molecular weight. The author also showed that cyclic structures in the alcohol group of fatty acid alcohol esters, tended to reduce the ignition quality of the fuel molecules with respect to straight or single-branched structures of the alcohol group. His work is an early account of the effects which the structure of the alcohol group has upon the auto-ignition characteristics of biodiesel molecules.

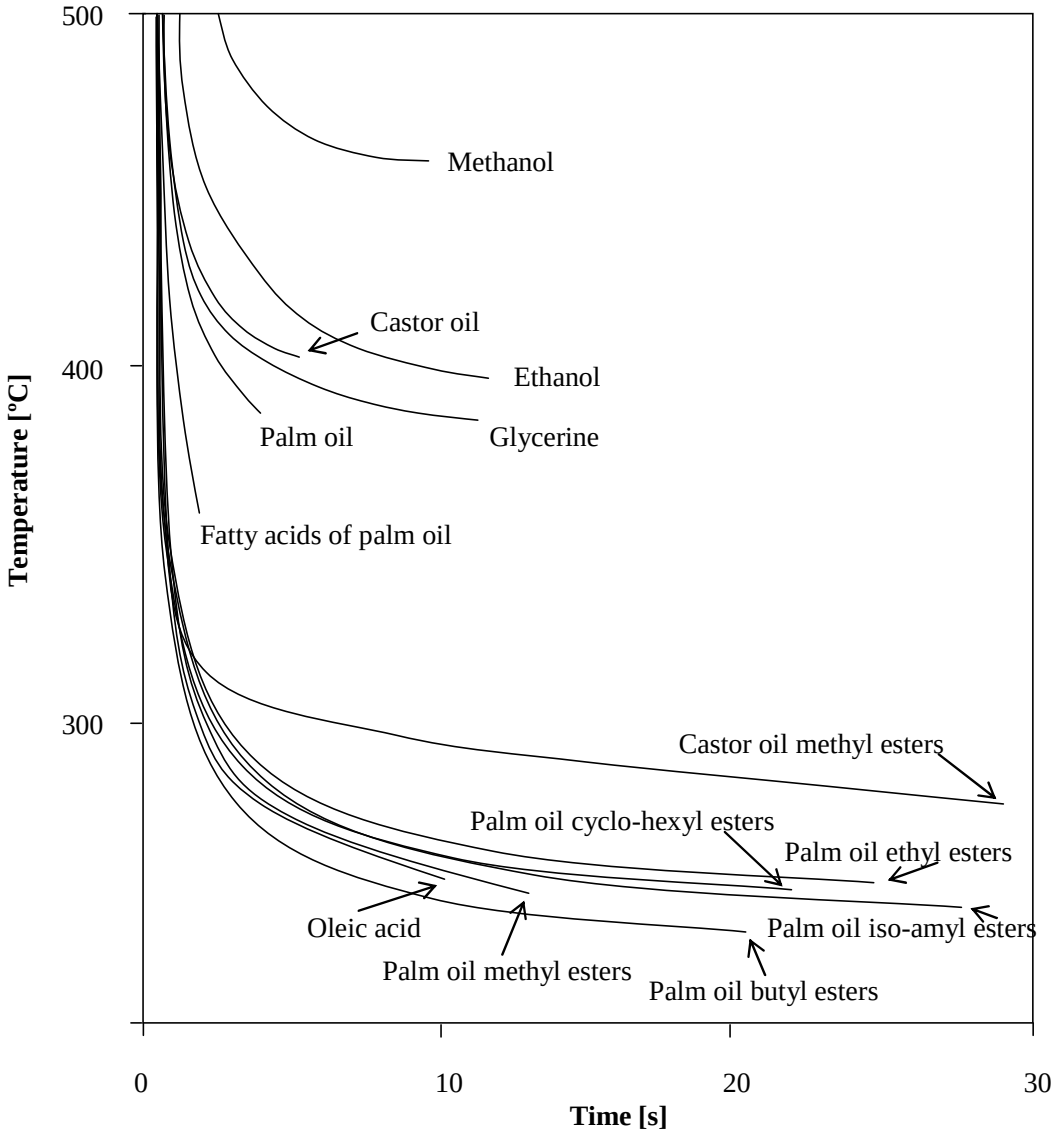

Figure 2.15 – Auto-ignition temperatures and delays for fatty acid esters of various alcohols. Adapted from Duport (1946)

The first systematic study of individual fatty acid esters carried out inside a diesel engine appears to have been carried out by Klopfenstein (1983), who synthesised 16 individual fatty acid esters which were tested for cetane numbers by an engine laboratory (Dresser Industries, Waukesha, Wisconsin, USA). No details are reported explicitly on the test methods used to obtain the data, but it is likely that ASTM D-613 method was used, as was the case in a later publication by the author. It appears that only the cetane numbers were recorded in these experiments. From the obtained data, the author

was able to report for the first time three very important trends in the effect of the molecular structure of fatty acid esters on their ignition quality. These were:

1. Cetane number increases with molecular weight of the fatty acid moiety.
2. Cetane number increases with molecular weight of the alcohols moiety.
3. Cetane number decreases with unsaturation of the fatty acid moiety.

Klopfenstein also confirmed that branching in the alcohol chain of the molecule significantly reduces the cetane number of the fuel, as had previously been suggested by the work of Duport (1946) by measurement of the minimum autoignition temperatures.

Johnston and Harrington (1983) carried out engine experiments on real vegetable oils transesterified with different alcohols. Their experiments confirmed that transesterification with normal alcohols of increasing chain-length leads to progressively better ignition quality of the fuel. The experiments also provided confirmation that branching within the alcohol chain reduces ignition quality with respect to un-branched alcohol chains of the same atomic make-up under real diesel engine conditions.

Klopfenstein (1985) carried out further experiments on the ignition quality of individual fatty acid alcohol esters. These experiments were carried out according to ASTM D-613 in a single cylinder CFR engine. The results confirmed previously observed trends on chain lengths of the alcohol chain and the fatty acid chain. Klopfenstein observed that increasing the molecular mass of the fatty acid moiety of the molecule produced a larger increase in cetane number than increasing the molecular mass of the alcohol moiety of the molecule by the same amount (see Figure 2.16). It was also confirmed that the raw fatty acids have lower cetane numbers than their monohydric alcohol esters.

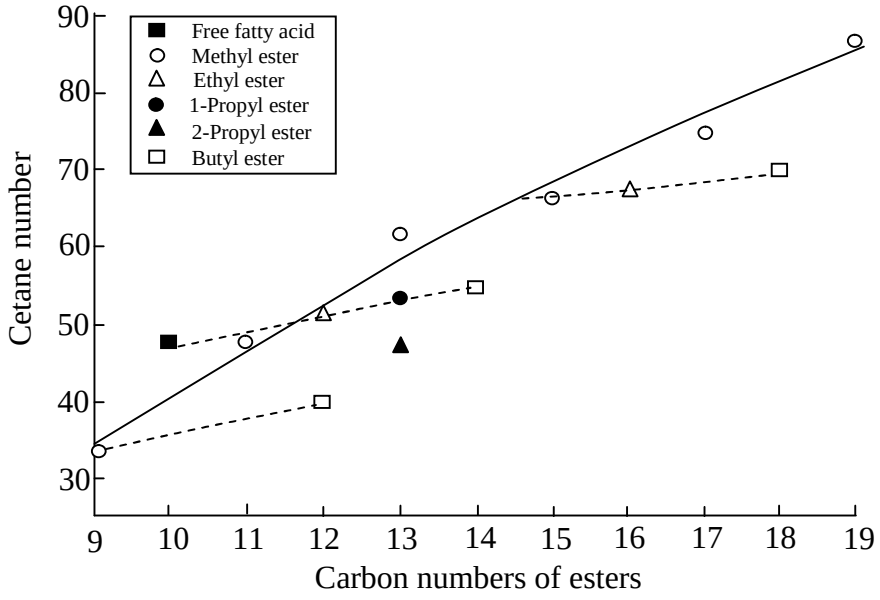

Figure 2.16 – Effect of molecular mass of fatty acid alcohol esters on cetane number, demonstrating the influence of chain length of alcohol chain versus that of the fatty acid chain of the molecule. Adapted from Klopfenstein (1985).

Harrington (1986) carried out qualitative predictions of the ignition quality of fatty acid alcohol esters with regards to their molecular structure, based on ignition quality data for different hydrocarbons obtained by Elliott et al. (1955) in a constant volume combustion bomb. Harrington (1986) also processed the experimental results obtained by Klopfenstein (1983) further. The author pointed out that from Klopfenstein's data it is visible that the relative position of the carbonyl group on the fatty ester chain has a distinct effect on cetane number. Harrington (1986) applied a correction in the cetane number due to the length of the fatty acid chain, derived from Klopfenstein's (1983) data and reported that good correlation exists between the relative position of the carbonyl group within the chain and the cetane number.

The author writes: 'the cetane rating is highest when the carbonyl 'side-chain' is closest to the end of the molecular chain, and lowest as the side-chain approaches the mid-point of the chain (RP = 0.5).' This is represented graphically in Figure 2.17.

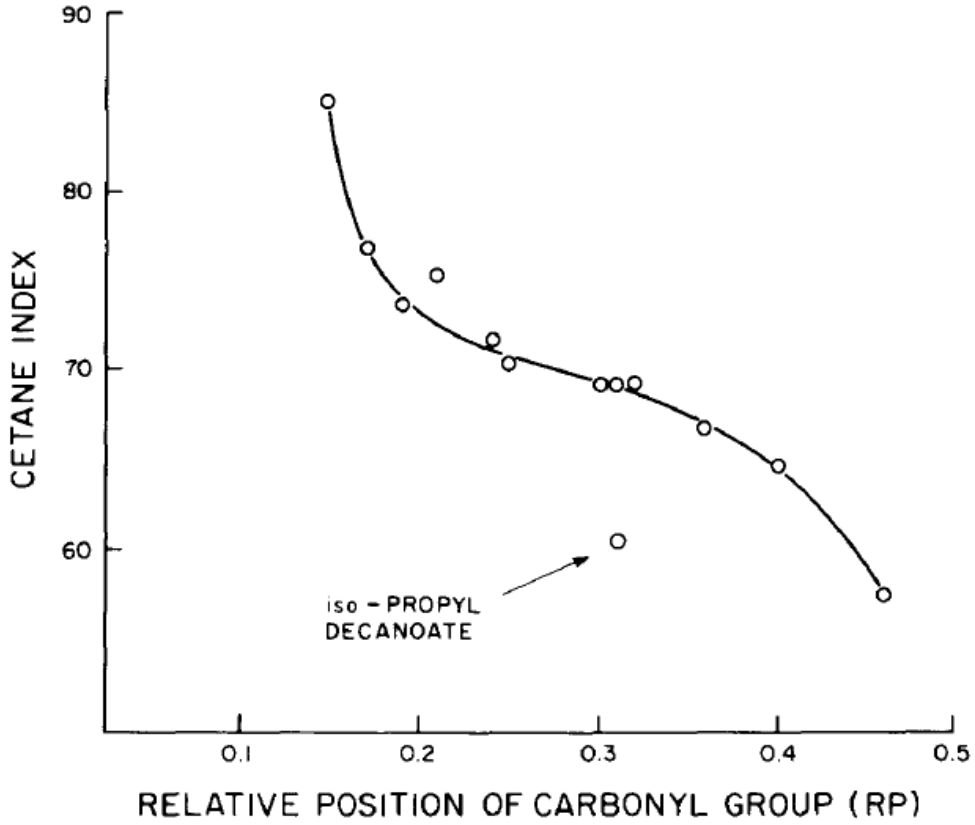

Figure 2.17 – Effect of relative position of carbonyl group in a saturated fatty acid monohydric alcohol ester on Cetane number. Harrington (1986).

Knothe et al. (1997) investigated the effect of the molecular structure of pure fatty acid alcohol esters on the ignition quality of the molecules in a constant volume ignition quality tester (IQT). The experiments provided reliable absolute values of Cetane number for 15 different fatty acid esters and four fatty acids (see Table 2.1). It was confirmed that the longer the chain length of the alcohol used in the transesterification process is, the higher the cetane number of the fuel molecule becomes, and that an increase in un-saturation of the fatty acid chain is correlated with a lower ignition quality. It

was also re-confirmed for four fatty acids that their ignition quality is lower than that of their respective monohydric alcohol esters.

Table 2.1 – Cetane numbers of various fatty esters determined in a combustion bomb. Adapted from Knothe et al. (1997).

	Acid	Methyl ester	Ethyl ester	Propyl ester	Butyl ester
Stearic (C18:0)	61.7	N/D	76.8	69.9	80.1
Oleic (C18:3)	46.1	55.0	53.9	55.7	59.1
Linoleic (C18:3)	31.4	42.2	37.1	40.6	41.6
Linolenic (C18:3)	20.4	22.7	26.7	26.8	28.6

2.7.2. Effect of molecular structure of biodiesel molecules on engine efficiency

Klopfenstein and Walker (1983[a]) synthesised nine individual fatty acid alcohol esters and carried out what appears to be the first account of engine experiments aimed at explaining the influence of the molecular structure of fatty acid alcohol esters on the diesel combustion process. Firstly, the authors determined the calorific value of these individual fatty acid alcohol esters samples in a combustion bomb. Secondly, a single cylinder direct-injection diesel engine which was run on these pure fatty acid alcohol esters at a specified load, and the volumetric flow rate of the fuel was measured. The data on the volumetric flow-rate was combined with the fuel density (which was taken from literature), the calorific value of the fuels and the engine work output, to calculate the thermal efficiencies achieved by the engine with these fuels. The authors found that the fuel-conversion efficiency of the engine increased progressively with shorter chain length of the molecules when running at constant brake load and speed (see Figure 2.18).

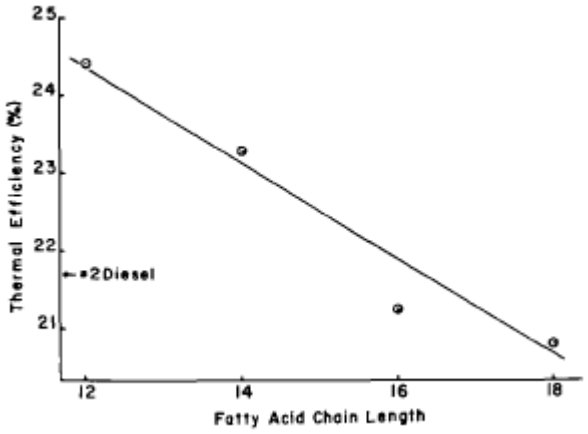

Figure 2.18 – Effect of chain length of saturated fatty acid methyl esters on thermal efficiency of a direct injection diesel engine, Klopfenstein and Walker (1983[a])

The authors concluded with respect to these experiments that: 'Although the energy content of the esters increases with chain length, the increased specific fuel consumption with increasing chain length produces a marked linear decrease in thermal efficiency. The reasons for this are not known.' The conclusion shows that despite observing a clear trend in the experiments, the absence of detailed pressure data and thermodynamic analysis of the engine cycle resulted in lack of understanding of the reasons for the changes in thermal efficiency. No clear trends were found for the effect of unsaturation on the thermal efficiency of the engine. It was reported that for varying degrees of saturation of a fatty acid methyl ester of constant chain length, the thermal efficiency of the engine first increased and then decreased again for a higher degree of saturation. The mono-unsaturated fatty acid methyl ester yielded the highest thermal efficiency. Klopfenstein and Walker (1983[a]) also investigated the effect of the alcohol chain length on the thermal efficiency and found that the efficiency increased when using an ethyl rather than a methyl ester, but then decreased again drastically when using a butyl ester. The results obtained for degree of saturation and alcohol chain length are not entirely clear in their trends, and some significant scatter exists in the results.

In a later publication the same year, Klopfenstein and Walker (1983[b]) reported that for fatty acid chain lengths below 12 carbon atoms the efficiency of the engine peaks at around 10 carbon atoms and then decreases again (see Figure 2.19).

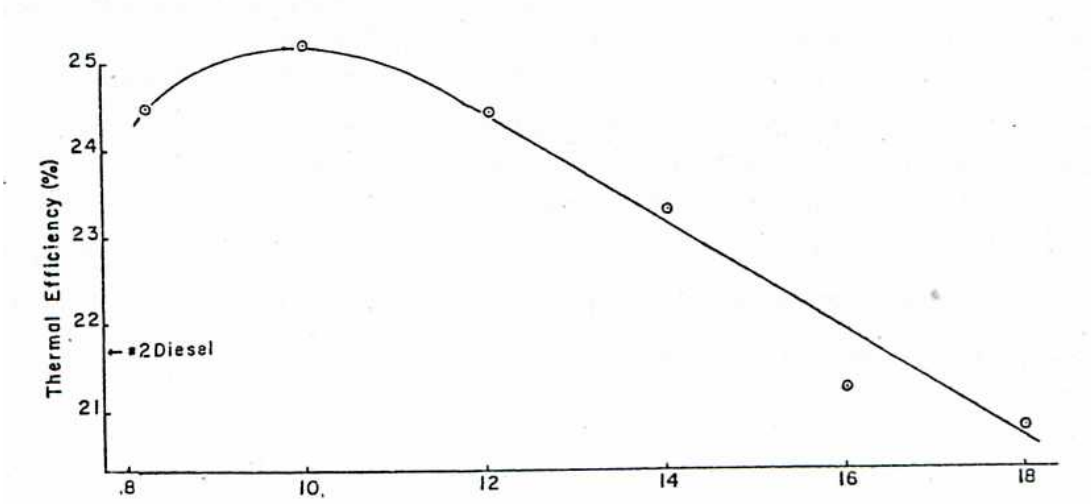

Figure 2.19 – Effect of fatty acid chain length on engine efficiency. Klopfenstein and Walker (1983[b])

It appears from the experiment reports that the cylinder pressure was not measured, and no information was known about the time of ignition or the phasing or duration of the combustion process. This lead to a lack of detailed thermodynamic understanding of the combustion process and its effect on the thermal efficiency of the engine. It is conceivable that the ignition quality of the various molecules may have played a substantial part in governing the thermal efficiency during these experiments. The thermal efficiency of the engine is highly dependent on the operating parameters of the engine such as injection timing, and that the optimal injection timing of a fuel

depends considerably on its ignition quality. Different trends for the fuel molecules may have been obtained if a different injection timing were applied, or if the injection timing had been optimised for each fuel molecule. Nevertheless, these experiments provided a valuable contribution on the combustion behaviour of individual fatty acid esters within a diesel engine.

2.7.3. Studies of the molecular structure of biodiesel molecules on pollutant emission

It has been reported by several researchers, that biodiesel fuels introduce distinct changes in the combustion behaviour of diesel engines and that their combustion is accompanied by certain traits in the patterns of exhaust gas emissions. It is generally reported that biodiesel fuels result in much lower emissions of particulate mass (PM), unburned hydrocarbons (UHC) and carbon monoxide (CO) with respect to fossil diesel fuel oil, and a small but significant increase in emissions of nitrogen oxides (NO_x).

Van den Abeele (1942) carried out the first opacity measurements to determine exhaust smoke levels in an engine fuelled with palm oil ethyl ester (biodiesel) and with fossil diesel fuel in comparison. Several engine loads were examined in this study. The author reported that if the same volume of fossil diesel fuel and biodiesel is injected into the combustion chamber, the exhaust gas from an engine fuelled on biodiesel is markedly less opaque than for fossil diesel fuel. But due to the lower calorific value of biodiesel, the engine produces less output power if the injected fuel volume is the same. The author carried out a second set of experiments in which the injected quantity for biodiesel was adjusted, so that the same indicated effective pressure was achieved for both fuels. The opacities which were measured for biodiesel at this condition were almost identical to those of diesel fuel.

Pischinger et al. (1982) carried out measurements of carbon monoxide, NO_x and smoke emissions from an IDI diesel engine. The authors observed that the combustion of biodiesel resulted in significantly lower emissions of carbon monoxide and smoke than fossil diesel fuel. A small increase (1.5% and 1.6%) in NO_x emissions was observed in two independent experiments.

Geyer et al. (1983) carried out experiments in a DI diesel engine in which the emissions of NO_x and aldehydes were measured. The authors reported a strong increase of around 75% in NO_x emissions for operation on biodiesel in comparison with fossil diesel fuel.

Mittelbach et al. (1985) carried out a comprehensive study of emissions from biodiesel fuels on a direct injection prototype engine with exhaust gas recirculation. The authors showed that the emissions of unburned hydrocarbons and total particulate mass were significantly reduced for operation on biodiesel fuel, whilst the emission of carbon monoxide remained relatively similar to that of fossil diesel fuel oil. The emission of NO_x was increased by about 22% on average from the value for fossil diesel fuel oil (see Figure 2.20).

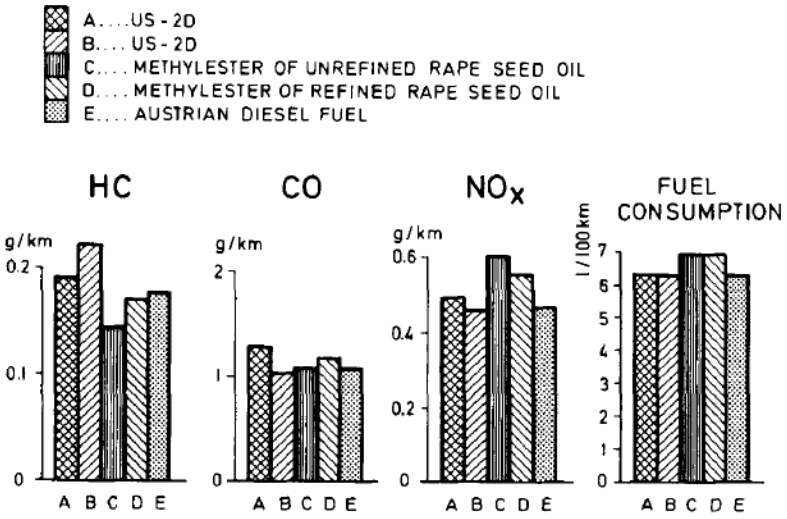

Figure 2.20 – Exhaust gas emissions of biodiesel fuel compared to fossil diesel fuel oil. Mittelbach et al. (1985).

The results obtained by Mittelbach et al. (1985) show reasonable agreement with numerous further studies carried out on the emissions characteristics of biodiesel (Schumacher, et al., 1996; Graboski & McCormick, 1998; Cheng, et al., 2006).

Graboski and McCormick (1998) compiled experimental NO_x and particulate mass data from two types of heavy duty direct injection diesel engines for blends of biodiesel and fossil diesel fuel. Their data showed that as the proportion of biodiesel to fossil diesel fuel is increased, the emission of NO_x also increased, whilst the emission of particulate matter decreased. The results obtained by Graboski and McCormick (1998) are shown in Figure 2.21 and Figure 2.22.

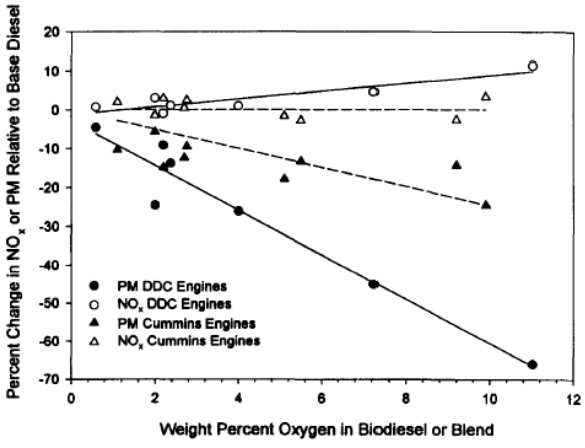

Figure 2.21 – Particulate and NO_x trends for direct injection heavy duty diesel engines powered by blends of biodiesel and fossil diesel fuel. Graboski and McCormick (1998).

Biodiesel (%)	10	20	30	50	100
NO_x	3.5	5.3	6.9	15.8	28.2
PM	−33.9	−24.1	−37.5	−26.8	−33.9
HC	−28	−32	−53	−50.7	−75.5
CO	−10.6	−8.1	−18.8	−6.9	−13.8
BSFC	1.9	2.2	3.2	8.5	12.4

Figure 2.22 – Table of particulate and NO_x emissions and brake specific fuel consumption (BSFC) relative to diesel fuel for direct injection heavy duty diesel engines powered by blends of biodiesel and fossil diesel fuel. Graboski and McCormick (1998).

Graboski et al. (2000, 2003) and McCormick et al. (2001) reported experiments in which the combustion of 14 different pure fatty acid alcohol esters was investigated in a heavy-duty diesel engine. The objective of the experiments was to determine the effect which the molecular structure of biodiesel fuel molecules had on the emission of NO_x and particulate mass. In particular the influence of the fatty acid chain length, the alcohol chain length, and the number of double bonds of the molecules were investigated. The tests were carried out on a Detroit diesel engine according to the U.S. heavy duty federal test procedure of 1991 calibration, which is optimised for fossil diesel fuel. The same injection calibration was used for all fuels, which is electronically controlled depending on the load and speed of the engine. The authors made the following observations: A decrease in fatty acid chain length and an increase in the number of double bonds within the fatty acid moiety of the molecules both resulted in an increase in NO_x emissions (Figure 2.23). According to the authors the effects of changing the alcohol chain length on NO_x emissions remained unclear from the experiments.

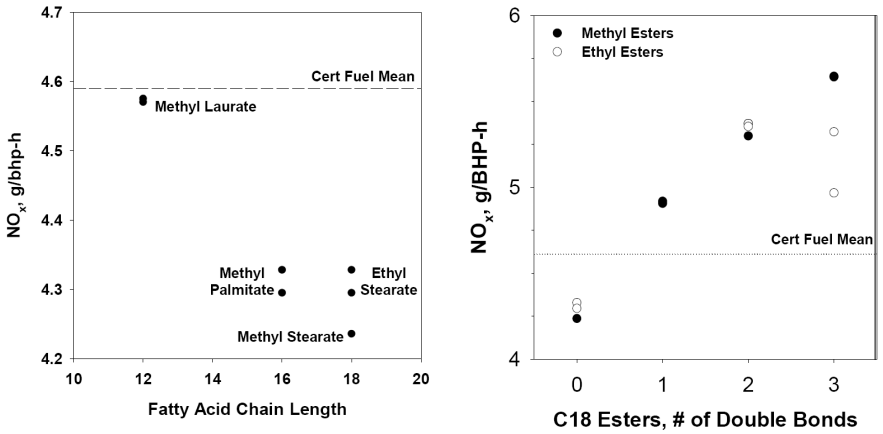

Figure 2.23 – Effect of fatty acid chain length and number of double bonds on NO_x emission at constant engine calibration in a heavy-duty direct injection diesel engine with electronic unit injection system. Graboski et al. (2003).

The results indicated that a reasonable correlation of NO_x emissions with the fuel cetane number existed. Ladommatos et al. (1996[a]) had shown that a lower cetane number of the fuel can lead to higher peak cylinder gas temperatures, and thus a higher amount of thermal NO_x formation during

combustion. In their study McCormick et al. (2001) carried out cetane number measurements on all their fuels which showed that a decrease in fatty acid chain length and an increase in number of double bonds within the fatty acid moiety both resulted in a decrease of cetane number. This confirmed previous results obtained by Klopfenstein (1983) and Knothe et al. (1997). It may thus be hypothesised that the results observed by Graboski et al. (2000, 2003) and McCormick et al. (2001) may be attributed to a large extent to differences in ignition quality of the various molecules. A plot of cetane number versus NO_x emissions for the experiments is shown in Figure 2.24.

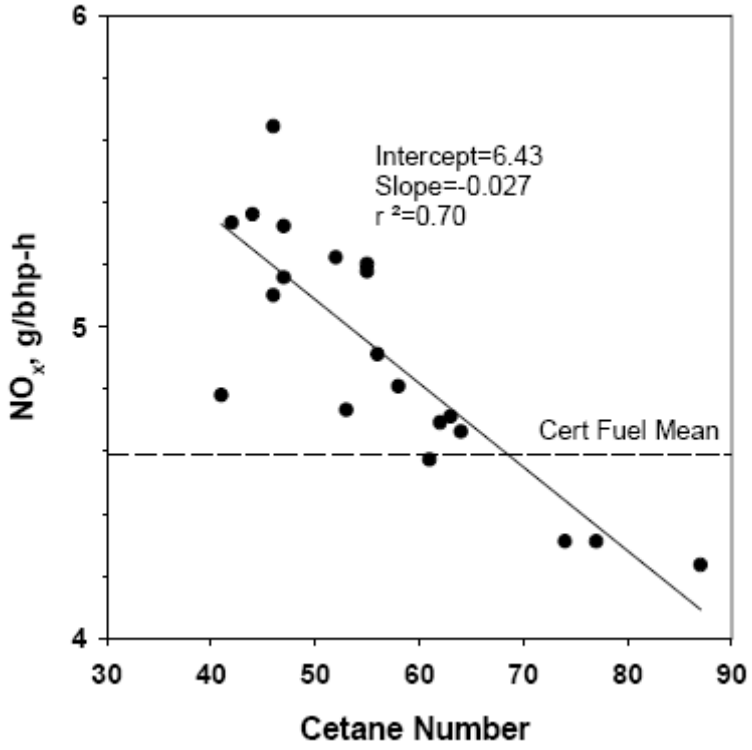

Figure 2.24 – Correlation between cetane number of fatty acid alkyl esters and NO_x emission. Graboski et al. (2003).

It thus remained unclear from the experiments carried out by Graboski et al. (2003), whether the observed increase in NO_x emissions was attributable to the lower ignition quality of the fuel, or whether other chemical or physical phenomena related to the molecular structure of the molecules may have played a role.

With regards to the emission of particulate matter from the engine, the authors observed that a decrease in fatty acid chain length and an increase in the number of double bonds within the fatty acid moiety of the molecules both resulted in an increase in particulate mass emissions (Figure 2.23). The results for fatty acid chain length and number of double bonds are shown in Figure 2.25. According to the authors, the effects of changing the alcohol chain length on particulate emissions remained unclear from the experiments.

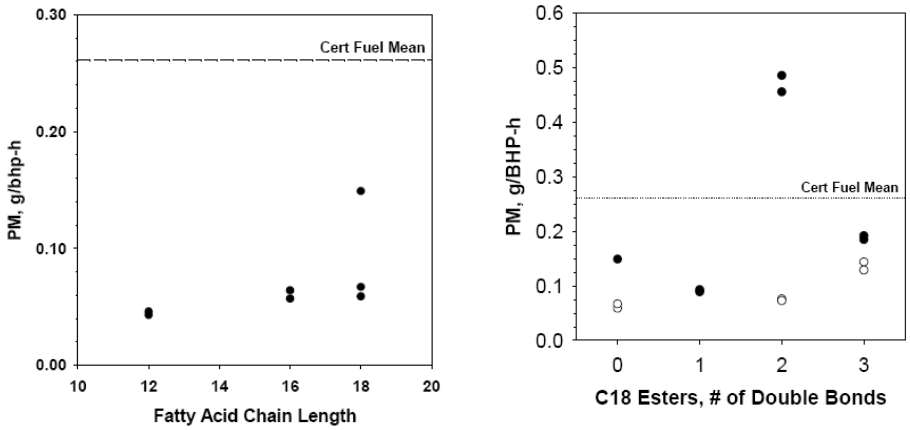

Figure 2.25 - Effect of fatty acid chain length and number of double bonds on particulate mass emission at constant engine calibration in a heavy-duty direct injection diesel engine with electronic unit injection system. Graboski et al. (2003).

The trends observed in Figure 2.25 may not be explained solely by differences in cetane number of the fuel molecules. Ladommatos et al. (1996[b]) had shown that an increase in fuel cetane number tends to result in an increase in smoke emissions due to a decrease in the premixed burn fraction (Figure 2.9). This mechanism may explain the increase in particulate matter emission for biodiesel molecules of longer fatty acid chain length which had a progressively higher cetane number, but can not explain the higher particulate emissions observed for the molecules with higher number of double bonds, which had a progressively lower cetane number. The chemical structure of the molecules may have played a significant part in governing the particulate emissions observed in these experiments. Ladommatos et al (1996[b]) had shown that hydrocarbon molecules with higher chain lengths and higher number of double bonds both displayed greater sooting tendencies during combustion. If an analogy regarding the sooting tendency between the hydrocarbon molecules studied by Ladommatos et al (1996[b]) and the fatty acid esters studied by Graboski et al. (2003) can be drawn, these results may help to explain the higher particulate emissions from the combustion of biodiesel molecules with longer fatty acid chain lengths and a higher number of double bonds.

Overall the study conducted by Graboski et al. (2003) represents one of the most complete accounts of the effects of molecular structure of fatty acid alkyl esters on diesel combustion. The results suggest that it may be interesting to discriminate the effects of cetane number of the molecules from other chemical characteristics of the biodiesel molecules in an attempt to gain increased understanding of the relative importance which various mechanism which govern the formation of NO_x and particulates.

The United States Environmental Protection Agency conducted a comprehensive analysis of the emission impacts of biodiesel using publicly available data. This investigation made use of statistical regression analysis to correlate the concentration of biodiesel in conventional diesel fuel with changes in regulated and unregulated pollutants. Most data in this study were taken from heavy duty engines. The results are shown in Figure 2.26.

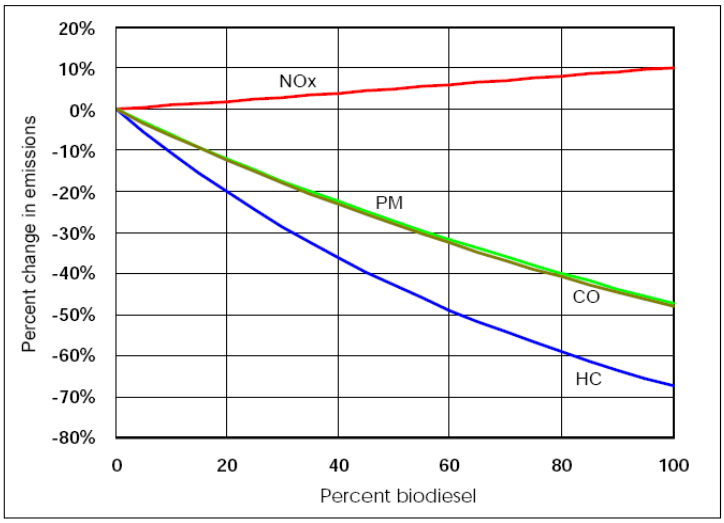

Figure 2.26 – Effect of biodiesel and diesel fuel blends on emissions from direct injection diesel engines. United States Environmental Protection Agency report (2002).

A detailed discussion on the causes for the observed increases in NO_x emissions with certain biodiesel fuels follows in the following section (2.7.4).

2.7.4. Theories for the observed increase in NO_x emissions from biodiesel in comparison to fossil diesel fuel

A number of hypotheses on the cause of the high NO_x emissions from the combustion of biodiesel fuel have been suggested. The literature currently published on the subject suggests four major hypotheses. These may be summarised as follows:

1. Advance in injection timing due to the higher bulk modulus of biodiesel.
2. High cetane number of biodiesel advances the point of ignition and causes a history of higher temperatures within the cylinder.
3. Increased formation of prompt NO_x (Fenimore, 1971) from high hydrocarbon radical concentration caused by double bonds in biodiesel molecules.
4. Increase in actual flame temperature due to lower soot radiative heat transfer of oxygenated molecules.
5. Elevated adiabatic flame temperature of biodiesel molecules, especially from unsaturated (double bonded) molecules.

The first theory noted above states that biodiesel incurs an advance in injection timing with mechanical injection systems compared to diesel fuel, due to its higher bulk modulus. This advance in injection timing results in an advance of ignition and heat release, causing higher combustion temperatures and longer residence times of the gases at high temperatures. This is said to be

responsible for the formation of larger amounts of thermally formed NO_x. Ziejewski et al. (1985) observed an anomalous advance in the injection timing of a mechanically injected direct injection diesel engine when operated on methyl ester compared to conventional fossil diesel fuel. The bulk modulus of fatty acid methyl esters reported by Gouw and Vlugter (1964), are generally of higher values than those of hydrocarbons typically present in fossil diesel fuel as those measured by Rolling and Vogt (1960). Tat et al. (2000) measured the bulk modulus of soybean methyl ester and two standard diesel fuels (US No.1 and US No.2 diesel fuel) and confirmed that the bulk modulus of the biodiesel fuel is significantly higher than that of fossil diesel fuel. The authors suggested that an increase in NO_x emissions from mechanically controlled fuel injection systems is caused by an advance in the fuel injection timing due to the higher bulk modulus of compressibility of biodiesel compared to fossil diesel fuel. The higher bulk modulus of the fuel (which is correlated to a higher speed of sound), decreases the delay between the pressure build up which is caused by the movement of the plunger in the fuel pump, and the mechanical opening of the injector needle. Monyem et al. (2001) showed that the emission of NO_x from a diesel Engine is very sensitive to the injection timing used when operating on biodiesel fuel, and that an advance of 3º CA can result in an increase of approximately 15% in NO_x emissions. Szybist and Boehman (2003) carried out an optical study on a mechanically injected engine in which the injector needle was forced open when a fuel pressure of 19.6 MPa applied to it. The authors observed that soybean methyl ester caused a 1º CA advance in injection timing with respect to fossil diesel fuel. This effect was attributed to the higher bulk modulus of the fuel, and was observed to advance the timing of ignition.

This theory provides a good explanation for the advance in injection timing observed by Ziejewski et al. (1985), and also partly an answer to the observed increases in NO_x reported by several researchers on engines employing mechanical injection systems. It is understood that this theory only applies to engines with fuel injection systems which rely on the transfer of a pressure wave from the pump to the injector as a means of injector actuation. This is the case for pump-line-nozzle injection systems in which the fuel is used as a medium to transmit positive opening pressure to the injector. An advance in injection timing has not been reported for injection systems not relying on the transmission of such a pressure wave from the pump to the injector, as is the case for as common rail systems. Choi et al. (1997) and Zhang and Boehman (2007) showed in experimental studies in which fuel injection rate or needle lift were measured that no advance in injection timing was observed for biodiesel when using a common rail fuel injection system.

Cheng et al. (2006) matched the injection timing of biodiesel and fossil diesel fuel, using optical access to the combustion chamber to verify that the injection timing was constant amongst these fuels. The authors observed that an increase in NO_x emissions for biodiesel fuel with respect to a primary reference diesel fuel of the same cetane number exists, even if the start of combustion and the cetane number and premixed-burn fraction are closely matched. This work provided evidence that effects other than just the advance in the injection timing or cetane number are responsible for increasing the amount of NO_x emission from the combustion of biodiesel in a compression ignition engine.

The second theory noted above was mentioned by Cheng et al. (2006). It assumes that the higher cetane number of biodiesel may result in an earlier ignition timing of the fuel, and thus cause higher temperature histories within the combustion chamber due to the earlier heat release near TDC. Several experimental studies have shown though that an increase in cetane number usually results in a lower premixed burn fraction and thus lower combustion peak cylinder temperatures. This typically results in lower NO_x emissions, despite the fact that this advances the time of ignition (Ladommatos, et al., 1996[a]; Szybist, et al., 2003 a; McCormick, et al., 2002). Based on these findings, this theory is likely to be unsustainable under typical engine operating conditions, with fuel injection occurring in the vicinity of TDC.

A third hypothesis that has been suggested for the observed increase of NO_x emissions of biodiesel compared to fossil diesel, is concerned with the formation of prompt NO_x via the reactions proposed by Fenimore (1971), due to high concentrations of fuel derived hydrocarbon radicals involved in the combustion process. Graboski et al. (2000) hypothesised that the formation of thermal NO_x via the Zeldovich mechanism is largely unaffected by the chemistry of the fuel, and that it may be possible that the observed increase in NO_x emission is due to prompt NO_x reactions caused by fuel radicals. Hess et al. (2005) advanced the hypothesis that because double bonds between carbon atoms in organic molecules have a greater tendency to promote radical formation than single bonds between carbon atoms, they may lead to a higher formation of prompt NO_x from fuel radicals via the mechanism described by Fenimore (1971). So far, no work has been conducted which appears to be able to disprove this theory. Graboski et al. (2000) and Hess et al. (2005) carried out experiments in which antioxidants were added to biodiesel fuels in an attempt to suppress the formation of free radicals thought to be involved in the formation of high concentrations of cyano compounds which could be responsible for increased levels of prompt NO_x formation from the combustion of biodiesel. Whilst some antioxidant substances caused visible reductions in NO_x emissions, several antioxidants tested by Hess et al. (2005) actually showed an increase in the amount of NO_x emissions. It is questionable whether these experiments provide any support for the hypothesis of elevated formation of prompt NO_x in biodiesel combustion. Whilst Graboski et al. (2000) and Hess et al. (2005) were trying to eliminate free radicals from the combustion reactions, it should be noted that it is these very reactions which tend to initiate and sustain the combustion process. Molecules such as 2-ethylhexyl nitrate or di-tert-butyl peroxide which have clearly been shown to successfully reduce NO_x in biodiesel by McCormick et al. (2002) are well-known initiator of radical reactions (Li & Simmons, 1986; Pritchard, 1989; Bornemann, et al., 2001) and thereby had the opposite effect on NO_x emission. Most importantly, Graboski et al. (2000) and Hess et al. (2005) failed to carry out a careful combustion analysis for these experiments. Based on the effect which 2-ethylhexyl nitrate has on the ignition process, it is conceivable that antioxidants may have detrimental effects on the ignition process. This could lead to a longer ignition delay and a higher premixed burn fraction, which has been shown to increase NO_x emissions based on the work of McCormick et al. (2002).
Ban-Weiss et al. (2007) showed in a modelling study that for methyl butanoate, which is a very short-chained fatty alkyl ester molecule, the relative effect of prompt NO_x is smaller than the

thermally motivated NO_x forming via the Zeldovich mechanism. Yet, the modelling showed that prompt NO_x is responsible for approximately 13% of total NO_x formed from the combustion of this molecule according to their numerical model. This portion of NO_x formation is of the order of the increases in NO_x emission observed for biodiesel fuels, suggesting that this theory can not be discredited.

A fourth hypothesis was proposed by McCormick et al. (1997) upon the suggestion made by Parker (1996) in a private communication: The author suggests that an increase in the flame temperature in either the premixed or diffusion burn regimes could be responsible for an increase in NO_x formation. It is suggested that despite the fact that the adiabatic flame temperatures of many oxygenated fuels are lower than that of diesel fuel, the actual flame temperature may be higher. This could be explained by the theory that biodiesel flames contain a lower amount of soot precursors and particulates, which are effective in reducing the flame temperature by heat radiation. This theory agrees with the observations made by several researchers (Pischinger, et al., 1982; Mittelbach, et al., 1985; Schumacher, et al., 1996; Graboski & McCormick, 1998), that biodiesel has a lower propensity to form particulate matter. Cheng et al. (2006) carried out an optical investigation in which the natural luminosity and spectrally filtered OH-chemiluminescence of the spray and combustion were recorded for biodiesel and a primary reference fuel representative of fossil diesel fuel. The primary reference fuel was composed of a binary mixture of n-hexadecane and 2,2,4,4,6,8,8-heptamethylnonane. Spectrally filtered OH-chemiluminescence was used to visualise the flame lift-off lengths for biodiesel and the reference fuel. An analytical spray model adopted from Siebers (1999) was used to estimate the local combustion stoichiometries at the lift-off lengths, which are thought to be representative of the stoichiometry at the fuel rich premixed flame, based on the combustion model reported by Dec (1997). The oxygen content of biodiesel was included in the calculation of the equivalence ratio. Due to the elevated oxygen content of biodiesel, it was found that the local equivalence ratio of biodiesel at the lift-off length of the spray was approximately 23 % lower compared to the primary reference fuel when averaged over the crank angles for which data were recorded. Based on these data, the authors calculated the adiabatic flame temperatures at these conditions. The results showed that the adiabatic flame temperature for methyl oleate was around 29K higher at 1325 K compared to 1296 K for the primary reference fuel. The authors suggest that these temperatures are too low for the formation of significant amounts of thermal NO_x via the Zeldovich mechanism, but note that the difference in temperature could affect the formation of prompt NO_x (Fenimore, 1971) which could be responsible for at least a portion of the observed NO_x increase. Further to this, the works of Flynn et al. (1999) and Cheng et al. (2002) suggest that the observed difference in mixture stoichiometry is likely to influence the formation of soot precursors and soot particles within the flame. Cheng et al. (2006) suggested that due to the lower equivalence ratios observed for biodiesel lift-off flames which would entail lower levels of soot, lower amounts of radiative heat transfer from biodiesel flames would occur. This could result in a higher actual flame temperature for biodiesel compared to fossil diesel fuel. Cheng et al. (2006) concluded that from this investigation it is not yet possible to conclude whether the higher NO_x emission stemmed

from differences in adiabatic flame temperature at the calculated combustion stoichiometry in the premixed combustion zone for the two fuels, or indirectly due to the lower amount of soot generated due to this variation in stoichiometry for biodiesel.

If soot-radiative heat transfer were the only effect causing the observed increase in NO_x emission from biodiesel fuel, it should be considered that unsaturated molecules appear to form higher amounts of NO_x than saturated molecules (McCormick, et al., 2005; Lapuerta, et al., 2008 a) yet it been shown that unsaturated molecules have a higher propensity to form soot during combustion in diffusion flames (McCormick, et al., 2001; Ladommatos, et al., 1996[a]). These two observations together somewhat contradict the theory that flames from hydrocarbons which produce lower soot necessarily produce higher amounts of NO_x, because unsaturated molecules are known to produce more soot, but yet they also produce higher amounts of NO_x. Mueller et al. (2009) demonstrated for the first time in a practical engine study that changes in soot radiative heat transfer does indeed result in small but measurable differences of NO_x emissions for soy methyl ester fuel. The experiments examined the effects of doping soy methyl ester with a polyaromatic fuel additive (phenantrene) which was used to generate higher amounts of soot radiation from its flames during combustion. The experiments showed that doping the fuel with 6% by weight of phenantrene resulted in an increase of up to 30% in spatially integrated natural luminosity of the flame, which was indicative of an increase in soot radiative heat transfer, and resulted in a measurable reduction of NO_x emissions of around 3%. Given that the spatially integrated natural luminosity of the flames from the combustion of biodiesel and fossil diesel fuel typically varies by less than 10%, whilst the emission of NO_x varies by more than 10%, it is unlikely that soot radiative heat transfer is the sole reason for the different NO_x emissions.

A fifth hypothesis was proposed by Ban-Weiss et al. (2007). It states that biodiesel, or certain types of biodiesel molecules, causes an increase in adiabatic flame temperature compared to fossil diesel fuel. Ban-Weiss developed a numerical model which simulates the combustion of a fuel jet entering a hot air mixture, similar to conditions found in a diesel engine. The authors studied the adiabatic flame temperatures of four hydrocarbons chosen to reveal the influence of double bonds in the molecular structure of the fuel molecules on NO_x emissions. The authors carried out a comparison in the adiabatic flame temperature between propane and propene. They found that the adiabatic flame temperature of propene was 49 K higher at 2782 K than that of propane at 2733 K, which resulted in an increase in NO_x emissions of 11% for propene compared to propane. A similar study was carried out on the two molecules methyl butanoate and methyl trans-2-butenoate, which are both fatty acid alkyl ester molecules. The peak flame temperature of methyl butanoate was found to be 2329 K, in comparison to the double bonded methyl trans-2-butenoate which had an adiabatic flame temperature of 2343 K. This increase in 14 K resulted in an increase of 21% of NO_x emissions according to the numerical model. Ban-Weiss et al. (2007) also carried out a sensitivity analysis using their numerical model to reveal the relative importance of various mechanisms for NO_x formation. It was found that if the Zeldovich mechanism was taken out of the numerical model, a

92% reduction in NO_x formation was observed. If the Fenimore mechanism was taken out of the model instead, a 13% reduction in NO_x emission took place. If both the Fenimore and the Zeldovich mechanisms were removed, the model showed a 92% reduction in NO_x emissions, which is the same result as when the Zeldovich mechanism alone was removed. From these results, the authors concluded that the Zeldovich mechanism is by far the most important source of NO_x formed in biodiesel combustion, and that the increases observed in experimental studies are due to an increase in adiabatic flame temperature caused mainly by the unsaturated biodiesel molecules. The calculations Ban-Weiss et al. (2007) are supported to some extent by the experimental work carried out by McCormick et al. (2005). McCormick carried out an experimental study with biodiesel fuels of different degrees of unsaturation - and thus of significantly different adiabatic flame temperatures - using an engine with electronically controlled common rail fuel injection system. Their experiments showed a progressive increase in NO_x emissions when using biodiesel fuel of higher degrees of unsaturation, which correlate with higher adiabatic flame temperatures. Lapuerta et al. (2008[a]) confirmed these findings and attributed these mainly to the longer ignition delay of biodiesel fuel with higher iodine number. As has been discussed previously (section 2.5.1) differences in ignition delay imply changes in heat release rates, stoichiometry and timing of the combustion process, and have been shown to have a significant effect on the emission of NO_x in the exhaust gas. It thus remains unclear whether these experimentally determined increases in NO_x emissions occurred due to an increase in the ignition delay or whether a difference in adiabatic flame temperature may have had an influence. Jha et al. (2007, 2008) carried out an experimental investigation using thermocouple measurements and applying thermal infrared imaging on wick generated open-air flames of biodiesel fuel molecules. Several individual methyl esters with different degrees of saturation were studied. The authors found that under these conditions, saturated methyl esters proved to have higher flame temperatures than unsaturated methyl esters. These findings contradict the modelling work carried out by Ban-Weiss et al. (2007) and Mueller et al. (2009), as well as the calculations presented in Chapter 5 of this thesis. Jha et al. (2007, 2008) also concluded that shorter-chained fatty acid alkyl esters had higher adiabatic flame temperatures than longer chained fatty acid alkyl esters. These findings again contradict the calculations presented in Chapter 5 of this thesis. It is not entirely clear what could cause the observed discrepancies between the results reported by Jha et al. (2007, 2008), the findings made by Ban-Weiss et al. (2007), Mueller et al. (2009) and the work presented in Chapter 5 of this thesis. According to the best judgement of the author, whilst relying on the authors own calculations, it is thought that the work presented by Ban-Weiss et al. (2007), Mueller et al. (2009) and the results presented in Chapter 5 of this thesis are correct.

It seems that agreement amongst researchers has not yet been found over the mechanisms and their relative importance by which biodiesel fuel may cause an increase in NO_x emission from diesel combustion.

2.8. Literature on the influence of the molecular structure of potential synthetic biofuel molecules produced from lignocellulose via biochemical pathways

The production of biofuels from lignocellulose via biochemical pathways could bring significant advantages over the sole production of fatty acid alkyl esters (biodiesel) discussed in the previous section. It opens up a more diverse source of raw materials, and can lead to a broader variety of fuel properties. Lignocellulose and cellulose constitute a significant proportion of land-based biomass, with the result that its production is undemanding in terms of particular plants or organisms to produce it. It may also be found more abundantly as 'waste' material from agricultural, industrial and domestic applications and could be made available from managed biotopes such as forests as long as a sustainable cycle of nutrients is instated. Several biochemical pathways for the conversion of lignocellulosic material into liquid fuels are conceivable. These shall be discussed in the following sections.

The most traditional pathway for the production of liquid fuels from lignocellulosic biomass is the hydrolysis of cellulosic material into fermentable sugars and subsequent fermentation of the sugars into ethyl alcohol (Kaltschmitt & Hartmann, 2001). The hydrolysis may be performed via acid catalysis using concentrated or dilute mineral acids such as sulphuric acid, or via enzymatic catalysis. A recent review of such technology is provided by Schacht (2008). The simplest type of fuel fermentation into ethanol may be carried out using yeast, such as the strain Saccharomyces Cerevisiae. The fuel product from this pathway is ethyl alcohol (ethanol). This could be used directly as an oxygenated additive to fossil diesel fuel as reported by Lapuerta (2008[b]). Its use as a pure fuel in a compression ignition engine implies significant changes to the combustion process and injection mechanism due to its low ignition quality, higher volatility and low lubricity. Higher compression ratios and adapted fuel injection systems will be necessary when using alcohol fuels of low ignition quality in diesel engines.

Two alternatives to traditional ethanol fermentation are the closely linked Acetone-Butanol-Ethanol (ABE) and Isopropanol-Butanol-Ethanol (IBE) fermentation processes using bacteria such as Clostridium Beijerinckii (Qureshi, 2008; Krouwel, et al., 1982). These fermentation processes allow not only the production of ethanol, but also that of acetone, isopropanol and butanol. Propanol or Butanol produced in such a way may be added to fossil diesel fuel in a blend, as has been reported from engine experiments by Karabektas and Hosoz (2009) or rapeseed oil as reported by Yoshimoto and Onodera (2002).

Recent years have seen the advent of metabolic engineering, which offers the opportunity to produce such alcohols via more direct biochemical pathways. Yomano et al. (1998) report that it is possible to produce ethanol using metabolically engineered Escherichia Coli bacteria. Atsumi and Liao (2007), Shen and Liao (2008) and Atsumi et al. (2008) further reported processes on the production

of propanol, butanol and higher alcohols as well as fatty acids using metabolically engineered E. Coli bacteria.

The alcohols obtained from lignocellulose may be processed further into a fuel of high cetane number such as ethers. D'Amore et al. (2007) and Manzer et al. (2007) have shown that the production of dibutyl ether is possible from either ethanol or butanol, by chemical reaction. Dibutyl ether has been successfully tried in engine experiments as an oxygenated and cetane improving additive to fossil diesel fuel (Sharavanan, et al., 2001) and pure rapeseed oil (Yoshimoto & Onodera, 2002).

A further fuel product which may be produced from lignocellulosic material via the production of alcohols, are acetals. The work of Charpentier and Mimoun (1978) has shown that it is possible to produce a variety of acetal molecules from primary or secondary alcohols via the formation of aldehydes or ketones as intermediate species. Oppenländer et al. (1979) reported what appears to be the first cetane numbers for 1,1-di-n-ethoxyethane at a value of 35 (BASF engine tests according to DIN-51773 test method). Oppenländer et al. (1979) proposed that acetals and polyethers derived from ethanol could be used as renewable diesel fuels. Bönnhof and Obenaus (1979), further reported cetane numbers for 3 acetal molecules (1,1-di-n-ethoxyethane, 1,1-di-n-butoxyethane and 1,1-di-n-butoxybutane) obtained in engine experiments. Capeletti et al. (2000) demonstrated the production of an acetal (1,1-di-n-ethoxyethane) from ethanol and acetaldehyde. A direct process for a generalised selective production process for acetals from primary alcohols has been reported by Bueno et al. (2007). The production of acetals from acetone and alcohols, has been described in the patent of Delfort and Marchal (2007).

2.8.1. Engine studies on fuels produced from lignocellulose via biochemical pathways

A number engine experiments have been carried out on fuels produced from lignocellulose via biochemical pathways. The present section focuses on the combustion of acetal molecules in particular. The combustion of alcohols and ethers is discussed in detail in section 2.9.1.

Several combustion and engine experiments with acetal molecules have been reported in the literature. The first reported account of an engine study with acetal fuels may be the patent of Oppenländer et al. (1979) in which the cetane number of 1,1-di-n-ethoxyethane was reported at a value of 35. Bönnhof and Obenaus (1979) reported the cetane numbers of 3 acetal molecules (1,1-di-n-ethoxyethane, 1,1-di-n-butoxyethane and 1,1-di-n-butoxybutane). The authors noted that no reduction in cetane number was observed when changing the molecular structure from 1,1-di-n-butoxybutane (CN = 105) to 1,1-di-n-butoxyethane (CN = 105), but that a strong reduction existed when changing the molecular structure to 1,1-di-n-ethoxyethane (CN = 44). Although the authors do not discuss this observation in detail, these results could be interpreted as providing an indication that the lateral moieties located to either side of the two oxygen atoms play a more important role in controlling the ignition quality of the molecules than the central carbon chain located between the

two oxygen atoms. Naegeli (1992) reported the first emissions from engine experiments using acetal blended fuels. Naegeli observed that a 20% blend of methylal (di-n-methoxymethane) in diesel fuel was shown to reduce smoke opacity by about 50% under start-up and high-idle running conditions. Sirman et al. (2000) reported a 52% reduction in particulate mass and a 4% reduction in NO_x emission from an engine operated on a blend of 15% methylal in diesel fuel, with respect to its operation on neat diesel fuel. Vertin et al. (1999) carried out an experimental engine study with blends (10-30% by volume) of di-n-methoxymethane in fossil diesel fuel. The authors reported significant reductions in particulate matter emissions with increasing amounts of methylal concentration in the fuel. It was also reported that no significant increase in cetane number was observed for increasing concentration of methylal within the diesel fuel blends. Cheng et al. (2001) carried out measurements of exhaust gas particulate emissions in terms of total mass, number density and mean particle diameter. They reported that the addition of methylal to diesel fuel results not only in a reduction in total particulate mass, but also in the reduction of the particle number density and mean particle diameter. Bertola and Boulouchos (2000) carried out experiments in a heavy-duty diesel engine with common-rail direct injection system with blends of di-n-methoxymethane (butylal) in fossil diesel fuel as well as pure butylal. They observed that the combustion of butylal had a lower fraction of heat release during the premixed combustion phase than diesel fuel. This was attributed to its higher ignition quality and shorter ignition delay. The authors also noted a significant reduction in exhaust gas opacity for engine operation with butylal in comparison with fossil diesel fuel, but no significant increases in NO_x emissions.

Nord and Haupt (2005) investigated the performance of a blend of 1,1-diethoxyethane as an additive in diesel fuel when used on a heavy-duty direct-injection diesel engine. By adding the acetal to diesel fuel, the ignition quality of the fuel was reduced slightly, i.e. from a cetane number of 52 to a cetane number of 51. The authors reported that by adding 1,1-diethoxyethane to the diesel fuel, a small reduction in engine power was recorded. Particulate number emissions were reported to decrease by 23%, whilst the total particulate mass emitted decreased by 35%. A decrease in NO_x emission by 3% was reported, whilst the emission of CO and UHC increased by 4% and 5% respectively. The authors also noted a 289% increase in acetaldehyde emissions, which was thought to be a product of partial decomposition of the 1,1-diethoxyethane.

Frusteri et al. (2007) carried out engine experiments with blends of 10% by volume 1,1-diethoxyethane in fossil diesel fuel. The authors reported that the blend of 1,1-diethoxyethane in diesel fuel had similar UHC, CO and NO_x emissions to diesel fuel, but showed a marked reduction in exhaust smoke emissions. Alseda et al. (2007) carried out experiments of homogeneous charge compression ignition combustion (HCCI) of diesel fuel, with the addition of 10-20% butylal in fossil diesel fuel. The authors reported that the addition of butylal retarded the time of autoignition in HCCI combustion mode, with respect to operation on diesel fuel, and that it resulted in a reduction in smoke emissions under these homogeneous charge conditions. This result appears to be in some disagreement with the work of Bertola and Boulouchos (2000), who reported a higher ignition quality for butylal than for diesel fuel. Given the fundamentally different method of charge preparation, this result may be explainable by differences therein.

2.9. Literature on influence of the molecular structure of potential synthetic biofuel molecules produced from lignocellulose via gasification

In 1902 Sabatier and Sendersen discovered the synthesis of methane gas by catalysing the reaction of hydrogen (H_2) and carbon monoxide (CO) over iron, nickel and cobalt catalysts (Sabatier & Sendersen, 1902; Sabatier, 1913). Their discovery laid the foundations to the synthesis of organic compounds from this mixture of gases.

In 1913 Mittasch and Schneider synthesised for the first time a mixture of liquid organic substances from a mixture of hydrogen and carbon monoxide gases. The product consisted of a mixture of alcohols, aldehydes, ketones and organic acids. The experiments were carried out at high pressures of the order of 100 atmospheres over a variety of transition metal catalysts including cerium, chrome cobalt and manganese. Mittasch and Schneider (1913) concluded that depending on the detailed experimental conditions and catalyst, varying mixtures of the above listed compounds could be produced. Further experiments resulted in an increased selectivity of the synthesis products, and eventually led to the discovery of the methanol synthesis from gaseous hydrogen and carbon monoxide (Mittasch, et al., 1923). At a similar time, Fischer and Tropsch (1924) confirmed and developed the synthesis of oxygenated organic compounds described by Mittasch and Schneider (1913) through independent experiments, and termed the described mixture of gaseous hydrogen and carbon monoxide used as reactants ‘synthesis gas’ and the mixture of oxygenated organic products ‘synthol’. Upon having produced considerable amounts of synthol, Fischer and Tropsch (1924) carried out engine experiments in a carburetted spark-ignition engine using this mixture of oxygenated organic compounds as a fuel, and noted satisfactory short-term performance.
In pursuit of an explanation of the mechanism responsible for the formation of synthol from synthesis gas, Fischer and Tropsch (1924, p.320) sought to clarify whether the formation of higher alcohols during the synthesis process occurred via the intermediate formation of methyl alcohol. To this end, they heated methyl alcohol in an autoclave to a temperature of 240 ºC in the presence of sodium. The experiment did not result in the formation of higher alcohols, but rather in the direct formation of dimethyl ether from methanol. This reaction, in conjunction with the methanol synthesis developed by Mittasch et al. (1923), provided a two-step path for the production of dimethyl ether from synthesis gas.

In further experiments, Fischer and Tropsch (1924) proceeded to lowering the pressure under which the synthesis gas was reacted to about 7 atmospheres and noted the formation of small amounts of oxygen-free hydrocarbons, which had been the ultimate aim of their investigations. Upon more experimentation, Fischer and Tropsch (1926) finally succeeded in producing liquid and even solid alkanes and alkenes of roughly controllable molecular size using iron and cobalt catalysts. The

reaction occurred at near atmospheric pressure and at low reaction temperatures of the order of 200ºC. It was observed that the lower the temperature of the reaction could be dropped - while still obtaining a reaction - the higher the molecular mass of the hydrocarbons would become. Together with adjustment of pressure, catalyst and the composition of the synthesis gas, this variation gave the process some degree of selectivity over the properties of the hydrocarbon products. Such hydrocarbon fuels produced from synthesis gas are commonly termed Fischer-Tropsch fuels.

The present description of fuel syntheses demonstrates that it is in principle possible to produce alcohols, ethers, alkanes and alkenes amongst other organic substances from a gaseous mixture of hydrogen and carbon monoxide. Synthesis gas, which represents the reactant for these processes, has traditionally been produced from mineral coal, but has recently received attention for its ability to be produced via the gasification of biomass. Its relative amounts of hydrogen and carbon monoxide are controllable through the addition or extraction of steam via the water-gas shift reaction.

$$CO + H_2O \leftrightarrow CO_2 + H_2$$

Equation 2.22

Since their early years of development, the synthesis processes described above have undergone substantial practical improvements in terms of process efficiency and product selectivity, and have recently been conducted with biomass as the initial reactant. Modern laboratory studies of Fischer-Tropsch fuels from wood have been reported to have been carried out since 2001 (Boerrigter, 2005; Carlowitz, 2005), with the first pilot-scale production facility of Fischer-Tropsch fuels from lignocellulose being operational since 2003 (Rudloff, 2005; Weitz, 2006). In addition to the production of Fischer-Tropsch fuels, Meyer (2005) reported the production of methanol from biomass via synthesis gas, Hu et al. (2005) have reported the synthesis of DME from Biomass synthesis gas and Waldheim et al. (2005) have reported the extraction of hydrogen from the synthesis gas for potential use as an automotive fuel. A review of potential thermal processes for the production of fuels from biomass has been published by Bridgwater (2003).

2.9.1. Engine studies on fuels produced from lignocellulose via gasification

This section provides a brief overview of previous experimental studies, carried out in compression-ignition engines to investigate the combustion behaviour of fuels that could potentially be derived from lignocellulosic biomass via gasification processes. Due to the variation in chemical properties of the fuel products that may be produced through this pathway, the section is further subdivided into chemical classes of potential fuels, namely alcohols, dimethyl ether, liquid ethers and Fischer-Tropsch hydrocarbon fuels.

Alcohols

Various alkyl alcohols of high molecular mass can be produced from lignocellulosic biomass via synthesis gas (Corain, et al., 1992; Qiu, et al., 2004; Hu, et al., 2007). Higher alcohols may be added to fossil diesel fuel in a blend, as has been reported from engine experiments by Karabektas and Hosoz (2009) or rapeseed oil as reported by Yoshimoto and Onodera (2002), but are also conceivable as pure fuels for compression ignition engines, under the provision that the engine is suitably adapted to the physical and chemical properties of the alcohols. Karabektas and Hosoz (2009) reported carried out experiments in which isobutanol was mixed with fossil diesel fuel in varying amounts. The authors reported that a decrease in brake thermal efficiency was observed in a diesel engine when operated on blends of 5% to 20% by volume iso-butanol in diesel fuel, with respect to the values obtained for neat diesel fuel when operated at the same engine calibration settings. The engine load was not kept constant in their experiments, but decreased by as much as 6% during operation with the iso-butanol blended diesel fuel. This could account for a proportion of the observed reduction in brake thermal efficiency. The authors further reported a decrease in NO_x and CO emissions, but an increase in UHC emissions for the isobutanol blended diesel fuels.

Yoshimoto and Onodera (2002) reported retarded ignition timing, an increase in peak combustion pressure, and reduced smoke emissions for rapeseed blends of propanol or butanol, when compared to operation with neat rapeseed oil. It was reported that an increase in brake thermal efficiency around 2% was observed for these blends (9-29% alcohol by volume) with respect to neat rapeseed oil.

Dimethyl ether

Dimethyl ether (DME) is the simplest of all ethers in terms of its molecular structure. Its molecules contain no carbon to carbon bonds, and approximately a third of their total mass is bound in oxygen atoms. The vapour pressure of DME (0.51 MPa at 293 K, BOC safety sheet for dimethyl ether) is higher than absolute atmospheric pressure, causing DME to flash-boil under atmospheric conditions, and to require pressurisation if it is to remain liquid.

DME has been suggested as a replacement for diesel fuel in compression ignition engines, due to its potential of achieving low levels of exhaust pollutant emissions, and its performance as sole fuel in a diesel engine was investigated (Fleisch, et al., 1995; Kapus & Ofner, 1995; Sorenson & Mikkelsen, 1995). Experiments demonstrated that DME results in a diesel combustion process of lower heat release rates, and with a lesser fraction of heat release occurring during the initial premixed combustion phase (Kajitani, et al., 1997) resulting in lower combustion noise (Kapus & Ofner, 1995). The engine efficiency of an engine fuelled on DME has been reported to be comparable to that achieved with operation on conventional diesel fuel (Kapus & Cartellieri, 1995; Tsuchiya & Sato, 2006).

Engine experiments have shown that very low levels of particulate emission are typically emitted by a diesel engine operated on DME as a fuel (Fleisch, et al., 1995; Kajitani, et al., 1997). Arcoumanis et al. 2008 have argued that any particulate emissions from a DME-fuelled engine result from the engine lubricating oil rather than from the fuel, although no proof of this hypothesis has so far been presented.

The emission of NO_x from DME-fuelled engines reported in the literature appears to vary depending on the engine design and operating conditions. Comparative studies between DME and diesel fuel have shown that, the combustion of DME can either result in lower (Fleisch, et al., 1995), similar (Egnell, 2001) or higher emissions of NO_x (Kajitani et al. 2002), than conventional fossil diesel fuel. The reasons for these changes are not entirely understood (Arcoumanis, et al., 2008). Lower emission of NO_x from DME compared to diesel fuel could be attributed to the shorter ignition delay of DME, which results in a lower premixed-burn fraction and lower peak gas temperatures. Kajitani et al. 1997 have suggested that higher NO_x emissions in their experiments conducted on an engine with mechanical fuel injection system could result from an earlier fuel injection resulting from a higher fuel feed pressure used for DME.

The emission of UHC from a DME in a diesel engine has generally been reported to be lower or similar to than for conventional diesel fuel (Fleisch, et al., 1995; Kajitani, et al., 1998), which may be attributed to the short ignition delay of DME, which avoids the formation of overly lean mixtures which fail to undergo full oxidation within the combustion chamber due to their lean stoichiometry.

Varying trends have been observed for the emission of CO from a DME in a diesel engine. Kajitani et al.(1998) reported lower CO for DME than for conventional diesel fuel, whilst Fleisch et al. (1995) reported very similar levels of CO in comparison to diesel fuel and Kapus and Cartellieri (1995) reported higher emission of CO than with conventional diesel fuel. The reasons for these discrepancies are not entirely clear. It could be argued that the high oxygen content and high ignition quality of DME together with its low volatility would be conducive to low levels of CO formation due to the reductions of fuel-rich areas within the fuel jet. Contrary to this, it could be argued that the higher volatility supports quenching of lean fuel air mixtures from which CO may result. This hypothesis seems unlikely under the consideration that if this mechanism was significantly responsible for elevated CO emissions, high emissions of UHC would also be expected, which is generally not reported within the published literature.

The high vapour pressure and low viscosity of DME are conducive to rapid fuel and air mixing when injected into a higher pressure environment typical of an internal combustion engine. Yu and Bae (2003) examined the spray characteristics of a DME spray from a high-pressure common rail system, and compared its behaviour with that of diesel fuel using the same injection system. It was observed that whilst DME exhibited characteristics strongly different to those of diesel fuel when it was injected into ambient gas conditions its behaviour became progressively more similar to that of diesel fuel when injected into higher gas pressures.

DME is especially suited for charge preparation employing direct injection of the fuel into the combustion chamber, under conditions at which the combustion chamber gases are at low temperatures and pressures, such as during the gas exchange processes and early stages of charge compression, due to its high volatility. The high volatility ensures fast vaporisation and can help avoid fuel-impingement on the combustion chamber walls, which may be important for conditions in which HCCI is to be operated.

It is known that the absence of fuel-rich gases beyond a certain stoichiometry limit suppresses the formation of soot during combustion (Kamimoto & Bae, 1988). The rapid fuel-air mixing, to which DME is conducive, in combination with the high fuel-bound oxygen content, can entirely eliminate the presence of such fuel-rich regions within the combustion chamber of a diesel engine. This could theoretically avoid the formation of carbonaceous soot from a diesel engine, according to the work of Miyamoto et al. (1998) and Flynn et al. (1999). It is further known that by reducing the occurrence of high temperatures, the formation of NO_x can be reduced, and even completely suppressed (Kamimoto & Bae, 1988). DME has a high cetane number in excess of 55 (Teng, et al., 2001), which results in a lower amount of premixed combustion, and a comparatively slow energy release to take place during conventional diffusion combustion typical of diesel engines. A slow energy release rate caused by high cetane number and low calorific value of the fuel is known to limit the maximum cylinder pressure and temperature, thereby keeping the formation of NO_x at comparatively low levels. A further reduction in NO_x levels can be achieved by switching the combustion mode from a near-stoichiometrically burning stratified diffusion flame to a lean homogeneously combusting mixture of fuel and air, usually referred to as homogeneous charge compression ignition (HCCI). DME is particularly conducive to this type of combustion, especially for direct injection of the fuel into the combustion chamber, due to its high volatility, which ensures fast vaporisation and can help avoiding fuel-impingement on the combustion chamber walls. This is particularly important if fuel injection occurs at times at which the combustion chamber gases are at low temperatures and pressures, such as during the gas exchange processes and early stages of charge compression.

The thermal conversion efficiency of DME in a compression ignition engine operated in diesel combustion mode is comparable to that of modern direct injection diesel engine (Arcoumanis, et al., 2008). Due to the lower fuel carbon content of the fuel, a lower emission of carbon dioxide (CO_2) is usually observed for a DME fuelled engine than for an engine fuelled with conventional diesel fuel oil.

Liquid ethers

Various liquid alkyl alcohols of high molecular mass can be produced from lignocellulosic biomass via synthesis gas (Snelling, 2003). Liquid alkyl ethers have similar advantages as dimethyl ether in terms of charge preparation due to their high volatility, but with the added advantage of being liquid under atmospheric conditions, allowing them to be stored without the need of pressurised tanks. A

number of ethers have already been tried as replacements for fossil diesel fuels in a number of engine studies. Engine experiments with Dibutyl ether have been reported, in which the fuel was used as an oxygenated and cetane improving additive to fossil diesel fuel (Sharavanan, et al., 2001) and pure rapeseed oil (Yoshimoto and Onodera, 2002). Sharavanan et al. (2001) reported that a reduction in smoke emissions from the engine was observed, together with an increase in brake thermal efficiency with respect to operation on neat fossil diesel fuel. Yoshimoto and Onodera (2002) reported advanced ignition timing, a reduction in peak combustion pressure, and reduced smoke emissions for rapeseed oil mixed with dibutyl ether when compared to operation on fossil diesel fuel. It was also reported that an increase in brake thermal efficiency was observed for rapeseed oil additised with di-n-butyl ether (9-33% by volume) with respect to neat rapeseed oil.

Fischer-Tropsch hydrocarbon fuels from Biomass

Recent years have seen the advent of Fischer-Tropsch diesel fuel oils derived from lignocelluslosic biomass, also termed biomass-to-liquid (BTL) fuels, synthesised in laboratories and pilot-scale production facilities (Boerrigter, 2005; Rudloff, 2005; Weitz, 2006). First experimental engine studies with fuel samples derived from these projects have been reported in modern diesel engines by Miers et al. (2005) and Ng et al. (2005). Miers et al. (2005) carried out experiments in a turbocharged direct-injected diesel engine. The authors observed a decrease in NO_x, CO, particulate mass and number emission as well as a reduction in ignition delay and brake specific fuel consumption when comparing a Fischer-Tropsch BTL diesel fuel with fossil US No. 2 diesel fuel. Ng, et al., (2005) similarly reported reductions in the premixed burn fraction, lower specific NO_x, UHC, CO and CO_2 emissions as well as a slight reduction in brake specific fuel consumption for Fischer-Tropsch BTL diesel fuel with respect to fossil US No. 2 diesel fuel. These initial engine studies indicate that Fischer-Tropsch BTL fuels provide improved engine performance as well as offering advantages in terms of greenhouse gas and pollutant emissions from the engine. An analysis of the overall greenhouse gas emissions including the processes of production, distribution and consumption of the fuel has been reported by van Vliet et al. (2009).

Chapter 3. Experimental apparatus

The apparatus with which the engine experiments were carried out is described in the present chapter. The experimental engine, fuel injection systems, measuring instruments such as pressure transducers, thermocouples, flow-meters, emissions analysers, particulate spectrometer and sampling unit, as well as the data acquisition systems were installed by the author for the purpose of the described experiments and future continuation-projects. A large proportion of the time spent on this project consisted in designing, ordering, constructing, installing and developing the described experimental apparatus.

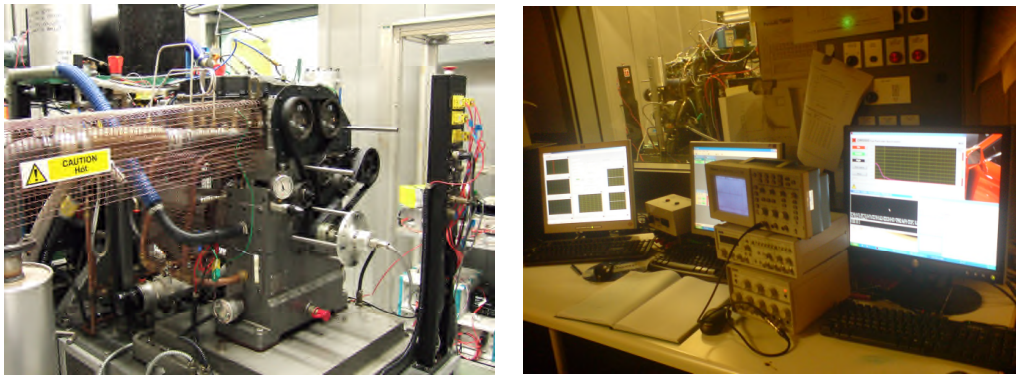

Figure 3.1 - Experimental engine test cell (l.) and engine control room (r.)

Figure 3.1 (l.) shows the experimental engine on its test bed in the engine test cell. Figure 3.1 (r.) shows the engine control room with the engine control and data acquisition systems in place.

3.1. Laboratory

The engine laboratory consisted of an engine test cell (Figure 3.1 (l.)), engine control room (Figure 3.1 (r.)), and a service corridor with gas-cabinet. A schematic of the laboratory is shown in Figure 3.2. The engine control and data acquisition systems were located in the engine control room, from which the engine and fuel systems are observable through armoured glass. The gas-analysing equipment was located in the service corridor, where it was supplied with the necessary calibration and service-gases from a purpose-built gas cabinet.

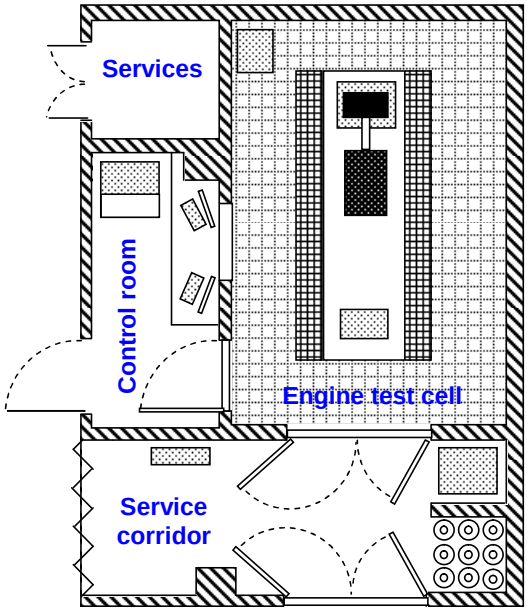

Figure 3.2 - Plan of the engine laboratory

The engine test cell services comprised single-and two-phase electrical power supplies, cooling-water, compressed air, ventilation, heating and exhaust gas extraction.

3.2. Engine

The test engine consisted of a custom-built 4-stroke naturally-aspirated single cylinder research engine with direct fuel injection. The engine was built using a generic research engine block (Ricardo Hydra) in conjunction with production engine parts from a 2.0 litre turbocharged automotive diesel engine (Ford Duratorq 2.0 CD132 130PS). The cylinder head, injector piston and cylinder were identical to those used in the production engine, to ensure that the combustion chamber geometry was representative of a typical current automotive diesel engine. The glow-plug of the original engine was replaced by a piezoelectric pressure transducer of virtually identical geometry, to allow for measurement of the pressure within the cylinder. The intake air and exhaust manifolds were each instrumented with a piezoresistive pressure transducer (Druck PTX-7517-3257), allowing absolute measurement of intake and exhaust manifold pressures respectively.

The combustion chamber comprised a flat roof with four valves and a centrally located injector in conjunction with a flat piston with centrally located omega-shaped piston bowl (see Figure 3.4). The fuel injector had six radially arranged nozzle holes of 154 μm diameter, and was controlled via solenoid-actuation. Its fuel was supplied and returned to a common-rail fuel system with electronic PID fuel pressure control (see section 3.3). The inlet-valve opening for normal engine operation occurred 5º CA before exhaust TDC, and the inlet-valve closing occurred 5 º CA after induction BDC. The exhaust valve opened 35º CA before expansion BDC, and closed at exhaust TDC (see Figure 3.3).

Table 3.1 - Engine Specification

Engine combustion chamber geometry	Ford Duratorq engine
Number of cylinders	1
Cylinder bore	86 mm
Crankshaft stroke	86 mm
Swept volume	499.56 cc
Compression ratio	15:1
Maximum cylinder pressure	150 bar
Piston design	Central ω-bowl in piston
Oil type	10W40
Water temperature	90 ° C
Minimum engine running speed	755 ± 5 rpm
Maximum engine speed	5500 ± 50 rpm

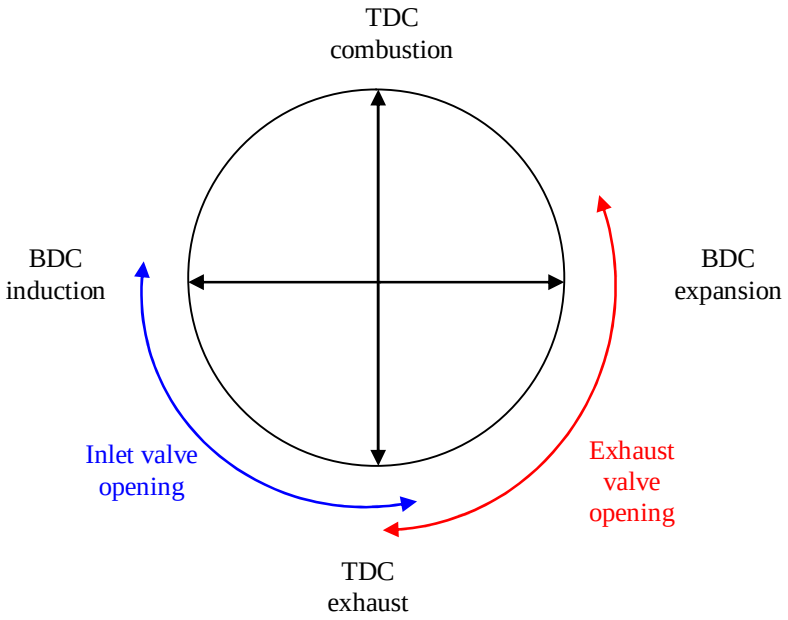

Figure 3.3 - Valve opening diagram

The intake air was inducted from the laboratory through an air filter, after which it passed through a positive displacement gas flow meter (Romet G40) and into a rigid damping chamber of approximately 60 litres volume. From the damping chamber, the intake air was fed into the intake port of the engine via a flexible intake runner of 52 mm internal diameter and 1.2 m length. Air pressure and temperature were measured at the flow-meter, and in the engine intake manifold.

The engine exhaust was extracted from the engine exhaust port via an exhaust pipe of 53 mm diameter, and discharged into the laboratory exhaust gas extraction system after having passed through an exhaust gas silencer box used to dampen acoustic noise. Exhaust pressure and temperature were measured 200 mm downstream of the engine exhaust valve. For a schematic of the engine intake air and exhaust gas systems, please see Appendix E.

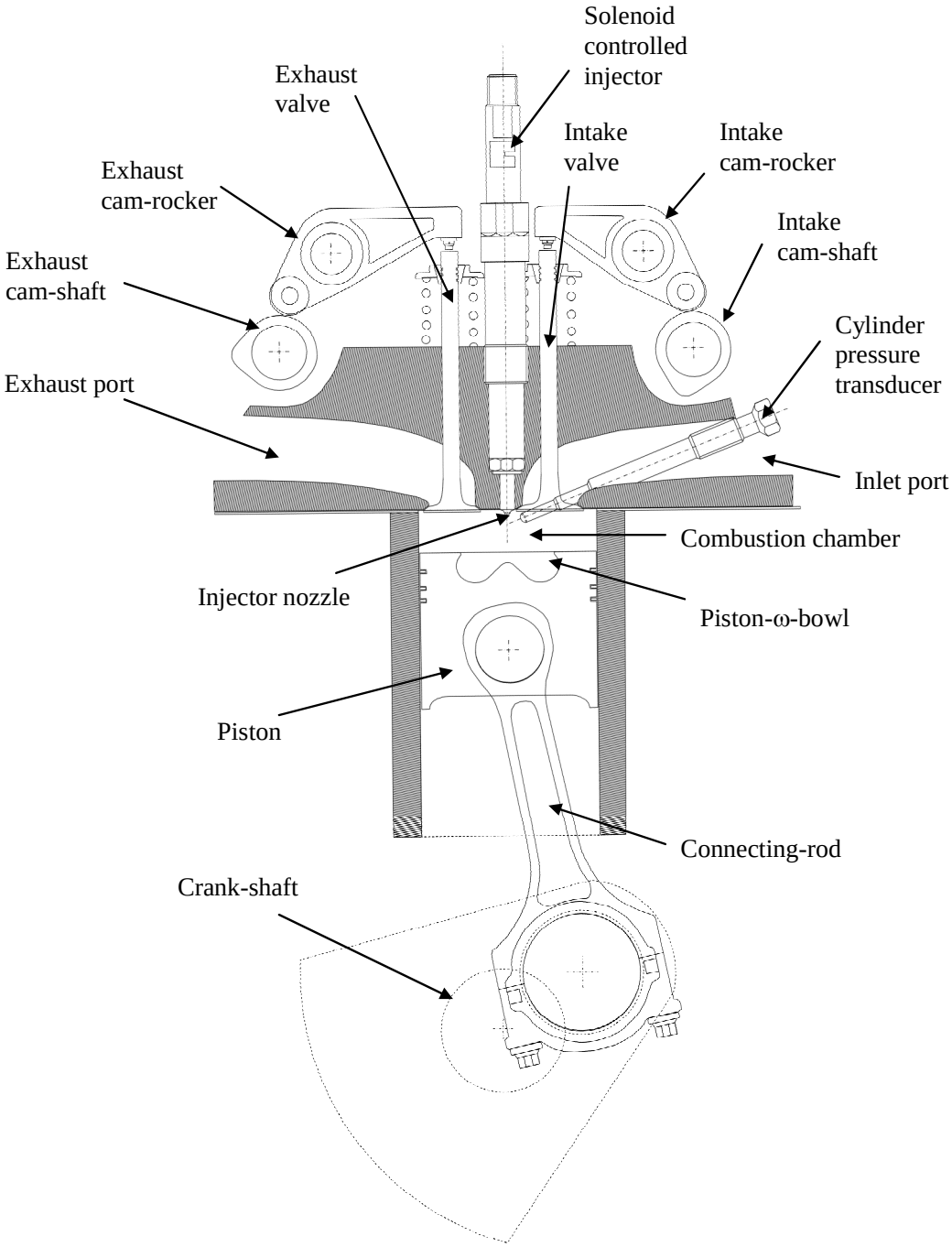

Figure 3.4 - Schematic of the combustion chamber

3.3. Direct-injection fuel injector characterisation

In order to establish the true ignition delay of the fuel, it was necessary to establish the precise moment of injection. There existed a small delay between the moment at which the current pulse was sent from the electronic fuel injection control unit through the solenoid of the injector, and the moment at which the spray exited the injector nozzle. The solenoid pulse for the opening of the injector was produced at the desired crank angle, and was measured using a current probe to be accurate within the resolution of the data acquisition system (0.2 º CA) at all engine speeds. The delay between this pulse, and when the spray started appearing at the injector nozzle was measured by passing a laser beam past the injector nozzle and using phototransistor to measure the obscuration of the beam.

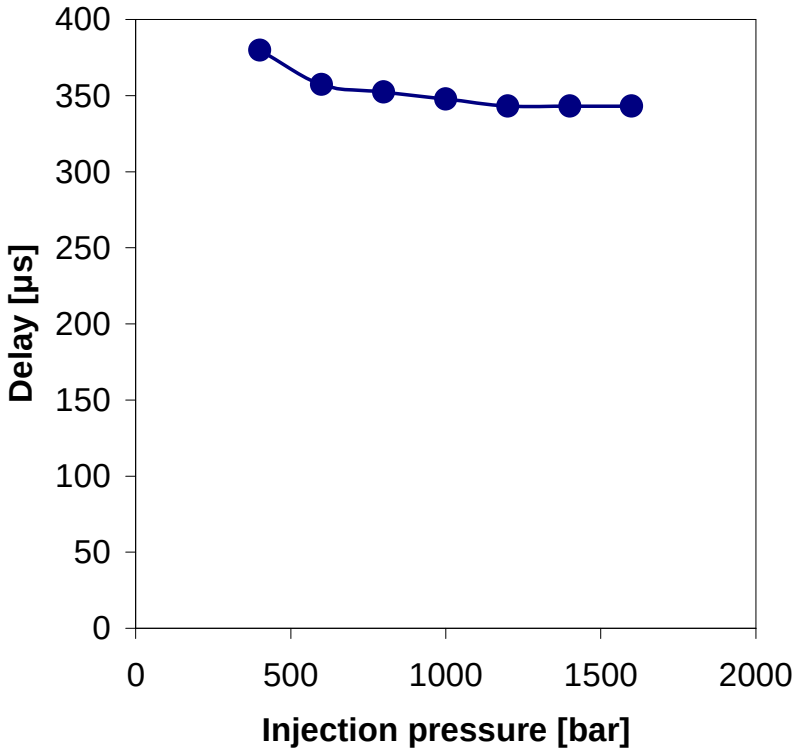

Figure 3.5 - Injector delay characterisation

The experiments were conducted by removing the injector from the engine, and clamping it within a rigid supporting frame which also carried the laser and phototransistor in order to minimise disturbances of the beam caused by vibrations. The injection pressure as well as the injector pulse duration and timing were controlled electronically via the injector driver and fuel control system (Emtronix EC-GEN 500) which in turn was controlled via a computer. The laser beam was passed directly past the opening of one of the holes of the injector, and was intercepted by a photodiode. The photodiode used a balancing circuit which allowed avoiding saturation of the photodiode by

balancing the base of the phototransistor with a variable voltage. When the laser beam was obscured slightly, the current through the phototransistor was reduced, and thus raised the voltage between the output connectors of the balancing circuit. This voltage was recorded with a sampling period of 14 μs using the 16-bit digital data acquisition system described in (section 3.7).

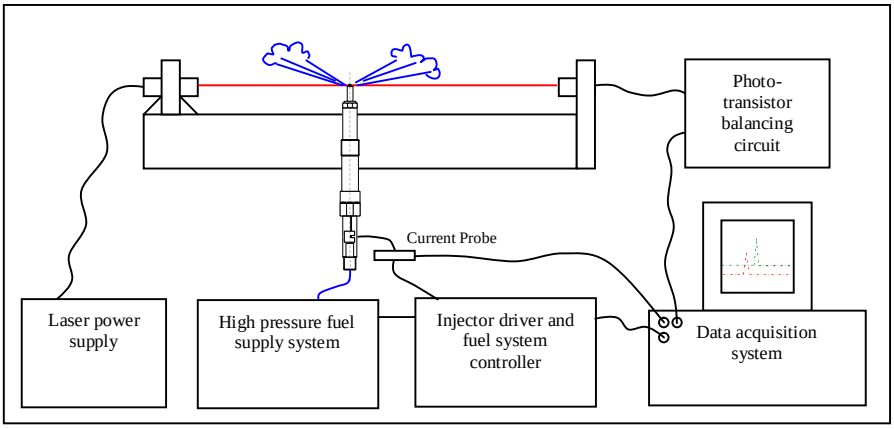

Figure 3.6 – Schematic of the experimental setup used for the injector delay characterisation

3.4. Fuel injection systems

During the course of this project, four laboratory fuel systems were developed and constructed:

1. Conventional common-rail fuel injection system for liquid fuels
2. Ultra low-volume fuel injection system
3. Intake-port injection system for liquid fuels
4. Common-rail fuel liquid injection system for gaseous fuels

Whilst the first two systems were designed and developed by the author, the intake port injection system for liquid fuels was developed in collaboration with Dr. Ramanarayanan Balachandran, and the original design for the fuel system for gaseous fuels was provided by Prof. Choongsik Bae of the Korean Advanced Institute of Science and Technology (KAIST).

3.4.1. Conventional common-rail fuel system for liquid fuels

The first fuel system consisted of a conventional laboratory fuel system for liquid fuels, and was similar to a fuel system used in practical automotive applications. It was designed for experiments requiring a continuous fuel flow over long periods of time, such as the high-load and high-speed experiments presented in section 5.3.9 of Chapter 5. The system had the capability of accurate control of fuel temperature and pressure and the capability of precise fuel-consumption metering. A schematic of this fuel system is Figure 3.7.

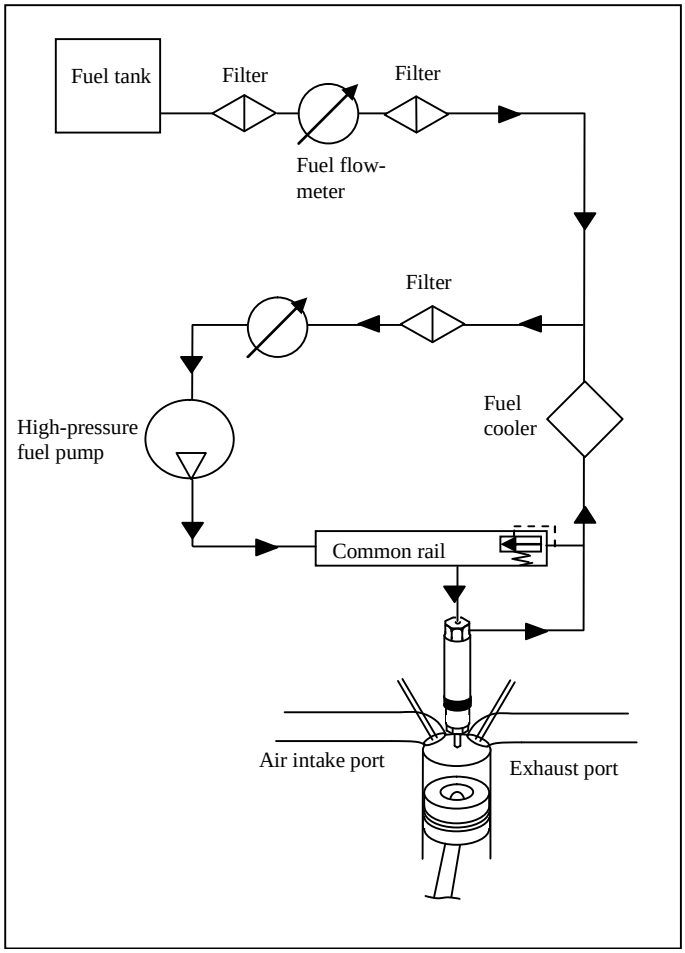

Figure 3.7 - Laboratory common rail fuel system for liquid fuels

3.4.2. Ultra low-volume fuel system

The aim of this project was to study the influence of the molecular structure of biofuels on the combustion in a diesel engine. The technique developed for this study was to combust pure samples of single-molecule biofuels in the engine and to correlate the observed changes in the combustion process with changes in the molecular structure of the fuel. The fuel samples necessary for this experimental approach needed to be purchased from specialist chemical suppliers if available or purposely synthesised. Due to the very high cost of such samples, only small quantities of these fuels could be obtained for the purpose of this project. The available quantities would not have sufficed to fill and operate a conventional common rail fuel system such as that described in section (3.4.1) in many cases. Furthermore, the necessity to clean the fuel system and to eliminate traces of the previous fuel sample before starting each new experiment would have required substantial amounts of fuel to be used for flushing of the fuel system, which further prohibited the use of a conventional common rail fuel system. In several cases, the fuel samples under investigation had unfavourable chemical or physical properties, such as low lubricity or being solid at room temperature, which would have made their use in a conventional diesel fuel system even more difficult. As a result of these challenges, a special fuel delivery system was developed which allowed small quantities of fuel to be injected with accurate control of fuel temperature and injection pressure through the engine's commercial solenoid injector. This ultra low-volume fuel system is shown in Figure 3.8.

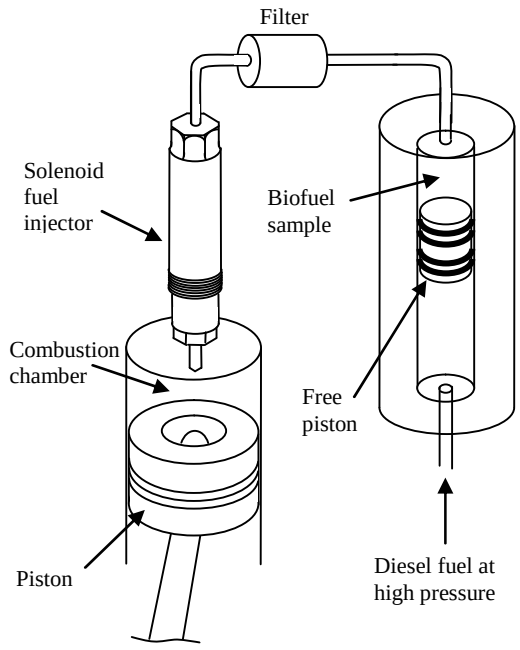

Figure 3.8 - Ultra-low volume fuel injection system

The ultra low-volume fuel system was capable of running engine tests with fuel-samples of less than 100 ml per test achieving injection pressures of up to 160 MPa and fuel temperature control within 2 K. The concept of this system was to use a common-rail diesel fuel system running on conventional diesel fuel as highly controllable hydraulic system to generate the injection pressure, without the conventional diesel fuel actually taking part in the combustion. The standard common rail diesel fuel system of the engine was thus used to control the pressure of a separate low-volume fuel delivery system containing the small fuel sample, which was in turn injected into the combustion chamber. A stainless steel hydraulic cylinder was developed to implement this idea. The hydraulic cylinder was divided into two chambers by a centrally located free piston which was able to move along the axis of the cylinder. The piston sealed the two opposing chambers against each other via four o-rings around its circumference as shown in Figure 3.9. One of the chambers was filled with the special fuel small sample under investigation, while the other chamber was fed with standard diesel fuel which was supplied and pressurised through the common rail fuel system of the engine. The cylinder was designed to withstand the maximum common rail pressure (160 MPa), and was designed to have high-pressure connections for fuel pipes at both ends.

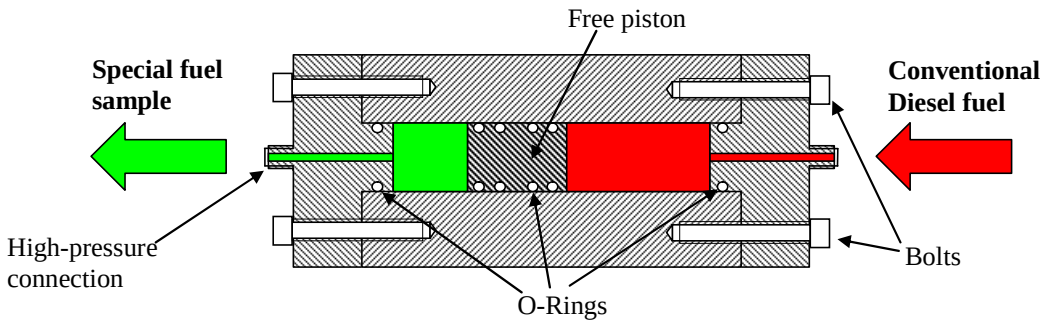

Figure 3.9 – Schematic of the free-piston cylinder used to transmit the injection pressure onto the biofuel samples

Because the piston was free to move along the cylinder axis, it transmitted the pressure from the fuel in the common rail directly onto the fuel sample without allowing any mixing of the two liquids to take place. Due to the free-piston having very little friction and only travelling at low velocities, the pressure in both chambers reached a state of near equilibrium, so that virtually no pressure differential existed across the piston. The operation of the remaining fuel system was similar to that of a standard common rail system used in production diesel engines. The main components were the high-pressure diesel fuel pump, the common rail, a fuel cooler, a fuel tank and a fuel flow-meter. A schematic of the free piston cylinder integrated into the conventional fuel system is shown in Figure 3.10. A feedback temperature control unit using proportional-integral-derivative (PID) control was used to raise the temperature of the fuel samples, if required.

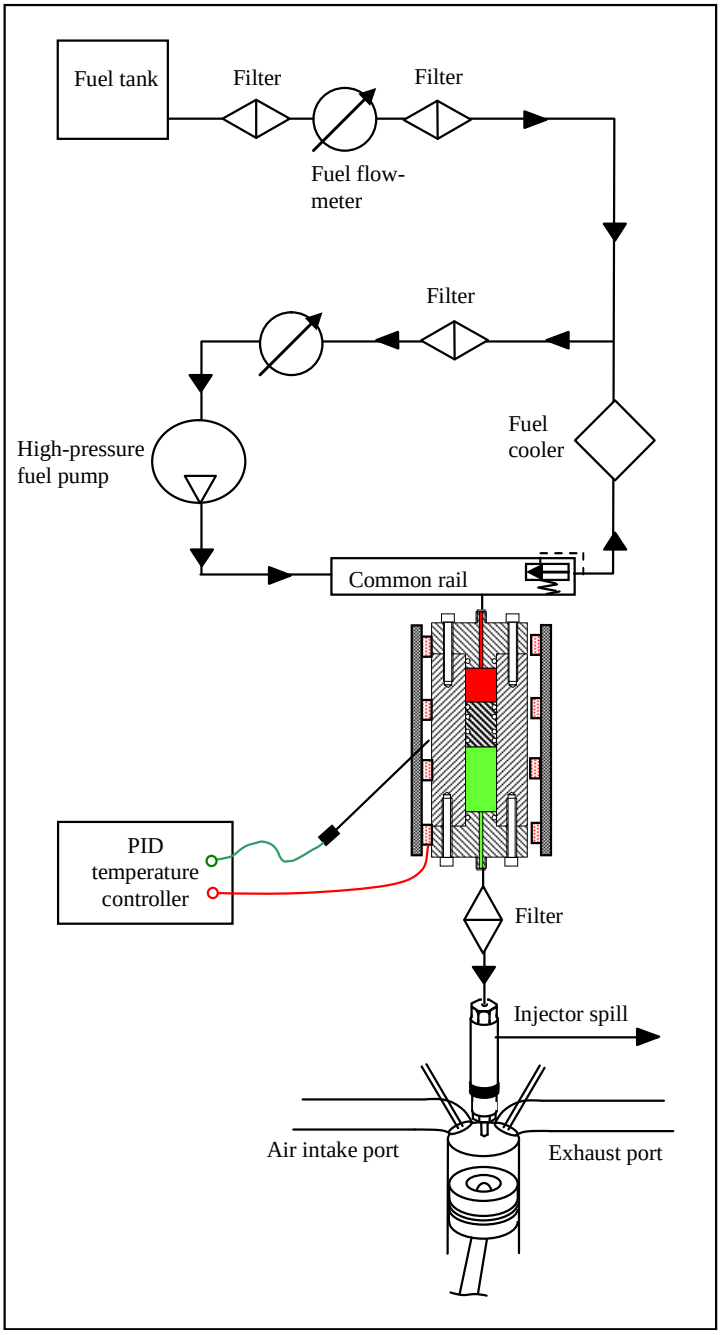

Figure 3.10 – Fuel system schematic of the ultra low-volume fuel system

The pump fed the common-rail with conventional diesel fuel at high pressure, which in turn supplied the right-hand chamber of the ultra low volume fuel injection system with conventional diesel fuel at the same pressure. The conventional automotive diesel fuel was thus used as the hydraulic medium to pressurize the small sample of test fuel. Any diesel fuel returned from the common rail and the pump, was cooled in the fuel cooler and directly returned to the inlet of the high-pressure pump. The consumption of the small quantity of sample fuel by the engine caused the free piston in the stainless steel cylinder to move to the left (see Figure 3.9), thus increasing the capacity of the normal diesel fuel within this cylinder, on the right side of the free piston. This caused a flow of fresh fuel supplied into this circuit from the normal diesel fuel tank which was measured using a positive-

displacement piston flow-meter. The spill-flow of the sample fuel from the injector was measured so that it could be subtracted from the total fuel consumption to yield the amount of fuel injected into the combustion chamber.

A photograph of the disassembled free-piston cylinder during its construction is shown in Figure 3.11.

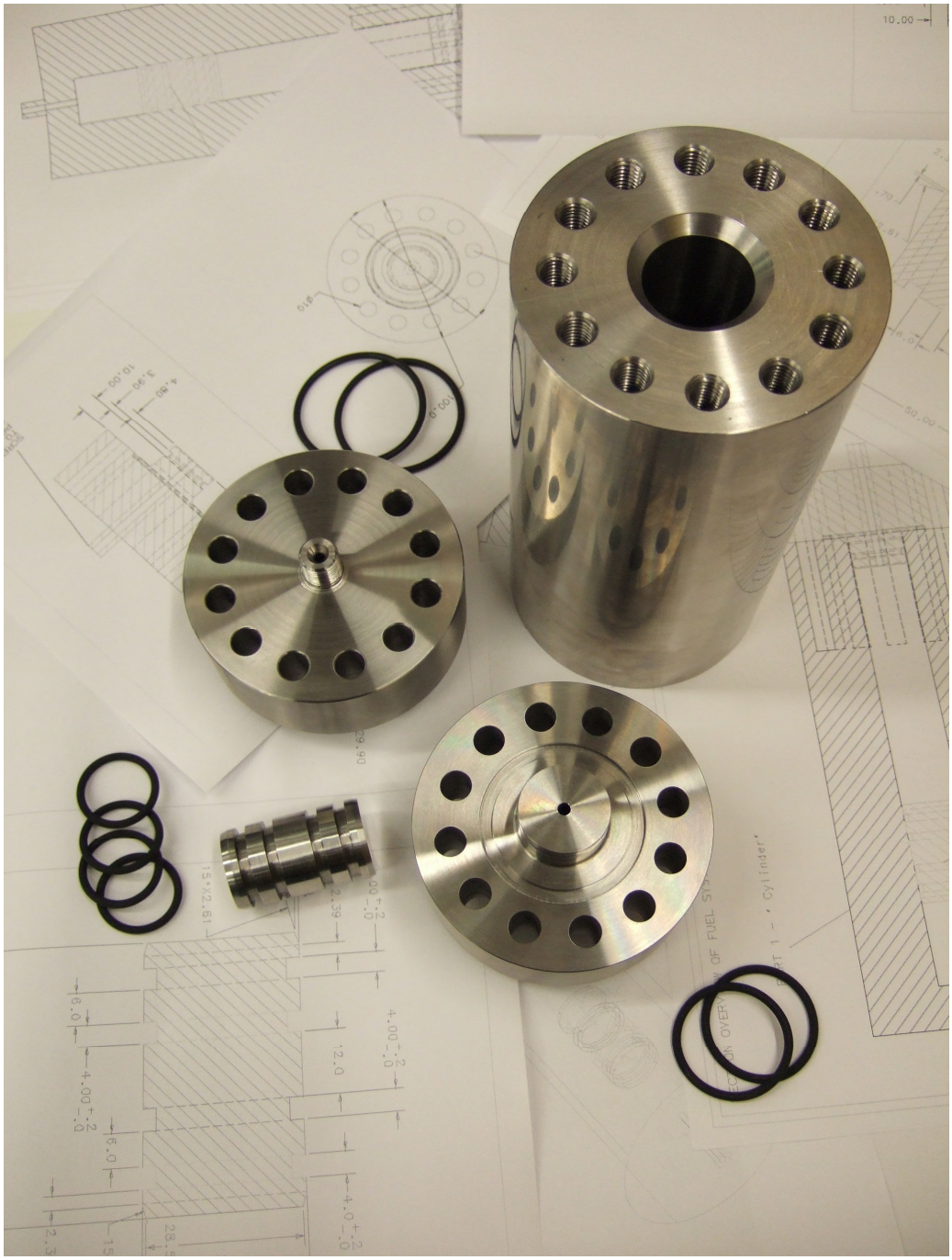

Figure 3.11 - Photograph of the disassembled free piston cylinder of the ultra low-volume fuel system

3.4.3. Intake-port injection system for liquid fuels

A fuel system was conceived for the preparation of homogeneous fuel-air mixtures in the intake port of the engine. This system used a low-pressure (3 bar) electronically controlled fuel injector as typically employed for the port injection of petrol in spark-ignition engines. A schematic of the fuel system is shown in Figure 3.12.

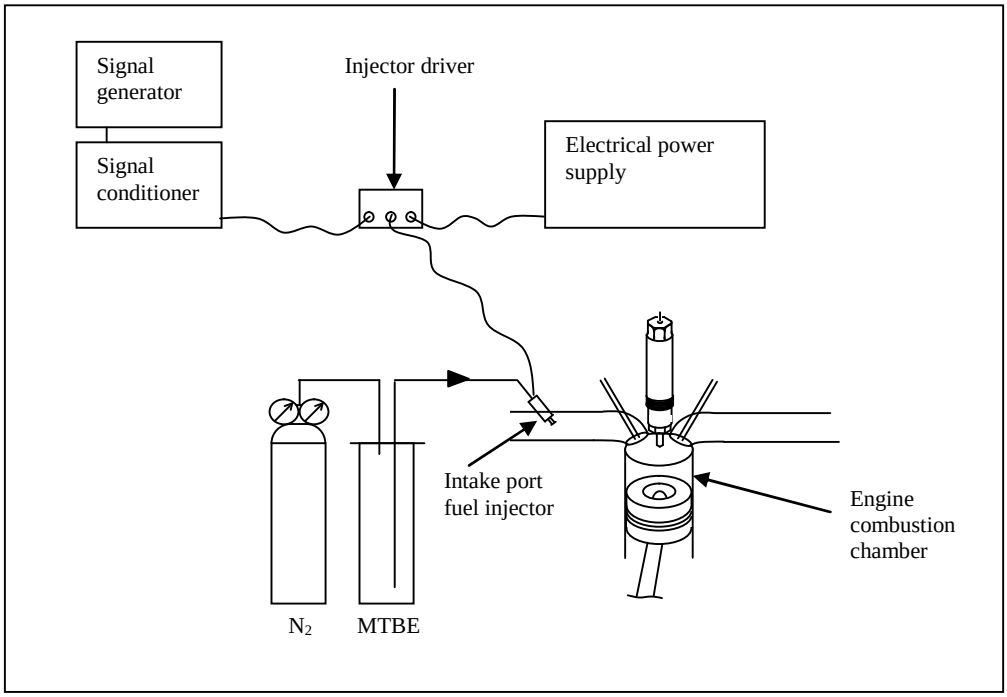

Figure 3.12 - Schematic of intake-port injection system for liquid fuels.

The fuel flow rate of the injection system was calibrated by Dr. Ramanarayanan Balachandran. The calibration was carried out by injecting the liquid fuel into a beaker and measuring the gravimetric fuel flow rate. This was achieved by weighing the beaker at regular time intervals and measuring the time taken for a given fuel mass increase. The system was calibrated for injection frequencies of 15, 20 and 30 Hz. The working fluid was commercial petrol used for spark-ignition engines. A plot of the calibration curve is shown in Figure 3.13.

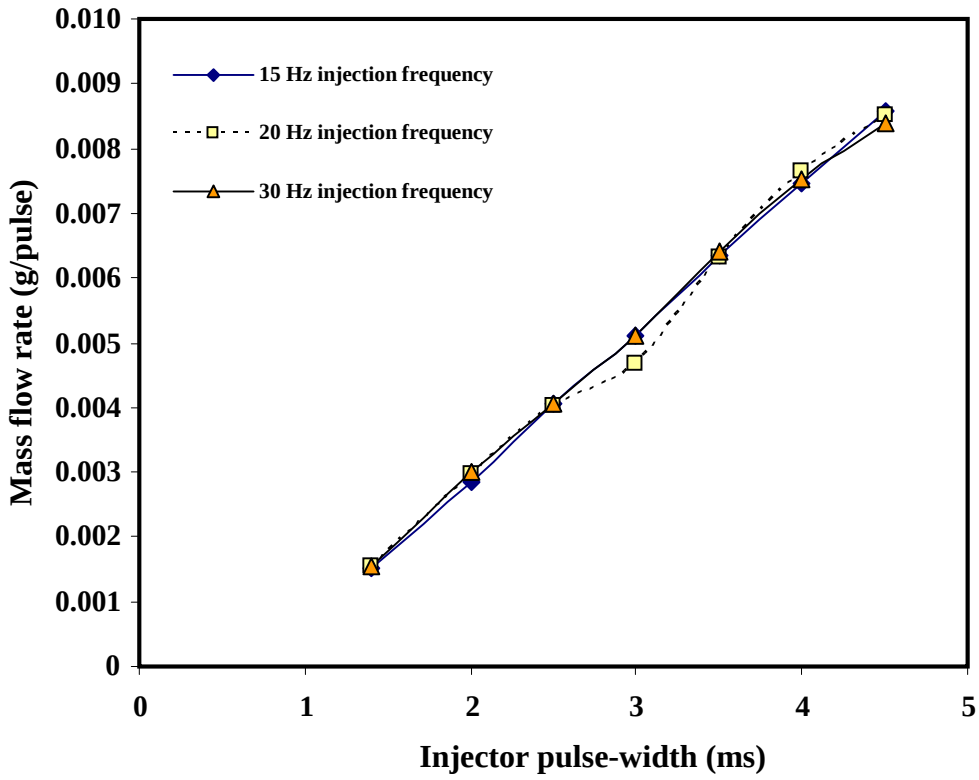

Figure 3.13 - Injector mass-flow rate calibration curve (Balachandran, 2006)

3.4.4. Common-rail fuel injection system for gaseous fuels

A pressurised fuel system which allowed the liquid-injection of fuels that are gaseous under atmospheric conditions was constructed and installed according to a design provided by Prof. Choongsik Bae of KAIST. The main purpose of this fuel system was the liquid-phase injection of dimethyl ether (DME) into the engine via its direct-injection diesel injector. Under operation with DME, the fuel system comprised a DME bottle and a nitrogen gas bottle, a visibility and settling chamber, two pneumatically driven high pressure pumps, a common rail, and a fuel injector (see Figure 3.14). The DME was supplied to the fuel system in liquid phase and was pressurised to 15 bar by a constant supply of nitrogen from the nitrogen gas bottle. The supply pressure of 15 bar was above the saturation pressure of DME at ambient temperature conditions, and was thus used to keep the DME liquid. Nitrogen was fed into the DME bottle via the vapour port of a DIN-1 valve mounted on the DME bottle, whilst the liquid DME was fed out of the DME bottle via the liquid port of the same DIN-1 valve. Both bottles were located in the gas cabinet of the laboratory (see Figure 3.2), and fed the DME into the engine test-cell via stainless steel pipes.

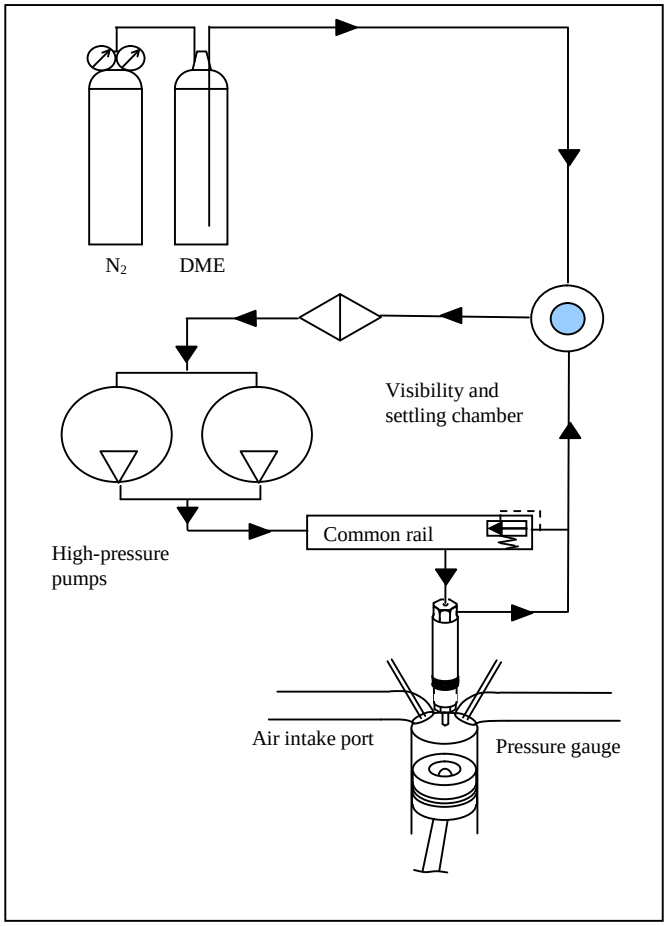

Figure 3.14 - Common rail fuel injection system for gaseous fuels

3.5. Measuring instruments

The dynamic cylinder pressure was measured using a piezoelectric pressure transducer (Kistler 6056AU38) and a charge amplifier (Kistler type 5011). The cylinder pressure was pegged during each combustion cycle at bottom dead centre using a piezoresistive pressure transducer (Druck PTX 7517-3257) located 160mm upstream of the inlet valves in the intake manifold. The geometric compression ratio of the engine was 15:1, and the air was naturally aspirated into the combustion chamber at atmospheric pressure. The exhaust gas was sampled 180 millimetres downstream of the exhaust valves using an automotive exhaust gas analysing system (Signal Instruments, Horiba MEXA 9100HEGR). The NO_x emissions were analysed using a chemiluminescence analyser, CO and CO_2 were measured using non-dispersive infrared analysers and a flame ionisation detector (FID) was used to measure the unburned hydrocarbon emissions. A differential mobility particle-size spectrometer (Cambustion DMS500) was used to measure the size distribution and concentration of the sub-micron particulates in the exhaust gas. The total mass emission of sub-micron particulates was calculated from their sizes and respective concentration in the exhaust gases using assumptions about their shape and density. For some investigations, particulate samples of

varying sizes were collected using a micro-orifice uniform distribution (MOUDI) aerodynamic cascade impactor. Detailed descriptions of all measuring instruments are provided in the following sections 3.5.1-3.5.5.

3.5.1. Pressure

The cylinder pressure was measured using a piezoelectric pressure transducer (Kistler 6056AU38) in combination with a charge amplifier (Kistler type 5011) and a 16 bit digital data acquisition system (National Instruments M-series 6251). The pressure transducer, charge amplifier and data acquisition system were calibrated together using a hydraulic dead-weight calibration system. The dead-weight calibration system uses the force from a known mass to generate hydraulic pressure on an oil circuit though a piston of known diameter. Details of the calibration and its results are shown in Appendix B.

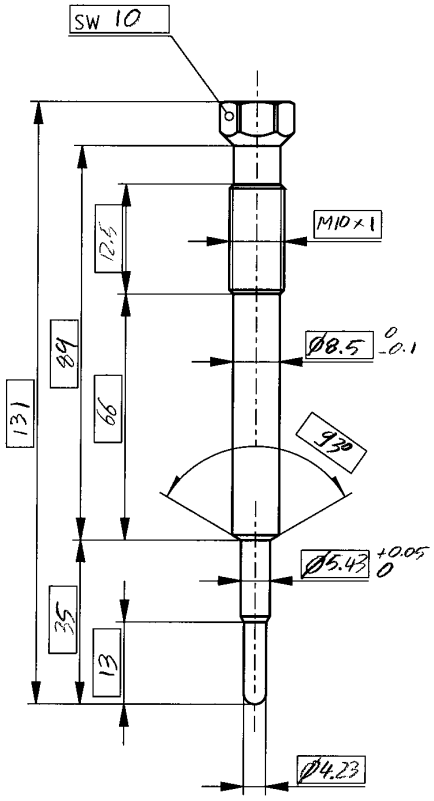

Figure 3.15 - Piezoelectric cylinder pressure transducer type 6056AU38 housing (Kistler, 2007)

Calibration (0-100 bar)	Transducer sensitivity	System sensitivity
Kistler Instruments UCL dead-weight calibration (N=3; σ = 0.00694554)	-19.10 pC/bar -18.97 pC/bar	15.00 V/bar 14.90 V/bar

The cylinder pressure was pegged each combustion cycle during open inlet valve at intake bottom dead centre using a piezoresistive pressure transducer (Druck PTX 7517-3257) located 160mm upstream of the inlet valves, in the intake manifold. This transducer was not only used for cylinder pressure pegging, but also to record the inlet manifold pressure of the engine at intervals of 0.2º CA. The piezoresistive transducer was calibrated by the manufacturer, and was guaranteed to have an accuracy of at least 0.15% within the operating conditions used.
The exhaust pressure was measured similarly to the inlet manifold pressure using a piezoresistive pressure transducer (Druck PTX 7517-3257).

3.5.2. Air flow rate

The air flow-rate was measured using a rotary positive displacement gas flow-meter (Romet G40). Calibration was carried out over a range of engine speeds for a certain engine valve-timing used. The calibration for normal engine valve-timing (shown in Figure 3.3) is shown in Figure 3.16 below.

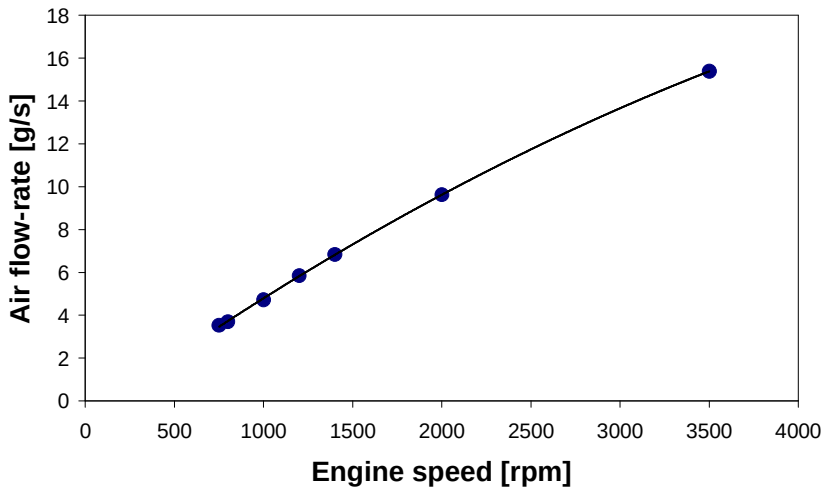

Figure 3.16 - Air flow rate of the engine versus engine speed

The air flow rate could be expressed as a function of engine speed by Equation 3.1, where x is the engine speed in rpm, and m is the mass of fresh air ingested by the engine in grams, and t is time in seconds.

$$\frac{dm}{dt}[g/s] = -4 \cdot 10^{-7} \cdot x^2 + 0.006 \cdot x - 0.8298$$

Equation 3.1

For retardation of the inlet valve timing at a constant engine speed of 1200 rpm, the air flow-rate through the engine was measured as shown in Figure 3.17.

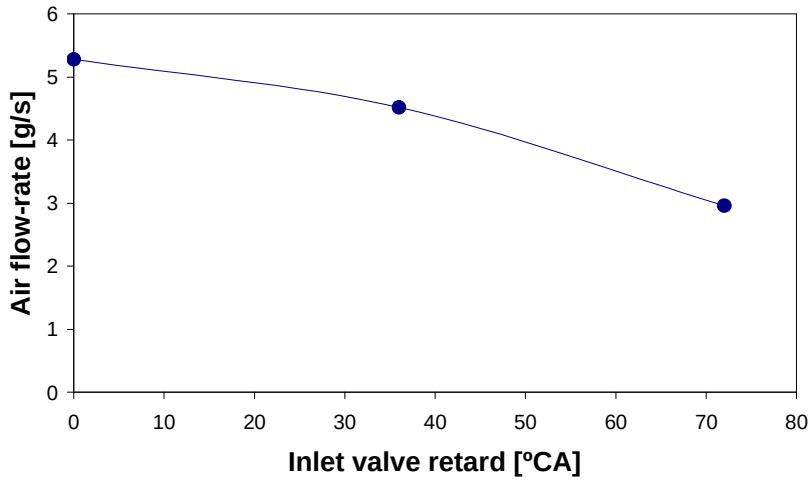

Figure 3.17 - Air flow-rate measurements for changes in inlet valve timing at an engine speed of 1200 rpm

The nominal error for the air flow rates used during the experiments was less than 0.2%.

3.5.3. Fuel flow rate

The fuel flow-rate was measured using a positive displacement piston flow-meter (Max machinery 213-310) as shown in the fuel-system schematic (Figure 3.7). Calibration was carried out by the manufacturer (see Appendix B for calibration certificate) and the instrument was sent-back to the supplier at a later date for re-calibration (see Appendix B for calibration certificate). The nominal error for the flow rates used during the experiments is less than 0.2%.

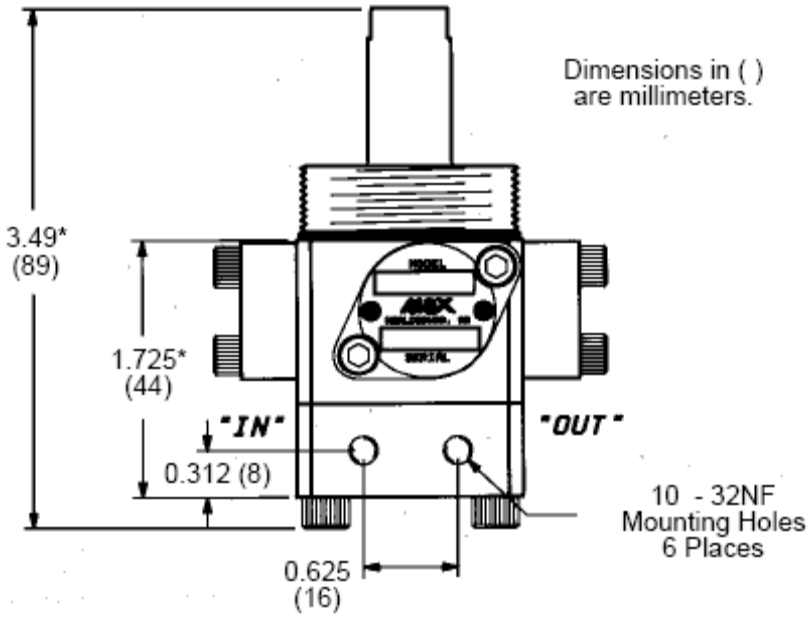

Figure 3.18 - Piston fuel flow-meter (Max machinery, 2003)

3.5.4. Inlet and exhaust gas concentrations

The concentration of individual gases present in the exhaust and intake streams, were measured using an automotive exhaust gas analyser rack (Signal Instruments multigas analyser rack or Horiba MEXA 9100HEGR). The analyser rack comprised instruments for the measurement of CO_2, CO, O_2, UHC, NO and NO_x. Figure 3.19 shows a schematic of the exhaust gas analyser rack.

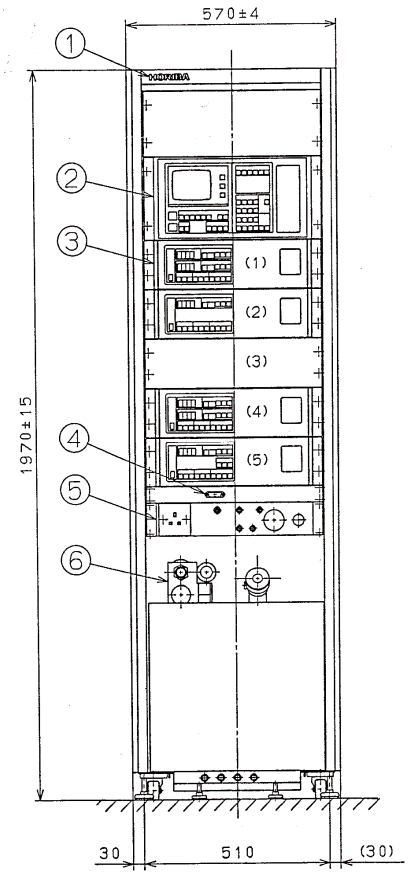

1 Analyser Rack

2 Flow controller

3 Analyser units:

(1) CO & CO_2 exhaust
(2) CO_2 inlet
(3) Blank panel
(4) UHC & O_2 exhaust
(5) NO/NO_x exhaust

4 Connector for gas divider

5 Sampling panel

6 Main sampling unit

Figure 3.19 – Horiba MEXA 9100HEGR exhaust gas analyser rack

The exhaust gas was sampled 180 millimetres downstream of the exhaust valves, and routed to the gas analyser via a heated sample line that was kept at a temperature of 190 ºC. Detailed background information on the analysing techniques are provided by Horiba (1984) and Zhao and Ladommatos (2001).

CO and CO_2 concentrations

The concentration of CO and CO_2 in the intake and exhaust streams were measured using a non-dispersive infrared (NDIR) absorptiometry analyser (Horiba AIA-120). The technique used by the analyser, relies on the principle that CO and CO_2 absorb infrared radiation, and indicates the concentration of CO or CO_2 in the sample gas by quantifying its absorption of infrared light at a known pressure. The absorbtion of infrared radiation is described by Beer's law which may be written as:

$$a_\lambda = 1 - e^{(-c_i Q_\lambda L)}$$

Where C_i is the concentration of species, Q_λ is the absorption efficiency, and L is the optical path length.

An infrared beam is generated by an incandescent infrared light source and filtered by optical filters to reduce it to a narrow wavelength band. Subsequent to passing through the filter, the beam is modulated by a rotating chopper wheel at a known frequency. The modulated infrared beam is projected through a transparent tube, through which sample gas is passed. Depending on the concentration of infrared-absorbing gas (i.e. CO or CO_2) present in the sample gas, more or less infrared radiation of that wavelength is absorbed. The remaining intensity of the infrared beam then proceeds to entering a hermetically sealed detection cell, which is filled with the type of gas to be detected (i.e. CO or CO_2).

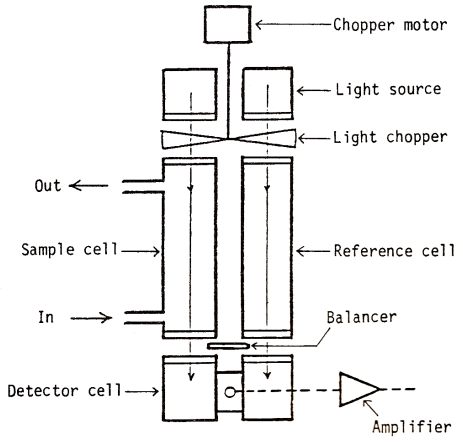

Figure 3.20 - NDIR CO/CO_2 gas analyser schematic (Horiba AIA-120 manual, 1984)

The gas in the detection cell absorbs infrared radiation causing a rise in temperature and pressure, which in turn results in an expansion of the gases in the cell via a flexible diaphragm. This expansion is detected by a capacitive probe on the diaphragm, which produces an electrical signal. The same procedure is applied to a second infrared beam, which passes through a reference cell

containing no infrared-absorbing gas, rather than sample gas from the engine. The difference in signal between the two detection cells yields a compound signal which may be correlated to the absolute concentration of infrared absorbing gas (i.e. CO or CO_2) within the sample gas tube. Selectivity between the two types of gases (i.e. CO or CO_2) is achieved by applying different wavelengths of infrared light to the sample gas, and compensating for the respective other gas using a compensation detector cell.

UHC concentration

The concentration of carbon atoms bound in unburned hydrocarbon molecules (UHC) in the exhaust gas, was measured using a flame ionisation detector (FID). The FID detects the amount of carbon atoms bound as hydrocarbon molecules within a stream of sample gas, by forcing the combustion of any hydrocarbon molecules present in the stream, in a hydrogen and air flame. The formation of positively charged ions and electrons produced by the combustion of the hydrocarbons is proportional to the amount of carbon atoms present in the hydrocarbon molecules prior to their combustion. The number of ions and electrons that are formed this way are collected by applying an electric field across the wake of the flame, using two electrodes of differing electric potential. The positively charged ions and the negatively charged electrons impact opposite electrodes, due to the different polarity of their electric charges, whereby a current is induced within the circuit that connects the two electrodes. This current is measured, and correlated through calibration to the amount of carbon atoms which were originally present as hydrocarbons in the sample stream.

O_2 concentration

The concentration molecular oxygen O_2 was measured using magneto-pneumatic gas analyser. The detection method relies on the fact that oxygen molecules have a stronger attraction to magnetic poles than other gases present in the exhaust stream, due to their higher paramagnetic susceptibility. Within the analyser, two electro-magnetic poles are alternatingly formed at two different positions, by the electrical excitation from two coils. The attraction of O_2 molecules to the site of the pole from the sample flow of gas temporarily reduces the nitrogen flow through the orifice located within the magnetic pole. The flow of nitrogen through the other pole remains unblocked, until the magnetic field is switched to the opposite pole and the flow reduction through the orifices is reversed.

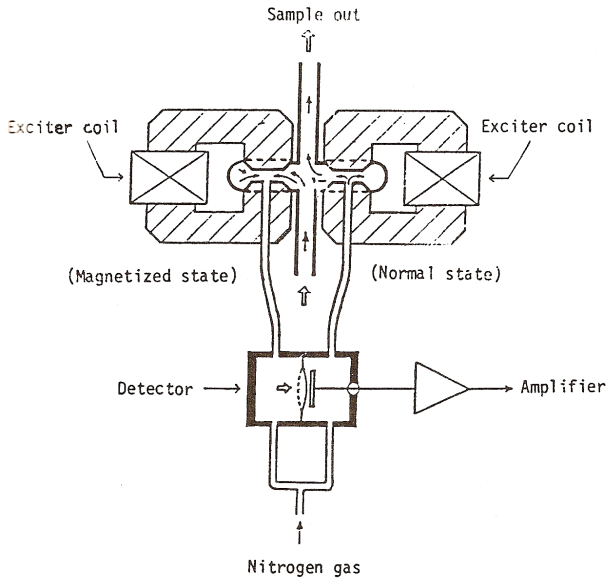

Figure 3.21 - Magneto-pneumatic O_2 detector (Horiba, 1984; FMA-120 analyser manual)

The reduction in nitrogen flow in either pole temporarily causes a higher back-pressure at that particular side of a diaphragm within the detector. The magnitude of the oscillations induced in the diaphragm by the resulting pressure oscillations is translated into an electrical signal, using the capacitive properties of the diaphragm. This signal is correlated to the concentration of O_2 within the sample gas.

NO and NO_x concentrations

The concentration of oxides of nitrogen (i.e. NO and NO_x) was measured using a chemiluminescence analyser. In this type of analyser, the sample gas is mixed with an excess quantity of ozone (O_3) under reduced pressure, which reacts with nitric oxide (NO) that may be present in the sample gas, to form nitrogen dioxide while accompanied by the emission of light. The detection of this light during the chemical reaction is used to quantify the concentration of NO that was initially present in the sample gas. The chemical reactions taking place may be described as:

$$NO + O_3 \rightarrow NO_2^* + O_2$$

Equation 3.2

$$NO_2^* \rightarrow NO_2 + hf$$

Equation 3.3

Where * designates an excited state, h is Planck's constant and f is the light frequency in Hertz.

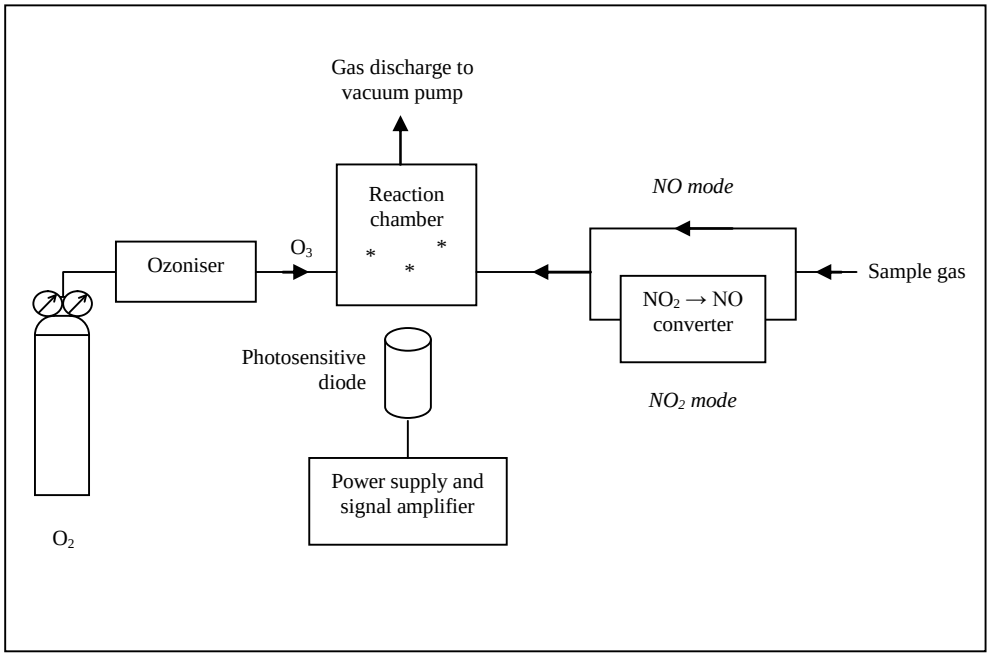

Figure 3.22 – NO and NO_2 chemiluminescence analyser schematic

Figure 3.22 shows a schematic of the analyser used for measuring the concentration of NO and NO_x in the sample gas. For the detection of NO_x rather than NO, the sample gas is passed through a NO_2 to NO converter, which reduces the NO_2 present in the sample gas to NO with the aid of a heated catalyst. The combined concentration of NO in the sample gas, after the NO_2 has passed through the NO_2 to NO converter, is thus equal to the sum of the concentrations of NO and NO_2 of the original sample gas taken from the engine. This makes it possible to detect the total concentration of NO_x. The analyser can be switched between the NO or the NO_x detection modes by routing the sample gas either directly into the reaction chamber (NO detection mode), or routing it via the NO_2 to NO converter (NO_x detection mode). The analyser is specified to have a maximum error of 1% of the operating range, and a response time of 2 seconds.

3.5.5. Exhaust gas particulates

A differential mobility particle-size spectrometer (Cambustion DMS 500) was used to measure the size distribution and mass of the sub-micron particulates in the exhaust gas. Separately, particulate samples having different sizes were collected in some experiments using a micro-orifice uniform distribution (MOUDI) aerodynamic cascade impactor.

Particulate number, size and mass

The number, size and mass of the particulates ranging from 5 – 1000 nm was measured using a differential mobility spectrometer (Cambustion DMS500). The principle of operation of the differential mobility is to classify and count the particles according to their specific ratio of electric charge to aerodynamic drag. The instrument was used to sample gas from the exhaust manifold, at a location of approximately 200 mm downstream of the exhaust valve of the engine. Upon entering the sample line of the differential mobility spectrometer, the exhaust gas was diluted at a ratio of 4:1 with a filtered and measured flow of compressed air in the primary diluter (Figure 3.23).

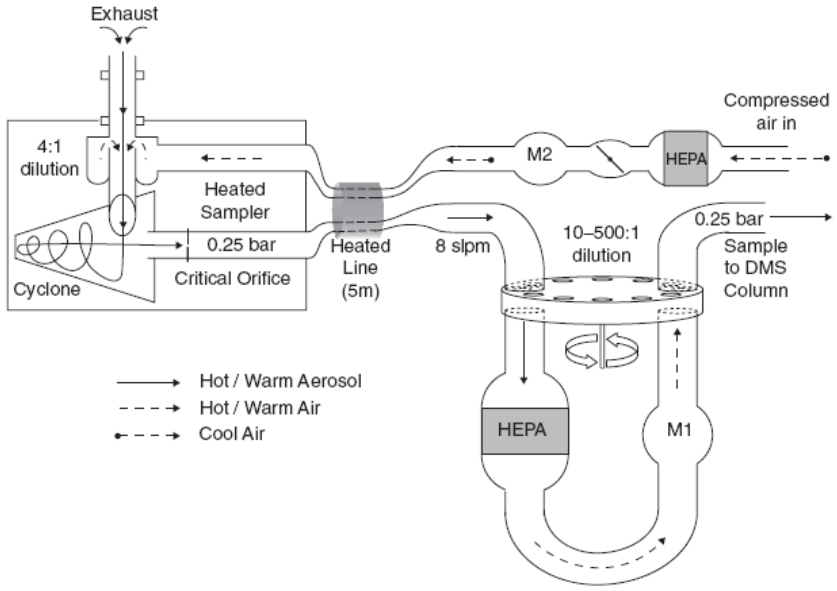

Figure 3.23 - Sampling system of the differential mobility spectrometer (Symonds et al. 2007). High efficiency particulate air filter (HEPA). Mass flow-meter (M).

After this primary dilution, the flow was passed through a cyclone separator in which particles larger than 1000 nm are removed from the sample gas by impaction. After the cyclone separator, the sample stream was passed through a restriction orifice, which induces a pressure drop in the stream, and reduces the pressure downstream of the orifice to around 0.25 bar. The sample gas is then passed through a heated flexible polytetrafluoroethylene (PTFE) sampling pipe, which carries the sample to a secondary rotating disc diluter. In this secondary diluter the sample is diluted by a ratio ranging from 20:1 to 500:1 with a filtered and metered flow of sample gas that has been passed through a high efficiency particulate air filter (HEPA). When emerging from this secondary dilution stage, the sample flow enters a corona discharge charger, which adds a negative electric charge to any particles suspended in the sample gas. The particles then enter the classifier column, where they are introduced into a laminar flow of particle-free air.

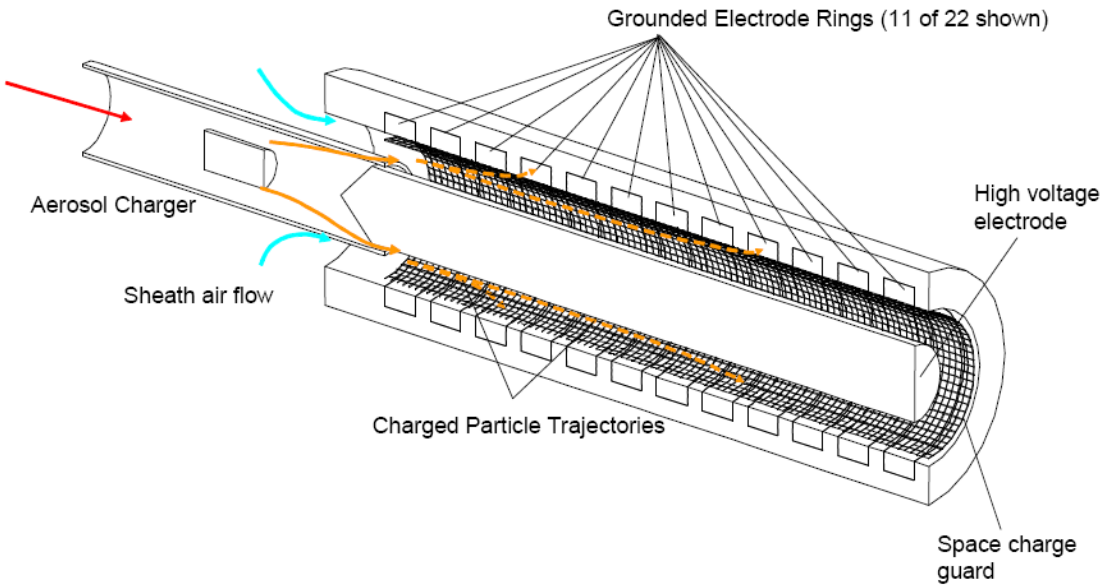

Figure 3.24 - Corona charger and classifier column with in the differential mobility spectrometer (Cambustion DMS 500 manual, 2004)

Within the classification column, the particles are deflected towards the electrode rings located on the exterior of the column by a high-voltage electrode located at the central axis of the column due to their electric charge. The location at which a particle impacts the exterior of the column, and thus the electrode ring upon which it discharges its charge, depends on the ratio of its aerodynamic drag to its electric charge. Since the charge and drag is known for particles of different sizes, their size and number may be determined by measuring the discharge currents at the grounded electrodes. The total particulate mass may be estimated by making an assumption about the density and shape of the particles. Empirical work has shown that good mass estimates can be achieved for diesel particulates using the particle mobility diameter (Park, et al., 2003, Symonds, et al., 2007). The relationship used to estimate particulate mass of the particles for this instrument was that proposed by Symonds et al. (2007). The relationship between particulate mass (m_p) and electrical mobility equivalent particulate diameter (D_{eme}) is described by Equation 3.4:

$$m_p[\mu g] = 1.535 \cdot 10^{-16} \cdot (D_{eme}[nm])^{3.19}$$

Equation 3.4

Figure 3.25 illustrates the effective density of the particulate matter as a function of the electrical mobility particulate diameter, as it is implemented by Equation 3.4.

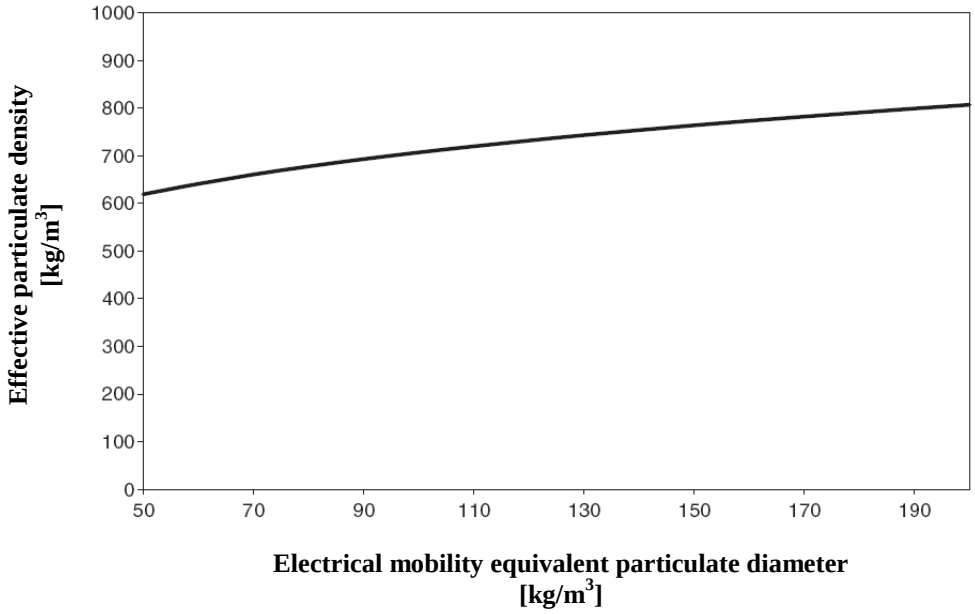

Figure 3.25 - Effective density of the particulate matter as a function of electrical mobility equivalent particulate diameter. Adapted from Symonds et al. (2007).

Collection of particulate samples

In order to conduct analyses on exhaust gas particulates that are able to yield information about the characteristics of the particles as a function of their size, particles needed to be collected and separated into different size groups. Such samples were necessary for analyses of optical, chemical and thermogravimetric nature. A practical instrument capable of accomplishing this task is the micro-orifice uniform distribution (MOUDI) aerodynamic cascade impactor (Figure 3.26), which was used to carry out this task. The instrument relies on the principle that particles of different sizes have varying aerodynamic mobility, which depends on their ratio of aerodynamic drag forces to their inertia. The particles are subjected to an air-flow of known velocity, which is accelerated through an array of nozzles situated prior to each impaction stage. After exiting this nozzle, the air stream is deviated sharply around the impaction membrane. Depending on their mobility, particles will be able to follow the air stream (small particles), or will be forced to impact on the impaction membrane (large particles). By specifying orifice diameters and the sample air flow it is possible to make accurate predictions about the size of particles which will impact each impaction stage. In this manner, the MOUDI aerodynamic cascade impactor allows collection of exhaust gas particles whilst simultaneously separating them according to their size.

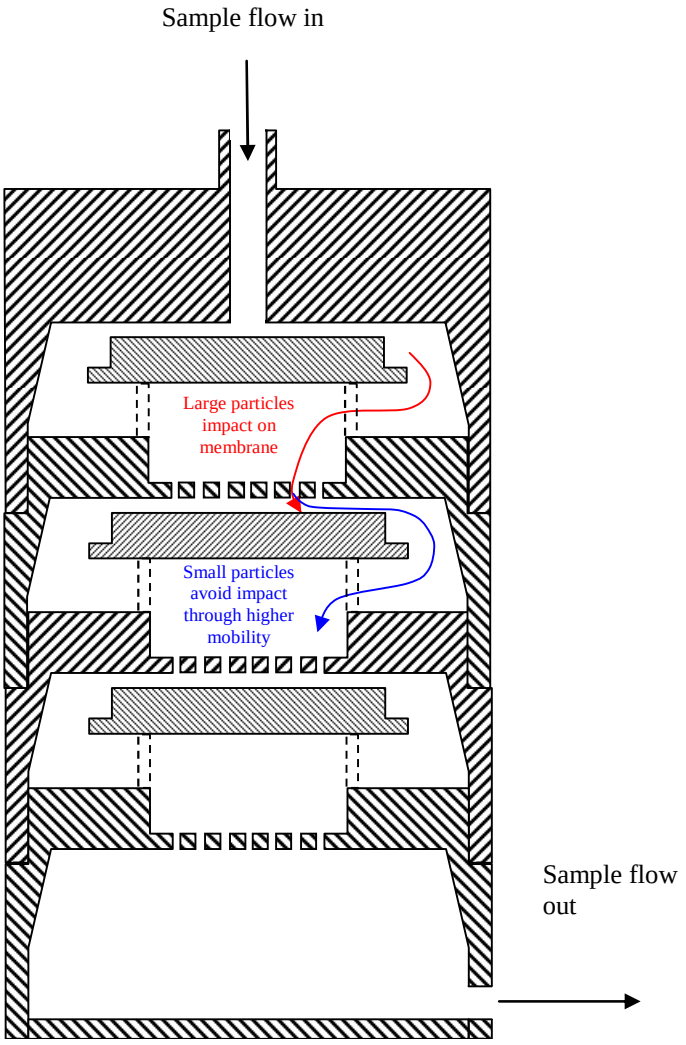

Figure 3.26 - Schematic of the MOUDI cascade impactor

3.6. Fuel injection control system

The fuel injection timing and injection pressure were controlled using an electronic fuel injection control system (Emtronix EC-GEN-500). The system uses signals from a Hall-effect sensor mounted on the flywheel and a Hall-effect sensor mounted on the camshaft to time the injection pulse sent to the solenoid in the injector. In an alternative configuration, the timing of the injection pulse may be timed using a TDC and a crank degree marker signal from the optical shaft encoder in conjunction with the signal from the Hall-effect sensor mounted on the camshaft. The system is capable of generating up to eight independently controllable pulses to the injector within one engine cycle, allowing up to eight independent fuel injections per cycle.

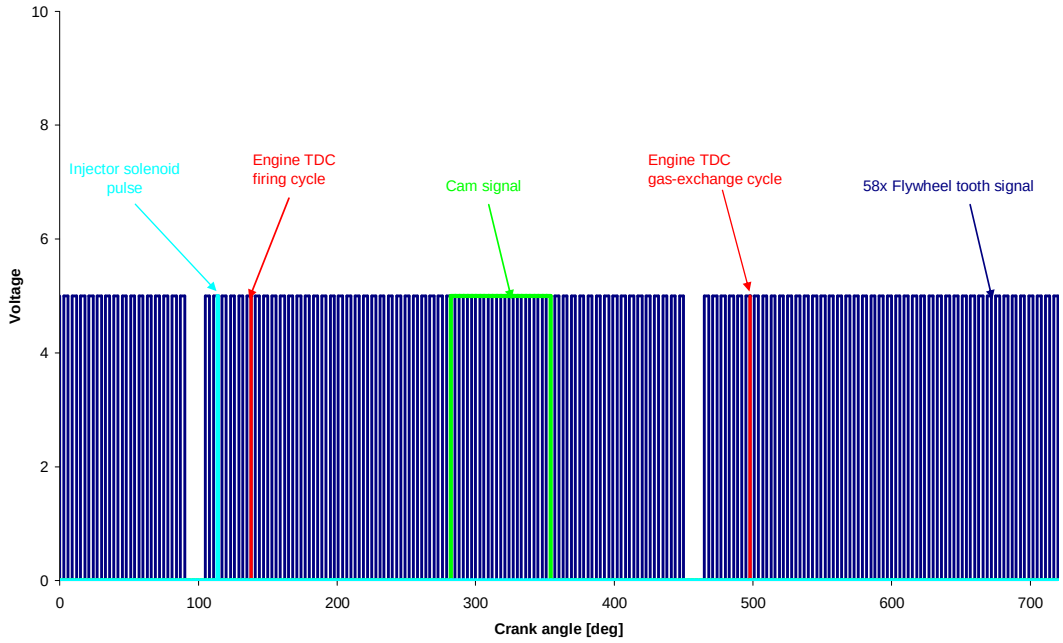

Figure 3.27 – Flywheel 58x signal and camshaft signal used to control the injection timing by the fuel injection control system.

Figure 3.27 shows a diagram of the signals used by the fuel injection control system to control the timing of the electric pulse sent to the solenoid of the injector.

The fuel pressure can be controlled via the fuel metering valve on the inlet port of the high-pressure pump, as well as through the pressure control valve mounted on the common rail. Under normal operating conditions, the fuel metering valve on the inlet port of the high-pressure pump is kept fully open, and the common rail pressure is exclusively controlled by controlling the pulse width modulation (PWM) on the pressure control valve located on the common rail.

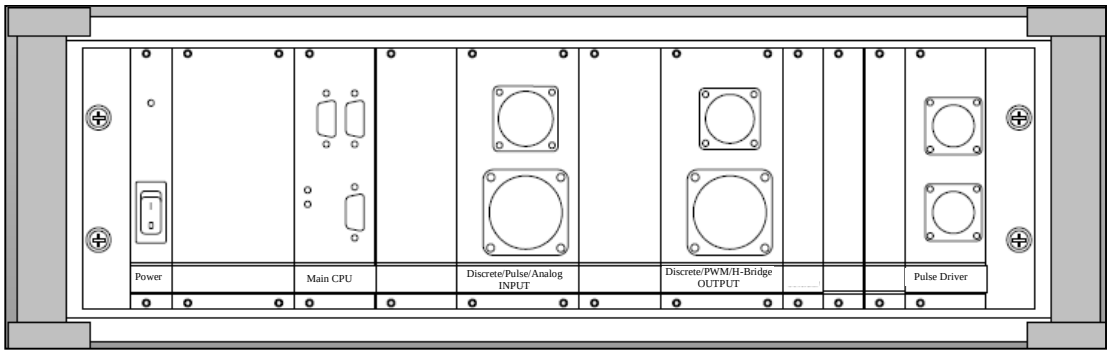

Figure 3.28 - Schematic of the injection control rack (Emtronix, 2004)

The common rail pressure was controlled using a proportional-integral-derivative (PID) feedback control loop using a pressure signal taken from a strain-sensitive variable-resistance semiconductor pressure transducer measuring the common rail pressure.

3.7. Data acquisition systems

The analogue signals for cylinder pressure, inlet manifold air pressure, exhaust pressure, fuel injection pressure and engine speed were recorded using a 16-bit digital data acquisition system (National Instruments M-series NI-6251). The system was capable of sampling the 5 analogue channels at a sampling rate of 200 kHz using a single analogue to digital converter (ADC) in conjunction with a multiplexer. The software controlling the data acquisition system was developed by the author within the software package Labview to suit the data acquisition and timing input signals. The data acquisition system was configured to acquire crank-angle resolved data for each engine cycle, which was accomplished by starting to record at a constant point during the engine cycle and proceeding by recording samples at 0.2º crank angle intervals within that cycle until the cycle ended. Timing of the recording process was achieved using three electric signals from the engine. The first two signals were supplied by an optical shaft encoder which encoded the crank-shaft rotation into 1800 increments using a square crank-degree marker (CDM) as the first signal and provided a square synchronisation pulse once every crankshaft revolution as the second signal. The synchronisation pulse was interfaced with the third signal, a square pulse from an optical sensor mounted on the camshaft through a solid state electronic AND gate. The resulting signal from the AND gate yielded a synchronisation pulse from the crank-shaft encoder once every engine cycle, rather than once every crankshaft revolution. This pulse was used as reference point within the engine cycle, to synchronise the data acquisition process with the engine cycle. The position of piston TDC within the cycle was specified in the data acquisition software by defining a crank-angle offset between the synchronisation pulse and TDC. Initially, the position of piston TDC was determined using static measurements with a dial gauge.

The data-acquisition system carried out segmentation of the data for each cycle and allowed real time display of the recorded data and any parameters calculated from this data. The software displayed crank-angle resolved cylinder pressure, inlet manifold pressure, exhaust pressure and fuel injection pressure for every recorded cycle during engine operation. The cylinder pressure was pegged each cycle by the data-acquisition software via the absolute pressure recorded in the exhaust gas manifold at a specified point within the engine cycle. The software used pre-input data about the engine geometry in conjunction with the instantaneous piston position to carry out real-time calculations of combustion parameters such as indicated mean effective pressure (IMEP), first and second derivatives of cylinder pressure, apparent heat release rate, cumulative heat release, mass fraction burnt, global cylinder temperature and the specific gas entropy. Low-pass filters could optionally be applied to the pressure, temperature and heat release data. The software also displayed engine speed, P-V and log-P-log-V diagrams of the engine cycle and incorporated algorithms for the detection of the timing of the start of combustion. Ensemble-averages of combustion parameters and electronic storage of the data in a specified spreadsheet format could also be carried out. Calibration of the dynamic engine TDC position could be conducted during engine operation using the global cylinder temperature and the specific gas entropy calculated from the cylinder pressure and engine geometry, according to the method developed by Tazerout et al. (1999). Details about the

mathematical methods used to calculate the most important engine parameters are provided in Chapter 4.

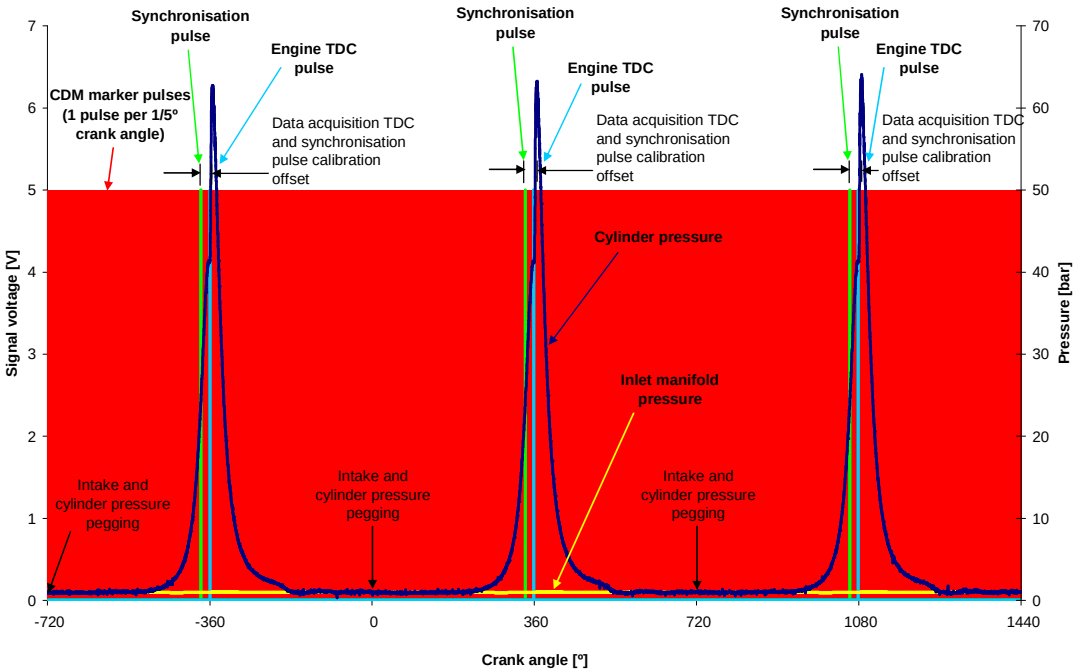

Figure 3.29 – Schematic of data acquisition signals

Chapter 4. Analytical methods applied to the experimental data

The present chapter describes the most important mathematical analyses carried out using the experimental data. These are the analysis of the cylinder pressure which leads to the calculation of the heat release rate, cumulative heat release rate, mass fraction burnt and global cylinder as well as the stoichiometric analysis of the combustion reactants and products from measured experimental data.

4.1. Cylinder pressure analysis and heat release

The cylinder pressure traces in their raw form provide information about the compression ratio and volumetric efficiency of the engine, the evaporation of fuel, the start of ignition, the duration and magnitude of the heat release of combustion as well as being indicative of the global gas temperatures during the engine cycle. In its raw form, cylinder pressure is usually recorded over the entire crank angle domain of the engine cycle and may be ensemble-averaged over a desired number of engine cycles at the same condition. This value, a function of the engine crank-angle, may simply be expressed as:

$$p$$

The first derivative with respect to crank angle may be expressed as:

$$\frac{dp}{d\theta}$$

The second derivative with respect to crank angle may be expressed as:

$$\frac{d^2p}{d\theta^2}$$

The second derivative of pressure may be used to determine the inflection point of cylinder pressure rise, which may be used to define the start of fuel ignition during the engine cycle. The following section will further show how the apparent heat release from the combustion may be calculated.

4.1.1. Cylinder volume calculation

A pre-requisite for the calculation of heat release rate is knowledge of the combustion chamber (also referred to as cylinder in this text) volume at all times during the engine cycle. The combustion chamber volume may be expressed as:

$$V = V_{clear} + \left[A_{bore}\left(l_{con} + r_{crank} - \sigma\right)\right]$$

Equation 4.1

Where A_{bore} is the cylinder bore area, V_{clear} is the clearance volume, r_{crank} is the crank radius, and s the instantaneous stroke.

The area is given by:

$$A_{bore} = \frac{D_{bore}^2}{4}\pi$$

Equation 4.2

And the instantaneous stroke is given by:

$$\sigma = a\cos(\theta) + \sqrt{l_{con}^2 - a^2\sin^2(\theta)}$$

Equation 4.3

Where θ is the crank angle from the TDC position.

4.1.2. Heat release of combustion

The heat release of combustion within the combustion chamber may be calculated by applying the first law of thermodynamics to the combustion chamber volume, by assuming that the cylinder contents display ideal gas behaviour. The cylinder contents are considered to be a single closed system. The apparent heat release is calculated assuming that no mass flow is occurring across the system boundary, and that the system is adiabatic for the calculation of the net heat release. The net heat release is the gross heat released by the combustion plus the heat transferred to the cylinder walls. Due to the temperature of the system being higher than that of its surroundings for most of the cycle, the heat transfer will occur spontaneously from the system to its surroundings by second law of thermodynamics. Hence the heat transferred to the cylinder walls will mostly assume a negative value by thermodynamic convention. This can be written as follows:

$$\frac{dQ_{net}}{d\theta} = \frac{dQ_{ch}}{d\theta} + \frac{dQ_{ht}}{d\theta}$$

Equation 4.4

By application of the first law of thermodynamics to the system, the net heat release rate must be equal to the rate at which work is done on the piston, plus the rate of change of sensible internal energy of the system. This can be written as:

$$\frac{dQ_{net}}{d\theta} = p\frac{dV}{d\theta} + \frac{dU_s}{d\theta}$$

Equation 4.5

Under the assumption that the system contents follow ideal gas behaviour, Equation 4.5 may be re-written as:

$$\frac{dQ_{net}}{d\theta} = p\frac{dV}{d\theta} + mc_v\frac{dT}{d\theta}$$

Equation 4.6

From the ideal gas law, pressure, volume, mass and temperature are related by the expression:

$$pV = mRT$$

Equation 4.7

Thus it follows that:

$$\frac{dp}{p} + \frac{dV}{V} = \frac{dT}{T}$$

Equation 4.8

So that equation 2.5 may be re-written as:

$$\frac{1}{R}(Vdp + pdV) = mdT$$

Equation 4.9

Equation 4.9 may be used to replace mdT in Equation 4.6, to yield:

$$\frac{dQ_{net}}{d\theta} = \left(1 + \frac{c_v}{R}\right) p\frac{dV}{d\theta} + \frac{c_v}{R} V\frac{dp}{d\theta}$$

Equation 4.10

Since the ratio of specific heats may be expressed as

$$\gamma = \frac{c_p}{c_v},$$

Equation 4.11

And the gas constant as

$$R = c_p - c_v,$$

Equation 4.12

$$\frac{dQ_{net}}{d\theta} = \frac{\gamma}{\gamma - 1} p\frac{dV}{d\theta} + \frac{1}{\gamma - 1} V\frac{dp}{d\theta}$$

Equation 4.13

Equation 4.13 is used to calculate the heat release rate of the combustion process. The algorithm encoded in the data acquisition and data processing programmes calculate $dQ_{net}/d\theta$ for every CA increment (usually 1/5 º crank-angle). The pressure p of any given increment is taken as the average value of the preceding value of pressure p_{n-1}, and that of the present value of pressure p_n. The value of $dp/d\theta$ is the difference in pressure between the values p_n, and p_{n-1}. Hence:

$$\frac{dp}{d\theta} = \frac{p_n - p_{n-1}}{d\theta}$$

Equation 4.14

The value of volume V, is calculated via the algorithm detailed in section 4.1.1., both for the present value of volume V_n, and the preceding value of volume V_{n-1}. The average of both values is used in Equation 4.13 for the calculation of the heat release rate. The value of dV/dθ is given by the difference between the present value of Volume V_n, and the preceding value of volume V_{n-1}. Thus:

$$\frac{dV}{d\theta} = \frac{V_n - V_{n-1}}{d\theta}$$

Equation 4.15

Both the averaging of pressure p and volume V by using the present and preceding values, in the differentiation yielding dp/dθ and that of dV/dθ result in a phase lead of magnitude dθ/2 of the heat release rate with respect to the pressure data.

The values of the ratio of specific heats are assumed to be constant for the compression process, and constant for the expansion process. At TDC the value of γ is switched from the compression value of γ to the expansion value of γ. For the compression process it has been recommended to use a value in the region of $\gamma_{comp} \approx 1.35$, and for the expansion process it is recommended to use a value in between $\gamma_{comp} \approx 1.26$ and $\gamma_{comp} \approx 1.30$ (Heywood, 1988, p. 510).

4.1.3. Cumulative heat release and mass fraction burnt

In order to obtain an indication of the accumulating fraction of the total value of chemical energy released by the fuel at any given crank angle, the cumulative heat release is calculated. This is done by integrating the HRR over the total area over which positive heat release is taking place between the start of injection and the moment of the exhaust valve opening. The Labview code requires the program user to enter the values of crank angle in between which the HRR-analysis and CHR-analysis are to be performed. The CHR is expressed by the integral of equation (2.9) over the desired crank angle domain; thus:

$$dQ_{ch} = \int_{\theta_{start}}^{\theta_{end}} \frac{dQ_{ch}}{d\theta} d\theta$$

Equation 4.16

4.1.4. Global cylinder gas temperature

The global gas temperature within the combustion chamber of the engine, may be estimated under the assumption of homogeneity and ideal gas behaviour of the cylinder contents, using Equation 4.17.

$$T_{gas} = \frac{p_{cyl} \cdot V_{cyl}}{n_{air} \cdot \tilde{R}}$$

Equation 4.17

Where $\tilde{R}$ is the universal molar gas constant.

The simplest assumption that may be used to estimate the global gas temperature is that the number of moles of the gas is constant throughout the engine cycle and is equal to the amount of moles of air inducted by the cylinder during each engine cycle. This assumption is more realistic if the combustion is very lean and the composition of the cylinder gas consists predominantly of air.

4.1.5. Indicated work per engine cycle and indicated mean effective pressure

The net indicated displacement work per engine cycle (W_i) is equal to the cyclic integral of pressure with respect to the cylinder volume over the entire crank-angle domain of the engine cycle.

$$W_i = \oint p \cdot dV$$

Equation 4.18

The indicated mean effective pressure (P_{IME}) of the engine cycle may be calculated from the net indicated displacement work and the swept volume of the engine.

$$P_{IME} = \frac{W_i}{V_d}$$

Equation 4.19

Where the swept volume is defined by the area of the bore and the piston-stroke as:

$$V_d = A_{bore} \cdot \sigma$$

Equation 4.20

4.2. Stoichiometric analysis of the combustion experiments

Definition of variables

Φ	fuel-air equivalence ratio
φ	molar coefficient of injected fuel
a	number of C atoms in one fuel molecule
b	number of H atoms in one fuel molecule
c	number of O atoms in one fuel molecule
d	number of N atoms in one fuel molecule
e	molar coefficient of air
g	molar coefficient of CO_2 in the exhaust gas
h	molar coefficient of CO in the exhaust gas
j	molar coefficient of O_2 in the exhaust gas
k	molar coefficient of N_2 in the exhaust gas
l	molar coefficient of NO in the exhaust gas
m	molar coefficient of NO_2 in the exhaust gas
s	molar coefficient of CH_4 in the exhaust gas
t	molar coefficient of H_2 in the exhaust gas
μ	molar coefficient of N_2 in the intake air
υ	molar coefficient of O_2 in the intake air
ω	molar coefficient of CO_2 in the intake air
π	molar coefficient of H_2O in the intake air
N_{air}	absolute number of moles of fresh air ingested by the engine per cycle
$N_{pollutant}$	absolute number of moles of pollutant emitted by the engine per cycle
M	absolute mass of pollutant molecules emitted per engine cycle
m’	mass of pollutant molecules emitted per net indicated output energy produced by the engine

Subscripts

i	associated with engine inlet gas mixture
e	associated with engine exhaust gas mixture

Superscripts

‘	denotes a dry molar coefficient, measured after the removal of water

4.3. The general combustion equation

The combustion of a fuel molecule comprising carbon, hydrogen, oxygen and nitrogen atoms in air containing O_2, N_2, CO_2 and H_20 in any proportions as its constituents, can be described by Equation 4.21 below:

$$\varphi \cdot C_a H_b O_c N_d + e \cdot (\upsilon \cdot O_2 + \mu \cdot N_2 + \omega \cdot CO_2 + \pi \cdot H_2O)$$
$$\Rightarrow$$
$$g_e \cdot CO_2 + h_e \cdot CO + j_e \cdot O_2 + k_e \cdot N_2 + l_e \cdot H_2O + m_e \cdot NO + q_e \cdot NO_2 + s_e \cdot CH_4 + t_e \cdot H_2$$

Equation 4.21

For lean or stoichiometric combustion, the term t_e may be assumed to be negligible. Thus $t_e \rightarrow 0$. Balancing the atoms on both sides, we now have the general combustion equation:

$$\varphi \cdot C_a H_b O_c N_d + e \cdot (\upsilon \cdot O_2 + \mu \cdot N_2 + \omega \cdot CO_2 + \pi \cdot H_2O)$$
$$=$$
$$g_e \cdot CO_2 + h_e \cdot CO + j_e \cdot O_2 + k_e \cdot N_2 + l_e \cdot H_2O + m_e \cdot NO + q_e \cdot NO_2 + s_e \cdot CH_4$$

Equation 4.22

4.3.1. System of four linear equations

The number of atoms present in the reactant species is equal to that of the number of atoms present in the product species. In particular, this balance of atoms is true for each type of atom present in the combustion reaction because no changes in the type of atoms occur, i.e. to the C, H, O and N atoms individually. The four atomic balances can be coupled together, and are sufficient to fully determine the combustion reaction. This can be done in matrix form, in which the matrix A is the matrix of coefficients for the four unknowns φ, e, k_e and l_e, b is the vector of the four unknowns, and c is the vector of constant terms.

$$[A]\cdot[b]=[c]$$

Equation 4.23

The solution to the vector of unknowns b in this system can be found by multiplying both sides of Equation 4.23 by the inverse of A, i.e. A^{-1}.

$$[b]=[A^{-1}]\cdot[c]$$

Equation 4.24

Writing the four simultaneous linear equations the balance of the C, H, O and N atoms, yields the matrix equation shown in Equation 4.24 below. The first row describes the carbon balance, the second row the hydrogen balance, the third row the oxygen balance and the fourth row describes the nitrogen balance.

$$\begin{bmatrix} a & \omega & 0 & 0 \\ b & 2\cdot\pi & 0 & -2 \\ c & (2\cdot\upsilon+2\cdot\omega+\pi) & 0 & -1 \\ d & 2\cdot\mu & -2 & 0 \end{bmatrix}\cdot\begin{bmatrix} \varphi \\ e \\ k_e \\ l_e \end{bmatrix}=\begin{bmatrix} g_e+h_e+s_e \\ 4\cdot s_e \\ 2\cdot g_e+h_e+2\cdot j_e+m_e+2\cdot q_e \\ m_e+q_e \end{bmatrix}$$

Equation 4.25

As shown in Equation 4.23 and Equation 4.24, this system may be solved by multiplying both sides of the equation by the inverse of A. This yields a solution to the vector of unknowns b as follows:

$$\begin{bmatrix} \varphi \\ e \\ k_e \\ l_e \end{bmatrix}=\left[\begin{bmatrix} a & \omega & 0 & 0 \\ b & 2\cdot\pi & 0 & -2 \\ c & (2\cdot\upsilon+2\cdot\omega+\pi) & 0 & -1 \\ d & 2\cdot\mu & -2 & 0 \end{bmatrix}\right]^{-1}\cdot\begin{bmatrix} g_e+h_e+s_e \\ 4\cdot s_e \\ 2\cdot g_e+h_e+2\cdot j_e+m_e+2\cdot q_e \\ m_e+q_e \end{bmatrix}$$

Equation 4.26

4.3.2. Calculation of the equivalence ratio Φ

In order to determine the equivalence ratio under which combustion is taking place, the combustion equation for complete combustion of the fuel at a stoichiometric fuel to air ratio needs to be found. Assuming stoichiometric conditions and complete combustion, so that the only species present in the exhaust gas are CO_2, N_2 and H_2O. The general combustion equation can thus be written as:

$$\varphi \cdot C_a H_b O_c N_d + e \cdot (\upsilon \cdot O_2 + \mu \cdot N_2 + \omega \cdot CO_2 + \pi \cdot H_2O) \Rightarrow g_e \cdot CO_2 + k_e \cdot N_2 + l_e \cdot H_2O$$

Equation 4.27

In order to calculate the stoichiometric fuel to air ratio, knowledge of the fuel composition in terms of its relative molar quantities of carbon, hydrogen, oxygen and nitrogen atoms, as well as the air composition in terms of its relative amounts of oxygen and nitrogen present. Thus, knowledge of the variables a, b, c, d and μ is required to balance Equation 4.27. For simplicity, φ will be defined as being equal to unity. Thus:

$$\varphi \equiv 1$$

Equation 4.28

The balance of carbon atoms

$$g_e = a + e \cdot \omega$$

Equation 4.29

The balance of hydrogen atoms

$$b + 2 \cdot \pi \cdot e = 2 \cdot l_e$$

Equation 4.30

$$l_e = \frac{b + 2 \cdot \pi \cdot e}{2}$$

Equation 4.31

The balance of oxygen atoms

$$c + e(2 \cdot \upsilon + 2 \cdot \omega + \pi) = 2 \cdot g_e + l_e$$

Equation 4.32

The balance of nitrogen atoms

$$d + 2 \cdot e \cdot \mu = 2 \cdot k_e$$

Equation 4.33

$$k_e = \frac{d + 2 \cdot e \cdot \mu}{2}$$

Equation 4.34

Combining the carbon, hydrogen and oxygen balances yields: Substituting Equation 4.29 and Equation 4.31 into Equation 4.32 yields:

$$c + e\left(2 \cdot \upsilon + 2 \cdot \omega + \pi\right) = 2 \cdot \left(a + e \cdot \omega\right) + \frac{b + 2 \cdot \pi \cdot e}{2}$$

Equation 4.35

$$\rightarrow \quad e = \frac{2 \cdot a + \frac{b}{2} - c}{2 \cdot \upsilon}$$

Equation 4.36

The molar coefficient e can thus be calculated from the amounts of carbon, hydrogen and oxygen atoms present in the fuel, i.e. the variables a, b, c and the variable υ, describing the relative oxygen content in the air.

4.3.3. The equivalence ratio Φ of a combustion experiment

As described earlier, the equivalence ratio is a measure of the relative amounts of fuel to air compared with the amounts of fuel to air for a stoichiometric mixture, and can be described by Equation 4.37 below.

$$\Phi = \frac{\varphi_{\exp eriment} \cdot e_{stoichiometric}}{\varphi_{stoichiometric} \cdot e_{\exp eriment}}$$

Equation 4.37

As Equation 4.37 demonstrates, knowledge of the molar mass of the fuel and air are thus not necessary for the calculation of the equivalence ratio. The coefficients φ and e are calculated via the solution of Equation 4.26 for experimental conditions, and Equation 4.28 and Equation 4.36 for stoichiometric conditions respectively.

A simplified model for the stoichiometric analysis of the combustion experiments was developed. On the basis of experimental measurements, this model yields the global equivalence ratio of combustion, the fuel and oxygen consumption of the engine, and the power- or fuel-specific emission of pollutant gases and particulate matter. At the heart of the stoichiometric analysis lies the combustion equation, which describes the chemical reactions taking place. The analytical model and solution process were developed in order to balance the combustion equation in terms of its carbon (C), hydrogen (H), oxygen (O) and nitrogen (N) atoms, from experimentally determined values of volumetric exhaust-gas concentrations and composition of fuel and oxidant streams. Further details about the detailed derivations of this stoichiometry analysis model can be found in Appendix A.

4.3.4. Simplified combustion model

For the purpose of practical combustion experiments in engines, the general combustion equation may be simplified by using a fixed oxygen concentration in the fresh intake air, and neglecting the small concentrations of H_2O and CO_2 in the fresh intake air. The simplified combustion model yields very similar results to the detailed combustion model, and commends itself for practical use due to its greater simplicity. The combustion of a fuel molecule comprising carbon, hydrogen, oxygen and nitrogen atoms in simplified air, consisting only of oxygen and nitrogen can thus be described by Equation 4.38:

$$\varphi \cdot C_a H_b O_c N_d + e \cdot (O_2 + \mu \cdot N_2) \Rightarrow g_e \cdot CO_2 + h_e \cdot CO + j_e \cdot O_2 + k_e \cdot N_2 + l_e \cdot H_2O + m_e \cdot NO + q_e \cdot NO_2 + s_e \cdot CH_4 + t_e \cdot H_2$$

Equation 4.38

For lean combustion, the term t_e is assumed to be negligible. Thus $t_e \rightarrow 0$. Balancing the atoms on both sides, we now have the general combustion equation:

$$\varphi \cdot C_a H_b O_c N_d + e \cdot (O_2 + \mu \cdot N_2) = g_e \cdot CO_2 + h_e \cdot CO + j_e \cdot O_2 + k_e \cdot N_2 + l_e \cdot H_2O + m_e \cdot NO + q_e \cdot NO_2 + s_e \cdot CH_4$$

Equation 4.39

4.3.5. Balancing the atoms in the combustion equation

The number of atoms present in the reactant species is equal to that of the number of atoms present in the product species. In particular, this balance of atoms is true for each type of atom present in the combustion reaction because no changes in the type of atoms occur, i.e. to the C, H, O and N atoms individually. Every atomic balance is described by one mathematical equation as shown below:

The balance of carbon atoms

Consider the simplified general combustion reaction given by Equation 4.39. The balance of carbon atoms is described by the following equation:

$$\varphi \cdot a = g_e + h_e + s_e$$

Equation 4.40

The balance of hydrogen atoms

The balance of hydrogen atoms in Equation 4.39 is described by:

$$\varphi \cdot b = 2 \cdot l_e + 4 \cdot s_e$$

Equation 4.41

This may be re-arranged as:

$$\varphi \cdot b - 2 \cdot l_e = 4 \cdot s_e$$

Equation 4.42

The balance of oxygen atoms

The balance of oxygen atoms in Equation 4.39 is described by:

$$\varphi \cdot c + 2 \cdot e = 2 \cdot g_e + h_e + 2 \cdot j_e + l_e + m_e + 2 \cdot q_e$$

Equation 4.43

This may be re-arranged as:

$$\varphi \cdot c + 2 \cdot e - l_e = 2 \cdot g_e + h_e + 2 \cdot j_e + m_e + 2 \cdot q_e$$

Equation 4.44

The balance of nitrogen atoms

The balance of nitrogen atoms in Equation 4.39 is described by:

$$\varphi \cdot d + 2 \cdot e \cdot \mu = 2 \cdot k_e + m_e + q_e$$

Equation 4.45

This may be re-arranged as:

$$\varphi \cdot d + 2 \cdot e \cdot \mu - 2 \cdot k_e = m_e + q_e$$

Equation 4.46

4.3.6. System of four linear equations

The four atomic balances can be coupled together, and are sufficient to fully determine the combustion reaction. This can be done in matrix form, in which the matrix A is the matrix of coefficients for the four unknowns φ, e, k_e and l_e, b is the vector of the four unknowns, and c is the vector of constant terms.

$$[A]\cdot[b]=[c]$$

Equation 4.47

The solution to the vector of unknowns b in this system can be found by multiplying both sides of Equation 4.49 by the inverse of A, i.e. A^{-1}.

$$[b]=[A^{-1}]\cdot[c]$$

Equation 4.48

Writing the four simultaneous linear equations of Equation 4.40, Equation 4.42, Equation 4.44, Equation 4.46 in matrix form, yields the matrix equation shown in Equation 4.49 below. The first row describes the carbon balance, the second row the hydrogen balance, the third row the oxygen balance and the fourth row describes the nitrogen balance.

$$\begin{bmatrix} a & 0 & 0 & 0 \\ b & 0 & 0 & -2 \\ c & 2 & 0 & -1 \\ d & 2\cdot\mu & -2 & 0 \end{bmatrix}\cdot\begin{bmatrix} \varphi \\ e \\ k_e \\ l_e \end{bmatrix}=\begin{bmatrix} g_e+h_e+s_e \\ 4\cdot s_e \\ 2\cdot g_e+h_e+2\cdot j_e+m_e+2\cdot q_e \\ m_e+q_e \end{bmatrix}$$

Equation 4.49

As shown in Equation 4.47 and Equation 4.48 before, this system may be solved by multiplying both sides of the equation by the inverse of A. This yields a solution to the vector of unknowns b as follows:

$$\begin{bmatrix} \varphi \\ e \\ k_e \\ l_e \end{bmatrix}=\begin{bmatrix} a & 0 & 0 & 0 \\ b & 0 & 0 & -2 \\ c & 2 & 0 & -1 \\ d & 2\cdot\mu & -2 & 0 \end{bmatrix}^{-1}\cdot\begin{bmatrix} g_e+h_e+s_e \\ 4\cdot s_e \\ 2\cdot g_e+h_e+2\cdot j_e+m_e+2\cdot q_e \\ m_e+q_e \end{bmatrix}$$

Equation 4.50

4.3.7. Calculation of wet molar fractions from dry molar fractions

The solution of the system of linear equations described in Equation 4.50, relies on the knowledge of the wet molar concentrations of CO, CO_2, O_2, NO, NO_2 and CH_4. Under laboratory conditions, it is usually most practical to measure dry concentrations of all exhaust gas concentration except CH_4. Thus, in order to fully solve Equation 4.50, the calculation of the wet molar concentrations of CO, CO_2, O_2, NO, NO_2 is necessary. This can be done by subtracting the water content from the dry molar fractions these gases, assuming that the water content in every of these gases is the same, as would be under ideal gas conditions. The equations relating the wet molar fractions to the dry molar fractions of each of these gases are thus as follows:

Wet molar fraction of CO_2

$$h_e = (1 - l_e) \cdot h'_e$$

Equation 4.51

Wet molar fraction of CO

$$g_e = (1 - l_e) \cdot g'_e$$

Equation 4.52

Wet molar fraction of O_2

$$j_e = (1 - l_e) \cdot j'_e$$

Equation 4.53

Wet molar fraction of NO

$$m_e = (1 - l_e) \cdot m'_e$$

Equation 4.54

Wet molar fraction of NO_2

$$q_e = (1 - l_e) \cdot q'_e$$

Equation 4.55

Equation 4.51 to Equation 4.55 emphasise that the calculation of the wet molar fraction of CO, CO_2, O_2, NO, NO_2 require knowledge of the fraction of water vapour present in the exhaust gas.

4.3.8. Exhaust gas water fraction

The fraction of water vapour present in the exhaust gas can be calculated from the hydrogen balance equation and the carbon balance equation, represented by Equation 4.56 and Equation 4.58 respectively, as shown in the following procedure:

Carbon atom balance

$$\varphi \cdot a = g_e + h_e + s_e$$

Equation 4.56

$$\varphi = \frac{g_e + h_e + s_e}{a}$$

Equation 4.57

Hydrogen atom balance

$$\varphi \cdot b = 2 \cdot l_e + 4 \cdot s_e$$

Equation 4.58

$$\varphi = \frac{2 \cdot l_e + 4 \cdot s_e}{b}$$

Equation 4.59

Carbon and hydrogen balances in conjunction: Equating the terms of Equation 4.57 to those of Equation 4.59, and solving for the exhaust gas water fraction l_e yields:

$$\frac{g_e + h_e + s_e}{a} = \frac{2 \cdot l_e + 4 \cdot s_e}{b}$$

Equation 4.60

$$b \cdot (g_e + h_e + s_e) = 2 \cdot a \cdot l_e + 4 \cdot a \cdot s_e$$

Equation 4.61

$$l_e = \frac{b \cdot (g_e + h_e + s_e) - 4 \cdot a \cdot s_e}{2 \cdot a}$$

Equation 4.62

Replacing the wet molar fractions of CO_2 and CO by the dry molar fraction of CO_2 and CO, as per Equation 4.51 and Equation 4.52 respectively yields:

$$l_e = \frac{b \cdot (1 - l_e) \cdot (g'_e + h'_e) + b \cdot s_e - 4 \cdot a \cdot s_e}{2 \cdot a}$$

Equation 4.63

$$2 \cdot a \cdot l_e = b \cdot g'_e + b \cdot h'_e - b \cdot l_e \cdot g'_e - b \cdot l_e \cdot h'_e + s_e \cdot (b - 4 \cdot a)$$

Equation 4.64

$$2 \cdot a \cdot l_e + b \cdot l_e \cdot g'_e + b \cdot l_e \cdot h'_e = b \cdot g'_e + b \cdot h'_e + s_e \cdot (b - 4 \cdot a)$$

Equation 4.65

$$l_e \cdot (2 \cdot a + b \cdot g'_e + b \cdot h'_e) = b \cdot g'_e + b \cdot h'_e + s_e \cdot (b - 4 \cdot a)$$

Equation 4.66

$$l_e = \frac{b \cdot g'_e + b \cdot h'_e + s_e \cdot (b - 4 \cdot a)}{2 \cdot a + b \cdot g'_e + b \cdot h'_e}$$

Equation 4.67

The fraction of water vapour present in the exhaust gas can thus be calculated from knowledge of the relative amounts of carbon and hydrogen atoms present in the fuel, in conjunction with the dry concentrations of CO_2, CO and the wet concentration of CH_4 in the exhaust gas. This completes the values necessary to fully determine the relative molar quantities of molecular species taking part in the combustion, according to the general combustion Equation 4.39.

4.3.9. Considerations on Nitrogen oxides

The exhaust gas concentration of NO is defined as m_e, and the exhaust gas concentration of NO_2 is defined as q_e. The total concentration of oxides of nitrogen (NO_x) shall be defined as the combined concentration of NO and NO_2, and shall be denoted by o_e. Thus:

$$o_e = q_e + m_e$$

Equation 4.68

Similarly, the ratio of the concentration of NO_2/NO, is given by υ_e. Thus:

$$\upsilon_e = \frac{q_e}{m_e}$$

Equation 4.69

The value of υ_e can be measured by operating the engine at steady state, and switching the nitrogen oxide analyser in between NO and NO_2 measurement modes. In cases in which the time available to take this measurement is limited, e.g. during experiments with very small quantities of fuels, an assumption for this value can be made. This assumption is based upon the values provided by Heywood (1988, p.577-578). In this case NO_2 is assumed to be 10% of the total NO_x (i.e. υ_e=1/9).
The concentration of NO (m_e) and the concentration of NO_2 (q_e) may thus be represented by the concentration of NO_x (o_e) and the ratio of NO and NO_2, υ_e. Thus, rearranging Equation 4.68 gives:

$$q_e = o_e - m_e$$

Equation 4.70

Equation 4.70 may be re-written as:

$$q_e = o_e - \frac{m_e}{q_e} q_e$$

$\rightarrow$

Equation 4.71

$$q_e + \frac{m_e}{q_e} q_e = o_e$$

$\rightarrow$

Equation 4.72

$$q_e \left(1 + \frac{m_e}{q_e} \right) = o_e$$

$\rightarrow$

Equation 4.73

Substituting Equation 4.69 for q_e and m_e yields the molar fraction of NO_2 as a function of the values o_e and υ_e:

$$q_e = \frac{o_e}{\left(1 + \frac{1}{\upsilon_e} \right)}$$

Equation 4.74

Similarly the molar fraction of NO (m_e) may thus be expressed as a function of o_e and υ_e:

$$m_e = \frac{o_e}{(1 + \upsilon_e)}$$

Equation 4.75

4.3.10. Calculation of the equivalence ratio Φ

In order to determine the equivalence ratio under which combustion is taking place, the combustion equation for complete combustion of the fuel at a stoichiometric fuel to air ratio needs to be found. Assuming stoichiometric conditions and complete combustion, the only species present in the exhaust gas are CO_2, N_2 and H_2O. The general combustion equation can thus be written as:

$$\boxed{\begin{array}{c}\varphi \cdot C_a H_b O_c N_d + e \cdot \left(O_2 + \mu \cdot N_2\right) \\ \Rightarrow \\ g_e \cdot CO_2 + k_e \cdot N_2 + l_e \cdot H_2O\end{array}}$$

Equation 4.76

In order to calculate the stoichiometric fuel to air ratio, knowledge of the fuel composition in terms of its relative molar quantities of carbon, hydrogen, oxygen and nitrogen atoms, as well as the air composition in terms of its relative amounts of oxygen and nitrogen present. Thus, knowledge of the variables a, b, c, d and μ is required to balance Equation 4.76. For simplicity, φ will be defined as being equal to unity. Thus:

$$\varphi \equiv 1$$

Equation 4.77

The balance of carbon atoms yields

$$g_e = a$$

Equation 4.78

The balance of hydrogen atoms yields

$$b = 2 \cdot l_e$$

Equation 4.79

$$l_e = \frac{1}{2} \cdot b$$

Equation 4.80

The balance of oxygen atoms yields

$$c + 2 \cdot e = 2 \cdot g_e + l_e$$

Equation 4.81

$$e = \frac{2 \cdot g_e + l_e - c}{2}$$

Equation 4.82

Replacing g_e and l_e through Equation 4.78 and Equation 4.80 yields:

$$e = \frac{2 \cdot a + \frac{b}{2} - c}{2}$$

Equation 4.83

The molar coefficient e at stoichiometric conditions can thus be calculated from the amounts of carbon, hydrogen and oxygen atoms present in the fuel, i.e. the variables a, b and c.

The balance of nitrogen atoms yields

$$d + 2 \cdot e \cdot \mu = 2 \cdot k_e$$

Equation 4.84

$$k_e = \frac{d + 2 \cdot e \cdot \mu}{2}$$

Equation 4.85

Since φ and e have now been defined, the equivalence ratio Φ of the experiment may now be calculated as shown in the following section.

The equivalence ratio Φ of a combustion experiment

The equivalence ratio is a measure of the relative gravimetric amounts of fuel to air compared with the gravimetric amounts of fuel to air for a stoichiometric mixture.

$$\Phi = \frac{\left(\frac{m_{fuel}}{m_{air}}\right)_{Experiment}}{\left(\frac{m_{fuel}}{m_{air}}\right)_{Stoichiometric}}$$

Equation 4.86

The relative mass of the fuel and air taking part in the combustion reaction is defined by the reaction coefficients of fuel and air, and the relative molecular masses of fuel and air. Care must be taken in referring to the molar mass of air, since air is not a homogeneous fluid, but in this model consists of N_2 and O_2 molecules in the relative quantities described by the variable μ. Thus, the molecular mass of air shall be taken as the average weight of a generic air molecule, having taken into consideration the relative amounts of N_2 and O_2 present in the air, as per Equation 4.92 further below.

$$\left(\frac{m_{fuel}}{m_{air}}\right)_{Experiment} = \frac{\varphi_{Experiment} \cdot \left(m_{C_aH_bO_cN_d}\right)}{e_{Experiment} \cdot (1+\mu) \cdot m_{\frac{O_2+\mu \cdot N_2}{1+\mu}}}$$

Equation 4.87

$$\left(\frac{m_{fuel}}{m_{air}}\right)_{Stoichiometric} = \frac{\varphi_{Stoichiometric} \cdot \left(m_{C_aH_bO_cN_d}\right)}{e_{Stoichiometric} \cdot (1+\mu) \cdot m_{\frac{O_2+\mu \cdot N_2}{1+\mu}}}$$

Equation 4.88

$$\Phi = \frac{\varphi_{Experiment} \cdot e_{Stoichiometric}}{\varphi_{Stoichiometric} \cdot e_{Experiment}}$$

Equation 4.89

As Equation 4.89 demonstrates, knowledge of the molar mass of the fuel and air are thus not necessary for the calculation of the equivalence ratio. The coefficients φ and e are calculated via the solution of Equation 4.50 for experimental conditions, and Equation 4.77 and Equation 4.83 for stoichiometric conditions respectively.

The gravimetric fuel-air ratio

The gravimetric fuel to air ratio ($FAR_{gravimetric}$) describes the mass of fuel, divided by the mass of air. The molar mass of a fuel molecule or the average mass of an air molecule, can both be calculated from the mass of the atoms of which the molecules comprise. The gravimetric fuel to air ratio ($FAR_{gravimetric}$) can thus be found using Equation 4.90.

$$FAR_{gravimetric} = \frac{m_{fuel}}{m_{air}} = \frac{\varphi \cdot \left(m_{C_aH_bO_cN_d}\right)}{e \cdot (1+\mu) \cdot m_{\frac{O_2+\mu \cdot N_2}{1+\mu}}}$$

Equation 4.90

Table 4.1 below shows the molar masses of the atoms used in the combustion reaction.

Atom	C	H	O	N
Molar mass [g/mol]	12.0107	1.00794	15.9994	14.00674

Table 4.1 – Molar masses of atoms involved in the combustion process

The molar mass of a fuel molecule and the average mass of an air molecule can thus be calculated as follows:

Molar mass of a fuel molecule of the composition $C_aH_bO_cN_d$:

$$m_{C_aH_bO_cN_d} = 12.0107 \cdot a + 1.00794 \cdot b + 15.9994 \cdot c + 14.00674 \cdot d$$

Equation 4.91

Molar mass of an air molecule of the mean composition:

$$\frac{O_2 + \mu \cdot N_2}{1+\mu}$$

May be expressed by the following relation:

$$m_{\frac{O_2+\mu \cdot N_2}{1+\mu}} = \frac{2 \cdot 15.9994 + 2 \cdot \mu \cdot 14.00674}{1+\mu}$$

Equation 4.92

Calculation of fuel consumption

The fuel consumption can be calculated from knowledge of the composition of the exhaust gas and the air-flow through the engine.

$$m_{fuel} = m_{air} \cdot \frac{\varphi_{Experiment} \cdot \left(m_{C_aH_bO_cN_d}\right)}{e_{Experiment} \cdot (1+\mu) \cdot m_{\frac{O_2+\mu \cdot N_2}{1+\mu}}}$$

Equation 4.93

The relative amount of N_2 and O_2 in the air μ, must be known from measurement or literature, the stoichiometry coefficients $\varphi_{Experiment}$ and $e_{Experiment}$ are found through Equation 4.50, whilst the molecular mass of the fuel molecule and the mean molecular mass of air are calculated via Equation 4.91 and Equation 4.92 respectively. Depending on whether the mass of air refers to the mass of air going through the engine per engine revolution, engine cycle, or time unit, the corresponding amount of fuel of the same unit may be calculated via Equation 4.93

4.3.11. Calculation of energy-specific gas and pollutant emissions and oxygen consumption

In order to determine the absolute amount of gases consumed and emitted by the engine, it is necessary to reference any measured gas concentration to an absolute amount of gas. An absolute value of the amount of intake air ingested by the engine was measured experimentally, using a positive displacement air flow meter. Any pollutant gas concentrations are measured in the exhaust gas. Thus knowledge about an absolute value of the number of exhaust gas molecules, rather than of the intake air molecules is necessary. The solution of the stoichiometry model presented in Equation 4.50, relates the specific amount of exhaust gas molecules to the amount of fresh intake air molecules. Thus, from the amount of air ingested by the engine, and measurement of the exhaust gas concentrations, the total amount of exhaust gas can be calculated via the stoichiometry model previously described.

Referring to the general combustion reaction presented by Equation 4.39, the total number of intake air molecules is described by the term:

$$\mathrm{I} = e \cdot (1+\mu)$$

Equation 4.94

The total number of exhaust gas molecules is described by the term:

$$\mathrm{E} = g_e + h_e + j_e + k_e + l_e + m_e + q_e + s_e$$

Equation 4.95

Thus the ratio of exhaust gas molecules versus fresh intake air may be described as:

$$\frac{\mathrm{E}}{\mathrm{I}} = \frac{g_e + h_e + j_e + k_e + l_e + m_e + q_e + s_e}{e \cdot (1 + \mu)}$$

Equation 4.96

Calculation of energy-specific pollutant emissions

This can be used to calculate the absolute number of moles of pollutant molecules $N_{pollutant}$ emitted from the engine per engine cycle, via Equation 4.97 below. The variable f_e represents a generic concentration of a gas or pollutant gas, and may be substituted by any of the following variables {g_e, h_e, j_e, k_e, l_e, m_e, q_e, s_e}, and N_{air} represents the number of moles of fresh air ingested by the engine per cycle:

$$N_{Pollutant} = N_{air} \cdot \frac{E}{I} \cdot f_e$$

Equation 4.97

The absolute mass of the pollutant molecules emitted from the engine per cycle can be obtained by multiplying the absolute number of moles of pollutant molecules emitted per cycle by the molar mass of the particular pollutant molecules, designated by $(m)_{\text{Pollutant Molecule}}$ in Equation 4.98 below:

$$M_{pollutant} = N_{air} \cdot \frac{E}{I} \cdot f_e \cdot (m)_{Pollutant\,Molecule}$$

Equation 4.98

The mass of pollutant molecules emitted from the engine per net indicated output energy produced by the engine can be calculated by as follows:

$$m'_{pollutant} = \frac{M_{pollutant}}{W_i}$$

Equation 4.99

Where W_i is the net indicated displacement work per engine cycle.

Calculation of oxygen consumption

Finally, the total number of oxygen molecules O_2 consumed by the engine may be calculated via the total number of oxygen atoms bound in new molecular species other than oxygen described by Equation 4.100.

$$N_{O-consumed} = N_{air} \cdot \frac{E}{I} \cdot \left\{2 \cdot g_e + h_e + l_e + m_e + 2 \cdot q_e\right\}$$

Equation 4.100

Whilst the total number of O_2 molecules consumed by the engine is equal to half the number of oxygen atoms consumed. This is described by Equation 4.101.

$$N_{O_2-consumed} = N_{air} \cdot \frac{E}{I} \cdot \frac{\left\{2 \cdot g_e + h_e + l_e + m_e + 2 \cdot q_e\right\}}{2}$$

Equation 4.101

And the total mass of oxygen consumed can be calculated by multiplying the number of moles of O_2 molecules consumed by the molar mass of molecular oxygen, m_{O_2}.

$$m_{Oxygen} = N_{O_2-consumed} \cdot m_{O_2}$$

Equation 4.102

EGR considerations

The volumetric EGR rate shall be denoted by ε, and shall be defined as: The number of moles of exhaust gases that are re-circulated into the intake gas stream, divided by the sum of itself plus the number of moles of fresh intake air molecules. The fuel is excluded from this fraction by this definition. The EGR rate can be estimated using knowledge of the fresh intake air composition, the intake gas concentrations of CO_2 after the EGR has been added, and the exhaust gas concentration of CO_2.

Hot EGR (wet)

EGR shall be referred to as 'hot-EGR' if the exhaust gas is recirculated directly into the gas stream ingested by the engine, so that no water or other gas is eliminated by condensation. For hot EGR, the volumetric EGR rate is equal to the wet concentration of CO_2 in the gas mixture ingested by the engine, divided by the wet concentration of CO_2 in the exhaust gas. This is true for a simplified composition of air as assumed throughout this combustion model, which does not contain any CO_2 as described by the general combustion Equation 4.38 and Equation 4.39.

The intake gas concentration of CO_2 after the EGR has been added is measured on a dry basis. The same is true for the exhaust gas concentration of CO_2. Thus, in order to determine the EGR rate exactly, the wet concentration of CO_2 must be calculated from the dry concentration of CO_2. In the case of the exhaust gas, the wet concentration of CO_2 can be calculated using Equation 4.51 in conjunction with Equation 4.67. In the case of the intake gas concentration of CO_2 after the EGR has been added, the following derivation may be used to calculate the wet concentration of CO_2 in the intake gas after mixing with recirculated exhaust gas has taken place:
If hot EGR is used, the volumetric EGR rate can thus be measured as:

$$\varepsilon_{hot} = \frac{g_i}{g_e} = \frac{g'_i \cdot (1 - l_i)}{g'_e \cdot (1 - l_e)}$$

Equation 4.103

Assuming that the fresh atmospheric air is dry, as has been throughout the entire model, the concentration of water in the intake gas mixture can be described by the concentration of water in the exhaust gas and the EGR rate:

$$l_i = l_e \cdot \varepsilon_{hot}$$

Equation 4.104

Substituting Equation 4.104 into Equation 4.103, yields:

$$\varepsilon_{hot} = \frac{g'_i \cdot (1 - l_e \cdot \varepsilon_{hot})}{g'_e \cdot (1 - l_e)}$$

Equation 4.105

Progressively rearranging this gives an expression for the hot EGR rate (Equation 4.109) based on the dry intake and exhaust gas concentrations.

$$\varepsilon_{hot} = \frac{g'_i - l_e \cdot g'_i \cdot \varepsilon_{hot}}{g'_e \cdot (1 - l_e)}$$

Equation 4.106

$$\varepsilon_{hot} + \varepsilon_{hot}\left(\frac{l_e \cdot g'_i}{g'_e \cdot (1 - l_e)}\right) = \frac{g'_i}{g'_e \cdot (1 - l_e)}$$

Equation 4.107

$$\varepsilon_{hot}\left(1 + \frac{l_e \cdot g'_i}{g'_e \cdot (1 - l_e)}\right) = \frac{g'_i}{g'_e \cdot (1 - l_e)}$$

Equation 4.108

$$\varepsilon_{hot} = \frac{\frac{g'_i}{g'_e \cdot (1 - l_e)}}{\left(1 + \frac{l_e \cdot g'_i}{g'_e \cdot (1 - l_e)}\right)}$$

Equation 4.109

The hot EGR rate can thus be calculated on the basis of the dry intake and exhaust CO_2 concentrations and knowledge of the exhaust water concentration le, which was calculated previously using Equation 4.67.

Cold EGR (dry)

The EGR passes through a water-cooled heat exchanger which cools the EGR gas to intake air temperature and extracts most of the water from the exhaust gas (see Figure 4.1).

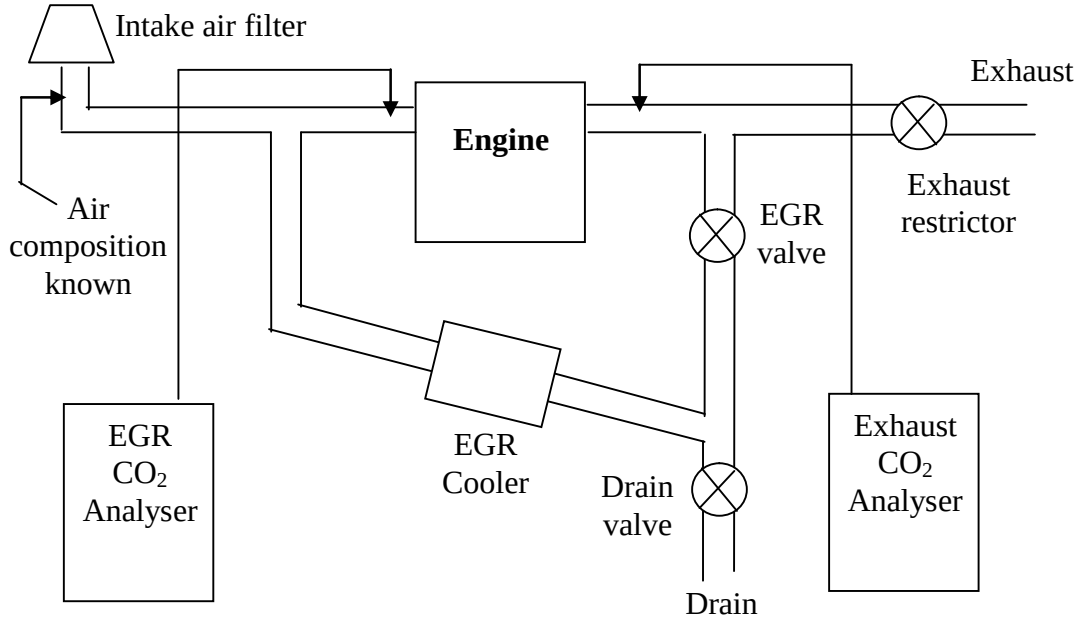

Figure 4.1 – Cold-EGR configuration on the test engine

If the EGR is cooled so that all water is extracted from the gas, and subsequently brought back to the temperature of the fresh air taken into the engine from the atmosphere, then both the intake and exhaust gas, which are mixed together to form the gas mixture that is ingested into the engine, are completely dry. Under these circumstances, and assuming that the fresh intake air contains no CO_2 itself, as consistently done throughout this model, the cold EGR rate may be determined from the dry concentration of CO_2 in the gas mixture ingested into the engine after the addition of EGR, and the dry concentration of CO_2 in the exhaust gas only. This may be written as:

$$\varepsilon_{cold} = \frac{g'_i}{g'_e}$$

Equation 4.110

It is of course not practical to extract all water out of the exhaust gas. If the exhaust gas is cooled to the temperature of the atmospheric air, the water content will at least be similar to that of the ambient air. Since the water content of the ambient air is assumed to be negligible within this model, it is fair to assume that the water content of the cooled EGR gas may also be ignored.

4.3.12. Particulate matter measurements

Particulate measurements on the engine were carried out using a differential particulate spectrometer. The spectrometer measures particulate number, and correlates this to the mass of the particulates to these using an estimate for density and shape factor of the particulates. The instrument yields calibrated readings in terms of particulate number and mass per cc of exhaust gas at standard temperature and pressure (i.e. 273.15 K and 1 atm absolute pressure). In order to calculate the total particulate number and mass data, the total amount of exhaust gas emitted from the engine is thus calculated, assuming ideal gas behaviour. Thus the exhaust gas volume may be calculated as:

$$V_{Exhaust} = \frac{N_{Exhaust} \cdot R \cdot T}{p_{atm.}}$$

Equation 4.111

Where:

$$N_{Exhaust} = N_{air} \cdot \frac{E}{I}$$

Equation 4.112

N_{air} is the total number of moles of fresh intake air flow measured through the engine, and E/I is calculated as per Equation 4.96.

4.3.13. Number of moles of fresh intake air

The number of moles of fresh intake air can be measured using a positive displacement volumetric air-flow meter at known conditions of pressure and temperature, and applying the ideal gas law:

$$p \cdot V = n \cdot R \cdot T$$

Equation 4.113

Thus:

$$N_{air} = \frac{R \cdot T_{air}}{p_{air} \cdot V_{air}}$$

Equation 4.114

The stoichiometric analysis models have been encoded for ‘Matlab 6.1’ The source codes for four versions of the model can be found in electronic format on a CD (Appendix G).

Chapter 5. The influence of molecular structure of fatty acid monoalkyl esters on diesel combustion

The present chapter describes a series of experiments conducted on a single-cylinder research engine investigating the influence of molecular structure on the combustion behaviour of fatty acid alcohol ester (biodiesel) molecules under diesel engine conditions. The fuels employed in these experiments consisted in various samples of pure individual fatty acid alcohol ester molecules of different structure, as well as several mixtures of such molecules. The latter consisted in biodiesel fuels produced by the transesterification of naturally occurring plant oils or animal fat with a monohydric alcohol.

It was observed that the molecular structure of the fuel significantly influenced the formation of NO_x and particulate matter and their respective concentration in the exhaust gas. The influence on the formation of NO_x in particular, appeared to be exerted firstly through the effect which the molecular structure had on the auto-ignition delay occurring after the fuel was injected into the combustion chamber, and secondly through the flame temperature at which the various molecules burned. The emission of particulates on the other hand showed correlation with the number of double bonds in the fuel molecules for the case of larger accumulation mode particles, and with the boiling point of the fuel samples for the case of the smaller, nucleation mode particles.

The effect of ignition delay on the exhaust emissions of these pollutants was isolated by adding the ignition promoting molecule 2-ethylhexyl nitrate to some of the fuel samples in closely specified concentrations, so as to equalise the ignition delay for the relevant fuel samples. The removal of the ignition delay as a main influence on the combustion process enabled the observation of the lesser effects of adiabatic flame temperature.

5.1. Introduction

The combustion of biomass-derived liquid fuels such as biodiesel has gained significant importance in practical combustion systems such as diesel engines. An understanding of the physical and chemical processes occurring during their combustion, especially those which significantly influence the thermal efficiency and the formation of pollutants is important, not least, for the development of better alternatives.

Biodiesel is defined as a liquid hydrocarbon fuel composed of fatty acid monohydric alcohol esters whose molecular composition may change according to the feed-stocks used for the fuel synthesis (Chavanne, 1937). Differences in molecular structure influence the physical and chemical processes occurring during the atomisation, vaporisation and combustion of the fuel after it is injected into the combustion chamber. These differences lead to distinctive patterns in fuel energy release rates and pollutant formation from various molecules.

Several researchers have reported that the combustion of biodiesel in diesel engines tends to result in lower emissions of particulate mass (PM), unburned hydrocarbons (UHC) and carbon monoxide (CO) with respect to fossil diesel fuel, along with a small increase in the emission of nitrogen oxides (NO_x) (Pischinger, et al, 1982; Geyer et al, 1983; Geyer, et al., 1984; Mittelbach, et al., 1985; Schumacher, et al., 1996; Graboski & McCormick, 1998; Graboski, et al., 2000; Graboski, et al., 2003; Zhang & Boehman, 2007). The reasons for these changes are still not fully understood, and are expected to depend in detail on the mixture of chemical species present in the biodiesel fuel.

It is generally accepted that the low particulate mass emission from biodiesel is a result of the fuel-bound oxygen, which lowers the oxygen equivalence ratio (Φ) of combustion in the fuel-rich zones of the fuel spray, and aids the oxidation of soot and its precursors. An optical study of biodiesel flames has shown that Φ at the lift-off length of biodiesel-fuelled diesel engine flames is significantly lower than for a primary reference fuel representative of fossil diesel fuel, if the fuel-bound oxygen of biodiesel is taken into account (Cheng, et al., 2006). This could provide a plausible explanation for the lower rate of formation of soot and its precursors within the fuel-rich premixed flames of the combustion process. The fuel-bound oxygen content and the type of functional moiety by which the oxygen is bound, have both been reported to play a significant role in the reducing the formation of soot from the diesel combustion process (Pepiot-Desjardins, et al., 2008).

The low emission of unburned hydrocarbons associated with biodiesel fuel is commonly attributed to its high ignition quality and thus its short ignition delay, which reduces the formation of overly lean mixtures from the fuel spray. Lean mixtures of fuel in air that are too lean to support autoignition or flame propagation, can form by over-mixing of the fuel spray with its surrounding air, during excessively long ignition delay periods (Heywood, 1988, pp. 622-623; Ladommatos, et al., 1996[a]). These are thought to be a major source of incomplete combustion products such as UHC, due to their failure of undergoing combustion.

The reduction in the emission of CO from biodiesel is generally explained by a leaner combustion stoichiometry in terms of the oxygen equivalence ratio Φ, as previously described with regards to the soot emissions.

The reasons behind the elevated NO_x emissions from the combustion of biodiesel are not yet as clear. A number of hypotheses have been advanced on the cause of the high NO_x emissions from the combustion of biodiesel. Detailed reviews of the literature on the subject have been written (Graboski & McCormick, 1998; United States Environmental Protection Agency, 2002; Lapuerta, et al., 2008[a]). Five main hypotheses appear to provide the most plausible explanations, and shall be discussed in the ensuing section:

Firstly, an advance in the fuel injection timing due to biodiesel has been reported in engines utilising mechanical injection systems in which the fuel is used as a medium of timing the injection. In these types of engines, actuation of the injector is achieved by transmitting a pressure wave from the plunger of the fuel pump to the injector. This actuation method incurs a small delay due to the compressibility of the fuel. It has been demonstrated by measurements of the physical properties, that biodiesel has lower compressibility, quantified by a higher bulk modulus, and a higher speed of

sound than fossil diesel fuel. Engine experiments have shown that the lower compressibility and higher speed of sound of biodiesel fuel can significantly shorten the injection delay with respect to fossil diesel fuel. This results in an advanced start of injection of biodiesel fuel with respect to fossil diesel fuel (Ziejewski, et al., 1985; Gouw & Vlugter, 1964; Rolling & Vogt, 1960; Tat, et al., 2000; Monyem & van Gerpen, 2001; Szybist & Boehman, 2003). This advance in injection timing leads not only to higher peak cylinder temperatures, but also to an advanced timing of this maximum cylinder temperature (Szybist, et al., 2005). An earlier timing of peak temperature is thought to allow for a longer period of time during which the condition of the combustion are conducive to the formation of NO_x, before the reactions are frozen in the expansion stroke. Studies carried out using common rail fuel injection systems have shown that this phenomenon does not apply to modern electronically controlled common rail injection systems (Choi, et al., 1997; Zhang & Boehman, 2007; Cheng, et al., 2006), but that an observed increase in NO_x emissions still persists.

Secondly, it has been suggested that the observed increase in NO_x emission may be attributable to the higher cetane number of biodiesel with respect to fossil diesel fuel. According to this theory, the higher cetane number of biodiesel would lead to a shortening of the ignition delay, which in turn is responsible for advancing the timing of combustion (Scholl & Sorenson, 1993; Zhang & van Gerpen, 1996). Experimental studies have shown though, that under conditions at which the start of injection or the start constant start of combustion are constant, and both occurs in the vicinity of top-dead centre, a decrease in ignition delay will commonly lead to a reduction of NO_x emissions (Ladommatos, et al., 1996[a]; McCormick, et al., 2002). Specifically under such operating conditions, the theory that cetane number increases NO_x emissions does not appear to be sustainable.

Thirdly, it has been suggested that 'prompt NO' formed via the mechanisms described by Fenimore (1971) could be more pronounced in the combustion for biodiesel than in that of fossil diesel fuel (McCormick, et al., 2006). This could be attributed to a higher propensity of biodiesel to form hydrocarbon radicals in fuel rich premixed flames. A recent numerical study employing the well-mixed balloon model (Ban-Weiss, et al., 2007) showed that in the combustion of methyl butanoate, which is a short-chained fatty acid alkyl ester molecule, the Fenimore mechanism is expected to account for approximately 13% of total NO_x formation. It is also well known that prompt NO plays an important role in diesel-like fuels such as kerosene (Fenimore, 1971). Clear evidence that biodiesel, or certain of its species, significantly increase prompt NO formation with respect to fossil diesel fuel has not yet been found.

A fourth theory suggests that the actual flame temperature of biodiesel may be higher than that of fossil diesel fuel, mainly due to lower soot radiative heat transfer from biodiesel flames (Cheng, et al., 2006). It is generally agreed that whilst the combustion of biodiesel produces lesser amounts of soot than fossil diesel fuel, it also tends to produce higher amounts of NO_x (Pischinger, et al., 1982; Mittelbach, et al., 1985; Schumacher, et al., 1996). This could lead to the assumption that the lesser formation of NO_x in fossil diesel fuel may be due to a reduction in flame temperatures from soot radiative heat transfer. Cheng et al. (2006) provided evidence from an optical study that supports this theory.

A fifth hypothesis could be advanced, which suggests that differences in the adiabatic flame temperature between certain biodiesel species and fossil diesel fuel are responsible for an increase in thermally formed NO_x. Ban-Weiss et al (2007) carried out a numerical study on combustion, comparing a double bonded and a single bonded fatty acid alkyl ester molecule. The authors found that the peak flame temperature of the double bonded methyl trans-2-butanoate was 14 K higher than that of the single-bonded methyl butanoate. This change in temperature was found to result in an increase of 21% of NO_x emissions from the combustion event, according to the numerical model. Cheng et al. (2006) carried out calculations of adiabatic flame temperature for a single biodiesel component (methyl oleate) and a primary reference diesel fuel blend consisting of hexadecane and heptamethylnonane. A comparison between these two fuels showed that no significant differences in adiabatic flame temperature existed at stoichiometric conditions (Φ=1), but the calculations were limited to only one monounsaturated biodiesel molecule. Mueller (2008) confirmed by calculation, that the adiabatic flame temperature of polyunsaturated biodiesel molecules is significantly higher than that of a primary reference fuel consisting of hexadecane and heptamethylnonane. Despite these findings, this work also suggested, solely on the basis of the ratio of carbon to hydrogen atoms of the individual fuels, that commercial diesel fuel consisting of a wide variety of hydrocarbon species, would be expected to have a higher adiabatic flame temperature than several polyunsaturated biodiesel molecules. McCormick et al. (2005) carried out an experimental study with biodiesel fuels of different degrees of unsaturation and thus of significantly different adiabatic flame temperatures using an engine with electronically controlled common rail fuel injection system. Their experiments showed a progressive increase in NO_x emissions when using biodiesel fuel of higher degrees of unsaturation, which correlate with higher adiabatic flame temperatures. Lapuerta et al. (2008[a]) confirmed these findings and attributed these mainly to the longer ignition delay of biodiesel fuel with higher iodine number. Due to the differences in ignition delay, which imply differences in heat release rates, stoichiometry and timing of the combustion process, it thus remains unclear whether this observed increase in NO_x occurred due to an increase in the ignition delay or whether a difference in adiabatic flame temperature may have an influence.

The subject of the present chapter is an experimental study of how the molecular structure of biodiesel molecules influences their combustion in a diesel engine when the time of injection or the timing of ignition of the fuel are precisely controlled. In particular the effects of ignition delay were discriminated from those of flame temperature by equalising the ignition delay of the various fuels via the addition of the ignition promoting molecule 2-ethylhexyl nitrate (2-EHN) in small, varying concentrations. This eliminated the ignition delay as a variable, allowing the weaker effects of flame temperature to be revealed and quantified. Exhaust gas concentrations of NO_x, unburned hydrocarbons (UHC), carbon monoxide (CO), Carbon dioxide (CO_2), oxygen (O_2) and sub-micron particulate matter were measured. Results for the biodiesel molecules were compared with those of standard fossil diesel fuel at the same experimental conditions.

5.2. Experimental methods

5.2.1. Apparatus

Some of the fuels samples were only available in quantities that were insufficient for use with a conventional diesel engine injection system, and several of them were crystalline solids at room temperature. The special fuel injection system described in Chapter 3 was used to carry out these experiments. The solution devised was to retain the conventional engine injection system but not use it to inject the test fuels into the combustion chamber. Instead, the conventional injection system was used to generate the hydraulic injection pressure for a separate low-volume fuel injection system, as shown in Figure 3.8. Small quantities of sample bio fuels (~100ml) where pressurised to 45 MPa using this arrangement, although the system was able to achieve injection pressures above 100 MPa. The fuels were injected into the engine combustion chamber through a solenoid-controlled injector with six holes of 154 μm diameter each. The low-volume fuel system was heated via a PID-controlled heating system to a temperature of 353 ± 2 K. This made sure that all fuel samples were injected in liquid state and at the same temperature.

The dynamic cylinder pressure was measured using the piezoelectric pressure transducer (Kistler 6056AU38) and charge amplifier (Kistler type 5011) described in Chapter 3. The cylinder pressure was pegged each combustion cycle at bottom dead centre using a piezoresistive pressure transducer (Druck PTX 7517-3257) located 160mm upstream of the inlet valves in the intake manifold. The geometric compression ratio of the engine was 15, and the air was naturally aspirated into the combustion chamber at atmospheric pressure. The exhaust gas was sampled 180 mm downstream of the exhaust valves and analysed using an automotive exhaust gas analyser. The NO_x was measured using a chemiluminescence analyser, CO and CO_2 concentrations were measured using non-dispersive infrared analysers and, oxygen concentration was measured using a paramagnetic oxygen analyser a flame ionisation detector was used to measure the unburned hydrocarbons, as described in Chapter 3. A differential mobility spectrometer (Cambustion DMS500) was used to measure the size distribution and mass of the sub-micron particulates in the exhaust gas. Particulate samples having different sizes were collected using a set of micro-orifice uniform distribution (MOUDI) aerodynamic cascade impactor.

5.2.2. Fuel molecules investigated

Two different types of fuel samples were used in the experiments: Firstly, eight samples of single molecule fatty acid alkyl esters were used to investigate the effects of fatty acid chain length, degree of un-saturation of the fatty acid moiety, and the effect of alcohol chain length. Secondly four mixtures of such molecules were tested, which contained the above eight and other fatty acid alkyl esters in different proportions. For the purpose of this chapter, the former shall be referred to as ‘single molecule fatty acid esters’ (SMFAE) and the latter four mixtures shall be referred to as

'natural biodiesel' (NB) fuel samples. The molecular structures of the SMFAE samples are shown in Figure 5.1, and salient physical and chemical properties of these are given Table 5.2. Molecular composition and salient properties of the NB fuel samples are given in Table 5.3. The combustion experiments for the SMFAE fuels are presented in sections 5.3.1-5.3.4. The samples were used to study three distinct aspects of molecular structure:

1. Influence of chain length of the fatty acid moiety
2. Influence of chain length of degree of unsaturation of fatty acid moiety
3. Influence of chain length of alcohol moiety

First, the effect of fatty acid chain length was studied using 5 samples of SMFAE representing fully saturated methyl ester molecules of chain lengths between 12 and 22 carbon atoms. Second, the effect of degree of fatty acid chain un-saturation was investigated using three SMFAE containing 18 carbon atoms in the fatty acid chain, and zero, one and two double bonds respectively. And third, the effect of alcohol chain length was studied using two SMFAE, a methyl and an ethyl ester of oleic acid. Both molecules contained 18 carbon atoms and one double bond in their fatty acid moiety, but distinguished themselves by having one and two carbon atoms in their alcohol chain respectively. The four NB fuel samples consisted of methyl esters of rapeseed oil, palm oil, jatropha oil and tallow respectively. Details on their fatty acid ester compositions and physical and chemical properties are shown in Table 5.3. The combustion experiments for the NB fuels are presented in section 5.3.6. Alongside all fuel samples, tests with a fossil refinery diesel fuel to EN 590 standard were carried out, to provide a basis for comparison. This fuel shall be referred to as 'fossil diesel fuel' throughout the chapter. Detailed properties of this fossil diesel fuel are shown in Table 5.2 and Table 5.3.
The fuels were subjected to three series of experiments:

1. Constant injection timing
2. Constant ignition timing
3. Constant ignition delay

In the first series of experiments, the time of injection for all fuel samples was fixed. Due to their different ignition characteristics, the time of ignition of each molecule varied accordingly. The common point of injection was chosen so that ignition of the fossil diesel fuel would occur at top-dead-centre (TDC) of the engine cycle. In the second series of experiments, the time of ignition was kept constant for all fuel samples. This was achieved by adjusting the time of injection for each sample, so that ignition would occur at TDC. In the third series of experiments all fuel samples were subjected to the same injection timing, the same ignition timing (at TDC) and thus, the same ignition delay. This was achieved by adding the ignition promoting molecule 2-EHN in varying small concentrations to the fuel samples, until their ignition delay was equalised. The fuel samples to which 2-EHN was added will be referred to as 'doped' fuels.

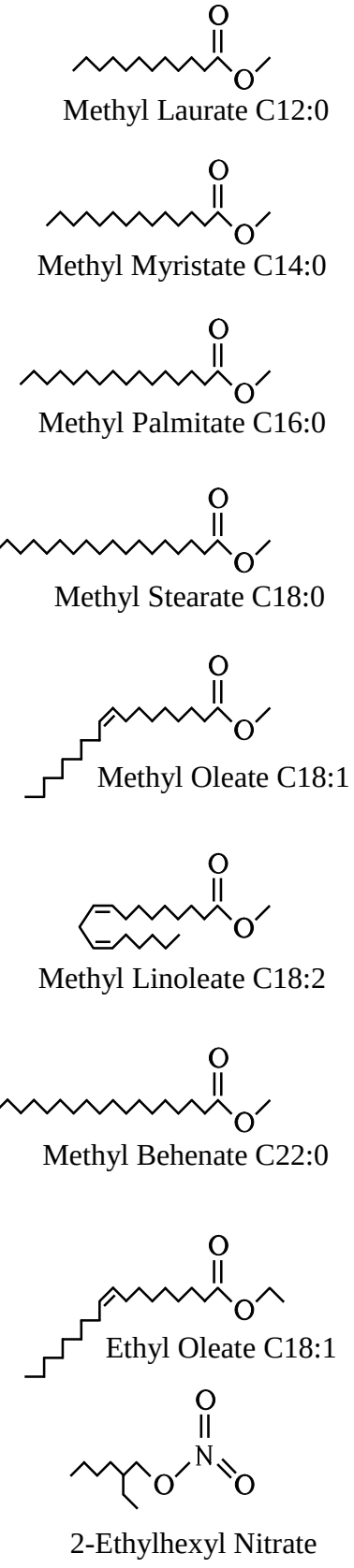

Figure 5.1 - Molecules used for the experimental investigations

Table 5.1 – Experimental conditions

Constant injection timing:

	I.M.E.P. [MPa]	Engine speed [rpm]	Injection timing [ºCA BTDC]	Ignition timing [ºCA BTDC]	Injection pressure [MPa]	Indicated Thermal η [%]
Diesel fuel	0.4	1200	7.1	TDC	45	31.70
C12:0 M	0.4	1200	7.1	0.4	45	33.49
C14:0 M	0.4	1200	7.1	0.8	45	33.61
C16:0 M	0.4	1200	7.1	1.6	45	33.97
C18:0 M	0.4	1200	7.1	1.8	45	33.87
C22:0 M	0.4	1200	7.1	1	45	32.80
C18:1 M	0.4	1200	7.1	-0.2	45	33.19
C18:2 M	0.4	1200	7.1	-2	45	32.71
C18:1 E	0.4	1200	7.1	-0.3	45	32.71
Diesel fuel	0.4	1200	7.1	TDC	45	32.45

Constant ignition timing:

	I.M.E.P. [MPa]	Engine speed [rpm]	Injection timing [ºCA BTDC]	Ignition timing [ºCA BTDC]	Injection pressure [MPa]	Indicated thermal η [ ]
Diesel fuel	0.4	1200	7.1	TDC	45	31.70
C12:0 M	0.4	1200	7.4	TDC	45	32.88
C14:0 M	0.4	1200	7.2	TDC	45	32.90
C16:0 M	0.4	1200	6.8	TDC	45	33.57
C18:0 M	0.4	1200	6.3	TDC	45	32.87
C22:0 M	0.4	1200	6.7	TDC	45	32.80
C18:1 M	0.4	1200	7.5	TDC	45	32.41
C18:2 M	0.4	1200	9	TDC	45	32.23
C18:1 E	0.4	1200	7.6	TDC	45	32.29
Diesel fuel	0.4	1200	7.1	TDC	45	32.45

Constant ignition delay:

	I.M.E.P. [MPa]	Engine speed [rpm]	Injection timing [ºCA BTDC]	Ignition timing [ºCA BTDC]	Injection pressure [MPa]	Indicated thermal η [ ]	2-EHN treatment rate [ppm]
Diesel fuel	0.4	1200	6.2	TDC	45	33.12	21066
C12:0 M	0.4	1200	6.2	TDC	45	33.82	11057
C14:0 M	0.4	1200	6.2	TDC	45	33.73	5066
C16:0 M	0.4	1200	6.2	TDC	45	33.85	1130
C18:0 M	0.4	1200	6.2	TDC	45	32.58	0
C18:1 M	0.4	1200	6.2	TDC	45	33.88	17601
C18:2 M	0.4	1200	6.2	TDC	45	33.27	36942
C18:1 E	0.4	1200	6.2	TDC	45	33.19	15473
Diesel fuel	0.4	1200	6.2	TDC	45	33.19	21066

Table 5.2 – Thermochemical properties of fatty acid monohydric alcohol esters and diesel fuel

		Fossil diesel fuel	C12:0 Methyl laurate	C14:0 Methyl myristate	C16:0 Methyl palmitate	C18:0 Methyl stearate	C18:1 Methyl oleate	C18:2 Methyl linoleate	C22:0 Methyl behenate	C18:1 Ethyl oleate	2-EHN
Upper heating value	***[kJ/kg]***	45820	37913	38852	39119	40210	40032	39613	41631	-	-
Lower heating value	***[kJ/kg]***	42980	35306	36202	36443	37501	37436	37148	38872	-	27364[1]
Carbon (Theoretical)	***[m/m %]***	-	72.84	74.32	75.50	76.45	76.97	77.49	77.9	77.36	54.84
Hydrogen (Theoretical)	***[m/m %]***	-	12.23	12.48	12.67	12.83	12.24	11.64	13.08	12.34	9.78
Oxygen (Theoretical)	***[m/m %]***	-	14.93	13.20	11.83	10.72	10.79	10.87	9.02	10.3	27.39
Nitrogen (Theoretical)	***[m/m %]***	-	0	0	0	0	0	0	0	0	7.99
Carbon (Measured)	***[m/m %]***	86.68	73.02	74.35	-	-	76.99	77.43	-	-	-
Hydrogen (Measured)	***[m/m %]***	13.32	12.23	12.44	12.57	12.73	12.20	11.58	-	-	-
Oxygen (Measured)	***[m/m %]***	0.07	14.76	13.21	-	-	10.80	10.99	-	-	-
Density @ 15°C	***[g/ml]***	0.834	0.873	0.870	0.867[2]	0.868[2]	0.896	0.891		0.87[3]	0.963
Viscosity @ 40 ° C (*20% vol. sample in diesel fuel)	***[mm^2/s]***	2.564	2.425	3.273	2.778*	2.986*	4.518	3.745	-	-	-
Cetane No.	-	49.8	62[4]	71[4]	81[4]	89[4]	62[4]	42[4]	-	65[4]	-
Normal B.Pt.	***[°C]***	-	262[5]	323[5]	338[5]	352[5]	349[5]	366[5]	394[5]		-
Melting Point	***[°C]***	-	4.5-5	18	32-35	37-41	-20	-35	-	-32	-
Iodine number	[g/100g]	-	0	1	1	0	94	176	3	81.7[6]	-

[1] Oxley et al. (2001)
[2] Graboski et al. (2000)
[3] Sigma-Aldrich chemical company (2004)
[4] Murphy et al. (2004)
[5] Yuan et al. (2005)
[6] Knothe (2002)

Table 5.3 - Physical properties and molecular composition of biodiesel

		RME	PME	JME	TME	Fossil diesel fuel
Upper heating value	MJ/kg	39.98	39.82	39.5	39.98	45.82
Lower heating value	MJ/kg	37.40	37.18	36.94	37.44	42.98
Carbon	%	77.2	76.2	76.71	76.3	86.6
Hydrogen	%	12.15	12.5	12.04	12.15	13.4
Oxygen	%	10.9	11.2	12.00	10.9	0.07
Total	%	100.3	99.9	100.8	99.4	100.1
Density @ 15 deg C	[g/ml]	0.883	0.876	0.888	0.878	0.834
Viscosity	[mm2/s]	4.492	N/A	5.227	4.415	2.564
Cetane No.	[ ]	52.2	N/A	57.8	57.2	49.8
Pour point	[° C]	-12	18	-	9	-
Iodine number	[gI/100g]	110	51	-	77	-
2-EHN in Constant ignition delay experiments	[m/m %]	1.09	0	0	0.71	0.58
FAME composition (EN14103)	[m/m %]					
C12:0		0	0.2	0	0.2	-
C14:0		0.1	1.1	0	1.2	-
C16:0		4.6	43.0	12.6	18.9	-
C16:1		0.3	0.2	0.8	2.1	-
C18:0		1.8	4.7	5.9	8.9	-
C18:1		60.7	40.1	35.8	44.4	-
C18:2		19.1	9.5	28.8	15.7	-
C18:3		8.3	0.2	0.2	2.8	-
C20:0		0.6	0.4	0.2	0.3	-
C20:1		1.4	0.2	0.1	0.8	-
C22:0		0.3	0	0.1	0.1	-
C22:1		0.3	0	0	0	-
C24:0		0.1	0	5.1	0	-
C24:1		0.1	0	0.1	0	-
Other		0.4	0.4	0	1.8	-
Total		98.1	100.0	89.7	97.2	-
Total saturates		7.5	49.4	23.9	29.6	-

5.3. Experimental Results

5.3.1. Effect of fatty acid chain length

The first structural characteristic of the molecules under investigation, was that of fatty acid chain length. Samples of five saturated methyl esters of variable fatty acid chain length (12, 14, 16, 18 and 22 carbon atoms) and fossil diesel fuel were tested under three experimental conditions. First all fuel samples were injected at the same crank angle timing within the engine cycle (7.1º crank angle (CA) before top-dead-centre (BTDC)). The timing of injection was chosen so that ignition would occur at TDC for fossil diesel fuel. The injected fuel quantity for each molecule was chosen so as to obtain the same indicated work during the complete cycle (i.e. all the molecules were tested at constant indicated mean effective pressure (IMEP)).

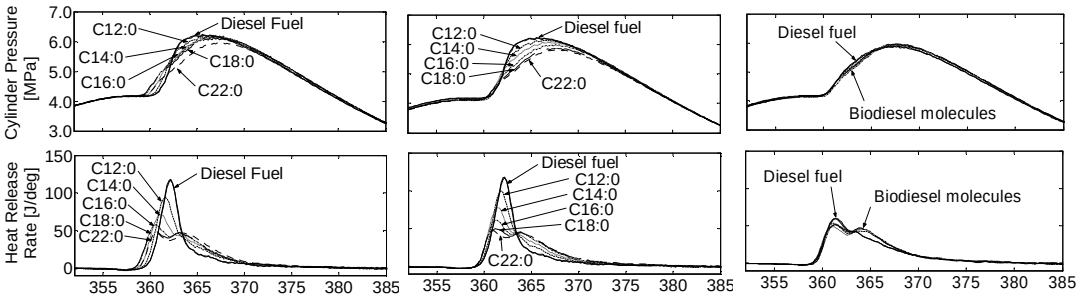

Figure 5.2 - Cylinder pressure and heat release rates for molecules of different fatty acid chain lengths

The length of the fatty acid chain strongly influenced the ignition delay periods of the injected molecules. As can be seen in Figure 5.2 a longer fatty acid chain length resulted in a shorter ignition delay. When all molecules were injected at the same timing during the cycle, it can be seen in Figure 5.3 that molecules with longer fatty acid chain lengths produced less NO_x during their combustion than shorter chained molecules. These findings are in agreement with those of Graboski et al. (2003). The different ignition delays of the individual molecules meant that the ignition of the fuel occurred at different times during the cycle, at which the cylinder volume and pressure were slightly different. Since the timing of injection was held constant, the entire combustion process was thus advanced or retarded within the engine cycle.

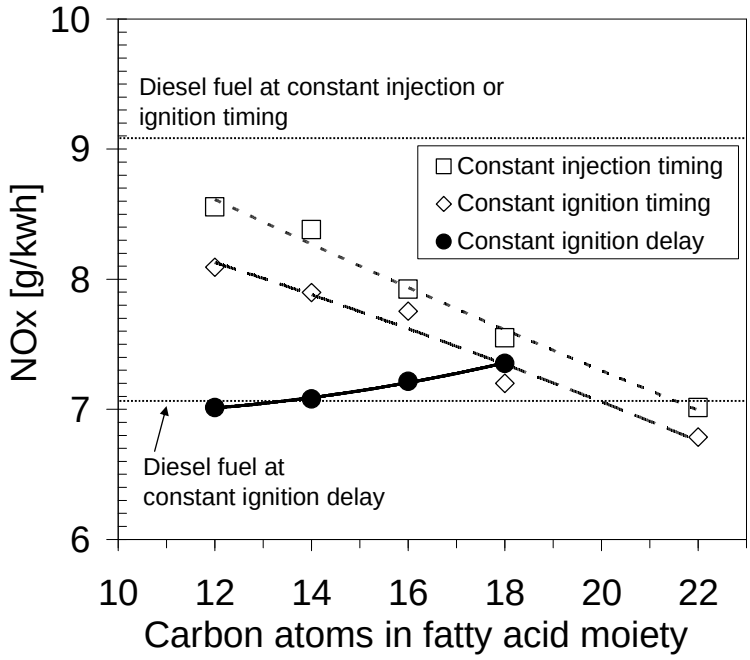

Figure 5.3 – NO_x emissions for molecules of different fatty acid chain lengths

A second experiment was carried out in which the time of injection was adjusted for every fuel so that the ignition of all fuels would occur at the same time; that is at TDC. The cylinder pressure traces and heat release rates for this experiment can be seen in the centre of Figure 5.2, and the corresponding NO_x and particulate mass emissions are shown in Figure 5.3 and Figure 5.4 respectively. The patterns of heat release and emissions remained essentially the same as those for the constant injection timing experiments. Figure 5.4 shows that the emission of particulate mass was significantly greater for the longest molecule (behenic acid methyl ester) than for any other SMFAE molecule. It is suspected that this high emission of particulate mass derives from the high viscosity of this molecule and inadequate atomisation of the fuel spray, since the temperature at which it was injected was only 25 K above its melting point.

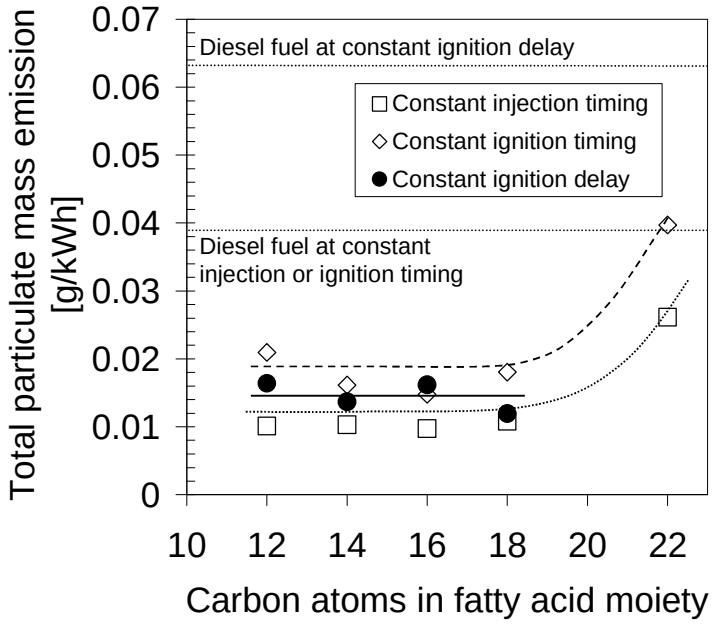

Figure 5.4 – Particulate mass emissions for molecules of different fatty acid chain lengths

The NO_x emission for the different molecules is shown in Figure 5.3 to have a clear trend, which remains the same when the engine operation was changed from constant injection timing to constant ignition timing. Figure 5.3 and Figure 5.3 suggest shorter chained molecules burned with longer ignition delays, higher maximum heat release rates and produced higher NO_x emissions than longer chained molecules. This is in agreement with other experimental studies which had shown that for fuels with longer ignition delay a greater proportion of the fuel burns in premixed mode which, in turn, raises peak combustion temperatures and NO_x emissions (Ladommatos et al. 1996[a]; Szybist an Boehman, 2003. It may thus be of interest to understand how the exhaust emissions are affected by the structure of the molecule if the injection and ignition timing, as well as the ignition delay were the same; thus removing the substantial effect which ignition delay has on NO_x emission. A third set of experiments was carried out, in which the fuel samples were additised with the ignition promoting molecule 2-EHN (see Figure 5.1 for molecular structure and Table 5.2 for properties) in varying concentrations to equalise the ignition quality of all fuel samples.

The recorded cylinder pressure, heat release rates, NO_x and particulate mass emissions are shown on the right hand side of Figure 5.3, and in Figure 5.4 and Figure 5.4, respectively. It can be seen that once the effect of ignition delay is removed, the cylinder pressure and heat release histories were very similar for all SMFAE samples. A clear distinction could still be made with respect to fossil diesel fuel, which had a higher maximum heat release rate, and shorter combustion duration. The heat release patterns show that the combustion of fossil diesel fuel had a slightly higher proportion of heat released in the premixed combustion phase which directly followed ignition, compared to the SMFAE samples. This is likely to be due to the fossil diesel fuel having a higher calorific value per

unit volume than SMFAE and a lower viscosity. A shorter injection period was required for the fossil diesel fuel than for the SMFAE fuels to yield the same IMEP during the experiments. This is because a lower fuel volume needed to be injected to provide a similar amount of calorific energy to the engine. Since a similar total amount of fuel energy was introduced into the combustion chamber, the shorter injection period indicates that the rate at which fuel energy is introduced into the combustion chamber, was higher for fossil diesel fuel than it was for any of the SMFAE fuels. The fuel injection had not ceased by the time at which ignition occurred, for any fuel. The ignition delay period was the same for all fuels. This meant that at the end of the ignition delay period, a higher amount of fuel energy had been introduced into the combustion chamber for the fossil diesel fuel, than it had been for the SMFAE fuels. Thus at the time of ignition, more fuel energy was available for combustion. This is believed to be the reason for the slightly higher peak heat release rate observed for fossil diesel fuel during the premixed combustion phase, which directly ensued the ignition.

An interesting observation could be made when considering the NO_x emissions for the molecules of varying fatty acid chain lengths. It was observed that fatty acid monohydric alcohol esters with shorter fatty acid chain lengths produced lesser amounts of NO_x in their combustion than longer chained molecules, provided that their ignition delay is the same. Previous experiments carried out at constant injection timing and constant ignition timing had shown the opposite trend. This indicates that the differences in NO_x emissions produced in the former experiments, were predominantly caused by differences in ignition characteristics. From this observation it can be deduced that ignition delay played a dominant role in the formation of NO_x by controlling the global heat-release patterns and combustion stoichiometry. The third experiment, in which the ignition delays were equalised, removed this effect and highlighted a secondary effect which had previously been masked by the prevailing role of the ignition delay. This effect is thought to be one of flame temperature, and is layered below that of the ignition delay, as will be discussed later on.

A further observation was that the shorter-chained molecules which were treated with higher concentrations of 2-EHN (which introduces fuel-bound nitrogen to the fuel samples) produced lower amounts of NO_x than those fuel samples containing lesser amounts of 2-EHN. This indicates that fuel-bound nitrogen plays a comparatively small role in NO_x formation under the present experimental concentrations. This may suggest a subordinated role of prompt NO_x formation via nitrogen-containing fuel radicals in these experiments, since an increase in fuel-bound nitrogen may be expected to result in an increase of such species. This observation is also important in that it supports the use of 2-EHN as a valid experimental tool for equalising the ignition delay, even when studying the formation of NO_x.

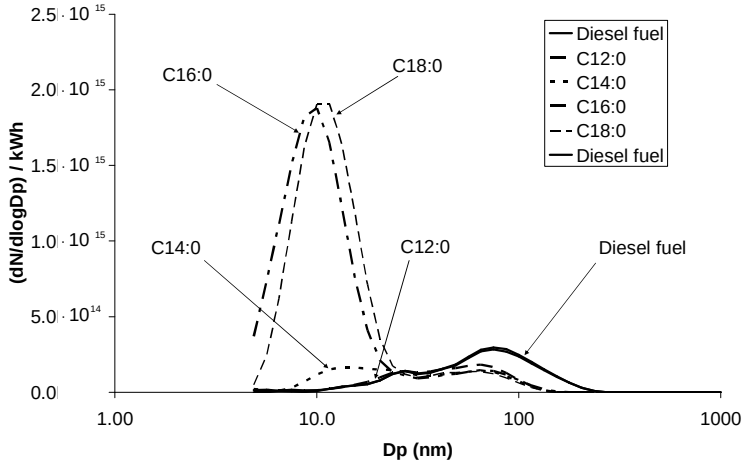

Figure 5.5 – Particulate size distribution for experiments with constant ignition delay

Figure 5.5 shows how the fatty acid molecule chain length affects the size distribution of sub-micron particulates. It can be seen that the total particulate mass emitted from fossil diesel fuel is much larger than that for the SMFAE molecules due to higher number of accumulation mode particles in the range of 40 to 200 nm diameter. The longer chained molecules produced a higher number of very small particles of the order of 5-40 nanometres diameter. It remained unclear from these experiments what the make-up of these particles was. It could be speculated that they may consist of unburned fuel droplets which condense in the exhaust gas. The author has no clear proof of this theory. This speculation could be supported by the fact that the longer chained molecules have a progressively lower vapour pressure and higher boiling point, which could result in a greater amount of condensation. This shall be discussed in more detail in section 5.3.5. Additional experimental results can be found in Appendix C.

5.3.2. Effect of number of double bonds

The second structural effect of the molecules that was investigated was the degree of unsaturation of the molecules, which is reflected in the number of double bonds in the fatty acid chain. It is known from cetane number experiments that more unsaturated fatty acid alkyl ester molecules have a lower ignition quality than saturated fatty acid alkyl ester molecules (Klopfenstein, 1983; Klopfenstein, 1985; Knothe, et al., 1997; Knothe, et al., 2003).

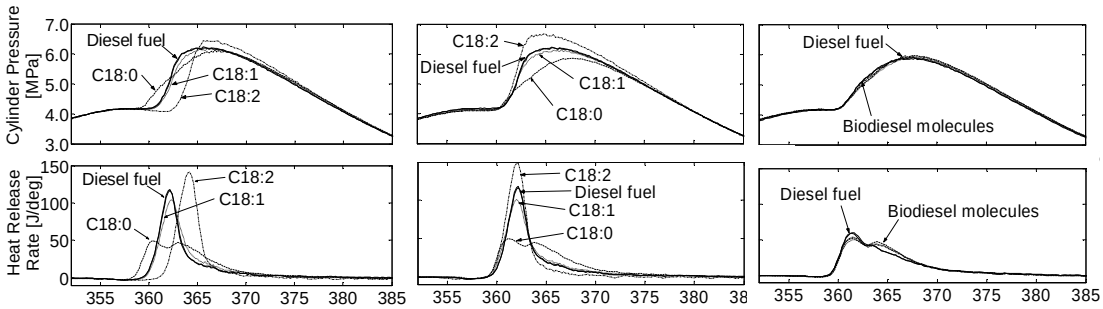

Figure 5.6 - Cylinder pressure and heat release rates for molecules of different number of double bonds

Three fatty esters with a fatty acid chain containing 18 carbon atoms and zero, one and two double bonds respectively, as well as fossil diesel fuel, were tested. In the first series of experiments, all fuels were injected into the combustion chamber at 7.1 º crank-angle before TDC. The pressure traces and heat release rates on the left hand side of Figure 5.6 show that the ignition delays and fraction of fuel burnt in premixed combustion were significantly different for the three degrees of saturation of the SMFAE molecules. The longest ignition delay was experienced by the polyunsaturated methyl ester (C18:2, i.e. two double bonds). The mono-unsaturated methyl ester (C18:1) had a similar ignition delay to fossil diesel fuel, and the saturated methyl ester (C18:0) had the shortest ignition delay. Figure 5.7 shows that the polyunsaturated fatty acid ester molecule (C18:2) produced the largest amount of NO_x emission. As mentioned before, it is well documented that fuels with a longer ignition delay tend to produce higher amounts of NO_x in diesel combustion (Ladommatos, et al., 1996[a]; McCormick, et al., 2002).

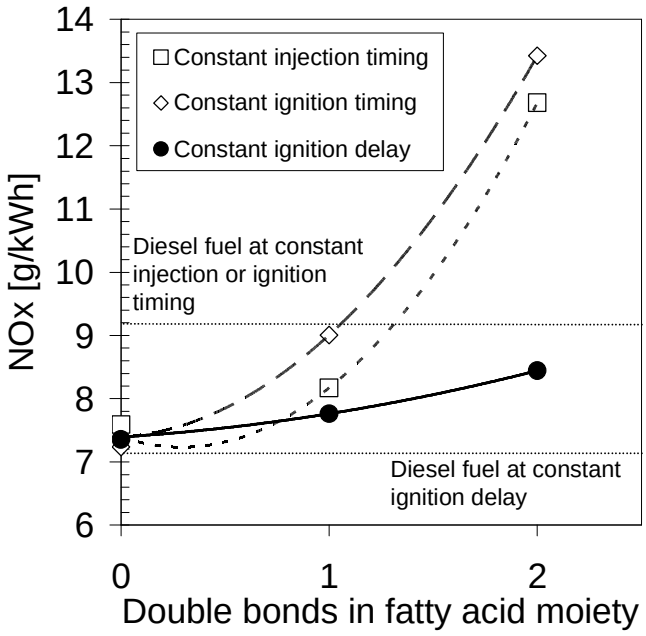

Figure 5.7 – NO_x emissions for molecules with different number of double bonds

Figure 5.7 shows that NO_x emission increases with number of double bonds in fatty acid alkyl ester molecules, when the ignition delay is not specifically controlled. This agrees with the findings of Lapuerta et al. (2008[a]). However, it is still unclear from these experiments, whether the higher emission of NO_x stems solely from the longer ignition delay of the less saturated molecules. The effect of the double bonds on the formation of particulate mass is shown in Figure 5.8. More unsaturated molecules had longer ignition delay, thus allowing more fuel-air mixing to take place before ignition, and consequently for a greater proportion of the fuel energy to be released under premixed combustion conditions. Despite the fact that better fuel-air mixing is generally understood to lead to a reduction in particulate formation (Ladommatos, et al., 1996[a]; Schulz, et al., 1999), the emission of particulate matter clearly increases with greater number of double bonds within the fatty acid moiety of the ester molecules. This is in reasonable agreement with the results reported by Graboski et al. (2003) who have shown a similar trend. It has been reported in experiments conducted on real biodiesel fuels though (Lapuerta, et al., 2008[a]), that an increase in iodine number can in some instances result in a decrease of particulate mass emissions. The reasons for these discrepancies are not clear, but could be rooted in differences in experimental conditions. It may be speculated that in the former case, the particulate emission is predominantly influenced by the higher chemical propensity of the unsaturated molecules to form soot, whilst in the latter case, the lower particulate emission is predominantly a consequence of the lower ignition quality of the less saturated fuels and may be attributable to a longer ignition delay, and better fuel-air mixing; leading to leaner premixed combustion.

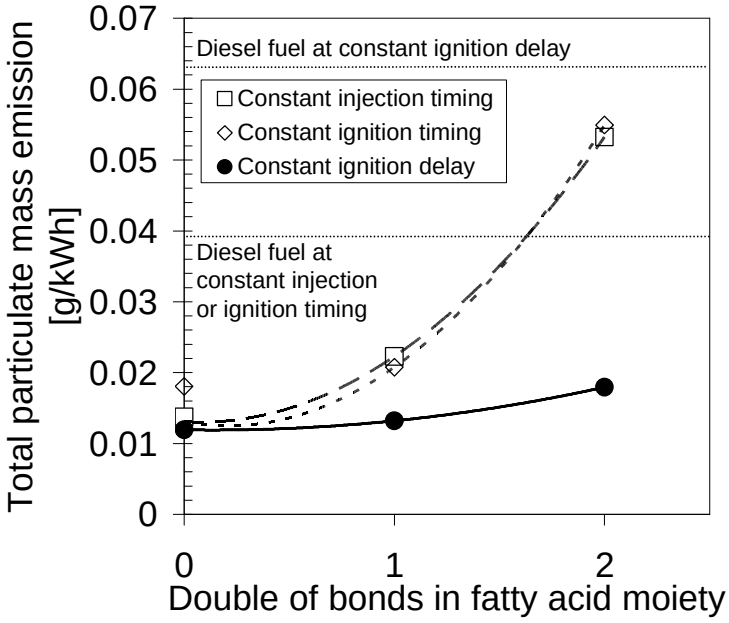

Figure 5.8 – Particulate mass emissions for molecules with different number of double bonds

A second experiment was carried out in which the time of ignition was equalised for all fuels. This was done by adjusting the time of injection according to the individual ignition delay of the each molecule, so that ignition would always occur at TDC. The results are shown in Figure 5.6 and were very similar to those obtained for the constant injection timing experiments. Figure 5.6 shows that the peak cylinder pressures and heat release rates for the unsaturated molecules were significantly higher than for the saturated fatty acid esters and occurred slightly earlier during the cycle. The higher peak cylinder pressures and heat release rates are accompanied by higher NO_x emissions as would be expected. The mono-unsaturated ester (C18:1) produced a similar amount of NO_x as fossil diesel fuel. The fully saturated fatty ester (C18:0) produced a significantly lower amount of NO_x than fossil diesel fuel and the poly-unsaturated fatty ester (C18:2) produced significantly higher amount of NO_x than fossil diesel fuel. The emission of total particulate mass for the constant ignition timing experiments is shown in Figure 5.8. As observed for the constant injection timing experiments, the constant ignition timing tests showed that progressively higher amounts of particulate mass are formed with increasing number of double bonds. This result may be explained by the fact that the less saturated molecules have a higher chemical propensity to form soot. The double bonds in the molecules provide a more direct path to the formation of ethene and ethyne during the thermal decomposition of the molecules, both of which are known precursors to carbonaceous soot (Dobbins, et al., 1998).

A third experiment was carried out, in which 2-EHN was added to the individual fuel samples until the same ignition delay was obtained for all fuels. The right hand side of Figure 5.6 shows that the cylinder pressure and heat release patterns are now almost indistinguishable for all SMFAE molecules. The higher concentrations of NO_x measured for the less saturated molecules in this experiment, can thus not be attributed to a shift towards premixed combustion. It is visible that there remains, after the removal of the effect of ignition delay, a second effect which still causes elevated

NO_x concentration traceable in the exhaust gas. This third set of experiments thus provides evidence that the elevated NO_x formation from the combustion of unsaturated fatty acid alcohol ester molecules is not solely due to the longer ignition delay that they experience, but that there exists a further reason.

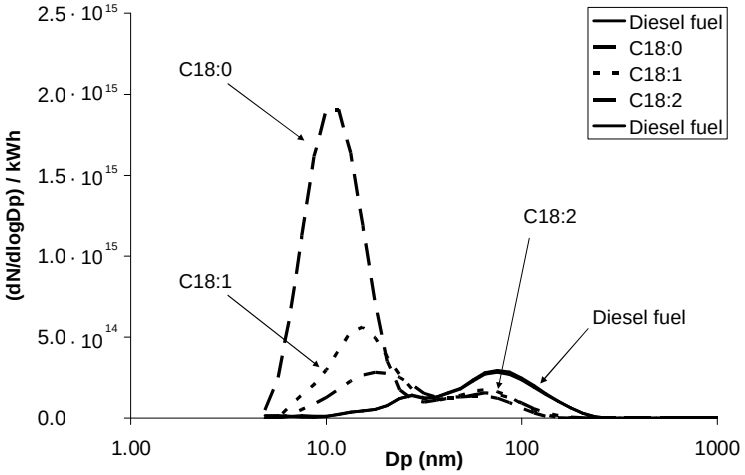

Figure 5.9 – Particulate size distribution for molecules with different number of double bonds

Figure 5.8 shows the total particulate mass emitted for this set of experiments. It is clear that fossil diesel fuel has a much higher propensity of forming soot than any of the SMFAE molecules when the ignition delay is the same for both types of fuels. This is likely to be due to the lower oxygen content of fossil diesel fuel. A comparison amongst the individual SMFAE molecules shows that when the ignition delay is constant, molecules with a higher number of double bonds exhibit a higher propensity of forming particulate mass. As mentioned previously, the double bonds in the molecules are likely to provide a direct path to the formation of carbonaceous soot via the formation of ethene and ethyne during the thermal decomposition of the molecule. Both of these species are known precursor molecules to carbonaceous soot. It should be noted, with regards to the validity of the experimental approach, that the more unsaturated molecules (containing more double bonds) had been subjected to higher concentrations of 2-EHN than the saturated molecule. 2-EHN contains a significantly higher fraction of oxygen by weight than any of the fatty acid methyl esters, and would be expected to suppress the formation of soot. Yet, the more unsaturated molecules containing higher amounts of 2-EHN produced higher amounts of soot. This may suggest that the formation of soot was not significantly influenced by the addition of the 2-EHN. The size distribution of the sub-micron particulates can be seen in Figure 5.9. It is clearly visible that the reason for the elevated total particulate mass from fossil diesel fuel and unsaturated fatty ester molecules is due to greater number of accumulation mode particles in the range of about 40 and 200 nanometres in diameter. The more saturated molecules were found to emit large numbers of nucleation mode particles, which were about 5-40 nanometres in diameter. As observed before, the particulate number density of these nucleation mode particles appears to correlate with the boiling points of the fuel molecules. This would suggest that condensation of unburned fuel may play a significant role in the formation of these small particles.

5.3.3. Effect of alcohol chain length

The effect which the chain length of the alcohol moiety has on the combustion of fatty acid alkyl esters was studied in a third series of experiments. Two fatty acid alcohol ester molecules were used; C18:1 methyl ester (methyl oleate) and C18:1 ethyl ester (ethyl oleate), in addition to fossil diesel fuel. The experiments were very similar to those for the fatty acid chain length and degree of saturation: one at constant injection timing for all fuels, one at constant ignition timing, and one at constant ignition delay. The cylinder pressures and heat release rates are shown in Figure 5.10. It is visible that the cylinder pressure and heat release curves are relatively similar, and that only a small difference in ignition quality exists between the methyl and the ethyl esters of oleic acid. The ethyl ester was subject to a slightly shorter ignition delay than the methyl ester.

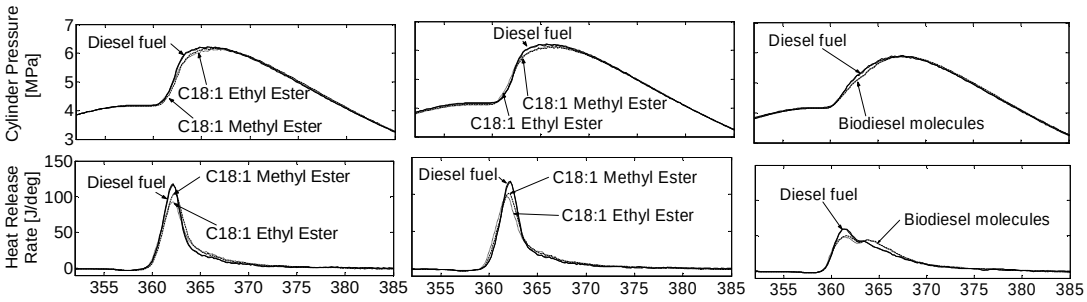

Figure 5.10 – Cylinder pressure and heat release rates for molecules with different alcohol chain lengths

For the experiments in which the injection timing and the ignition timing were held constant, the combustion of the ethyl ester thus produced slightly lower peak combustion chamber pressures than the methyl ester. This is reflected in the fact that the methyl oleate produces slightly larger amounts of NO_x than the ethyl oleate (Figure 5.11). This is in agreement with the findings of Lapuerta et al. (2008[b]). In the third experiment, in which the ignition delay was equalised for all fuels by the addition of 2-EHN, methyl oleate still produced marginally higher concentrations of NO_x than ethyl oleate (Figure 5.11). This may be attributable to its higher adiabatic flame temperature.

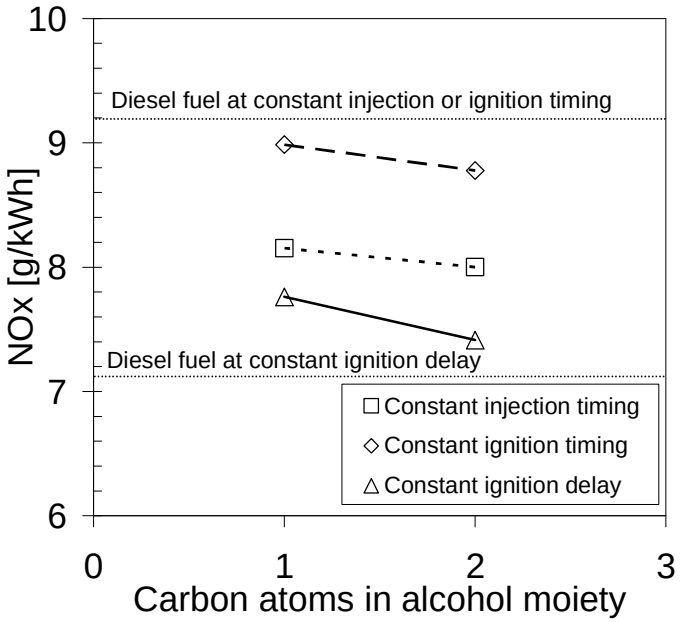

Figure 5.11 - NO_x emissions for molecules with different alcohol chain-lengths

Ethyl oleate emitted slightly more particulate mass than methyl oleate in all three experiments, even when the ignition delay was constant (see Figure 5.12). The reasons for the slightly higher emission of particulate mass from the ethyl ether are not entirely clear, but four hypotheses could provide a tentative explanation: Firstly, in the two experiments ('constant injection timing' and 'constant ignition timing') in which the ignition delay was not controlled, it is likely that there is a significant influence of ignition delay. The ethyl ester was subjected to a shorter ignition delay, so that its combustion would be expected to exhibit a slightly lesser amount of fuel-air premixing before ignition occurs, accompanied by a subtle shift towards diffusion controlled combustion. This is likely to result in richer conditions in the premixed flames, which encourage the formation of soot and its precursors. Secondly, the methyl ester contains slightly more oxygen by mass than the ethyl ester. This would be expected to improve its ability to oxidise soot precursors forming in the fuel-rich regions of the spray. Thirdly, the methyl ester is expected to exhibit slightly higher adiabatic flame temperatures than the ethyl ester as shall be shown later (see section 5.3.7), which may be responsible for a higher rate of oxidation of soot in the flame front. Fourthly, it may be speculated that the thermal decomposition of the ethyl ester may advantage the formation intermediate species which are more conducive to the formation of soot than that of the methyl ester (e.g. ethene). A higher probability of the ethyl ester to form such intermediate species may be reflected in a higher propensity of forming soot.

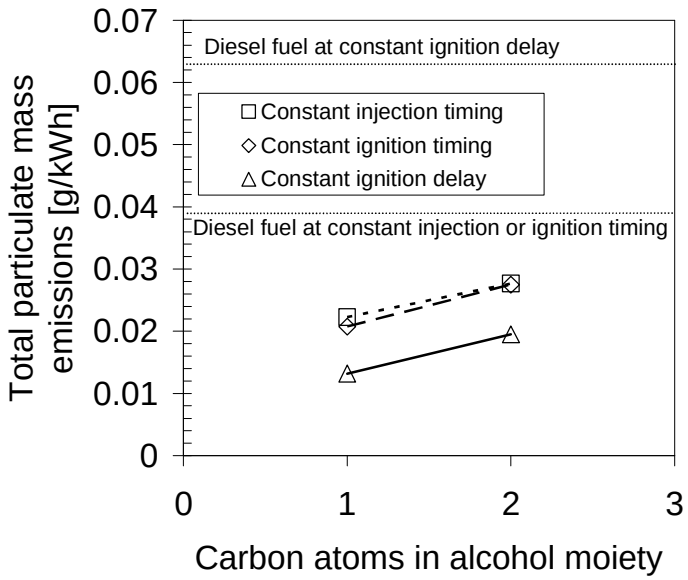

Figure 5.12 – Particulate mass emissions for molecules with different alcohol chain-lengths

Figure 5.13 shows the particulate size distribution for the series of experiments that were carried out at constant ignition delay. It is clearly visible that the fossil diesel fuel forms a much larger number of accumulation size particles of the order of 40-200 nanometres than the two SMFAE molecules. This explains the higher particulate mass emission from fossil diesel fuel in comparison to the SMFAE (see Figure 5.12). The ethyl ester formed marginally higher number of accumulation mode particulates of the order of about 40-200 nanometres diameter than the methyl ester, which is the reason for the higher total mass of the particulate emissions, shown in Figure 5.12. Both SMFAE molecules formed a large number of very small particles of the order of around 5-40 nanometres diameter. The methyl ester was observed to produce a larger amount of these particles than the ethyl ester in all three experiments, carried out at different conditions (constant injection timing, constant ignition timing and constant ignition delay). As previously noted for other molecules, this may be attributable to an increased amount of condensation of unburned fuel taking place. The slightly higher boiling point of the methyl ester compared to the ethyl ester may be conducive to a more pronounced formation of small condensed fuel droplets, or to the accumulation of fuel onto small soot particulates.

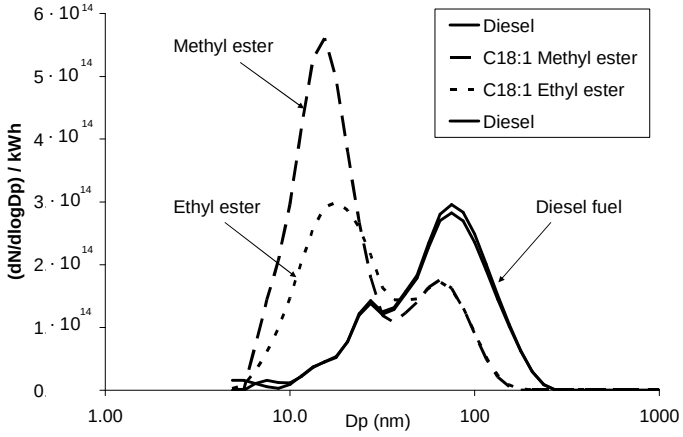

Figure 5.13 – Particulate size distribution for molecules with different alcohol chain-lengths

5.3.4. Effect of fuel oxygen content on total particulate mass emission

Figure 5.14 illustrates the influence of the fuel oxygen content on the emission of particulate mass for all experiments conducted on the SMFAE fuel samples and the fossil diesel fuel.

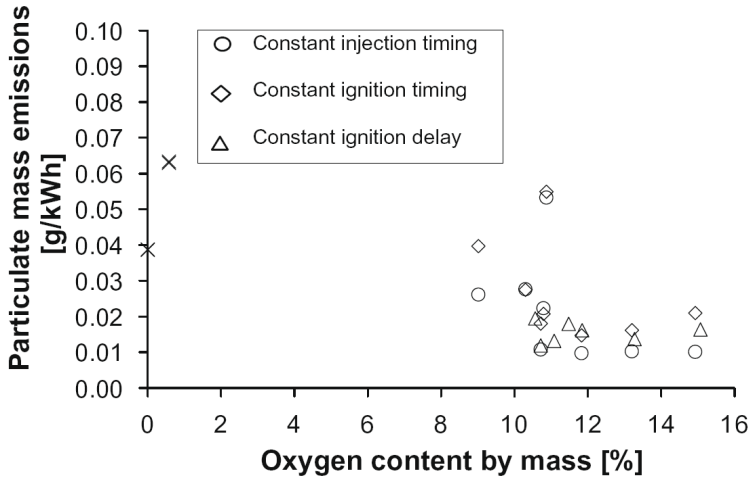

Figure 5.14 - Influence of fuel oxygen content on total particulate mass emissions

It can be seen that some degree of correlation may exist between the oxygen content of the fuel and particulate mass emissions. It should be noted that oxygen is not the exclusive factor affecting the formation of particulate mass. The experiments conducted on the number of double bonds in the fatty acid moiety have highlighted another significant influence. Introducing double bonds into the fatty acid moiety of the molecules increases the propensity of the molecules to form soot (Figure 5.8). The influence of the double bonds was clearly visible despite the fact that, under unadditised conditions (constant injection timing and constant ignition timing experiments), the more saturated molecules have a slightly lower oxygen content than those with more double bonds.

5.3.5. Influence of fuel standard boiling point on nucleation mode particulate number density

Figure 5.15 shows the relationship between the particulate number density of the nucleation mode particulates generated by all SMFAE samples in the experiments presented in sections 5.3.1-5.3.3 and their corresponding standard boiling points. The results show that as the boiling points of the individual fatty acid esters increase, a progressively higher number density of fine particles (5-40nm) was recorded by the mobility spectrometer. It should be noted that the number density of nucleation mode particles is not closely correlated with the total emission of particulate mass. This is because the nucleation mode particles do not bear a considerable amount of mass, due to their small size. The bulk of the total particulate mass is carried by the larger accumulation mode particles. The

correlation between the number density of nucleation mode particles and boiling point of the fuel (Figure 5.15) would support the theory that a large proportion of the nucleation mode particles may consist of liquid fuel droplets. It could be speculated that these form through condensation of unburned fuel during the late stages of the expansion of the cylinder charge, when temperatures drop below the boiling point of the fuel.

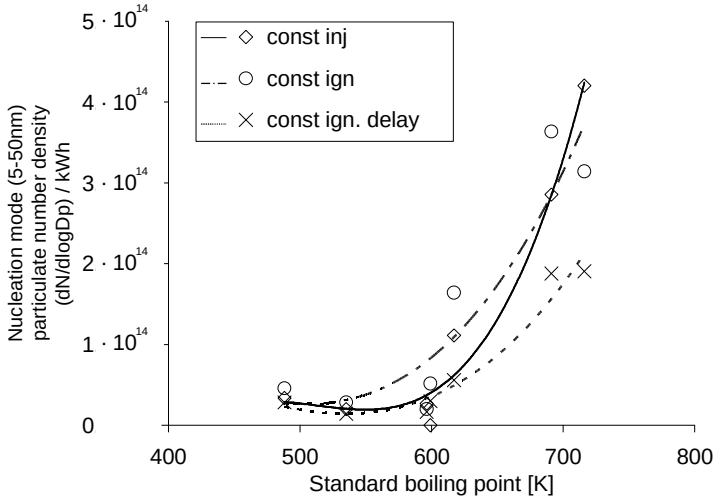

Figure 5.15 – Correlation between normal boiling point and nucleation mode particulate number density

5.3.6. Experiments with natural biodiesel (NB) fuel samples

In order to examine whether the observed structural effects of the SMFAE molecules were applicable to biodiesel fuels produced from natural fat products and alcohols, tests on four different NB fuel samples were carried out. These samples consisted of mixtures of fatty acid alkyl esters in different proportions (see Table 5.3). The oils and fat used for the transesterification process were palm oil, rapeseed oil, jatropha oil, and tallow, while the alcohol was methanol in all cases. Relevant properties of the NB samples were measured and are shown in Table 5.3.

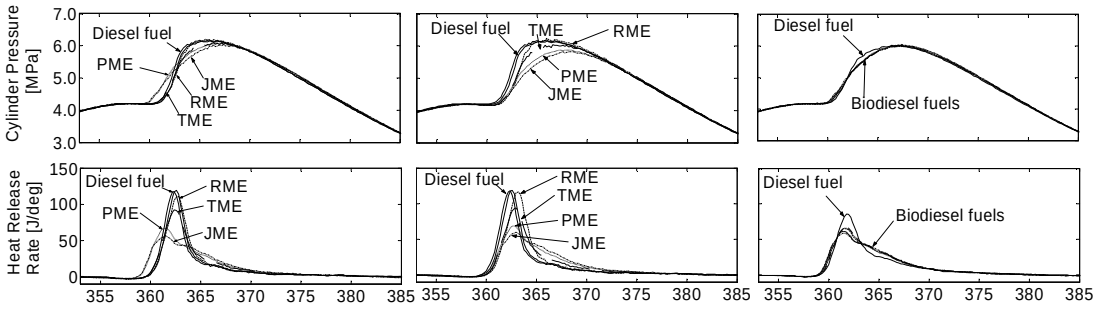

Figure 5.16 – Cylinder pressure and heat release rates for four biodiesel fuels and fossil diesel fuel

Figure 5.16 shows the cylinder pressure and heat release rates for experiments at constant injection timing, constant ignition timing and constant ignition delay. The palm oil methyl ester (PME) and the jatropha oil methyl ester (JME) had the shortest ignition delay in the unadditised experiments, followed by the tallow methyl ester (TME), rapeseed oil methyl ester (RME) and the fossil diesel fuel. For the experiments at constant injection timing and constant ignition timing, the total NO_x emissions show good correlation with the values of peak heat release rate as can be seen by comparing Figure 5.17 and Figure 5.16. The JME and PME had practically identical ignition characteristics, but the JME produced lower peak heat release rates and cylinder pressures due to its slightly lower calorific value. RME produced significantly higher NO_x emissions than the other NB fuels, even when the ignition delay was held constant.

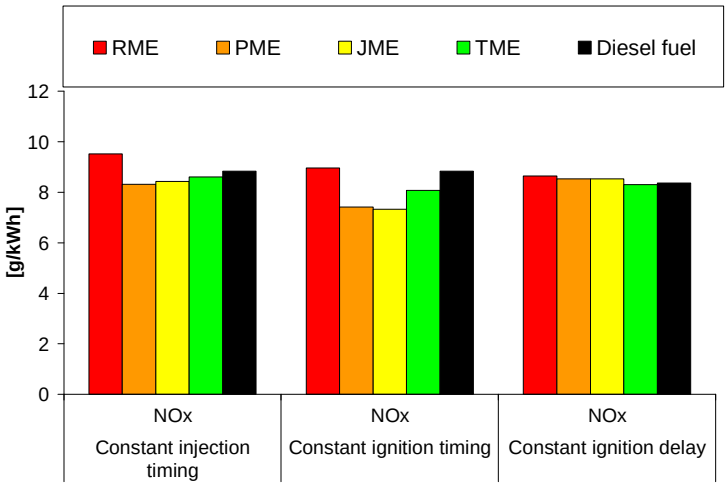

Figure 5.17 – NO_x emissions for four biodiesel fuels and fossil diesel fuel

Figure 5.18 shows that RME also produced the highest amount of particulate mass amongst the biodiesel fuels in all three experiments, even when the ignition delay was equalised. When the effect of ignition delay was removed, the TME produced the lowest amount of particulate mass, followed by the JME, PME and RME in this order. Fossil diesel fuel produced significantly more particulate mass than all NB samples in all experiments, which may be attributed to its lower oxygen content.

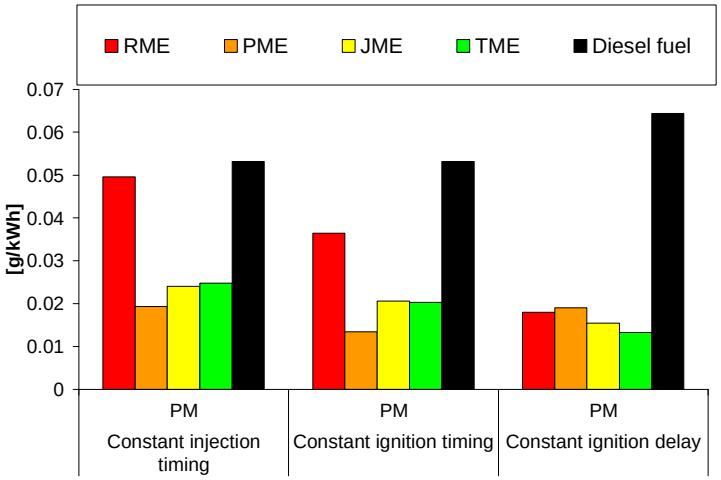

Figure 5.18 – Particulate mass emissions for four biodiesel fuels and fossil diesel fuel

Figure 5.19 shows the particulate size distribution for the experiments with constant ignition delay. Whilst the differences in total particulate mass seen in Figure 5.18 stem from differences in accumulation mode particles of the order of about 40-200 nanometres in size, clear patterns in the emission of very fine particles were observed which are not reflected in the total mass data. JME produced a large number of very fine particles, followed by PME, RME and finally TME. It is thought that these fine particles may consist mainly of condensed droplets of unburned fuel.

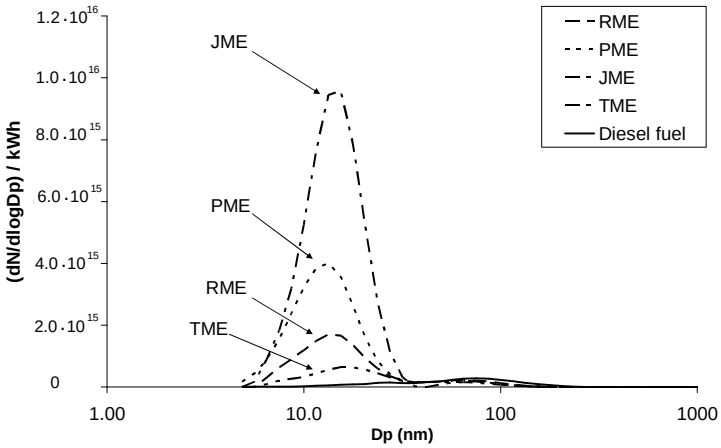

Figure 5.19 – Particulate size distribution for four biodiesel fuels and fossil diesel fuel

It should be recalled from the earlier experiments, that the nucleation mode particulate number density for individual fatty acid ester molecules was highest for the long-chained fully saturated fatty acid methyl esters. The formation of a high number of nucleation mode particles appears to be linked to the high boiling points of these fuel molecules. An interesting finding emerges when considering the fatty acid methyl ester composition of the four NB fuels in Table 5.3. The unusually high formation of nucleation mode particles from the jatropha methyl ester visible in Figure 5.19 may be linked to the high content (5.1%) of lignoceric acid (C24:0) methyl ester present in the jatropha NB fuel.

With regards to the total particulate mass emitted, it can be seen that the RME generally produces the highest amount of particulate mass in all experiments as well as producing the highest amount of specific emission of NO_x in all experiments. The fatty acid methyl ester composition (Table 5.3) shows that the RME contains by far the highest amount of unsaturated methyl esters (90.2% unsaturates) out of the four NB fuels. As the experiments with individual fatty acid methyl ester molecules had previously shown, these double-bonded molecules are likely to result in higher emissions of particulate mass due to their high propensity of forming soot precursors, as well as resulting in higher NO_x emissions. This suggests that the results obtained for the SMFAE molecules are able to explain some of the observations made for the combustion of the NB fuels which consist of mixtures of various fatty acid ester molecules.

5.3.7. Effects of ignition delay, adiabatic flame temperature and soot radiative heat transfer on NO_x formation

In the described experiments, the time of injection and the time of ignition of the fuel were accurately controlled in order to study the effects of combustion on NO_x emissions. Three distinct and layered phenomena were observed to significantly influence the exhaust gas emission of NO_x. The first one, which is the most influential, is the ignition delay. The second one appears to be one of the adiabatic flame temperature. A third phenomenon, soot-radiative heat transfer, may also be identifiable.

The first phenomenon is that of ignition delay. In diesel combustion, the magnitude of the ignition delay governs the proportion of fuel energy released in premixed combustion mode, the premixed burn fraction. This has been identified as a major influence on NO_x emission (Musculus, 2004). For constant load operation at either fixed start of injection or fixed start of combustion, the ignition delay has been shown to correlate well with NO_x emissions (Ladommatos, et al., 1996[a]). The mechanisms by which the ignition delay and premixed-burn fraction influences the formation of NO_x are not fully understood (Musculus, 2004). Optical diagnostics and crank-angle resolved in-cylinder gas sampling experiments have shown that nitric oxide is not significantly formed during the early premixed combustion phase, but forms specifically in the later diffusion flames of the mixing-controlled combustion phase (Voiculescu & Borman, 1978; Musculus, 2004; Dec & Canaan, 1998). It is believed that the premixed combustion occurs under too fuel-rich conditions to be conducive to significant amounts of nitric oxide formation (Dec & Espey, 1995). In some instances it has been shown, that if a higher proportion of fuel is burned in the rapid premixed combustion mode, this can lead to higher global cylinder gas temperatures which are conducive to higher amounts of thermal NO_x formation (Ladommatos, et al., 1996[a]). These higher temperatures influence not only the later stages of the premixed combustion phase, but also the subsequently occurring diffusion flames during which NO_x is mainly believed to be formed. If these peak temperatures occur earlier during the engine cycle, the time period over which conditions are conducive to NO formation may be prolonged. It is still doubtful whether this theory may provide a full explanation to the observed phenomenon, leading to further hypotheses about the relation between premixed burn-fraction and NO_x formation. It has been suggested that under sufficiently long ignition delay conditions, some of the premixed combustion may well become lean enough to support some nitric oxide formation (Musculus, 2004). It could also be hypothesised that a longer ignition delay of the fuel may also be reflected in longer lift-off lengths of the flames. This may cause more air-entrainment into the burning fuel spray. It is thought that additional air entrainment may lower the flame soot-loading. A lower flame soot-loading is in turn thought to cause higher flame temperatures because less heat may be dissipated from the flames via soot-radiative heat transfer ((Musculus, 2004; Cheng, et al., 2006).

A high correlation between ignition delay and NO_x emission was observed in the current experiments, as is illustrated in Figure 5.20.

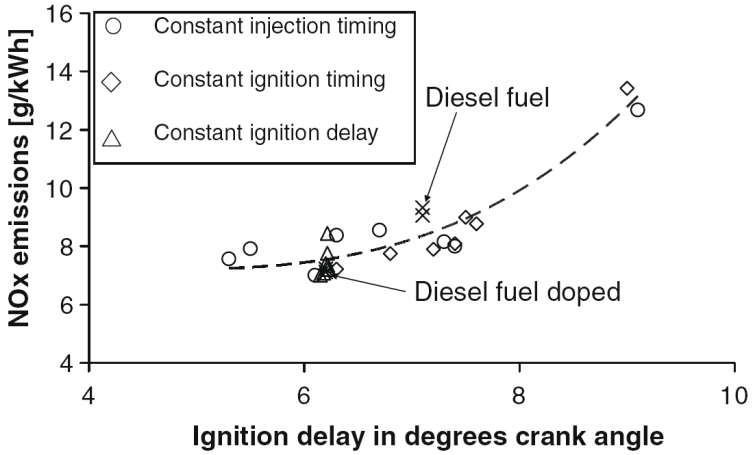

Figure 5.20 – Specific emission of NO_x versus ignition delay in crank angle degrees for all experiments with individual biodiesel molecules and fossil diesel fuel

The data presented in Figure 5.20 comprise the eight SMFAE molecules, as well as the fossil diesel fuel at all three experimental conditions (constant injection timing, constant ignition timing, and constant ignition delay). It can be seen in Figure 5.21 that the ignition delay controlled the fraction of heat released in premixed combustion mode and influenced the maximum heat release rate. The premixed burn fraction and peak heat release rate in turn influenced the magnitude of the peak global cylinder temperature and the timing at which this occurred.

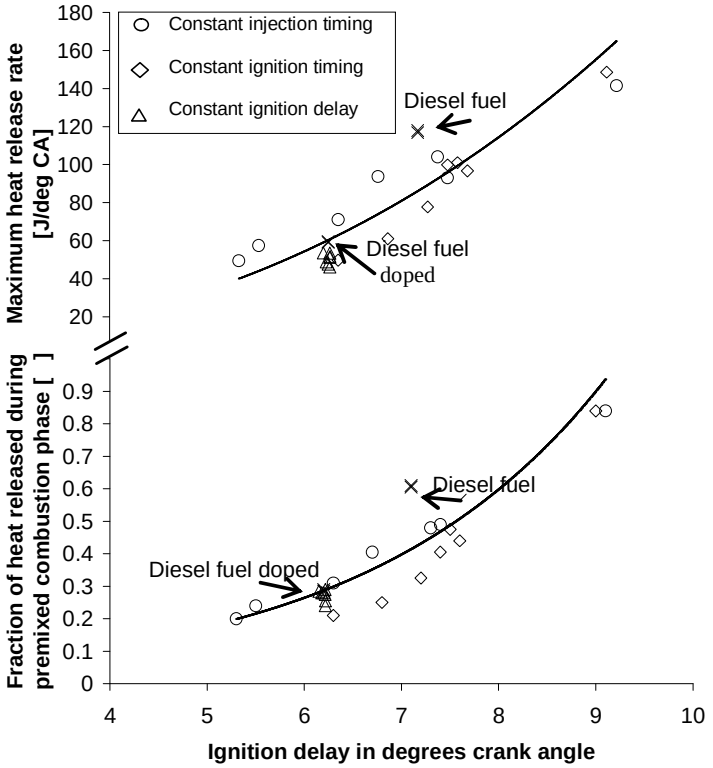

Figure 5.21 - Relationship between ignition delay and the proportion of heat released in premixed combustion and the maximum heat release rate during premixed combustion for all experiments with individual biodiesel molecules and fossil diesel fuel

The relation between NO_x emission and peak global cylinder temperature is illustrated in Figure 5.22. Figure 5.23 illustrates the relation between NO_x emission and the timing of the peak global temperature on a crank-angle basis. It is possible that other factors such as changes in local equivalence ratio (Φ) and changes in soot-radiative heat transfer due to differences in ignition delay may have influenced the formation of NO_x. Detailed examination of Figure 5.20-Figure 5.23 shows that if the ignition delay is equalised (constant ignition delay experiments), all other factors shown to correlate significantly with the emission of NO_x in these figures (i.e. the maximum heat release rate, the premixed burn fraction, the peak global gas temperature and its timing), become essentially constant. This indicated that these factors are strongly linked to ignition delay under the described experimental conditions. The ignition delay is defined by the time taken for auto-ignition to occur for each type of fatty acid alkyl ester molecule with air, and was strongly dependent on molecular structure.

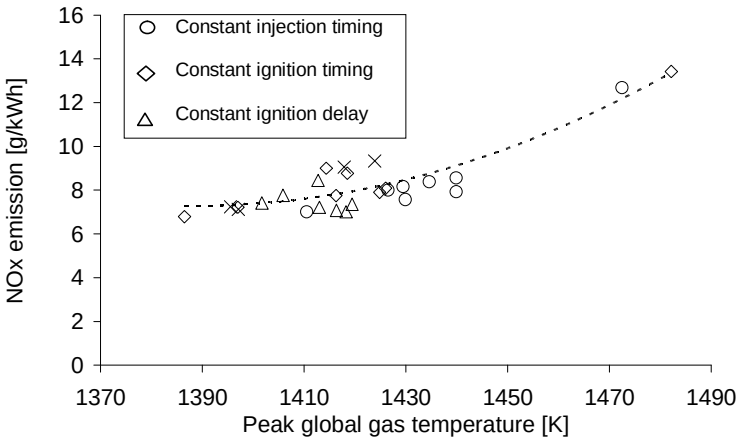

Figure 5.22 - NO_x emissions versus peak global temperature

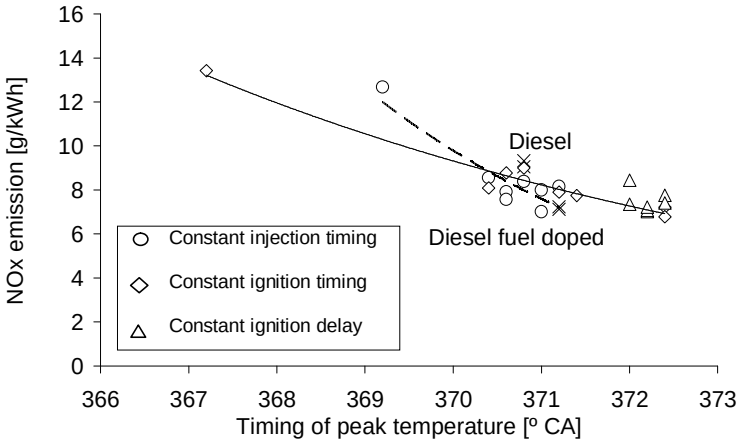

Figure 5.23 - NO_x emissions versus timing peak global temperature

The second phenomenon observable in the experimental results was that of adiabatic flame temperature. The effect of adiabatic flame temperature on NO_x emissions appears to be subordinated to that of ignition delay under certain conditions, and can be masked by this larger effect (Figure

5.3). The effect of ignition delay on NO_x emission was removed by equalising the ignition delay using 2-EHN as an additive, revealing the effect of adiabatic flame temperature, as shown in Figure 5.24. Figure 5.24 shows that a good correlation exists between the adiabatic flame temperatures of the molecules and the emission of NO_x, once the effect of ignition delay is removed. The adiabatic flame temperature was calculated for a stoichiometric mixture of the respective fuel with air ($\Phi = 1$) at constant pressure without any dissociation; the combustion products thus consisting only of CO_2, H_2O and N_2. The product mixture enthalpy is estimated using constant specific heats evaluated at the average flame temperature defined as:

$$T_{C_p} = \frac{1}{2}\left(T_i + T_{ad}\right)$$

Equation 5.1

Where T_i is the initial temperature of the reactants, and T_{ad} is the adiabatic flame temperature.

The calculation of adiabatic flame temperature is described in detail by Turns (1996, p. 32-35). The values presented in Figure 5.24 were calculated from an initial temperature T_i = 881 K. This is the peak air temperature achieved through isentropic compression of air at a constant ratio of specific heats (γ = 1.4) from standard atmospheric conditions (1 atm, 298.15 K) through a volumetric compression ratio of 15. This value is in fair agreement with the experimentally measured values at TDC during motoring of the engine at the same compression ratio. The enthalpy of formation of the fatty acid alkyl esters molecules in the case of Figure 5.24 were taken from the quantum chemistry calculations of Osmont et al. (2007) for the fatty acid monoalkyl esters, and Zeng et al. (2007) for the 2-EHN. The values of specific heat capacity of the products which were used to determine the product mixture enthalpy, were taken from the data provided by Turns (1996, p.514-546). The so calculated value of T_{ad} was used to re-estimate T_{c_p} in an iterative process, until the value of T_{ad} converged to within 1/10 K. It is expected that these simplified theoretical calculations predict values of adiabatic flame temperatures significantly above those occurring with dissociation taking place, but that the trend amongst the samples would be sustained.

The adiabatic flame temperature values presented in Figure 5.25 were calculated using experimentally determined values of enthalpy of combustion via the calorific value of the fuel. This was done to include the NB fuels and diesel fuel, for which no theoretical data on enthalpy of formation were available. The calorific value of the fuel samples was determined using bomb calorimetry (DIN 51900-2) from diluted samples of 1/5 fatty acid alkyl ester in 4/5 fossil diesel fuel. This was done for the NB fuels, fossil diesel fuel, as well as for the SMFAE samples. The calorific value obtained for all fuels are presented in Table 5.2 and Table 5.3 (except for the value for ethyl oleate, which was taken from Keffler & McLean (1935). The values shown in Figure 5.25 and Figure 5.24 show a maximum difference of 27 K between specific molecules. The general trend shows reasonable agreement between both methods.

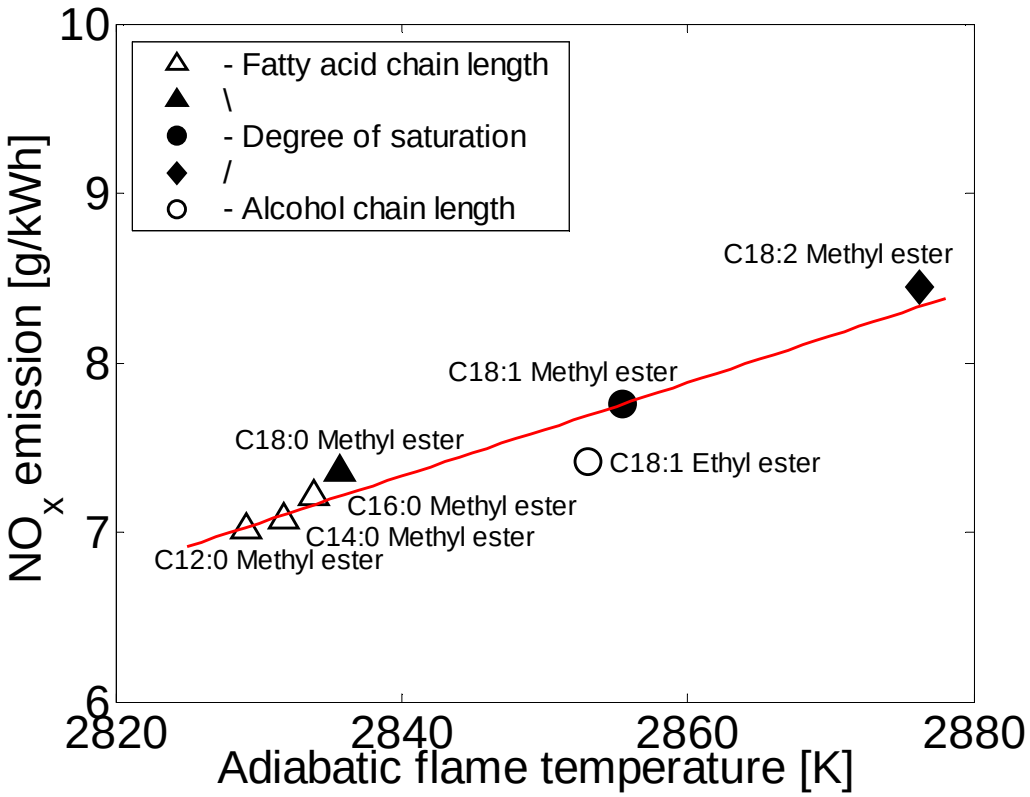

Figure 5.24 - Relationship between measured NO_x emission and calculated adiabatic flame temperature at constant pressure for a stoichiometric air-fuel mixture (Φ=1) with no dissociation; combustion starting at 881 K and 4.5 MPa. Engine running condition 1200 rev/min engine speed and 0.4 MPa IMEP; ignition delay equalised to 6.2 °CA for all fatty acid monoalkyl molecules

Figure 5.25 shows the effect of adiabatic flame temperature when the ignition delay is equalised for two series of experiments: the SMFAE fuel samples and the NB fuels. These two series of experiments had different ignition delays. The reason for this is that in each case, the ignition delay was equalised to that of the fuel with the shortest ignition delay, within that group of fuel samples. In the case of the SMFAE fuels the ignition delay was constant at 6.2° crank angle and in the case of the NB fuels at 6.7° crank angle. The fossil diesel fuel was tested in both series of experiments with different concentrations of 2-EHN.

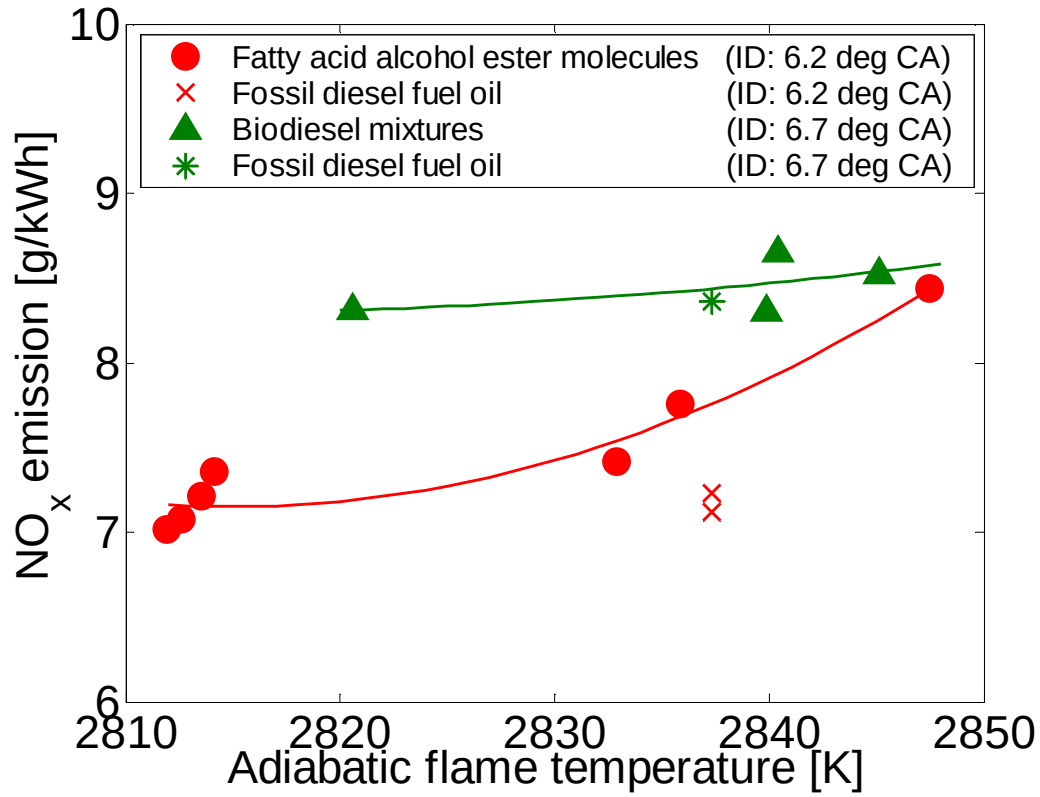

Figure 5.25- Relationship between measured NO_x emission and calculated adiabatic flame temperature at constant pressure with no dissociation (Φ=1). Engine running condition 1200 rev/min engine speed and 0.4 MPa IMEP; ignition delay (ID) equalised to 6.2 °CA for all pure molecules, and ignition delay equalised to 6.7 °CA for biodiesel fuels from natural oils and fat. Combustion starting at 881 K and 4.5 MPa.

Figure 5.25 shows that as the ignition delay becomes shorter, the gradient of the correlation of NO_x emission with adiabatic flame temperature becomes steeper. This would suggest that as the ignition delay becomes shorter, the influence of premixed burn fraction is reduced, and the influence of the adiabatic flame temperature on the total emission of NO_x becomes stronger. This means that for fuels of higher ignition quality, the adiabatic flame temperature plays a more significant role in governing the formation of NO_x. A similar increase in the influence of adiabatic flame temperature could be hypothesised for engine operating conditions involving a lesser proportion of premixed combustion and a higher proportion of diffusion controlled combustion.

An interesting observation from Figure 5.7 and Figure 5.8 is that some of the molecules tested tended to produce both higher NO_x and particulate emissions. For example, this is observed in the case of the unsaturated (double bonded) molecules where NO_x and particulates increase with greater degree of unsaturation resulting in a positive correlation between NO_x and particulates. It could therefore be suggested that the effect of radiative heat transfer from soot is in this case subordinated to the effect of adiabatic flame temperature in controlling the exhaust gas emission of NO_x in these experiments.

However this third phenomenon, of soot-radiative heat transfer, may still be distinguishable in the experimental results presented. Figure 5.25 tentatively implies that the emission of NO_x from diesel fuel does not quite lie with the trend observed for the SMFAE molecules, or for the NB fuels. This could suggest that the effect of adiabatic flame temperature may still not fully explain the observed increase of NO_x emissions with respect to fossil diesel fuel. It is tentatively hypothesised that this difference may be attributed to a difference in soot radiative heat transfer between diesel fuel and the biodiesel molecules as suggested by Cheng et al. (2006).

5.3.8. Analysis of particulate matter

A simple analysis of the particulate matter was conducted to investigate the physical nature of the particulate matter and to explain the formation of the high number of very fine particles around 5-40 nm in diameter. This was done in an effort to understand whether the small nucleation mode particles (5-40 nm) consisted of carbonaceous soot or another material, such as volatile organic matter deriving from unburned fuel. For this purpose the particles were classified and collected according to aerodynamic size by inertial impaction on the MOUDI aerodynamic cascade impactor. This was done for two of the fuels: the stearic acid methyl ester to represent a SMFAE fuel with high boiling point (C18:0 methyl ester, which formed the largest number of small particles) and fossil diesel fuel.

In order to simplify the analysis, two samples of particulate matter from each fuel were examined, one to represent the nucleation mode particles of the order of 10-18 nanometres in diameter, and one to represent the accumulation mode particles around 100 nanometres in diameter. The particulate samples were analysed using transmission and scanning electron microscopy (TEM & SEM), thermogravimetric analysis (TGA) and energy dispersive X-ray photoelectron spectroscopy (XPS).

Transmission- and scanning electron microscope images

Upon optical examination using TEM and SEM, the particulate matter collected from the combustion of fossil diesel fuel and methyl stearate appeared to consist mainly of large agglomerations of primary carbon particles. It was found that some particles collected on the impaction stages which were supposed to contain only particles of 5-40 nanometres in diameter, were much larger than expected, and often in the range of several hundred nanometres diameter. Since the individual particles lay far apart from each other upon the membrane onto which they were impacted, it is believed that they did not agglomerate on the membrane itself, but that they formed at such size within the engine. This is an indication that the inertial impactor did not separate the particles as accurately as it was aimed in the experiment. Similar difficulties with accurate particle separation have been reported by Stein et al. (1994) and Park et al. (2003).

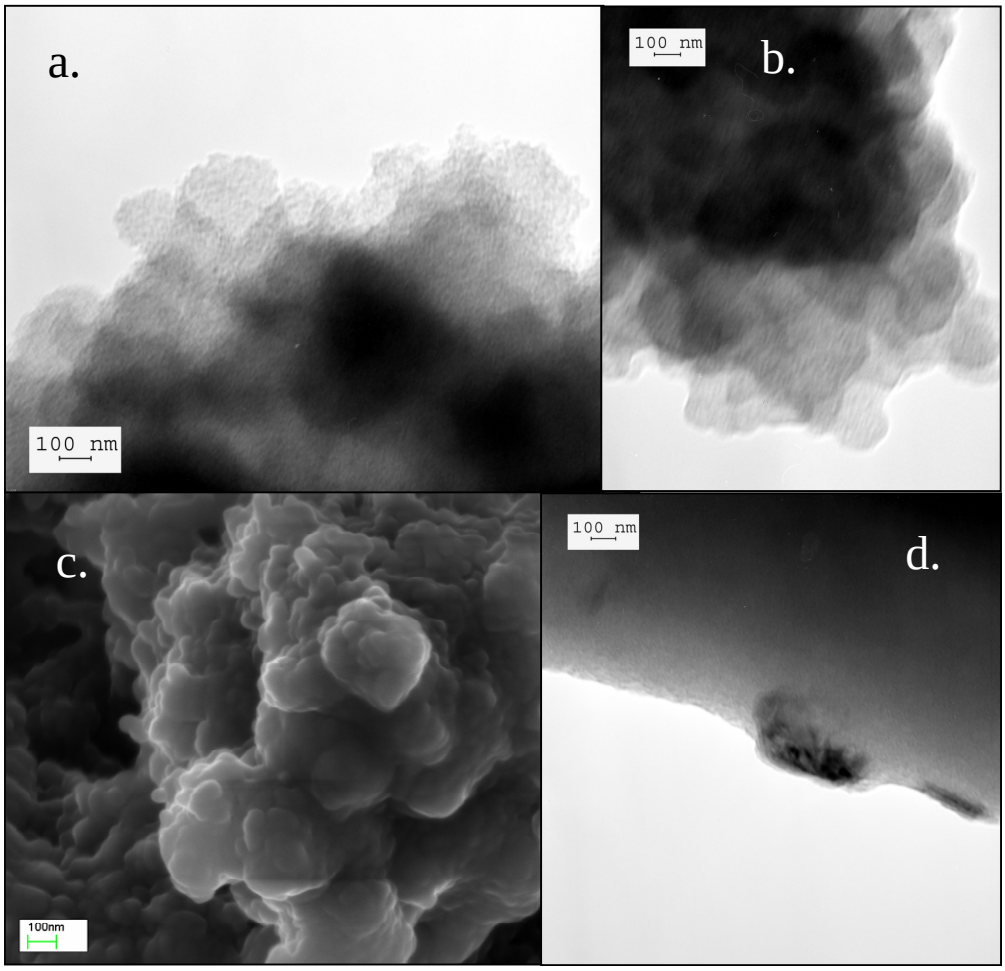

Figure 5.26 – TEM and SEM micrographs particulates from the combustion of fossil diesel fuel (a., c.) and TEM micrographs from the combustion of methyl stearate (b., d.). Larger particles are shown in figures a. and b., smaller particles are shown in figures c. and d.

Figure 5.26 a. and b. show TEM micrographs of particulates that were collected on the accumulation mode impaction stage of the MOUDI (40-200nm nominal size). Figure 5.26 a. shows a particulate produced by the combustion of fossil diesel fuel whilst Figure 5.26 b. one produced by the combustion of methyl stearate. Both particulates have a similar granular structure consisting of primary particles forming larger clusters. It is visible that the particulates produced from the combustion of methyl stearate shown in Figure 5.26 b. have a smoother surface than those produced by fossil diesel fuel, shown in Figure 5.26 a. This could be an indication of a higher fraction of condensed fuel being adsorbed onto the particulates. A similar observation has been reported by other researchers (Boehman, et al., 2005).

Figure 5.26 c. and d. show SEM and TEM micrographs of particulates that were collected on the nucleation mode impaction stage of the MOUDI (10-18nm nominal size). Figure 5.26 c. shows a SEM image for a particle produced by the combustion of fossil diesel fuel, whilst Figure 5.26 d. shows a TEM image of particulate matter produced by the combustion of methyl stearate. It was generally observed that the smaller particles collected on the nucleation mode impaction stages (10-

18 nanometres diameter nominal size), were smoother in surface structure, than those collected on the accumulation mode impaction stages (56-100nm nominal size). This may suggest a higher fraction of volatile organic compounds adsorbed on the particulates. The nucleation mode impaction stages for methyl stearate (10-18nm) included some particles (Figure 5.26 d.) which did not follow the general pattern of clusters of carbonaceous primary particles previously observed in Figure 5.26 a.-c. These particles had a smooth surface and may be crystalline in structure. It could be tentatively hypothesised that they represent particles consisting of crystallised fuel droplets, but this could not be proven by the optical examination carried out.

Thermogravimetric analysis

Thermogravimetric analysis was conducted on particulate samples collected in the nucleation stage (10 to 18nm) and one of the accumulation stages (320 to 560nm) of the micro-orifice uniform distribution (MOUDI) aerodynamic cascade impactor. The filters used as a substrate for the collection of the particulates were made of pure, binder-free quartz, heat resistant up to 1093°C, and had previously been heat-treated to remove traces of organic compounds (Tissuquartz Filters, Pallflex). The particulate mass collected for one sample was approximately 5mg. In the analysis of the results, the thermogravimetric mass loss recorded for a blank filter was subtracted from that of a filter loaded with particulates, in an effort to eliminate any mass loss effects attributable to the quartz filter itself. The particulates on their filter substrate were heated at a rate of 5°C/min from 25°C to 800°C in a flow of pure nitrogen gas. Figure 5.27 shows, that the finer particulates started losing their volatile mass fraction at a comparatively low temperature of 40ºC, whilst the coarser particulates required a higher temperature of around 120ºC. These observations suggest that the finer particulates contained either lighter volatile fractions or a higher water fraction which vaporised at lower temperatures than those of the coarser particles.

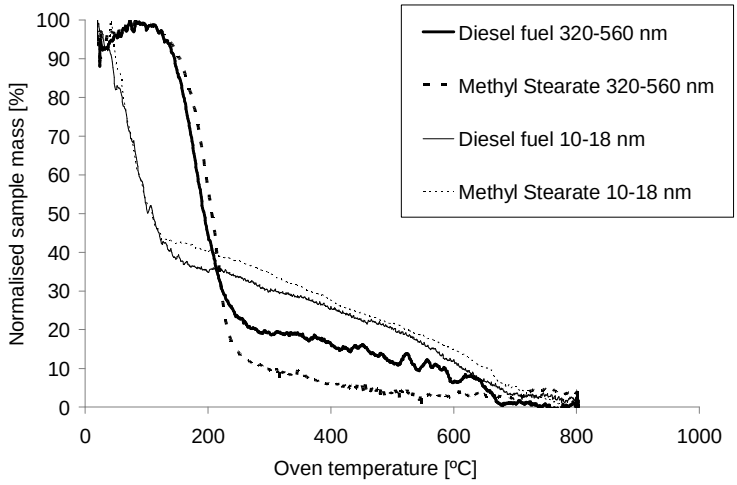

Figure 5.27 - Thermogravimetric analysis of nucleation and accumulation mode particulates separated and collected by a micro-orifice uniform distribution (MOUDI) aerodynamic cascade impactor

X-ray photoelectron spectra

X-ray photoelectron spectroscopy (XPS) spectroscopy was carried out on the particulates using an excitation voltage of 5 kV. The XPS was performed separately for particulates produced by the combustion of fossil diesel fuel and methyl stearate respectively. The particles from either fuel were further separated into nucleation mode (10-18nm) and accumulation (56-100nm) mode particulates using the MOUDI aerodynamic cascade impactor. The results are summarised in Figure 5.28. The particulates produced by methyl stearate gave a larger elemental count of oxygen than those produced by the combustion of fossil diesel fuel. Elemental analysis of the original fuels before combustion, shows that the stearate molecules contained 10.72% by mass of oxygen while the fossil diesel fuel only contained 0.07% by mass of oxygen. There appears to be a correlation between the oxygen content of the fuel, and the oxygen content of the particulates produced by the combustion of the fuel. The particulate samples showed oxygen contents of 6-8% for methyl stearate, and of 4-5% for fossil diesel fuel. This is in fair agreement with the oxygen contents reported in other studies (Williams, et al., 2006; Song, et al., 2006; Popovicheva, et al., 2006). Figure 5.28 further shows that for both fuels, the oxygen to carbon ratio for the finer (nucleation) particles is greater than that for the coarser (accumulation) particles. It could be speculated that the higher oxygen content of the finer nucleation mode particles may be attributable to a higher fraction of condensed fuel.

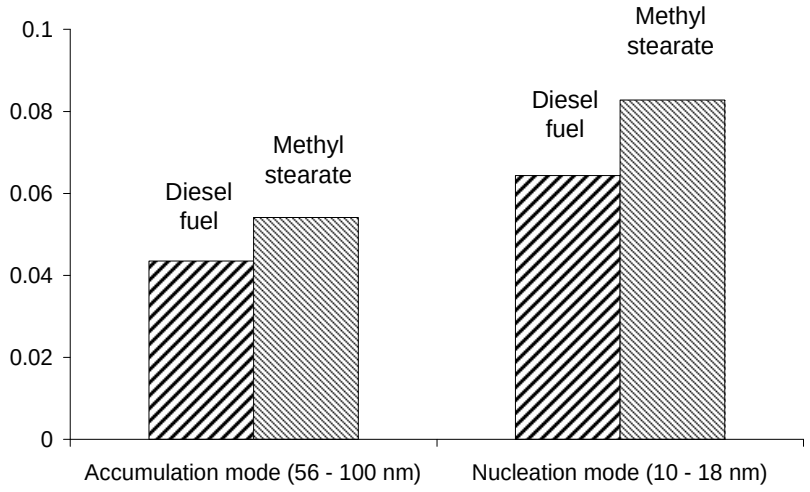

Figure 5.28 - Relative quantity of XPS detection counts of oxygen versus carbon atoms

5.3.9. Experiments with biodiesel and its blends with diesel fuel at higher engine loads and speed with pilot injection

A further series of experiments was carried out in order to examine the behaviour of biodiesel fuels and its blends with fossil diesel fuel. The tests were intended to verify some of the trends observed in sections 5.3.1 - 5.3.7 at higher engine loads and speeds, under engine operating conditions that are more representative of practical engine applications. The experiments were conducted on blends in fossil diesel fuel of 0%, 5%, 10% 50% and 100% jatropha methyl ester (JME) and tallow methyl ester (TME). The tests were conducted at three combinations of higher loads and engine speeds, and employed a split-injection strategy, consisting of a pilot fuel injection and a main fuel injection. The engine operating conditions are summarised in Table 5.4.

Table 5.4 - High engine speed and load operating conditions for blends of JME & TME in fossil diesel fuel

		Condition 1	Condition 2	Condition 3
IMEP	**[bar]**	4	8	8
Engine speed	**[rpm]**	2000	2000	3500
Injection pressure	**[bar]**	450	1200	1400
Pilot injection timing	**[° CA BTDC]**	31	36	42
Nominal pilot duration	**[µs]**	342	270	280
Pilot energy	**[J]**	180	300	600
Main injection timing	**[° CA BTDC]**	10	9	12
Nominal main duration	**[µs]**	770	1360	1650

It should be noted that during the course of these experiments the engine was operating under less stable conditions than for all other experiments presented in this thesis. The reason for the unsteady engine operation was a fluctuation in the fuel injection pressure of up to 40 bar around the nominal injection pressure, as a consequence of unstable operation of the common-rail control system. The tests were carried out using the conventionally operating common rail injection system described in Chapter 3, section 3.4.1. The reason for this instability in injection pressure was an excessively high pressure drop through the fuel cooler situated in the fuel return line of the common rail, which caused a pressure build-up in the fuel return line, and prevented adequate release of the return fuel from the common rail. The problem was resolved, subsequently to these results being recorded, by re-designing the fuel cooler to produce a lower pressure drop. The main effects of the unsteady injection pressure were fluctuating fuel flow readings, unsteady cylinder pressure traces and erratic NO_x readings. The trends in the heat release rates and particulate emissions proved comparatively insensitive to these fluctuations. It was decided to present the data from these experiments despite these shortcomings, bearing in mind that the stability of the engine was compromised.

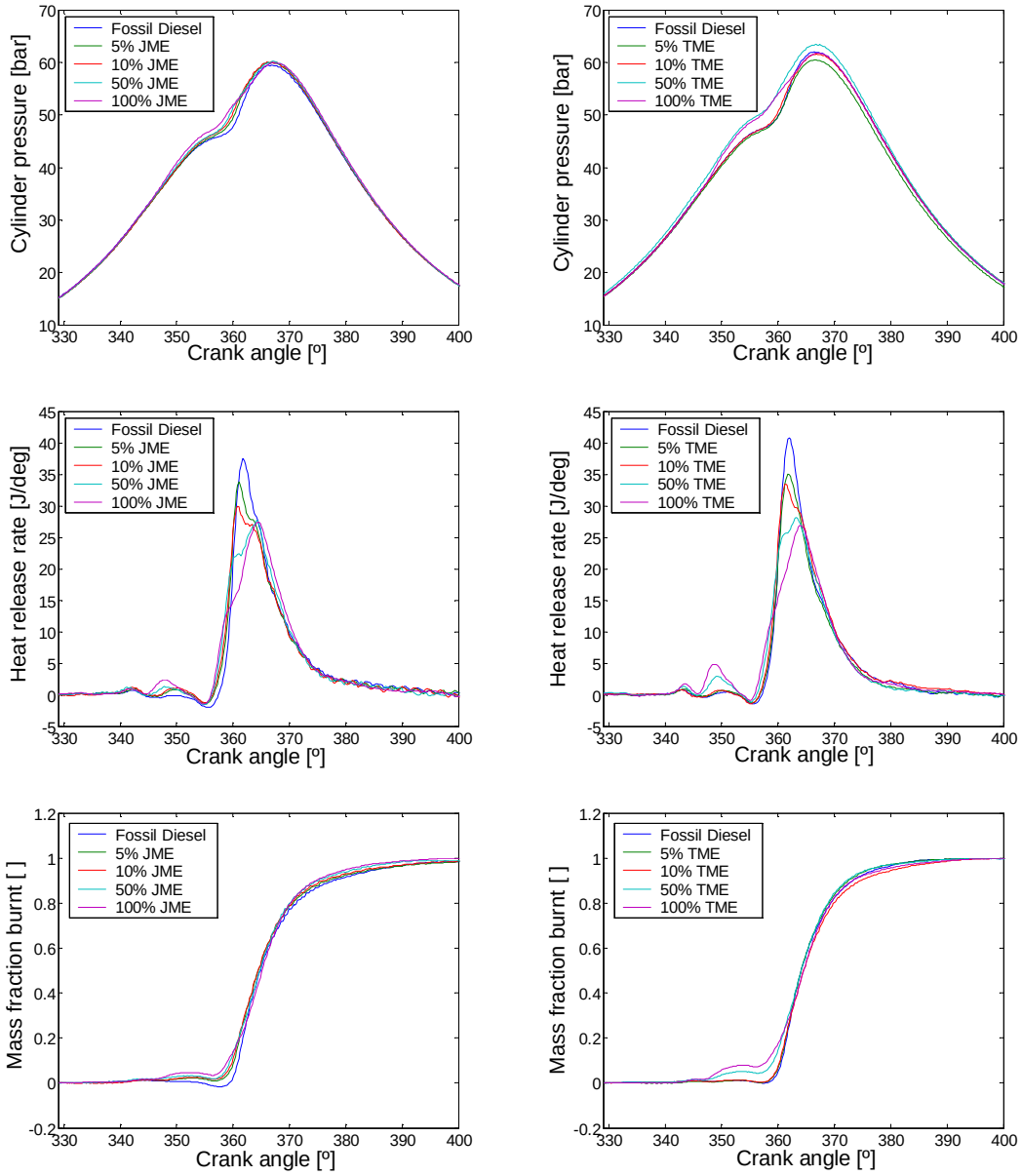

Figure 5.29 – Condition 1: High-load high-speed engine running condition showing cylinder pressure, heat release rates and mass fraction burnt analysis for JME blends (l.h.s.) and TME blends (r.h.s.) in fossil diesel fuel

The pilot injection was adjusted for every fuel sample in an attempt to keep the amount of energy injected during the pilot injection constant. This was done as follows: The main injection was switched-off, and the pilot injection was moved to the timing of the main injection (e.g. 10 º BTDC for condition 1; see Table 5.4 for other conditions). The pilot injection was then switched on and its duration was adjusted until the total heat released during combustion reached the pre-determined value of 180 Joules. The timing of the pilot injection was then returned to its nominal value (e.g. 31º BTDC, see Table 5.4 for other conditions) and the main injection was subsequently switched on.

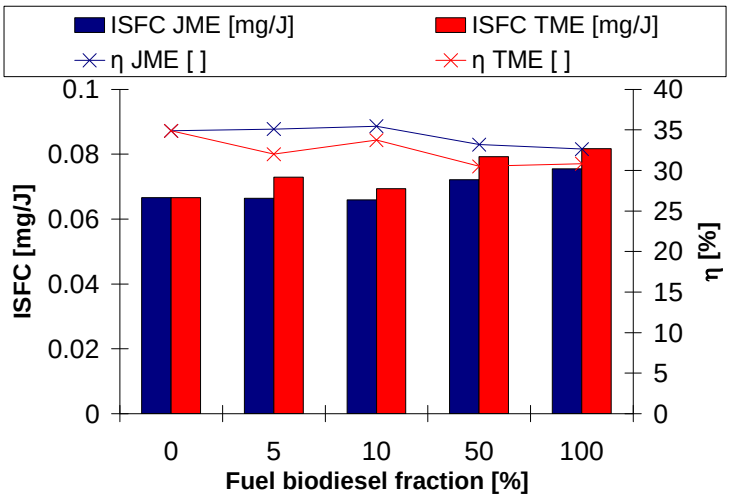

Figure 5.30 - Condition 1: ISFC and indicated thermal efficiency of JME & TME blends in fossil diesel fuel

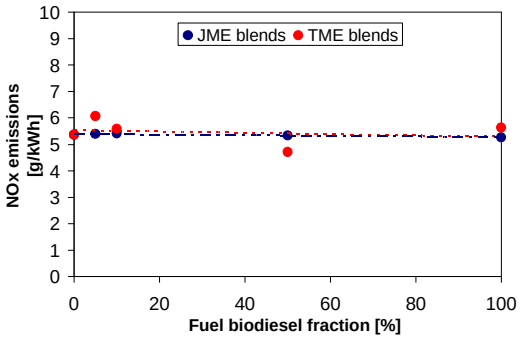

Figure 5.31 - Condition 1: NO_x emissions of JME and TME blends

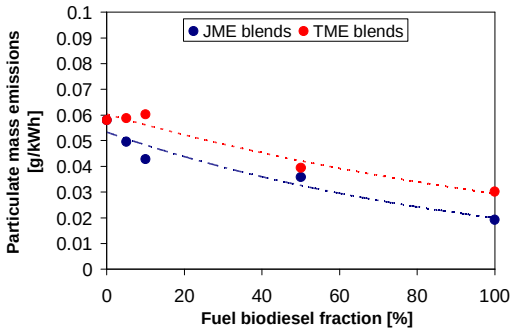

Figure 5.32 – Condition 1: Particulate mass emissions of JME and TME blends

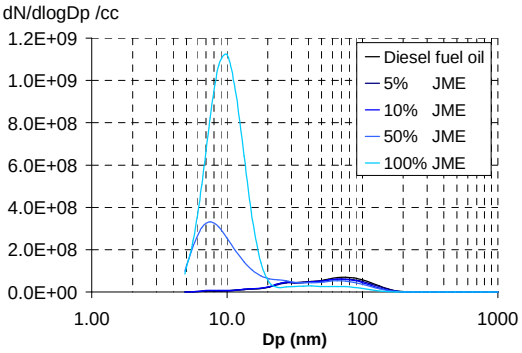

Figure 5.33 - Condition 1: Particulate size distribution of JME blends in diesel fuel

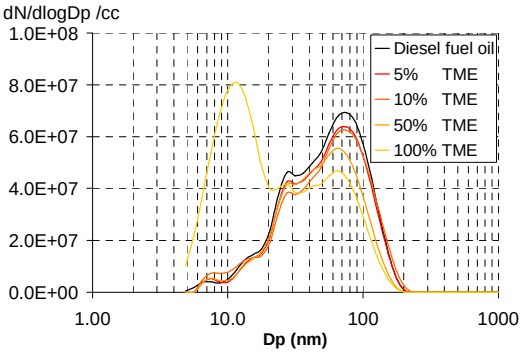

Figure 5.34 - Condition 1: Particulate size distribution of TME blends in diesel fuel

The duration of the main injection was then adjusted to yield the total nominal IMEP (e.g. 4 bar for Condition 1, see Table 5.4 for other conditions). This procedure was carried out for every fuel sample in this set of experiments, in order to try keeping the fuel energy injected into the combustion chamber during the pilot injection near-constant.

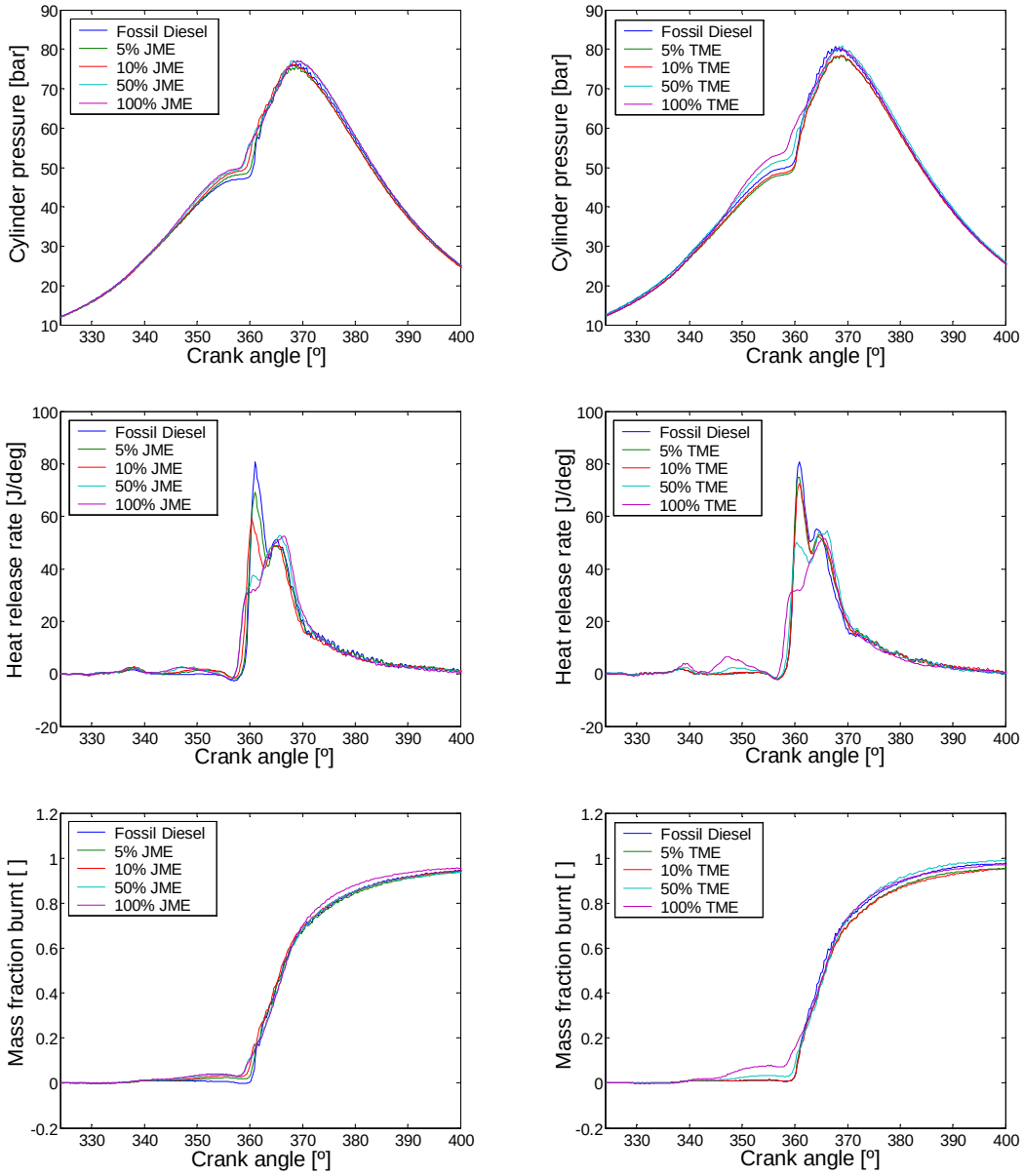

Figure 5.35 - Condition 2: High-load high-speed engine running condition showing cylinder pressure, heat release rates and mass fraction burnt analysis for JME blends (l.h.s.) and TME blends (r.h.s.) in fossil diesel fuel

A number of relatively clear trends could be observed in the data. The heat release rate of combustion depicted in Figure 5.29, Figure 5.35, Figure 5.41 shows that two separate heat release phases were discernible which corresponded to heat released from the pilot fuel injection and from the main fuel injection respectively. As the biodiesel content (JME or TME) in the fuel was increased, a progressively higher peak heat release was recorded during the pilot fuel combustion phase and a progressively lower heat release was recorded during the combustion of the fuel from the main injection.

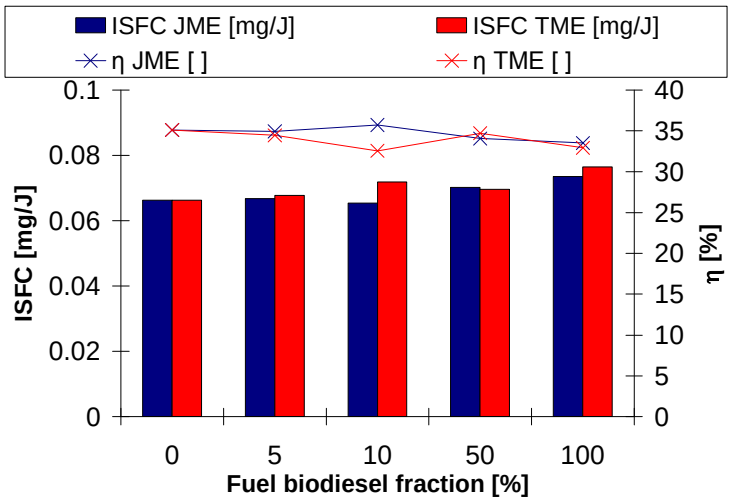

Figure 5.36 - Condition 2: ISFC and indicated thermal efficiency of JME & TME blends in fossil diesel fuel

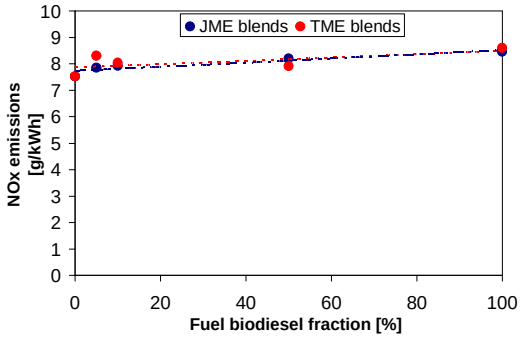

Figure 5.37 - Condition 2: NO_x emissions of JME and TME blends

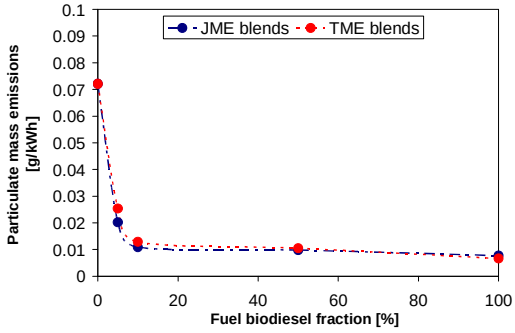

Figure 5.38 – Condition 2: Particulate mass emissions of JME and TME blends

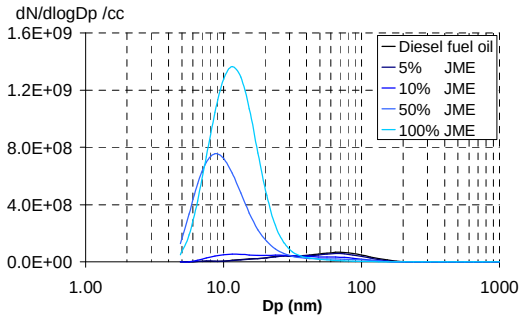

Figure 5.39 - Condition 2: Particulate size distribution of JME blends in diesel fuel

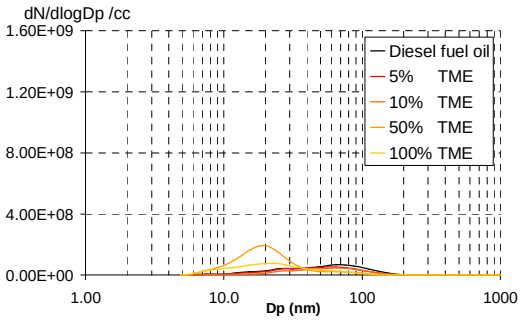

Figure 5.40 - Condition 2: Particulate size distribution of TME blends in diesel fuel

This may be attributed to the higher ignition quality of biodiesel (CN_{JME} = 57.8, CN_{JME} = 57.2) in comparison to fossil diesel fuel (CN_{JME} = 49.8), which resulted in a shorter ignition delay of the fuel injected during the pilot injection.

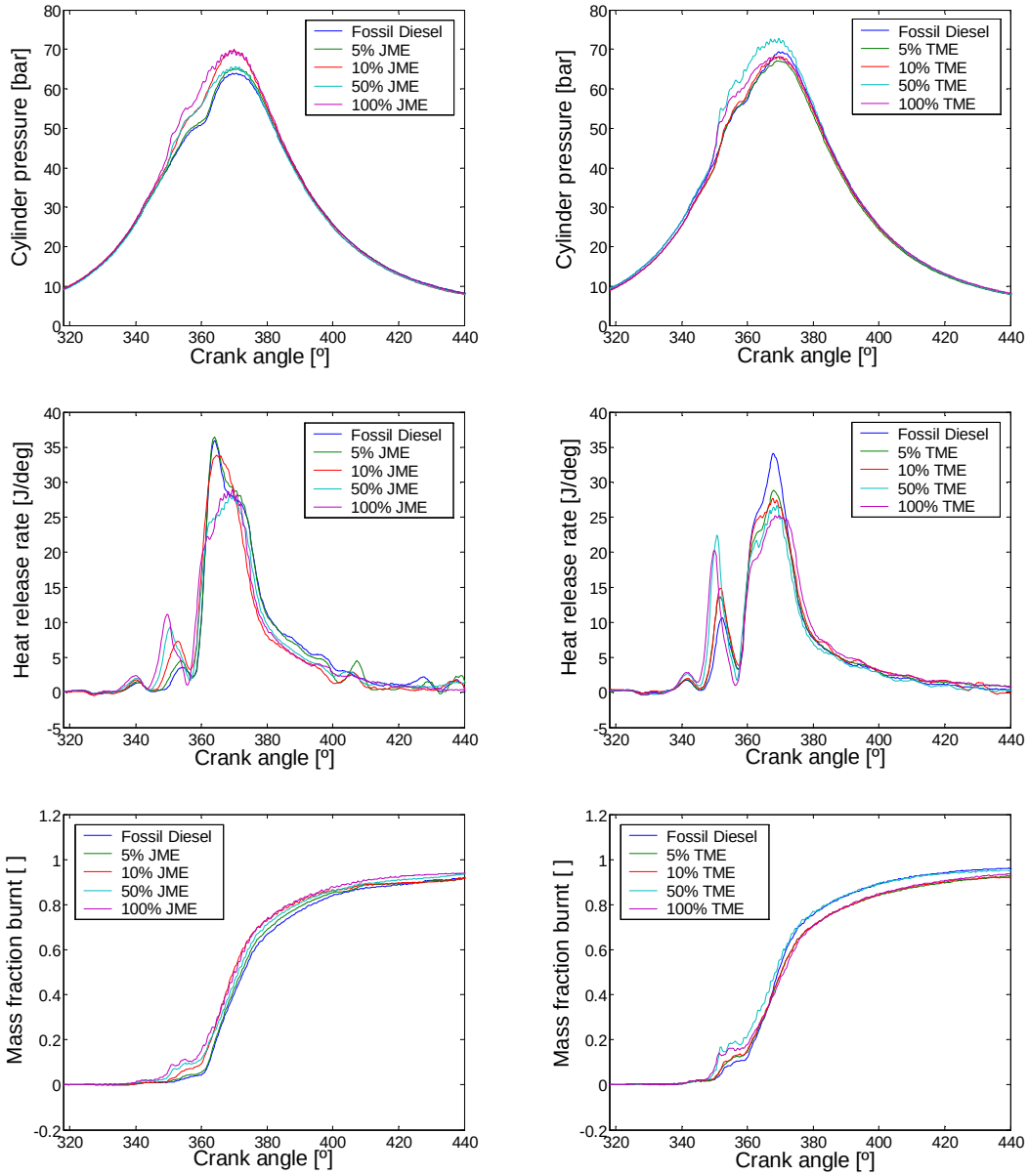

Figure 5.41 - Condition 3: High-load high-speed engine running condition showing cylinder pressure, heat release rates and mass fraction burnt analysis for JME blends (l.h.s.) and TME blends (r.h.s.) in fossil diesel fuel

The shorter ignition delay for the biodiesel blends is thought to have allowed a lesser proportion of the pilot-injection fuel to have mixed excessively with air, and thus resulted in a lesser portion of fuel having failed to ignite. This is thought to have resulted in a larger amount of heat being released for biodiesel during the pilot combustion phase than for fossil diesel fuel. In consequence, the combustion chamber pressures and temperatures after the pilot combustion phase became higher for the biodiesel fuels than for the diesel fuel, which in conjunction with the higher ignition quality of the ester fuels, reduced the ignition delay of the main fuel injection, and resulted in a smoother main combustion phase with lower peak heat release rates.

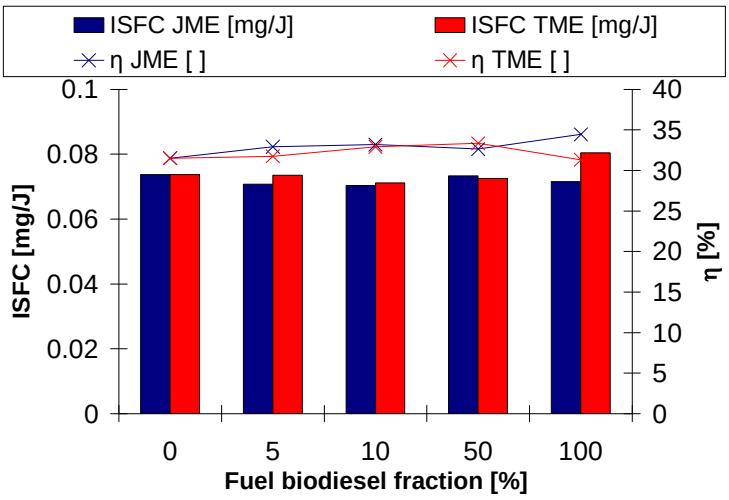

Figure 5.42 - Condition 3: ISFC and indicated thermal efficiency of JME & TME blends in fossil diesel fuel

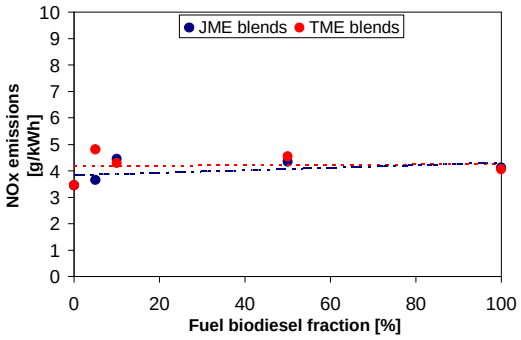

Figure 5.43 - Condition 3: NO_x emissions of JME and TME blends

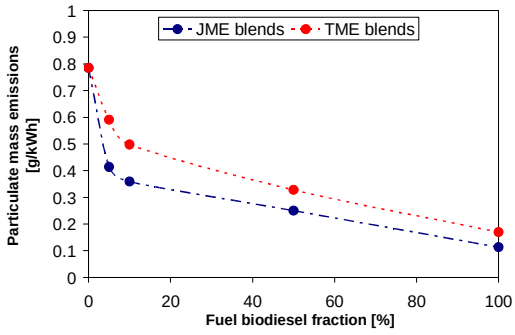

Figure 5.44 – Condition 3: Particulate mass emissions of JME and TME blends

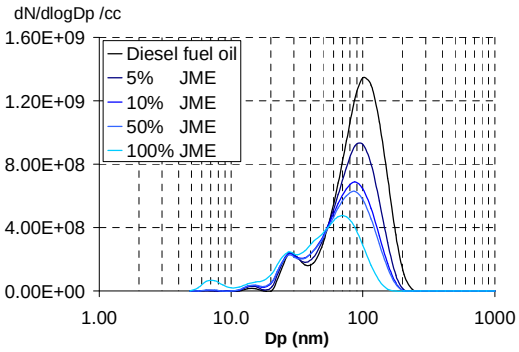

Figure 5.45 - Condition 3: Particulate size distribution of JME blends in diesel fuel

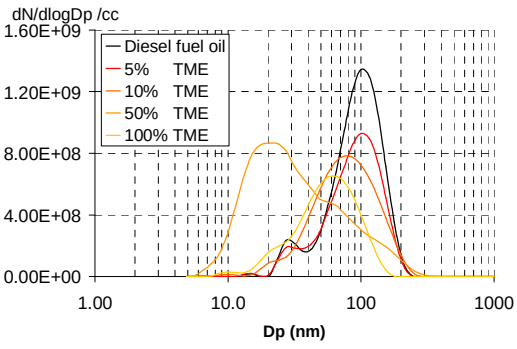

Figure 5.46 - Condition 3: Particulate size distribution of TME blends in diesel fuel

In order to produce the same indicated load, biodiesel required 11-17% longer injection duration than fossil diesel fuel, which resulted in a slightly longer duration of heat release during the main combustion phase for biodiesel than for diesel fuel. It is visible from the shape of the heat release traces presented in Figure 5.29, Figure 5.35 and Figure 5.41 that under these higher load conditions

with pilot injection, a significantly larger portion of the total heat release took place in diffusion combustion mode than for the earlier single-injection experiments presented in sections 5.3.1-5.3.3. It has been discussed in section 5.3.7, that as the proportion of heat released in the diffusion-controlled combustion phase increases, the adiabatic flame temperature gains in relative importance with respect to the effect of premixed burn fraction as an influence on NO_x formation. The NO_x emission for the experiments with pilot injection is shown in Figure 5.31, Figure 5.37 and Figure 5.43. The results show that switching the fuel from fossil diesel fuel to biodiesel resulted in a relatively similar level of NO_x emissions, although a minor increase in NO_x emissions may be discernable amongst the data, especially for the higher-load conditions conducted at an IMEP of 8 bar. This increase in NO_x should be considered with caution, due to the relatively unstable operation of the engine, but it is possible that this marginal increase in NO_x emission may be attributable to the slightly higher adiabatic flame temperature of the two biodiesel fuels. The adiabatic flame temperature from initial conditions of T_i = 881 K and p_i = 45 bar was calculated to be 2845 K for JME, 2840 K for TME and 2837 K for fossil diesel fuel (see Turns (1996, p.32-35)).

The emission of total particulate mass from the experiments is presented in Figure 5.32, Figure 5.38 and Figure 5.44. The data show that a clear reduction in particulate mass emissions occurred as the biodiesel content of the fuel was increased, and that the reduction was more pronounced under higher load conditions (8 bar IMEP) than at the lower load operation (4 bar IMEP). The reductions in total particulate mass emissions may be attributed to the oxygen content of the fuel which supports the oxidation of soot and its precursors within the fuel rich core of the fuel spray. The size spectral density of the particulate mass is shown in Figure 5.33, Figure 5.39 and Figure 5.45 for the combustion of JME blends, and in Figure 5.34, Figure 5.40 and Figure 5.46 for the combustion of TME blends. The results indicate that an increase in biodiesel fuel content (TME or JME) resulted in a notable decrease of accumulation mode particulate emissions. This is particularly clearly visible in Figure 5.34 due to its reduced ordinate scale, which emphasises the differences in the amount of accumulation mode particles.

The size spectral density of the particulates shows that JME produced a significantly larger amount of nucleation mode particles (5-40 nm diameter) than TME and diesel fuel. This confirmed the findings previously shown in section 5.3.6 (Figure 5.19), which showed that JME produced a significantly larger amount of nucleation mode particles (5-40 nm diameter) than TME and diesel fuel under single-injection engine operating conditions. As discussed in section 5.3.5, the boiling point of a fuel is thought to exert a strong influence on the formation of such nucleation mode particles (Figure 5.15), since these are believed to be largely formed by condensation of unburned fuel in the exhaust gases. The high content (5.1% by mass) of lignoceric acid (C24:0) methyl ester present in JME, is thought to have been the main cause of the high emission of nucleation mode particles from the combustion of JME. Lignoceric acid methyl ester is estimated to have a normal boiling point of 687 K (Yuan, et al., 2005), which is higher than the exhaust gas temperature of 583 K recorded for JME when operating at 2000 rpm and 4 bar IMEP. These findings suggest that some of the observations made for the single-injection experiments in sections 5.3.1-5.3.6 are also applicable to higher load and speed engine operation with pilot injection.

5.4. Conclusions

The ignition delay of the fatty acid monoalkyl ester molecules depended strongly on their molecular structure. An increase in the length of the fatty acid moiety, an increase in the saturation of the fatty acid moiety and an increase in the length of the alcohol moiety, all resulted in a decrease of the ignition delay.

The formation of NO_x during the diesel combustion process of the fatty acid monoalkyl esters was found to be controlled by several, layered effects. The first and most significant effect on the formation of NO_x was that of the ignition delay, which controlled the relative amounts of heat released during the premixed combustion phase and the diffusion-controlled combustion phase. The proportion of heat released during the premixed combustion phase was defined as the premixed burn fraction. An increase in the premixed burn fraction resulted in a strong increase of NO_x emissions. The second most significant effect on NO_x emissions was that of the adiabatic flame temperature of the fuel. This only became clearly visible once the effect of ignition delay was removed. The theoretical adiabatic flame temperature of the fuel molecules at $\Phi = 1$ and constant pressure with no dissociation, was found to correlate well with the measured emission of NO_x when the ignition delay was constant (Figure 5.24). The adiabatic flame temperature depended in detail on the molecular structure of fuel. Increasing the length of the fatty acid moiety, increasing the number of double bonds in the fatty acid moiety and decreasing the length of the alcohol moiety resulted in an increase in adiabatic flame temperatures for the molecules tested. Further to the effects which the ignition delay and the adiabatic flame temperature had on NO_x emission, it was observed that the effect soot radiative heat transfer may have played a role of tertiary importance.

The relative importance of the influence of the premixed burn fraction and the adiabatic flame temperature on NO_x emission appeared to shift towards that of adiabatic flame temperature as the ignition delay became shorter (Figure 5.25). This suggests that for fuels of higher ignition quality (i.e. shorter ignition delay), the adiabatic flame temperature played an increasingly significant role in governing the total emission of NO_x.

According to current literature (Graboski, et al., 2003), molecules with shorter fatty acid moieties produce more NO_x in diesel combustion. The experiments presented in this chapter showed that the reason for this higher emission of NO_x was their longer ignition delay (Figure 5.3). It was demonstrated that if the ignition delay was equalised for all molecules, fatty acid monoalkyl ester molecules with shorter fatty acid moieties actually produced less NO_x than those with longer fatty acid moieties, due to their lower adiabatic flame temperatures.

The emission of accumulation mode soot particles was positively correlated with the number of double bonds present in the fatty acid moiety of the molecules. The emission of nucleation mode particles showed positive correlation with the boiling points of the individual fatty acid methyl ester molecules. This observation gave some indication that the high number of nucleation mode particles produced by the fatty acid methyl ester molecules may have consisted to a large extent of unburned fuel droplets.

Chapter 6. The combustion of acetal molecules produced via biochemical synthesis from lignocellulose

Acetals are liquid hydrocarbon compounds that could be used as fuels for diesel engines. They could be produced from cellulosic biomass through a combination of biochemical and chemical synthesis steps. A background discussion on potential production methods is provided in section 2.8 of Chapter 2. Various pathways for the synthesis of acetals are conceivable, but usually the formation of monohydric alcohols of low molecular mass such as methanol, ethanol, propanol or butanol represents a necessary intermediate step in their production process. The cellulose may thus be converted into alcohols, and the alcohols may thereafter be used for the synthesis of acetal molecules. The synthesis of acetals from alcohols is described in detail by Charpentier and Mimoun (1978), and occurs via the formation of aldehydes or ketones as intermediate species. Depending on the reactants used, and the detailed conditions under which the synthesis is carried out, a multitude of different acetal molecules can be synthesised with similar production efficiencies.

The combustion behaviour of most acetal molecules which could be produced via this method, has not been documented. Depending on their detailed molecular structure, it is to be expected that the various molecules exhibit different combustion characteristics. In order to identify and develop fuel molecules conducive to high thermal efficiency of the engine cycle, and to low pollutant formation, it is necessary to understand how their molecular structure affects the combustion process. Such an understanding allows tailoring the fuel synthesis methods to selectively synthesise acetal molecules for a particular type of combustion process.

The experimental study described in this chapter, is aimed at understanding how the molecular structure of acetal fuels influences their combustion behaviour in a diesel engine under various conditions. For this purpose, thermodynamic and stoichiometric analyses of the combustion of individual molecules were carried using the instrumented single-cylinder research engine described in Chapter 3. The results of these analyses are described in the present chapter.

6.1. Molecule synthesis

A simple fuel synthesis process shall be described in this section. This process can be used to produce acetal molecules from cellulosic biomass, and provides an overview of the types of molecules that can be synthesised. The combustion characteristics of individual molecules will be discussed in the ensuing sections of this chapter (sections 6.2 and 6.3).
The synthesis process of acetal molecules from cellulosic biomass may be segmented into five main synthesis steps:

1. Pre-treatment of the lignocellulosic biomass for hydrolysis
2. Hydrolysis of the cellulose using mineral acids and enzymes into sugars
3. Isopropanol-butanol-ethanol (IBE) fermentation of the sugars into alcohols
4. Separation of the alcohols from the fermentation broth
5. Synthesis of acetal molecules from alcohols

The first step in the synthesis process consists of pre-treating the lignocellulosic biomass in preparation for hydrolysis of the cellulose (Mosier, 2006). This can either be done by milling of the lignocellulosic material into fine powder, or by treating it with superheated steam under high pressure, as employed in the Stake or Lotech processes (Roehr, 2001; Kaltschmitt and Hartmann, 2001). This pre-treatment of the biomass makes the cellulose physically accessible to the enzymes or catalysts used to hydrolyse the cellulose into sugars.
The second step consists in the hydrolysis of the cellulose into fermentable (usually monomer) sugars. This can be achieved by the addition of acids or enzymes acting as catalysts in the process. Acid catalysis is usually the faster process, whilst enzymatic catalysis generally gives a higher yield of fermentable sugars (Kaltschmitt and Hartmann, 2001). Significant improvements are expected to be made in the development of enzymatic catalysis in the coming years, and due to its higher sugar yield, this method is considered to be the most promising pathway for the future (Schacht, 2008). In enzymatic catalysis, the cellulose is broken down under the consumption of water, from the large polymer that is cellulose, into many monomer sugars. These sugar molecules are directly fermentable into alcohols.
The third step consists of the fermentation of sugars into alcohols. The types of alcohols produced in the process can be governed by the type of microorganism used to carry out the fermentation, and by the detailed environmental conditions under which the fermentation is carried out. By using strains of the bacterium Clostridium Beijerinckii, the anaerobic isopropanol-butanol-ethanol (IBE) fermentation process can be carried out. In this process 1-butanol, 2-propanol and ethanol are formed as the main products amongst small quantities butyric and acetic acid (Krouwel, 1982). The alcohols provide the basis for the synthesis of the acetal molecules.
The fourth step consists in extracting the alcohols produced by the fermentation process from the aqueous solution that is the fermentation broth. This process can be achieved using a multitude of

processes such as gas-stripping, liquid to liquid extraction, adsorption, ultra-filtration, reverse-osmosis, perstraction and pervaporation (Kawedia, et al., 2000). Pervaporation is commonly perceived to be the best method for the extraction of the alcohols from the fermentation broth (Qureshi, et al., 2001; Kawedia, et al., 2000). It requires the least amount of energy input, and can be continuously performed alongside the fermentation process in the form of extractive fermentation, because it is not harmful to the microorganisms carrying out the fermentation. In the process of pervaporation, the products of the fermentation are extracted from the liquid phase of the fermentation broth through a membrane. The membrane is contacted with the liquid fermentation broth, and the products are extracted through it, using a vacuum on the other side of the membrane. The alcohols which are isolated from the fermentation broth via this process may be further purified via distillation. They provide the reactants for the final step in the production process; that is the reaction into acetals.

The fifth and final process consists in the chemical reaction of alcohols into acetals. This process is the most interesting single step from the point of view of the combustion characteristics of the fuel, because it gives the largest influence in governing the molecular structure of the acetal molecules. The detailed conditions under which the synthesis reactions take place may be varied according to the type of product yield that is required. The works of Charpentier and Mimoun (1978), and Bueno et al. (2007) have shown that both single-step and two-step conversion processes are possible. In both cases, the alcohols are oxidised into aldehydes or ketones using atmospheric oxygen. These aldehydes or ketones are then further reacted with alcohol molecules, to produce acetal molecules (Charpentier & Mimoun, 1978). Depending on the types of alcohol used for the initial oxidation process, and on the types of alcohols used for the subsequent reaction with the aldehydes or ketones, the molecular structure of the final acetal molecules is governed.

The following paragraph provides a description of the two generalised reaction steps used in the synthesis process of acetals from alcohols.

The first sub-step (A) in converting alcohols into acetal molecules consists in the oxidation of an alcohol with dioxygen which can be extracted from the atmosphere. This reaction may be catalysed using a catalyst consisting of two salts or complexes of transition metals (e.g. $RuCl_3$ and $Cu(ClO_4)_2$). The general chemical reaction equation may be written as:

A)

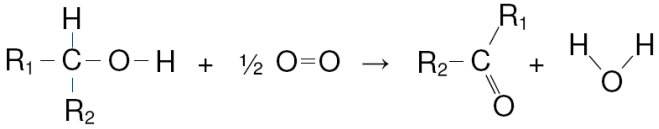

The second sub-step (B) in converting alcohols into acetal molecules consists in the reaction of the product formed in the first reaction step (A) with further alcohol molecules. This reaction yields the acetal molecule as the final product:

B)

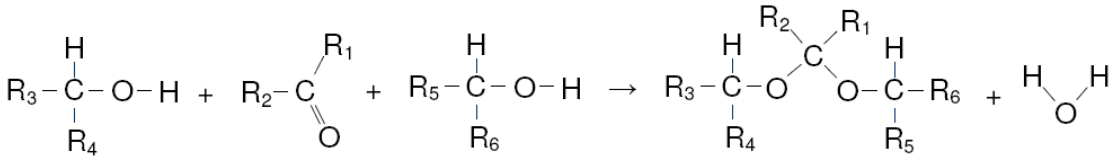

The two reaction steps (A) & (B) show that under the consumption of 3 alcohol molecules and ½ dioxygen molecule, 1 acetal molecule and 2 molecules of water are produced. The structure of the acetal molecule depends in detail on the types of alcohols used as the reactants.

The following section is aimed at illustrating the production process using two examples.
In this first example, 3 molecules of 1-butanol are converted into di-n-butyl acetal (1,1-dibutoxybutane) via the intermediate formation of the aldehyde butyraldehyde. In the first sub-step, the primary alcohol is oxidised to butyraldehyde. This may be written as:

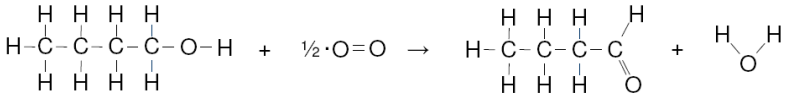

In the second sub-step, the aldehyde produced in the first sub-step is reacted with two primary molecules of 1-butanol to produce the final product: di-n-butyl acetal (1,1-dibutoxybutane):

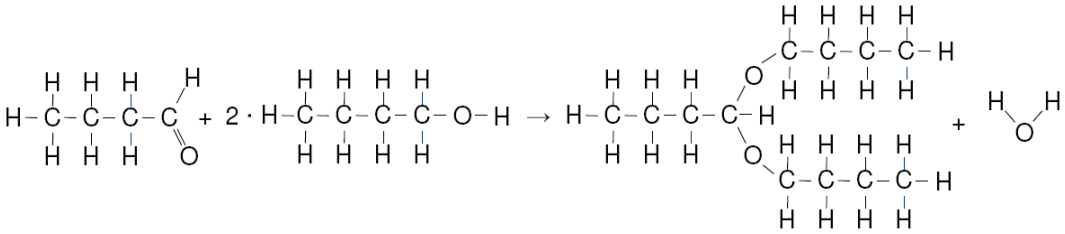

A second example: 1 molecule of 2-butanol and 2 molecules of 1-ethanol are converted to the acetal 2,2-diethoxybutane via the intermediate formation of the ketone butanone. In the first sub-step, the alcohol 2-butanol is oxidised to 2-butanone. This may be written as:

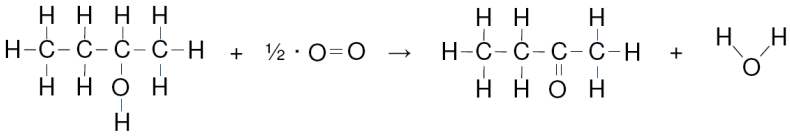

In the second sub-step, the ketone produced in the first sub-step is reacted with two primary alcohol molecules (1-ethanol) to produce the final product 2,2-diethoxybutane:

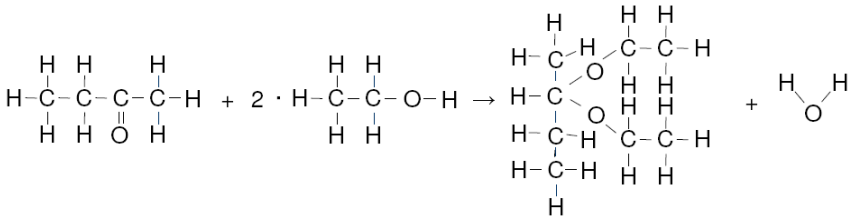

Both of the above examples represent syntheses of molecules whose combustion behaviour was experimentally investigated in the following section.

6.2. Initial experimental study

In an initial screening study, four acetal molecules, one ether molecule and fossil diesel fuel oil were tested in a series of experiments aimed at clarifying their combustion behaviour. The four acetal molecules were chosen to represent molecules likely to be produced via the synthesis pathways described in section 6.1 from primary and secondary alcohol versions of methanol, ethanol, propanol and butanol. The ignition promoting molecule 2-ethylhexyl nitrate (2-EHN) was used in certain experiments alongside these molecules to control the ignition delay experienced by the fuel.

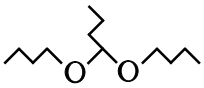

1,1 Dibutoxybutane

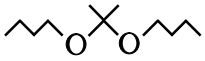

2,2 Dibutoxypropane

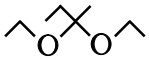

2,2 Diethoxybutane

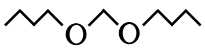

Di-n-butoxymethane

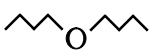

Di-n-butyl ether

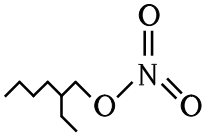

2-Ethylhexyl nitrate

Figure 6.1 – Structure of fuel molecules used in the initial screening study

The physical and chemical properties of the molecules varied according to their molecular structure. Salient properties of the fuel samples are given in Table 6.1. In comparison to fossil diesel fuel, the acetal molecules had a high oxygen content, and their lower heating values were significantly lower. All of the acetal molecules had a slightly higher density than fossil diesel fuel. The ignition quality of the fuel samples was determined using three different test methods. Table 6.1 shows that the measured values of cetane number depended strongly on the methodology with which the ignition quality was measured. The cetane numbers determined using the ignition quality tester (IQT) correlated best with the behaviour observed in the engine.

Table 6.1 - Thermochemical properties of the fuels

Molecule name		**1,1 Dibutoxy butane**	**2,2 Dibutoxy propane**	**2,2 Diethoxy butane**	**Di-n-butoxy methane**	**Di-n-butyl ether**	**Fossil diesel fuel**
Sum formula		**$C_{12}H_{26}O_2$**	**$C_{11}H_{24}O_2$**	**$C_8H_{18}O_2$**	**$C_9H_{20}O_2$**	**$C_8H_{18}O$**	**-**
Lower heating value	**[kJ/kg]**	35475	34891	32582	33253	38044	42980
Carbon	**[%]**	71.23	70.16	65.71	67.45	73.78	86.6
Hydrogen	**[%]**	12.95	12.85	12.41	12.58	13.93	13.5
Oxygen	**[%]**	15.81	16.99	21.88	19.97	12.29	0.07
Density	**[g/ml]**	0.838	0.839	0.845	0.842	0.772	0.8341
Cetane No. (CFR method)		71.6	73.5	26.1	84.5	72.2	49.8
Cetane No. (BASF method)		87.3	86.8	-	90.3	67.6	-
Cetane No. (IQT)		80.5	76.2	50.9	70.3	88.8	53.4

The acetal molecules had cetane values which were higher and lower than that of fossil diesel fuel, depending on their molecular structure. 1,1-Dibutoxybutane had the highest ignition quality, followed by 2,2-dibutoxybutane and di-n-butoxymethane, all of which had a higher cetane number than the fossil diesel fuel. 2,2-Diethoxybutane had the lowest ignition quality amongst the acetals, which was even lower than that of the fossil diesel fuel. The ether molecule had a significantly higher ignition quality than all other fuels.

The molecules were tested under three closely controlled conditions. The engine rotational speed and load were kept constant in all experiments at an engine speed of 1200 rpm and an indicated load of 4 bar IMEP. The three experimental conditions consisted of constant injection timing, constant ignition timing and constant ignition delay. For the experiments conducted at constant ignition delay, both the injection timing as well as ignition timing were kept constant. Detailed data on the experimental conditions can be found in Appendix D. An overview of the experimental conditions is given Table 6.2.

Table 6.2 - Overview of experimental conditions

Engine speed: 1200 rpm Engine load: 4 bar IMEP	Constant injection timing		Constant ignition timing		Constant ignition delay		
	Injection timing [º CA BTDC]	Ignition timing [º CA BTDC]	Injection timing [º CA BTDC]	Ignition timing [º CA BTDC]	Injection timing [º CA BTDC]	Ignition timing [º CA BTDC]	2-EHN conc. [vol. %]
Fossil diesel fuel oil	7.10	TDC	7.1	TDC	5.40	TDC	4.0
Di-n-butyl ether	7.10	1.68	5.4	TDC	5.40	TDC	0.0
1,1 Dibutoxy butane	7.10	1.18	5.9	TDC	5.40	TDC	0.4
2,2 Dibutoxy propane	7.10	0.88	6.1	TDC	5.40	TDC	0.8
2,2 Diethoxy butane	7.10	-2.23	9.3	TDC	5.40	TDC	16.0
Di-n-butoxy butane	7.10	0.68	6.4	TDC	5.40	TDC	2.0
Fossil diesel fuel oil	7.10	TDC	7.1	TDC	5.40	TDC	4.0

In order to allow unambiguous reference to the structural features of the acetal molecules, the group of atoms located between the two oxygen atoms of the molecules shall be referred to as 'central moiety' and the group of atoms located to either side of the two oxygen atoms shall be referred to as 'lateral moieties' in this thesis. Figure 6.2 illustrated this definition using the molecule 1,1-dibutoxybutane as an example.

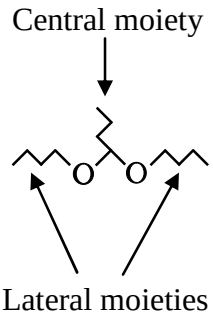

Figure 6.2 - Nomenclature of structural features of the acetal molecules

6.2.1. Constant injection timing experiments

In the first series of experiments, all fuels were injected at a fixed timing within the combustion cycle, at 7.1º crank angle (CA) before top-dead-centre (BTDC). The amount of fuel injected was adjusted so that each type of fuel would develop the same indicated load of 4 bar IMEP. The engine speed was 1200 rpm for all experiments. Figure 6.3 shows the combustion chamber pressures, heat release rates and mass fraction burnt analyses for the individual fuel molecules.

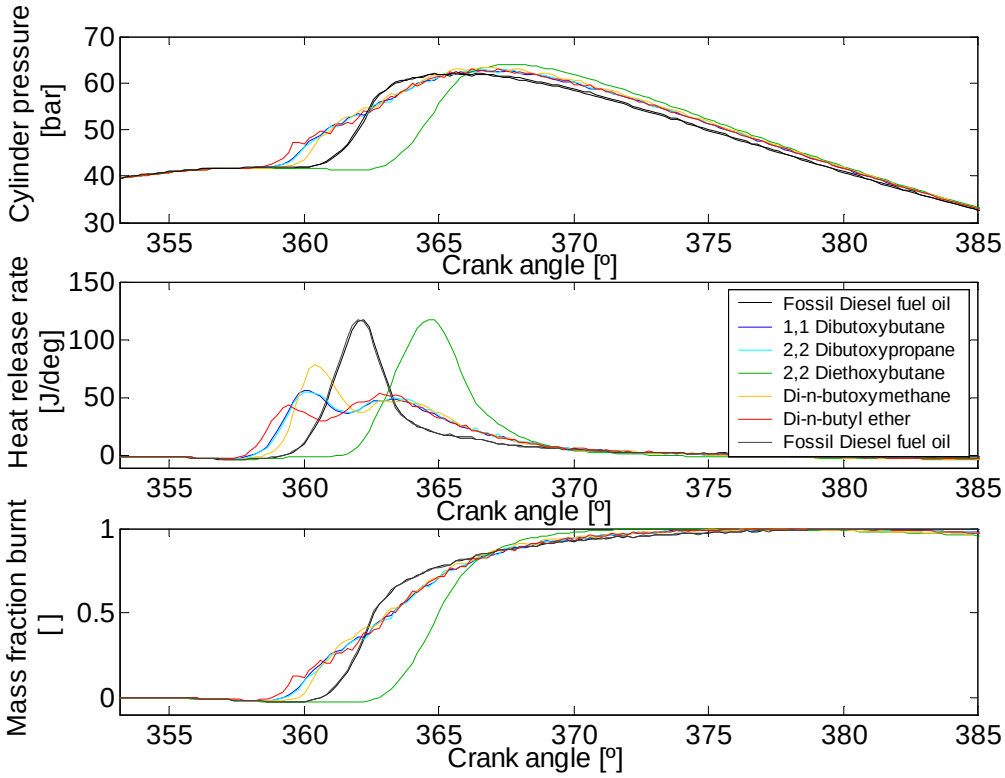

Figure 6.3 - Cylinder pressure, heat release rate and mass fraction burnt for constant injection timing experiments at 1200 rpm and 4 bar IMEP.

The cylinder pressure and heat release rates show that the molecules underwent different ignition delays after injection, depending on their propensity to undergo thermal decomposition. The ignition delay had a large effect on the rate of heat released from the combustion. It deferred the onset of the heat release from the start of fuel injection, and controlled the magnitude as well as the shape of the heat release rate. Figure 6.1 shows, that as the ignition delay was reduced, the peak heat release rate was lowered, and two distinctive peaks of heat release formed. These two peaks represent the initial pre-mixed combustion phase which directly ensued the ignition, and the later mixing-controlled combustion phase whose heat release rate was limited by the rate of mixing of the fuel with the surrounding air. It is visible that di-n-butyl ether had a significantly shorter ignition delay than any of the acetal molecules, and that it was the only molecule whose peak heat release rate during the premixed combustion phase was lower than its peak heat release rate during the diffusion controlled

combustion phase. Figure 6.3 shows that amongst the acetal molecules, 1,1-dibutoxybutane had the shortest ignition delay, followed by 2,2-dibutoxypropane, and di-n-butoxymethane, all of which had a shorter ignition delay than fossil diesel fuel oil. The acetal molecule with the longest ignition delay by far was 2,2-diethoxybutane. The ignition delay of 2,2-diethoxybutane was even longer than that of fossil diesel fuel, which is reflected by a significantly later phasing of combustion, and a very rapid heat release (Figure 6.3).

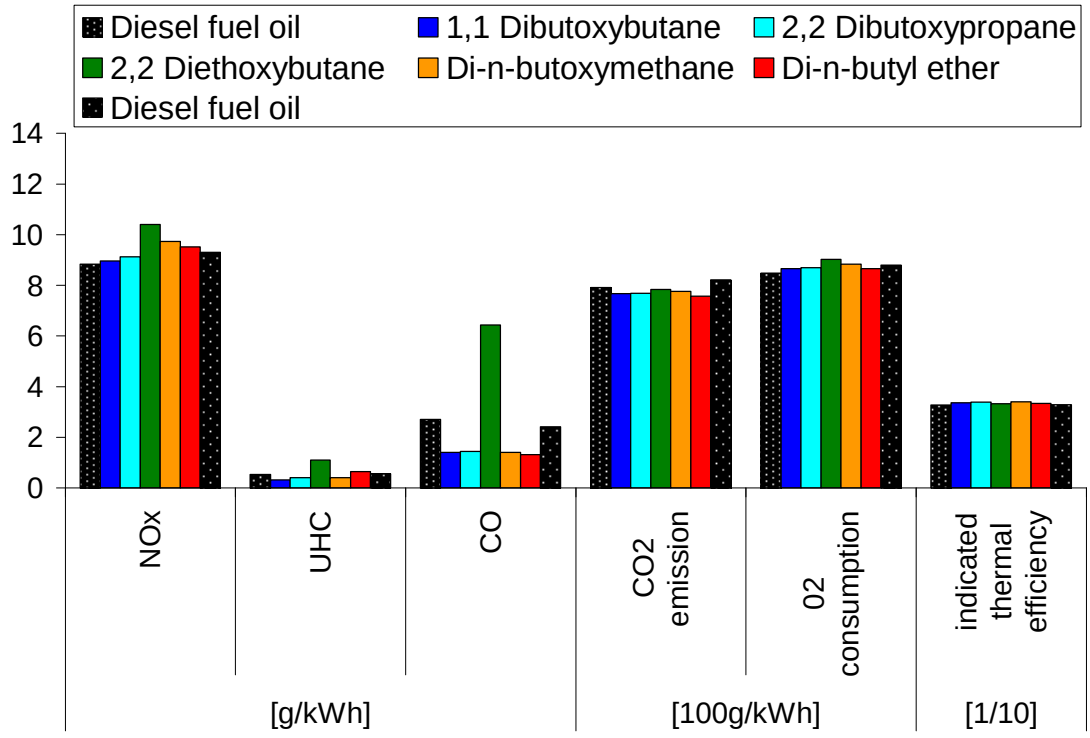

Figure 6.4 - Emission of gaseous pollutants and indicated thermal efficiency of the engine for constant injection timing experiments

The emission of gaseous pollutants and the indicated thermal efficiency of the engine at constant injection timing are presented in Figure 6.4. The results show that amongst the acetal molecules, a good correlation existed between the peak heat release rate (Figure 6.3) and the emission of NO_x (Figure 6.4). Looking at the gaseous pollutant emissions of the acetal molecules amongst themselves, it is clearly visible that the molecules, 2,2-diethoxybutane showed the most distinct emission patterns. 2,2-diethoxybutane produced by far the highest emission of NO_x, UHC, CO amongst the tested fuels. It also had the highest emission of CO_2 and the lowest indicated thermal efficiency amongst the acetal molecules.

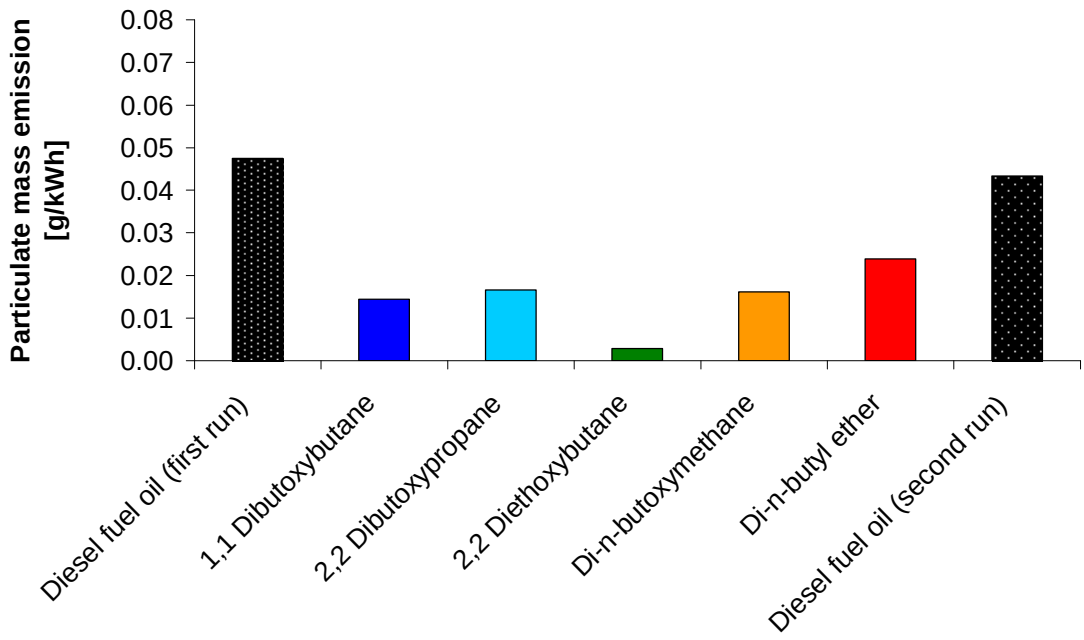

Figure 6.5 - Emission of total particulate mass from the engine for experiments conducted at constant injection timing

Figure 6.5 shows the total particulate mass emitted from the experiments. It can be seen that fossil diesel fuel oil emitted far more particulate mass than any of the oxygenated single-molecule samples. This is likely to have been due to two main reasons: Firstly, the higher oxygen content of the oxygenated single-molecule fuel samples, was conducive to the oxidation of soot and its precursor molecules. Secondly, the single-molecule samples did not contain any double-bonded or aromatic molecular species, which are strongly conducive to the formation of soot (Pepiot-Desjardins, et al., 2008). Figure 6.5 shows that the molecule with the longest ignition delay, produced the least amount of particulate mass by far. This can be explained by the increased amount of fuel and air mixing which the fuel spray experiences before ignition occurs. An increased amount of fuel and air mixing during the ignition delay reduced the fuel rich regions within the spray. This reduced the amount of fuel subjected to pyrolysis which occurs in the absence of sufficient oxygen, and thus resulted in a reduction of soot formed by this mechanism. Further analysis with respect to the formation of soot and the ignition delay will be shown in section 6.4.4 (Figure 6.38).

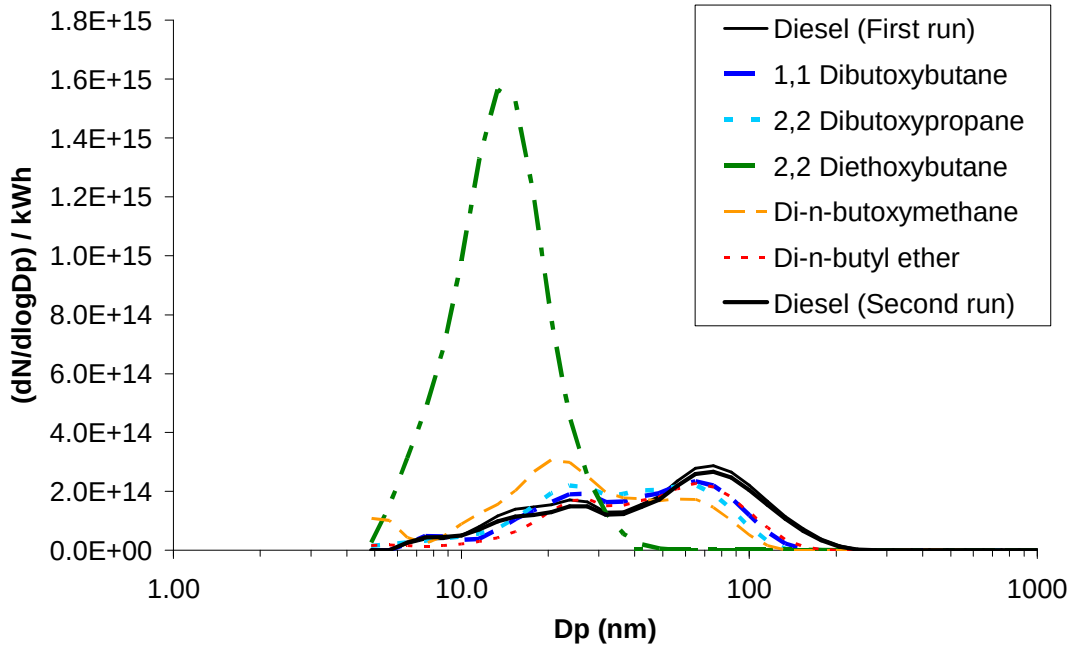

Figure 6.6 - Size spectral density of sub-micron particulate matter for experiments conducted at constant injection timing

Figure 6.6 shows the size spectral density of the sub-micron particulate matter. Fossil diesel fuel produced the most significant number of large, accumulation type particles of a diameter larger than 100 nm. These large particles were mostly responsible for the high particulate mass emissions diesel fuel, that are shown in Figure 6.5. The size spectral density of particulates shown in Figure 6.6 clearly indicates that the two acetal molecules with the longest ignition delays (2,2-diethoxybutane and di-n-butoxymethane) formed the largest number of small particles between 5 and 40 nm in diameter. This was particularly prominent for the 2,2-diethoxybutane, which had the longest ignition delay. Figure 6.4 suggests that 2,2-diethoxybutane also exhibited the highest emission of unburned hydrocarbons, which may have played a role in causing this high emission of nucleation mode particles, since these are believed to consist predominantly of volatile organic compounds such as unburned fuel (Kittelson, 1998). For the molecule 2,2-diethoxybutane, the absence of significant amounts of particles larger than about 50 nm is also clearly noticeable. This absence of larger accumulation mode particles from the combustion of 2,2-diethoxybutane, allows explaining the low total particulate mass emission previously observed in Figure 6.5 for this molecule.

6.2.2. Constant ignition timing experiments

In the second series of experiments, the ignition of the fuel was kept constant at the same point during the combustion cycle, at top-dead-centre (TDC). Due to the different ignition qualities of the fuels, the time of injection was adjusted for each fuel, so that ignition would occur at TDC in each case. The amount of fuel injected was optimised so that each type of fuel would develop the same indicated load of 4 bar IMEP. The engine speed was 1200 rpm for all experiments. Figure 6.7 shows the combustion chamber pressures, heat release rates and mass fraction burnt analyses for the individual fuel molecules.

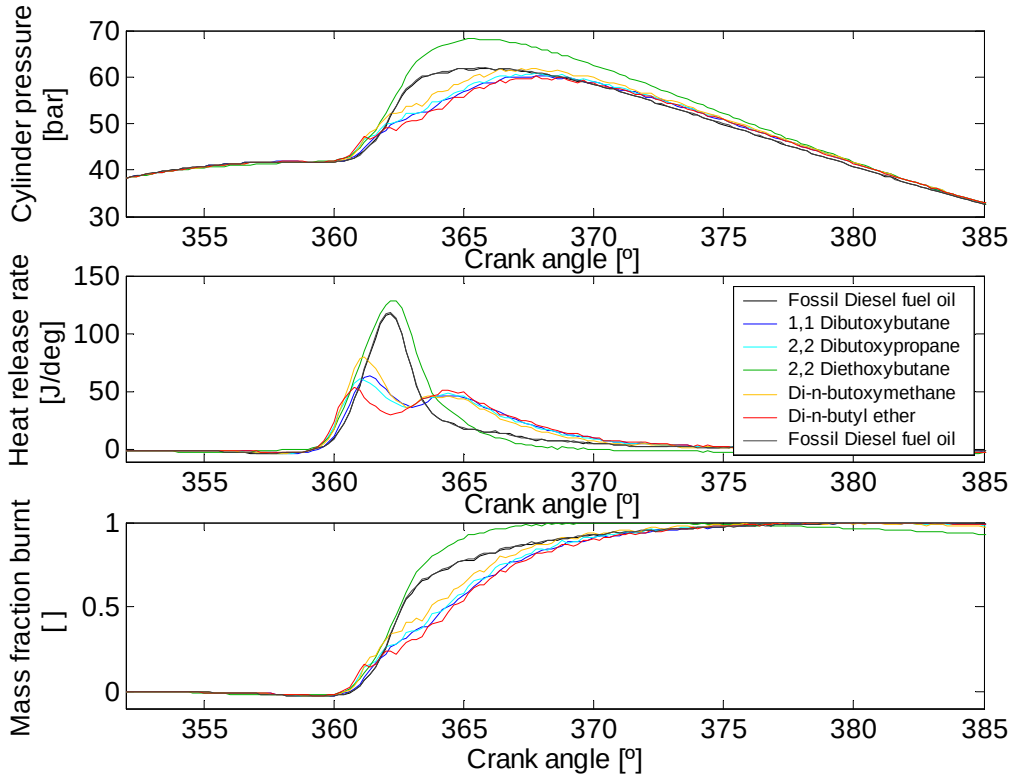

Figure 6.7 - Cylinder pressure, heat release rate and mass fraction burnt for constant ignition timing experiments at 1200 rpm and 4 bar IMEP.

The cylinder pressure traces and heat release rates show that the differences in ignition delay (Table 6.2) between the fuels, which had been previously observed in the constant injection timing experiments (Figure 6.3), lead to stark differences of cylinder pressure in the constant ignition timing experiments (Figure 6.7). Those fuels which experienced a longer ignition delay underwent more significant mixing with air during the ignition delay period, allowing more fuel to be ready for combustion once ignition occurred. This resulted in a faster combustion and more rapid heat release for these fuels. Due to the faster heat release, the maximum cylinder pressures and global cylinder temperatures were higher for those fuels which experienced a longer ignition delay.

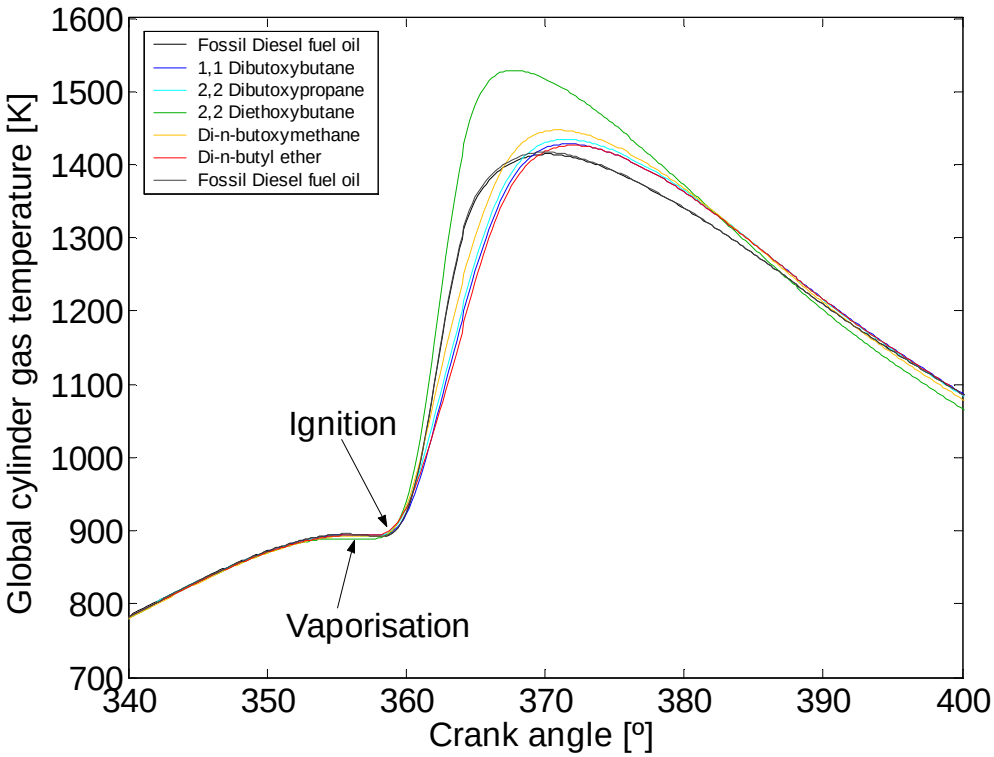

Figure 6.8 - Global cylinder gas temperature history for experiments at constant ignition timing.

The global cylinder gas temperature history traces are shown in Figure 6.8. The traces were calculated based on the assumption that the temperature of the gases was equal across the entire combustion chamber, and that the number of moles of gas present in the cylinder was equal to that of the air ingested into the cylinder during each cycle. The global gas temperature was thus calculated according to the relationship described by Equation 4.17. It can be seen that up to the point of ignition (TDC) the global cylinder gas temperatures showed a very similar development amongst the fuels. Those fuels with the longest ignition delays (2,2-diethoxybutane and di-n-butoxymethane) exhibited slightly lower gas temperatures just prior to TDC. This marginally lower temperature is indicative of the higher amount of fuel vaporisation taking place for these two fuels. The fuel vaporisation resulted in slight cooling of the cylinder charge due to the latent heat of vaporisation needed to take the fuel from its liquid to its vapour phase. The amount of vaporisation increased progressively over time, and was thus more pronounced for fuels with a longer ignition delay. The development of global gas temperature following the point of ignition was primarily governed by the heat release of the fuels shown at the centre of Figure 6.7. It can be seen that those fuels with higher heat release rate reached significantly higher global gas temperatures.

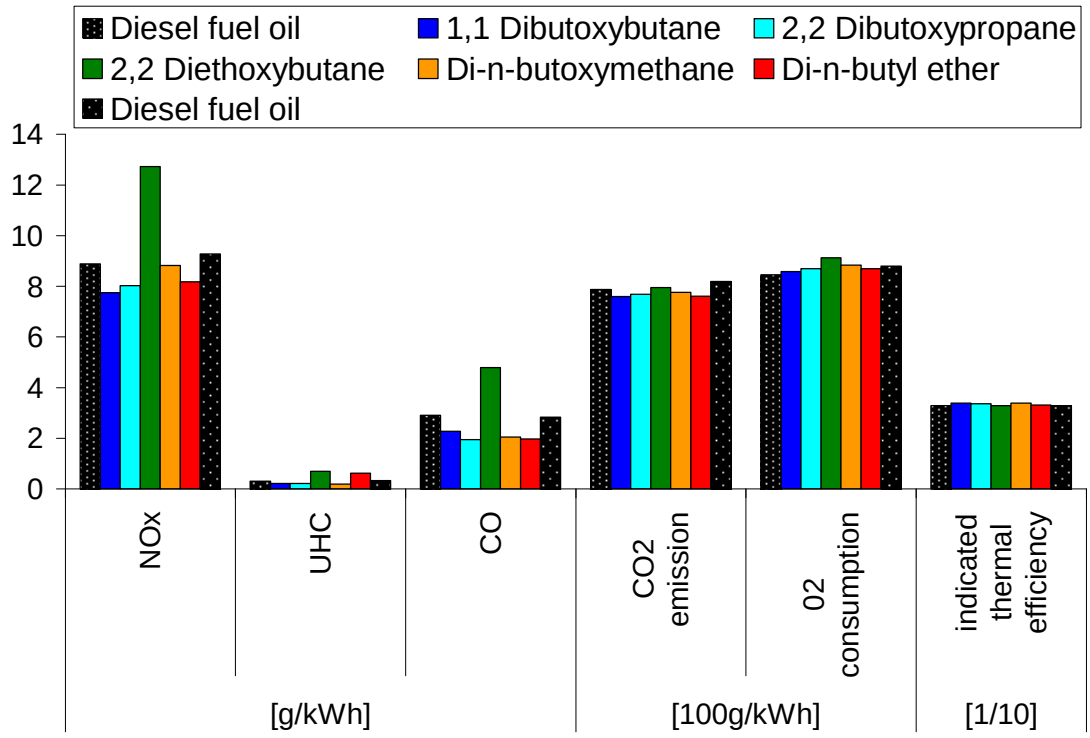

Figure 6.9 - Emission of gaseous pollutants and indicated thermal efficiency of the engine for constant ignition timing experiments

The emission of gaseous pollutants and the indicated thermal efficiency of the engine at constant ignition timing are presented in Figure 6.9. The results show that the differences in NO_x emissions between the acetal molecules which had previously been observed for the constant injection timing experiments (Figure 6.4) are further increased for the experiments with constant ignition timing. Amongst the acetal molecules, the emission of NO_x shows good correlation with the peak global cylinder gas temperatures reached during the combustion process, which are presented in (Figure 6.8). Although the temperatures shown in Figure 6.8 are too low to significantly contribute to the thermal formation of NO_x, the local temperatures of the flames forming during the combustion process within this global environment will be significantly higher, and would be able to participate in the formation of NO_x. Figure 6.9 shows that the molecule 2,2-diethoxybutane formed the highest concentration of UHC and CO in the exhaust gas. This is likely to be attributable to the low ignition quality of the fuel, which is likely to have resulted in the formation of overly lean mixtures of fuel and air during the long ignition delay period. Overly lean mixtures of fuel and air are known to be unable to support full fuel oxidation and result in the formation of incomplete reaction products (Heywood, 1988, pp. 620-622.) The data presented in Figure 6.9 also indicate that the 2,2-diethoxybutane had a slightly higher emission of CO_2 and a lower thermal efficiency. The reasons for this are not immediately obvious. The rapid combustion just after TDC, which occurred with the molecule 2,2-diethoxybutane, resulted in an engine cycle which was closer to the ideal isochoric (Otto) cycle than those of any of the other fuels, since its combustion occurred almost at a constant volume. Thus, from the theoretical point of view of cycle analysis, the molecule 2,2-diethoxybutane should have exhibited the highest indicated efficiency and the lowest emission of CO_2. Careful

analysis of the cylinder pressure trace and the global cylinder gas temperature (Figure 6.8) reveal that during the later stages of expansion (after 385 º CA), the cylinder pressure and temperature dropped below those recorded for the combustion of the other fuels. It is believed that the combustion of 2,2-diethoxybutane, which resulted in very high cylinder pressures and temperatures immediately after TDC, experienced a higher amount of losses in terms of cylinder gas mass and heat than the combustion of other fuels. The mechanism by which gas was lost from the combustion chamber is likely to have consisted primarily of blowby past the cylinder rings, whilst the mechanism responsible for heat losses is likely to have consisted predominantly of heat transfer to the cylinder walls via convection and radiation. Blowby is strongly encouraged by higher cylinder gas pressures, whilst heat losses from the cylinder gas are encouraged by higher cylinder gas temperatures. It could therefore be expected that the combustion of fuels involving higher cylinder pressures and temperatures such as that of 2,2-diethoxybutane are likely to experience higher losses in terms of cylinder gas mass and heat. These higher losses appeared to have had a stronger effect in reducing thermal efficiency of the engine than the more rapid combustion of 2,2-diethoxybutane was able to improve cycle efficiency by bringing the cycle closer to the isochoric (Otto) cycle.

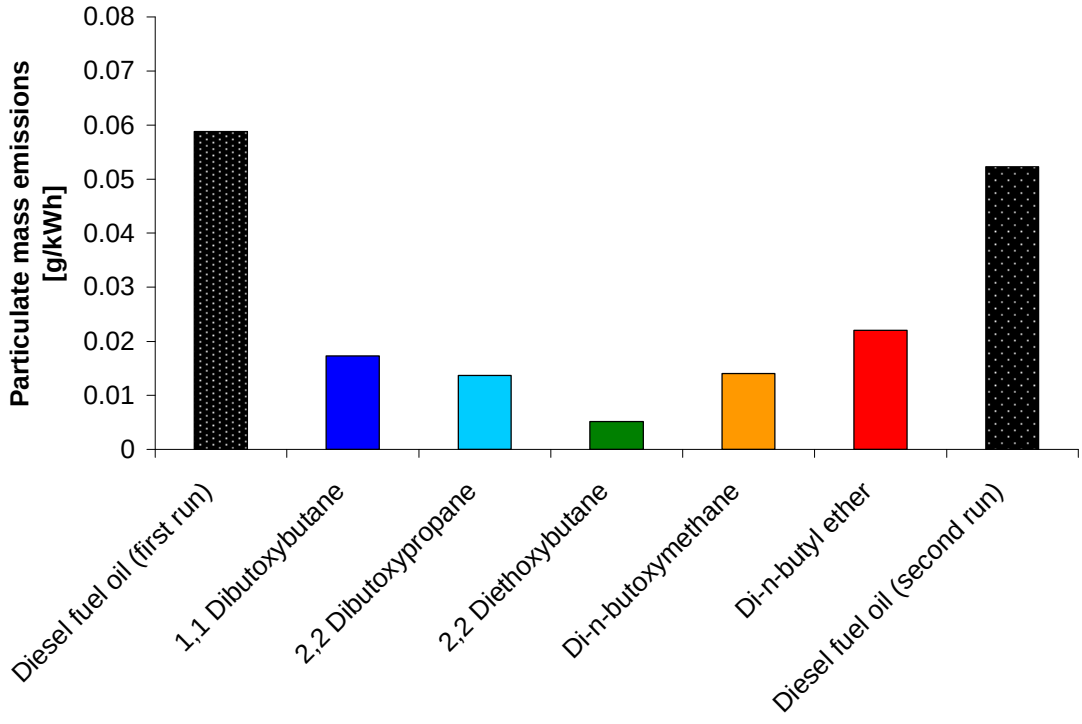

Figure 6.10 - Emission of total particulate mass from the engine for experiments conducted at constant ignition timing

Figure 6.10 shows the particulate mass emission from the engine for the experiments conducted at constant ignition timing. Similarly to the results obtained for the constant injection timing experiments (Figure 6.5), the data show that the oxygenated single-molecule fuel samples produced significantly lower amounts of soot than the diesel fuel. Some indication exists that amongst the oxygenated fuels, those with a longer ignition delay tended to produce lower amounts of particulate

mass due to their enhanced mixing with air, which is possible during their longer ignition delay. As observed in the previous experiments (Figure 6.5), the data shown in Figure 6.10 illustrates that the molecule 2,2-diethoxybutane formed the lowest amount of particulate mass.

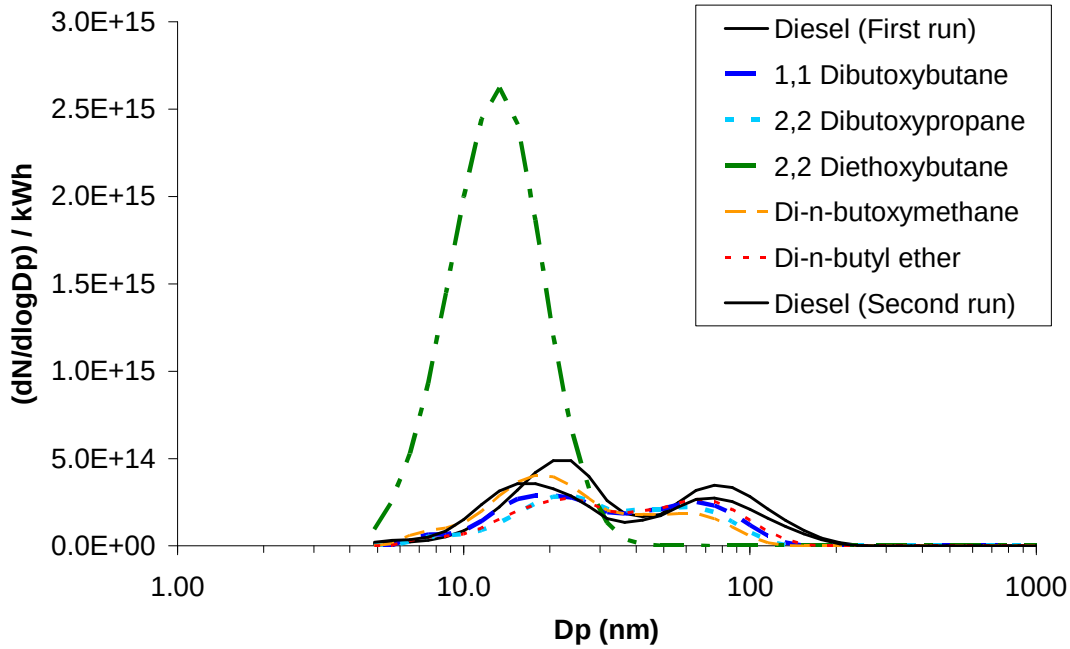

Figure 6.11 - Size spectral density of sub-micron particulate matter for experiments conducted at constant injection timing

Figure 6.11 shows the size spectral density of the sub-micron particulate matter. As observed for the experiments with constant injection timing (Figure 6.6), it can be seen that the combustion of fossil diesel fuel produced a significantly larger number of accumulation mode particulates than any of the other fuels. This was reflected in larger emissions of total particulate mass from diesel fuel, as shown in Figure 6.10. It is prominent that the combustion of 2,2-diethoxybutane produced hardly any particulates larger than 50 nm in diameter, and that it produced a very high number of nucleation mode particles of 5-40 nm in diameter. The molecule di-n-butoxymethane shows some sign of developing a similar nucleation particle mode and of producing a reduced amount of particulates in accumulation mode.

6.2.3. Constant ignition delay experiments

In the third series of experiments, the ignition delay of the fuels was equalised through the addition of the ignition improving additive 2-EHN to the fuel samples in varying concentrations. The same time of injection and the same time of ignition were used for all fuels. The amount of fuel injected was optimised so that each type of fuel would develop the same indicated load of 4 bar IMEP. The engine speed was 1200 rpm for all experiments. Figure 6.12 shows the combustion chamber pressures, heat release rates and mass fraction burnt analyses for the individual fuel molecules.

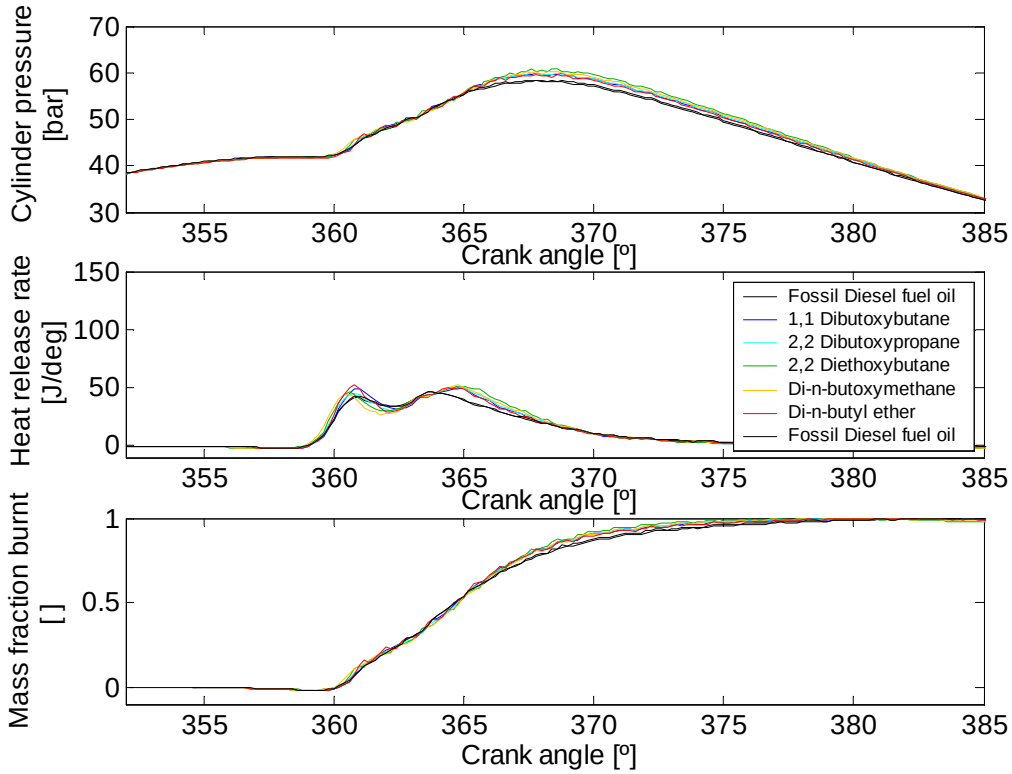

Figure 6.12 - Cylinder pressure, heat release rate and mass fraction burnt for constant ignition delay experiments at 1200 rpm and 4 bar IMEP.

The data presented in Figure 6.12 show that once the ignition delay was equalised, the differences in heat release patterns between the fuels were substantially reduced. There still existed noticeable differences in the heat release rates pattern between the oxygenated fuels as a group and the fossil diesel fuel. The oxygenated molecules showed only minute differences amongst themselves. These differences consisted primarily in the magnitude of the first peak of heat release that was attributable to the premixed combustion phase, and in the duration of the second heat release phase that was attributable to the mixing-controlled combustion phase. The very small differences visible in the premixed combustion phase do not appear to correlate clearly with any of the fuel properties. It is believed that they can be attributed to the limited accuracy with which the ignition delay was controlled via the ignition improving additive, as well as small differences in the calorific values of

the fuels. Some clear differences were observed in the duration of the mixing-controlled combustion phase which, although small, showed good correlation with the calorific value of the fuels. Those fuels with the lowest calorific value required the longest injection duration, for the engine to develop the same indicated load. This prolonged duration of injection was clearly reflected in a lengthening of the mixing controlled combustion phase as is visible through careful examination of the heat release rates presented in Figure 6.12.

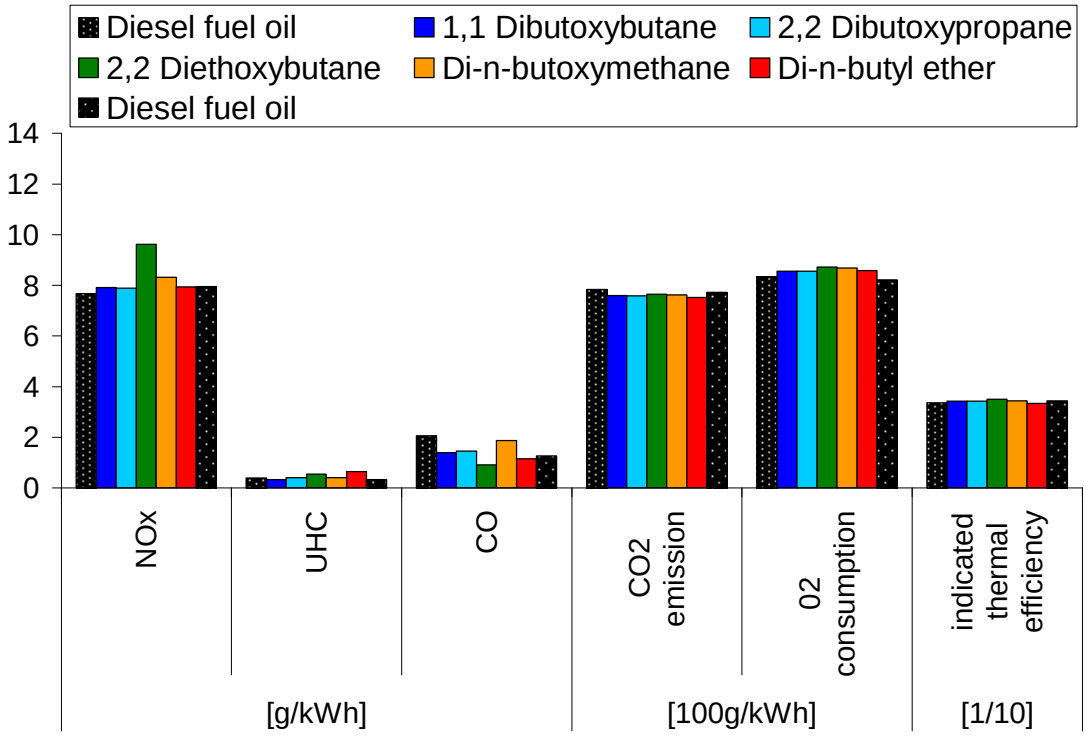

Figure 6.13 - Emission of gaseous pollutants and indicated thermal efficiency of the engine for constant ignition delay experiments

Figure 6.13 shows the emission of gaseous pollutants for the individual fuel samples at constant ignition delay. Significant differences between the fuels, particularly in the emission of NO_x are visible despite the similar heat release patterns of the fuels. The most prominent difference was the substantially high emission of NO_x from the combustion of the molecule 2,2-diethoxybutane. To a lesser degree, the molecule di-n-butoxymethane also showed a noticeably higher formation of NO_x than most of the other fuels. Since the heat release patterns between the fuels were not significantly different from each other, it is likely that this effect may be attributed to an effect of the flame temperature or NO_x from formation fuel-bound nitrogen. It is possible that the ignition improving additive added to some of the fuel samples may have contributed to NO_x formation through fuel bound nitrogen, as a result of the high amount of nitrogen present in the ignition improving additive.

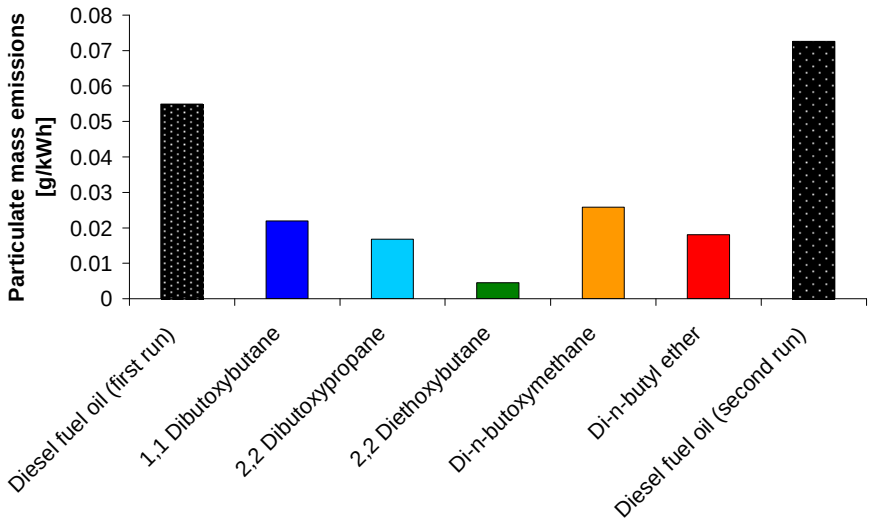

Figure 6.14 - Emission of total particulate mass from the engine for experiments conducted at constant ignition delay

The emission of total particulate mass from the experiments conducted at constant ignition delay is shown in Figure 6.14. Despite the removal of significant differences in the ignition delay patterns, differences in the emission of total particulate mass remained. The most notable difference is that the oxygenated molecules produced less particulate mass than the fossil diesel fuel oil.

The size-spectral density of the particulate matter shown in Figure 6.15 suggests that the higher emission of particulate mass from the fossil diesel fuel was caused by the high emission of accumulation mode particles between 100 and 200 nm in size. Amongst the oxygenated molecules, the number density of particulates emitted in the accumulation mode was negatively correlated with the amount of ignition improving additive (2-EHN) added to the fuel samples. The high oxygen content of the fuel additive could be responsible for reducing the amount of accumulation mode particles formed by introducing oxygen into the fuel-rich core of the burning fuel jet.

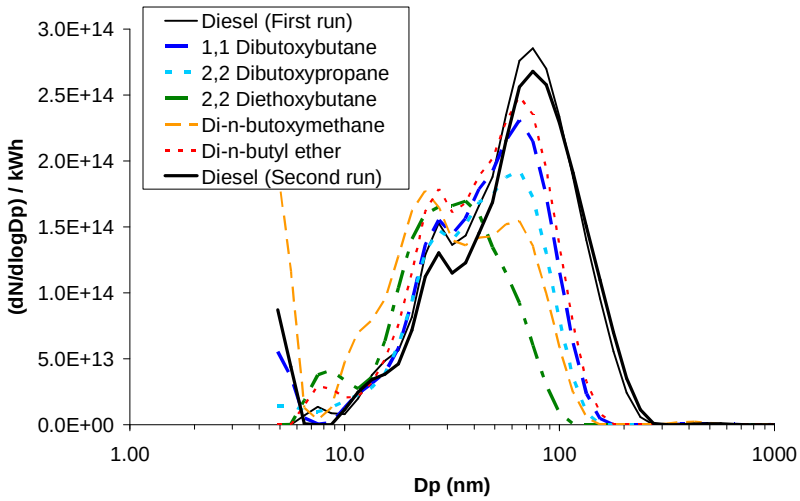

Figure 6.15 - Size spectral density of sub-micron particulate matter for experiments conducted at constant ignition delay

6.2.4. Conclusions of the initial study

The initial study was concerned with investigating the general combustion behaviour of acetal molecules that could be produced via the synthesis methods described in section 6.1. It was shown that the ignition quality of the acetal molecules, which was quantified by their ignition delay, depended strongly on their molecular structure. All oxygenated molecules with the exception of 2,2-diethoxybutane had a significantly higher ignition quality than fossil diesel fuel oil. All acetals had an inferior ignition quality to di-n-butyl ether, which was also tested in the experiments for comparison.

Detailed trends on how the molecular structure of the acetals influenced their ignition delay were observed: The experiments showed that the ignition delay of the acetals was shortened if the central moiety of the acetal molecules was lengthened. The influence which the number of carbon atoms in the central moiety had on the ignition delay was demonstrated using the molecules di-n-butoxymethane and 1,1-dibutoxybutane. The molecule 1,1-dibutoxybutane, which comprised a central moiety of four carbon atoms in a straight chain, had a shorter ignition delay than the molecule di-n-butoxymethane, whose central moiety consisted of a single carbon atom.

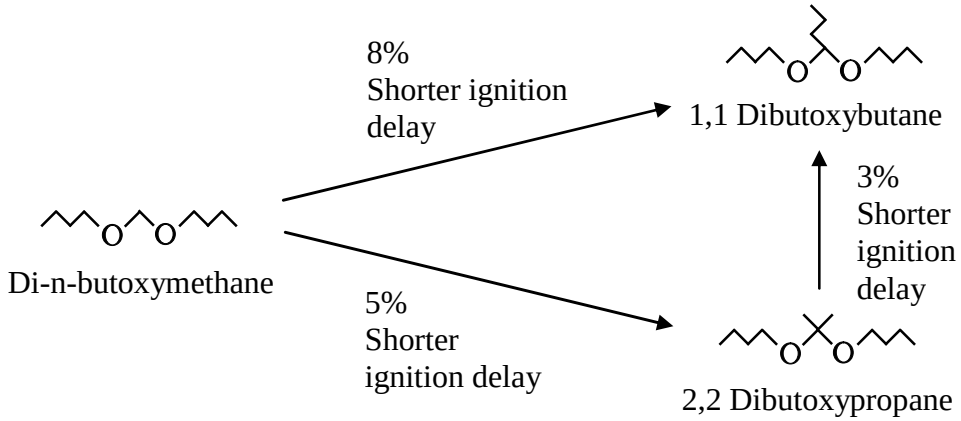

Figure 6.16 - Qualitative assessment of the effect of central moiety on ignition delay of acetal molecules

Experiments conducted with the molecules di-n-butoxymethane and 2,2-dibutoxybutane showed, that the ignition delay was shortened when the number of carbon atoms of the central moiety was increased from one to three. This occurred even though the central moiety of three carbon atoms was branched in structure. The molecule 1,1-dibutoxybutane was subject to a shorter ignition delay than the molecule 2,2-dibutoxypropane. This could suggests that straightening of the central moiety tended to shorten the ignition delay of the molecule (See Figure 6.16). Because the chain was simultaneously lengthened and straightened when changing the structure from the molecule 2,2-dibutoxypropane to the molecule 1,1-dibutoxybutane, it could not be quantified to which extent each

of these two structural changes was responsible for the improvement in ignition quality. Further experiments (described in section 6.3) were carried out to clarify this issue.

The gaseous pollutant emission from the experiments showed that the acetal molecules with the lowest ignition quality (longest ignition delay) produced the highest amount of NO_x during their combustion. This longer ignition delay increased the peak heat release rates of combustion and raised the peak global gas temperatures of the cycle. The fuels incurring a longer ignition delay also produced significantly lower amounts of particulate mass during their combustion. This observation was attributed to increased mixing of the fuel spray with air taking place at longer ignition delays. A longer ignition delay has been shown to decrease the equivalence ratio of the premixed combustion region (Musculus, 2004), and to result in longer lift-off lengths of the flames (Siebers, 1999). Longer lift-off lengths of the flames increase air-entrainment and decrease the equivalence ratio at the lift-off length of the fuel spray. This is thought to cause lower soot-formation in the flames as a result of increased soot oxidation (Musculus, 2004).

In an effort to remove the differences in ignition delay, the fuels were subjected to a series of experiments in which the ignition delay was equalised. This was achieved by adding the ignition improving additive 2-EHN to the fuel samples in varying concentrations. The experimental results showed that once the ignition delay was equalised, the oxygenated molecules showed almost indistinguishable heat release patterns amongst themselves, whilst minor differences between the heat release characteristics of fossil diesel fuel and the oxygenated molecules persisted. The emission of gaseous pollutants showed that although the heat release characteristics of the acetal molecules had been equalised, significantly higher formation of NO_x was still observed for the same molecules that had shown higher formation of NO_x in the constant injection timing and constant ignition timing experiments. Since the fuel samples which had the longest ignition delays in the constant injection timing and constant ignition timing experiments were additised with the largest quantities of 2-EHN, it is possible that the additive may have played a role in the higher formation of NO_x from these fuel samples. Various reasons for this observation are conceivable. Firstly, 2-EHN contains a high level of fuel-bound nitrogen. Fuel bound nitrogen can result in higher NO_x emissions due to the increased formation of nitrogen containing hydrocarbon radicals from nitrogen contained in the fuel, as has been described by Miller and Bowman (1989). Secondly, calculations showed that the addition of 2-EHN to the fuel samples increased their adiabatic flame temperature. Analysis of the adiabatic flame temperature of the fuel samples, which includes the effect of the added 2-EHN, suggests that under these conditions of equal ignition delay, the emission of NO_x correlates reasonable well with the adiabatic flame temperature of the fuel samples (section 6.4, Figure 6.37). Higher flame temperatures would be expected to increase the formation of NO_x (Miller & Bowman, 1989).

The particulate emission from the experiments carried out at a constant ignition delay showed more similar emission levels amongst the acetal molecules than for those experiments carried out at

constant injection timing and at constant ignition timing. This confirmed that the differences in particulate mass formation observed in the previous experiments were largely attributable to differences in the amount of fuel-air mixing as a resulting of the different ignition delays. Small differences amongst the fuels were still observable in the number density of accumulation mode particles (100-200 nm). The number density of these particles correlated well with the amount of ignition improving additive (2-EHN) added to the fuel samples. The high oxygen content of 2-EHN is thought to have contributed to increased oxidation of soot precursors within in the fuel-rich core of the spray.

The experiments suggested that the ignition quality of the molecules was more sensitive to certain features of the molecular structure than to others. Changing the length and structure of the central moiety located between the two oxygen atoms (di-n-butoxymethane, 1,1-dibutoxybutane, 2,2-dibutoxypropane) only had a small influence on the ignition quality of the acetal molecules. Changing the length of the lateral moieties of the acetals molecules was observed to exert a more significant effect on the ignition quality, than changing the length of the central moiety. The molecule 2,2-diethoxybutane which had two carbon atoms in its lateral moieties had a markedly lower ignition quality than any of the other acetal molecules, which had four carbon atoms in their lateral moieties. It could thus be hypothesised that the structure of the lateral moieties located to either side of the two oxygen atoms, played a more influential role in controlling the ignition quality of the molecules than the structure of the central moiety, located between the two oxygen atoms.

6.3. A detailed study of molecular structure on combustion

The initial study was concerned with investigating the general combustion behaviour of acetal molecules that could be produced via the fuel synthesis described in section 6.1. This study gave an idea of someof the mechanisms involved in controlling the combustion characteristics of acetal molecules. The results allowed classifying the acetals in terms of their general combustion behaviour with respect to fossil diesel fuel and a normal ether molecule and gave insights into how changes in the molecular structure influence the combustion behaviour of the molecules. Due to the limited coherency in the molecular structure amongst the fuel molecules, the number of definite conclusions about the influences of specific structural characteristics on the combustion process was limited.

A more detailed study was conducted to understand the effects of specific changes in the molecular structure on the combustion behaviour of acetal molecules. Three molecules were purposely designed for this study, the fuels were synthesised, and their combustion behaviour was studied under similar experimental conditions as those employed for the previous study.

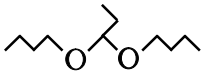

1,1 Dibutoxypropane

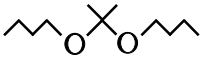

2,2 Dibutoxypropane

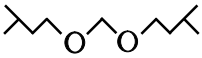

3-Methyl-1-(3-methylbutoxymethoxy) butane

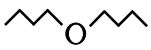

Di-n-butyl ether

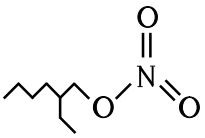

2-Ethylhexyl nitrate

Figure 6.17 - Molecular structure of acetal fuels

Figure 6.17 shows the structure of the molecules used in the experiments. The molecules consisted of 1,1-dibutoxypropane, 2,2-dibutoxypropane and 3-methyl-1-(3-methylbutoxymethoxy)butane. Di-n-butyl ether and fossil diesel fuel oil were tested alongside these acetal molecules to provide a basis for comparison, and to link these experiments to the previous study. The three acetal molecules had a constant number of carbon, hydrogen and oxygen atoms, but the atoms formed a different

molecular structure in each molecule. This allowed eliminating differences in the number of specific atoms and molecular mass amongst the molecules, and allowed focussing the study on structural differences between the molecules. Salient thermochemical and physical properties of the fuels are shown in Table 6.3.

Table 6.3 - Thermochemical properties of the three acetal fuels

Molecule name		**1,1 Dibutoxy propane**	**2,2 Dibutoxy propane**	**3-methyl-1-(3-methylbutoxy methoxy) butane**	**Di-n-butyl ether**	**Fossil diesel fuel**
Sum formula		$C_{11}H_{24}O_2$	$C_{11}H_{24}O_2$	$C_{11}H_{24}O_2$	$C_8H_{18}O$	-
Upper heating value	**[kJ/kg]**	37800	37760	37920	-	-
Lower heating value	**[kJ/kg]**	35020	35000	35140	38044	42980
Carbon	**[%]**	70.16	70.16	70.16	73.78	86.6
Hydrogen	**[%]**	12.85	12.85	12.85	13.93	13.5
Oxygen	**[%]**	16.99	16.99	16.99	12.29	0.07
Density	**[g/ml]**	0.837	0.839	0.835	0.772	0.8341
Viscosity	**[mm^2/s]**	-	-	-	-	2.564
Cetane No. (IQT)		78.67	71.41	57.97	88.8	53.4
Standard boiling point	**[ºC]**	207.3	194.6	219.8	142.5	167.1-362.3

The first aim of this study was to clarify the effect of branching of the central moiety, on the ignition and combustion characteristics of the acetal molecules. The molecules 1,1-dibutoxypropane and 2,2-dibutoxypropane have the same number of carbon atoms in their central moiety, but distinguish themselves by their degree of branching within that moiety. 1,1-Dibutoxypropane had a straight-chained central moiety, whilst 2,2-dibutoxypropane had a branched central moiety. The combustion differences observed between the molecules 1,1-dibutoxypropane and 2,2-dibutoxypropane illustrated the effects which this change in molecular structure had on their combustion behaviour. The second aim of this study was to show the relative importance which the central moiety and the lateral moieties for the ignition quality of the molecules. This was done by comparing the two molecules 2,2-dibutoxypropane and 3-methyl-1-(3-methylbutoxymethoxy)butane with each other. In the molecule 2,2-dibutoxypropane the branching was positioned at the central moiety located between the two oxygen atoms. In the molecule 3-methyl-1-(3-methylbutoxymethoxy)butane the branching was positioned at the ends of the lateral moieties. Branching at the ends of the chain was used to provide an obstacle to the thermal decomposition mechanism. By moving the branching from one part of the molecule to another, it was hoped to gain some understanding of the relative importance of the individual parts of the molecule for the ignition quality of the molecule. The

initial study had led to the hypothesis that the lateral moieties were more important to the ignition quality of the molecules than the central moiety, indicating that thermal decomposition of the molecules may occur predominantly via the lateral moieties. This was studied in further detail using these experiments.

Table 6.4 - Overview of experimental conditions

Engine speed: 1200 rpm Engine load: 4 bar IMEP	**Constant injection timing**		**Constant ignition timing**		**Constant ignition delay**		
	Injection timing [° CA BTDC]	**Ignition timing [° CA BTDC]**	**Injection timing [° CA BTDC]**	**Ignition timing [° CA BTDC]**	**Injection timing [° CA BTDC]**	**Ignition timing [° CA BTDC]**	**2-EHN conc. [vol. %]**
Fossil diesel fuel oil	7.10	TDC	7.1	TDC	5.4	TDC	4.00
Di-n-butyl ether	7.10	1.70	5.4	TDC	5.4	TDC	0.00
1,1 Dibutoxy propane	7.10	0.98	6.1	TDC	5.4	TDC	0.60
2,2 Dibutoxy propane	7.10	0.88	6.2	TDC	5.4	TDC	0.79
3-methyl-1-(3-methylbutoxymethoxy) butane	7.10	-0.04	7.15	TDC	5.4	TDC	1.80
Fossil diesel fuel oil	7.10	TDC	7.1	TDC	5.4	TDC	4.00

The molecules were tested under three experimental conditions, as shown in Table 6.4. The conditions consisted of constant injection timing, constant ignition timing and constant ignition delay, as in the previous study. For the experiments conducted at constant ignition delay, the injection timing as well as ignition timing were kept constant, by additising the fuel samples with the ignition promoting molecule 2-EHN in varying concentrations.

6.3.1. Constant injection timing experiments

In the constant injection timing experiments, all fuels were injected at the same point during the cycle (7.1º CA BTDC). This common time of injection was chosen so that the ignition would occur at TDC when fossil diesel fuel oil was used for the experiments. The amount of fuel injected was adjusted so that each type of fuel would develop the same indicated load of 4 bar IMEP. The engine speed was 1200 rpm for all experiments. Figure 6.18 shows the combustion chamber pressures, heat release rates and mass fraction burnt analyses for the individual fuel molecules.

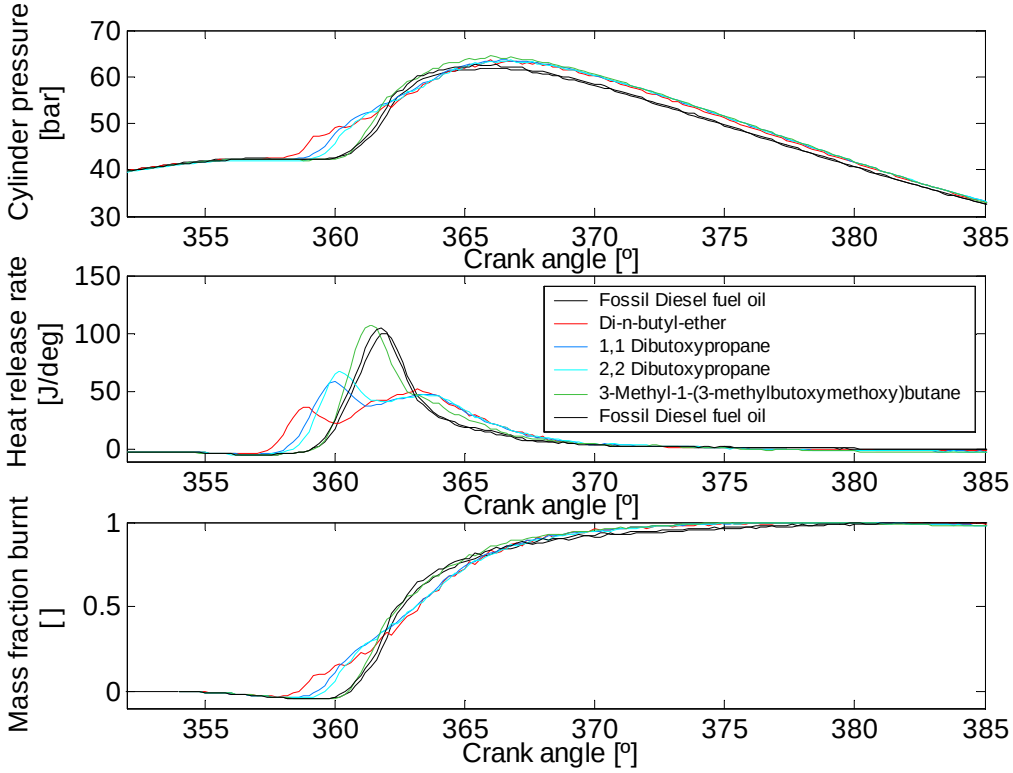

Figure 6.18 - Cylinder pressure, heat release rate and mass fraction burnt for constant injection timing experiments at 1200 rpm and 4 bar IMEP

Figure 6.18 shows that the individual molecules had significantly different ignition delays. Di-n-butyl ether clearly had the shortest ignition delay of all fuels. 1,1-Dibutoxypropane had the shortest ignition delay amongst the acetal molecules, closely followed by 2,2-dibutoxypropane, whilst 3-methyl-1-(3-methylbutoxymethoxy)butane had by far the longest ignition delay. The data demonstrate how the ignition quality of the fuel was influenced by its molecular structure. If the central moiety of the molecule was changed from a straight configuration (1,1-dibutoxypropane) to a branched configuration (2,2-dibutoxypropane) of the same number of carbon atoms, the ignition quality was slightly reduced. This observation unequivocally clarified the observations previously made with the molecules 1,1-dibutoxypropane and 2,2-dibutoxypropane in the initial experimental study of acetal molecules (section 6.2). It showed that branching of the central moiety increased the

ignition delay of the molecule, even if the number of atoms in the central moiety remained equal. A further observation was made by examination of the ignition behaviour of the molecule 3-methyl-1-(3-methylbutoxymethoxy)butane. Under the assumption that branching at the end of a carbon chain provides an obstacle to chemical decomposition, the relative importance of decomposition via the central moiety and the lateral moieties was investigated. This was done by moving the location of the branching from the central moiety (2,2-dibutoxypropane) to the carbon chains to either side of the two oxygen atoms (3-methyl-1-(3-methylbutoxymethoxy)butane).

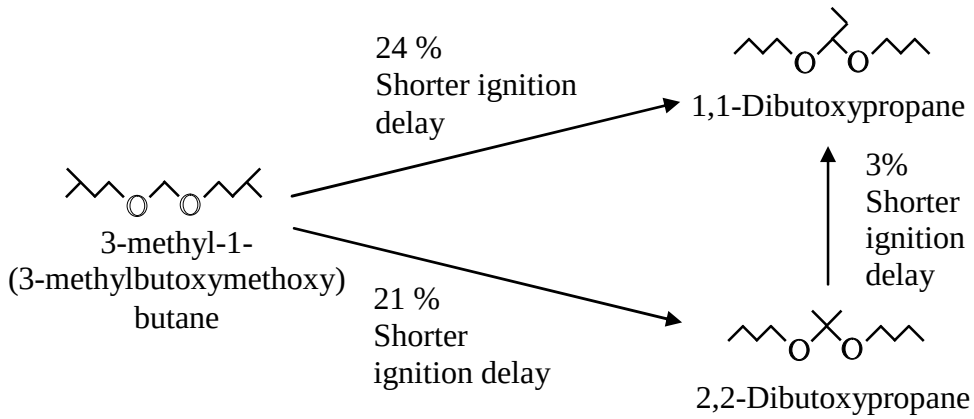

Figure 6.19 – Effect of molecular structure on ignition delay of acetal molecules composed of the same atoms

The cylinder pressure histories and heat release rates recorded for the experiments (Figure 6.18) showed that the ignition delay increased by more than twice the amount when changing the molecular structure of the fuel from 2,2-dibutoxypropane to molecule 3-methyl-1-(3-methylbutoxymethoxy)butane than when changing it from 1,1-dibutoxypropane to 2,2-dibutoxypropane. This could suggest that thermal decomposition of the molecule via its lateral-moieties is more critical to the ignition delay than decomposition via the central moiety.

The emission of gaseous pollutants from the engine experiments and the indicated thermal efficiency are shown in Figure 6.20. It can be seen that contrary to the observations made in the initial study (section 6.2), lower emissions of NO_x were recorded for the di-n-butyl ether than for the 2,2-dibutoxypropane in these experiments (the molecule 2,2-dibutoxypropane was tested in both studies). The experimental results thus showed a discrepancy between the initial study and the present more detailed study. The reasons for this discrepancy are not clear, but the results observed in the present more detailed study, appear to be more plausible. The lower emissions of NO_x from the di-n-butyl ether may readily be explained by its shorter ignition delay with respect to the 2,2-dibutoxypropane. It still remains unclear though why the relative magnitude in emission of NO_x between the two molecules changed between the two studies. The two most significant parameters which were changed in between the study described in section 6.2 and the present study (section 6.3) were the fuel injector and the chemiluminescence exhaust gas emissions analyser. Both had to be replaced due to mechanical failure during experiments that were undertaken in between the two studies.

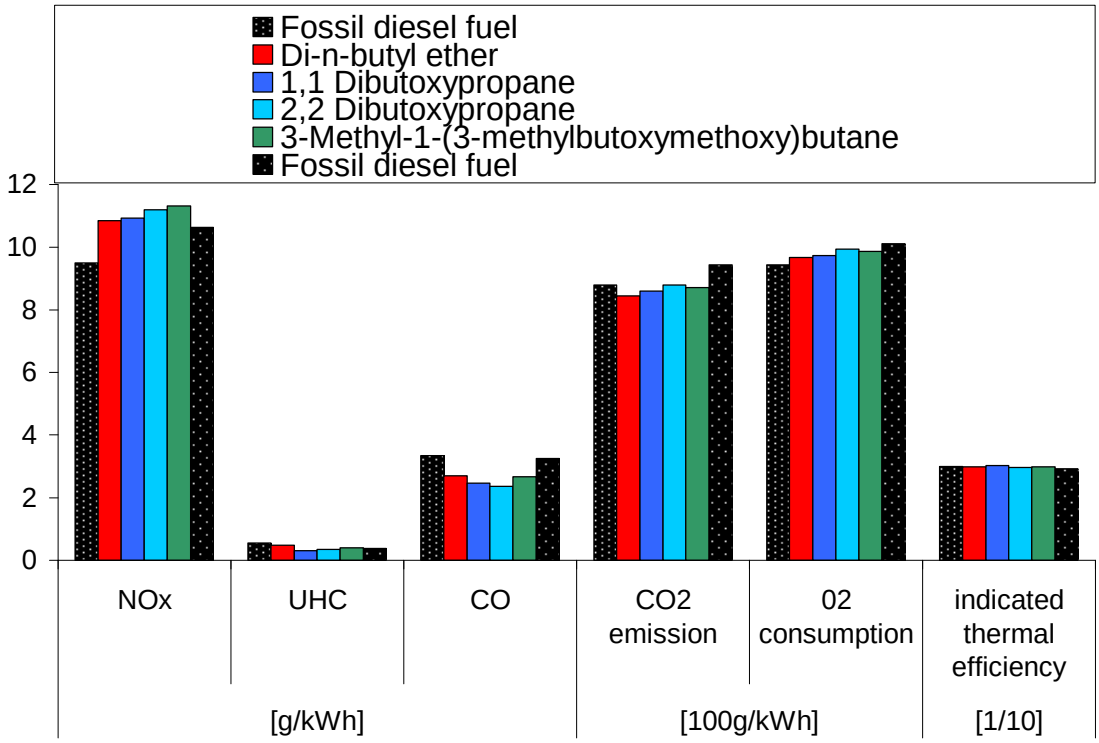

Figure 6.20 - Emission of gaseous pollutants and indicated thermal efficiency of the engine for constant injection timing experiments

The analysis of exhaust gases (Figure 6.20.) showed that the oxygenated molecules produced relatively similar levels of NO_x emissions. Amongst the oxygenated molecules, the relative magnitude of NO_x emissions showed good correlation with the ignition delay of the molecules. Fossil diesel fuel however, produced the lowest emissions of NO_x amongst the fuels despite its relatively long ignition delay. This observation is also in good agreement with the initial experimental study (section 6.2). As will be discussed in more detail in section 6.4.4, this could be due to differences in soot-radiative heat transfer between the diesel fuel and the oxygenated fuels. Figure 6.21 shows that diesel fuel produced significantly higher soot emissions than the oxygenated fuels. If it may be assumed that higher exhaust gas particulate emission are indicative of higher soot-concentration within the flames during combustion, diesel fuel would be expected to have a higher soot-concentration within its flames than the oxygenated fuels. The presence of soot in the flames has been shown to lower the temperature of the flames through radiative heat transfer from the soot particles and thereby lower the formation of NO_x (Mueller, et al., 2009). The soot emission measurements shown in Figure 6.21 provide some support for this theory.

Figure 6.22 shows the size spectral density of the particulates. The results indicate that amongst the acetal molecules, the emission of nucleation mode particles was positively correlated with the emission of unburned hydrocarbons and with the ignition delay of the fuel samples. A higher unburned hydrocarbon concentration in the exhaust gases may have assisted the formation of nucleation mode particles through increased condensation of hydrocarbon vapours.

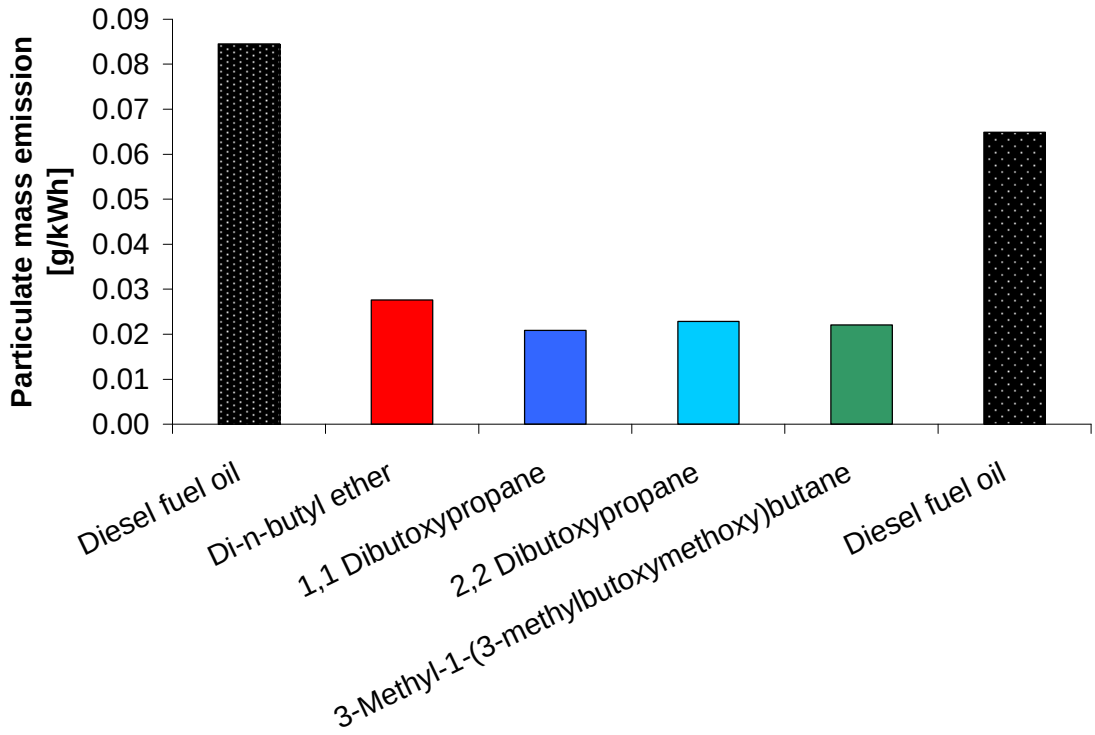

Figure 6.21 - Emission of total particulate mass from the engine for experiments conducted at constant injection timing

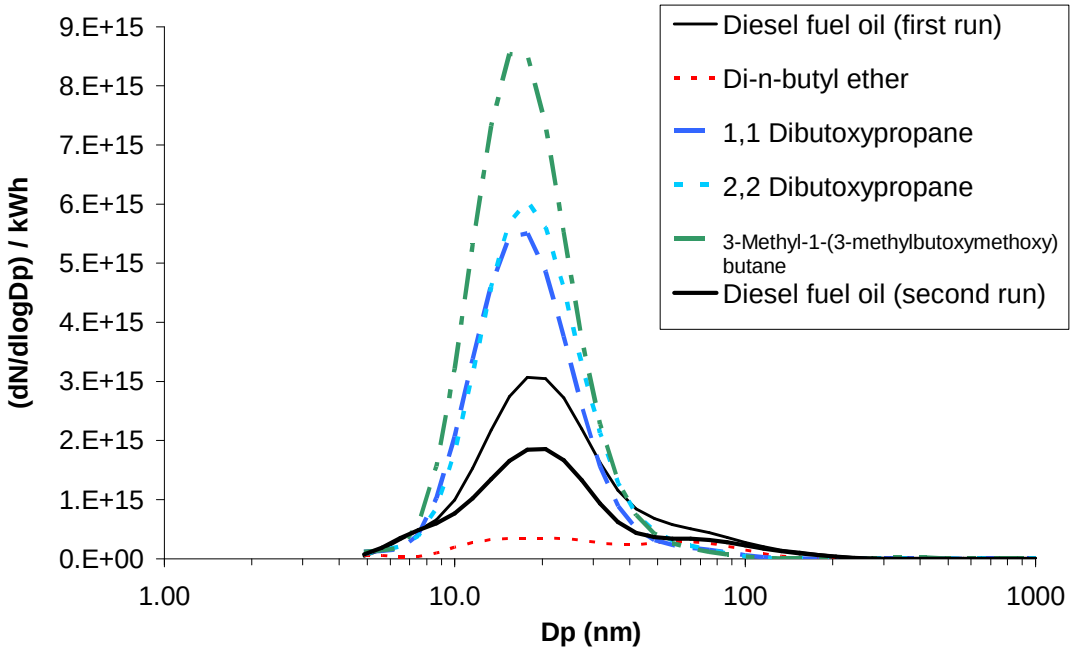

Figure 6.22 - Size spectral density of sub-micron particulate matter for experiments conducted at constant injection timing

6.3.2. Constant ignition timing experiments

In the constant ignition timing experiments, the ignition timing of all fuels was equalised by adjusting the time of injection, so that ignition would occur at the same point during the combustion cycle, at top-dead-centre (TDC). The amount of fuel injected was adjusted so that every type of fuel would develop the same indicated load of 4 bar IMEP. The engine speed was 1200 rpm for all experiments. Figure 6.23 shows the combustion chamber pressures, heat release rates and mass fraction burnt analyses for the individual fuels.

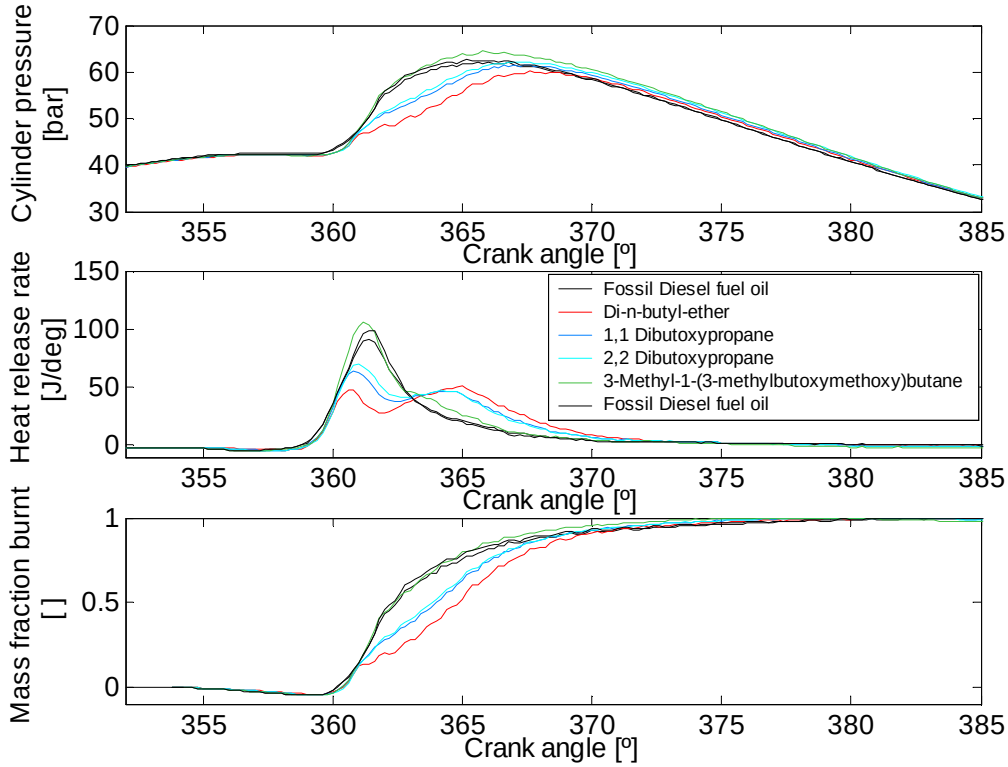

Figure 6.23 - Cylinder pressure, heat release rate and mass fraction burnt for constant ignition timing experiments at 1200 rpm and 4 bar IMEP

Figure 6.23 shows the cylinder pressure, heat release rates and mass fraction burnt from the experiments. The heat release rates showed similar patterns to those observed for the experiments carried out at constant injection timing in Figure 6.18 (section 6.3.1), with the exception that in the constant injection timing experiments the start of heat release occurred at different times during the cycle, whilst in the constant ignition timing experiments the start of heat release occurred at the same time for all fuels. As in the experiments with constant injection timing, di-n-butyl ether clearly had the shortest ignition delay. 1,1-Dibutoxypropane had the shortest ignition delay amongst the acetal molecules and was closely followed by 2,2-dibutoxypropane. 3-Methyl-1-(3-methylbutoxymethoxy)butane had by far the longest ignition delay. Figure 6.23 shows that the heat release rates of the fuels changed, depending on the ignition delay which the fuels underwent. As the ignition delay became longer, the combustion process shifted from a predominantly diffusion-

controlled combustion process (di-n-butyl ether) to predominantly premixed combustion (3-methyl-1-(3-methylbutoxymethoxy)butane). The shift towards premixed combustion caused the peak heat release rate during the pre-mixed combustion phase to increase significantly. This increase in the rate of heat release caused fuel molecules with a longer ignition delay to undergo faster combustion than those with a shorter ignition delay. This led to higher peak pressures and temperatures for molecules with a longer ignition delay, as previously demonstrated in Figure 6.8 for the molecules tested in the initial series of experiments (section 6.2). The higher global gas temperatures are thought to have lead to a higher formation of NO_x. The emission of NO_x and other gaseous pollutants from these experiments is shown in Figure 6.24.

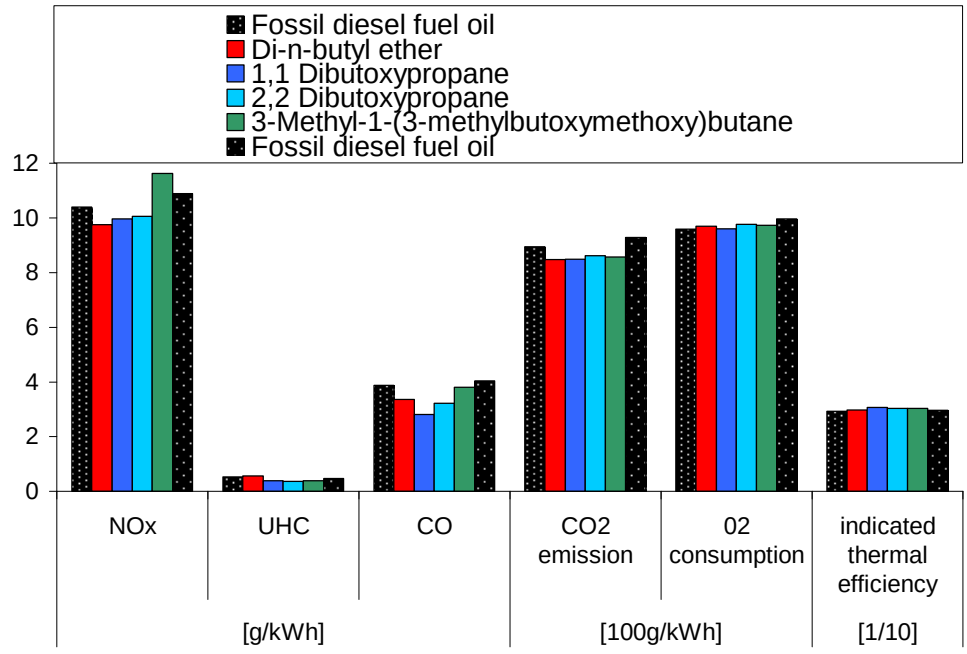

Figure 6.24 - Emission of gaseous pollutants and indicated thermal efficiency of the engine for constant ignition timing experiments

Figure 6.24 shows that the emission of NO_x from the engine correlated well with the peak heat release rates and peak combustion chamber pressures shown in Figure 6.23. Amongst the acetal molecules, 1,1-dibutoxypropane produced the lowest amount of NO_x emissions. 2,2-Dibutoxypropane produced slightly more NO_x than 1,1-dibutoxypropane, but both molecules still produced significantly less NO_x than fossil diesel fuel under this experimental condition. The molecule 3-methyl-1-(3-methylbutoxymethoxy)butane produced markedly higher amounts of NO_x than 1,1-dibutoxypropane, 2,2-dibutoxypropane or fossil diesel fuel oil. Figure 6.23 shows that although 3-methyl-1-(3-methylbutoxymethoxy)butane had a comparable ignition delay to fossil diesel fuel, its heat release during the premixed combustion phase and during the mixing-controlled combustion phase were consistently higher than for diesel fuel. This is likely to have been due to the higher volatility and lower boiling point of 3-methyl-1-(3-methylbutoxymethoxy)butane (219.8 ºC at 1 atm) with respect to fossil diesel fuel oil (only 35.9 % by volume of the diesel fuel boils at 250 ºC at 1 atm). The lower boiling point of 3-methyl-1-(3-methylbutoxymethoxy)butane is thought to have aided evaporation and mixing of the fuel with air, causing a more rapid combustion process.

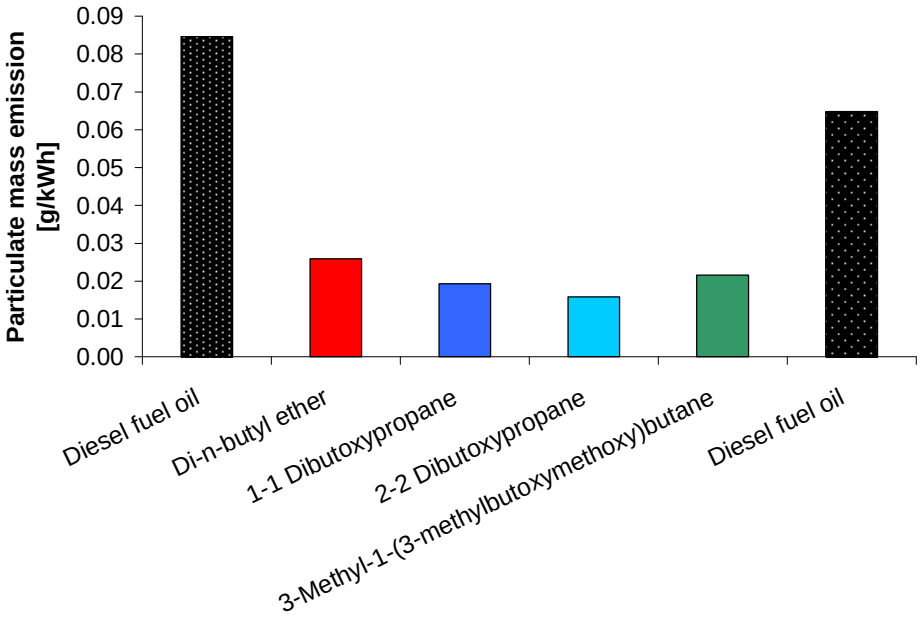

Figure 6.25 - Emission of total particulate mass from the engine for experiments conducted at constant ignition timing

Figure 6.25 shows the total particulate mass emission from the experiments conducted at constant ignition timing. Similarly to the experiments conducted at constant injection timing, the most important observation that can be made from the data is that the fossil diesel fuel produced higher amounts of particulate matter than any of the acetal molecules or the ether. This is likely to be due to the higher oxygen content of the acetal and ether molecules, which assists the oxidation of soot and its precursors in the fuel-rich regions of the flames. Figure 6.26 shows the size spectral density of the particulate matter. The size spectral density of the particulates showed similar patterns to those observed for the constant injection timing experiments (section 6.3.1). As for the experiments conducted at constant injection timing there appeared to be some degree of correlation between the emission of nucleation mode particles and the ignition delay for the oxygenated fuel samples.

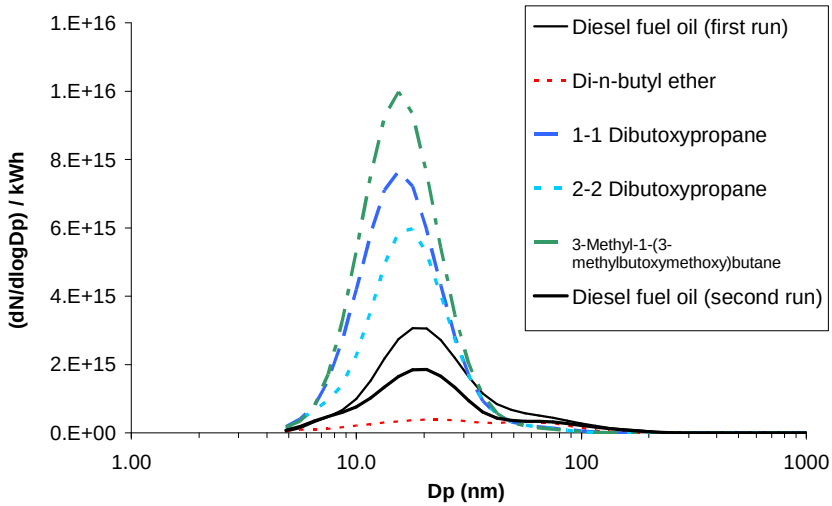

Figure 6.26 - Size spectral density of sub-micron particulate matter for experiments conducted at constant ignition timing

6.3.3. Constant ignition delay experiments

In the third series of experiments, the ignition delay of the fuels was equalised through the addition of the ignition improving molecule 2-EHN to the fuel samples in varying concentrations. The same time of injection and the same time of ignition were used for all fuels. The amount of fuel injected was optimised so that each type of fuel would develop the same indicated load of 4 bar IMEP. The engine speed was 1200 rpm in all experiments. Figure 6.27 shows the combustion chamber pressures, heat release rates and mass fraction burnt analyses for the individual fuel molecules.

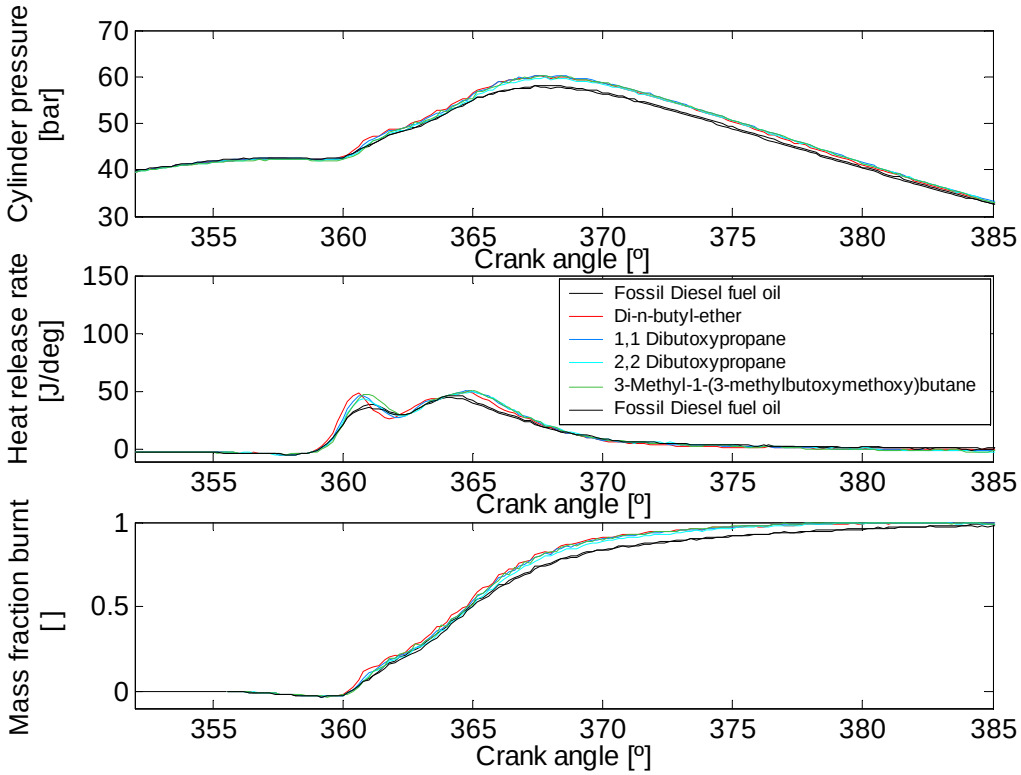

Figure 6.27 - Cylinder pressure, heat release rate and mass fraction burnt for constant ignition delay experiments at 1200 rpm and 4 bar IMEP

Figure 6.27 shows that once the ignition delay was equalised for all fuels, their heat release characteristics became very similar. Significant differences in the heat release rates remained visible between the fossil diesel fuel and the oxygenated fuel molecules. The oxygenated molecules showed higher peak heat release rates than the fossil diesel fuel oil during the premixed combustion phase and during the mixing-controlled combustion phase. This is thought to have occurred as a result of faster fuel-air mixing having taken place for the oxygenated molecules than for the fossil diesel fuel due to their higher volatility. The oxygenated fuels each had a single boiling point which lay between 142.5 ºC (di-n-butyl ether) and 219.8 ºC (3-methyl-1-(3-methylbutoxymethoxy)butane) at atmospheric pressure. The fossil diesel fuel oil, which consisted of a large variety of hydrocarbon compounds, had a boiling point range spanning from 167-362 ºC. At atmospheric pressure and a

temperature of 250 ºC, all oxygenated molecules would have been in a gaseous state, whilst only 35.9 % of the total volume of fossil diesel fuel would have become gaseous. The lower boiling points of the oxygenated fuels, which are indicative of their higher volatility, are thought to have allowed faster evaporation and more rapid mixing with air to have taken place.

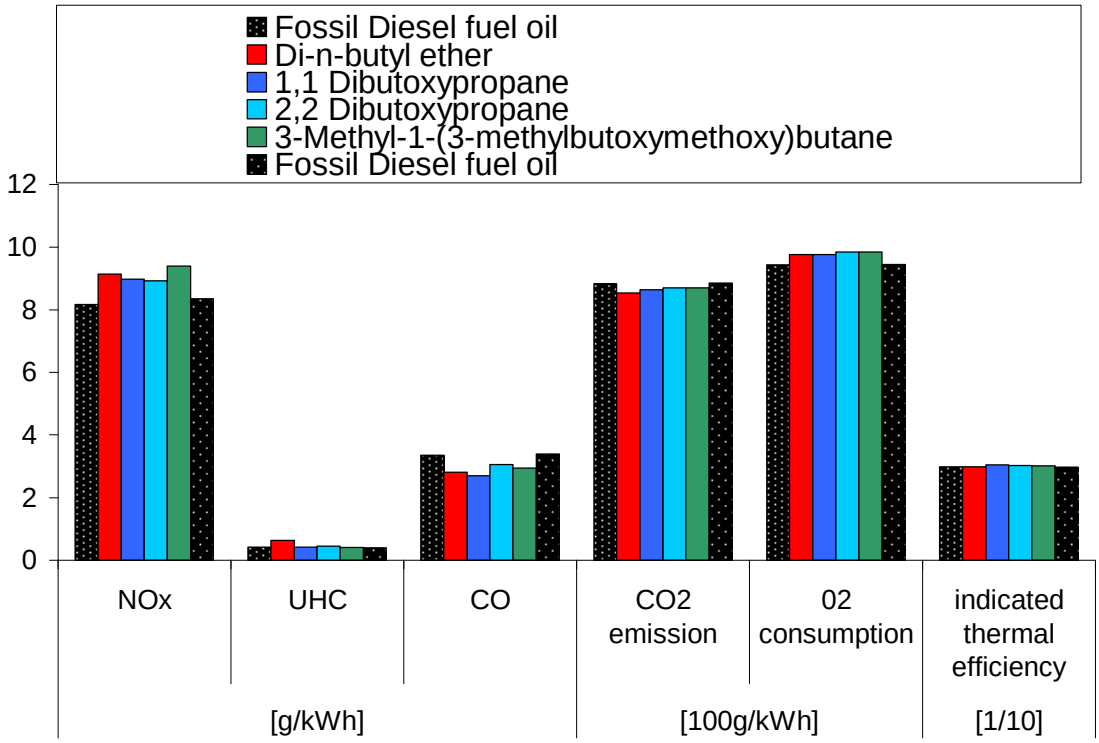

Figure 6.28 - Emission of gaseous pollutants and indicated thermal efficiency of the engine for constant ignition delay experiments

The emission of exhaust gases and the indicated thermal efficiency of the engine are shown in Figure 6.28. It can be seen that when the ignition delay of the fuels was equalised, fossil diesel fuel produced significantly lesser amounts of NO_x than the oxygenated fuel molecules. The data indicate that the thermal efficiencies recorded for the oxygenated molecules, especially for the 1,1-dibutoxypropane, were marginally higher than that recorded for fossil diesel fuel.

Figure 6.29 depicts the total particulate mass emissions from the experiments. The data show that the oxygenated fuels produced significantly lower amounts of particulate mass than fossil diesel fuel. It is though that the oxygen present in the ether and acetal molecules reduced the equivalence ratio within the fuel-rich core of the fuel jet during combustion, whereby it increased the oxidation of soot and its precursor molecules. The increased oxidation of soot and its precursors for the oxygenated fuels is thought to have resulted in reduced emissions of particulate mass from the engine.

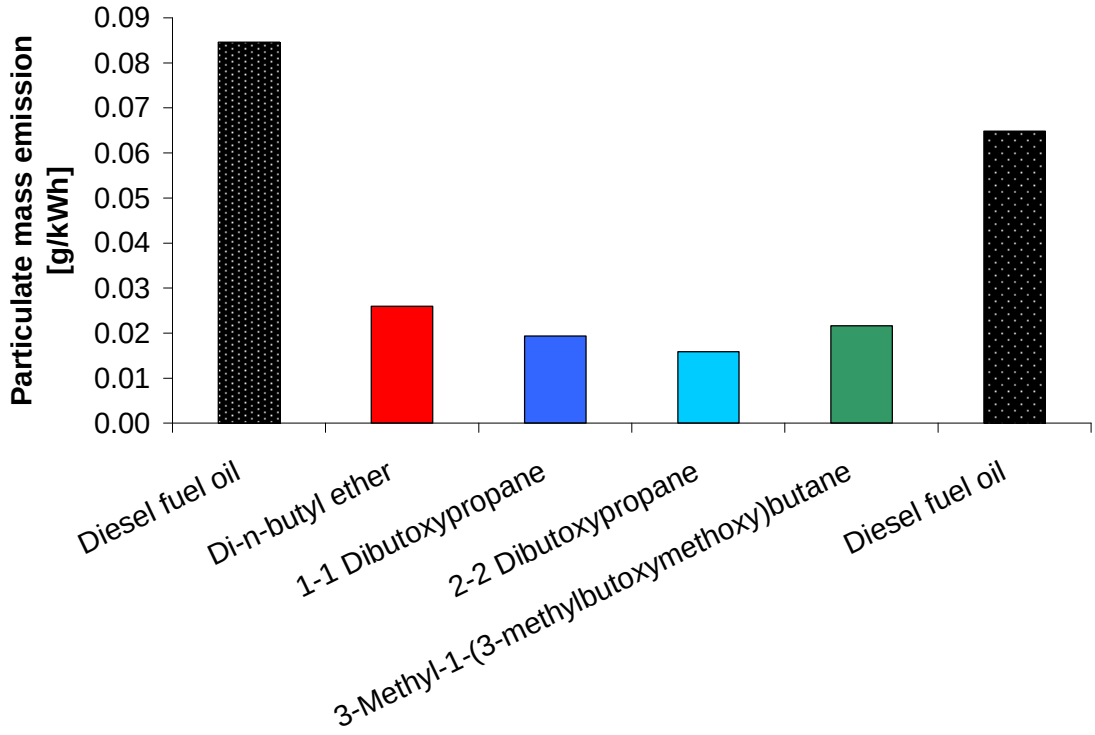

Figure 6.29 - Emission of total particulate mass from the engine for experiments conducted at constant ignition delay

The size spectral density of the sub-micron particulate matter is shown in Figure 6.30. It can be seen that once the ignition delay was equalised, a reasonable correlation existed between the boiling points of the fuels and the size spectral density of nucleation mode particles (5-40nm diameter).

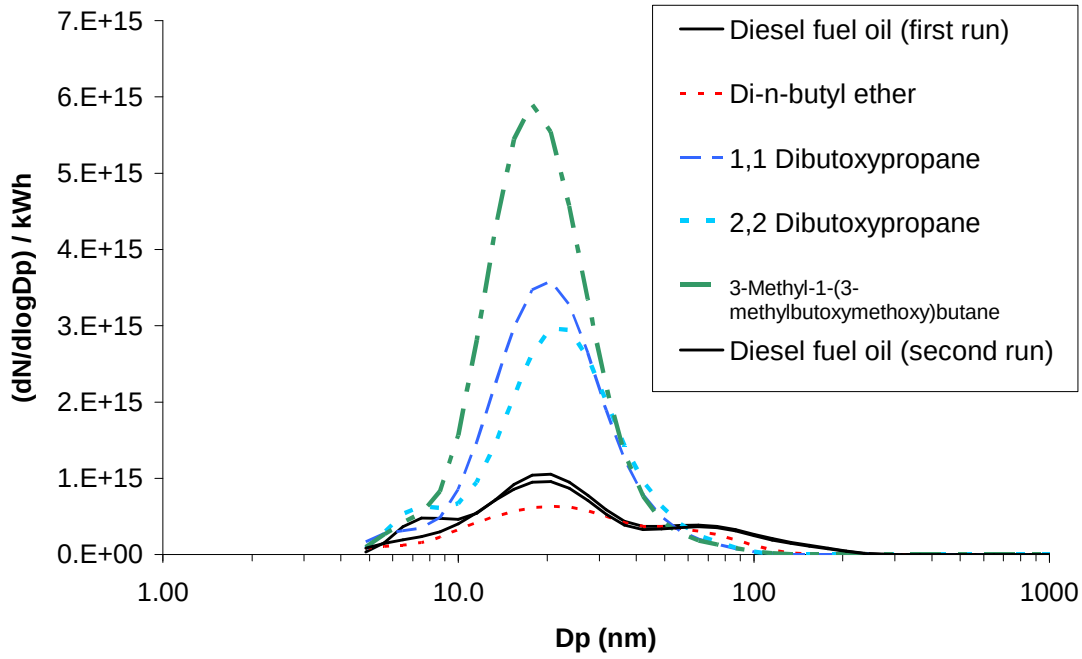

Figure 6.30 - Size spectral density of sub-micron particulate matter for experiments conducted at constant ignition delay

6.4. Conclusions of the two studies

The combustion behaviour of several acetal molecules was studied in two consecutive series of experiments. In the first series of experiments four acetal molecules which could be produced via the synthesis methods described in section 5 were examined for their combustion behaviour and compared with fossil diesel fuel oil and a normal ether molecule. In a second study, detailed changes in the molecular structure of acetals of the same atomic composition were studied using three additional molecules. Conclusions drawn from both studies in conjunction are presented in this section.

6.4.1. Influence of molecular structure on auto-ignition

The experiments showed that the molecular structure of the acetal molecules had a significant influence on their ignition delay. This is illustrated in Figure 6.31. Figure 6.31 shows how individual changes in the molecular structure of acetal molecules affected their ignition behaviour. The following paragraph provides a discussion of the individual structural changes amongst the molecules, and how these affected the ignition delay. The molecule di-n-butoxymethane, will be used as the starting point for this discussion, due to its basic structure which is common to most tested molecules. Di-n-butoxymethane comprises two normal butyl groups as lateral moieties and a simple central moiety consisting of a methyl group. A comparison between di-n-butoxymethane and 3-methyl-1-(3-methylbutoxymethoxy)butane shows that the addition of a carbon atom to each of the two lateral-moieties, in such a manner that a branched end to the lateral-moiety was created, decreased the ignition quality of the molecule, and lead to an increase in the ignition delay from 889 μs to 993 μs. This result leads to two conclusions about the influence of the molecular structure on the ignition process. Firstly, the lateral moieties of the molecules play a significant role in the thermal decomposition and ignition of the molecule. Secondly, the thermal decomposition of the molecule via these lateral moieties is inhibited to some degree by the branching of these lateral moieties.

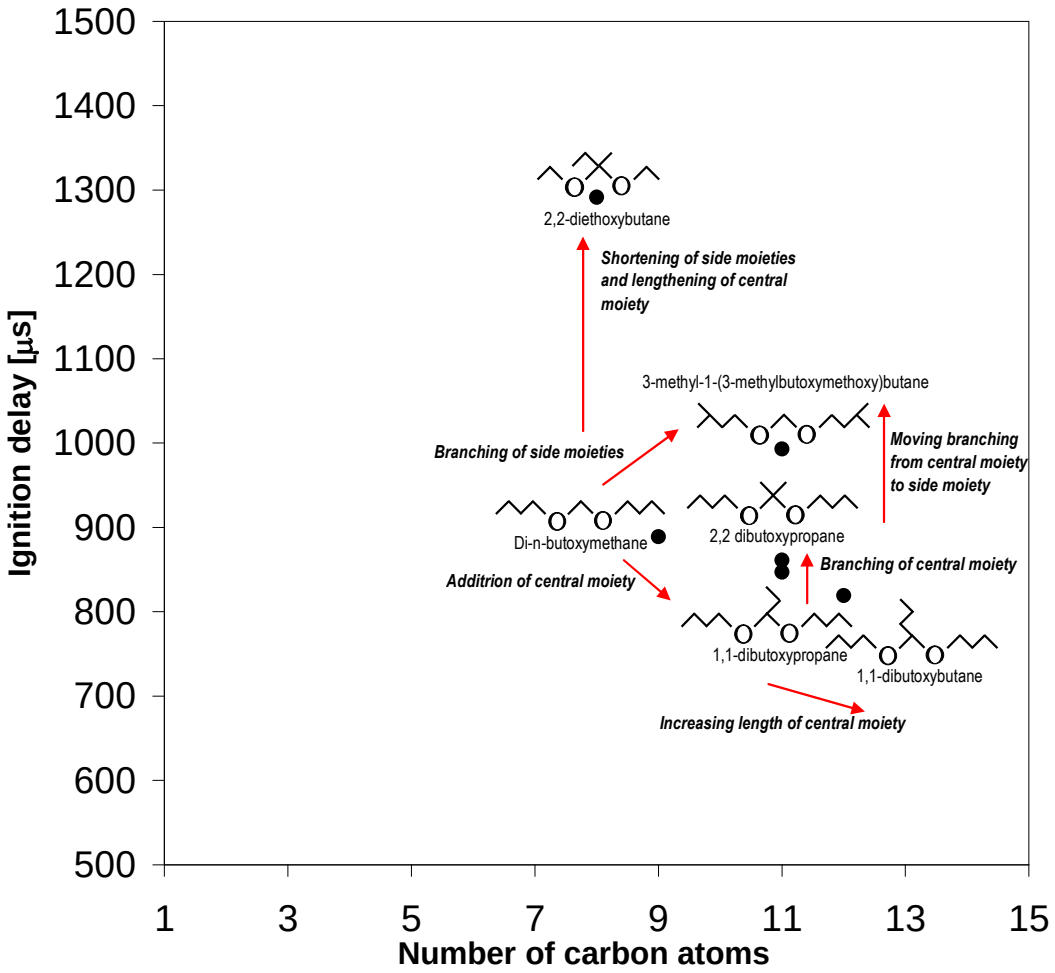

Figure 6.31 - Ignition delay and molecular structure at (T_{ign}=881 K and p_{ign}=4.5 MPa)

A different result was obtained when adding two carbon atoms in a branched configuration to the central moiety of di-n-butoxymethane, which formed the molecule 2,2-dibutoxypropane. When implementing this structural change from di-n-butoxymethane to 2,2-dibutoxypropane, the ignition delay was reduced from 889 to 861 µs. This reduction in ignition delay occurred even though the two carbon atoms were arranged in a branched configuration. Changing the molecular structure from the molecule 2,2-dibutoxypropane to 1,1-dibutoxypropane resulted in a further reduction of ignition delay from 861 to 847 µs. This shows that by changing the structure of the central moiety from a branched configuration to a straight configuration improved the auto-ignition quality further.

A further effect can be observed when examining the influence of the length of the central moiety on the ignition delay. A comparison of the molecule 1,1-dibutoxypropane with the molecule 1,1-dibutoxybutane shows that increasing the length of the central moiety by one carbon atom decreased the ignition delay from 847 µs for 1,1-dibutoxypropane to 819 µs for 1,1-dibutoxybutane.

The molecule with the longest ignition delay by far, was 2,2-diethoxybutane with 1292 µs. A comparison of di-n-butoxymethane with 2,2-diethoxybutane shows that two structural changes distinguish the two molecules from each other, which makes interpretation of the results more difficult. Two conjectures based on observations from the results presented so far can be used in an attempt to clarify the effect of the structural changes between these two molecules on their ignition

delay. Firstly, when changing the structure from di-n-butoxymethane to 2,2-diethoxybutane, a central moiety of three additional carbon atoms, with some degree of branching is added. Secondly, the lateral moieties are shortened from four to two carbon atoms. It had been shown previously (by comparing di-n-butoxymethane with 2,2-dibutoxypropane) that the addition of a central moiety, even if it is branched, lead to significant shortening of ignition delay. On the premise of this observation, the addition of the central moiety alone when changing the structure from di-n-butoxymethane to 2,2-diethoxybutane should lead to a reduction in ignition delay. Yet, the ignition delay was increased significantly when changing the molecular structure from di-n-butoxymethane to 2,2-diethoxybutane. Therefore, the second structural change, which consisted in a reduction of the length of the lateral moieties from four to two carbon atoms, must have been responsible for the observed decrease in ignition quality. This conjecture indicates that the length of the lateral moieties may have had a stronger impact on the auto-ignition quality of the molecules than the central moiety.

6.4.2. Influence of molecular structure on heat release

The experiments in these two studies indicated that the ignition delay had the strongest effect in governing the rate of heat release from the fuel molecules. The longer the ignition delay was, the more time was available for fuel-air mixing to take place prior to ignition. A greater amount of fuel-air mixing having taken place prior to ignition allowed higher amounts of heat to be released during the initial pre-mixed combustion phase, as a result of greater amounts of fuel having mixed to within their flammability limits with air.

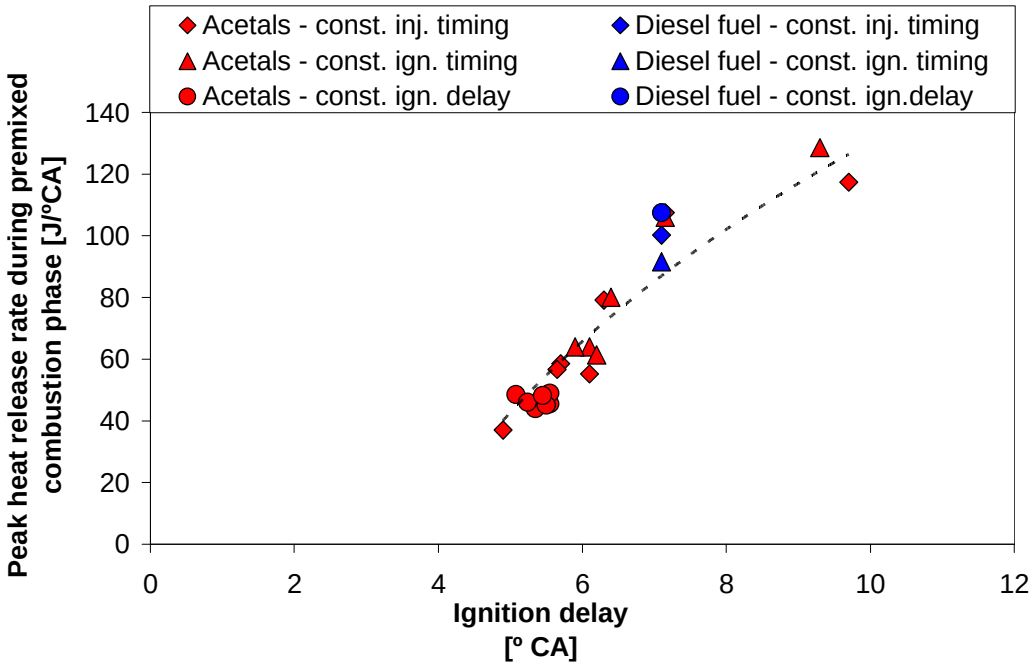

Figure 6.32 – Influence of ignition delay on the peak heat release rate of the fuel during the premixed combustion phase

Figure 6.32 illustrates the correlation between the ignition delay and the peak heat-release rate during the premixed combustion phase. The data suggest that most of the heat release characteristics of the fuels can be explained by their ignition delay under these conditions.

6.4.3. Influence of molecular structure on adiabatic flame temperature

The adiabatic flame temperature for a stoichiometric mixture of fuel and air with no dissociation, was calculated for all the molecules tested in this study according to the procedure delineated by Turns (1996, p. 32-35). Due to the lack of availability of data on the enthalpies of formation or combustion for these molecules in the published literature, the adiabatic flame temperatures were calculated on the basis of experimentally determined values of enthalpy of combustion. These measurements were carried out via bomb calorimetry according to the UK Institute of Petroleum's (IP12) standard.

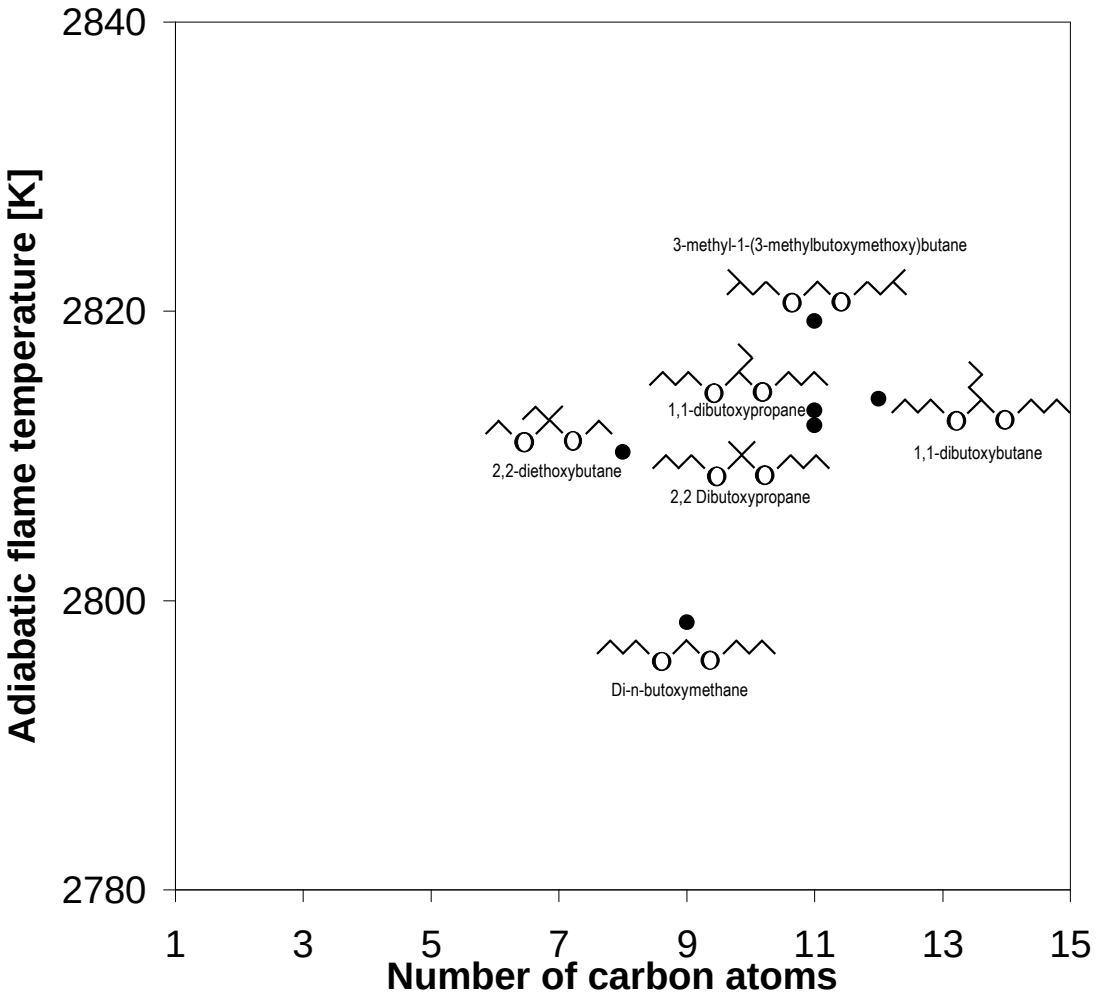

Figure 6.33 - Adiabatic flame temperature of the acetal molecules at stoichiometric mixture with air for combustion starting at temperature of 881 K

Previous experiments (see Chapter 5) had suggested that experimentally determined values of enthalpy of combustion may provide a reasonable indication of adiabatic flame temperature, though they may be less accurate than theoretically determined values. The results from the calculation of adiabatic flame temperature of the acetal molecules are shown in Figure 6.33. The largest difference in adiabatic flame temperature (21 K) occurred between the molecules di-n-butoxymethane which had the lowest adiabatic flame temperature and 3-methyl-1-(3-methylbutoxymethoxy)butane which had the highest adiabatic flame temperature. The differences amongst the other molecules were relatively small, so that a relatively similar behaviour in terms of pollutant formation would be expected. Analysis of the influence of adiabatic flame temperature on the formation of NO_x shall be presented in Figure 6.37 of the following section.

6.4.4. Influence of molecular structure on the emission of gaseous pollutants and particulates

The molecular structure of the fuel molecules played an important part in the formation and emission of pollutants from the diesel combustion process. It had been shown in Figure 6.31 that the ignition delay of the fuel strongly depended on the structure of the fuel molecules. Figure 6.32 had shown that the ignition delay was an important factor in controlling the peak heat-release rates during the premixed combustion phase. Figure 6.34 shows that some correlation exists between the heat release rates of the combustion process and the exhaust gas emission of NO_x. Because the NO_x emissions recorded in two studies were slightly different from one another (this may depend on the conditions of the engine intake air (temperature, atmospheric pressure and humidity), the NO_x emissions recorded during the initial study were normalised with respect to the second study using the value of NO_x emitted for the same standard diesel fuel, which was testes in both sets of experiments.

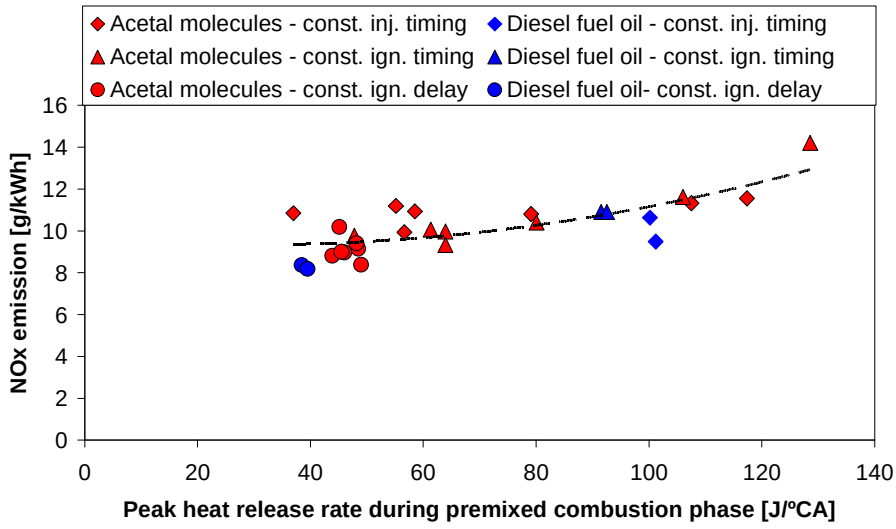

Figure 6.34 – Influence of peak heat release rate during the pre-mixed combustion phase on NO_x emissions

Figure 6.34 shows that some degree of correlation exists between NO_x emissions and peak heat release rate during the pre-mixed combustion phase, especially under conditions of constant ignition timing. This is because higher peak heat release rates typically lead to higher combustion temperatures.

Since most of the NO_x formation during the combustion process of an internal combustion engine may be attributed to thermal NO_x via the Zeldovich mechanism, there usually exists a strong correlation between the combustion temperature and the emission of NO_x. It should be noted that the magnitude of the heat release rates from the combustion of the fuel does not necessarily lead to higher combustion temperatures. The timing of the heat release during the engine cycle may also play an important role in determining the combustion temperatures.

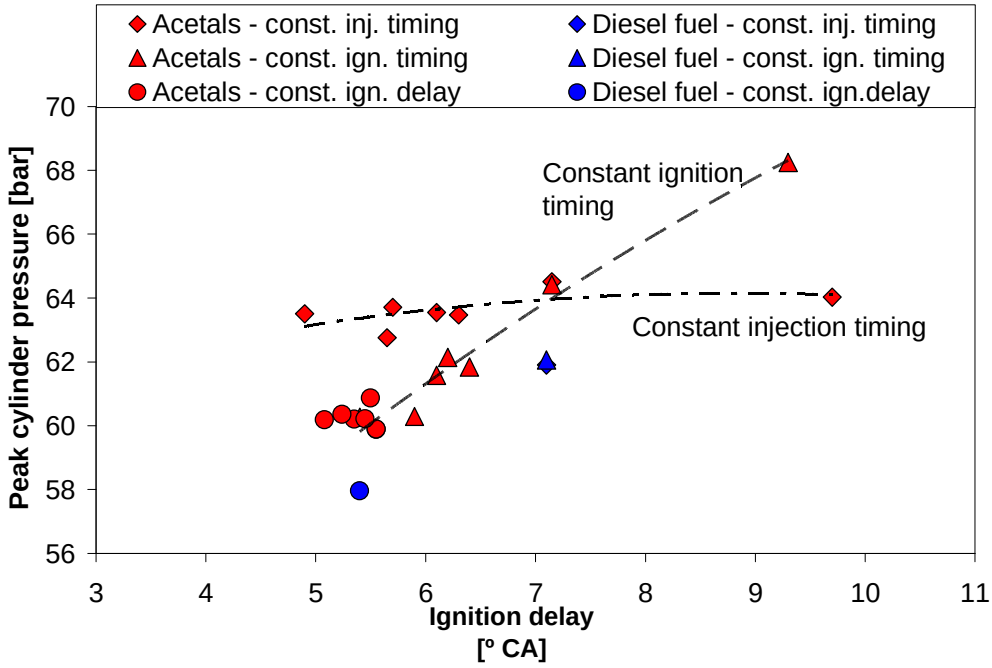

Figure 6.35 - Influence of ignition delay on peak-cylinder pressure

This is demonstrated in Figure 6.35, which shows that if the injection timing is kept constant, the peak cylinder pressure (which is correlated with temperature of the combustion) is only mildly influenced by the ignition delay, whilst for experiments conducted at constant ignition timing there exists a strong correlation between peak cylinder pressure and ignition delay. If the experiments are carried out with a constant time of ignition, fuels with a longer ignition delay and thus a higher heat release rate (see Figure 6.32) will induce higher combustion temperatures. However, if the experiments are carried out at constant injection timing, the higher peak heat release rates are almost entirely compensated by the later timing of this heat release rate, so that only marginally higher cylinder pressures (and temperatures) are achieved.

Figure 6.36 shows the correlation of peak cylinder pressure with the emission of NO_x from the engine. As previously done for Figure 6.34, the NO_x emissions from the initial study were normalised using the emission of NO_x from the fossil diesel fuel oil as standard and adjusted to the level of the second study. It can be observed that a high degree of correlation exists between peak

cylinder pressure and the emission of NO_x. This correlation appears to be independent of the type of fuel (diesel fuel oil or acetal fuel).

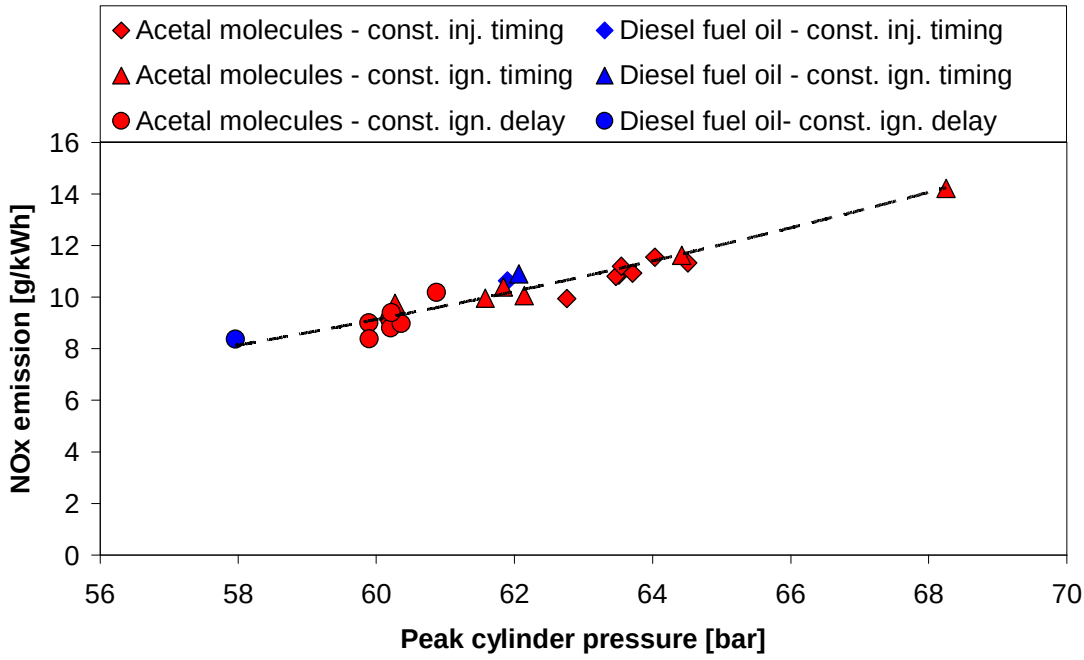

Figure 6.36 – Correlation between peak cylinder pressure and emission of NO_x in the engine exhaust gas

The correlation between peak cylinder pressure and the emission of NO_x may be explained by the relation between cylinder pressures and combustion temperatures, previously described in Equation 4.17. It is generally accepted that the principal source of NO_x in the combustion of near-stoichiometric fuel-air mixtures is the oxidation of atmospheric nitrogen via the Zeldovich mechanism (Heywood 1988, p.572), which is strongly dependent on the combustion temperature (Turns, 1996, p.144). The rate of formation of NO_x, and well as the equilibrium concentration of NO_x are both increased by higher combustion temperatures. The higher formation of NO_x at higher peak cylinder pressures in Figure 6.34 may thus be explained by the occurrence of higher combustion temperatures under these conditions.

By equalising the ignition delay, the peak cylinder pressures amongst the acetal molecules became almost constant (Figure 6.12 and Figure 6.27). This rendered the effect which the peak cylinder pressure exerted on the emission of NO_x almost constant. Under these conditions, the adiabatic flame temperature of the molecules appears to show some correlation with the formation of NO_x. This is illustrated in Figure 6.37 which shows a plot of the engine exhaust gas NO_x emissions versus the adiabatic flame temperature for a stoichiometric mixture of the respective fuel molecule with air.

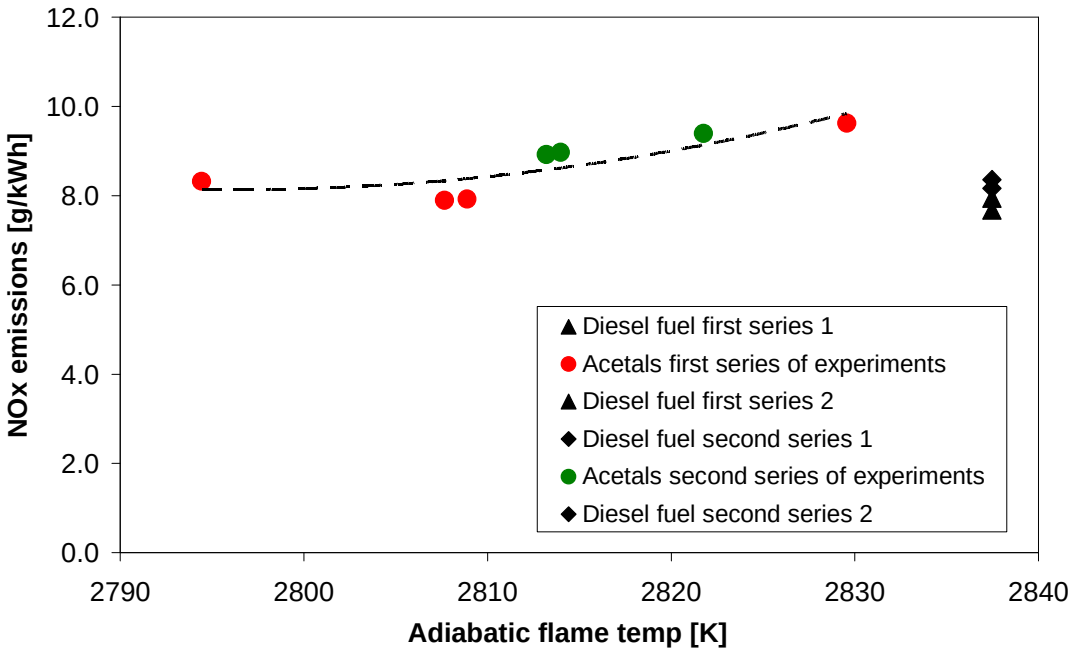

Figure 6.37 - NO_x emission and adiabatic flame temperature for acetal molecules and fossil diesel fuel at constant ignition delay conditions

The peak cylinder pressures of the fossil diesel fuel oil at this condition were slightly lower than those of the acetal molecules, as a result of a slower heat-release from the diesel fuel. So, although fossil diesel fuel has a higher adiabatic flame temperature than any of the acetal molecules, the emission of NO_x from its combustion was visibly lower. Figure 6.12 and Figure 6.27 had previously shown that the combustion process of diesel fuel was visibly slower than that of the acetal molecules, which was reflected in its lower heat release rates and lower peak cylinder pressures.

A further reason could be that the fossil diesel fuel produced significantly higher amounts of soot in its flames than the oxygenated acetal fuels. The presence of soot in the flames has been shown to be able to reduce flame temperatures through radiative heat transfer from the soot particles. Lower flame temperatures caused by soot-radiative heat transfer have been shown to reduce the formation of NO_x (Musculus, 2004; Cheng et al., 2006 and Mueller, et al., 2009). Although this theory cannot be proven to apply to these experiments, because no direct soot measurements of the flames were carried out, the soot measurements of the exhaust gas provided some support to this hypothesis, under the assumption that a correlation exists between the soot loading of the flames and the particulate concentration in the exhaust gas. The total particulate mass emission from the acetal molecules and the fossil diesel fuel for all experiments are shown in Figure 6.38.

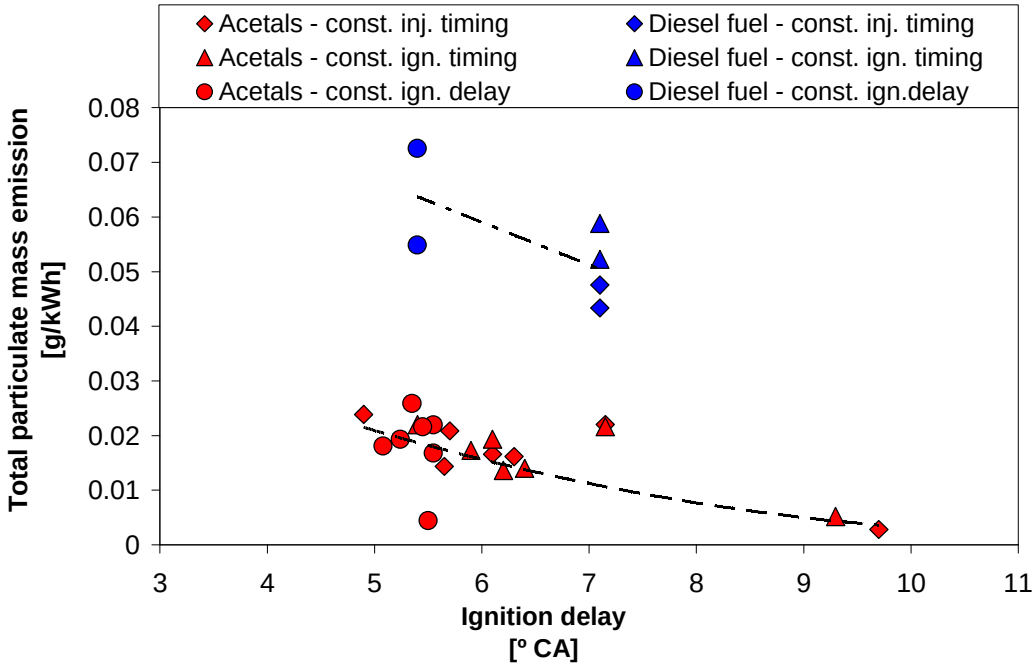

Figure 6.38 - Total particulate mass emissions of acetal molecules and fossil diesel fuel

Figure 6.38 shows that a large difference existed the in levels of total particulate mass emissions between the acetal fuels and the diesel fuel. This observation suggests that the fuel-bound oxygen carried by the acetal molecules, was very effective in lowering the emission of particulate mass from the engine. Figure 6.38 also shows that a good correlation existed between the ignition delay of the fuels, and the emission of total particulate mass from the engine. As the ignition delay increased, more time was available for mixing of the fuel with the surrounding air, before ignition occurred. The improved mixing is thought to have introduced air-bound oxygen into the fuel-rich regions of the fuel spray, and to have reduced the emission of soot through increased soot-oxidation.

The analysis of the combustion experiments has shown that in order to minimise the emission of NO_x from diesel-type combustion of acetal molecules, the ignition delay as well as the adiabatic flame temperature should be minimised. Within the ranges of adiabatic flame temperature and ignition delay tested, the experiments showed that minimising the ignition delay was of greater importance than minimising the adiabatic flame temperature to obtain low levels of NO_x. Figure 6.39 shows a map of the ignition delay and adiabatic flame temperature of the acetal molecules which provides some guidance as to which type of molecules would be most suitable for minimising the formation of NO_x during their combustion in diesel engines. In order to minimise the emission of NO_x molecules should be positioned as far as possible towards the origin of Figure 6.39 in order to reduce ignition delay and adiabatic flame temperature.

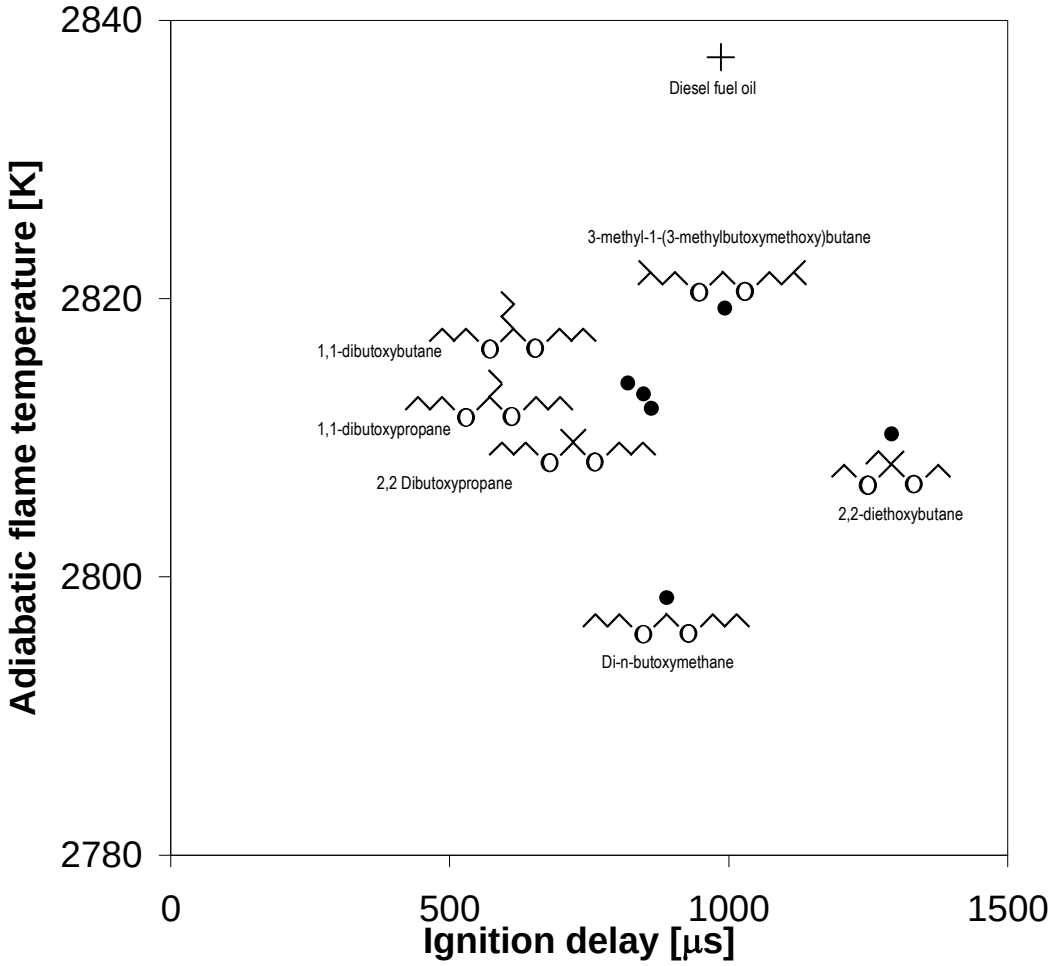

Figure 6.39 - Map of ignition delay and adiabatic flame temperature of the acetals

6.5. Summary

The combustion behaviour of several acetal molecules was studied in two consecutive series of engine experiments. The following summarising statements can be made:

1. Acetal molecules could potentially be produced from lignocellulosic biomass. Based on their combustion characteristics acetals could be used as a replacement of fossil diesel fuel oil in diesel engines. Potential technical problems regarding compatibility of acetals with materials used in the fuel system or potential problems caused by low fuel lubricity may require further investigation.
2. The combustion process of acetal molecules was more rapid than that of fossil diesel fuel under conditions of equal ignition delay, which may be due to their higher volatility resulting in faster fuel-air mixing.

3. Acetal molecules generally tend to produce significantly lower amounts of particulate matter than conventional diesel fuel.
4. Acetals produced higher amounts of NO_x than conventional diesel fuel under conditions of constant ignition delay, which is likely to have been a result of their faster combustion process and higher heat release rates. It is also possible that lower soot radiative heat transfer may have played a part in the high NO_x emissions from acetals under these conditions.
5. The ignition quality of acetal molecules depended strongly on the molecular structure. Acetal molecules can have higher or lower ignition quality than fossil diesel fuel. The lateral moieties of the acetal molecules appeared to have the strongest effect on ignition quality. Increasing the length of the lateral moieties of the acetal molecules strongly increased ignition quality. Branching the lateral moieties of the acetal molecules strongly decreased ignition quality. The addition of a central moiety to the acetal molecules increased ignition quality. Changing the central moiety of the acetal molecules from a branched configuration to a straight configuration increased ignition quality. Increasing the length of the central moiety of the acetal molecules increased ignition quality.
6. The adiabatic flame temperature of acetal molecules tended to be lower than that of fossil diesel fuel. Branching the lateral moieties of the acetal molecules strongly increased adiabatic flame temperature. The addition of a central moiety to the acetal molecules strongly increased adiabatic flame temperature. Changing the central moiety of the acetal molecules from a branched configuration to a straight configuration slightly decreased adiabatic flame temperature. Increasing the length of the central moiety of the acetal molecules slightly increased adiabatic flame temperature.

Chapter 7. The combustion of synthetic ethers and alcohols produced via catalytic reaction from synthesis gas

This chapter describes experiments on the combustion of various synthetic fuels, which could be produced via the gasification of biomass. The focus lies primarily on the use of oxygenated substances, based on the discussion of production methods provided in Chapter 2 (section 2.4). The fuels comprise ethers, alcohols, glymes, and two hydrocarbons, namely an alkane and an alkene. The experiments were carried out in the laboratory engine described in Chapter 3 and were conducted in three experimental studies: The first study (section 7.1) is aimed at characterising the combustion characteristics of liquid ethers and alcohols of high molecular mass. The fuels tested in this initial study consisted of four oxygenated molecules with the common chemical sum formula $C_{10}H_{22}O$, but with distinct molecular structures, which separates them into two liquid ethers and two liquid alcohols of high molecular mass. The second experimental study (section 7.2) is concerned with the diesel combustion process of dimethyl ether (DME) and its differences in terms of heat release and emissions with respect to fossil diesel fuel. The third experimental study (section 7.3) is a brief comparison of several ethers and glymes of varying molecular weights.

7.1. The combustion of $C_{10}H_{22}O$ alcohol and ether molecules in a diesel engine

The fuel molecules utilised in the first experimental study had the same number of carbon, hydrogen and oxygen atoms, but different molecular structure. They consisted of two ethers and two alcohols of the molecular sum formula $C_{10}H_{22}O$ with the molecular structures shown in Figure 7.10.

The molecules were chosen to represent chemical substances of two functional groups; ethers and alcohols. For each functional group, two isomer molecules were used, to highlight effects other than from the functional group. The ethers comprised a symmetrical normal-ether and a branched isomer of this ether. The alcohols comprised a primary alcohol which bore its hydroxyl group on the first carbon atom, and a secondary alcohol whose hydroxyl group was attached to the second carbon atom. Table 7.1 shows the densities, boiling points and cetane numbers of the four compounds.

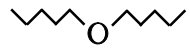

Di-n-pentyl ether
(Normal ether)

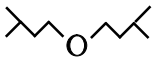

Di-iso-pentyl ether
(Isomer ether)

1-Decanol
(Primary alcohol)

2-Decanol
(Secondary alcohol)

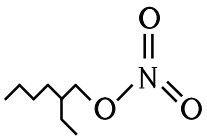

2-Ethylhexyl nitrate

Figure 7.1 – Molecular structure of the $C_{10}H_{22}O$ ethers and alcohols

Four main sets of experiments were carried-out. The first three sets of experiments were carried out at an engine speed of 1200 rpm and an IMEP of 0.1 MPa, whilst the final set of experiments was carried out at 2000 rpm engine speed and 0.4 MPa IMEP. The first set of experiments used a single fuel injection with a constant injection timing, whilst in the second set of experiments the injection timing was adjusted to obtain a constant start of ignition for all fuels. A third set of experiments was carried out, in which the ignition improving additive 2-EHN was added to the fuels, to obtain a constant ignition delay. The three initial sets of experiments employed a single fuel injection. The fourth set of experiments used a more realistic running condition, at higher engine load and speed. This running condition featured, in addition to the main injection, a pilot injection. During all experiments, the engine IMEP was adjusted to a constant value between all fuels. In addition to the four oxygenated fuels, the engine was run on conventional diesel fuel according to EN590 standard (European Committee for Standardization, 2004) withinin each set of experiments, to provide a basis for comparison. Two repeat tests were carried out with fossil diesel fuel, one at the start of each experimental set and the other at the end of the experimental set, so as to detect any drift in the engine running conditions and instrumentation during the experiments.

Table 7.1 - Properties of the fuel samples

Fuel name	Density [g/ml]	Boiling point [°C]	Cetane number (IQT - from 5% blend) [ ]
1-Decanol	0.829	231	50
2-Decanol	0.827	211	41
Di-n-pentyl ether	0.785	187	162
Di-iso pentyl ether	0.778	173	112
Fossil diesel fuel	0.833	167-359	51

7.1.1. Constant injection timing

In the first set of experiments, the injection timing (single injection) was fixed at 7 º crank angle (CA) before top-dead-centre (BTDC). This injection timing provided ignition at TDC when the engine was operating on conventional diesel fuel. The injection duration was adjusted for each fuel, in order to obtain the same IMEP for all fuels. The running parameters are summarised Table 7.2.

Table 7.2 - Experimental conditions at constant injection timing

IMEP	1.0	bar
Engine speed:	1200	rpm
Injection pressure:	450	bar
Single injection timing:	7	º CA BTDC
Coolant temperature:	84 ±1	°C
Inlet air temperature:	30 ±1	°C

The cylinder pressure data for the experiments are shown in Figure 7.2. It can be seen in Figure 7.2 that significant variations in ignition delay existed between the four oxygenated molecules, which caused the start of combustion to be shifted between the fuels. The normal ether showed by far the shortest ignition delay, followed by the isomer ether, the EN590 diesel fuel, the primary alcohol and the secondary alcohol in this order. The heat release rate of those fuels that had an earlier start of ignition was moderated to some extent by the shorter mixing process of the fuel with the air. This can be seen in the heat release analysis presented in Figure 7.3, which shows that the normal ether exhibited the earliest start of ignition, along with the longest combustion duration and the lowest heat release rates. The secondary alcohol displayed the latest start of combustion, along with the shortest combustion duration and the highest peak heat release rate. Those fuels with a later start of combustion burned with higher peak heat release rates due to a higher degree of mixing having taken place before the start of ignition, so that more fuel had formed a combustible mixture at the time when ignition occurred. Figure 7.4 illustrates that a good correlation existed between the ignition delay and the peak heat release rate of each fuel.

Combustion of $C_{10}H_{22}O$ alcohols and ethers at constant injection timing

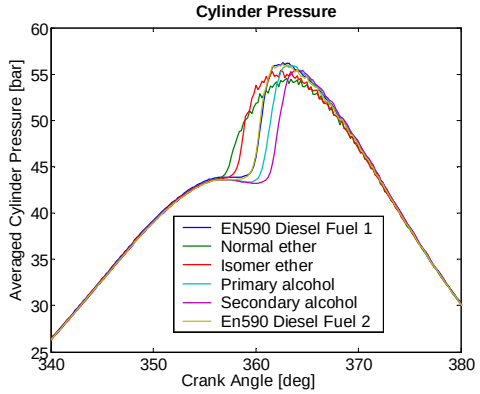

Figure 7.2 - Cylinder pressure for constant injection timing experiments at 1200 rpm and 1 bar IMEP

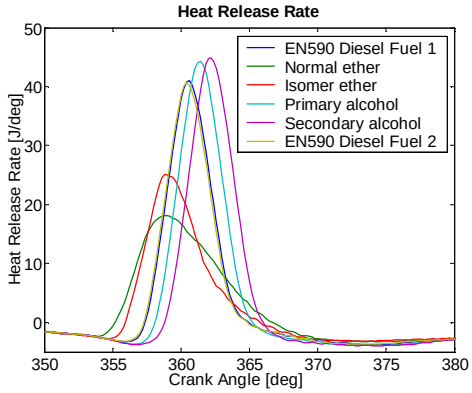

Figure 7.3 - Apparent heat release rate for constant injection timing experiments at 1200 rpm and 1 bar IMEP

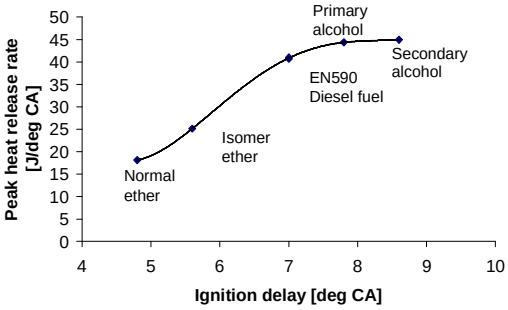

Figure 7.4 - Effect of ignition delay on peak heat-release rate of the fuel for constant injection timing experiments at 1200 rpm and 1 bar IMEP

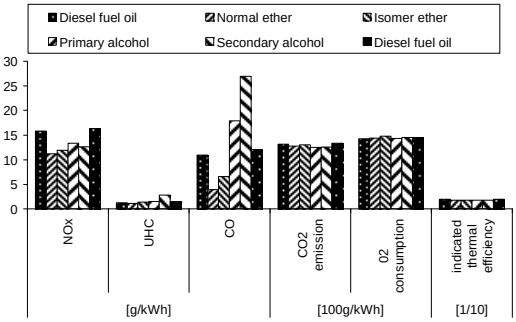

Figure 7.5 - Exhaust gas emissions for constant injection timing experiments at 1200 rpm and 1 bar IMEP

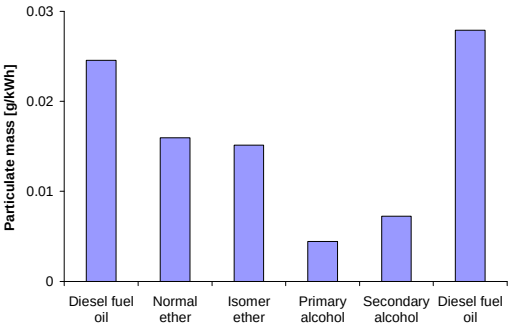

Figure 7.6 - Total particulate emissions for constant injection timing experiments at 1200 rpm and 1 bar IMEP

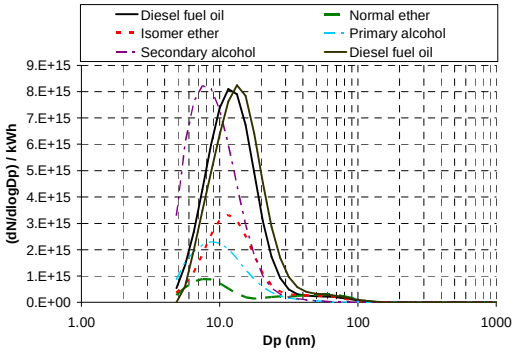

Figure 7.7 - Size spectral density of particulate emissions between 5nm and 1000nm for constant injection timing experiments at 1200 rpm and 1 bar IMEP

Figure 7.5 shows the gaseous pollutant emission, oxygen consumption and thermal efficiency of the engine for each of the fuels. The NO_x emission levels (Figure 7.5) for the four sample fuels seem to reflect the differences in ignition delay between the four fuels to some extent, with the two alcohols showing higher NO_x levels than the two ethers. The NO_x emission levels of all of the oxygenated fuels were lower than those of fossil diesel fuel, despite their ignition delays being both longer and shorter than fossil diesel fuel. This could be an indication of the lower adiabatic flame temperatures of the oxygenated fuels.

It is not entirely clear though why the secondary alcohol produced lower NO_x emission than the primary alcohol, despite having a longer ignition delay. A possible explanation could be hypothesised as follows: In this series of experiments, most of the fuel was burned in premixed combustion mode, as a result of the very low engine load applied (1 bar IMEP). This can be verified by the shape of the heat release curves in Figure 7.3 which are typical of a premixed combustion event, and can be deduced from the fuel injection timing data, which revealed that fuel injection had ceased before ignition had occurred. Figure 7.4 shows that for the fuels exhibiting an ignition delay shorter than 8° CA, a longer ignition delay was positively correlated with a higher peak heat release rate, suggesting that the premixed combustion under these conditions takes place under fuel-rich conditions, and required more fuel-air mixing for an increase in the peak heat release rate. This trend flattened out progressively, and almost ceased to have an effect beyond 8° CA. Thus, only a minor increase in peak heat release rate was recorded between the primary alcohol and the secondary alcohol. This could suggest that for the primary alcohol, sufficient pre-mixing of all the fuel had already been achieved, and that any further mixing beyond this point resulted in a large proportion of the premixed combustion taking place under fuel-lean conditions. It can be seen from the emissions of unburned hydrocarbons (UHC) in Figure 7.5 that the emission of UHC increases drastically for the secondary alcohol, which has an ignition delay in excess of 8° CA. The increase in UHC emissions is indicative of the formation of overly lean fuel-air mixtures before ignition occurred (see discussion in section 2.5.3 of Chapter 2). This could lead to the hypothesis that the combustion of the secondary alcohol had taken place to a large extent under fuel lean conditions (considerable stratification of the fuel air mixture would be expected within the premixed combustion phase (Musculus, 2004)). These fuel-lean conditions would result in a decrease of the adiabatic flame temperature due to an excess of air, and could result in lower levels of NO_x formation due to a reduction in gas temperatures. The CO emission levels showing similar trends to those for UHC for the four sample fuels, which would suggests that over dilution at the spray fringe resulted both in ignition failure as well as partial-burn of some of the injected fuel.

The emission of particulate matter is shown in Figure 7.6 in terms of mass emitted and in Figure 7.7 in terms of its size spectral density. Figure 7.6 shows that the two ethers produced significantly more total particulate mass than the two alcohols did. This may be attributed to some extent to a higher amount of fuel-air mixing habving taken place for the combustion of the alcohols prior to ignition having taken place, due to their longer ignition delay. The particulate size distribution shown in

Figure 7.7 indicates that a significantly lower amount of accumulation mode particulates was produced by the two alcohols than by the two ethers. This can be explained by a greater amount of fuel-air pre-mixing prior to ignition. Amongst the ethers, the normal ether produced a higher amount of particulate mass than the isomer ether (Figure 7.6), due to a higher number density of accumulation mode particulates (Figure 7.7). The lower emission of accumulation mode particulates (40-200 nm) from the combustion of the isomer ether than from the combustion of the normal ether may be attributed to better fuel-air mixing for the isomer ether as a result of its longer ignition delay.

A different trend is observable amongst the two alcohols, where the secondary alcohol produced a higher amount of particulate matter, despite exhibiting a longer ignition delay than the primary alcohol. The particulate size distribution shown in Figure 7.7 shows that in this case, the higher particulate mass emission may not be attributed to an increase in the accumulation mode number density of particulates, but rather due to an increase in the number density of nucleation mode particles. The work of Kittelson (1998) has shown that the nucleation mode particles consist predominantly of unburned hydrocarbons, and not of carbonaceous soot. Their formation can not be explained by the same mechanisms as that of carbonaceous soot. It is believed that these particles form predominantly during cooling of the exhaust gases through condensation of unburned fuel (Kittelson 1998). The higher emission of particulate mass from the secondary alcohol thus stems predominantly from the emission of droplets of unburned hydrocarbons with the exhaust gases. These are formed due to the high concentration of unburned hydrocarbons in the exhaust gas (see Figure 7.5), and arise from over-dilution of the fuel spray during the long ignition delay period.

As mentioned previously, maintaining the injection timing constant for all four sample fuels caused the ignition timing to be different for the four fuels. This led to the heat release of combustion to be offset from one another, and the combustion to take place in different combustion chamber volumes.

7.1.2. Constant ignition timing

A simple way of offsetting the different ignition delays for the four sample fuels is to ensure that the point of ignition for all fuels is the same. This was done in a second set of experiments in which the time of ignition for all fuel samples was maintained within a window of 0.5° CA with respect to that of the diesel fuel.

Table 7.3 - Experimental conditions at constant ignition timing

IMEP	1.0	bar
Engine speed:	1200	rpm
Injection pressure:	450	bar
Fixed ignition timing:	1.8	º CA BTDC
Coolant temperature:	84 ±1	°C
Inlet air temperature:	30 ±1	°C

In order to clarify the effect which the oxygen atoms have upon the combustion process, two additional molecules which did not contain any oxygen were tested alongside the ethers and alcohols. These were a normal-alkane and a primary alkene with the same number of carbon atoms as the ethers and alcohols. The running parameters for these experiments are summarised in Table 7.3.

The pressure traces in Figure 7.8 show that whilst the time of ignition was now equalised for all fuels, the individual fuels burned with varying peak cylinder pressures whilst yielding the same IMEP value of 1 bar. This was because the heat release rates varied significantly amongst the fuels, as shown in Figure 7.9. Figure 7.10 shows that the reason for the different peak heat release rates was primarily attributable to differences in the ignition delay. Those fuels with shorter ignition delays had less time for fuel-air mixing prior to ignition, resulting in a moderation of the peak heat release rates. The fuels with a shorter ignition delay and lower heat release rate burned for a longer duration than those with a higher heat release rates in order to produce the same IMEP. The cylinder pressure traces for the slower burning fuels showed slightly higher pressures than the fast burning fuels towards the end of their combustion, which was where the lost IMEP due to a slower burn rate around TDC was recovered, so that the overall IMEP produced remained the same for all fuels.

Combustion of $C_{10}H_{22}O$ alcohols and ethers at constant ignition timing

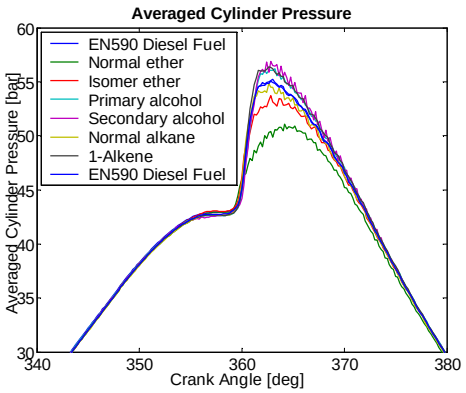

Figure 7.8 - Cylinder pressure for constant ignition timing experiments at 1200 rpm and 1 bar IMEP

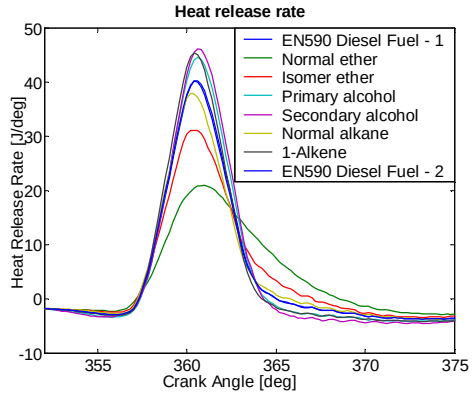

Figure 7.9 - Apparent heat release rate for constant ignition timing experiments at 1200 rpm and 1 bar IMEP

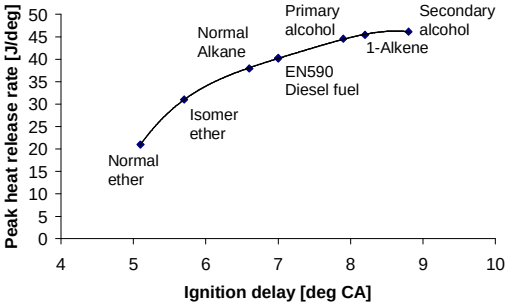

Figure 7.10 - Peak heat release rate versus ignition delay rate for constant ignition timing experiments at 1200 rpm and 1 bar IMEP

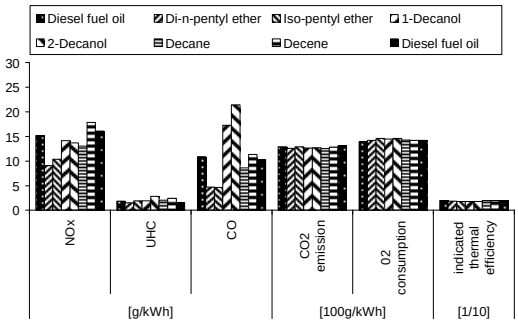

Figure 7.11 - Exhaust gas emissions for constant ignition timing experiments at 1200 rpm and 1 bar IMEP

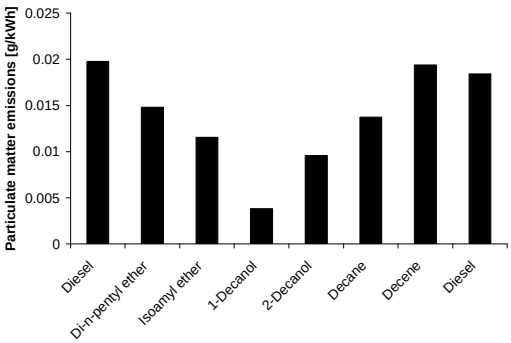

Figure 7.12 - Total particulate matter mass emissions for constant ignition timing for constant ignition timing experiments at 1200 rpm and 1 bar IMEP

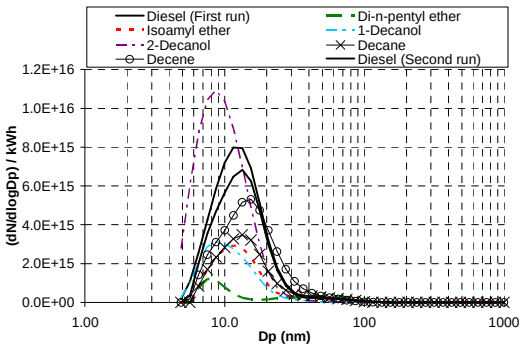

Figure 7.13 - Size spectral density of particulate emissions between 5nm and 1000nm

The exhaust gas emissions for the constant ignition timing experiments in Figure 7.11 showed similar trends to those measured for the constant-injection-timing set experiments. All oxygenated fuel molecules produced lower NO_x emissions than the reference diesel fuel. The normal-ether produced the lowest NO_x emissions of all, followed by the iso-ether, the secondary alcohol and the primary alcohol in the listed order. The reasons for this trend appear to be the same as those delineated in detail in section 7.1.1, with changes in the peak heat release rates for the two ethers and the primary alcohol, and the formation of lean mixtures for the 2-decanol being responsible for the differences in NO_x formation. The ignition delay differences still remain an important influence on the NO_x exhaust levels, but the higher NO_x emissions cannot be entirely explained by the heat release characteristics of the fuels. The primary alcohol and the secondary alcohol show very similar heat release profiles to the 1-alkene, but the measured NO_x emissions for normal-alkene are significantly higher than that of the two alcohols, which may be indicative of a lower flame temperature for the two alcohols.

The total particulate matter emissions are shown in Figure 7.12. The total particulate emissions from all single-component fuel samples were lower than those of the reference diesel fuel. The oxygenated molecules had lower particulate emissions than the non-oxygenated samples, with the exception that the normal-alkane actually had lower particulate emissions than the normal-ether. This effect is likely to have been due to the extremely short ignition delay of the normal-ether, which gave it little time to mix with air before ignition occurred. Overall, the particulate matter emissions showed similar trends to those observed for the constant-injection-timing set of experiments.

The size-spectral density of the particulates is shown in Figure 7.13. The two alcohols, which exhibited the lowest particulate mass emissions, had a high number of very fine particulates around 10-40 nm in size (nucleation mode) but only very small amounts of larger particulates in the size range of 40-100nm (accumulation mode). As discussed in section 7.1.1, this trend may be explained by the longer ignition delay experienced by the alcohol fuels, which resulted in a greater amount of fuel-air mixing prior to ignition, thus forming less accumulation mode particles (consisting predominantly of carbonaceous soot). The longer ignition delay also resulted in larger amounts of gaseous UHC emissions and thus also in a higher size spectral density of nucleation mode particles (which are likely to consist of condensed hydrocarbon droplets).

7.1.3. Constant ignition delay

The first set of experiments examined how the individual molecules behaved when injected at a fixed point during the cycle, thus keeping pressure, temperature and cylinder volume constant at the time of injection. The second experiment examined how the fuels behaved if the injection was adjusted, so that ignition of the fuels would occur at the same point during the cycle, thus keeping pressure, temperature and cylinder volume similar at the time when ignition occurred. Both experiments comprised different ignition delays for the individual fuels, to which a large proportion in the combustion differences could be attributed. The ignition delay affected the heat release characteristics and combustion stoichiometry of the fuels, which were responsible for most of the differences in exhaust gas and particulate emissions. In order to quantify the effect which the ignition delay has on the combustion process, and to reveal differences between the fuels once this had been removed, a third set of experiments was carried out. The ignition promoting additive 2-EHN was added in varying concentrations to the fuels, to keep the ignition delay constant for all fuels. The normal ether had the shortest ignition delay in the previous experiments, and was not additised. The other fuels were additised to match the ignition delay of the normal ether. Due to the extremely high cetane number of the normal ether, a substantial amount of 2-EHN had to be added to the other fuels. The treatment rates are given in Table 7.4 below.

Table 7.4 - Treatment rates of fuels with 2-EHN

Normal ether	0.0	[vol. %]
Isomer ether	2.9	[vol. %]
Primary alcohol	11.1	[vol. %]
Secondary alcohol	14.1	[vol. %]
EN 590 diesel fuel	9.1	[vol. %]

Unfortunately, the addition of substantial amounts of 2-EHN ($C_8H_{17}N0_3$) significantly changed the percentage of oxygen content of the fuels which had the molecular formula $C_{10}H_{22}O$ and the diesel fuel. It also introduced nitrogen into the fuel samples. This was an obvious drawback of the experimental technique used and its effects will be addressed in detail in the discussion of the results. The engine running conditions were similar to the tests carried out at constant injection timing and constant ignition timing, and where carried out at 1 bar IMEP and 1200 rpm. An overview of the conditions is given in Table 7.5.

Table 7.5 - Experimental conditions at constant ignition delay

IMEP	1.0	bar
Engine speed:	1200	rpm
Injection pressure:	450	bar
Fixed injection timing:	5.1	º CA BTDC
Fixed ignition timing:	2.2	º CA BTDC
Coolant temperature:	85 ±1	°C
Inlet air temperature:	27 ±1	°C

Examination of the pressure traces (Figure 7.14) reveals that by matching the ignition delay closely within a small window of crank angle, the pressure history of the combustion process became very similar for the various fuel blends. This was because matching the ignition delay (Figure 7.16) caused the heat release rates of the fuels to become almost identical (Figure 7.15). As observed in the previous experiments in sections 7.1.1 and 7.1.2, the exhaust gas analysis (Figure 7.17) shows that ethers and alcohols produced lower NO_x emissions than fossil diesel fuel. Figure 7.17 shows that ethers produced less NO_x emissions than alcohols even under conditions of constant ignition delay. It is thought that this is to some extent attributable to the lower adiabatic flame temperature of the ethers with respect to the alcohol fuels.

Combustion of $C_{10}H_{22}O$ alcohols and ethers at constant ignition delay

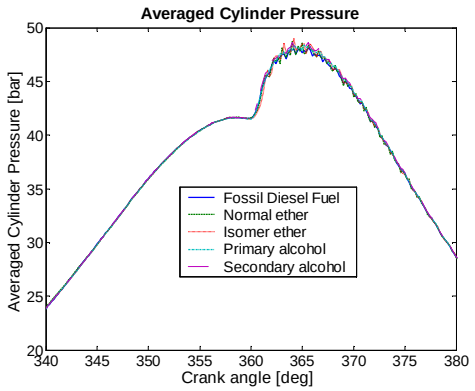

Figure 7.14 - Cylinder pressure for constant ignition delay experiments at 1200 rpm and 1 bar IMEP

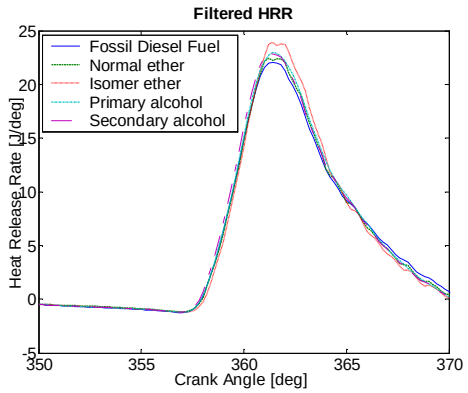

Figure 7.15 - Apparent heat release rate for constant ignition delay experiments at 1200 rpm and 1 bar IMEP

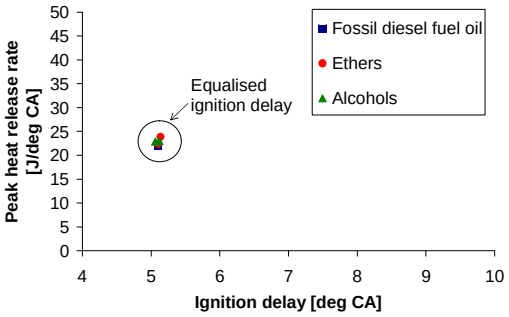

Figure 7.16 - Peak heat release rate versus ignition delay rate for constant ignition delay experiments at 1200 rpm and 1 bar IMEP

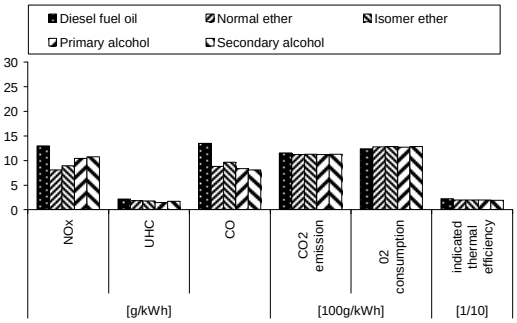

Figure 7.17 - Exhaust gas emissions for constant ignition delay experiments at 1200 rpm and 1 bar IMEP

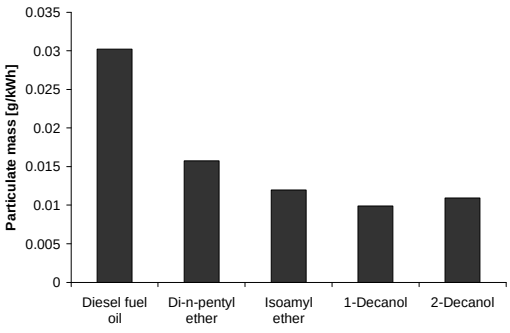

Figure 7.18 - Total particulate matter mass emissions for constant ignition delay for constant ignition timing experiments at 1200 rpm and 1 bar IMEP

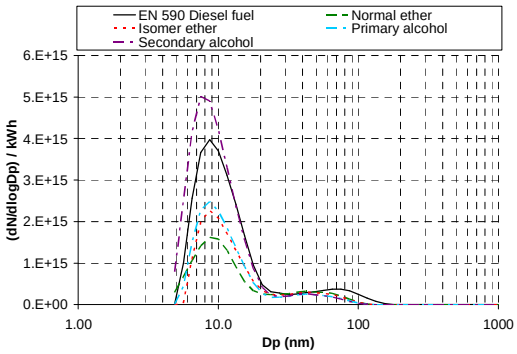

Figure 7.19 - Size spectral density of particulate emissions between 5nm and 1000nm

Figure 7.18 shows the total submicron particulate mass emissions at constant ignition delay. The previous experiments had already shown that all oxygenated fuels produced less sub-micron particulate mass than fossil diesel fuel, irrespective of whether their ignition delays were longer or shorter than that of diesel fuel. This is confirmed in Figure 7.18, which shows that the oxygenated fuels produced lesser amounts of total particulate mass than diesel fuel, when their ignition delay was equal. The earlier sets of experiments had also shown, that alcohols produced lower particulate mass emissions than ethers of the same molecular sum formula $C_{10}H_{22}O$ at their natural ignition delays. Figure 7.18 shows that the ethers still produced higher particulate mass emissions than the alcohols, but that the differences became smaller once the ignition delay was held constant. As in the previous experiments, the primary alcohol showed lower particulate mass emissions than the secondary alcohol, despite the fact that in the current set of experiments its oxygen content was higher due to the addition of larger amounts of 2-EHN. This suggests that the primary alcohol had a lower tendency of forming sub-micron particulate emissions than the secondary alcohol. Amongst the two ether molecules it can be seen that the normal ether produced higher particulate matter emissions than the branched isomer ether. This result may be attributable to the higher oxygen content of the branched isomer ether in this set of experiments, which was a result of its higher treatment rates with 2-EHN. In order to visualise the effect of the oxygen content, the total sub-micron particulate emissions were plotted against oxygen content in Figure 7.20.

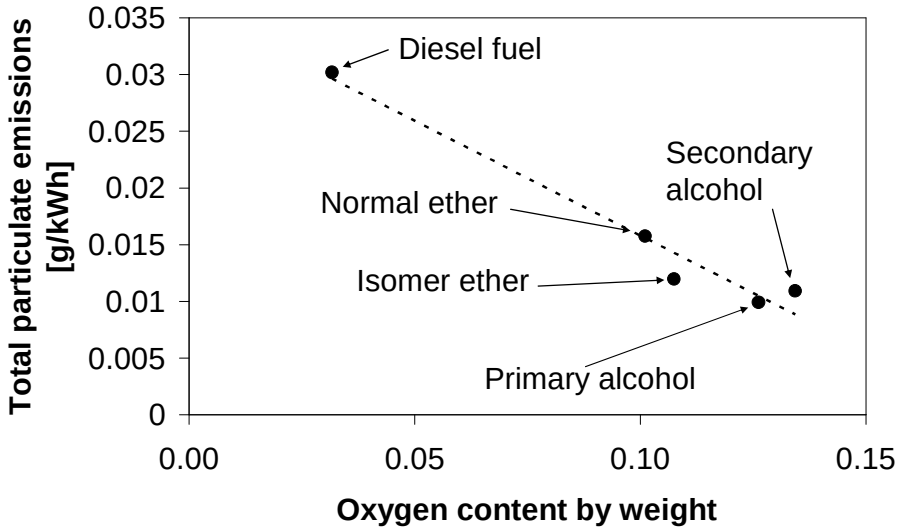

Figure 7.20 – Total particulate emissions between 5nm and 1000nm versus oxygen content of fuels additised with 2-EHN under constant ignition delay conditions

Figure 7.20 shows a linear least-squares line fitted to the particulate matter emissions of the four synthetic fuel molecules and the fossil diesel fuel. A linear effect of fuel oxygen content was assumed in order to visualise the trend of oxygen content. It should be noted that the present study is very limited in terms of available data points, and the linear correlation is merely indicative of a trend. It should further be noted that treatment of the fuels with 2-EHN not only introduces oxygen into the fuel sample, but that the 2-EHN may also exert a chemical effect. No attempt shall be made to fully explain such a potential chemical effect on the basis of the limited experimental data

available in this study. It appears though, that some of the reduction in particulate emission between the individual fuels may be attributed to changes in the oxygen content of the fuel sample, due to the addition of varying amounts of 2-EHN. For example the primary alcohol produced significantly less particulate mass emissions than the normal ether molecule, but this reduction appears to correlate with an increase in oxygen content due to the higher amount of 2-EHN present in the alcohol.

The particulate size distribution at constant ignition delay is shown in Figure 7.19. Diesel fuel formed by far the largest number of accumulation mode particulates. Amongst the oxygenated molecules, the normal ether had the highest number of accumulation mode particulates, followed by the isomer ether, the secondary alcohol and the primary alcohol. This trend reflects the trend observed in total particulate mass emissions previously shown in Figure 7.18. The differences in emission of nucleation mode particles amongst the fuels became smaller in comparison to the experiments in sections 7.1.1 and 7.1.2, with removal of the effect of ignition delay. Minor differences amongst the fuels still remained, indicating that the alcohols generally had a higher propensity of form nucleation mode particles, which may be an effect of their higher boiling points.

7.1.4. Experiments with pilot injection at higher load

A fourth set of experiments was carried out at a higher load and higher engine speed using a pilot injection. The injection timing of the pilot and the main injections was held constant in these experiments, while their durations were adjusted to yield the same IMEP for all fuel types.

Table 7.6 - Engine operating conditions

IMEP	4.0	bar
Engine speed:	2000	rpm
Injection pressure:	450	bar
Pilot injection timing:	31	º CA BTDC
Pilot energy injected:	180	J
Main injection timing:	10	º CA BTDC
Coolant temperature:	84 ±1	°C
Inlet air temperature:	30 ±1	°C

The pilot injection was adjusted for every fuel sample in an attempt to keep the amount of energy injected during the pilot injection constant. This was done as follows: The main injection was switched-off, and the pilot injection was moved to the timing of the main injection (i.e. 10 º BTDC). The pilot injection was then switched on and its duration adjusted until the total heat released during combustion reached the pre-determined value of 180 Joules. The timing of the pilot injection was then returned to its nominal value (i.e. 31 º BTDC) and the main injection was subsequently switched on. The duration of the main injection was then adjusted to yield a total IMEP of 4 bar. This procedure was carried out for every fuel sample in the set of experiments in order to try keeping the fuel energy injected into the combustion chamber during the pilot injection near constant (it should be noted that the pilot energy measurement was carried out at 10 º BTDC to improve the sensitivity and precision with which the pilot energy release was measured due to better combustion at this injection timing).

Combustion of $C_{10}H_{22}O$ alcohols and ethers with pilot injection

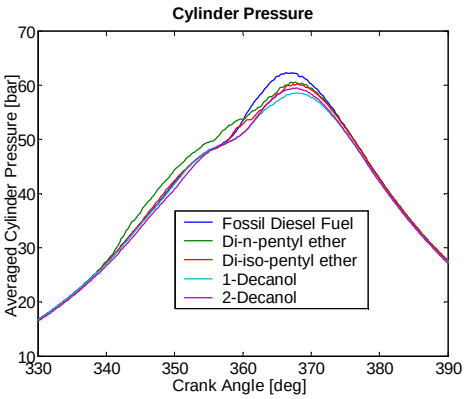

Figure 7.21 - Cylinder pressure for pilot injection experiments at 2000 rpm and 4 bar IMEP

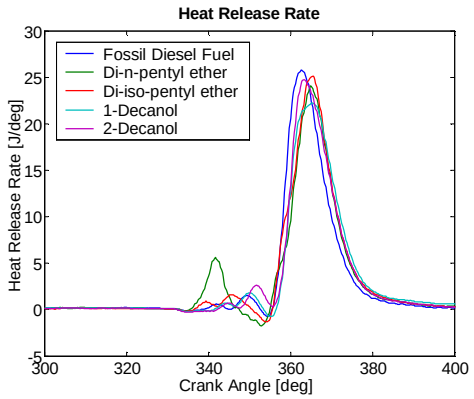

Figure 7.22 – Apparent heat release rate for pilot injection experiments at 2000 rpm and 4 bar IMEP

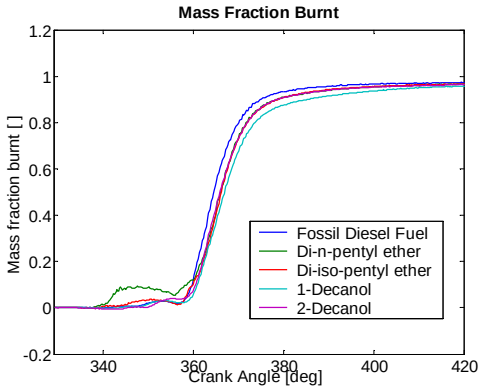

Figure 7.23 - Mass fraction burnt analysis for pilot injection experiments at 2000 rpm and 4 bar IMEP

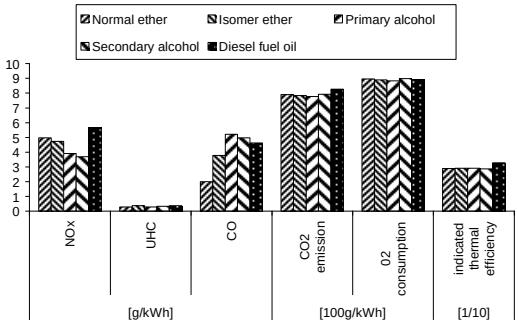

Figure 7.24 - Exhaust gas emissions for pilot injection experiments at 2000 rpm and 4 bar IMEP

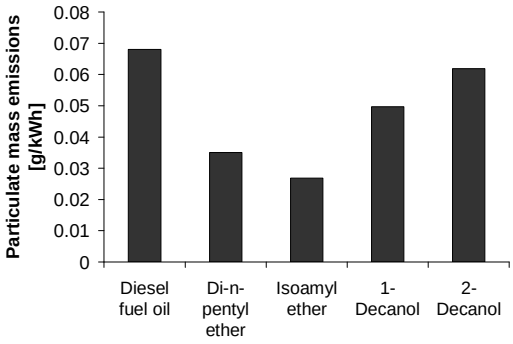

Figure 7.25 - Total particulate emissions for pilot injection experiments at 2000 rpm and 4 bar IMEP

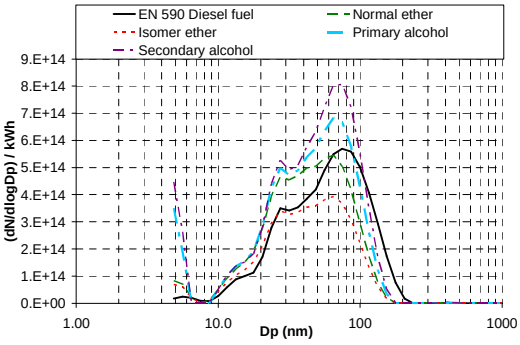

Figure 7.26 - Size-spectral Size spectral density of particulate emissions between 5nm and 1000nm analysis for pilot injection experiments at 2000 rpm and 4 bar IMEP

Figure 7.22 shows the apparent heat release rate of the combustion for the various fuels. It is visible that the introduction of a pilot injection caused the ignition timing of the main combustion phase to occur at a similar time for all fuels, and that the differences in peak heat release rates between the individual compounds were reduced. The heat release rates of the pilot fuel combustion however, still reveal clear differences in timing and magnitude. All fuels with the exception of the normal-ether showed some degree of cool-flame heat release during the pilot combustion phase. The normal-ether clearly had the earliest visible heat release, and no distinction between the cool and hot flame heat release phases during the pilot injection phase. As was the case for the single injection experiments discussed before, the oxygenated compounds had lower NO_x emissions than the reference diesel fuel. This time however, the order was exactly reversed. The secondary alcohol had the lowest NO_x emissions of the oxygenated blends, followed by the primary alcohol, the isomer ether, and the normal-ether.

In the single injection experiments, the two alcohols had lower total particulate emissions than the ethers. But when a pilot injection was used, the ethers showed lower particulate matter emissions than the two alcohols. The trend amongst themselves was still the same as for the single injection tests: The iso-ether had lower total particulate emissions than normal-ether, and the primary alcohol had lower total particulate emissions than the secondary alcohol.

The particulate size distribution (Figure 7.26) showed a coherent pattern amongst the synthetic fuel molecules and a slightly different pattern for the diesel fuel. It is visible from the figure that the majority of the particulates were of magnitudes between 10 and 200nm with a peak around 65nm for the oxygenated molecules and 75nm for the reference diesel fuel. As had previously been observed for the single injection experiments, the alcohols seemed to produce a larger amount of ultra-fine particulates in the region of 5nm diameter. The particulate spectrometer is unable to resolve particulates of smaller size than this, but it appears that the alcohols also produced a significant number of particulates below this size at this running condition.

Figure 7.25 shows that fossil diesel fuel produced higher amounts of particulate mass than any of the oxygenated fuel molecules. Amongst the oxygenated molecules the isomer ether formed the lowest amount of particulate mass, followed by the normal ether, the primary alcohol and the secondary alcohol.

7.2. The diffusion combustion of dimethyl ether in a diesel engine

The combustion of dimethyl ether (DME) was studied experimentally in a direct injection diesel engine. A background discussion about the potential advantages of dimethyl ether as a fuel can be found in section 2.9.1 of Chapter 2. Thermodynamic and stoichiometric analyses of the combustion of DME are described in this chapter, and the results compared with those obtained for fossil diesel fuel oil under the same conditions. The experiments were carried out on the instrumented single-cylinder research engine (described in section 3.2. of Chapter 3) with a specifically built fuel injection system (described in section 3.4.4 of Chapter 3). The molecular structure of DME is presented in below.

Figure 7.27 - Molecular structure of di-methyl ether

The DME was injected into the combustion chamber in its liquid phase under pressurised conditions using the electronically controlled solenoid injector and common rail system presented section 3.4.4 of Chapter 3. The experiments carried out on fossil diesel fuel were conducted using the same injector and common rail, but with the conventional injection system described in 3.4.1 of Chapter 3.

The DME was supplied by a gas supply company (BOC chemical company) and had an assay of at least 95% (BOC chemical company, 2000). DME had a vapour pressure of 510 kPa at the standard temperature of 293.15 K, and a boiling point of 248 K, meaning that DME was gaseous under standard atmospheric conditions. A lubricity improving additive was added to the DME in a concentration of 1000 ppm (apart from section 7.2.2 where this is further specified) to protect the injection system from excessive wear. The lubricity-improving additive consisted of a straight-chain alkyl ester mixture of an average molecular weight of 250 g/mol (Sugano, 2008).

All experiments were carried out at an engine speed of 1200 rpm and whilst the engine was developing an indicated load of 4 bar IMEP. The injection duration was adjusted for each condition, and thus also the amount of fuel injected into the combustion chamber, so that the engine would develop this constant load under all conditions.

Table 7.7 - Fuel properties of dimethyl ether and fossil diesel fuel oil

		Fossil diesel fuel oil	Dimethyl ether (DME)
Molecular formula		-	C_2H_6O
Cetane number	**[ ]**	54.3	65
Autoignition temperature	**[° C]**	-	235 [1]
Lower heating value	**[kJ/kg]**	43040	28430 [2]
Carbon proportion	**[% m/m]**	86.3	52.1
Hydrogen proportion	**[% m/m]**	13.7	13.1
Oxygen proportion	**[% m/m]**	-	34.7
Density	**[kg/m3]**	833.0	660.0
Viscosity	**[mPas]**	2.1658 @ 40 ºC	0.123
Sulphur content	**[ppm]**	3	-
Initial boiling point	**[° C]**	178	-24.8
Final boiling point	**[° C]**	351	-24.8
Mono-aromatics	**[% m/m]**	15.5	-
Di-aromatics	**[% m/m]**	1.5	-
Tri-aromatics	**[% m/m]**	0.3	-

[1] BOC chemical company (2000)

[2] Hu et al. (2005)

7.2.1. Effect of injection timing and injection pressure

The diesel diffusion combustion of the simplest ether, DME, was studied at various injection pressures and injection timings, and its combustion was compared with that of diesel fuel. The injection pressures used were 25 MPa and 40 MPa, whilst the injection timing was varied between 20 º crank angle (CA) before top-dead-centre (BTDC) to 4 º CA after top-dead-centre (ATDC) in incremental steps. The DME used in this series of experiments was additised with the alkyl ester lubricity additive in a concentration of 1000 ppm to protect the fuel injection system from excessive wear. All experiments were carried out at the IMEP of 400 kPa and at the same engine speed of 1200 rpm. The cylinder pressure traces for the combustion of DME and their corresponding heat release rates for injection pressures of 25 and 40 MPa and injection timings at 15º, 10º, 5º and 0º CA BTDC are shown in Figure 7.28.

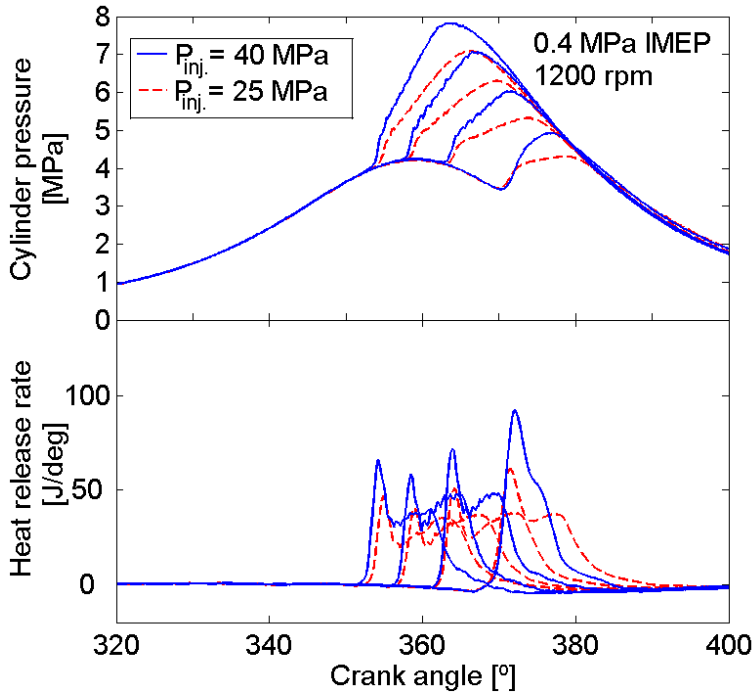

Figure 7.28 - Cylinder pressure and heat release rates for diffusion combustion of DME in a diesel engine. Injection pressures were 25 and 40 MPa, and injection timings 15º, 10º, 5º and 0º CA BTDC.

The fuel injection pressure significantly influenced the cylinder pressure traces and heat release rates of the combustion of DME, as is shown in Figure 7.28. An increase in the injection pressure from, 25 MPa to 40 MPa resulted in distinctly higher peak cylinder pressures and higher heat release rates of combustion. The higher injection pressure resulted in an increase in fuel flow-rate through the injector nozzle, shorter injection duration, and more rapid introduction of the DME into the combustion chamber. This is thought to have allowed more rapid mixing of the DME with air, leading to higher rates of combustion. It has been reported that increased fuel injection pressure results in increased spray tip penetration and thus better mixing of the fuel with air (Yu & Bae, 2003). The higher cylinder pressures were thus caused by higher cylinder gas temperatures, which in turn are a result of the higher rates of heat release from combustion of the fuel, due to its faster mixing with surrounding air. A similar trend was observed for the combustion of diesel fuel, as is shown in Figure 7.29.

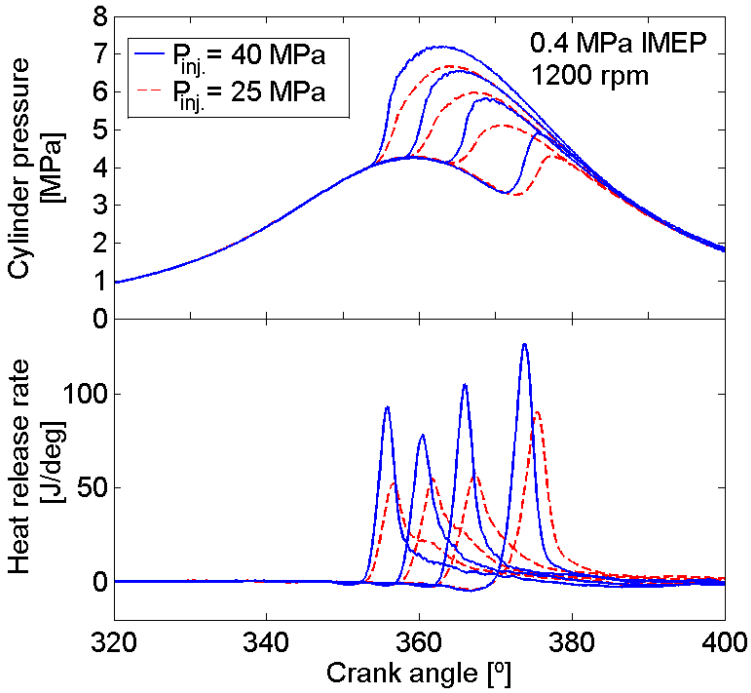

Figure 7.29 - Cylinder pressure and heat release rates for diffusion combustion of diesel fuel in a diesel engine. Injection pressures were 25 and 40 MPa, and injection timings 15º, 10º, 5º and 0º CA BTDC.

Evidence for the higher global gas temperatures was provided by the higher emission of NO_x from the engine at higher fuel injection pressures, as is shown in Figure 7.32. The effect of injection timing on the cylinder pressure and heat release rates was principally one of combustion phasing. The earlier the fuel was injected, the earlier the combustion process took place. Under the present conditions this resulted in a larger proportion of total heat release occurring in the vicinity of TDC, which represented the point of peak mechanical compression of the cylinder charge. The coincidence of mechanical compression from the piston with heat release from the combustion process thus increased the peak cylinder temperatures and pressures of the cylinder charge at earlier injection timings (Figure 7.28 and Figure 7.29). The higher gas temperatures which are thought to have occurred for earlier fuel injection timings were reflected by higher formation of NO_x from the combustion of DME or diesel fuel under these conditions, as is visible in Figure 7.32. A direct comparison of the cylinder pressure traces for the combustion of DME and diesel fuel for injection pressures of 25 and 40 MPa and injection timings at 15º, 10º, 5º and 0º CA BTDC is presented in Figure 7.30.

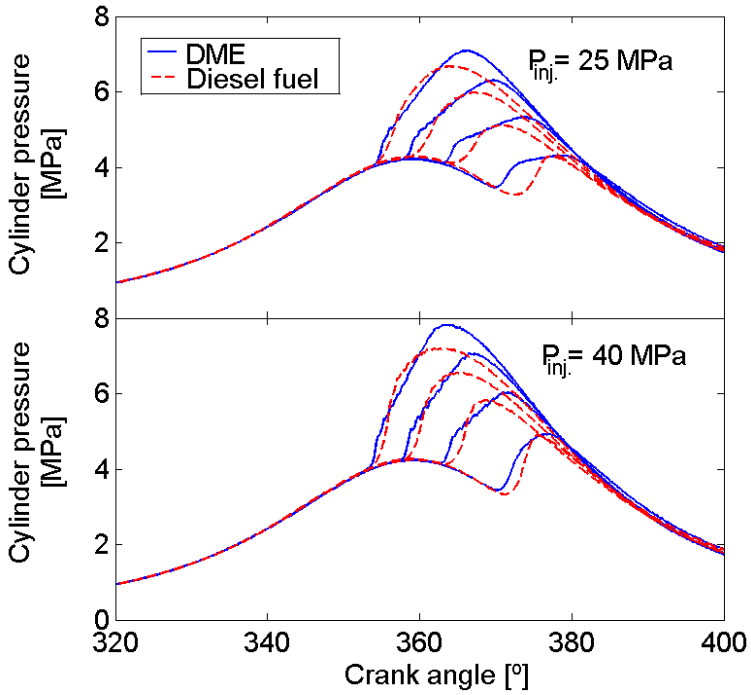

Figure 7.30 - Comparison between cylinder pressure traces for the diffusion combustion of DME and diesel fuel. Injection pressures were 25 and 40 MPa, and injection timings 15º, 10 º, 5 º and 0 CA BTDC.

The direct comparison shows that the combustion of DME resulted in higher peak cylinder pressures than diesel fuel under comparable conditions. The peak temperatures occurred towards the end of the combustion process. The reasons for this observation are not entirely clear, but a tentative explanation for this phenomenon may be hypothesised as follows. For the engine to develop the same indicated load under operation on both fuels, the injection of DME needed to be 50 % longer than the injection of diesel fuel, due to the lower calorific value of DME on a volumetric basis. The injection duration was verified using the electrical pulse length applied to the solenoid of the injector. Consequently, at the time at which the injection of diesel fuel ceased, the injection of DME was yet to proceed for a further third of its total duration. At this point in time, the heat release of neither of the fuels was yet complete, but their further heat release proceeded at different rates. Whilst the combustion of diesel fuel proceeded to the burnout stage of the diffusion flame as a result of the cessation of fuel injection, the combustion of DME was still proceeding at a steady rate, due to the sustained injection of fuel into the combustion chamber. This caused the heat release of DME to proceed at a higher rate than the combustion of diesel fuel during the final stages of the combustion process, resulting in higher peak cylinder pressures for the combustion of DME. Diesel fuel exhibited a significantly higher total heat release after the end of injection than DME, and its heat release continued for a significantly longer duration than any detectable heat release from the combustion of DME. It is thought that this higher heat release during the final burnout stages for the combustion of diesel fuel may have been a result of a higher amount of incomplete combustion products having formed as a result of pyrolysis within the fuel-rich core of the diesel flame. Such combustion products comprising of soot, carbon monoxide and unburned hydrocarbons may have

contained a significant amount of the total combustion energy. This energy may have been released when these combustion products were allowed to mix with sufficient amounts of air under high temperature conditions present during the burnout stages of the diffusion flame. The formation of such pyrolysis products in the fuel-rich core of the DME spray is thought to have been much lower due the high oxygen content and better ignition quality of DME.

Figure 7.30 shows that cylinder pressure traces recorded for DME and for diesel fuel exhibited distinct patterns in their shape. The combustion of diesel fuel led to a rounded cylinder pressure trace, whilst the combustion of DME led to a more angular pressure trace consisting of relatively straight lines separated by a distinctive kink. The heat release rates of combustion (Figure 7.28) indicated that DME tended to burn in two distinct phases, the premixed combustion phase ensuing the ignition delay, and the later diffusion-controlled combustion phase. The two heat release phases are reflected by the two discrete peaks in the heat-release rate, representing the pre-mixed and diffusion combustion phases respectively. The transition between the two combustion phases was marked by an inflection in the heat release rate, which manifested itself as a kink in the cylinder pressure trace. DME displayed a more pronounced separation between the premixed and mixing controlled heat release phases than the combustion of diesel fuel. It is thought that this may be attributed to two main reasons. First, the ignition quality of DME was significantly higher than that of diesel fuel, in that its cetane number was 65, compared to 54 for diesel fuel as shown in Table 7.7. Its higher cetane number reduced the ignition delay, so that for similar mixing rate of fuel with air, less fuel had premixed with air at the time of ignition. This allowed less fuel to burn during the pre-mixed combustion phase, thus forcing the fuel to burn in diffusion controlled combustion mode. A second reason for the more pronounced diffusion controlled combustion phase of DME with respect to diesel fuel was its lower calorific value per unit volume of fuel. In order to operate the engine at the same load, it was necessary to introduce a similar amount of calorific energy into the combustion chamber for diesel fuel and DME. Due to the lower calorific value of DME per unit volume, the injection duration for DME was approximately 50% longer than that for diesel fuel. Thus, at the time of ignition, a smaller proportion of the overall fuel energy had been introduced into the combustion chamber for DME than it had been for diesel fuel. A smaller proportion of fuel energy was thus available for combustion during the premixed combustion phase, and consequently a larger proportion of the total heat release was forced to occur in the diffusion-controlled combustion mode.

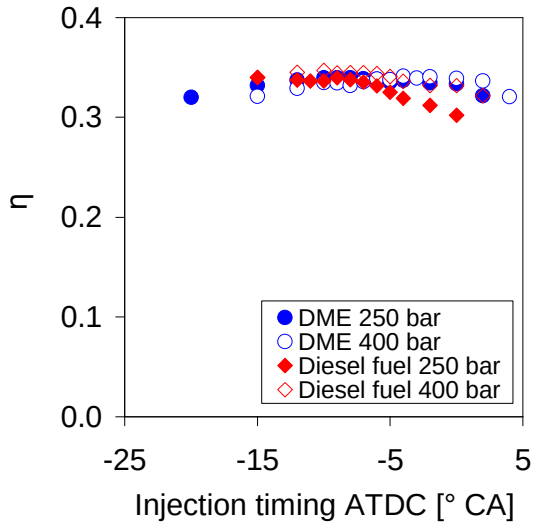

Figure 7.31 - Indicated engine efficiency for diffusion combustion mode operation of DME and Diesel fuel under different injection pressures in a diesel engine

A plot of the indicated thermal efficiency of the engine for DME and diesel fuel can be seen in Figure 7.31. The lowest fuel consumption for DME was recorded for an injection timing of 8 º CA BTDC at an injection pressure of 25 MPa, whilst for an injection pressure of 40 MPa the lowest fuel consumption was recorded for an injection timing of 4º CA BTDC. For diesel fuel, the optimum injection timings for low fuel consumption were slightly earlier; i.e. at 9 º CA BTDC for 25 MPa injection pressure and 10 º CA BTDC for an injection pressure of 40 MPa. It can be seen that the indicated thermal efficiencies were relatively similar for DME and diesel fuel. An increase in injection pressure resulted in a slight increase of thermal efficiency. This increase in efficiency was more pronounced in the case of diesel fuel than it was in the case of DME.

The pollutant emissions recorded for the diffusion combustion of DME and diesel fuel are shown in Figure 7.32. The emission of NO_x showed clear tends with respect to injection pressure of and injection timing of both fuels. In both cases an advance in injection timing and an increase in injection pressure tended to result in an increase in NO_x emission. Detailed examination of the NO_x emissions in Figure 7.32 reveals that DME produced slightly higher emissions of NO_x than diesel fuel at the same injection pressure and injection timing. Similar observations have previously been reported in the literature (Kajitani, et al., 2002; Konno, et al., 1999). The theoretical adiabatic flame temperature for stoichiometric conditions at constant pressure combustion without any dissociation is lower for DME than it is for fossil diesel fuel and can not explain the differences in NO_x emissions. The adiabatic flame temperature was calculated to be 2354 K for DME and 2363 K for the fossil diesel fuel. The calculations were performed using the thermochemical data presented in Table 7.7 for each fuel, and the procedure outlined by Turns (1996, p. 32-35). The adiabatic flame temperature of DME was thus calculated to be 9 K lower than that of the fossil diesel fuel and can therefore not explain the higher NO_x formation of DME with respect to diesel fuel. Direct comparison of the cylinder pressure traces for the combustion of DME and diesel fuel for injection pressures of 25 and 40 MPa and injection timings at 15 º, 10 º, 5º and 0º CA BTDC in Figure 7.30

reveals that for the same injection timing, the combustion of DME resulted in higher peak combustion pressures. The higher combustion chamber pressures are indicative of higher gas temperatures, which in turn are conducive to higher amounts of thermal NO_x formation via the Zeldovich mechanism. The likely reason for the higher emission of NO_x from the combustion of DME in comparison to diesel fuel is thus the higher peak gas temperature depicted in Figure 7.30. It is also possible that in addition to the higher cylinder pressure, differences in soot radiative heat transfer may have an effect on the relative amounts of NO_x formation between diesel fuel and DME. A higher soot loading in the flames of fossil diesel fuel may contribute to a reduction of the actual flame temperature of the diesel fuel. This theory is tentatively supported by the measurements of total particulate mass concentration in the exhaust gas of DME and diesel fuel. Figure 7.32 shows that fossil diesel fuel produced a significantly higher soot mass concentration in the exhaust gas than DME. It must be stressed that exhaust gas measurements of soot are clearly not direct measurements of the soot loading of the flames, but they can provide at least a tentative indication of the comparative soot loading within the respective flames.

The emission of particulate mass for the combustion of DME and diesel fuel is presented in Figure 7.32. Figure 7.32 shows that the combustion of DME resulted in almost negligible emissions of particulate mass, whilst the combustion of diesel fuel resulted in particulate mass emissions that were several orders of magnitude higher under similar conditions. This may be attributed to the formation of soot and its precursors within the fuel rich core of the combusting diesel fuel spray, whilst the high oxygen content of DME allowed full oxidation of soot and its precursors to take place, due to its high oxygen content. The low emission of particulate mass from DME was independent of injection timings and injection pressures. The combustion of diesel fuel on the contrary produced significant emissions of particulate mass, which showed noticeable trends with injection timing and injection pressure. An increase in injection pressure of diesel fuel from 40 MPa to 25 MPa resulted in reduction in particulate mass emissions of approximately one order of magnitude. This reduction in particulate mass emissions is thought to have been attributable to better fuel atomization, improved air entrainment into the fuel spray, and an increase in premixed burn fraction, resulting in an improved oxidation of soot and its precursors within the fuel-rich core of the spray. An advance in injection timing of diesel fuel tended to result in a reduction of particulate mass emissions emitted from the combustion of diesel fuel at both injection pressures. This reduction in particulate mass is thought to have been a result of the higher cylinder gas temperatures which occured in the post-flame gases under conditions of advanced injection timing. Higher cylinder gas temperatures during the later stages of combustion, in which the soot-carrying post-flame gases undergo dilution with sufficient oxygen in the lean cylinder charge, are known to increase the oxidation of soot (Tree & Svensson, 2007).

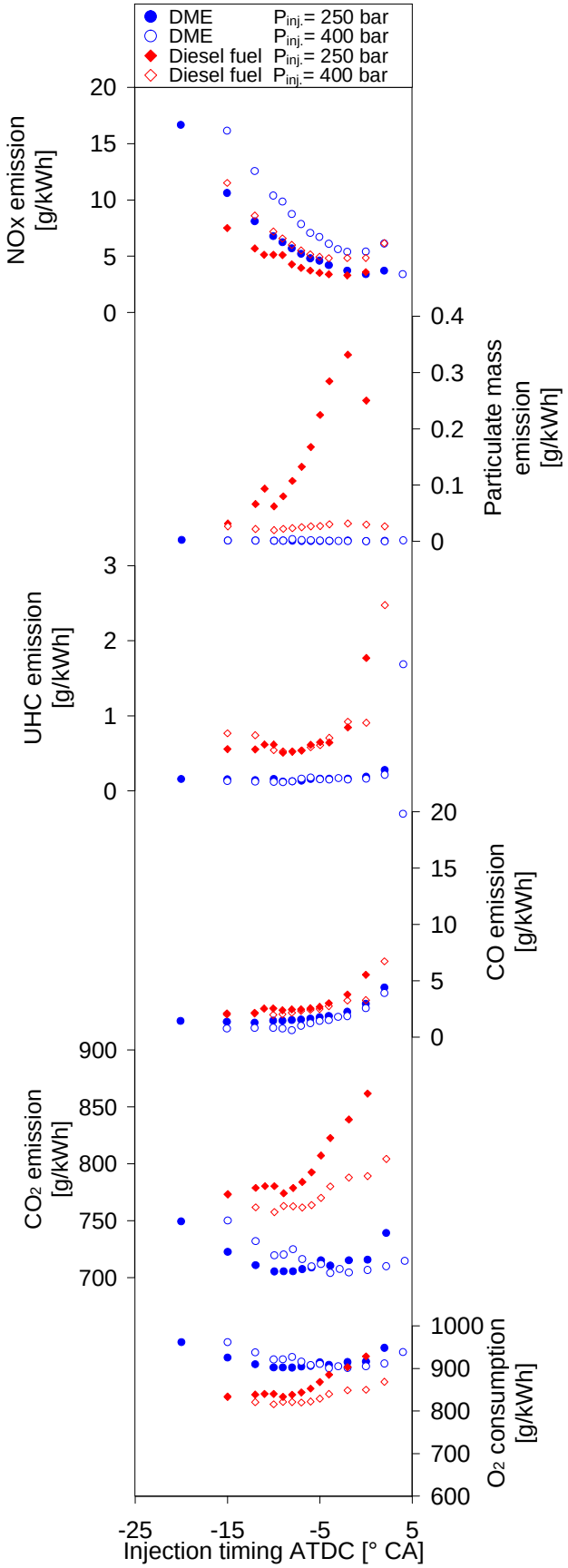

Figure 7.32 - Exhaust gas emissions for diesel combustion of DME and diesel fuel

The size spectral density of the particulate mass emissions between 5 and 1000 nm are shown in Figure 7.35 (a-d). Figure 7.35 (a and b) show the size spectral density of particulates for the combustion of DME at 25 MPa and 40 MPa injection pressure respectively. Figure 7.35 (c and d) show the size spectral density of particulates for the combustion of diesel fuel at 25 MPa and 40 MPa injection pressure respectively. It should be noted that a concentration of about 1000 ppm of alkyl-ester lubricity additive was present in the DME used for these experiments.

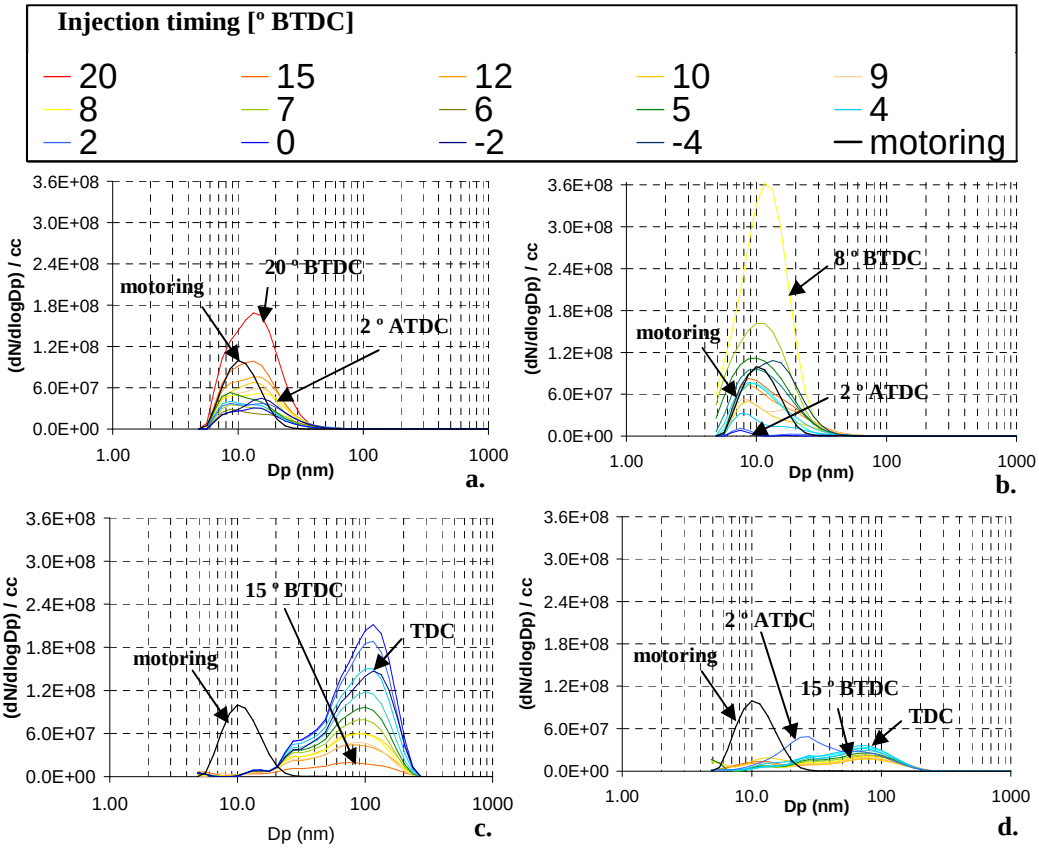

Figure 7.33 - Size spectral density of particulate matter for combustion of DME (a. and b.) and Diesel fuel (c. and d.) at injection pressures of 25 MPa (a. and c.) and 40 MPa (d.). The injection timings ranged from 20 ° BTDC to 4 ° ATDC

The most important result shown in Figure 7.33 was that the combustion of DME only produced small nucleation mode particles of the order of 5-40 nm in diameter, whilst the combustion of diesel fuel produced considerable amounts of accumulation mode particles of 40-200 nm in diameter. It has been reported that the smaller nucleation mode particles (5-40 nm) typically consist of volatile organic compounds, sulphites and water, but may contain some carbon soot and ash, whilst the larger accumulation mode particles (40-200 nm) consists predominantly of carbonaceous soot, with possible adsorbed organic compounds, sulphites and water (Kittelson, 1998). Nucleation mode particles (5-40 nm) carry considerably less mass than accumulation mode particles (40-200 nm) for a given size spectral density, due to their smaller volume. The differences in particle size shown in Figure 7.35 explain why the emission of particle mass from the combustion of DME were only a small fraction (0.2-10%) of the total particulate mass emitted by diesel fuel. The total level of

particulate mass emitted from the combustion of DME was close to the level of particulate matter recorded for mere motoring of the engine at that particular engine speed, without any fuel injection occurring. The injection pressure did not appear to significantly influence the emission of nucleation mode particles (5-40 nm) emitted from DME, as can be seen by comparison of Figure 7.33 (a and b).

The effects which the fuel injection pressure and injection timing had on the size spectral density of nucleation mode particles (5-40 nm) emitted from engine operation on DME, and the accumulation mode particles (40-200 nm) formed by the combustion of diesel fuel appeared to be fundamentally different. An advance in the fuel injection timing for DME resulted in a slight increase in the size spectral density of nucleation mode particles, as shown in Figure 7.33 (a and b). An advance in fuel injection timing of diesel fuel resulted in a notable reduction of accumulation mode particle emission from the engine, as shown in Figure 7.33 (c and d). An increase in the fuel injection pressure for the combustion of DME resulted in a minor increase of particulate mass emission. For diesel fuel, an increase in the fuel injection pressure resulted in a strong reduction of the accumulation mode particle emissions, as can be seen by comparison of Figure 7.33 (c and d). This indicates that the formation mechanisms for these two types of particle emissions were fundamentally different.

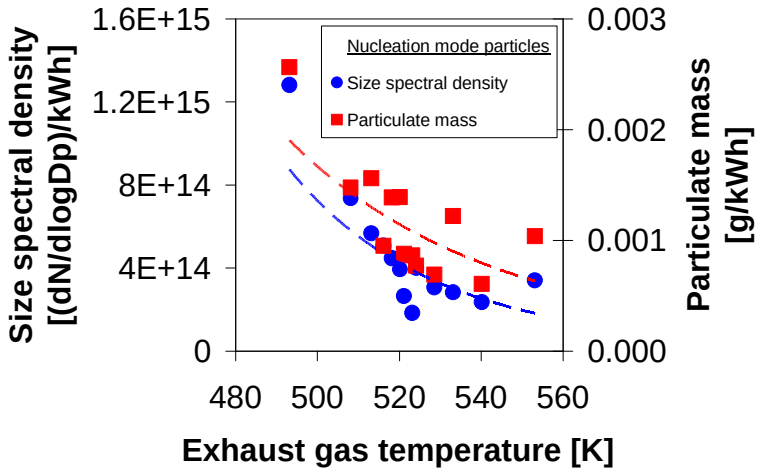

Figure 7.34 - Effect of exhaust gas temperature on nucleation mode particles from the combustion of DME with 1000 ppm straight-chained alkyl-ester lubricity additive

The mechanisms by which the combustion of diesel fuel leads to the emission of carbonaceous soot particles has been well documented (Tree & Svensson, 2007). The reasons for the emissions of the nucleation mode particles (5-40 nm) from the combustion of DME are less apparent, especially since DME is gaseous under the conditions encountered in the exhaust gas. It has been suggested that due to the high oxygen content of DME, smokeless combustion may be expected in a diesel engine, which would imply that no carbonaceous soot would be formed (Miyamoto, et al., 1998). If the nucleation mode particles do not consist of carbonaceous soot, it is likely that they may consist of organic compounds, sulphites, water or ash. Considering that the DME did not contain any sulphur, the formation of these particles from sulphites appears unlikely, leaving only organic compounds, water or ash as likely constituents. Figure 7.34 shows that the emission of the

nucleation mode particles (5-40 nm) from engine operation on DME was correlated with the exhaust gas temperature. A lower exhaust gas temperature resulted in a higher size-spectral density and mass emission of nucleation mode particles. This is an indication that the formation of these particles was the result of condensation of vapours within the combustion chamber or exhaust. If the particles formed through condensation, they are likely to have consisted predominantly of organic compounds or of water. The source of potential organic compounds is not entirely clear. DME is gaseous under the conditions encountered in the exhaust gas. Unburned DME is thus unlikely to have been the cause of these particulates. It is possible that the engine lubricating oil or the alkyl-ester fuel lubricity additive present in the DME may have been responsible for the formation of condensates within the exhaust gases. It may also be argued that leakage from the injector could contribute to the formation of particulates. Further investigations were necessary to investigate the potential sources of these nucleation mode particles. The emission of nanoparticles was measured when the engine was motored without any fuel injection taking place. Figure 7.33 showed that mere motoring of the engine produced a similar emission of nucleation mode particles (5-40 nm) as that recorded during fuelling of the engine with DME. The particles recorded during motoring of the engine cannot have derived from any component of the fuel, due to its absence. It is thought that the nucleation mode particles emitted during motoring of the engine consisted of a mist of engine lubricating oil, forming within the combustion chamber as a result of the cylinder bore lubrication and the rapid reciprocating movement of the piston. It remains unclear exactly how small lubricating oil droplets could have formed. One tentative explanation could be that engine lubricating oil was flung off the piston rings when the piston reversed at TDC. A further, more plausible explanation could be, that the collapse of cavitation, which has been shown to occur within the engine lubricating oil film on the trailing edge of the piston rings (Dellis & Arcoumanis, 2004), could have caused such small oil droplets to form. When the engine was fired on diesel fuel, these nucleation mode particles which appeared to derive from the engine lubricating oil were removed, as can be seen in Figure 7.33 (c and d). The mechanism by which this removal occurred is not entirely clear. It is possible that the oil droplets were oxidised by the combustion process, or that they may have been adsorbed onto the larger accumulation mode soot particles (40-200 nm), which were present under these conditions when operating on diesel fuel. If oxidation was the principal mechanism by which the oil particles were removed, the question arises why the combustion of DME did not have a similar effect. It will be shown in section 7.2.2 of this chapter that the engine lubrication oil and the fuel lubricity-improving additive, may both have contributed to the formation of liquid nucleation mode particles in the exhaust gases, and that no visible carbonaceous soot was produced by the combustion of DME.

The emission of unburned hydrocarbons from the combustion of DME in the engine was significantly lower than that of diesel fuel under all operating conditions, as is shown in Figure 7.32. This is likely to have been due to the higher ignition quality and shorter ignition delay of the DME which would have reduced over-dilution of the fuel spray prior to combustion. A shorter ignition delay has been known to reduce the amount of fuel forming an excessively lean fuel-air mixture that may fail to ignite at the fringes of the fuel spray (Heywood, 1988; Ladommatos, et al., 1996[a]). For

the combustion of DME, the minimum emission of UHC was recorded for fuel injection at 9º CA BTDC. For this injection timing, the lowest peak heat release rate was measured, indicating that the fuel underwent the shortest ignition delay under these conditions. Figure 7.32 also shows that the concentration of CO in the exhaust gas was lower for the combustion of DME than it was for the combustion of diesel fuel. This is likely to have been due to the higher oxygen content of DME (Table 7.7), which may have reduced the local equivalence ratio in fuel rich areas of the fuel spray, in which CO was likely to form. The emission of UHC and CO increased for both fuels if the injection timing was retarded towards the point of misfire. This indicated a deterioration of combustion efficiency of the fuels, due to insufficient time for combustion, lower temperatures and quenching of the flames induced by the expansion and cooling of the cylinder charge during the later stages of the expansion stroke. Figure 7.35 d) shows that the only operating point for which any significant emission of nucleation mode particles (5-40 nm) occurred for the combustion of diesel fuel was that for fuel injection at 2º CA ATDC, which was the latest injection timing reasonable combustion stability could be achieved for this fuel. The nucleation mode of particles around 5-40 nm in size were likely to have formed as a result of the high concentration of UHC present in the exhaust gases under these conditions, as shown in Figure 7.32. This result supports the hypothesis that the nucleation mode particles may predominantly have consisted of condensed droplets of unburned fuel.

7.2.2. Effect of straight-chain alkyl ester fuel lubricity-improving additive on sub-micron particulate emissions

During the experiments presented so far, it was observed that the operation of the engine on DME which had been additised with a concentration of 1000 ppm alkyl ester lubricity additive had resulted in the emission of a large number of nucleation mode particles of approximately 5-40 nm in diameter. The origin and formation mechanism of these particles remained unclear. One possibility is that these particulates consisted of droplets of the alkyl ester lubricity-improving additive which may have condensed into liquid droplets due to cooling of the combustion chamber gases during expansion. A further possibility is that these particles consisted of droplets of engine lubrication oil which had formed as a result of oil splash or collapsing cavitation within the engine lubricant oil film due to the rapid reciprocating movement of the piston. In order to establish whether the emission of nucleation mode particles could have been caused by the lubricity additive, a series of experiments were conducted in which the engine was operated with DME containing different concentrations of this additive. Neat DME, and DME with progressively increasing concentrations of alkyl ester additive were injected into the combustion chamber at 25 MPa injection pressure and an injection timing of 8º CA BTDC, which was the optimum injection timing for minimum fuel consumption at this injection pressure. The experiments showed that if no lubricity-improving additive was present in the DME, virtually particle-free combustion could be achieved under diffusion-combustion conditions, as can be seen in Figure 7.35. This provided an indication that

under these conditions the engine lubrication oil droplets had been visible during motoring of the engine were to a large extent oxidised by the combustion of DME. As the alkyl ester lubricity additive was introduced into the fuel, and its concentration was gradually increased from 50 to 5000 ppm, the number of nucleation mode particles emitted increased progressively. This result suggested that the lubricity-improving additive was involved in the formation of nucleation mode particles. The experiments were also carried out for a higher injection pressure of 40 MPa.

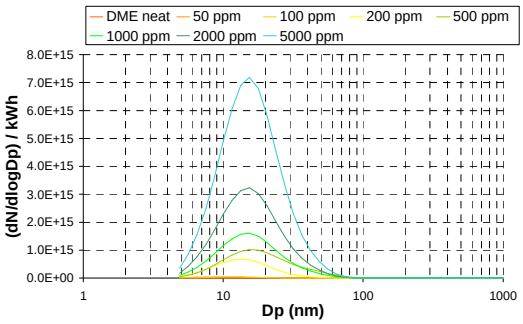

Figure 7.35 – Size spectral density of particulates for DME containing different concentrations of a silicon-based lubricity additive injected at 250 bar pressure

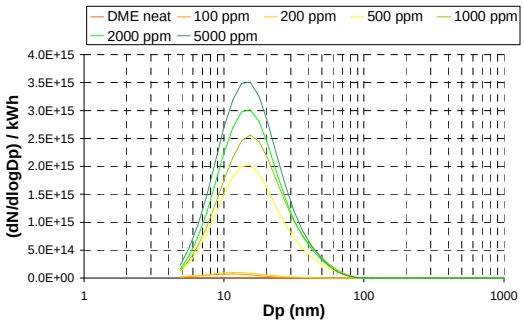

Figure 7.36 – Size spectral density of particulates for DME containing different concentrations of a silicon-based lubricity additive injected at 400 bar pressure

Figure 7.36 shows that similar results were obtained at this higher injection pressure. Despite the observed increase in number density of the nucleation mode particles due to an increased concentration of lubricity additive, only a relatively moderate increase in particulate mass from the combustion was recorded, as is illustrated in Figure 7.37.

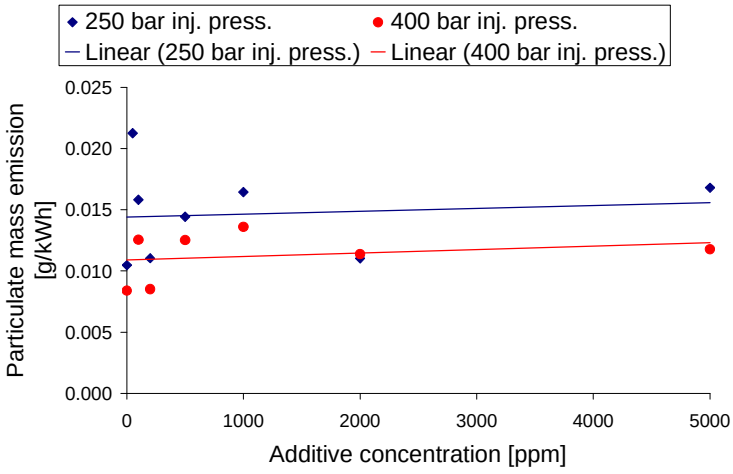

Figure 7.37 -Total particulate mass emissions from DME injected at different pressures with different lubricity additive concentrations

A sample of the particulate mass which had been formed during engine operation with 1000ppm concentration in diffusion combustion mode at 25 and 40 MPa injection pressure was collected using a MOUDI inertial impaction system. The optical appearance of the particulate mass was not

that of carbonaceous soot particles typical of diesel combustion, but rather that of viscous yellow liquid resembling engine oil or the alkyl-ester lubricity-improving additive. This liquid was analysed for its FTIR spectrum, and compared with that of the engine lubrication oil and with that of the lubricity-improving additive. Figure 7.38 shows a comparison of the three FTIR traces.

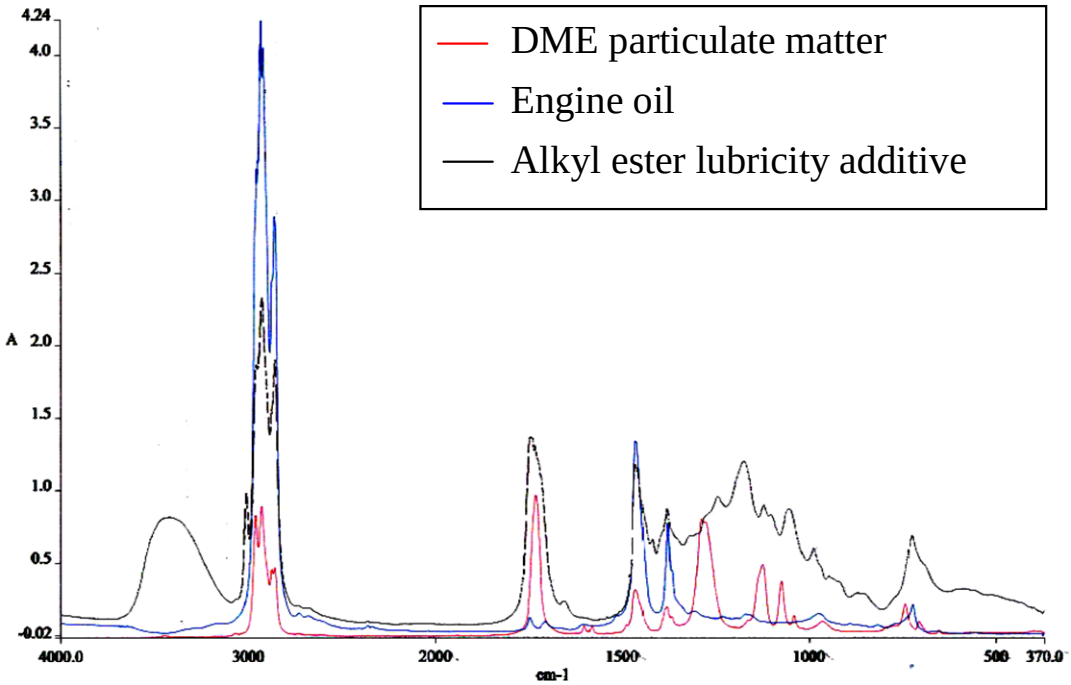

Figure 7.38 - FTIR absorbance spectrum of DME particulate matter formed with 1000ppm lubricity-improving additive concentration, pure engine fuel and pure lubricity-improving additive respectively

The FTIR analysis was not conclusive in that it did not identify either of the two liquids as the sole source of the particulates. The FTIR trace of the particulate mass showed some resemblance with both the lubricity-improving additive and with the engine lubrication oil. The visual appearance of the particulate matter on a polycarbonate membrane after being collected using MOUDI impactor is depicted by the photograph shown in Figure 7.39.

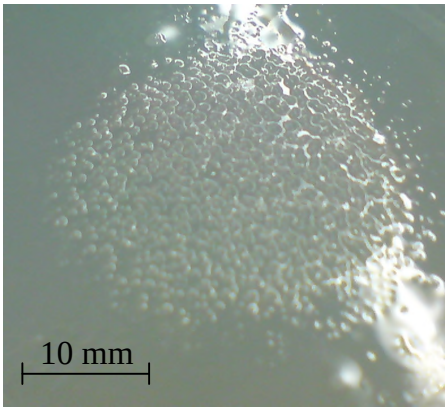

Figure 7.39 - Optical appearance of the particulate matter emitted by the diesel engine during operation on DME

7.3. The diffusion combustion of ethers and glymes in a diesel engine

In addition to the comparison of long-chained alcohols and ethers as well as dimethyl ether presented in the previous sections, a brief investigation was conducted on the diesel combustion of several ethers and glymes.

The four molecules were: dimethyl ether (DME), diethyl ether (DEE), ethylene glycol dimethyl ether (EGDME) and tri-ethylene glycol dimethyl ether (TEGDME). The four molecules were of varying chain length, and varying molecular mass. In addition ultra-low-sulphur fossil diesel fuel was tested to provide a basis for comparison.

Dimethyl ether (DME)

Diethyl ether (DEE)

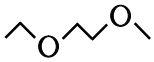

Ethylene glycol dimethyl ether (EGDME)

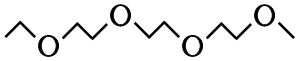

Tri-ethylene glycol dimethyl ether (TEGDME)

Figure 7.40 – Molecular structure of the ethers and glymes used as fuels

Table 7.8 - Engine running conditions

IMEP	4.0	bar
Engine speed:	2000	rpm
Injection pressure:	450	bar
Pilot injection timing:	31	º CA BTDC
Pilot energy injected:	180	J
Main injection timing:	10	º CA BTDC
Coolant temperature:	84 ±1	°C
Inlet air temperature:	30 ±1	°C

Combustion of ethers and glymes with pilot injection

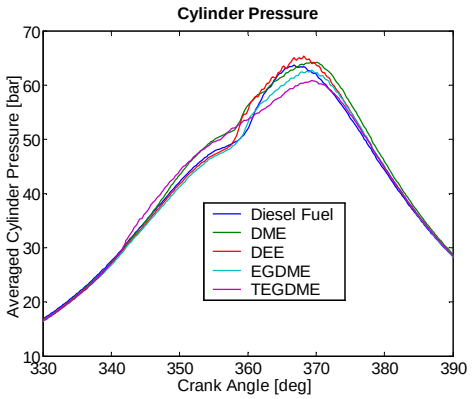

Figure 7.41 - Cylinder pressure for pilot injection experiments at 2000 rpm and 4 bar IMEP

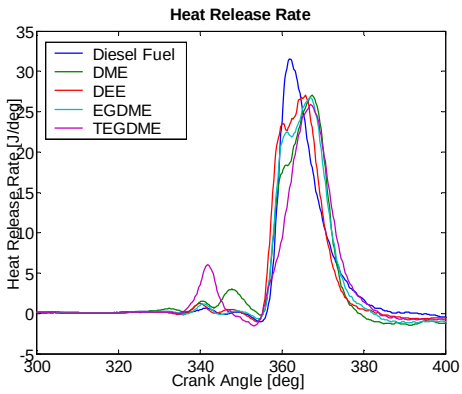

Figure 7.42 - Apparent heat release rate for pilot injection experiments at 2000 rpm and 4 bar IMEP

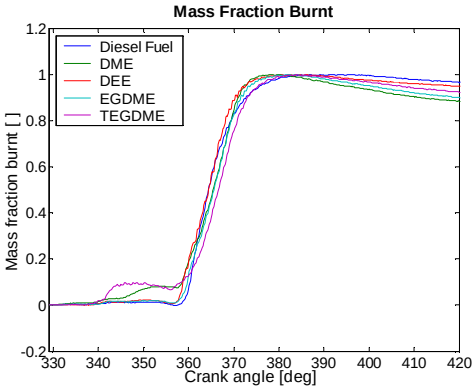

Figure 7.43 - Mass fraction burnt analysis for pilot injection experiments at 2000 rpm and 4 bar IMEP

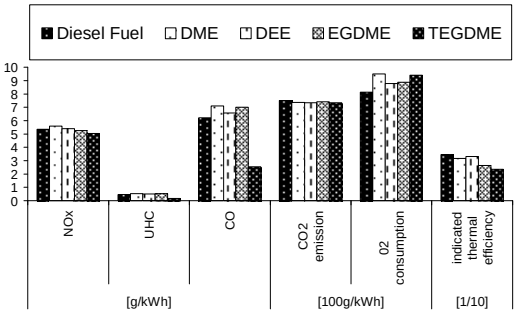

Figure 7.44 - Exhaust gas emissions for pilot injection experiments at 2000 rpm and 4 bar IMEP

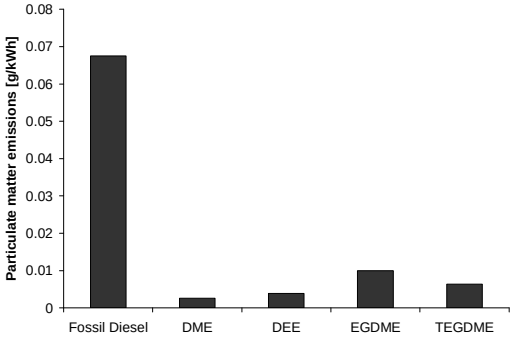

Figure 7.45 - Total particulate emissions for pilot injection experiments at 2000 rpm and 4 bar IMEP

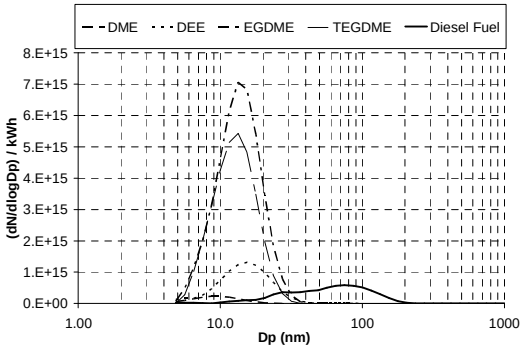

Figure 7.46 - Size-spectral Size spectral density of particulate emissions between 5nm and 1000nm analysis for pilot injection experiments at 2000 rpm and 4 bar IMEP

The experiments were carried out at the same engine running condition as that used in section 7.1.4 of this chapter for the four $C_{10}H_{22}O$ alcohols and ethers. All oxygenated fuels were additised with an alkyl-ester base lubricity improving additive (Infineum R655) to protect the injector from excessive wear.

The experimental conditions are summarised in Table 7.8. A pilot injection, which introduced an approximately constant amount of energy into the combustion chamber, was used in the same way as previously described in section 7.1.4 with regards to the experiments conducted on the $C_{10}H_{22}O$ ethers and alcohols. As for the experiments described in section 7.1.4, the duration of the main injection was adjusted to yield a constant IMEP for all fuels. The cylinder pressure traces shown in Figure 7.41 illustrate that the combustion of the various molecules resulted in different peak cylinder pressures amongst the fuels. These were due to differences in the patterns of heat released during the combustion of the pilot injection, as can be seen in Figure 7.42. It is clearly visible in Figure 7.42 and Figure 7.43 that the pilot fuel injected for the TEGDME combustion, burned in a single stage, and very early after its injection. This behaviour was very similar to that of the normal-ether (di-n-pentyl ether) in section 7.1.4, and was likely to have been an effect of the high cetane number of this molecule. Figure 7.42 also shows that a tendency existed for those fuels which released the largest amount of heat during the combustion of the pilot fuel, to exhibit a smoother rise in heat release rate during the main combustion phase.

The exhaust gas analysis in Figure 7.44 shows that some of the oxygenated molecules (DME and DEE) had slightly higher NO_x emissions than the diesel fuel. It can be seen that amongst the oxygenated molecules, those with a longer molecule length (and thus higher molecular mass), produced lower NO_x emissions than the shorter molecules. DEE showed relatively similar combustion characteristics to DME, with the added advantage that it was a liquid fuel, thus making it more practical to handle than the gaseous DME.

The exhaust gas analysis for particulates is shown in Figure 7.45 and Figure 7.46. Dimethyl ether produced the lowest particulate mass emissions, followed by diethyl ether, tri-ethylene glycol dimethyl ether and ethylene glycol dimethyl ether in this order. Figure 7.45 shows that the ethers and glymes tested in these experiments showed lower particulate mass emissions than the four long-chained ethers and alcohols of common sum formula $C_{10}H_{22}O$, which were discussed in section 7.1 of this chapter. It is probable that the lower particulate mass for this latter set of molecules was due to the higher ratio of oxygen atoms to carbon atoms. Tri-ethylene glycol dimethyl ether for example had 8 carbon atoms and 4 oxygen atoms in comparison to the 10 carbon atoms and 1 oxygen atom of the fuels tested in section 7.1. Fossil diesel fuel produced a high number of larger particulates in the range of 20-200 nm (Figure 7.46), whilst the oxygenated fuels produced hardly any accumulation mode particles, but a large amount of nucleation mode particles of 5-30 nm in diameter. The particulates towards the large-diameter-end of the spectrum contributed very strongly to the high mass loading, which explains the strong differences in overall soot production between fossil diesel fuel and the four oxygenated compounds. Both EGDME and TEGDME produced a very high number of particulates between 10 and 20 nm. Diethyl ether and dimethyl ether emitted significantly less particulates of this size, but it can be seen that their emissions in this range were still elevated

compared to that of refinery diesel fuel. It is possible that the lubricity improving additive which had been added to all of the oxygenated fuels may have been responsible for the larger number of nucleation mode particles. It is also possible that the higher boiling-point of the glymes with respect to the ethers may have played a role in their higher emission of nucleation mode particles.

7.4. Summary

In an attempt to investigate the effect of individual molecular structure of potential synthetic biofuel molecules, a brief study was conducted on four oxygenated molecules of the same number of carbon, hydrogen and oxygen atoms $C_{10}H_{22}O$, on DME and on four ethers and glymes of varying molecular mass. The results can be summarised as follows.

1. All oxygenated $C_{10}H_{22}O$ molecules produced lower NO_x emissions than the fossil diesel fuel at all conditions. DME produced higher NO_x emissions than fossil diesel fuel at comparable conditions.
2. All oxygenated molecules produced lower total particulate mass emissions than fossil diesel fuel.
3. The combustion of the simplest ether DME provided comparable engine efficiency as diesel fuel in diffusion combustion.
4. Soot-less combustion could be achieved when operating a diesel engine under diffusion combustion of DME.
5. An increase in the fuel injection pressure from 25 MPa to 40 MPa lead to a significant increase in the peak heat release and cylinder pressure rate for DME and diesel fuel, accompanied by a significant increase in NO_x concentration.
6. An increase in the fuel injection pressure from 25 MPa to 40 MPa lead to a significant reduction in total particulate mass formed from the combustion of fossil diesel fuel, but to no significant changes in particulate mass emission from the combustion of DME.
7. It was observed that an alkyl ester lubricity additive added to DME in concentrations ranging from 50-5000 ppm contributed to the emission of small nucleation mode particles (around 5-40 nm in diameter). The experiments suggested that these particles may have consisted of droplets of this additive which had condensed in the exhaust gas. The experiments also suggested that droplets from the engine lubricant oil may hace contributed to the formation of nucleation mode particles.
8. Diethyl ether was observed to have similarly good combustion characteristics as DME, with the added advantage of being liquid at atmospheric conditions.

Chapter 8. Biofuels in lean homogeneous-charge compression-ignition (HCCI) combustion

The experiments described so far have shown that the formation of NO_x and particulate matter occurring in the diesel combustion process, present some of the most severe problems of pollutant emission from diesel engines. The formation of NO_x occurs predominantly above temperatures of 1800 K, whilst the formation of carbonaceous soot occurs principally in rich fuel-air mixtures at temperatures above 1650 K. By avoiding the occurrence of high temperatures, and fuel-rich gases beyond a certain stoichiometry and temperature, the formation of NO_x and soot during combustion can be suppressed (Kamimoto & Bae, 1988).

It has thus been proposed to operate engines on the combustion heat of a lean, homogeneous mixture of fuel and air that is ignited through heating by polytropic compression of the gases (Onishi, et al., 1979; Najt & Foster, 1983; Thring, 1989). Such a fuel-air mixture can undergo a multistage ignition process (Griffiths, 1971) or single stage ignition (Dec, 2009), depending on the molecular species present in the fuel. Alkane fuels of higher molecular mass than methane and ethane, exhibit a tendency for a two-stage ignition process and two distinct phases of heat release (Benson, 1960; Glassman & Yetter, 2008), because they undergo rapid oxidation within two distinct temperature bands (the low-temperature heat release (LTHR) and high temperature heat release (HTHR) phases). The two temperature bands are divided by an intermediate temperature region in which oxidation progresses slowly, and may be endothermic. Other fuels such as methane, ethane, or branched hydrocarbons of higher molecular mass (e.g. iso-octane) do not undergo oxidation within the low temperature region, and only show a single-stage ignition process (Glassman & Yetter, 2008; Dec, 2009).

As discussed in section 2.1.5 of Chapter 2, several problems exist in the implementation of HCCI combustion in compression ignition engines. The most severe difficulties are posed by controlling the time of ignition under varying engine loads, speeds and operating temperatures, and by the preparation of a homogeneous mixture of fuel and air, when the fuel is directly injected into the combustion chamber. Also, the energy release arising from the rapid combustion of a homogeneously premixed mixture of fuel and air taking place throughout the combustion chamber may cause excessive rates of pressure rise. The present chapter looks into how biofuels of various molecular structures could provide potential solutions to some of these problems.

8.1. Fatty acid alkyl ester molecules

The first type of biofuel whose behaviour was studied in HCCI combustion mode was biodiesel; a mixture of fatty acid alkyl ester molecules. The fuel samples consisted of tallow methyl ester blended with diesel fuel in varying proportions.

The fuel was injected directly into the combustion chamber, using the electronically controlled solenoid injector and fuel system described in section 3.4.1 of Chapter 3. Three injections of short duration and high injection pressure (1600 bar) were employed to minimise fuel impingement on the combustion chamber walls. Fuel injection occurred during the early stages of the compression stroke, at 150º, 120º and 90º CA BTDC. The engine was operated at a constant load of 4 bar IMEP, and speed of 2000 rpm for all experiments. An overview of the experimental running conditions is given Table 8.1.

Table 8.1 - Experimental conditions

IMEP	4.0	bar
Engine speed:	2000	rpm
Injection pressure:	1600	bar
First injection timing	90	º CA BTDC
Nominal first duration:	420	µs
Second injection timing	120	º CA BTDC
Nominal second duration:	420	µs
Third injection timing	150	º CA BTDC
Nominal third duration:	420	µs

Cylinder pressure traces and heat release rates of the experiments are presented in Figure 8.1. All fuels exhibited a two-stage ignition process with two heat release peaks, indicative of the low-temperature and high temperature combustion phases. The low temperature combustion phase started around 23º CA BTDC and the high temperature combustion phase around 15º CA BTDC. The fatty acid alkyl esters produced lower peak cylinder pressures and lower peak heat release rates than fossil diesel fuel. Their combustion duration was significantly longer. It can be seen in Figure 8.1, that whilst all samples produced the same indicated engine load, the fossil diesel fuel showed a markedly shorter and more intense heat release than the biodiesel fuels. The cylinder pressure traces and heat release rates recorded for blends of TME with fossil diesel fuel indicate that these correlated with the proportion of biodiesel present in the fuel blends.

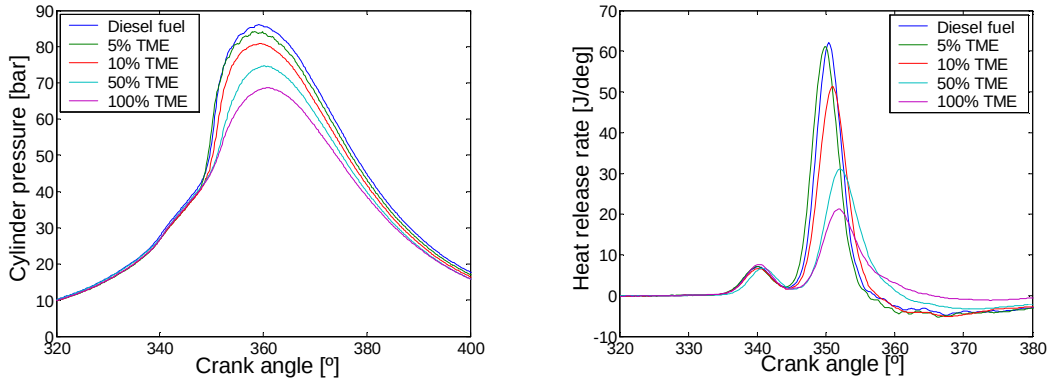

Figure 8.1 - Cylinder pressure traces and heat release rates for TME biodiesel fuels, their respective blends with fossil diesel fuel and pure diesel fuel.

Figure 8.2 shows the NO_x and particulate mass emissions recorded for fossil diesel fuel, biodiesel, and varying percentages of biodiesel blended within fossil diesel fuel. It is visible that the emission of NO_x and the emission of particulate matter increased, as the proportion of biodiesel within the fuel increased.

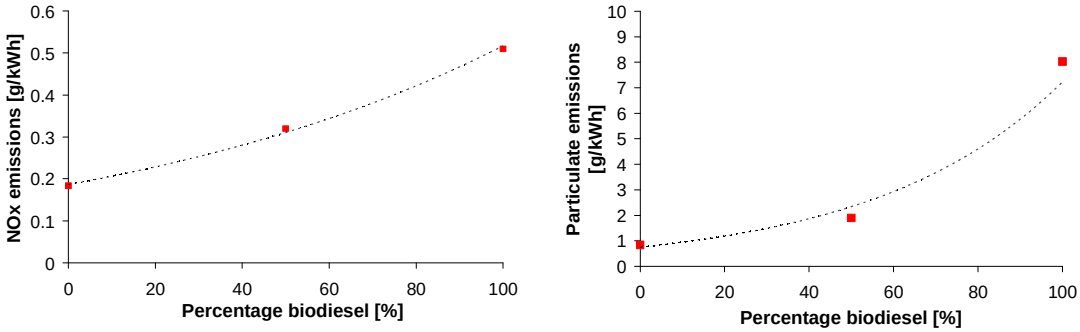

Figure 8.2 - NO_x and Particulate mass emissions for TME biodiesel fuels, their respective blends with fossil diesel fuel and pure diesel fuel.

On an absolute level, the emission of NO_x in this HCCI combustion mode is significantly lower than for operation of the engine in conventional diesel combustion mode. Emission levels of NO_x for operation of this engine in conventional diesel combustion mode at 2000 rpm and 4 bar IMEP were typically more than an order of magnitude higher (see section 5.8 of Chapter 5). The level of particulate matter emissions from the engine under this operating condition were at a remarkably high level. Typical emission levels of this engine, when operated in conventional diesel combustion mode at 2000 rpm and 4 bar IMEP, are of the order of 0.05 g/kWh. Thus the emissions shown in Figure 8.2 for direct injection HCCI combustion were about a hundred times higher than that of normal diesel engine operation. This level of particulate emission was, aside from being a serious concern in terms of pollutant emission, an indication of inadequate charge preparation within the combustion chamber. It is thought that these high levels of particulate emissions arose due to wetting of the piston and cylinder walls with liquid fuel, caused by excessive liquid penetration of the fuel spray and lack of fuel evaporation. This was a result of fuel injection taking place under insufficiently high pressures and temperatures of the combustion chamber gases, which occurred

during the early compression stroke. The particulates are thought to have been formed predominantly from liquid-film fires on the piston and combustion chamber walls, and possibly from the combustion of large liquid droplets which may have formed due to liquid fuel splashing off the piston. It is thought that the lower heat release observed for the biodiesel fuels in comparison to fossil diesel fuel could not be ascribed to differences in the rates of reaction between the two types of fuel. Instead, it is thought that the observed differences derived from poorer fuel-air mixing of the biodiesel occurring during charge preparation. It is believed that the prolonged heat release period observed for the biodiesel fuels stemmed from the liquid-film fires on the piston and combustion chamber walls described above, as well as from the combustion of any large droplets of fuel that may have survived throughout the compression stroke, or that may be formed as splash from the piston motion.

The reason for the slower evaporation was that the fatty acid alkyl ester fuels had significantly higher boiling points than fossil diesel fuel, which reduced their ability to evaporate and mix with the combustion chamber air. The distillation range of the fossil diesel fuel was in the range of 167-362 ºC, whilst the boiling points of the tallow methyl ester were in the range of 262-394 ºC. It has been shown experimentally that an increase in the fuel boiling point can result in increased liquid phase fuel spray penetration within the combustion chamber (Canaan et al. 1998). In addition to the lower volatility of biodiesel, its higher viscosity, may lead to the formation of larger droplets within the spray, and reduced evaporation. The kinematic viscosity of the tallow methyl ester (υ_{TME} = 4.4 mm^2/s) was significantly higher than that of fossil diesel fuel (υ_{diesel} = 2.6 mm^2/s). Hiroyasu (1985) and Ejim et al. 2007 have shown that increased fuel viscosity can result in an increase of the mean droplet diameter, which may also lead to increased droplet penetration before complete droplet evaporation can occur (Iyer et al. 2002). The increase in boiling point range together with an increase in fuel viscosity is thought to have lead to a reduction in fuel vaporisation when switching from fossil diesel fuel to biodiesel, and consequently to increased wall wetting. The indicated thermal efficiency of the engine during these experiments was of the order of 23%, which was significantly lower than for operation in conventional diesel combustion mode (~35%). Three major conclusions can be drawn from these experiments: Firstly, the low emission of NO_x and the two-stage ignition process of the charge demonstrated that the majority of the engine power derived from fuel combusting as a premixed homogeneous mixture of fuel and air. Secondly, the emission of particulate matter indicated that the occurrence of combustion chamber wall wetting in direct injection HCCI combustion can be a serious concern, and that changes in the fuel volatility strongly affected the amount of wall wetting taking place. Thirdly, under the present engine operating conditions, biodiesel represented a significantly worse fuel than fossil diesel fuel for HCCI combustion, due to its higher boiling point and higher viscosity. It was observed that the present types of biodiesel fuels were highly unsuited for HCCI operation. On the basis of these conclusions, and the work of Knothe (2005), it is believed that if biodiesel was to be used for HCCI engine operation, short-chained polyunsaturated fatty acid methyl esters would be most suitable. Their lower boiling points and lower viscosities, would be expected to reduce fuel wall-impingement and their lower cetane number would be expected to retard the ignition timing further towards TDC.

8.2. Acetal molecules

Acetals are liquid oxygenated molecules with slightly higher volatility and lower viscosity than fossil diesel fuel that could potentially be produced from lignocellulosic biomass. The behaviour of acetal fuels, was studied in HCCI combustion with particular attention to the influence of their molecular structure. In the experiments, three acetal molecules of the common molecular sum formula $C_{11}H_{24}O_2$ (discussed in section 6.3 of Chapter 6) and fossil diesel fuel were tested in direct injection compression ignition engine using the special low-volume fuel injection system (described in 3.4.2 of Chapter 3). The experiments were carried out at an engine speed of 1200 rpm and under the generation of an IMEP of 4 bar. The time of ignition was kept constant at TDC for all fuels molecules by employing varying amounts of cooled EGR gas. The three acetal molecules used for this study are shown in Figure 8.3 and the engine operating conditions are summarised in Table 8.2.

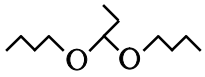

1,1 Dibutoxypropane

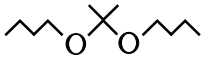

2,2 Dibutoxypropane

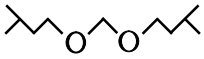

3-Methyl-1-(3-methylbutoxymethoxy) butane

Figure 8.3 - Molecular structure

The molecular structure of the fuels shows that whilst all three molecules had the same number of carbon, hydrogen and oxygen atoms, their differences lay in the branching of their molecular structure. This has been described in further detail in section 6.3 of Chapter 6. The molecule 1,1-dibutoxypropane represented the least-branched configuration of acetal molecule. The molecule 2,2-dibutoxypropane contained branching in its central moiety, whilst the molecule 3-Methyl-1-(3-methylbutoxymethoxy)butane contained branching in its lateral moieties. As discussed in section 6.3 of Chapter 6, these differences lead to variations in cetane numbers amongst the molecules. The cetane numbers were determined in an IQT using a 50% volumetric mixture in conventional diesel fuel and are presented in Table 8.2. The differences in ignition quality led to varying amounts of EGR being required to achieve a constant time of ignition at TDC for all molecules. Table 8.2 shows that the rates of cooled EGR needed to achieve fuel ignition around TDC were negatively correlated with the cetane numbers of the fuels. 1,1-Dibutoxypropane and 2,2-dibutoxypropane required similarly high EGR rates, whilst 3-methyl-1-(3-methylbutoxymethoxy)butane required a markedly lower EGR rate to retard ignition to TDC. The highest EGR rate had to be applied to 1,1-dibutoxypropane.

Table 8.2 - Experimental conditions

	LHV [kJ/kg]	CN [ ]	Engine speed [rpm]	IMEP [bar]	Injection pressure [bar]	Injection timing [° CA BTDC]	Ignition timing [ ]	EGR rate [%]	Indicated η
1,1 Dibutoxypropane	35020	79	1200	4	450	360	TDC	0.442	0.266
2,2 Dibutoxypropane	35000	71	1200	4	450	360	TDC	0.437	0.291
3-Methyl-1-(3-methylbutoxymethoxy) butane	35140	58	1200	4	450	360	TDC	0.406	0.301
Fossil diesel fuel	42980	50	1200	4	450	360	TDC	0.398	0.271

The cylinder pressure traces and heat release rates in Figure 8.4 and Figure 8.5 show that the variation in ignition quality and applied EGR rates between the fuels was reflected in their heat release behaviour. All fuels exhibited a two-stage ignition process with low-temperature and high temperature heat release phases respectively (Figure 8.5). The first heat release peak shown in Figure 8.5 represents the low-temperature combustion phase, and the second heat release peak represents the high-temperature combustion phase. 1,1-Dibutoxypropane showed the earliest and highest peak heat release rate during the low-temperature combustion phase, closely followed by 2,2-dibutoxypropane, whilst the molecule 3-methyl-1-(3-methylbutoxymethoxy)butane displayed a distinctly lower heat release rate during this phase (Figure 8.5). The lower heat release rate of 3-methyl-1-(3-methylbutoxymethoxy)butane during the low-temperature combustion resulted in lower cylinder pressures than for the other acetal molecules at the late stages of compression just before TDC (Figure 8.4). Glassman & Yetter (2008) and Dec (2009) have reported that low temperature heat release is typical of un-branched alkane molecules of high molecular mass. It may be suggested that the heat release of the un-branched lateral moieties of the two molecules 1,1-dibutoxypropane and 2,2-dibutoxypropane contributed significantly towards this similarity with un-branched alkanes, whilst this characteristic was visibly less pronounced for the molecule 3-methyl-1-(3-methylbutoxymethoxy)butane, due to branching of its lateral moieties. The lateral moieties may have been more important than the central moiety to the overall heat release behaviour of the molecule, because they carried about four times as much mass than the central moiety, and thus bore a significantly higher amount of chemically bound energy. This could help explain why the molecules 1,1-dibutoxypropane and 2,2-dibutoxypropane, which had no branching in their lateral moieties, exhibited a significantly higher amount of low-temperature heat release than the molecule 3-methyl-1-(3-methylbutoxymethoxy)butane, which had branched lateral moieties.

The second peak of heat release rate shown in Figure 8.5 represents the high-temperature combustion process. This high-temperature combustion occurred just after TDC, and showed significant variations in its intensity and duration amongst the various acetal molecules. 3-Methyl-1-(3-methylbutoxymethoxy)butane had by far the highest peak heat release rate during the high-temperature combustion phase, followed by 2,2-dibutoxypropane and 1,1-dibutoxypropane. The latter two molecules exhibited similarly low heat release rates. This trend, which was correlated with the ignition quality of the fuels, may be explained by the variations in EGR rates amongst the fuels.

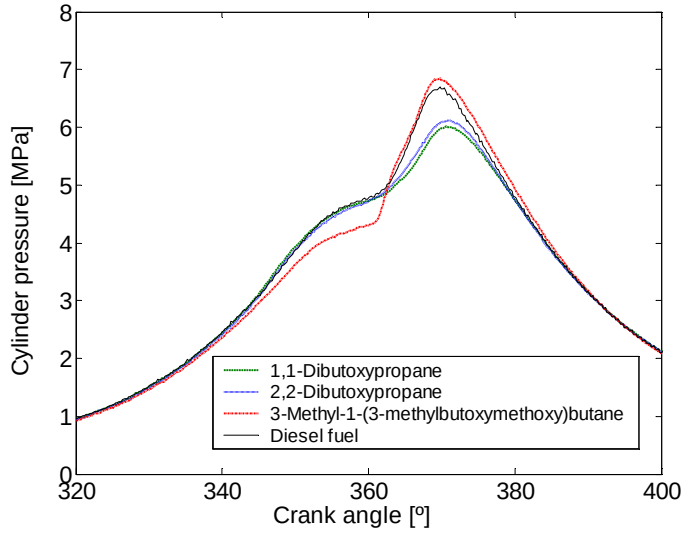

Figure 8.4 - Cylinder pressure for HCCI experiments with acetal molecules at constant ignition timing of TDC, controlled via EGR. Engine speed 1200 rpm, engine load 4 bar IMEP

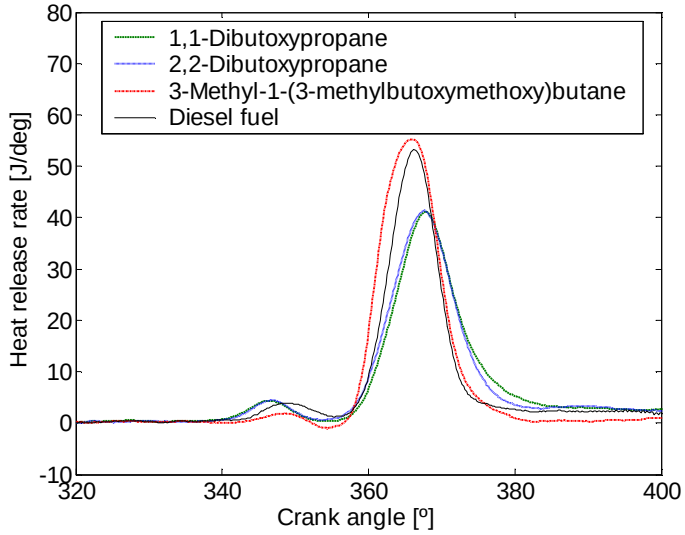

Figure 8.5 - Apparent heat release rate of acetal molecules at constant ignition timing of TDC, controlled via EGR. Engine speed 1200 rpm, engine load 4 bar IMEP

The molecule 3-methyl-1-(3-methylbutoxymethoxy)butane was subjected to the lowest EGR rate, whilst 1,1-dibutoxypropane was subjected to the highest EGR rate amongst the three acetal molecules. It is known that cooled EGR tends to reduce the reaction rates of combustion, of homogeneous fuel and air mixtures, and to result in lower heat release rates of combustion (Shi, et al., 2006; Kim & Lee, 2006). Thus, the higher levels of EGR applied to 1,1-dibutoxypropane and 2,2-dibutoxypropane in comparison to 3-methyl-1-(3-methylbutoxymethoxy)butane were the likely cause of the progressively lower heat release rates observed for these fuels during the high-temperature combustion phase. The reduction in rate of reaction was due to the dilution of the fuel-air mixture with inert gases, which reduced the concentration of reactants within the gas. It has been

well documented that a reduction in concentration of reactants can result in a decrease in reaction rates (Benson, 1960).

The emission of gaseous pollutants, oxygen consumption and thermal efficiency of the engine are shown in Figure 8.6. The emission level of NO_x for HCCI combustion of the acetal fuels was reduced to less than a hundredth of the NO_x emission when operating the engine on fossil diesel fuel in conventional diesel combustion mode. The absolute concentrations of NO_x within the exhaust gas were below 10 ppm for all fuels. This confirms that combustion was taking place under lean conditions, and that the emission of NO_x may be eliminated by lean HCCI combustion.

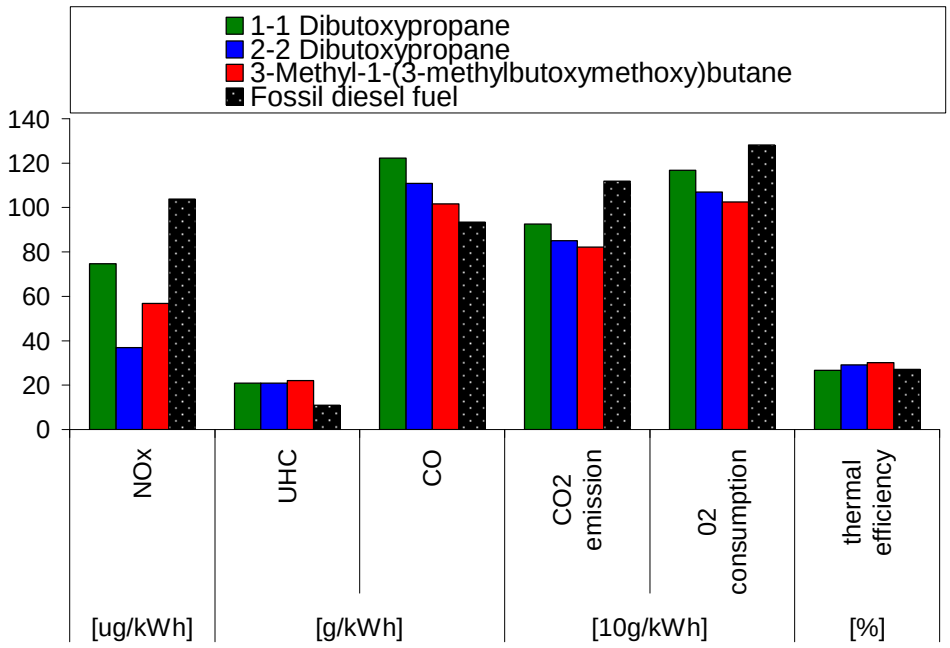

Figure 8.6 - Gaseous exhaust pollutant emissions and thermal efficiency during HCCI operation at 1200 rpm and 4 bar IMEP with three acetal molecules and fossil diesel fuel.

A new problem of this combustion mode was posed by the formation of markedly higher levels of products of incomplete oxidation, which indicated a low combustion efficiency. The emission of UHC was almost 100 times higher and the emission of CO were about 25 times higher than for operation of the same engine under conventional diesel combustion mode with fossil diesel fuel (see Chapter 5). These pollutants may in practice be oxidised to H_2O and CO_2 by use of a lean oxidation catalyst during after-treatment of the exhaust gases. It should be noted though, that their oxidation within the exhaust gas system also represents a waste of their chemical energy for power-generation purposes.

All acetal fuels produced lower CO_2 emissions and had a lower O_2 consumption than fossil diesel fuel. This could predominantly be ascribed to the higher hydrogen to carbon (H/C) ratio of the acetals in comparison to fossil diesel fuel. In the case of the molecule 3-methyl-1-(3-methylbutoxymethoxy)butane, and to some extent in the case of the molecule 2,2-dibutoxypropane, this could also be attributed to a higher thermal conversion efficiency of the engine cycle. The molecule 3-methyl-1-(3-methylbutoxymethoxy)butane displayed the highest thermal efficiency of all fuels tested within this series of experiments. This is thought to have been due to two reasons.

Firstly, the lower ignition quality of the molecule 3-methyl-1-(3-methylbutoxymethoxy)butane reduced the requirement for cooled recirculated exhaust gas, necessary to obtain ignition of the charge around TDC of the engine cycle. This resulted in slightly higher combustion efficiency, as is visible from the lower CO emissions shown in (Figure 8.6). Secondly, 3-methyl-1-(3-methylbutoxymethoxy)butane was more volatile than fossil diesel fuel, which would have resulted in better fuel evaporation, and less fuel being wasted as UHC emissions as a result of fuel impingement on the combustion chamber walls. Thirdly, 3-methyl-1-(3-methylbutoxymethoxy)butane displayed less low-temperature heat release prior to TDC, and a faster heat release rate just after TDC than any other fuel (Figure 8.5). This made its engine cycle resemble more that of an ideal isochoric cycle than was the case for the other fuels. The ideal isochoric cycle had been shown in section 2.2 of Chapter 2 to provide optimum cycle efficiency.

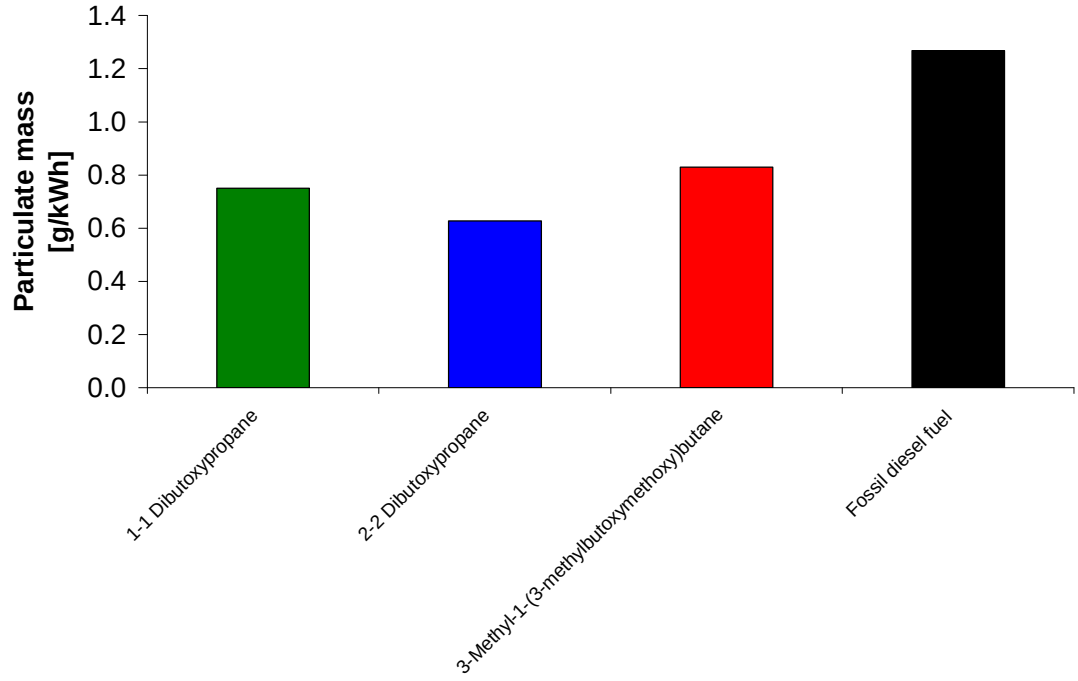

Figure 8.7 - Total particulate matter emissions during HCCI operation at 1200 rpm and 4 bar IMEP with three acetal molecules and fossil diesel fuel.

The total emission of particulate matter for the individual fuels is shown in Figure 8.7. All acetal molecules produced lower particulate matter emissions than fossil diesel fuel. The experiments presented in section 8.1 had suggested that the volatility of the fuel was very important for the avoidance of particulate formation through fuel impingement. The boiling point of all acetal molecules (195-220 ºC) lay below the 50% boiling point of fossil diesel fuel (271 ºC), indicating that a more complete evaporation was likely to have taken place, and that less fuel impinged on the combustion chamber walls. It should be noted that the total particulate mass emission for the acetal molecules under this condition was approximately 20 times higher than the particulate mass emissions of the same engine running on fossil diesel fuel in conventional diesel combustion mode.

The size spectral density of the particulate matter is shown in Figure 8.8. The particles produced by the HCCI combustion of the acetal molecules showed a bimodal distribution, with the particle size

of the smaller mode ranging from 10-100 nm in diameter, and the particle size of the larger mode ranging from about 100-300 nm. 1,1-Dibutoxypropane and 3-methyl-1-(3-methylbutoxymethoxy)butane produced an almost identical spectrum of the particles, whilst 2,2-dibutoxypropane produced slightly smaller particles in the finer and the coarser modes. Fossil diesel fuel produced a tri-modal distribution, with the smallest mode having particle diameters between 5-10 nm, the intermediate mode having particle diameters between 10-100 nm, and the larges particulate mode having diameters between 100-300nm. The higher particulate mass emission produced fossil diesel fuel with respect to the acetal fuels (Figure 8.7) could mainly be ascribed to the emission of a higher number of large particles of the order of 300 nm in diameter, which carried a large proportion of the total particulate mass.

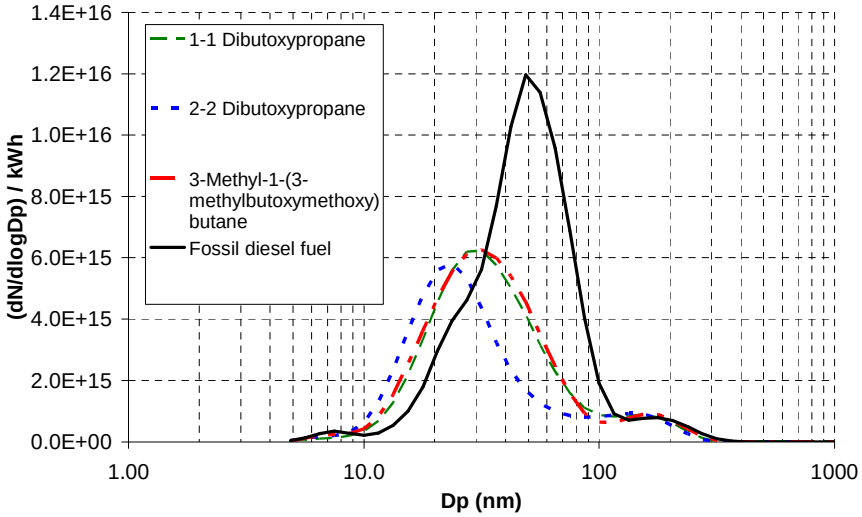

Figure 8.8 - Size spectral density of particulate matter

Several conclusions may be drawn from the experimental study described above. Firstly, acetal molecules provided some advantages over fossil diesel fuel in HCCI combustion mode. These consisted in improved thermal efficiency, lower NO_x, CO and CO_2 and particulate mass emissions. This results is in stark contrast to the performance of biodiesel fuel (fatty acid alkyl esters) presented in section 8.1, which indicated a worsening of all these parameters. The main advantage of acetal fuels over biodiesel fuels for their operation in HCCI combustion mode appeared to be their higher volatility, which lead to better fuel vaporisation and improved charge preparation. The experiments presented in section 8.1 and section 8.2, demonstrated that an adequate molecular structure of biofuels is invaluable to achieving successful HCCI combustion operation. Secondly, the experiments showed that by design of the molecular structure of the molecules it is possible to modulate the chemical and physical properties of the molecules to achieve more efficient HCCI operation. An example for such a process within this experimental study was the design and synthesis of the molecule 3-methyl-1-(3-methylbutoxymethoxy)butane. When designing the molecule it was hoped that its branching on the lateral moieties would result in a lower ignition quality of the fuel. This lead to a lower requirement for recirculated exhaust gas, and made the HCCI combustion process more efficient.

8.3. Ether molecules

Ethers are organic molecules consisting of two alkyl groups bound by a common oxygen atom. As a result of their inability to form hydrogen bonds amongst their molecules, ethers are characterised by low boiling points, low enthalpies of vaporisation and high vapour pressures (Morrison & Boyd, 1992, p.238). Ethers thus particularly commend themselves as fuel for HCCI combustion due to their high volatility (Teng, et al., 2001), which allows adequate vaporisation of the fuel and appropriate mixing of the fuel with air to take place during charge preparation. The experiments presented in section 8.1 had suggested that for direct injection HCCI combustion the volatility of the fuel was of principal importance to charge preparation and to the avoidance of fuel impingement on the combustion chamber walls.

In addition to high volatility, a suitable auto-ignition temperature of the fuel is of principal importance to engine efficiency, since it is crucial to the ignition timing of the fuel-air charge, and thus to the phasing of combustion within the thermodynamic cycle. The auto-ignition temperatures of ethers in air are highly variable, which allows high flexibility in matching the auto-ignition temperature of the fuel to the engine operating conditions. The auto-ignition temperature of ethers depends in detail on the structure of the alkyl groups of the molecules. Alkyl groups of high mass and straight-chained structure cause the ether molecules to have a low ignition temperature, whilst alkyl groups of lower mass and branched structure are conducive to high ignition temperatures and strong resistance to auto-ignition (Yaws, 2001). A suitable choice of ether fuel molecules may thus be used to adjust the time of ignition towards the point of peak geometric compression, as shall be described in the ensuing experimental results.

The HCCI combustion experiments were conducted with a variety of ethers of different molecular structures: dimethyl ether (DME), diethyl ether (DEE), diisopropyl ether (DIPE) and methyl tert-butyl ether (MTBE). The HCCI combustion behaviour of these ethers and the possibilities of controlling the ignition timing through various methods were studied. Control of ignition timing was achieved through varying rates of cooled exhaust gas recirculation (EGR), changes in the effective compression ratio, and variations in the molecular composition of the fuel. Adjustments in the molecular composition of the fuel were observed to provide an effective way of controlling the ignition timing of HCCI combustion whilst still achieving reasonably high thermal efficiencies. The experimental results were compared with the combustion of petroleum-derived diesel oil. Salient properties of the ethers are shown Table 8.3.

Table 8.3 – Fuel Properties

	Fossil diesel fuel oil	***Dimethyl ether (DME)***	***Diethyl ether (DEE)***	***Diisopropyl ether (DIPE)***	***Methyl-tertiary butyl ether (MTBE)***
Molecular formula	-	C_2H_6O	$C_4H_{10}O$	$C_6H_{14}O$	$C_5H_{12}O$
Cetane number	*54.3*	*65*	*150*	-	-
Autoignition temperature	-	*235° C* [1]	*160 ° C*	*441 ° C*	*374 ° C*
Lower heating value	*43040 kJ/kg*	*28430 kJ/kg*[2]	*33900 kJ/kg*[3]	*29104 kJ/kg* [4]	*34903 kJ/kg*[5]
Carbon proportion	*86.3 % mass*	*52.14 % mass*	*64.82% mass*	*70.53% mass*	*68.13% mass*
Hydrogen proportion	*13.7 % mass*	*13.13 % mass*	*13.60% mass*	*13.81% mass*	*13.72% mass*
Oxygen proportion	-	*34.73 % mass*	*21.59% mass*	*15.66% mass*	*18.15% mass*
Density	*833 kg/m^3*	*660 kg/m^3*	*706 kg/m^3*	*724 kg/m^3*	*740 kg/m^3*
Viscosity	*2.17 mPas @ 40 deg C*	*0.12 mPas*	*0.23 mPas @ 20 deg C*	*0.32 mPas*	*0.67 mPas @ 20 deg C*
Sulphur content	*3 ppm*	-	-	-	-
Initial boiling point	*178 ° C*	*-25 ° C*	*35 ° C*	*68 ° C*	*55 ° C*
Final boiling point	*351 ° C*	*-25 ° C*	*35 ° C*	*69 ° C*	*55 ° C*
Mono-aromatics	*15.5*	-	-	-	-
Di-aromatics	*1.5*	-	-	-	-
Tri-aromatics	*0.3*	-	-	-	-

[1] BOC chemical company (2000)
[2] Hu et al. (2005)
[3] Anand & Mahalakshmi (2008)
[4] Shell Chemicals (2001)
[5] Emel'yanov et al. (2001)

8.3.1. Influence of the molecular structure of the ether

An initial study was conducted on the effect of molecular structure of three volatile ethers in direct injection HCCI combustion, and the results were compared with those of fossil diesel fuel. The three ether molecules consisted in dimethyl ether (DME), diethyl ether (DEE) and diisopropyl ether (DIPE). The molecular structure of the molecules is illustrated in Figure 8.9.

Dimethyl ether (DME)

Diethyl ether (DEE)

Diisopropyl ether (DIPE)

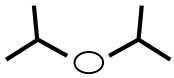

Figure 8.9 - Molecular structure of the ethers

The ignition timing of all fuels was controlled using cooled EGR or intake air heating so that the ignition of the high temperature combustion phase occurred around TDC for all fuels. All experiments were conducted at the same geometric compression ratio of 15:1, the same engine speed of 2000 rpm, and under the development of the same engine load of 400 kPa. Details of the engine operating condition are given in Table 8.4.

Table 8.4 – HCCI running conditions for effect of molecular structure

Combustion type	HCCI	
Compression ratio	15:1	
IMEP	400	kPa
Engine speed	2000	rpm
Injection pressure	45	MPa
Injection timing	120	° BTDC
Coolant temperature	84 ±3	°C
	EGR rate	**Intake air temperature**
Diesel fuel	43 %	25 °C
DME	61 %	23 °C
DEE	78 %	21 °C
DIPE	0 %	165 °C

The combustion chamber pressure and heat release rates of combustion from the experiments are shown in Figure 8.10. The pressure traces show that the highest peak pressure amongst the ethers was recorded for the combustion of DIPE, followed by DME, and that the lowest peak pressure trace was recorded for DEE. The combustion of diesel oil produced a similar pressure trace to that of DME. The heat release rates in Figure 8.10 illustrate that these variations in combustion chamber pressure were due to strong variations in the velocity of combustion amongst the fuels. DIPE produced by far the fastest combustion process with the highest heat release rates and the shortest combustion duration. The slowest combustion was recorded for DEE which produced the lowest heat release rates and had the longest combustion duration. Table 8.4 shows that the reduction in heat release rates was correlated with an increase in EGR rate, indicating that the combustion reactions were slowed down as a result of a dilution of the reactants through EGR gas. In the experiment using DIPE as fuel, the higher intake air temperature may also have contributed towards the faster rate of combustion.

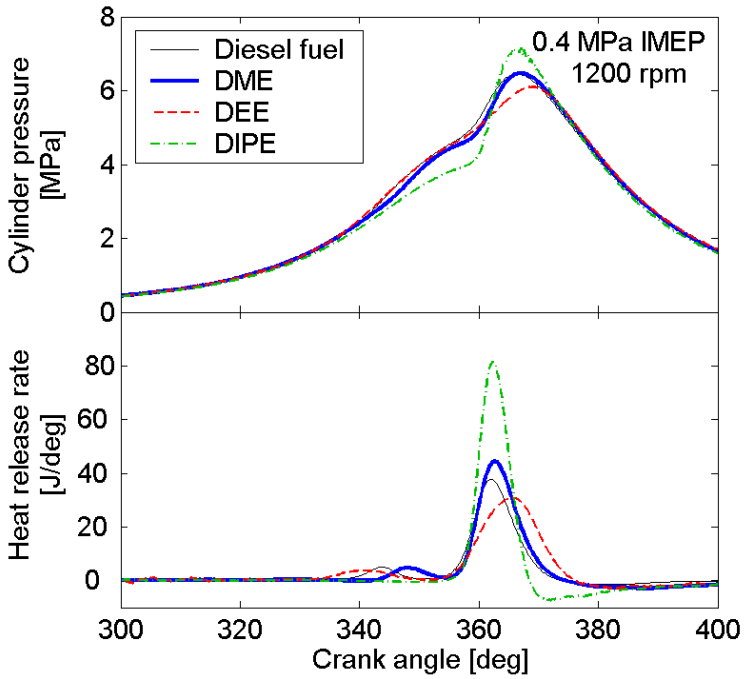

Figure 8.10 - Cylinder pressure and heat release rate for volatile ethers and diesel fuel in direct injection HCCI combustion mode

The heat release rates in Figure 8.10 show that fuels released significantly different proportions of heat released during the low temperature combustion phase, depending on their molecular structure. The two ethers with straight alkyl groups (DME and DEE), showed significant heat release during the low temperature combustion phase, whilst the branched ether (DIPE) only displayed a single high temperature combustion phase. Figure 8.10 suggests that the apparent heat release rate for the combustion of DIPE became negative for a short period of time after TDC. This was not en effect of combustion, but was attributable to heat transfer from the combustion chamber gases to the walls and piston. Figure 8.11 shows the emission of gaseous pollutants and the indicated thermal efficiency of the engine.

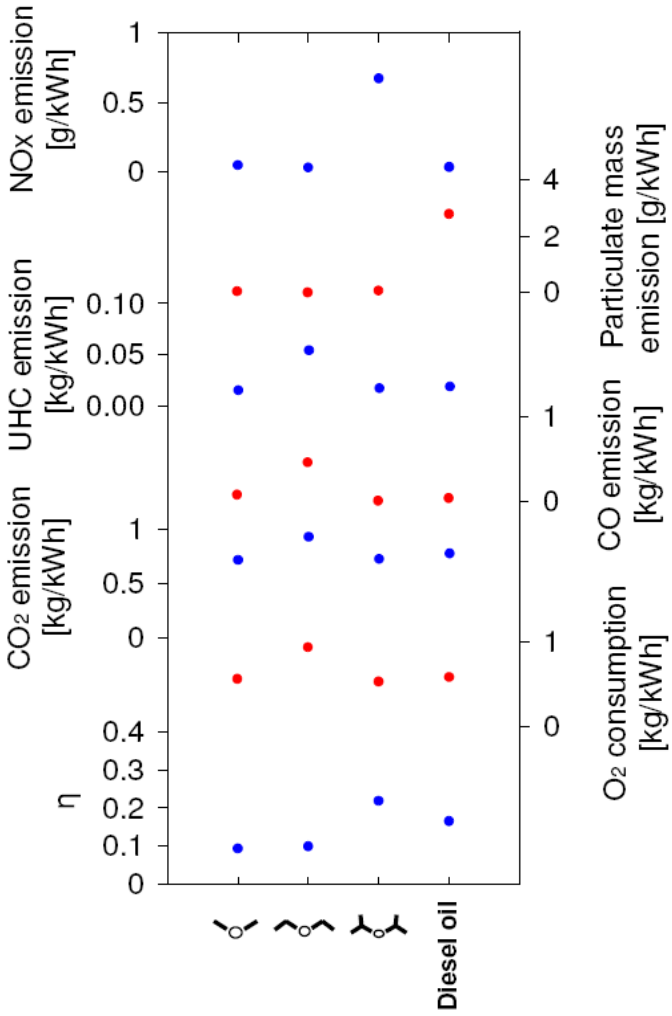

Figure 8.11 - Gaseous exhaust emissions for three volatile ethers and diesel fuel for direct injection HCCI combustion

All fuels exhibited extremely low emissions of NO_x in comparison with diffusion combustion operation of the engine (Chapter 5, 6, 7), confirming the advantages of HCCI combustion for low NO_x emission. DIPE was the only fuel to produce a notable amount of NO_x amongst the fuels. This may be explained by the higher intake air temperature and lower EGR rate applied to its combustion process, both of which would have resulted in an increase of combustion temperatures. Figure 8.11 shows that all ethers produced low levels of particulate mass emissions in HCCI combustion. The size spectral density of the particulates is shown in Figure 8.12.

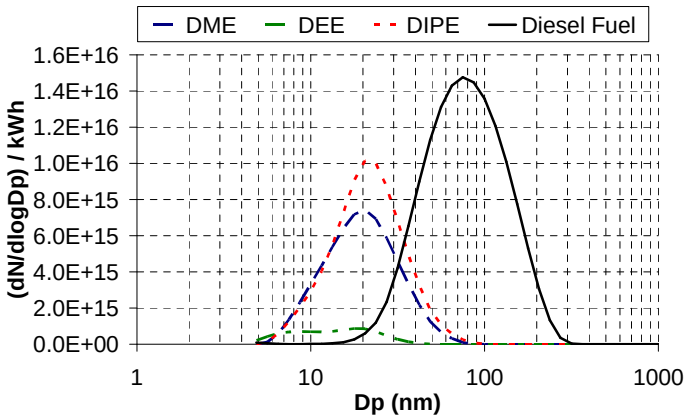

Figure 8.12 - Size spectral density of particulate emissions between 5nm and 1000nm for ethers in HCCI combustion

The HCCI combustion of diesel oil under these conditions produced an extremely high level of particulate mass emissions, which exceeded that of engine operation under diffusion combustion mode by far. This was due to fuel impingement of the diesel oil on the combustion chamber walls as a result its low volatility. It should be noted that the injection system and combustion chamber were not purposely adapted for operation of direct injection HCCI combustion. The low cylinder pressures and temperatures into which the fuel was injected during the early compression stroke resulted in a long liquid length of the fuel spray, slow evaporation of the fuel droplets, and fuel impingement on the cylinder walls and piston. Although this may have been improved to some extent by better design and operating strategies of the engine, the present experiments nevertheless highlighted the importance of fuel volatility when injecting the fuel early during the compression stroke.

The effect which the addition of EGR had on pollutant emissions was visible when considering the combustion data from the molecules DEE, which was subjected to the highest level of EGR. Figure 8.11 shows that this straight-chained ether produced the highest emission levels of carbon monoxide and unburned hydrocarbons, whilst also exhibiting the lowest emission of NO_x. This is likely to have been caused by the high EGR rate to which it was subjected. The EGR is thought to have lowered combustion temperatures through dilution of the reactants with inert gases, and to have lowered the reaction rate and the combustion efficiency. Conversely it can be seen that DIPE which was not subjected to any charge dilution through EGR, and was instead subjected to intake air heating, displayed the lowest emissions of carbon monoxide, unburned hydrocarbons, and the highest emission of NO_x. The highest thermal efficiencies were measured for those fuels with the lowest EGR rates in these experiments. It is thought that this was predominantly a result of the higher combustion efficiency of these fuels due to their lower emission of UHC and CO, and due to the increased combustion speed and higher gas temperatures of the cycle during heat addition.

8.3.2. Ignition control of lean homogeneous ether air mixtures

In order to obtain high thermal efficiency of the engine under HCCI conditions, it is desirable to obtain ignition of the charge when the piston is situated at TDC. The ensuing experiments were aimed at comparing various methods of controlling the ignition timing, and their influences on engine operation. First, the effects which cooled EGR had on the ignition timing were studied. Second, the effects of effective compression ratio on ignition timing were studied.

Influence of EGR

A brief study on the ignition timing of DME in lean HCCI combustion under the influence of cooled EGR was conducted. The engine was operated at a constant IMEP of 100 kPa and an engine speed of 1200 rpm. Figure 8.13 shows the cylinder pressure and heat release rates for HCCI combustion of DME for three different EGR rates.

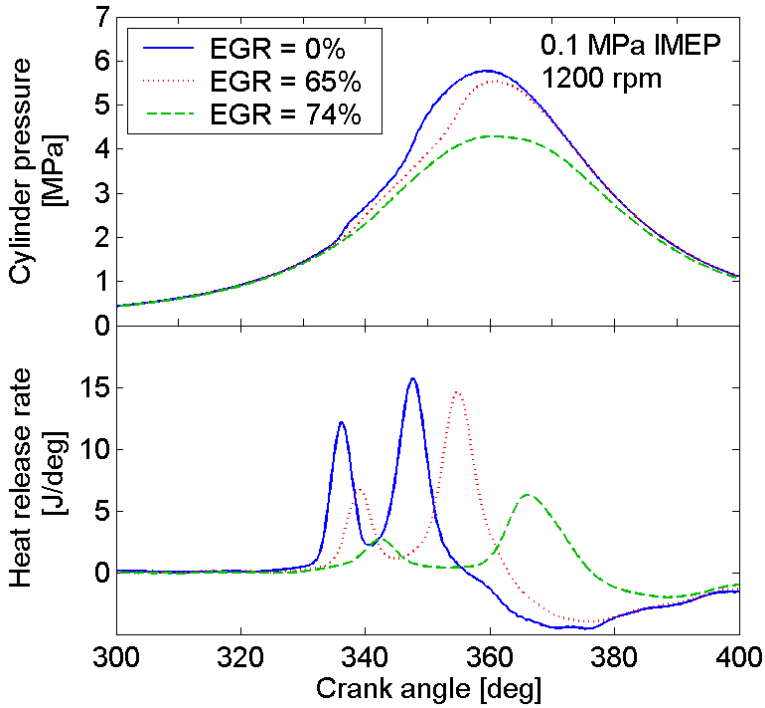

Figure 8.13 – Cylinder pressure and heat release rate for HCCI combustion of DME with varying EGR rates.

The heat release in all experiments showed two distinct peaks of heat release, illustrating the low temperature and high temperature combustion phases. An increase in EGR rate resulted in a progressive retardation of combustion timing, accompanied by a reduction in peak heat release rates,

and in a prolongation of the combustion process. The reduction in heat release rates illustrates that the combustion reactions were slowed down as a results of the dilution of the reactants by EGR gas. It was also observed that an increase in EGR rate shifted the two phases of combustion further apart from one another. The negative heat release rates observed around TDC were due to heat transfer from the charge gases to the combustion chamber walls, which were not accounted for in the heat release analysis. Exhaust gas emissions of NO_x, UHC, CO, CO_2, and O_2 and the indicated engine efficiency for the experiments are shown in Figure 8.14.

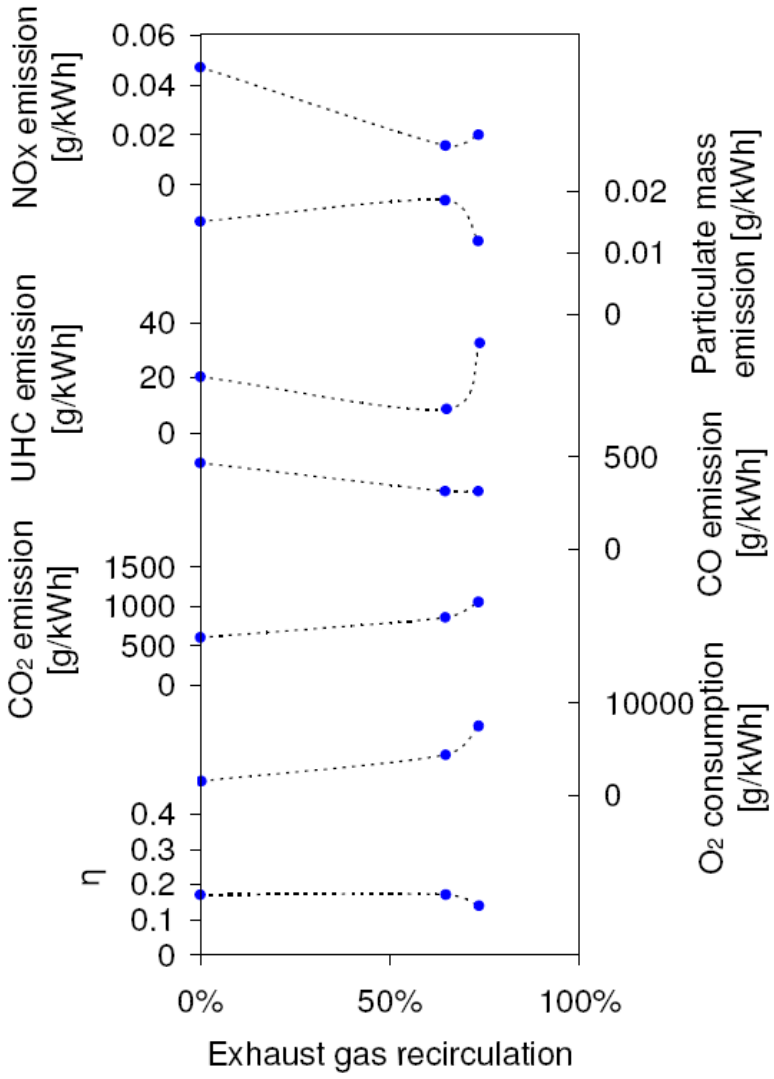

Figure 8.14 - Emissions characteristics for HCCI combustion of DME with varying EGR rates

Figure 8.14 demonstrates that although an initial increase in thermal efficiency was observed when increasing the EGR rate from 0% to 65%, a further increase in EGR rate to 74% resulted again in a reduction of efficiency of the engine. The highest thermal efficiency thus occurred for an EGR rate of 65%. It is thought that the initial increase in thermal efficiency may be attributed to later phasing

of ignition towards TDC, whilst the subsequent reduction in efficiency, when increase the EGR rate to 74%, may be attributed to a strong deterioration in combustion efficiency as a result of the dilution of the reactants and the lower combustion temperatures. The low combustion efficiency was suggested by a high emission of UHC, as shown in Figure 8.14. The experiments illustrated that although EGR was effective at retarding the time of ignition, high rates of EGR resulted in a deterioration of thermal efficiency of the engine due to a reduction in combustion efficiency. The size spectral density of the particulate matter in Figure 8.15 shows that mainly nucleation mode particles 5-40 nm in diameter were produced under this engine operating condition.

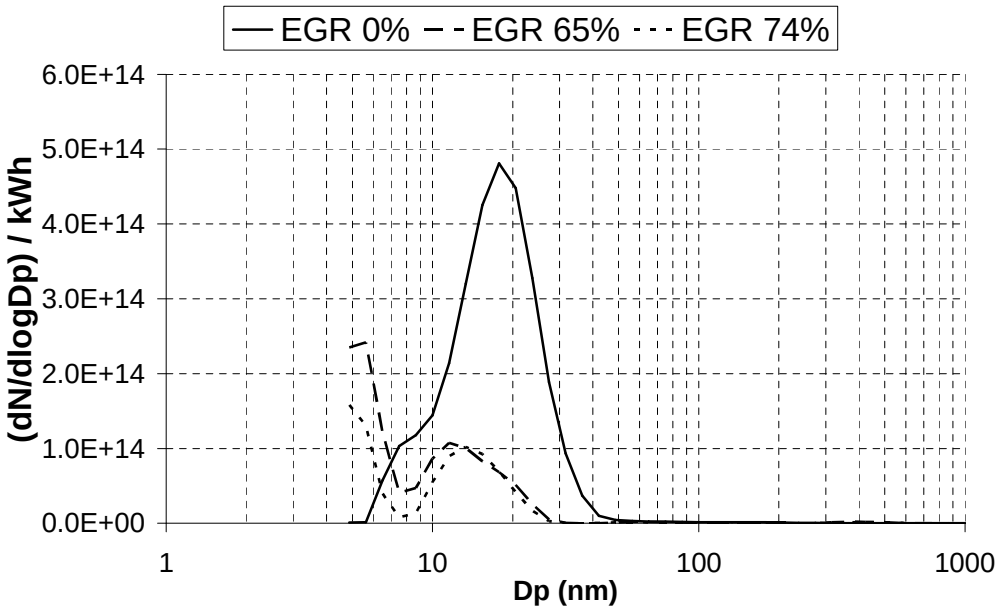

Figure 8.15 - Particulate size spectral density for HCCI combustion of DME with varying EGR rates

Particulates of that size would be expected to predominantly consist of volatile organic compounds and water droplets (Kittelson, 1998), indicating that the formation of carbonaceous soot may be largely absent under this engine operating condition with DME.

Influence of effective compression ratio controlled by inlet valve timing

The effective compression ratio of the engine may be used to control the ignition timing of HCCI combustion by changing the pressures and temperatures to which the charge is subjected during compression. This can be achieved by variation of the time of intake valve closure during the compression stroke. Compression of the charge is only achieved if the valves of the cylinder are closed. Keeping the intake valve open during the earlier stages of the compression stroke can be used to reduce the effective compression ratio of the engine, whilst simultaneously reducing the mass of gases trapped during each cycle. The effects of changing the effective compression ratio of the engine by means of late intake valve closure were studied in this series of experiments.

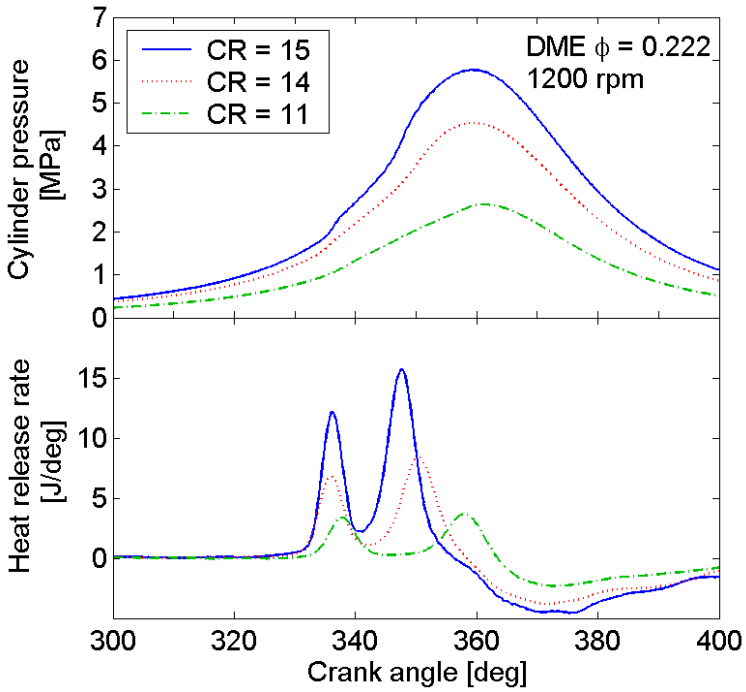

Figure 8.16 - Cylinder pressure and heat release rate for HCCI combustion of DME with varying effective compression ratio by changes in the intake valve timing

The tests were conducted at an engine speed of 1200 rpm and a constant equivalence ratio (Φ=0.222). Operation of the engine at a constant equivalence ratio implied that the engine load changed considerably amongst the individual experiments because a variation in the mass of air trapped within the combustion chamber required the amount of fuel injected into the air to vary accordingly. Operation of the engine at higher effective compression ratio thus resulted in a higher engine load than operation at lower effective compression ratio. It should be noted that since a constant intake valve opening duration of 205º CA was used in these experiments, a partial vacuum was created in the combustion chamber at the beginning of the intake stroke when retarded valve timings were used (Figure 8.17).

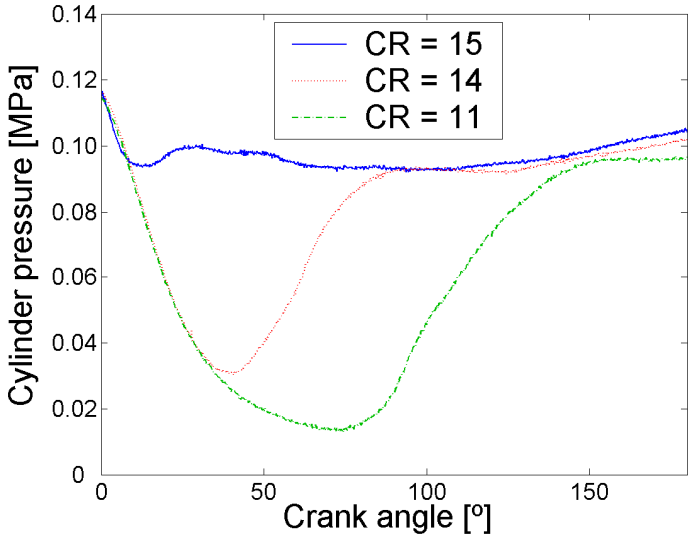

Figure 8.17 - Vacuum at the start of the intake stroke

This vacuum resulted in a reduction of the net engine load due to increased pumping work. In a practical application, this problem could be overcome by increasing opening duration of the intake valve through a valve-train with variable valve-opening duration. It was thus chosen to present values of gross IMEP for these experiments involving changes in valve timing rather than values of net IMEP. These values were also used to calculate the specific pollutant emissions of the engine. All other experiments employed values of net IMEP. The values of gross IMEP for these experiments are given in Table 8.5.

Table 8.5 - Gross IMEP for different inlet valve retardation

Compression ratio (CR)	15	14	11
Inlet valve retardation [º CA]	0	36	72
Gross IMEP [kPa]	951	487	65

The effective compression ratio of the engine was 15:1 for normal valve timing, 14:1 for a 36 º CA retardation of inlet valve timing and 11:1 for a 72 º CA retardation of inlet valve timing. The cylinder pressure traces and heat release rates of combustion are shown in Figure 8.16. It can be seen in Figure 8.16 that a reduction in effective compression ratio of the engine resulted in significantly lower combustion chamber pressures throughout the cycle. The heat release rates in Figure 8.16 show that as the effective compression ratio was lowered, the ignition timing was delayed, the peak heat release rates were reduced, and the two distinct heat release phases moved further apart from each other. Similar results have been reported by Jang and Bae (2009). The retardation in combustion timing which was incurred as a result of reduced compression ratio remained relatively small because an increase in intake charge temperature occurred simultaneously

to the reduction in compression ratio. This is because for operation with retarded intake valve timing part of the intake air was returned from the cylinder to the intake port during the period of open valve compression, after having absorbed heat from the intake valves and combustion chamber walls. A total increase in intake charge temperature from 315 K to 330 K was measured at a distance of 150 mm from the intake valves within the intake port as the compression ratio was reduced from 15 to 11. It is thought that an even more significant increase in intake air temperature would have occurred at a closer distance to the intake valves. The specific pollutant emissions and engine efficiency are shown in Figure 8.18.

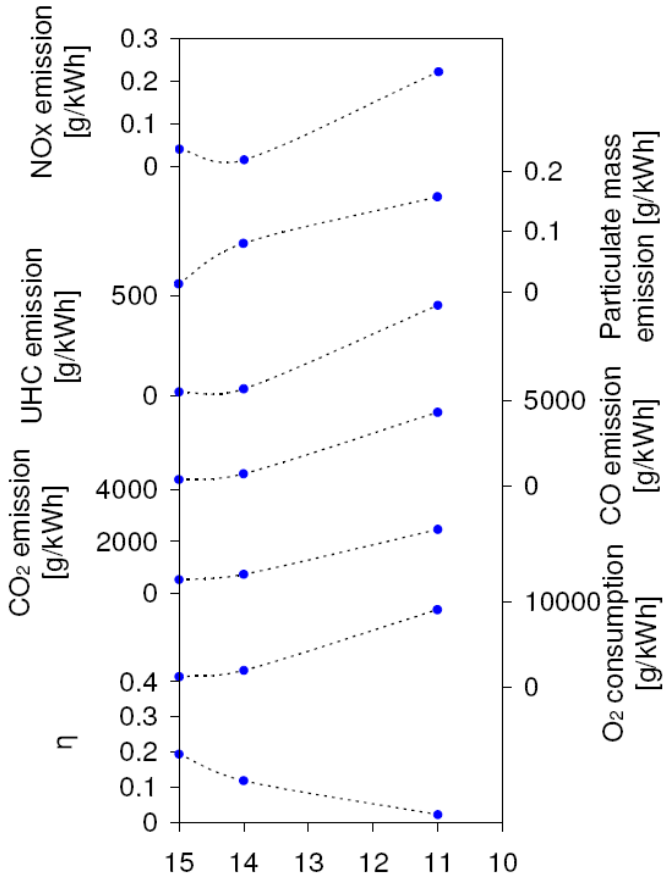

Figure 8.18 - Emissions characteristics for HCCI combustion of DME with varying effective compression ratio by changes in the intake valve timing

It can be seen that the emission of all pollutants increased as the effective compression ratio was reduced by later intake valve timing. The indicated efficiency of the engine reduced significantly as the compression ratio was reduced. The experiments demonstrate that whilst intake valve timing was moderately effective at delaying the time of ignition of the charge, it resulted in a strong reduction in thermal efficiency of the engine and higher specific emission of pollutants when a constant equivalence ratio was maintained.

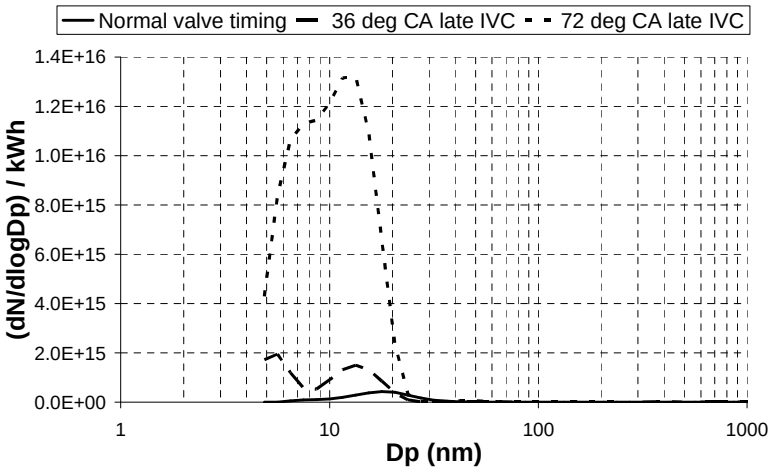

Figure 8.19 - Size spectral density of particulates for HCCI combustion of DME with varying effective compression ratio by changes in the intake valve timing

The size spectral density of the particulate matter is shown in Figure 8.19. It can be seen that the experiments produced predominantly small nucleation mode particles (5-40 nm), but no significant amount of larger particles. This could be an indication that the particles produced by the engine under these conditions consisted predominantly of volatile organic particles, and that no substantial amount of soot was formed.

8.3.3. Homogeneous charge compression ignition of dimethyl ether with vapour of methyl-tertiary butyl ether as ignition suppressant

The experiments on the molecular structure shown in section 8.3.1 demonstrated that the structure of ether molecules had a strong effect on their ignition quality under HCCI conditions. It was observed that the straight-chained ethers DME and DEE had excessively high ignition qualities, requiring large amounts of cooled EGR to retard their ignition timing towards TDC. High rates of EGR were shown to have detrimental effects on combustion efficiency in section 8.3.2, and may result in reduced thermal efficiency of the engine. Branched ethers on the contrary had low ignition qualities, and required additional heating of the intake air to achieve ignition. In the following experiment, a mixture of varying proportions of a straight-chained ether and a branched ether were used to adjust the ignition quality of the ether fuel so that ignition of the charge could be obtained around TDC without the need for EGR or intake air heating. A direct-injected homogeneous mixture of DME and methyl-tertiary butyl ether (MTBE) were premixed with air in the combustion chamber using the experimental arrangement shown in section 3.4.3 in conjunction with the experimental arrangement shown in 3.4.4 of Chapter 3. DME was injected at 25 MPa directly into the combustion chamber at the start of the intake stroke, whilst MTBE was injected at 0.3 MPa into the aspirated intake air at a

position 1.2m upstream of the intake air valves. The engine speed was 1200 rpm for all mixtures. The equivalence ratio of DME was kept constant at Φ_{DME} = 0.222 (as shown in Table 8.6), whilst the equivalence ratio of the MTBE was increased in five progressive steps from Φ_{MTBE} = 0.000 to Φ_{MTBE} = 0.073. The total equivalence ratio of DME and MTBE in combination was increased from Φ_{Total} = 0.222 to Φ_{Total} = 0.40 as the addition of MTBE was increased. The engine load was thus not constant. An overview of the engine IMEP produced by the engine under these conditions is given Table 8.6.

Table 8.6 - IMEP for different equivalence ratios of MTBE

Φ	0.00	0.0357	0.0499	0.0624	0.0727
IMEP (kPa)	88	316	363	401	391

Figure 8.20 shows the combustion chamber pressure and heat release rate histories of the combustion.

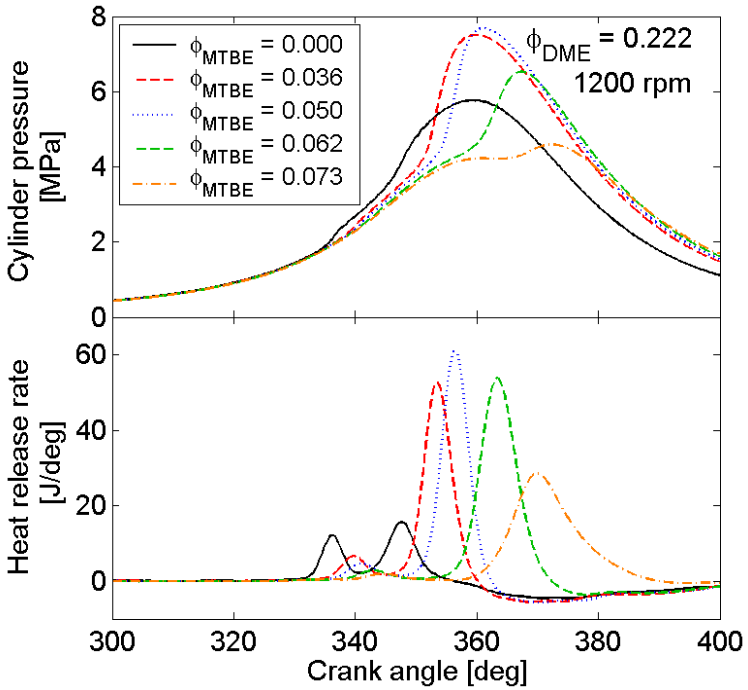

Figure 8.20 - Cylinder pressure and heat release rate for HCCI combustion of DME with varying concentration of MTBE in the intake air

Despite an incremental rise in the overall equivalence ratio from Φ_{Total} = 0.222 to Φ_{Total} = 0.40 by the addition of MTBE, the time of ignition was progressively retarded as the amount of MTBE was increased. It can be observed in Figure 8.20 that the low-temperature heat release was progressively suppressed by the addition of MTBE, whilst retardation in the high-temperature heat release phase occurred. The peak heat release rate of the high-temperature combustion phase was increased as the equivalence ratio of the MTBE was increased from Φ_{MTBE} = 0.000 to Φ_{MTBE} = 0.036 and then to

Φ_{MTBE} = 0.050, but subsequently reduced again upon a further increase of the MTBE equivalence ratio to Φ_{MTBE} = 0.062 and then to Φ_{MTBE} = 0.073. Figure 8.21 shows that the highest thermal efficiency was achieved for an MTBE equivalence ratio of Φ_{MTBE} = 0.062. It can be seen from the emission of gaseous pollutants in Figure 8.21 that for the highest two values of equivalence ratio of MTBE, which retard the combustion beyond TDC, a slight increase in the concentration of UHC was observed in the exhaust gas, indicating a deterioration of the combustion efficiency. It is thought that MTBE was responsible for eliminating radicals forming as a result of the thermal decomposition of DME molecules, thereby delaying, and finally entirely suppressing the combustion process.

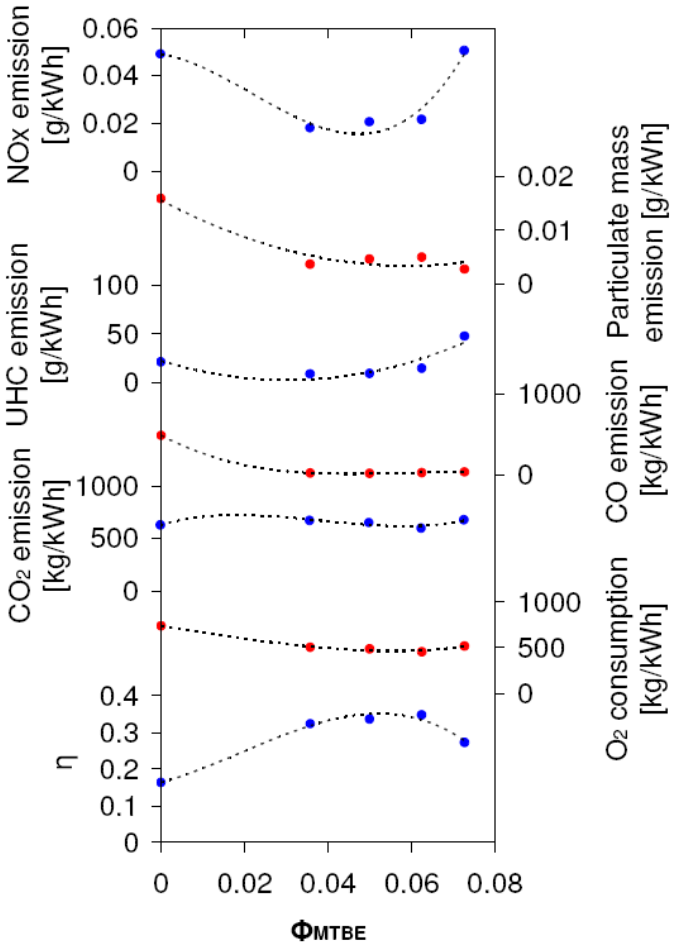

Figure 8.21 - Gaseous exhaust emissions for HCCI combustion of DME with varying amounts of MTBE

The MTBE was thus used to control the time of ignition of the charge. This suggests that a binary mixture of two ether molecules with different ignition characteristics could be used in conjunction to control the load as well as the time of ignition of the HCCI combustion of volatile ethers in an internal combustion engine. Comparison between the efficiency and pollutant emission data of these experiments with those for diffusion combustion presented in Chapters 5, 6 and 7 shows that HCCI combustion was able to achieve similarly high thermal efficiencies, whilst producing NO_x emissions

that were two orders of magnitude lower, and whilst still producing lower particulate emissions than for diffusion operation with diesel fuel.

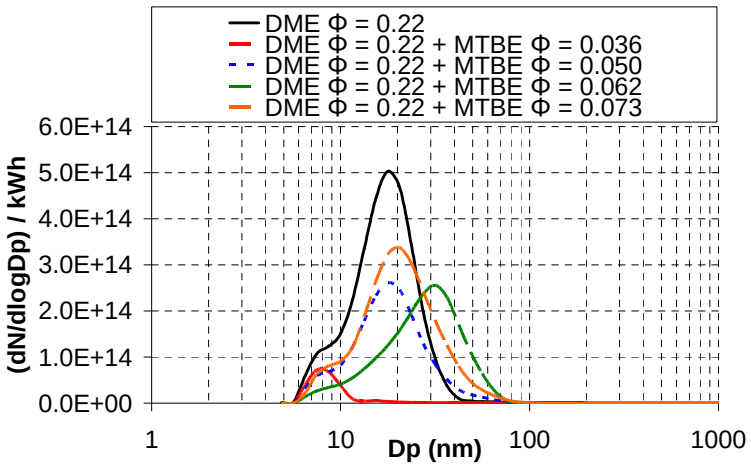

Figure 8.22 - Particulate size density for HCCI combustion of DME with varying amounts of MTBE

The particulate size spectral density in Figure 8.22 shows that the experiments produced a single mode of particles between 5 and 80 nm in diameter. UHC and CO emissions were considerably higher for HCCI combustion than for diffusion combustion.

8.3.4. Homogeneous charge compression ignition of a direct-injected binary mixture of diethyl ether and di-iso-propyl ether

The experiments presented in 8.3.3 had shown that a binary mixture of two ether molecules with different ignition characteristics could be used to control the time of ignition of HCCI combustion by separate injection at two different locations. DME was a fuel that was gaseous under atmospheric conditions. A further series of experiments was carried out to prove that liquid ethers may equally be used to achieve this type of combustion, and to prove that both fuels may be premixed to form a single fuel before being injected directly into the cylinder. Diethyl ether (DEE) and diisopropyl ether (DIPE) were mixed on a volumetric basis in six incremental steps consisting of one, two three, four and five fifths DIPE in DEE. The engine speed was 1200 rpm and the engine load was kept constant at 100 kPa. The fuel quantity injected per cycle was adjusted in each case, so that this constant engine load was achieved under all conditions. The cylinder pressure and heat release histories of the experiments are shown in Figure 8.23.

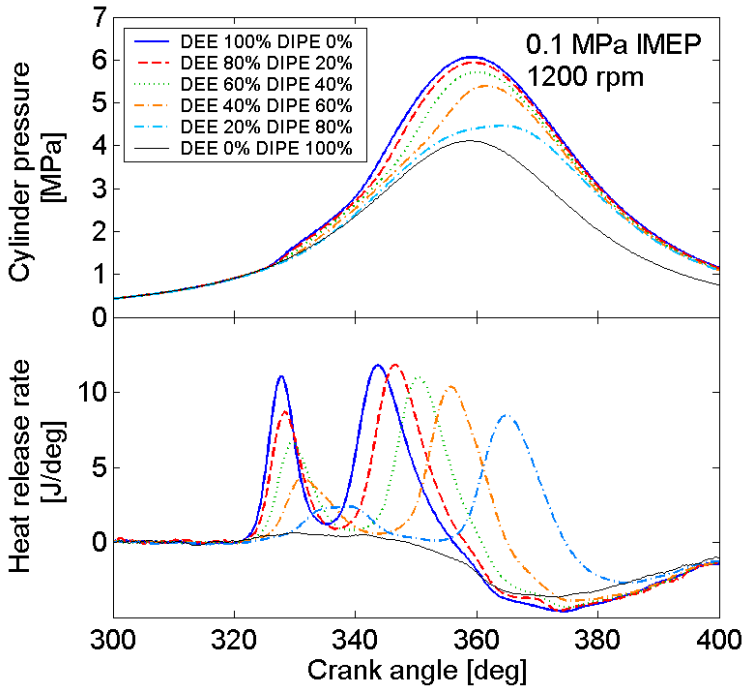

Figure 8.23 - Cylinder pressure and heat release rate for HCCI combustion of DEE with varying concentration of DIPE in the intake air

The combustion chamber pressure and heat release rates show that as the proportion of DIPE in DEE increased, the ignition was progressively retarded. An increase in the proportion of DIPE suppressed the proportion of heat released during the low temperature combustion. The value of the heat released during the later high-temperature heat-release phase remained nearly constant.

The mixture of 1/5 DEE and 4/5 DIPE by liquid volume gave the best combustion phasing for this engine with a geometric compression ratio of 15:1. As observed in section 8.3.3 for the mixtures of DME and MTBE, the combustion efficiency deteriorated slightly for mixtures containing high concentrations of the branched ether molecule. This was reflected in the increasing emission of UHC, especially for the 80% mixture of DIPE in DEE, as can be seen in Figure 8.24.

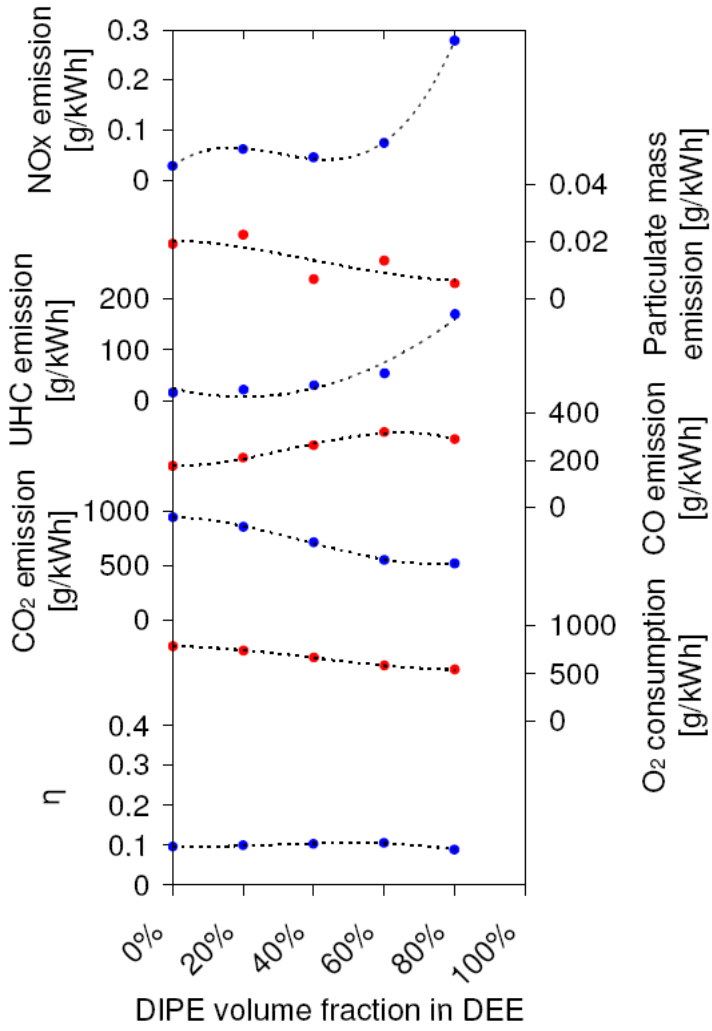

Figure 8.24 - Exhaust gas concentration for HCCI combustion of DEE and DIPE in varying proportions

The highest thermal efficiency was achieved for a mixture of 2/5 DEE and 3/5 DIPE due to the better combustion efficiency and lower emission of UHC. The thermal efficiencies measured in this series of experiments were significantly lower than for the diffusion combustion experiments presented in Chapters 5, 6 and 7 or the homogeneous charge experiments presented in sections 8.3.3. The reason for this low efficiency is thought to be the lower engine load, which has been reported to reduce efficiency considerably (Dec, 2009). The emission of particulate mass showed only little variation for the mixtures of DEE and DIPE as can be seen in Figure 8.24.

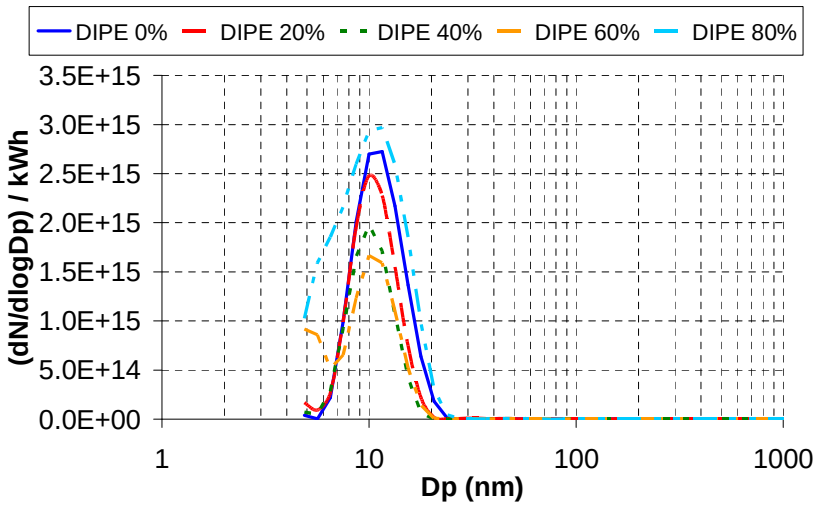

Figure 8.25 - Size spectral density of particulates for HCCI combustion of direct injected mixtures of DEE and DIPE

The particulate size spectral density depicted in Figure 8.25 illustrates that only very fine particles of the order of 5 and 30 nm diameter were generated. These are likely to have consisted of volatile organic matter rather than of carbonaceous soot. The experiments demonstrated that it was possible to control the ignition timing of HCCI combustion by varying the composition of an ether fuel consisting of a binary mixture of a straight-chained and a branched ether. The concept worked even when using liquid ethers under direct fuel injection into the combustion chamber, resulting in low NO_x and particulate emissions, with the potential for high thermal efficiencies.

8.4. Conclusions

The following conclusions can be drawn from the experiments:

1. Biodiesel appeared to be unsuitable for HCCI operation as a result of its low volatility, which entailed problems of charge preparation.
2. Acetals had significantly better HCCI combustion characteristics than biodiesel.
3. The HCCI combustion of DME in a diesel engine was able to produce virtually NO_x free exhaust gas.
4. The particulate mass emitted for direct injection HCCI combustion of either DME or diesel fuel was always slightly higher than that of the same fuel in diffusion combustion mode. This is thought to have been a result of poor charge preparation. The HCCI combustion of DME produced less particulate mass than the diffusion combustion of diesel fuel with the added advantage of very low NO_x levels.

5. Cooled EGR was used to control the ignition timing of a homogeneous charge of ethers and air. The main drawback was a deterioration of combustion efficiency for very high rates of EGR.
6. A change in the effective compression ratio was used to control the ignition timing of a homogeneous charge of DME and air in HCCI combustion.
7. The molecular structure of ethers had an important influence on their ignition and combustion characteristics. An increase in the alkyl chain length of ethers lead to an increase in ignition quality of the molecule, whilst branching of the alkyl chain lead to a severe reduction of ignition quality.
8. A binary mixture of two volatile ethers of different ignition quality, which resulted from their differences in molecular structure, was successfully used to control the ignition timing of HCCI combustion in a diesel engine.

Chapter 9. Summary, conclusions, claims of originality and recommendations for future work

9.1. Summary and conclusions

An investigation into the influence of the molecular structure of various types of biofuels on the combustion process in compression ignition engines was carried out. Experimental studies were conducted on fatty acid monoalkyl esters, acetals, alcohols and ethers as potential biofuels. Particular attention was given to the development of heat release from the combustion process, and the formation of NO_x and other gaseous pollutant emission, as well as particulate matter. The experiments were conducted under diffusion combustion conditions, which are typical of traditional diesel engines, as well as under homogeneous charge compression ignition combustion conditions, which may see future application in internal combustion engines. It was observed in both instances that the molecular structure of biofuels could be used to control the combustion process. Detailed conclusions regarding the experiments are presented in the ensuing sections.

Conclusions regarding the combustion of fatty acid monoalkyl esters under diesel engine conditions

The influence of the molecular structure of fatty acid monoalkyl esters on their combustion characteristics in a direct injection diesel engine was studied experimentally. The concept of the experimental study was to record the combustion of a sample of a single fatty acid monoalkyl ester at a time, and to systematically vary the molecular structure of this single-molecule fuel, to resolve the effects of specific structural characteristics. This allowed studying the effect which the length of the fatty acid moiety had on their combustion, the effect which the number of double bonds in the fatty acid moiety had on their combustion, and the effect which the length of the alcohol moiety had on their combustion.

The results showed that the ignition delay of the fuel molecules was strongly affected by the molecular structure of individual fatty acid monoalkyl ester molecules. Increasing the length of the fatty acid moiety, increasing saturation of the fatty acid moiety and an increasing the length of the alcohol moiety, all decreased the ignition delay.

The formation of NO_x during the diesel combustion process was found to be controlled by several, layered effects. The most dominant role was that of ignition delay of the fuel molecules, which determined the relative amounts of heat released during the premixed combustion phase and during the diffusion controlled combustion phases. A higher degree of premixed combustion was observed to strongly increase NO_x formation. The secondary effect was that of adiabatic flame temperature, which only became clearly visible once the effect of ignition delay was removed. The adiabatic

flame temperature depended on the structure of the molecules. The theoretical adiabatic flame temperature at Φ=1 and constant pressure with no dissociation was found to correlate with the measured specific concentration of NO_x in the exhaust gas when the ignition delay was constant. The effect of soot radiative heat transfer may have played a role of tertiary grade in the formation of NO_x in the present experiments. The experiments indicated that the relative importance on NO_x emissions between the influence of the adiabatic flame temperature and the influence of the premixed burn fraction shifted towards the adiabatic flame temperature as the ignition delay became shorter. This implied that for fuels of higher ignition quality, the adiabatic flame temperature played a more significant role in governing the formation of NO_x.

According to current literature (Graboski, et al., 2003), molecules with shorter fatty acid chains were known to produce more NO_x in diesel combustion than molecules with longer fatty acid chains. It was observed in these experiments that the reason for this was the longer ignition delay of the shorter chain fatty acid molecules. The experiments showed that if the ignition delay was equalised for all molecules, shorter fatty acid chains in biodiesel molecules actually produced less NO_x, due to their lower adiabatic flame temperature.

The experiments showed that the number of double bonds present in the fatty acid moiety of the molecules was strongly correlated with the emission of accumulation mode soot particles. It was observed that the specific particulate number concentration of nucleation mode particles in the exhaust gas correlated well with the boiling points of the individual fatty acid methyl ester molecules. This observation gave some indication that the high number of nucleation mode particles, produced by the diesel combustion of fatty acid methyl ester molecules, may have consisted predominantly of liquid fuel.

Conclusions regarding the combustion of acetal molecules under diesel engine conditions

The influence of molecular structure of acetals on their combustion behaviour in a direct injection diesel engine was studied experimentally. Two consecutive series of engine experiments were carried out to complement each other. The results showed that the molecular structure of the acetal molecules influenced their ignition delay. Increasing the length of the lateral moieties strongly decreased the ignition delay of the acetals. Branching the lateral moieties of the acetals strongly decreased their ignition delay. The addition of a central moiety to the acetals decreased ignition delay. Changing the central moiety of from a branched configuration to a straight configuration decreased the molecule's ignition delay. Increasing the length of the central moiety decreased ignition delay. The lateral moieties appeared to have the strongest effect on ignition quality, which may suggest that the reactivity of acetals relies largely on decomposition via the lateral moieties of the molecules.

The results showed that acetal molecules produced significantly lower amounts of particulate matter than fossil diesel fuel under all experimental conditions used. Under conditions of constant ignition

delay, acetal molecules tended to produce marginally higher amounts of NO_x than fossil diesel fuel. This was predominantly attributed to the faster heat release of acetals with respect to fossil diesel fuel, which could be due to faster fuel-air mixing of the acetals, as a result of their higher volatility. It is possible that reduced soot-radiative heat transfer in the flames of the acetals may also have contributed to the increase in NO_x emissions.

The adiabatic flame temperature of acetal molecules generally tended to be lower than that of fossil diesel fuel, and depended in detail on their molecular structure. Branching of the lateral moieties strongly increased the adiabatic flame temperature of the acetals. The addition of a central moiety to the acetal molecules strongly increased their adiabatic flame temperature. Changing the central moiety from a branched configuration to a straight configuration slightly decreased the adiabatic flame temperature. Increasing the length of the central moiety slightly increased the adiabatic flame temperature.

Conclusions regarding the combustion of ethers and alcohols under diesel engine conditions

In an attempt to investigate the effect of molecular structure of various potential biofuels that could be produced from synthesis gas, a series of investigations were conducted. The fuels consisted of four oxygenated molecules of the same number of carbon, hydrogen and oxygen atoms $C_{10}H_{22}O$, DME as well as four ethers and glymes of varying molecular mass. The results can be summarised as follows: All oxygenated molecules of the common sum-formula $C_{10}H_{22}O$ produced lower NO_x emissions than the fossil diesel fuel under all tested experimental conditions. DME produced higher NO_x emissions than fossil diesel fuel. This was attributed to higher peak cylinder temperatures as a result of faster fuel-air mixing of DME compared to diesel fuel. All oxygenated molecules produced lower total particulate mass emissions than diesel fuel. The combustion of DME appeared to result in soot-less combustion. For the combustion of DME in particular, an increase in the fuel injection pressure from 25 MPa to 40 MPa lead to a significant increase in the peak heat release rate for DME and diesel fuel, which was accompanied by a significant increase in NO_x concentration. No significant changes in particulate mass concentration from the combustion of DME were observed when increasing the fuel injection pressure from 25 MPa to 40 MPa. The addition of an alkyl ester lubricity additive to DME in concentrations ranging from 50-5000 ppm contributed to the emission of small nucleation mode particles (around 5-40 nm in diameter). The experiments suggested that these particles may consist of droplets of this additive condensing in the exhaust gas. Droplets from the engine lubricant oil may also have contributed to the formation of nucleation mode particles. The molecule diethyl ether was observed to have similarly good combustion characteristics as DME, with the added advantage of being liquid under atmospheric conditions.

Conclusions regarding the combustion of biofuels under HCCI combustion conditions

Several potential biofuels were tested under HCCI combustion conditions. The experiments indicated that the production of synthetic biofuels might allow designing biofuels with characteristics that are suitable for HCCI combustion. The experiments showed that direct-injection HCCI combustion with high thermal efficiency and low emission of NO_x and particulates was possible with fuels of high volatility, such as ethers of low molecular mass, and potentially, with acetals of low molecular mass. Fuels with low volatilities such as biodiesel or conventional diesel fuel resulted in poor fuel-air mixing through slow evaporation of the fuel, and caused high amounts of fuel impingement on the combustion chamber walls. This led to unacceptably high particulate emissions.

The most volatile ether, DME, emitted virtually no NO_x emissions under HCCI operating conditions, whilst also producing relatively low particulate emissions. The main drawback when using DME as HCCI fuel in conjunction with the compression ratio of 15:1 of this engine was excessively early fuel ignition. This resulted in poor combustion phasing. Changing the effective compression ratio through late intake valve closure was used to control the ignition timing of DME HCCI combustion to some extent. However, as a result of considerable heat transfer from the engine to the fresh intake air under conditions of late intake valve closure, this method of controlling the combustion phasing was relatively ineffective. Cooled EGR could be used more successfully to control the ignition timing in HCCI combustion mode. The main drawback was a deterioration of combustion efficiency for high rates of EGR. The experiments showed that the molecular structure of the fuels could be used successfully to control their time of ignition under HCCI operating conditions. A binary mixture of two volatile ethers of different molecular structure, and thus of ignition qualities, was successfully used to control the time of ignition of HCCI combustion. Controlling the time of ignition through the ignition quality of the fuel resulted in high engine efficiency due to improved combustion phasing. The ignition quality of the fuels was thus adjusted via the molecular composition of the fuel.

9.2. Claims of originality

In order to carry out experiments with high fuel injection pressures (>100 MPa) with small quantities of fuels, a novel type of fuel injection system has been designed built, and used in experiments on the influence of molecular structure on diesel combustion. A follow-on EPSRC-funded Ph.D. project ('CASE' award) has already started at UCL, which uses this novel injection technique as basis for the experiments.

According to current literature (Graboski, et al., 2003), fatty acid monoalkyl ester molecules with shorter fatty acid moieties produce more NO_x in diesel combustion than fatty acid monoalkyl ester molecules with longer fatty acid moieties. The experiments presented in this chapter showed that the reason for this higher emission of NO_x was their longer ignition delay (Figure 5.3). It was demonstrated that if the ignition delay was equalised for all molecules, fatty acid monoalkyl ester molecules with shorter fatty acid moieties actually produced less NO_x than those with longer fatty acid moieties, due to their lower adiabatic flame temperatures.
The theoretical adiabatic flame temperature of the fuel molecules at $\Phi = 1$ and constant pressure with no dissociation, was found to correlate well with the measured emission of NO_x when the ignition delay was constant (Figure 5.24).

The sponsor company BP has filed a patent application on the reduction of NO_x emissions using short-chained fatty acid alkyl ester molecules in conjunction with a cetane improving additive such as 2-EHN, based on the findings outlined in Chapter 5 of this thesis.

'Use, method and composition'.

Applicant:	BP Oil International Limited [GB]	
Inventors:	Allan, R. E. (BP Oil UK Limited Technology Centre)	
	Schonborn, A. (University College London)	
Application:	European Patent Office	
Patent №:	EP20071006 (A1)	(Published 17th June 2009)
Appl. №:	07254679.9 – 1213	(Date: 03.12.07)
	07254964.5 – 1213	(Date: 19.12.07)

The first study conducted on acetal molecules had suggested that it was possible to control the ignition quality of acetal fuels through their molecular structure. The molecule 3-methyl-1-(3-methylbutoxymethoxy)butane (which does not have a registered CAS number) was designed for the second study, to provide an obstruction to thermal decomposition, and to exhibit a lower cetane number than other molecules of the same sum formula $C_{11}H_{24}O_2$ (i.e. 1,1-Dibutoxypropane & 2,2-dibutoxypropane). This provided a more adequate ignition temperature of this fuel molecule under HCCI operation than the other two molecules, and thereby resulted in increased thermal efficiency under HCCI operation.

Experiments were conducted which showed that the molecular structure of ethers could be used systematically to control the ignition quality of the molecules under HCCI operation. This was demonstrated using the molecules dimethyl ether (DME), diethyl ether (DEE) and diisopropyl ether (DIPE). The ensuing experiments showed that the molecular composition of an ether fuel could be used systematically to control the ignition phasing of an ether-air mixture under HCCI operating conditions. This was demonstrated using binary mixtures of DME with methyl-tert buty ether (MTBE) and DEE with DIPE. An internal combustion engine which was able to control the molecular structure of the ether fuel at its disposition, could, as demonstrated in the described experiments, govern the time of ignition of HCCI combustion through the molecular composition of the ether fuel.

Three peer-reviewed papers written on the basis of the work conducted during this project have been accepted for publication by the time this thesis was written:

1. Schönborn A., Ladommatos N., Williams J., Allan R., Rogerson J. (2007). Effects on Diesel Combustion of the Molecular Structure of Potential Synthetic Biofuel Molecules. SAE technical paper, No. 2007-24-0125, 2007.
2. Schönborn A., Ladommatos N., Allan R., Williams J., Rogerson J. (2008). Effect of the molecular structure of individual fatty acid alcohol esters (biodiesel) on the formation of NO_x and particulate matter in the Diesel combustion process. SAE technical paper, No. 2008-01-1578; also published as: SAE International Journal of Fuels and Lubricants. 1 (1) 2009, pp. 849-872.
3. Schönborn A., Ladommatos N., Williams J., Allan R., Rogerson J. (2009). The influence of molecular structure of fatty acid monoalkyl esters on Diesel combustion. Combustion and Flame, 156 (7), pp.1396-1412.

Papers on the combustion of acetal fuels and the nanoparticle emission of DME are in preparation.

9.3. Recommendations for future work

A multitude of questions have arisen during th is work, which remain unanswered. The possibilities of investigating new types of fuel molecules remain largely unexplored. The following paragraph is aimed at providing recommendations for further work, based on the observations made during the experiments presented herein.

Further investigations into how the molecular structure of alkyl esters affects combustion could be used to improve the combustion characteristics of biodiesel fuels. The structure of the alcohol moiety of the molecules leaves further room for investigation. The work presented herein only provided a brief investigation into the effect of the alcohol moiety on the combustion behaviour of fatty acid alkyl esters. The development of the production of alcohols from cellulose using synthesis gas formation (Corrain, et al., 1992; Qiu, et al., 2004; Hu et al., 2007) or biochemical synthesis (Qureshi 2008, Krouwel et al. 1982) as production pathways are expected to provide a supply of alcohols of higher molecular mass as raw material for biofuels. The effects of using such alcohols of higher molecular mass in the production of fatty acid alcohol esters (biodiesel) could be explored in engine experiments. Furthermore, the effect of adding a hydroxyl group to the fatty acid moiety of biodiesel molecules could be studied. Hydroxyl groups would be present in the fatty acid moiety of biodiesel molecules, when using ricinoleic acid as raw material for the production of biodiesel. Ricinoleic acid is an important constituent of the esters present in castor oil. It would be of interest to explore the effects of adding one, two or more hydroxyl groups, and to vary the respective position of this group along the fatty acid moiety chain.

The present work has indicated that the nucleation mode nanoparticles of diameters ranging from 5-30 nm consist predominantly of volatile hydrocarbons. Little agreement has so far been reached on the mechanisms and composition of these particles (Tobias, et al., 2001; Kirchner, et al., 2009; Arcoumanis, et al., 2008). Optical examination of the particulate matter produced by the combustion of DME had suggested that the particulate matter produced during operation on DME consisted almost entirely of engine oil and lubricity-improving additive. Further experiments in which this particulate matter is collected during motoring of the engine and during engine firing of the engine could provide further insights into the mechanism involved in their formation. The experiments could be augmented by spray experiments with DME with lubricity-improving additive in a spray chamber.

The development of further liquid biofuel molecules with high volatility and an ignition quality suitable for HCCI operation in high compression ratio engines, such as the molecule 3-methyl-1-(3-methylbutoxymethoxy)butane which was developed for its lower ignition quality, should be further pursued. The charge preparation and effects of fuel volatility on charge-preparation of such fuels could be visualised in an optically accessible spray chamber or engine.

References:

Alseda, D. Montagne, X. Dagaut, P., 2007. Homogeneous charge compression ignition: formulation effect of a Diesel fuel on the initiation and the combustion - Potential of acetals impact in a Diesel base fuel. SAE technical paper, No. 2007-24-0018.

Amann, C.A. Siegla, D.C., 1981. Diesel Particulates - What They Are and Why. Aerosol Science and Technology. 1 (1), pp.73-101.

Anand, R. Mahalakshmi, N.V., 2008. Simultaneous reduction of NOx and smoke from a direct-injection diesel engine with exhaust gas recirculation and diethyl ether, Proc. Inst. Mech. Eng. Part D, J. Automobile Engineering, 221: (1), pp. 109-116.

Aoyagi, Y. Kamimoto, T. Matsui, Y. Matsuoka, S., 1980. A Gas Sampling Study on the Formation Processes of Soot and NO in a DI Diesel Engine. SAE technical paper, No. 800254; SAE Transactions, vol. 89, 1980.

Arcoumanis, C. Bae, C. Crookes, R. Kinoshita, E., 2008. The potential of di-methyl ether (DME) as an alternative fuel for compression-ignition engines: A review. Fuel, 87 (7), pp.1014-1030.

Atsumi, S. Hanai, T. Liao, J.C., 2008. Non-fermentative pathways for synthesis of branched-chain higher alcohols as biofuels. Nature. 451 (3), pp.86-89. [doi:10.1038/nature06450]

Atsumi, S. Liao, J.C., 2008. Metabolic engineering for advanced biofuels production from Escherichia coli. Current opinion in Biotechnology. 19 (5), pp.414-419.

Balachandran, R., 2006. Port fuel injector calibration. Private communication. 11th May.

Ban-Weiss, G.A. Chen, J.Y. Buchholz, B.A. Dibble, R.W., 2007. A numerical investigation into the anomalous slight NOx increase when burning biodiesel; A new (old) theory, Fuel Processing Technology, 88 (7), pp.659-667.

Baumert, K.A., Herzog, T. Pershing, J., 2005. Navigating the Numbers: Greenhouse gas data and international Policy. Washington, USA: World Resources Institute. ISBN 1-56973-599-9. Available at: http://www.wri.org/publication/navigating-the-numbers [Accessed 25th May, 2009]

Benson, S.W., 1960. The Foundations of Chemical Kinetics. New York, USA: McGraw-Hill Book Company.

Bertola, A. Boulouchos, K., 2000. Oxygenated Fuels for Particulate Emissions Reduction in Heavy-Duty DI-Diesel Engines with Common-Rail Fuel Injection. SAE technical paper, No. 2000-01-2885.

BOC chemical company, 2000. Special gases data safety sheet for dimethyl ether. Product MSDS No. 302-00-0015BOC(U), Version 1.01., Manchester, UK: BOC.

Boehman, A.L. Song, J. Alam, M., 2005. Impact of Biodiesel Blending on Diesel Soot and the Regeneration of Particulate Filters. J. Energy & Fuels, 19 (5), pp.1857-1864.

Boerrigter, H., 2005. Large scale production of Fischer-Tropsch diesel from biomass. In: Synthetic Biofuels: Technologies, potentials, prospects, Wolfsburg, Germany, 3rd-4th November, 2004. Münster, Germany: Landwirtschaftsverlag. ISBN-3-7843-3346-X..

Bone, J., 2008. UN peacekeeper killed in Haiti riots over food prices. The Times, London, 14th April.

Bönnhof, K. Obenaus, F., 1979. Dieselkraftstoff. German patent publication No. 2911411, Filed on 23rd March 1979, Published 25th September 1980.

Bornemann, H. Scheidt, F. Sander, W., 2002. Thermal Decomposition of 2-Ethylhexyl Nitrate (2-EHN). J Chem. Kinet., 34, pp.34–38.

Bridgwater, A.V., 2003. Renewable fuels and chemicals by processing of biomass. Chemical Engineering Journal, 91 (2–3), pp.87–102.

Bruwer, J.J. van Boshoff, B.D. Hugo, F.J.C. du Plessis, L.M. Fuls, J. Hawkins, C. van der Walt, A.N. Engelbrecht, A., 1980. Sunflower Seed Oil as an Extender for Diesel Fuel in Agricultural Tractors. In: Symposium of the South African Institute of Agricultural Engineers, 11th June.

Bueno, A. C. Gonçalves, J. A. Gusevskaya, E. V., 2007. Palladium-catalyzed oxidation of primary alcohols: Highly selective direct synthesis of acetals, Applied Catalysis, A: General, 329, pp.1–6.

Cambustion Instruments, 2004. DMS500 Fast Particulate Spectrometer: User Manual. Version 2.0. Cambridge, United Kingdom: Cambustion Ltd.

Canaan, R. E. Dec, J. E. Green, R. M. Daly, D. T., 1998. The Influence of Fuel Volatility on the Liquid-Phase Fuel Penetration in a Heavy-Duty D.I. Diesel Engine. SAE technical paper, No. 980510, 1998.

Capeletti, M.R. Balzano, L. de la Puente, G. Laborde, M. Sedran, U., 2000. Synthesis of acetal (1,1-diethoxyethane) from ethanol and acetaldehyde over acidic catalysts. Applied Catalysis, A: General, 198 (1-2), Letters, pp.1-4.

Carlowitz, O., 2005. Die CUTEC-Btl-Versuchsanlage zur Herstellung biogener Kraftstoffe. In: Synthetic Biofuels: Technologies, potentials, prospects, Wolfsburg, Germany, 3rd-4th November, 2004. Münster, Germany: Landwirtschaftsverlag. ISBN-3-7843-3346-X.

Çengel, Y. A., Boles, M. A., 1998. Thermodynamics: An Engineering Approach. 3rd edition. New York, USA: McGraw-Hill. ISBN-0-07-115247-4.

Chancellor, W.J. Raubach, N., 1981. Vegetable Oil Methyl Esters for Fuel. In: Alcohol and Vegetable Oil as alternative Fuels, 7th-9th April 1981 Raleigh, NC, USA, pp.267-273.

Charpentier, R. Mimoun, H., 1978. Préparation de dérivés carbonylés par oxidation d'alcools par l'oxygène moléculaire [Preparation of carbonyl compounds via the oxidation of alcohols with molecular oxygen]. French patent application No. 7815671. Publication No. 2460907. Filed on 24th May 1978. Published 30th January 1981. [Equivalent UK patent: Manufacture of carbonyl compounds, Patent No. GB2022582 (A), 1978].

Chavanne, C.G., 1937. Procédé de transformation d'huiles végétales en vue de leur utilisation comme carburants. [Process for the transformation of vegetable oils with regard to their utilisation as fuels]. Brevet d'invention / Octrooibewijs No. 422877. [Belgian patent No. 422877]. Brussels, Belgium 1937.

Chavanne, G., 1943. Sur un Mode d'Utilisation Possible de l'Huile de Palme à la Fabrication d'un Carburant Lourd [On a method of possible utilization of palm oil for the manufacture of a heavy

fuel. original text in French, no translation found]. Bulletin de la Société Chimique de France. 5éme serie,10 (1-2), pp.52–58.

Cheng, A.S. Upatnieks, A. Mueller, C.J., 2006. Investigation of the impact of biodiesel fuelling on NO_x emissions using an optical direct injection Diesel engine. Int. J. Engine Res., Vol. 7.

Cheng, A.S. Damm, C.J. Sawyer, R.F. Dibble, R.W. Lucas, D. Koshland, C.P., 2001. The effect of oxygenate-in-diesel blends and Fischer-Tropsch diesel on particulate matter emissions from compression-ignition engines. In: Proceedings of the Second Joint Meeting of the U. S Sections of the Combustion Institute, Oakland, March, Session 6, paper 10.

Cheng, A.S. Dibble, R.W. Buchholz, B.A., 2002. The effect of oxygenates on diesel engine particulate matter. SAE technical paper, No. 2002-01-1705.

Cheng, A.S. Upatnieks, A. Mueller, C.J., 2006. Investigation of the impact of biodiesel fuelling on NOx emissions using an optical direct injection Diesel engine. Int. J. Engine Research, 7 (4), pp.297-318.

Choi, C.Y. Bower, G.R. Reitz, R.D., 1997. Effects of Biodiesel Blended Fuels and Multiple Injections on D.I. Diesel Engine. SAE technical paper, No. 970218.

Choi, C.Y. Reitz, R.D., 1999. An experimental study on the effects of oxygenated fuel blends and multiple injection strategies on DI diesel engine emissions. Fuel, 78 (11), pp.1303-1317.

Choi, M.Y. Hamins, A. Mulholland, G.W. Kashiwagi, T., 1994. Simultaneous optical measurement of soot volume fraction and temperature in premixed flames. Combustion and Flame, 99 (1), pp.174-186.

Corain, B. Basato, M. Zecca, M. Braca, G. Raspolli-Galletti, A.M. Lora, S. Palma, G. Guglielminotti, E., 1992. Direct synthesis of alcohols from n-olefins and syngas in the liquid phase catalyzed by rhodium supported on crosslinked acrylic resins. Journal of Molecular Catalysis, 73, pp.23-41.

D'Amore, M.B. Manzer, L.E. Miller, E.S. Dicosimo, R. Knapp, J.P., 2007. Process for making dibutyl ethers from aqueous 1-butanol. United States Patent Application. Application No. 11/818,353, Publication No. US2009/0036716 A1. Filed 13th June 2007, Published 5th February 2009.

Dec J. E., Espey C., 1998. Chemiluminescence Imaging of Autoignition in a DI Diesel engine. SAE technical paper, No. 982685.

Dec, J.E. Canaan, R.E., 1998. PLIF Imaging of NO Formation in a DI Diesel Engine. SAE technical paper, No. 980147.

Dec, J.E. Espey, C., 1995. Ignition and early soot Formation in a DI Diesel Engine Using Multiple 2-D Imaging Diagnostics. SAE technical paper, No. 950456; SAE Transactions, 104 (3), pp.853-875.

Dec, J.E., 1997. A Conceptual Model of DI Diesel Combustion Based on Laser-Sheet Imaging, SAE technical paper, No. 970873.

Dec, J.E., 2009. Advanced compression-ignition engines - understanding the in-cylinder processes. Proceedings of the Combustion Institute, 32 (2), pp.2727-2742.

Delfort, B. Marchal, R., 2007. Procédé de transformation de biomasse en produits renfermant des groupements acetals et leur utilisation comme biocarburants. French Patent FR2921385 (A1).

Delichatsios, M.M., 1972. The Kinetics of CO Emissions from an Internal Combustion Engine. Science Masters Thesis, Massachusetts Institute of Technology, Cambridge, MA, USA, June 1972.

Dellis, P. Arcoumanis, C., 2004. Cavitation development in the lubricant film of a reciprocating piston-ring assembly. Proceedings of the Institution of Mechanical Engineers, Part J: Journal of Engineering Tribology. 218 (3), pp.157-171.

Diesel, R., 1892. Arbeitsverfahren und Ausführungsart für Verbrennungskraftmaschinen [Working process and its realisation for combustion engines]. German patent No. 67207, filed on 28th February, 1892. Approved 23th February 1893.

Diesel, R., 1893 a. Theory and construction of a rational heat Motor. Translated from German by Bryan Donkin, E. & F.N. Spon, London, New York, 1894. [Original text: Diesel R., 1893. Theorie und Konstruktion eines rationellen Wärmemotors. Berlin, Germany: Springer]

Diesel, R., 1893 b. Verbrennungskraftmaschine mit veränderlicher Dauer der unter wechselndem Überdruck stattfindenden Brennstoffeinführung [Combustion engine with introduction of fuel over a variable duration and under variable overpressures]. German patent No. 82168, filed on 30th November, 1893. Approved 12th July 1895.

Diesel, R., 1912. The Diesel Oil-Engine and its industrial importance particularly for Great Britain. Proceedings of the Institution of Mechanical. Engineers, Parts 1-2, pp.179-280.

Diesel, R., 1913. Die Entstehung des Dieselmotors. Berlin, Germany: Verlag von Julius Springer.

Dobbins, R.A. Fletcher, R.A. Chang, H.-C., 1998. The Evolution of Soot Precursor Particles in a Diffusion Flame. Combustion and Flame, 115 (3), pp.285-298.

Dolan, D.F. Kittelson, D.B., Whitby, K.T., 1975. Measurements of diesel exhaust particle size distributions, ASME paper, Winter annual meeting of the American power conference, 5, 1975.

Duport, R., 1946. Étude sur la Température d'Auto-Inflammation des Combustibles pour Moteurs Diesel [Study on the auto-ignition temperature of fuels for Diesel engines , original text in French, no translation found]. Oléagineux, 3, pp149-153.

Egnell, R., 2001. Comparison of Heat Release and NOx Formation in a Diesel Engine Running on DME and Diesel Fuel. SAE technical paper, No.2001-01-0651.

Ejim, C.E. Fleck, B.A. Amirfazli, A., 2007. Analytical study for atomization of biodiesels and their blends in a typical injector: Surface tension and viscosity effects. Fuel, 86 (10-11), pp.1534-1544.

Elliott, M.A. Hurn, R.W. Trimble, H.M., 1955. Autoignition of fuels in a constant-volume bomb: Effects of operating variables and fuel structure. Proceedings of the American Petroleum Institute, 35 (3), pp.361-373.

Emel'yanov, V.E. Deineko, P.S. Nikitina, E.A. and Grebenshchikov, V.P., 1991. Methyl tert-butyl ether as a component of aviation gasolines. Chemistry and Technology of Fuels and Oils, 27 (9), pp.484-486.

Espey, C. Dec, J.E. Litzinger, T.A. Santavicca, D.A., 1994. Quantitative 2-D Fuel Vapour Concentration Imaging in a Firing D.I. Diesel Engine Using Planar Laser-Induced Rayleigh Scattering, SAE technical paper, No. 940682.

Espey, C. Dec, J.E. Litzinger, T.A. Santavicca, D.A., 1997. Planar Laser Rayleigh Scattering for Quantitative Vapour-Fuel Imaging in a Diesel Jet. Combustion and Flame, 9 (1-2), p.65-78.

European Biodiesel Board, 2006. EU Biodiesel production growth hits record in 2005: EBB publishes annual Biodiesel production statistics. Brussels, Belgium: European Biodiesel Board press release, 25th April. Available at: http://www.ebb-eu.org/EBBpressreleases/EBB%20press%20release%202005%20statistics%20(final).pdf [Accessed 25th May 2009]

European Committee for Standardization, 2004. Automotive fuels —Diesel — Requirements and test methods. EN 590:2004. London, UK: British Standards Institution.

European parliament and council of the European union, 2009. Directive 2009/28/EC of the European parliament and of the council of 23 April 2009 on the promotion of the use of energy from renewable sources and amending and subsequently repealing Directives 2001/77/EC and 2003/30/EC. Official Journal of the European Union. English edition, L140, 16. ISSN 1725-2555, 5th June. Available at: http://eur-lex.europa.eu/LexUriServ/LexUriServ.do?uri=OJ:L:2009:140:0016:0062:EN:PDF [Accessed 29th June 2009]

Fenimore, C.P., 1971. Formation of nitric oxide in premixed hydrocarbon flames. In: 13th Symposium (International) on Combustion, pp.373-379, The Combustion Institute, Pittsburgh, PA, USA.

Fischer, F. Tropsch, H., 1926. Über die direkte Synthese von Erdölkohlenwasserstoffen bei gewöhnlichem Druck. [About the synthesis of petroleum hydrocarbons at ordinary pressure]. 1. Mitteilung, Ber. Dtsch. Chem. Ges., 59, pp.830-831.

Fischer, F. Tropsch, H., 1926. Über die direkte Synthese von Erdölkohlenwasserstoffen bei gewöhnlichem Druck. [About the synthesis of petroleum hydrocarbons at ordinary pressure]. 2. Mitteilung, Ber. Dtsch. Chem. Ges., 59, pp.832-836.

Fischer, F., 1924. Die Umwandlung der Kohle in Öle. Berlin, Germany: Borntraeger. [Original text in German, English Translation by R. Lessing: F. Fischer, 1925. The Conversion of Coals into Oils. London, UK: Ernst Benn Limited]

Fischer, F., 1930. Über die Entwicklung unserer Benzinsynthese aus Kohlenoxyd und Wasserstoff bei gewöhnlichem Druck, Brennstoff-Chem., 11 pp.489-501.

Fischer, F., 1932. Kenntniss der Kohle. Berlin, Germany: Gebrüder Bornträger.

Fleisch, T. McCarthy, C. Basu, A. Udovich, C. Charbonneau, P. Slodowske, W. Mikkelsen, S.E. McCandless, J.C. 1995. A new clean diesel technology: demonstration of ULEV emissions on a navistar diesel engine using a new alternative fuel. SAE technical paper, No. 950061; SAE Transactions, 104 (4), pp.42–53.

Flynn, P.F. Durrett, R.P. Hunter, G.L. zur Loye, A.O. Akinyemi, O. C. Dec, J.E. Westbrook, C.K., 1999. Diesel Combustion: An Integrated View Combining Laser Diagnostics, Chemical Kinetics and Empirical Validation. SAE technical paper, No. 1999-01-0509.

Freedman, B. Bagby, M.O., 1989. Heats of Combustion of Fatty Esters and Triglycerides. Journal of the American Oil Chemists' Society. 66 (11), pp.1601-1605.

Frusteri, F. Spadaro, L. Beatrice, C. Guido, C., 2007. Oxygenated additives production for diesel engine emission improvement, Chemical Engineering Journal, 134, pp.239–245.

Geyer, S.M. Jacobus, M.J. Lestz, S.S., 1983. Single-cylinder Diesel engine study of raw and transesterified vegetable oils. In: Vegetable oil as Diesel fuel, Seminar III, US Department of Agriculture, Agricultural Research service, Northern Agricultural Energy Centre, Peoria, ILL., USA, October 19-20, pp.157-162.

Geyer, S.M. Jacobus, M.J. Lestz, S.S., 1984. Comparison of Diesel Engine Performance and Emissions from Neat and Transesterified Vegetable Oils. Transactions of the American Society of Agricultural Engineers, 27, pp.375-381.

Glassman, I. Yetter, R.A., 2008. Combustion. 4th Edition, Amsterdam, The Netherlands: Elsevier, ISBN 978-0-12-088573-2.

Gouw, T.H. Vlugter J.C., 1964. Physical Properties of Fatty Acid Methyl Esters. IV. Ultrasonic Sound Velocity. J. Am. Oil Chem. Soc., 41 (8), pp.524-526.

Graboski, M.S. McCormick, R.L. 1998. Combustion of fat and vegetable oil derived fuels in diesel engines. Progress in Energy and Combustion Science, 24 (2), pp.125-164.

Graboski, M.S. McCormick, R.L. Alleman, T.L. Herring, A.M., 2000. Effect of Biodiesel Composition on NOx and PM Emissions from a DDC Series 60 Engine, National Renewable Energy Laboratory, Report under contract No. ACG-8-17106-02.

Graboski, M.S. McCormick, R.L. Alleman, T.L. Herring, A.M., 2003. The Effect of Biodiesel Composition on Emissions from a DDC Series 60 Diesel Engine, National Renewable Energy Laboratory, Report No. NREL/SR-510-31461.

Griffiths, J.F. Gray, B.F. Gray, P., 1971. Multistage ignition in hydrocarbon combustion: Temperature effects and theories of nonisothermal combustion. Symposium (International) on Combustion, 13 (1), pp.239-248.

Harrington, K.J., 1986. Chemical and Physical Properties of Vegetable Oil Esters and their Effect on Diesel Fuel Performance. Biomass, 9 (1), pp.1-17.

Hess, M. Haas, M.J. Foglia, T.A. Marmer, W.N., 2005. Effect of Antioxidant Addition on NOx Emissions from Biodiesel. Journal of Energy and Fuels, 19 (4), pp.1749-1754.

Heywood, J. B. Fay, J. A., Linden, L.H., 1971. Jet Aircraft Air Pollutant Production and Dispersion. AIAA J., 9 (5), pp.841-850.

Heywood, J.B., 1988. Internal Combustion Engine Fundamentals. New York, USA: McGraw-Hill, ISBN 0-07-100499-8.

Higgins, B. S. Mueller, C. J. Siebers, D. L., 1999. Measurements of Fuel Effects on Liquid-Phase penetration in DI Sprays. SAE technical paper, 1999-01-0519.

Hilliard, J.C. Wheeler, R.W., 1979. Nitrogen Dioxide in Engine Exhaust. SAE technical paper, No. 790691; SAE Transactions, 88, 1979.

Hiroyasu, H., 1985. Diesel Engine Combustion and Its Modeling. Diagnostics and Modeling of Combustion in Reciprocationg Engines. In: Proceedings of COMODIA 85 Symposium. Tokyo 4th-6th September.

Horiba Instruments, 1984. MEXA 9100HEGR instructions manual. Kyoto, Japan: Horiba.

Houghton H.G., 1959. Cloud Physics: Not all questions about nucleation, growth, and precipitation of water particles are yet answered. Science, 129 (3345), pp.307-313.

Howard, J.B. Wersborg, B.L. Williams, G.C., 1973. Coagulation of carbon particles in flames. Faraday Symposia of the Chemical Society, 7, pp.109-119. [DOI: 10.1039/FS9730700109]

Hu J., Wang Y., Cao C., Elliott D.C., Stevens D.J., and White J.F., 2005. Conversion of Biomass Syngas to DME Using a Microchannel Reactor. Ind. Eng. Chem. Res., 44 (6), pp.1722-1727. [DOI: 10.1021/ie0492707].

Hu, J. Wang, Y. Cao, C. Elliott, C. Stevens, D.J. White, J.F., 2007. Conversion of biomass-derived syngas to alcohols and C2 oxygenates using supported Rh catalysts in a microchannel reactor. Catalysis Today, 120, pp.90-95.

Hura, H.S. Glassman, I., 1988. Soot Formation in Diffusion Flames of Fuel/Oxygen Mixtures. In: Proceedings of the 22nd Synposium (International) on Combustion, The Combustion Institute, Pitsburgh, PA, USA, pp.371-388.

Hwang, W. Dec, J. Sjöberg, M., 2008. Spectroscopic and chemical-kinetic analysis of the phases of HCCI autoignition and combustion for single- and two-stage ignition fuels. Combustion and Flame, 154 (3), pp.87-409.

Infineum petroleum additive company, 2006. Safety data sheet for lubricity additive Infineum R655. Abingdon, UK: Infineum UK limited.

Iyer, V. A. Abraham, J. Magi, V., 2002. Exploring injected droplet size effects on steady liquid penetration in a Diesel spray with a two-fluid model. International Journal of Heat and Mass Transfer, 45 (3), pp.519-531.

Jang, J. Bae, C., 2009. Effects of valve events on the engine efficiency in a homogeneous charge compression ignition engine fueled by dimethyl ether. Fuel, 88 (7), pp.1228-1234.

Janulis, P., 2004. Reduction of energy consumption in biodiesel fuel life cycle. Renewable Energy, 29 (6), pp. 861–871.

Jha, S.K. Fernando, S.D. To, F.S.D, 2007. Flame temperature analysis of biodiesel blends and components. Annual meeting, American Society of Agricultural and Biological Engineers, Paper No. 076234.

Jha, S.K. Fernando, S.D. To, F.S.D, 2008. Flame temperature analysis of biodiesel blends and components. Fuel, 87 (10-11), pp.1982-1988.

Johnston, R.R.M. Harrington, K.J., 1983. Rapid Ignition Quality Testing. In: Vegetable oil as Diesel fuel, Seminar III, US Department of Agriculture, Agricultural Research service, Northern Agricultural Energy Centre, Peoria, ILL., USA, 19th-20th October, pp.130-137.

Johnston, R.R.M., 1983. Rapid ranking of Diesel ignition quality. In: 2nd National Conference on Fuels from Crops, Melbourne, SAE Australasia, pp. 1-16.

Kajitani, S. Chen, C.L. Oguma, M. Alam, M. Rhee, K.T., 1998. Direct Injection Diesel Engine Operated with Propane - DME Blended fuel. SAE technical paper, No. 982536.

Kajitani, S. Chen, Z. Oguma, M. Konno, M., 2002. A study of low compression-ratio di-methyl ether diesel engines. International Journal of Engine Research, 3 (1), pp.1–11.

Kajitani, S. Zhili, C. Konno, M. Rhee, K.T., 1997. Engine Performance and Exhaust Characteristics of Direct-Injection Diesel Engine Operated with DME. SAE technical paper, No.972973.

Kaltschmitt, M. Hartmann, H., 2001. Energie aus Biomasse: Grundlagen, Techniken und Verfahren [Energy from Biomass: Fundamentals, Techniques and Processes. Original text in German]. Berlin, Germany: Springer-Verlag. ISBN 3-540-64853-4, 2001.

Kamimoto, T. Bae, M., 1988. High Combustion Temperature for the Reduction of Particulate in Diesel Engine. SAE technical paper, No.880423.

Kamimoto, T. Kobayashi H., 1991. Combustion processes in diesel engines. Progress in Energy and Combustion Science, 17 (2), pp.163-189.

Kapus, P. Ofner, H., 1995. Development of fuel injection equipment and combustion system for DI diesels operated on di-methyl ether. SAE technical paper, No. 950062; SAE Transactions, 104 (4), pp.54–59.

Kapus, P.E. Cartellieri, W.P., 1995. ULEV Potential of a DI/TCI Diesel Passenger Car Engine Operated on Dimethyl Ether. SAE technical paper, No.952754.

Karabektas, M. Hosoz, M., 2009. Performance and emission characteristics of a diesel engine using isobutanol - diesel fuel blends. Renewable Energy, 34 (6), pp.1554-1559.

Kawedia, J.D. Pangarkar, V.G. Niranjan, K., 2000. Pervaporative stripping of acetone, butanol and ethanol to improve ABE fermentation. Bioseparation, 9 (3), pp.145-154. [10.1023/A:1008129713552]

Keffler, L. McLean, J. H., 1935. Homology in long-chain compounds I. Oleic acid and the n-alkyl oleates. J. Soc. Chem. Ind., 54 (21), pp.178-185.

Kent, J.H. Wagner, H.G., 1985. Temperature and fuel effects in sooting diffusion flames. In: Proceedings of the 20th Synposium (International) on Combustion, The Combustion Institute, Pitsburgh, PA, USA, pp.1007-1015.

Khatri, N.J. Johnson, J.H., Leddy, D.G., 1978. The characterization of the hydrocarbon and sulfate fractions of diesel particulate matter, SAE technical paper, No. 780111; SAE Transactions, 87, pp.469.

Kim, D.S. Lee, C.S., 2006. Improved emission characteristics of HCCI engine by various premixed fuels and cooled EGR. Fuel, 85 (5-6), pp.695-704.

Kirchner, U. Scheer, V. Vogt, R. Kägi, R., 2009. TEM study on volatility and potential presence of solid cores in nucleation mode particles from diesel powered passenger cars. Journal of Aerosol Science, 40 (1), pp.55-64.

Kistler Instruments, 2007. Technical drawing of pressure transducer 6056AU38 housing. Winterthur, Switzerland: Kistler.

Kittelson D.B., 1998. Engines and Nanoparticles: A Review. J. Aerosol Sci., 29 (5-6), pp. 575-588.

Kittelson, D.B. Dolan, D.F. Verrant, J.A., 1978. Investigation of a diesel exhaust aerosol, SAE technical paper, No. 780109.

Klopfenstein, W.E. Walker, H. S., 1983[a]. Efficiencies of Various Esters of Fatty Acids as Diesel Fuels. Journal of the American Oil Chemists' Society, 60 (8), pp.1596-1698.

Klopfenstein, W.E. Walker, H.S. 1983[b]. Effects of Structure of Fatty Acid Esters on Efficiencies as Diesel Fuels. In: Vegetable oil as Diesel fuel, Seminar III, US Department of Agriculture, Agricultural Research service, Northern Agricultural Energy Centre, Peoria, ILL., USA, 19th-20th October, pp.102-103.

Klopfenstein, W.E., 1983. Relationship Between Cetane Number and Structure for Fatty Acid Esters. In: Vegetable oil as Diesel fuel, Seminar III, US Department of Agriculture, Agricultural Research service, Northern Agricultural Energy Centre, Peoria, ILL., USA, 19th-20th October, pp.104-105.

Klopfenstein, W.E., 1985. Effect of Molecular Weights of Fatty Acid Esters on Cetane Numbers as Diesel Fuels. Journal of the American Oil Chemists' Society, 62 (6), pp.1029-1031.

Knothe G., 2005. Dependence of biodiesel fuel properties on the structure of fatty acid alkyl esters. Fuel Processing Technology, 86 (10), pp.1059-1070.

Knothe, G. Bagby, M.O. Ryan, T.W.III., 1997. Cetane Numbers of Fatty Compounds: Influence of Compound Structure and of various Potential Cetane Improvers. SAE technical paper, No. 971681.

Knothe, G. Matheaus, A.C. Ryan, T.W., 2003. Cetane numbers of branched and straight-chain fatty esters determined in an ignition quality tester. Fuel, 82 (8), pp.971-975.

Knothe, G., 2002. Structure Indices in Fatty Acid Chemistry. How Relevant Is the Iodine Value? J. Am. Oil Chem. Soc., 79 (9), pp.847-854.

Kobayashi, K. Yamaguchi E., 1921. Artificial Petroleum from Fish Oils, J. Chem. Ind. (Japan), 24, pp.1399–1420; [as cited in: Chem. Abstr. 16: 2983 (1922)].

Kobayashi, K., 1921[a]. Artificial Petroleum from Soybean, Coconut, and Chrysalis Oils and Stearin. J. Chem. Ind. (Japan), 24, pp.1421–1424.

Kobayashi, K., 1921[b]. Artificial Petroleum from Fish Oils. Kogyo-Kwagaku Zasshi [The Journal of Chemical Industry], [Published English translation of the original Japanese article], 24, 12/286, pp.107–110.

Konno, M. Kajitani, S. Oguma, M. Iwase,T. Shima, K.-I., 1999. NO Emission Characteristics of a CI Engine Fueled with Neat Dimethyl Ether. SAE technical paper, No. 1999-01-1116.

Krisnangkura, K., 1986. A Simple Method For Estimation of Cetane Index of Vegetable Oil Methyl Esters. Journal of the American Oil Chemists' Society, 63 (4), pp.552-553.

Krouwel, P.G. Groot, W.J. Kossen, N.W.F. van der Laan, W.F.M., 1982. Continuous isopropanol-butanol-ethanol fermentation by immobilized Clostridium beijerinckii cells in a packed bed fermenter. Enzyme and Microbial Technology, 5 (1), pp.46-54.

Ladommatos, N. Abdelhalim, S. Zhao, H., 2000. The effects of exhaust gas recirculation on diesel combustion and emissions. International Journal of Engine Research, 1 (1), pp.107-126.

Ladommatos, N. Parsi, M. Knowles, A., 1996[a]. The effect of fuel cetane improver on diesel pollutant emissions. Fuel, 75 (1), pp.8-14.

Ladommatos, N. Rubenstein, P. Bennett, P., 1996[b]. Some effects of molecular structure of single hydrocarbons on sooting tendency, Fuel, 75 (2), pp.114-124.

Lapuerta, M. Armas, O. Rodríguez-Fernández, J., 2008[a]. Effect of biodiesel fuels on diesel engine emissions. Progress in Energy and Combustion Science, 34 (2) pp.198-223.

Lapuerta, M. Armas, O. Rodríguez-Fernández, J., 2008[b]. Emissions from a diesel-bioethanol blend in an automotive diesel engine. Fuel, 87 (1), pp.25-31.

Lapuerta, M. Armas, O. Rodríguez-Fernández, J., 2008[c]. Effect on the Degree of Unsaturation of Biodiesel Fuels on NOx and Particulate Emissions. SAE technical paper, No. 2008-01-1676.

Lapuerta, M. Herreros, J.M Lyons, L.L. García-Contreras, R. Briceño, Y., 2008[d]. Effect of the alcohol type used in the production of waste cooking oil biodiesel on diesel performance and emissions. Fuel, 87 (15-16), pp.3161-3169.

Lavoie, G.A. Heywood, J.B. Keck, J.C., 1970. Experimental and Theoretical Investigation of Nitric Oxide Formation in Internal Combustion engines. Combustion Science and Technology, 1, pp.313-326.

Leigh-Haag, A., 2007. Algae bloom again. Nature, 447, pp.520-521. [doi:10.1038/447520a].

Li, T.-M., Simmons, R.F., 1986. The action of Ignition improvers in Diesel fuels. In: 21st Symposium (International) on Combustion, The Combustion Institute, pp.455-462.

Lipkea, W.H. Johnsen, J.H. Vuk, C.T., 1978. The physical and Chemical Character of Diesel Particulate Emissions – Measurement Techniques and Fundamental Considerations. SAE technical paper, No. 780108.

Lü, X.-C. Chen, W. Huang, Z., 2005. A fundamental study on the control of the HCCI combustion and emissions by fuel design concept combined with controllable EGR. Part 2. Effect of operating conditions and EGR on HCCI combustion. Fuel, 84 (9), pp.1084-1092.

Machrafi, H. Cavadias, S. Gilbert, P., 2008. An experimental and numerical analysis of the HCCI auto-ignition process of primary reference fuels, toluene reference fuels and diesel fuel in an engine, varying the engine parameters. Fuel Processing Technology, 89 (11), pp.1007-1016.

Mailhe A., 1923. Preparation of Motor Fuel from Vegetable Oils, J. Usines Gaz, 46, pp.289–292; [as cited in: Chem. Abstr. 17: 197 (1923)].

Mallamo, F. Badami, M. Millo, F., 2005. Effect of Compression Ratio and Injection Pressure on Emissions and Fuel Consumption of a Small Displacement Common Rail Diesel Engine. SAE technical paper, No. 2005-01-0379.

Mantell, C.L., 1968. Carbon and Graphite Handbook. New York, USA: John Wiley and Sons.

Manzer, L.E. D'Amore, M.B. Miller, E.S., 2007. Process for making dibutyl ethers from aqueous ethanol. International Patent Application published under the patent cooperation treaty. World Intellectual property Organization. International Publication No. WO 2008/069982 A2, Publication No. US2009/0036716 A1. International filing date 30th November 2007, International publication date 12th June 2008.

Martin, A., 2008. Biofuels getting blame for high food prices. International Herald Tribune, New York, 15th April.

Martin, G.B. Berkau, E.E., 1971. An investigation of the conversion of various fuel nitrogen compounds to NO in oil combustion. In: Paper presented at 70th AIChE National Meeting, San Francisco, CA, USA, August.

Mathot, R.E., 1921. L'utilisation des huiles végétales pour la force motrice. [The use of vegetable oils for motive power. Original text in French]. Bull. Mat. Grasses Inst. Colon. Marseille, pp.116–128.

Mayer, W. J. Lechman, D.C. Hilden, D.L., 1980. The contribution of engine oil to diesel exhaust particulate emissions, SAE technical paper, No. 800256; SAE Transactions, 89, pp.1190.

Max Machinery, 2003. Instructions manual series 210 positive displacement flowmeters. Healdsburg, CA, USA: Max Machinery.

McCormick, R.L. Alvarez, J.R. Graboski, M.S. Tyson, K.S. Vertin, K., 2002. Fuel Additive and Blending Approaches to Reducing NOx Emissions from Biodiesel. SAE technical paper, No. 2002-01-1658.

McCormick, R.L. Graboski, M.S. Alleman, T.L. Herring, A.M. Tyson, K.S., 2001. Impact of Biodiesel Source Material and Chemical Structure on Emissions of Criteria Pollutants from a Heavy-Duty Engine. Environmental Science and Technology, 35 (9), pp.1742–1747.

McCormick, R.L. Ross, J.D. Graboski, M.S., 1997. Effect of Several Oxygenates on Regulated Emissions from Heavy-Duty Diesel Engines. Environmental Science and Technology, 31 (4), pp.1144-1150.

McCormick, R.L. Tennant, C.J. Hayes, R.R. Black, S. Ireland, J. McDaniel, T. Williams, A. Frailey, M., 2005. Regulated Emissions from Biodiesel Tested in Heavy-Duty Engines Meeting 2004 Emissions Standards. SAE technical paper, No. 2005-01-2200.

McCormick, R.L. Williams, A. Ireland, J. Brimhall, M. Hayes, R. R., 2006. Effects of Biodiesel Blends on Vehicle Emissions, National Renewable Energy Laboratory, Report No. NREL/MP-540-40554.

Medalia, A.I. Heckman, F.A., 1969. Morphology of aggregates-II. Size and shape factors of carbon black aggregates from electron microscopy, Carbon 7, p.567.

Meyer, B. Dimming, T. Radig, W., 2005. Die BTL-Pilotanlage an der TU Freiberg - ein Zwischenbericht. In: Synthetic Biofuels: Technologies, potentials, prospects, Wolfsburg, Germany, 3rd-4th November, 2004. Münster, Germany: Landwirtschaftsverlag. ISBN-3-7843-3346-X.

Miers, S.A. Ng, H. Ciatti, S.A. Stork, K., 2005. Emissions, Performance, and In-Cylinder Combustion Analysis in a Light-Duty Diesel Engine Operating on a Fischer-Tropsch, Biomass-to-Liquid Fuel. SAE technical paper, No 2005-01-3670.

Miller, J.A. Bowman, C.T., 1989. Mechanism and modelling of nitrogen chemistry in combustion. Progress in Energy and Combustion Science, 15 (4), pp287-338.

Milliken, R.C., 1962. Journal of Physical Chemistry, 66, pp.794-799.

Mittasch, A. Pier, M. Winkler, K., 1923. Ausführung organischer Katalysen [Procedure of organic catalyses]. German patent No. 415686, Filed 24th July 1923, Published 27th July 1925. [Corresponding English language patents: UK Patent Specification No. 229,715, and US Patent specification 1,569,775].

Mittasch, A. Schneider, C., 1913. Verfahren zur Darstellung von Kohlenwasserstoffen und deren Derivaten [Procedure for the synthesis of hydrocarbons and their derivatives]. German patent No. 293787, 8th March 1913, Approved 23rd August 1916.

Mittelbach, M. Tritthart, P. Junek, H., 1985. Diesel fuel derived from vegetable oils, II, Emission tests using rape oil ester. Energy in Agriculture, 4, pp.207-215.

Miyamoto, N. Ogawa, H. Nurun, N.M. Obata, K. Arima, T., 1998. Smokeless, high NOx, high thermal efficiency and low noise diesel combustion with oxygenated agents as main fuel. SAE technical paper, No. 980506.

Monyem, A. Van Gerpen, J.H., 2001. The effect of biodiesel oxidation on engine performance and emissions. Biomass and Bioenergy. 20 (4) pp.317–325.

Morrison, R. T. Boyd, R. N. 1992. Organic Chemistry, 6th Edition. London, UK: Prentice-Hall, ISBN-0-13-643669-2.

Mosier, N., Wyman C., Dale B., Elander R., Lee Y. Y., Holtzapple M., Ladisch M., 2005. Features of promising technologies for pretreatment of lignocellulosic biomass. Bioresource Technology, Vol. 96, Issue 6, pp. 673-686, April 2005.

Mueller C.J., 2008. Radiative heat transfer and other effects on the biodiesel NOx increase, in: Proceedings of the 2008 Biodiesel Technical Workshop, New Orleans, LA, 22nd October.

Mueller, C.J. Boehman, A.L., Martin, G.C., 2009. An Experimental Investigation of the Origin of Increased NOx Emissions When Fuelling a Heavy-Duty Compression-Ignition Engine with Soy Biodiesel. SAE technical paper, No. 2009-01-1792.

Murphy, M.J. Taylor, J.D. McCormick, R.M., 2004. Compendium of Experimental Cetane Number Data, National Renewable Energy Laboratory, Report No. NREL/SR-540-36805.

Musculus, M.P.B., 2004. On the Correlation between NOx Emissions and the premixed Burn. SAE technical paper, No. 2004-01-1401.

Naber, J.D. Siebers, D.L., 1996. Effects of Gas Density and Vaporization on Penetration and Dispersion of Diesel Sprays. SAE technical paper, No.960034; SAE Transactions, 105 (3), pp.82-111.

Naegeli, D., 1992. Fuel Additives for Smoke Reduction in Diesel Engines. Report 03–130, San Antonio, TX, USA: Southwest Research Institute.

Najt, P.M. Foster, D.E., 1983. Compression-Ignited Homogeneous Charge Combustion. SAE technical paper, No. 830264.

Ng, H. Biruduganti, M. Stork, K., 2005. Comparing the Performance of SunDieselTM and Conventional Diesel in a Light-Duty Vehicle and Heavy-Duty Engine. SAE technical paper, No 2005-01-3776.

Nord, K. E. Haupt, D., 2005. Reducing the Emission of Particles from a Diesel Engine by Adding an Oxygenate to the Fuel. Environmental Science and Technology, 39 (16), pp.6260-6265.

Onishi, S. Jo, S.H. Shoda, K. Jo, P.D. Kato, S., 1979. Active thermo-atmosphere combustion (ATAC) - A new combustion process for internal combustion engines. SAE technical paper, No. 790501.

Oppenländer, K. Merger, F. Strickler, R. Hovemann, F. Schmidt, H. Starke, K., 1979. Verwendung von Polyäthern und Acetalen auf der Basis von Äthanol als Dieselkraftstoffe sowie diese Komponenten enthaltende Dieselkraftstoffe. German patent publication No. 2906604, Filed on 21st February 1979, Published 4th September 1980.

Osmont, A. Catoire, L. Gökalp, I., 2007. Thermochemistry of methyl and ethyl esters from vegetable oils. Int. J. Chemical Kinetics, 39 (9), pp.481-491.

Oxley, J.C. Smith, J.L. Rogers, E. Ye, W. Aradi, A.A. Henly, T.J., 2001. Heat-Release Behaviour of Fuel Combustion Additives. Energy & Fuels, 15 (5), pp.1194-1199.

Palmer, H.B. Cullis, H.F., 1965. The Chemistry and Physics of Carbon. Vol.1, New York, USA: Dekker.

Park, K. Cao, F. Kittelson, D.B. McMurry, P.H., 2003. Relationship between particle mass and mobility for diesel exhaust particles. Environmental Science and Technology, 37, pp.577–583.

Park, K. Kittelson , D.B. McMurry , P.H., 2003. A Closure Study of Aerosol Mass Concentration Measurements: Comparison of Values Obtained with Filters and by Direct Measurements of Mass Distributions. Atmospheric Environment, 37 (9-10), pp.1223-1230.

Parker, T.E., 1996. Private communication [As referenced by McCormick et al. (1997)].

Pepiot-Desjardins, P. Pitsch, H. Malhotra, R. Kirby, S.R. Boehman, A.L., 2008. Structural group analysis for soot reduction tendency of oxygenated fuels. Combust. Flame, 154 (1-2), pp.191-205.

Pierpont, D.A. Reitz, R.D., 1995. Effects of Injection Pressure and Nozzle Geometry on D.I. Diesel Emissions Performance. SAE technical paper, No. 950604.

Pischinger, G.H. Siekmann, R.W. Falcon, A.M. Fernandes, F.R., 1982. Methylesters of Plant Oils as Diesel Fuels, either straight or in blends. In: Vegetable Oil Fuels proceedings of the Int. Conf. on Plant and vegetable oils and fuels. ASAE 4-82, Fargo, ND, USA, 2nd-4th August, pp.198-208.

Pischinger, R. Cartellieri W., 1972. Combustion system Parameters and their Effects upon Diesel Engine Exhaust Emissions. SAE technical paper No.720756; SAE Transactions, vol. 81, 1972.

Popovicheva, O.B. Persiantseva, N.M. Kuznetsov, B.V. Rakhmanova, T. A. Shonija, N. K. Suzanne, J. Ferry, D., 2003. Microstructure and Water Adsorbability of Aircraft Combustor Soots and Kerosene Flame Soots: Toward an Aircraft-Generated Soot Laboratory Surrogate. J. Phys. Chem., A, 107 (47), pp.10046-10054.

Pritchard, H.O., 1989. Thermal decomposition of Isooctyl Nitrate. Combustion and Flame, 75 (3-4), pp.415-416.

Pryde, E.H., 1981. Vegetable Oil vs. Diesel Fuel: Review of International Research. In: Alcohol and Vegetable Oil as alternative Fuels, Raleigh, NC, USA, 7th-9th April, pp.217-224.

Qiu, X.Q. Tsubaki, N. Fujimoto, K. Zhu, Q.M., 2004. Oxygenate synthesis from 1-hexene and syngas over supported cobalt catalysts, Fuel processing technology, 85, pp.1193-1200.

Qureshi, N. Meagher, M.M. Huang, J. Hutkins, R.W., 2001. Acetone butanol ethanol (ABE) recovery by pervaporation using silicalite–silicone composite membrane from fed-batch reactor of Clostridium acetobutylicum. Journal of Membrane Science, Vol.187, Issues 1-2, pp 93-102. 15 June 2001.

Qureshi, N. Ezeji, T.C. Ebener, J. Dien, B.S. Cotta, M.A. Blaschek, H.P., 2008. Butanol production by Clostridium Beijerinckii: Part I. Use of acid and enzyme hydrolyzed corn fiber. Bioresource Technology, 99 (13), pp.5915-5922.

Roehr, M., 2001. The Biotechnology of Ethanol: Classical and Future Applications. New York, USA: Wiley-VCH, ISBN-3527301992, 2001.

Rolling, R.E. Vogt, C.J., 1960. The adiabatic Bulk Modulus of Normal Paraffin Hydrocarbons from Hexane to Hexadecane. J. Basic Eng., 82, pp.635-644.

Rudloff, M., 2005. SunDiesel - made by CHOREN - Erfahrungen und neueste Entwicklungen. In: Synthetic Biofuels: Technologies, potentials, prospects, Wolfsburg, Germany, 3rd-4th November, 2004. Münster, Germany: Landwirtschaftsverlag. ISBN-3-7843-3346-X.

Sabatier, P. Sendersen, J. B., 1902. Nouvelles Synthèses du Méthane [New Methane Syntheses], Compt. Rend. 134, pp.514-516.

Sabatier, P., 1922. La Catalyse en Chimie Organique. Paris, France: Béranger. 1913. [English translation: P. Sabatier, 1922. Catalysis in Organic Chemistry, Company, New York, USA: D. Van Nostrand].

Sakurai, H. Park, K. McMurry, P.H Zarling, D.D. Kittelson, D.B. Ziemann, P.J., 2003 a. Size-Dependent Mixing Characteristics of Volatile and Nonvolatile Components in Diesel Exhaust Aerosols. Environ. Sci. Technol., 37 (24), pp.5487-5495. [DOI: 10.1021/es034362t].

Sakurai, H. Tobias, H.J. Park, K. Zarling, D. Docherty, K.S. Kittelson, D.B. McMurry, P.H. Ziemann P.J., 2003 b. On-line measurements of diesel nanoparticle composition and volatility. Atmospheric Environment, 37 (9-10), pp.1199-1210.

Sato, M., 1922. Preparation of a Liquid Fuel Resembling Petroleum by the Distillation of the Calcium Salts of Soybean Oil Fatty Acids, J. Chem. Ind. (Japan), 25, pp.13–24; [as cited in: Chem. Abstr. 16: 2984 (1922)].

Schacht, C. Zetztl, C. Brunner, G., 2008. From plant materials to ethanol by means of supercritical fluid technology. The Journal of Supercritical Fluids, 46 (3), pp.299-321.

Schneider, J. Hock, N. Weimer, S. Borrmann, S. Kirchner, U. Vogt, R. Scheer V., 2005. Nucleation Particles in Diesel Exhaust: Composition Inferred from In Situ Mass Spectrometric Analysis. Environ. Sci. Technol., 39 (16), pp.6153-6161. [DOI: 10.1021/es049427m].

Scholl, K.W. Sorenson, S.C., 1993. Combustion of soybean oil methyl ester in a direct injection diesel engine. SAE technical paper, No. 930934.

Schulz, H. Bandeira, G. De Melo, Ousmanov, F., 1999. Volatile organic compounds and particulates as components of diesel engine exhaust gas. Combustion and Flame, 118 (1-2), pp.179-190.

Schumacher, L.G. Borgelt, S.C. Fosseen, D. Goetz, W. Hires, W.G., 1996. Heavy-duty engine exhaust emission tests using methyl ester soybean oil/diesel fuel blends. Bioresource Technology, 57 (1), pp.31-36.

Searchinger, T. Heimlich, R. Houghton, R.A. Dong, F. Elobeid, A. Fabiosa, J. Tokgoz, S. Hayes, D. Yu, T.-H., 2008. Use of U.S. Croplands for Biofuels Increases Greenhouse Gases Through Emissions from Land-Use Change, Science, 319, pp.1238-1240, 29th February. [DOI: 10.1126/science.1151861].

Service, R.F., 2008. Eyeing oil, Synthetic Biologists Mine Microbes for Black Gold. Science, 322 (5901), pp.522-523, 24th October [DOI: 10.1126/science.322.5901.522]

Sharavanan, A. Jaishanker, D. G.Saravanan, C., 2001. Improved Performance and Reduced Emissions in a D. I. Engine by Fuel Additives, SAE technical paper, No. 2001-01-2504.

Sheehan, J. Dunahay, T. Benemann, J. Roessler, P., 1998. A Look Back at the U.S. Department of Energy's Aquatic Species Program – Biodiesel from Algae, National Renewable Energy Laboratory, NREL/TP-580-24190. Golden, CO, USA: NREL. Available at: http://www.nrel.gov/biomass/pdfs/24190.pdf [Accessed: 25th May, 2009]

Shell chemicals, 2001. Isopropyl ether, Data Sheet IS 3.5.1A.

Shen, C.R. Liao J.C., 2008. Metabolic engineering of Escherichia coli for 1-butanol and 1-propanol production via the keto-acid pathways. Metabolic Engineering, 10 (6), pp.312-320.

Shi, L. Cui, Y. Deng, K. Peng, H. Chen, Y., 2006. Study of low emission homogeneous charge compression ignition (HCCI) engine using combined internal and external exhaust gas recirculation (EGR). Energy, 31 (14), pp.2665-2676.

Shudo, T. Ono, Y., 2002. HCCI Combustion of Hydrogen, Carbon Monoxide and Dimethyl Ether. SAE technical paper, No. 2002-01-0112.

Siebers, D. Higgins, B. Pickett, L., 2002. Flame lift-off on direct injection diesel fuel jets: Oxygen concentration effects. SAE technical paper, No. 2002-01-0890.

Siebers, D. L., 1999. Scaling liquid-phase fuel penetration in diesel sprays based on mixing-limited vapourisation. SAE technical paper, No. 1999-01-0528.

Siekmann, R.W. Pischinger, G.H. Joseph, H.Jr., 1983. Nonregulated exhaust emissions of Volkswagen's IDI Engine fuelled with transesterified or refined soybean oil either straight or blended into Gasoil. Vegetable oil as Diesel fuel, Seminar III, US Department of Agriculture, Agricultural Research service, Northern Agricultural Energy Centre, Peoria, ILL., USA, , October 19-20, pp.153-156.

Sigma-Aldrich Chemical Company, 2004. Safety Data Sheet for Ethyl Oleate.

Sirman, M. Owens, E. Whitney, K., 1998. Emissions Comparison of Alternative Fuels in an Advanced Automotive Diesel Engine. Southwest Research Institute report for DOE and US Army TARDEC, Interim report TFLRF 338. San Antonio, TX, USA: Southwest Research Institute.

Sison, K. Ladommatos, N, Song, H. Zhao, H., 2007. Soot generation of diesel fuels with substantial amounts of oxygen-bearing compounds added. Fuel, 86 (3), pp.345-352.

Smith, O.I., 1981. Fundamental of Soot formation in Flames with Application to Diesel Engine Particulate emissions. Progress in Energy and Combustion Science, 7 (4), pp.275-291.

Snelling, J. Curtis, C.W. Park, Y.K., 2003. Synthesis of higher carbon ethers from olefins and alcohols I. reactions with methanol, Fuel processing technology, 83 (1-3), pp.219-234.

Solbrig, C.E. Litzinger, T.A., 1990. The Effect of Intake Charge Temperature on Combustion and Emissions in an Optically Accessible DI Diesel Engine With and Without Swirl. SAE technical paper, No. 902060.

Solomon, S. Qin, D. Manning, M. Marquis, M. Averyt, K. Tignor, M.M.B. Miller, H.L. Jr. Chen, Z., 2007. Climate Change 2007: The Physical Science basis. IPCC WGI Fourth Assessment Report. Intergovernmental Panel on Climate Change. Cambridge, UK: Cambridge University Press. ISBN: 978-0-521-70596-7.

Song, J. Alam, M. Boehman, A.L. Kim. U., 2006. Examination of the oxidation behaviour of Biodiesel soot. Combustion and Flame, 146 (4), pp.589-604.

Sorenson, S.C. Mikkelsen, S.E., 1995. Performance and emissions of a 0.273 liter direct injection diesel engine fueled with neat dimethyl ether. SAE technical paper, No. 950064; SAE Transactions, 104 (4), pp.80-90.

Stein, S.W. Turpin, B. J. Cai, X. Huang, P.-F. McMurry, P.H., 1994. Measurements of relative humidity-dependent bounce and density for atmospheric particles using the DMA-impactor technique. Atmospheric Environment, 28 (10), pp.1739-1746.

Stone, R., 1999. Introduction to Internal Combustion Engines. Third Edition. Basingstoke, UK: Palgrave Publishers Ltd. ISBN 0-333-74013-0.

Street, J.C Thomas, A., 1955. Carbon Formation in Pre-mixed Flames. Fuel. 34, p.4.

Sugano, H.Y., 2008. Gas oil composition. European patent application EP 2006360 (A1). International publication number WO 2007/114026. Date of filing 11th March 2007. Date of publication 24th December 2008. European patent office.

Symonds, J.P.R. Reavell, K.S.J. Olfert, J.S. Campbell, B.W. Swift, S.J., 2007. Diesel-soot mass calculation in real-time with a differential mobility spectrometer, Journal of Aerosol Science, 38, pp.52-68.

Szybist, J. Boehman, A. 2003. Behavior of a Diesel Injection System with Biodiesel Fuel. SAE technical paper No. 2003-01-1039.

Szybist, J.P. Boehman, A.L. Taylor, J.D. McCormick, R.L., 2005. Evaluation of formulation strategies to eliminate the biodiesel NOx effect. Fuel Processing Technology, 86 (10), pp.1109-1126.

Szybist, J.P. Bunting, B.G., 2005. Cetane Number and Engine Speed Effects on Diesel HCCI Performance and Emissions. SAE technical paper, No. 2005-01-3723.

Szybist, J.P. Song, J. Alam, M. Boehman, A.L., 2007. Biodiesel combustion, emissions and emissions control. Fuel Processing Technology, 88 (7), pp.679-691.

Tat, M.E. Van Gerpen, J.H. Soylu, S. Canakci, M. Monyem, A. Wormley, S., 2000. The Speed of Sound and Isentropic Bulk Modulus of Biodiesel at 21°C from Atmospheric Pressure to 35 MPa. J. Am. Oil Chem. Soc., 77 (3), pp.285-289.

Tazerout, M. Le Corre, O. Rousseau, S., 1999. TDC Determination in IC Engines Based on the Thermodynamic Analysis of the Temprature-Entropy Diagram, SAE technical paper, No. 1999-01-1489.

Teng, H. McCandless, J.C. Schneyer, J.B., 2001. Thermo-chemical characteristics of di-methyl ether - an alternative fuel for compression-ignition engines. SAE technical paper, No. 2001-01-0154; SAE Transactions, 110 (4), pp.96–106.

Thring, R.H., 1989. Homogeneous Charge Compression Ignition (HCCI) Engines. SAE technical paper, No.892068.

Tobias, H.J. Beving, D.E. Ziemann, P.J Sakurai, H. Zuk, M. McMurry, P.H. Zarling, D. Waytulonis, R. Kittelson, D.B., 2001. Chemical Analysis of Diesel Engine Nanoparticles Using a Nano-DMA/Thermal Desorption Particle Beam Mass Spectrometer. Environ. Sci. Technol., 35 (11), pp.2233-2243. [DOI: 10.1021/es0016654].

Tree D.R., Svensson K.I., 2007. Soot processes in compression ignition engines. Progress in Energy and Combustion Science, 33 (3), pp. 272-309.

Tsuchiya, T. Sato, Y., 2006. Development of DME Engine for Heavy-duty Truck. SAE technical paper, No.2006-01-0052.

Turns, S.R., 1996. An Introduction to Combustion: Concepts and Applications. New York, USA: McGraw-Hill. ISBN 0-07-911812-7.

Umakantha, N., 1974. Algae as fuel, Nature, 250 (5465), p.371. [DOI: 10.1038/250371b0]

United States Environmental Protection Agency, 2002. A comprehensive analysis of biodiesel impacts on exhaust emissions. United States Environmental Protection Agency, Report No. EPA420-P-02-001.

van den Abeele, M., 1942. L'Huile de Palme: Matière Première pour la Préparation d'un Carburant lourd utilisable dans les moteurs à combustion interne [Palm Oil: Raw material for the production of a heavy fuel for internal combustion engines, [original text in French]. Bulletin Agricole du Congo Belge, 33 (1), pp.3-90.

van Vliet, O.P.R. Faaij, A.P.C. Turkenburg, W.C., 2009. Fischer-Tropsch diesel production in a well-to-wheel perspective: A carbon, energy flow and cost analysis. Energy Conversion and Management, 50 (4), pp.855-876.

vander Wal, R.L., 2005. Soot Nanostructure: Definition, Quantification and Implications. SAE technical paper, No. 2005-01-0964.

Vertin, K.D. Ohi, J.M. Naegeli, D.W. Childress, K.H. Hagen, G.P. McCarthy, C.I. Cheng, A.S. Dibble, R.W., 1999. Methylal and Methylal-Diesel Blended Fuels for Use in Compression-Ignition Engines. SAE technical paper, No. 1999-01-1508.

Vogel, A. Reichmuth, M. Kaltschmitt M., 2005. Potenziale von Biokraftstoffen unter Berücksichtigung ökonomischer Aspekte [Prospectives of biofuels with consideration of economical aspects]. In: Synthetic Biofuels: Technologies, potentials, prospects, Wolfsburg, Germany, 3rd-4th November, 2004. Münster, Germany: Landwirtschaftsverlag. ISBN-3-7843-3346-X.

Voiculescu, I.A. Borman, G.L., 1978. An Experimental Study of Diesel Engine Cylinder-Averaged NOx Histories. SAE technical paper, No.780228; SAE Transactions, 87 (1), pp.1001-1014.

Vuk, C.T. Jones, M.A. Johnson, J.H., 1976. The measurement and analysis of the physical character of diesel particulate emissions, SAE technical paper, No. 760131.

Waldheim, L. Morris, M. Ståhl, K. Gårdmark, L., 2005. CHRISGAS PROJECT - Manufacture of a clean hydrogen-rich gas through biomass gasification and hot gas upgrading. In: Synthetic Biofuels: Technologies, potentials, prospects, Wolfsburg, Germany, 3rd-4th November, 2004. Münster, Germany: Landwirtschaftsverlag. ISBN-3-7843-3346-X.

Walton, J., 1938. The Fuel Possibilities of Vegetable Oils. Gas and Oil Power, 33. pp.167-168.

Waltz, E., 2009. Biotech's Green Gold? Nature Biotechnology, 27 (1), pp.15-18.

Wang M., Wu M., Huo H., 2007. Life-cycle energy and greenhouse gas emission impacts of different corn ethanol plant types, Environmental Research Letters, 2 (2), Bristol, UK: Institute of Physics (IOP) publishing, April–June 2007. Available at: http://www.iop.org/EJ/abstract/1748-9326/2/2/024001/ [Accessed: 25th May 2009]. [doi:10.1088/1748-9326/2/2/024001].

Wang, R., 1988. Development of Biodiesel fuel. Taiyangneng Xuebao, 9, pp.434-436. [As in: Chem. Abstr. 111: 26233 (1989)].

Weitz, M., 2005. Biokraftstoffe - Potenzial, Zukunftsszenarien und Herstellungsverfahren im wirtschaftlichen Vergleich. Reihe Nachhaltigkeit, Band 4, Hamburg, Germany: Diplomica. ISBN-10: 3-8324-9352-2.

Williams, A. McCormick, R.L. Hayes, R.R. Ireland, J. Fang, H.L., 2006. SAE technical paper, No. 2006-01-3280.

Wong, C.L. Steere, D.E., 1982. The Effects of Diesel Fuel Properties and Engine Operating Conditions on Ignition Delay. SAE technical paper, No. 821231.

Yaws, C. L., 2001. Chemical properties handbook: physical, thermodynamic, environmental, transport, safety, and health related properties for organic and inorganic chemicals., Norwich, NY, USA: Knovel, McGraw-Hill.

Yomano, L.P. York, S.W. Ingram, L.O., 1998. Isolation and characterization of ethanol-tolerant mutants of E. coli KO11 for fuel ethanol production. J.Ind. Microbiol.Biotechnol., 20, pp.132–138.

Yoshimoto, Y. Onodera, M., 2002. Performance of a Diesel Engine Fueled by Rapeseed oil Blended with Oxygenated Organic Compounds, SAE technical paper, No. 2002-01-2854.

Yu, J. Bae, C., 2003. Dimethyl ether (DME) spray characteristics compared to diesel in a common-rail fuel injection system. Proceedings of the Institution of Mechanical Engineers, Part D: Journal of Automobile Engineering. 217 (12), pp.1135-1144.

Yu, R.C. Shahed, S.M., 1981. Effects of Injection Timing and Exhaust Gas Recirculation on Emissions from a D.I. Diesel Engine. SAE technical paper, No.811234.

Yuan, W. Hansen, A.C. Zhang, Q., 2005. Vapour pressure and normal boiling point predictions for pure methyl esters and biodiesel fuels. Fuel, 84 (7-8), pp.943-950.

Zel'dovich, Y.B. Sadovnikov, P.Y. Frank-Kamenetskii, D.A., 1947. Okislenie azota gorenii [Oxidation of nitrogen in combustion. Translated from Russian by M. Shelef, Academy of Sciences of the USSR, Moscow, 1985].

Zeng, X. Chen, W. Liu, J., 2007. Molecular Structure, Electronic Structure and Heats of Formation of Explosive Sensitizers. Acta Phys.-Chim. Sin., 23 (2), pp.192-197.

Zhang, Y. Boehman, A.L. 2007. Impact of Biodiesel on NOx Emissions in a Common Rail Direct Injection Diesel Engine. J. Energy & Fuels, 21 (4), pp.2003-2012.

Zhang, Y. van Gerpen, J.H., 1996. Combustion analysis of esters of soybean oil in a diesel engine. SAE technical paper No. 960765.

Zhao, H. Ladommatos, N., 2001. Engine combustion Instrumentation and Diagnostics. Warrendale, PA, USA: Society of Automotive Engineers Inc. ISBN-0-7680-0665-1.

Ziejewski, M. Kaufman, K.K. Pratt, G.L. Goettler, H.J., 1985. Fuel Injection Anomalies Observed During Long-Term Engine Performance Tests on Alternate Fuels. SAE technical paper, No. 852089.

Appendix A. Theoretical derivations

Derivation of overexpanded thermodynamic cycle with isothermal combustion according to Diesel (1892) as a function of compression ratio and cut-off ratio

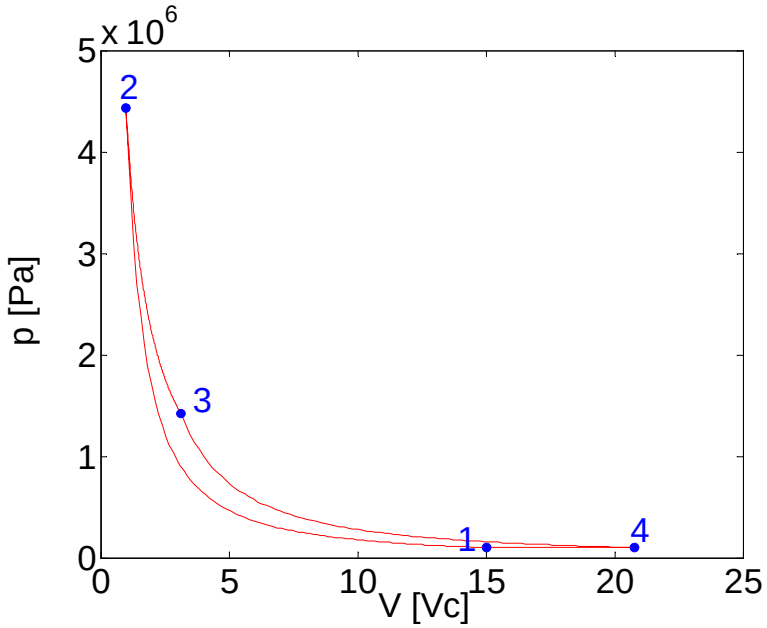

Figure A. 1- Indicator diagram for overexpanded thermodynamic cycle with isothermal combustion according to Diesel (1892)

For the cyclic process shown in Figure A. 1, the net indicated work done per cycle by the working fluid may be expressed by the cyclic integral of the pressure of the working fluid over its volume.

$$W_{cycle} = \oint p \cdot dV$$

The net indicated mean effective pressure (P_{IME}) may be defined by the net indicated work done per cycle divided by the volume of the working fluid.

$$P_{IME} = \frac{\oint p \cdot dV}{V_{swept}}$$

The indicated thermal efficiency of the cycle may be defined as the net specific work output of the cycle divided by the heat supplied to the working fluid per cycle. Thus:

$$\eta = \frac{w_{out}}{q_{in}} = \frac{q_{in} - q_{out}}{q_{in}} = \frac{{}_2q_3 - {}_4q_1}{{}_2q_3}$$

For isothermal expansion from point (2) to (3):

$${}_2q_3 = {}_2w_3$$

Hence the thermal efficiency may be re-written as:

$$\eta = \frac{{}_2 w_3 - {}_4 q_1}{{}_2 w_3}$$

Equation A. 1

Work done during the isothermal expansion process from point (2) to (3) is defined by the integral of pressure over the changes in volume. Hence:

$${}_2 w_3 = \int_2^3 p \cdot dv$$

Since pv = RT, and assuming that R and T remain constant throughout the isothermal expansion process, then the product of pv is constant. Thus:

$$p \cdot v = k$$

Hence the work done by the working fluid during the isothermal expansion from process from (2) to (3) may generally be expressed as:

$${}_2 w_3 = k \int_2^3 \frac{dv}{v} = k \cdot \ln\left(\frac{v_3}{v_2}\right)$$

More specifically the work done by the working fluid during the isothermal expansion from process from (2) to (3) may be expressed using the pressure and specific volume at point 2:

$${}_2 w_3 = p_2 v_2 \cdot \ln\left(\frac{v_3}{v_2}\right)$$

Equation A. 2

The heat rejected during the isobaric heat rejection process from (4) to (1) is defined by the change in enthalpy from points (4) to (1). Under the assumption that the specific heat capacity at constant pressure is constant with temperature, the change in enthalpy may be expressed by the specific heat capacity at constant pressure, and the temperature of the working fluid points (4) to (1). Thus:

$${}_4 q_1 = p_1\left(v_4 - v_1\right) + \left(u_4 - u_1\right) = h_4 - h_1 = c_p\left(T_4 - T_1\right)$$

Equation A. 3

By substituting Equation A. 2 and Equation A. 3 back into Equation A. 1, the indicated thermal efficiency of the cycle may be expressed as:

$$\eta = \frac{p_2 v_2 \cdot \ln\left(\frac{v_3}{v_2}\right) - c_p\left(T_4 - T_1\right)}{p_2 v_2 \cdot \ln\left(\frac{v_3}{v_2}\right)}$$

Equation A. 4

The compression ratio shall be defined as:

$$r = \frac{v_1}{v_2}$$

Equation A. 5

And the cut-off ratio shall be defined as:

$$r_c = \frac{v_3}{v_2}$$

Equation A. 6

Thus Equation A. 4 may be re-written as:

$$\eta = \frac{p_2 v_2 \cdot \ln\left(r_c\right) - c_p\left(T_4 - T_1\right)}{p_2 v_2 \cdot \ln\left(r_c\right)}$$

Equation A. 7

For isentropic expansion between points (3) and (4):

$$T_4 = T_3\left(\frac{p_4}{p_3}\right)^{\frac{\gamma-1}{\gamma}}$$

Equation A. 8

where:

$$p_3 = \frac{p_2 v_2}{v_3}$$

Equation A. 9

And since:

$$\frac{p_1 v_1}{T_1} = \frac{p_2 v_2}{T_2}$$

Then:

$$\frac{T_2}{T_1} = \frac{p_2 v_2}{p_1 v_1}$$

Equation A. 10

For polytropic compression between points (1) and (2):

$$p_1 \cdot {v_1}^{\gamma} = p_2 \cdot {v_2}^{\gamma}$$

So that:

$$\frac{p_2}{p_1} = \frac{{v_1}^{\gamma}}{{v_2}^{\gamma}} = r^{\gamma}$$

Equation A. 11

Substituting Equation A. 11 into Equation A. 10 yields:

$$\frac{T_2}{T_1} = \frac{v_2}{v_1} \cdot r^{\gamma} = r^{-1} \cdot r^{\gamma} = r^{\gamma - 1}$$

Equation A. 12

But since:

$$p_2 v_2 = \frac{T_2}{T_1} p_1 v_1$$

Equation A. 13

Substituting Equation A. 12 into Equation A. 13 yields:

$$p_2 v_2 = r^{\gamma - 1} \cdot p_1 v_1$$

Equation A. 14

Substituting Equation A. 14 into Equation A. 9 yields:

$$p_3 = \frac{r^{\gamma - 1} \cdot p_1 v_1}{v_3}$$

Equation A. 15

Substituting Equation A. 15 back into Equation A. 8 gives:

$$T_4 = T_3\left(\frac{p_4 v_3}{r^{\gamma-1}\cdot p_1 v_1}\right)^{\frac{\gamma-1}{\gamma}}$$

Since process (2) to (3) is isothermal, T_2 = T3. Hence:

$$T_4 = T_2\left(\frac{p_4 v_3}{r^{\gamma-1}\cdot p_1 v_1}\right)^{\frac{\gamma-1}{\gamma}}$$

Equation A. 16

For polytropic compression:

$$p_1 \cdot v_1^{\gamma} = p_2 \cdot v_2^{\gamma}$$

Hence:

$$\frac{p_2}{p_1} = \left(\frac{v_1}{v_2}\right)^{\gamma}$$

Equation A. 17

Subsituting Equation A. 17 into Equation A. 10 yields:

$$\frac{T_2}{T_1} = \frac{v_2}{v_1}\left(\frac{v_1}{v_2}\right)^{\gamma} = \left(\frac{v_1}{v_2}\right)^{\gamma-1} = r^{\gamma-1}$$

Hence:

$$T_2 = T_1 \cdot r^{\gamma-1}$$

Equation A. 18

Substituting Equation A. 18 into Equation A. 16 yields:

$$T_4 = T_1 \cdot r^{\gamma-1} \cdot \left(\frac{p_4 v_3}{r^{\gamma-1}\cdot p_1 v_1}\right)^{\frac{\gamma-1}{\gamma}}$$

Since p4 = p1 this may be reduced to:

$$T_4 = T_1 \cdot r^{\gamma-1} \cdot \left(\frac{v_3}{r^{\gamma-1}\cdot v_1}\right)^{\frac{\gamma-1}{\gamma}}$$

Equation A. 19

From the definition of cut-off ratio, i.e. Equation A. 6:

$$v_3 = r_c \cdot v_2$$

Substituting this into 27 yields:

$$T_4 = T_1 \cdot r^{\gamma-1} \cdot \left(\frac{r_c \cdot v_2}{r^{\gamma-1} \cdot v_1} \right)^{\frac{\gamma-1}{\gamma}}$$

From the definition of compression ratio, i.e. Equation A. 5. Hence:

$$T_4 = T_1 \cdot r^{\gamma-1} \cdot \left(\frac{r_c}{r^{\gamma-1} \cdot r} \right)^{\frac{\gamma-1}{\gamma}}$$

Which may be re-arranged to yield:

$$T_4 = T_1 \cdot r^{\gamma-1} \cdot \left(\frac{r_c}{r^{\gamma}} \right)^{\frac{\gamma-1}{\gamma}}$$

Equation A. 20

Since pv = RT, and in particular $p_2v_2=RT_2$, Equation A. 7 may be re-written as:

$$\eta = \frac{RT_2 \cdot \ln(r_c) - c_p(T_4 - T_1)}{RT_2 \cdot \ln(r_c)}$$

Equation A. 21

Substituting Equation A. 20 into Equation A. 21 yields:

$$\eta = \frac{RT_2 \cdot \ln(r_c) - c_p\left(T_1 \cdot r^{\gamma-1} \cdot \left(\frac{r_c}{r^{\gamma}} \right)^{\frac{\gamma-1}{\gamma}} - T_1 \right)}{RT_2 \cdot \ln(r_c)}$$

From Equation A. 18 again, this yields:

$$\eta = \frac{RT_1 \cdot r^{\gamma-1} \cdot \ln(r_c) - c_p\left(T_1 \cdot r^{\gamma-1} \cdot \left(\frac{r_c}{r^{\gamma}} \right)^{\frac{\gamma-1}{\gamma}} - T_1 \right)}{RT_1 \cdot r^{\gamma-1} \cdot \ln(r_c)}$$

Eliminating T_1 from the relation yields:

$$\eta = \frac{R \cdot r^{\gamma-1} \cdot \ln(r_c) - c_p\left(r^{\gamma-1} \cdot \left(\frac{r_c}{r^{\gamma}} \right)^{\frac{\gamma-1}{\gamma}} - 1 \right)}{R \cdot r^{\gamma-1} \cdot \ln(r_c)}$$

Rearranging the term $r^{\gamma-1}$ and the constant R within the equation yields:

$$\eta = \frac{\ln(r_c) - \frac{c_p}{R}\left(\left(\frac{r_c}{r^{\gamma}} \right)^{\frac{\gamma-1}{\gamma}} - \frac{1}{r^{\gamma-1}} \right)}{\ln(r_c)}$$

Equation A. 22

Since $\gamma = \frac{c_p}{c_v}$; and $R = c_p - c_v$:

$$\frac{c_p}{R} = \frac{1}{1 - \frac{1}{\gamma}}$$

Equation A. 23

Substituting Equation A. 23 into Equation A. 22 yields:

$$\eta = \frac{\ln(r_c) - \frac{1}{1 - \frac{1}{\gamma}}\left(\left(\frac{r_c}{r^\gamma}\right)^{\frac{\gamma-1}{\gamma}} - \frac{1}{r^{\gamma-1}}\right)}{\ln(r_c)}$$

which may be re-written as:

$$\eta = \frac{\ln(r_c) - \frac{\gamma}{\gamma - 1}\left(\left(\frac{r_c}{r^\gamma}\right)^{\frac{\gamma-1}{\gamma}} - r^{1-\gamma}\right)}{\ln(r_c)}$$

This yields:

$$\eta = 1 - \frac{\frac{\gamma}{\gamma - 1}}{\ln(r_c)}\left(\left(\frac{r_c}{r^\gamma}\right)^{\frac{\gamma-1}{\gamma}} - r^{1-\gamma}\right)$$

Thus the thermal efficiency of the isothermal combustion cycle described by Diesel (1892), may be expressed in terms of the ratio of specific heats of the working fluid γ, the compression ratio r, and the rc. This may be written as:

$$\eta_{Diesel1892} = 1 - \frac{\frac{\gamma}{\gamma - 1}}{\ln(r_c)}\left[\left(\frac{r_c}{r^\gamma}\right)^{\frac{\gamma-1}{\gamma}} - r^{1-\gamma}\right]$$

Equation A. 24

Derivation of cycle with isothermal combustion without overexpansion according to Diesel (1892) as a function of compression ratio and cut-off ratio

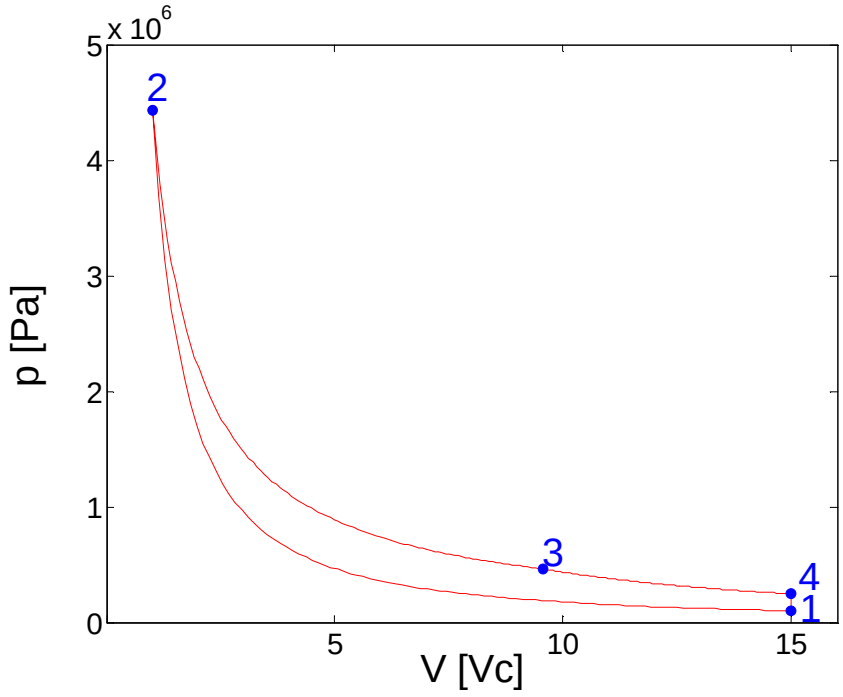

Figure A. 2- Indicator diagram for thermodynamic cycle with isothermal combustion without overexpansion according to Diesel (1892)

For the cyclic process shown in Figure A. 2, the net indicated work done per cycle by the working fluid may be expressed by the cyclic integral of the pressure of the working fluid over its volume.

$$W_{cycle} = \oint p \cdot dV$$

The net indicated mean effective pressure (P_{IME}) may be defined by the net indicated work done per cycle divided by the volume of the working fluid.

$$P_{IME} = \frac{\oint p \cdot dV}{V_{swept}}$$

The indicated thermal efficiency of the cycle may be defined as the net specific work output of the cycle divided by the heat supplied to the working fluid per cycle. Thus:

$$\eta = \frac{w_{out}}{q_{in}} = \frac{q_{in} - q_{out}}{q_{in}} = \frac{{}_2q_3 - {}_4q_1}{{}_2q_3}$$

For isothermal expansion from point (2) to (3):

$${}_2q_3 = {}_2w_3$$

Hence the thermal efficiency may be re-written as:

$$\eta = \frac{{}_2w_3 - {}_4q_1}{{}_2w_3}$$

Equation A. 25

Work done during the isothermal expansion process from point (2) to (3) is defined by the integral of pressure over the changes in volume. Hence:

$${}_2w_3 = \int_2^3 p \cdot dv$$

Since pv = RT, and assuming that R and T remain constant throughout the isothermal expansion process, then the product of pv is constant. Thus:

$$p \cdot v = k$$

Hence the work done by the working fluid during the isothermal expansion from process from (2) to (3) may generally be expressed as:

$${}_2w_3 = k\int_2^3 \frac{dv}{v} = k \cdot \ln\left(\frac{v_3}{v_2}\right)$$

More specifically the work done by the working fluid during the isothermal expansion from process from (2) to (3) may be expressed using the pressure and specific volume at point 2:

$${}_2w_3 = p_2v_2 \cdot \ln\left(\frac{v_3}{v_2}\right)$$

Equation A. 26

The heat rejected during the isochoric heat rejection process from (4) to (1) is defined by the change in internal energy from points (4) to (1). Under the assumption that the specific heat capacity at constant volume is constant with temperature, the change in internal energy may be expressed by the specific heat capacity at constant volume, and the temperature change of the working fluid points (4) to (1). Thus:

$${}_4q_1 = p_1(v_4 - v_1) + (u_4 - u_1) = (u_4 - u_1) = c_v(T_4 - T_1)$$

Equation A. 27

By substituting Equation A. 26 and Equation A. 27 back into Equation A. 25, the indicated thermal efficiency of the cycle may be expressed as:

$$\eta = \frac{p_2 v_2 \cdot \ln\left(\frac{v_3}{v_2}\right) - c_v\left(T_4 - T_1\right)}{p_2 v_2 \cdot \ln\left(\frac{v_3}{v_2}\right)}$$

Equation A. 28

The compression ratio shall be defined as:

$$r = \frac{v_1}{v_2}$$

Equation A. 29

And the cut-off ratio shall be defined as:

$$r_c = \frac{v_3}{v_2}$$

Equation A. 30

Thus Equation A. 28 may be re-written as:

$$\eta = \frac{p_2 v_2 \cdot \ln\left(r_c\right) - c_v\left(T_4 - T_1\right)}{p_2 v_2 \cdot \ln\left(r_c\right)}$$

Equation A. 31

T_4 may be calculated as follows. The polytropic compression between points may be described by the following relation using the ratio of specific heats γ:

$$p_1 \cdot v_1^{\gamma} = p_2 \cdot v_2^{\gamma}$$

Equation A. 32

$$\frac{p_2}{p_1} = \frac{v_1^{\gamma}}{v_2^{\gamma}}$$

Equation A. 33

But pv = RT, so that:

$$\frac{p_1 \cdot v_1}{T_1} = \frac{p_2 \cdot v_2}{T_2}$$

Therefore:

$$\frac{T_2}{T_1} = \frac{p_2 \cdot v_2}{p_1 \cdot v_1}$$

Equation A. 34

Substituting Equation A. 33 into Equation A. 34 yields:

$$\frac{T_2}{T_1} = \frac{{v_1}^{\gamma} \cdot v_2}{{v_2}^{\gamma} \cdot v_1} = \frac{v_1^{\gamma-1}}{v_2^{\gamma-1}} = \left(\frac{v_1}{v_2}\right)^{\gamma-1}$$

Considering the definition of the compression ratio, this yields:

$$\frac{T_2}{T_1} = r^{\gamma-1}$$

So that:

$$T_2 = T_1 \cdot r^{\gamma-1}$$

Equation A. 35

For isentropic expansion from point (3) to (4):

$$\frac{T_4}{T_3} = \left(\frac{P_4}{P_3}\right)^{\frac{\gamma-1}{\gamma}} = \left(\frac{v_3}{v_4}\right)^{\gamma-1}$$

Equation A. 36

From the definition of compression ratio, i.e. Equation A. 29 and cut-off ratio, i.e. Equation A. 30, and since:

$$v_4 = v_1$$

Equation A. 36 may be re-arranged to yield:

$$T_4 = T_3 \cdot \left(\frac{v_2 \cdot r_c}{v_1}\right)^{\gamma-1} = T_3 \cdot \left(\frac{r_c}{r}\right)^{\gamma-1}$$

Equation A. 37

Since the expansion process between points (2) and (3) is isothermal:

$$T_3 = T_2$$

Thus:

$$T_4 = T_2 \cdot \left(\frac{r_c}{r}\right)^{\gamma-1}$$

Equation A. 38

Substituting Equation A. 35 into Equation A. 38 yields:

$$T_4 = T_1 \cdot r^{\gamma-1} \cdot \left(\frac{r_c}{r}\right)^{\gamma-1}$$

Equation A. 39

Substituting Equation A. 28 back into yields:

$$\eta = \frac{p_2 v_2 \cdot \ln(r_c) - c_v\left(T_1 \cdot r^{\gamma-1} \cdot \left(\frac{r_c}{r}\right)^{\gamma-1} - T_1\right)}{p_2 v_2 \cdot \ln(r_c)}$$

Equation A. 40

Since pv = RT, and in particular $p_2v_2=RT_2$, Equation A. 40 may be re-written as:

$$\eta = \frac{R \cdot T_2 \cdot \ln(r_c) - c_v\left(T_1 \cdot r^{\gamma-1} \cdot \left(\frac{r_c}{r}\right)^{\gamma-1} - T_1\right)}{R \cdot T_2 \cdot \ln(r_c)}$$

Again substituting T_2 using Equation A. 35 yields:

$$\eta = \frac{R \cdot T_1 \cdot r^{\gamma-1} \cdot \ln(r_c) - c_v\left(T_1 \cdot r^{\gamma-1} \cdot \left(\frac{r_c}{r}\right)^{\gamma-1} - T_1\right)}{R \cdot T_1 \cdot r^{\gamma-1} \cdot \ln(r_c)}$$

Which may be simplified to:

$$\eta = \frac{R \cdot \ln(r_c) - c_v\left(\left(\frac{r_c}{r}\right)^{\gamma-1} - \frac{1}{r^{\gamma-1}}\right)}{R \cdot \ln(r_c)}$$

And:

$$\eta = \frac{\ln(r_c) - \frac{c_v}{R}\left(\left(\frac{r_c}{r}\right)^{\gamma-1} - \frac{1}{r^{\gamma-1}}\right)}{\ln(r_c)}$$

Equation A. 41

But since $\gamma = \frac{c_p}{c_v}$; and $R = c_p - c_v$:

$$\frac{c_v}{R} = \frac{1}{\gamma - 1}$$

Equation A. 42

Substituting Equation A. 42 back into Equation A. 41 yields:

$$\eta = \frac{\ln(r_c) - \frac{1}{\gamma - 1}\left(\left(\frac{r_c}{r}\right)^{\gamma-1} - \frac{1}{r^{\gamma-1}}\right)}{\ln(r_c)}$$

Which in turn may be reduced to:

$$\eta_{isothermal} = 1 - \frac{1}{\gamma - 1} \cdot \frac{1}{\ln(r_c)}\left[\left(\frac{r_c}{r}\right)^{\gamma-1} - r^{1-\gamma}\right]$$

Equation A. 43

Detailed stoichimetric analysis of combustion experiments

Definition of variables

Φ	fuel-air equivalence ratio
φ	molar coefficient of injected fuel
a	Number of C atoms in one fuel molecule
b	Number of H atoms in one fuel molecule
c	Number of O atoms in one fuel molecule
d	Number of N atoms in one fuel molecule
e	Molar coefficient of air
g	Molar coefficient of CO_2 in the exhaust gas
h	Molar coefficient of CO in the exhaust gas
j	Molar coefficient of O_2 in the exhaust gas
k	Molar coefficient of N_2 in the exhaust gas
l	Molar coefficient of NO in the exhaust gas
m	Molar coefficient of NO_2 in the exhaust gas
s	Molar coefficient of CH_4 in the exhaust gas
t	Molar coefficient of H_2 in the exhaust gas
μ	Molar coefficient of N_2 in the intake air
υ	Molar coefficient of O_2 in the intake air
ω	Molar coefficient of CO_2 in the intake air
π	Molar coefficient of H_2O in the intake air

Subscripts

i	associated with engine inlet gas mixture
e	associated with engine exhaust gas mixture

Superscripts

‘	denotes a dry molar coefficient, measured after the removal of water

The general combustion equation:

The combustion of a fuel molecule comprising carbon, hydrogen, oxygen and nitrogen atoms in air containing CO_2 and H_20 as constituents, can be described by Equation A. 44 below:

$$\varphi \cdot C_a H_b O_c N_d + e \cdot (\upsilon \cdot O_2 + \mu \cdot N_2 + \omega \cdot CO_2 + \pi \cdot H_2O)$$
$$\Rightarrow$$
$$g_e \cdot CO_2 + h_e \cdot CO + j_e \cdot O_2 + k_e \cdot N_2 + l_e \cdot H_2O + m_e \cdot NO + q_e \cdot NO_2 + s_e \cdot CH_4 + t_e \cdot H_2$$

Equation A. 44

For lean or stoichiometric combustion, the term t_e is assumed to be negligible. Thus $t_e \rightarrow 0$. Balancing the atoms on both sides, we now have the general combustion equation (Equation A. 45):

$$\varphi \cdot C_a H_b O_c N_d + e \cdot (\upsilon \cdot O_2 + \mu \cdot N_2 + \omega \cdot CO_2 + \pi \cdot H_2O)$$
$$=$$
$$g_e \cdot CO_2 + h_e \cdot CO + j_e \cdot O_2 + k_e \cdot N_2 + l_e \cdot H_2O + m_e \cdot NO + q_e \cdot NO_2 + s_e \cdot CH_4$$

Equation A. 45

Balancing the atoms in the combustion equation

Atoms are neither destroyed nor created during the combustion reaction, but merely regrouped with one another to form different molecular species. Thus the number of atoms present in the reactant species must be equal to that of the number of atoms present in the product species. In particular, this balance of atoms is true for each type of atom present in the combustion reaction because no changes in the type of atoms occur, i.e. to the C, H, O and N atoms individually. Every atomic balance is described by one mathematical equation as shown below:

The balance of carbon atoms

Consider the simplified general combustion reaction given by Equation A. 45. The balance of carbon atoms is described by the following equation:

$$\varphi \cdot a + e \cdot \omega = g_e + h_e + s_e$$

Equation A. 46

The balance of hydrogen atoms

The balance of hydrogen atoms in Equation A. 45 is described by:

$$\varphi \cdot b + 2 \cdot e \cdot \pi = 2 \cdot l_e + 4 \cdot s_e$$

Equation A. 47

This may be re-arranged as:

$$\varphi \cdot b + 2 \cdot e \cdot \pi - 2 \cdot l_e = 4 \cdot s_e$$

Equation A. 48

The balance of oxygen atoms

The balance of oxygen atoms in Equation A. 45 is described by:

$$\varphi \cdot c + e \cdot \left(2 \cdot \upsilon + 2 \cdot \omega + \pi\right) = 2 \cdot g_e + h_e + 2 \cdot j_e + l_e + m_e + 2 \cdot q_e$$

Equation A. 49

This may be re-arranged as:

$$\varphi \cdot c + e \cdot \left(2 \cdot \upsilon + 2 \cdot \omega + \pi\right) - l_e = 2 \cdot g_e + h_e + 2 \cdot j_e + m_e + 2 \cdot q_e$$

Equation A. 50

The balance of nitrogen atoms

The balance of nitrogen atoms in Equation A. 45 is described by:

$$\varphi \cdot d + 2 \cdot e \cdot \mu = 2 \cdot k_e + m_e + q_e$$

Equation A. 51

This may be re-arranged as:

$$\varphi \cdot d + 2 \cdot e \cdot \mu - 2 \cdot k_e = m_e + q_e$$

Equation A. 52

System of four linear equations

The four atomic balances can be coupled together, and are sufficient to fully determine the combustion reaction. This can be done in matrix form, in which the matrix A is the matrix of coefficients for the 4 unknowns φ, e, k_e and l_e, b is the vector of the four unknowns, and c is the vector of constant terms.

$$[A]\cdot[b]=[c]$$

Equation A. 53

The solution to the vector of unknowns b in this system can be found by multiplying both sides of Equation A. 53 by the inverse of A, i.e. A^{-1}.

$$[b]=[A^{-1}]\cdot[c]$$

Equation A. 54

Writing the four simultaneous linear equations of Equation A. 46, Equation A. 48, Equation A. 50 and Equation A. 52, in matrix form yields the matrix equation shown in Equation A. 54 below. The first row describes the carbon balance, the second row the hydrogen balance, the third row the oxygen balance and the fourth row describes the nitrogen balance.

$$\begin{bmatrix} a & \omega & 0 & 0 \\ b & 2\cdot\pi & 0 & -2 \\ c & (2\cdot\upsilon+2\cdot\omega+\pi) & 0 & -1 \\ d & 2\cdot\mu & -2 & 0 \end{bmatrix}\cdot\begin{bmatrix} \varphi \\ e \\ k_e \\ l_e \end{bmatrix}=\begin{bmatrix} g_e+h_e+s_e \\ 4\cdot s_e \\ 2\cdot g_e+h_e+2\cdot j_e+m_e+2\cdot q_e \\ m_e+q_e \end{bmatrix}$$

Equation A. 55

As shown in Equation A. 53 and Equation A. 54, this system may be solved by multiplying both sides of the equation by the inverse of A. This yields a solution to the vector of unknowns b as follows:

$$\begin{bmatrix} \varphi \\ e \\ k_e \\ l_e \end{bmatrix}=\begin{bmatrix}\begin{bmatrix} a & \omega & 0 & 0 \\ b & 2\cdot\pi & 0 & -2 \\ c & (2\cdot\upsilon+2\cdot\omega+\pi) & 0 & -1 \\ d & 2\cdot\mu & -2 & 0 \end{bmatrix}^{-1}\end{bmatrix}\cdot\begin{bmatrix} g_e+h_e+s_e \\ 4\cdot s_e \\ 2\cdot g_e+h_e+2\cdot j_e+m_e+2\cdot q_e \\ m_e+q_e \end{bmatrix}$$

Equation A. 56

Calculation of the equivalence ratio Φ

In order to determine the equivalence ratio under which combustion is taking place, the combustion equation for complete combustion of the fuel at a stoichiometric fuel to air ratio needs to be found. Assuming stoichiometric conditions and complete combustion, so that the only species present in the exhaust gas are CO_2, N_2 and H_2O. The general combustion equation can thus be written as:

$$\boxed{\begin{gathered}\varphi \cdot C_a H_b O_c N_d + e \cdot \left(\upsilon \cdot O_2 + \mu \cdot N_2 + \omega \cdot CO_2 + \pi \cdot H_2O\right) \\ \Rightarrow \\ g_e \cdot CO_2 + k_e \cdot N_2 + l_e \cdot H_2O\end{gathered}}$$

Equation A. 57

In order to calculate the stoichiometric fuel to air ratio, knowledge of the fuel composition in terms of its relative molar quantities of carbon, hydrogen, oxygen and nitrogen atoms, as well as the air composition in terms of its relative amounts of oxygen and nitrogen present. Thus, knowledge of the variables a, b, c, d and μ is required to balance Equation A. 57. For simplicity, φ will be defined as being equal to unity. Thus:

$$\varphi \equiv 1$$

Equation A. 58

The balance of carbon atoms

$$g_e = a + e \cdot \omega$$

Equation A. 59

The balance of hydrogen atoms

$$b + 2 \cdot \pi \cdot e = 2 \cdot l_e$$

Equation A. 60

$$l_e = \frac{b + 2 \cdot \pi \cdot e}{2}$$

Equation A. 61

The balance of oxygen atoms

$$c + e\left(2 \cdot \upsilon + 2 \cdot \omega + \pi\right) = 2 \cdot g_e + l_e$$

Equation A. 62

The balance of nitrogen atoms

$$d + 2 \cdot e \cdot \mu = 2 \cdot k_e$$

Equation A. 63

$$k_e = \frac{d + 2 \cdot e \cdot \mu}{2}$$

Equation A. 64

Combining the carbon, hydrogen and oxygen balances yields: Substituting Equation A. 59 and Equation A. 61 into Equation A. 62 yields:

$$c + e\left(2 \cdot \upsilon + 2 \cdot \omega + \pi\right) = 2 \cdot \left(a + e \cdot \omega\right) + \frac{b + 2 \cdot \pi \cdot e}{2}$$

Equation A. 65

$$c + e\left\{\left(2 \cdot \upsilon + 2 \cdot \omega + \pi\right)\right\} = 2 \cdot a + 2 \cdot e \cdot \omega + \frac{b}{2} + e \cdot \pi$$

Equation A. 66

$$e\left\{\left(2 \cdot \upsilon + 2 \cdot \omega + \pi\right) - 2 \cdot \omega - \pi\right\} = 2 \cdot a + \frac{b}{2} - c$$

Equation A. 67

Which may be resolved for e:

$$e = \frac{2 \cdot a + \frac{b}{2} - c}{2 \cdot \upsilon}$$

Equation A. 68

The molar coefficient e can thus be calculated from the amounts of carbon, hydrogen and oxygen atoms present in the fuel, i.e. the variables a, b and c. Equation A. 68 is thus very similar to Equation 4.83 in Chapter 4, with the added variable υ, describing the relative oxygen content in the air.

The equivalence ratio Φ of a combustion experiment

As described earlier, the equivalence ratio is a measure of the relative gravimetric amounts of fuel to air compared with the gravimetric amounts of fuel to air for a stoichiometric mixture, and can be described by Equation A. 69 and Equation A. 70 below.

$$\Phi = \frac{\left(\frac{m_{fuel}}{m_{air}}\right)_{Experiment}}{\left(\frac{m_{fuel}}{m_{air}}\right)_{Stoichiometric}}$$

Equation A. 69

$$\Phi = \frac{\varphi_{Experiment} \cdot e_{Stoichiometric}}{\varphi_{Stoichiometric} \cdot e_{Experiment}}$$

Equation A. 70

As Equation A. 70 demonstrates, knowledge of the molar mass of the fuel and air are thus not necessary for the calculation of the equivalence ratio. The coefficients φ and e are calculated via the solution of Equation A. 56 for experimental conditions, and Equation A. 58 and Equation A. 68 for stoichiometric conditions respectively.

The gravimetric fuel-air ratio

The gravimetric fuel to air ratio ($FAR_{gravimetric}$) describes the mass of fuel, divided by the mass of air. The molar mass of a fuel molecule or the average mass of an air molecule, can both be calculated from the mass of the atoms of which the molecules comprise. The gravimetric fuel to air ratio ($FAR_{gravimetric}$) can thus be found using Equation A. 71.

$$FAR_{gravimetric} = \frac{m_{fuel}}{m_{air}} = \frac{\varphi \cdot \left(m_{C_aH_bO_cN_d}\right)}{e \cdot \left(\upsilon + \mu + \omega + \pi\right) \cdot m_{air}}$$

Equation A. 71

Referring to the atomic masses given in Table 4.1, the molar mass of a fuel molecule and the average mass of an air molecule can thus be calculated as follows:

Molar mass of a fuel molecule of the composition $C_aH_bO_cN_d$:

$$m_{C_aH_bO_cN_d} = 12.0107 \cdot a + 1.00794 \cdot b + 15.9994 \cdot c + 14.00674 \cdot d$$

Equation A. 72

Molar mass of an air molecule of the mean composition $\frac{\upsilon \cdot O_2 + \mu \cdot N_2 + \omega \cdot CO_2 + \pi \cdot H_2O}{\upsilon + \mu + \omega + \pi}$:

$$m_{air} = \frac{15.9994 \cdot \left(2 \cdot \upsilon + 2 \cdot \omega + \pi\right) + 14.00674 \cdot \left(2 \cdot \mu\right) + 12.0107 \cdot \omega}{\upsilon + \mu + \omega + \pi}$$

Equation A. 73

Calculation of fuel consumption

The fuel consumption can be calculated from knowledge of the composition of the exhaust gas and the air-flow through the engine as per Equation A. 74.

$$m_{fuel} = m_{air} \cdot \frac{\varphi_{Experiment} \cdot \left(m_{C_a H_b O_c N_d}\right)}{e_{Experiment} \cdot \left(\upsilon + \mu + \omega + \pi\right) \cdot m_{air}}$$

Equation A. 74

The relative amount of O_2, N_2, CO_2 and H_2O in the air, described by υ, μ, ω and π respectively must be known from measurement or literature, the stoichiometry coefficients φ and e are found through Equation A. 56, whilst the molecular mass of the fuel molecule and the mean molecular mass of air are calculated via Equation A. 72 and Equation A. 73 respectively. Depending on whether the mass of air refers to the mass of air going through the engine per engine revolution, engine cycle, or time unit, the corresponding amount of fuel of the same unit may be calculated via Equation A. 74.

All other parameters can be calculated as per the simplified combustion model previously presented herein.

The stoichiometric combustion models have been encoded for ‘Matlab 6.1’ The source codes for four versions of the combustion model can be found in electronic format on a CD (Appendix G).

Appendix B. Instrument calibrations

Piezoresistive pressure transducer calibration in conjunction with the data acquisition system

Pressure sensor:

Date of calibration 11 October 2006
Calibrated by Alessandro Schönborn

KISTLER Type 6056AU38
SN 1445255
Kistler Calibration 0-100 bar: -19.10 pC/bar
Kistler Calibration 0-150 bar: -19.18 pC/bar

Charge Amplifier:

KISTLER Type 5011
tested 19.11.03
Calibration factors:
T = 1.91E1
S = 1.50E1 286.5

Data acquisition System:
NI 6251 Data acquisition card
Labview software

Dead weight calibration results:

Calibration gauge pressure:	100.8206	bar
Atmospheric pressure:	1011	mbar
Calibration temperature:	21	º C

Calibration factor:	**TEST 1**		**TEST 2**		**TEST 3**		**Standard deviation:**
[bar/volts]	**14.90838**	[bar/v]	**14.89608**	[bar/v]	**14.89665**	[bar/v]	**0.00694554**
							0.69455379
Error from kistler individual component calibration:	**0.349905**	%	**0.432142**	%	**0.428355**	%	
error in bar	0.349905	[bar]	0.432142	[bar]	0.428355	[bar]	Average of 3 tests:
transducer sensitivity	-18.9833		-18.9677		-18.9684		**-18.97314**
error [%]	-0.6108%		-0.6928%		-0.6890%		**-0.6642%**

Average Value: **14.9** [bar/v]

Engine air flow-rate calibration

Engine speed [rpm]	Time for 10 Pulses [s]	Pulses per second [1/s]	Air flow per second [m3/s]	P Romet [bar]	T Romet [deg C]	mass/sec [kg/s]	mass/sec [g/s]	Air per cylinder charg [m3]	[l]	Air per cylinder charge [kg]	[g]
750	371	0.026954	0.002695	1.09	17	0.003528	3.528158739	0.000431	0.431267	0.000556	0.556334
800	347	0.028818	0.002882	1.07	17	0.003703	3.702966911	0.000432	0.432277	0.000558	0.557637
1000	274.5	0.03643	0.003643	1.08	17.5	0.004717	4.716601477	0.000437	0.437158	0.000564	0.563934
1200	221.1	0.045228	0.004523	1.08	18	0.005846	5.845697281	0.000452	0.452284	0.000583	0.583446
1400	188.94	0.052927	0.005293	1.08	18	0.006841	6.840709585	0.000454	0.453659	0.000585	0.58522
2000	133.00	0.075188	0.007519	1.07	18	0.009628	9.627941561	0.000451	0.451128	0.000582	0.581955
3500	84.78	0.117952	0.011795	1.09	18	0.015386	15.38630703	0.000404	0.404408	0.000522	0.521686

Engine speed [rpm]	RETARDED IVC [deg CA]	Time for 10 Pulses [s]	Pulses per second [1/s]	Air flow per second [m3/s]	P Romet [bar]	T Romet [deg C]	mass/sec [kg/s]	mass/sec [g/s]	Volume Air per cylinder charg [m3]	[l]	Mass Air per cylinder charge [kg]	[g]
1200	0	226.8667	0.044079	0.004408	1.008	20	0.005281	5.281023	0.000441	0.440788	0.000528	0.528102
1200	36	265.1667	0.037712	0.003771	1.008	20	0.004518	4.518245	0.000377	0.377121	0.000452	0.451825
1200	72	404.6667	0.024712	0.002471	1.008	20	0.002961	2.960679	0.000247	0.247117	0.000296	0.296068

Max Machinery, Inc.
1420 Healdsburg Ave
Healdsburg, CA 95448 USA
(707) 433-7281 www.maxmachinery.com

CALIBRATION CERTIFICATE

FLOWMETER BASIC CALIBRATION

	Flowmeter	Transmitter
Model No:	213-310	284-512
Serial No:	C451410	403

Sales Order: XXXX
Customer: STOCK
Date: 10 Mar 2005 2:12:00 PM
Test Stand: 401
Tested By: SLY
Test Fluid: KEROSENE
Viscosity (CPS): 1.83 CPS
Temp (°C): 21°C
Proof Pressure: 3000 PSI
Avg. K-Factor: 114.20

ccm	pulses/cc	% Error	Limits
1800	113.88	-0.28	0.5
1500	113.9	-0.26	0.5
1000	114.08	-0.11	0.5
300	114.52	0.28	0.5
100	114.46	0.23	0.5
30	114.27	0.06	0.5
10	113.98	-0.19	0.5
3	113.14	-0.93	1.67
1	110.66	-3.10	5

Linearity Curve

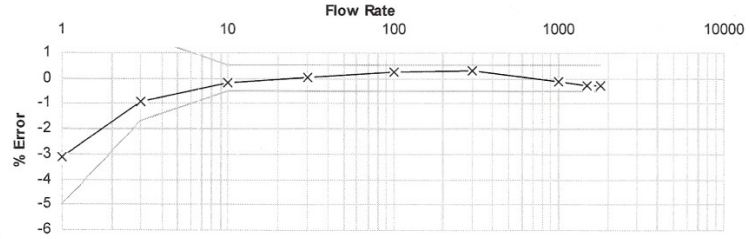

Pressure Drop

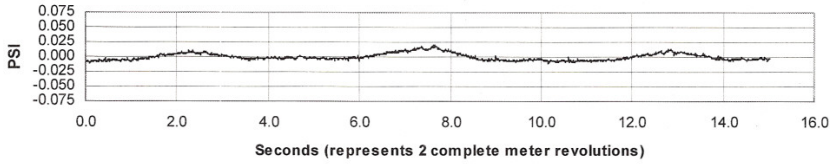

METER NOTES: The O-Rings Installed in this meter are **Viton**

FLOWMETER CONTAINS: RESIDUAL KEROSENE

For test stand 401 the uncertainty of the listed K-Factors is 0.123% with a 95% confidence. Calculations are available upon request.

Printed: 10 Mar 2005 2:38:51 PM

Figure B. 1 - Fuel flowmeter calibration certificate 10th March 2005

Calibration Report

Customer:	University College Londo	Job Number:	8713
Fluid:	isopar h	Save File Name:	max meter
Manufacturer:	Max Machinery	Model Number:	213-310
Serial Number:	C451410	Meter Tag:	
Meter Size:		End Fittings:	1.8" BSP
Bearing Type:		Sensor Type:	284 Transmitter
Sensor PN/SN:		Sensor Output:	
Ambient Temperature:	21.16 °C	Meter Density:	830.00 kg/m3

Meter Rate (l/min)	Meter Frequency (Hz)	Meter K-factor (p/lit)	Meter Viscosity (cSt)	Meter Pressure (bar)	Meter Temp (°C)
0.00303	5.72924	113286.30	7.04	5.00	21.08
0.00562	10.61974	113403.70	7.03	5.00	21.12
0.00999	18.89141	113480.46	7.02	5.00	21.15
0.01781	33.71905	113576.85	7.01	5.00	21.16
0.03076	58.20967	113526.69	7.01	5.00	21.17
0.06124	115.86827	113516.44	6.98	5.00	21.26
0.10428	197.80380	113811.68	7.01	5.00	21.19
0.19823	376.92095	114084.29	7.02	5.00	21.16

Calibrator Inv #:	MT99030169	Calibrated By:	J Thorne
Recal Date:	28/01/2006	Date:	29/06/2007
Procedure:		Certified By:	

Traceability:

Notes:

Figure B. 2 - Fuel flowmeter calibration certificate 28th January 2006

Appendix C. Additional experimental results

Fatty acid alkyl ester molecules with varying fatty acid chain lengths at constant injection timing

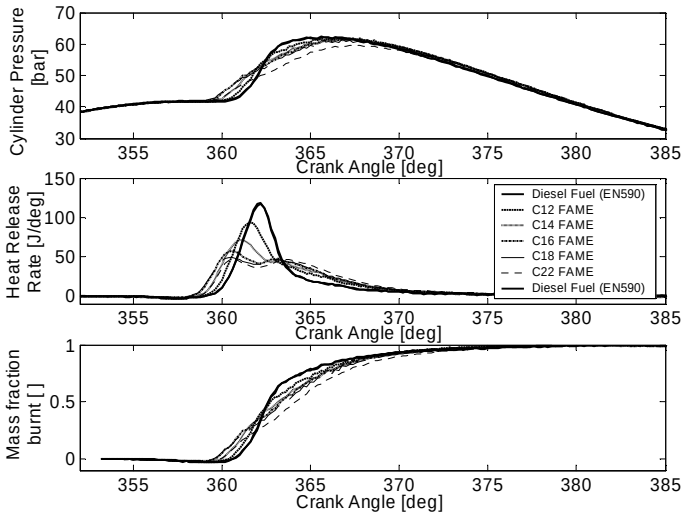

Figure C. 1- Effect of fatty acid chain length on cylinder pressure, net heat release rate and mass fraction burnt at constant injection timing

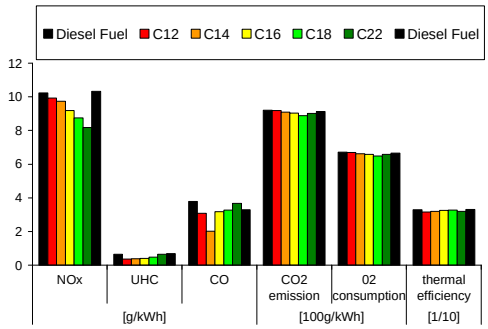

Figure C. 2 - Effect of fatty acid chain length on gaseous exhaust emissions and indicated thermal efficiency at constant injection timing

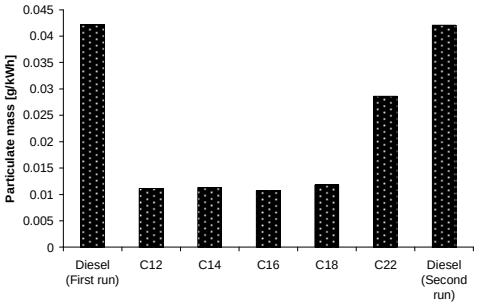

Figure C. 3 - Effect of chain length on total particulate matter emissions for constant injection timing

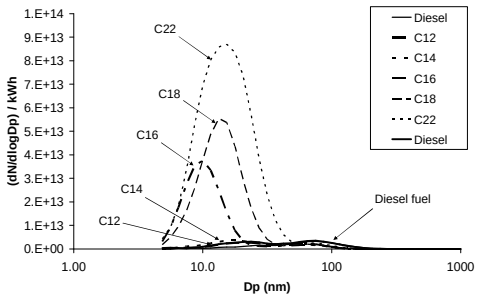

Figure C. 4- Particulate size distribution for constant injection timing

Fatty acid alkyl ester molecules with varying fatty acid chain lengths at constant ignition timing

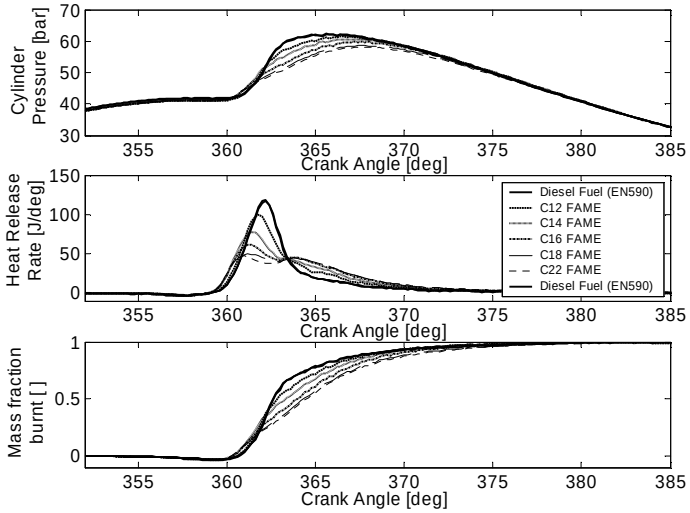

Figure C. 5- Effect of fatty acid chain length on cylinder pressure, net heat release rate and mass fraction burnt at constant ignition timing

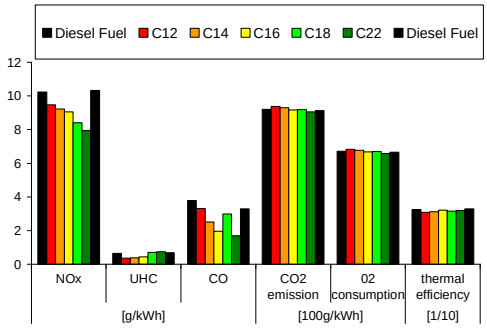

Figure C. 6-Effect of fatty acid chain length on gaseous exhaust emissions and indicated thermal efficiency at constant ignition timing

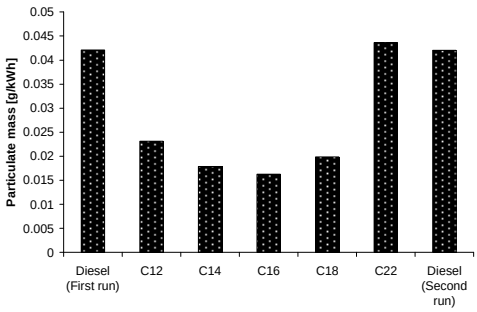

Figure C. 7 - Effect of chain length on total particulate matter emissions for constant ignition timing

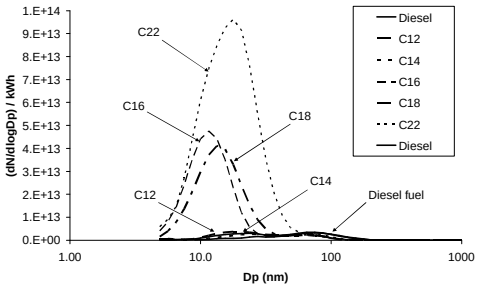

Figure C. 8- Particulate size distribution for constant ignition timing

Fatty acid alkyl ester molecules with varying fatty acid chain lengths at constant ignition delay

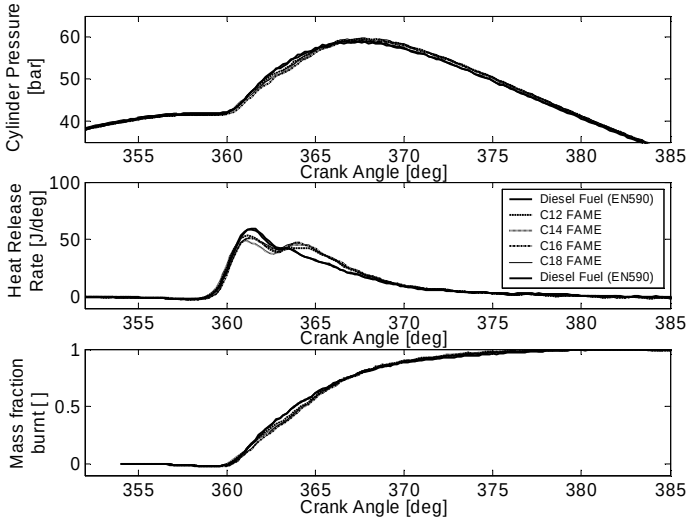

Figure C. 9 - Effect of fatty acid chain length on cylinder pressure, net heat release rate and mass fraction burnt at constant ignition delay

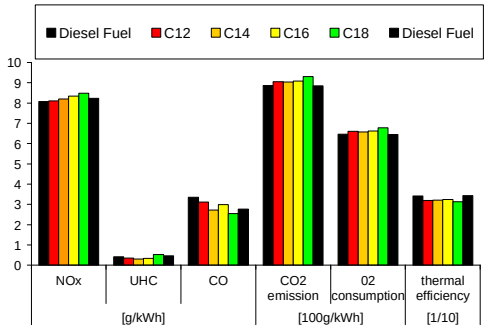

Figure C. 10 - Effect of fatty acid chain length on gaseous exhaust emissions and indicated thermal efficiency at constant ignition delay

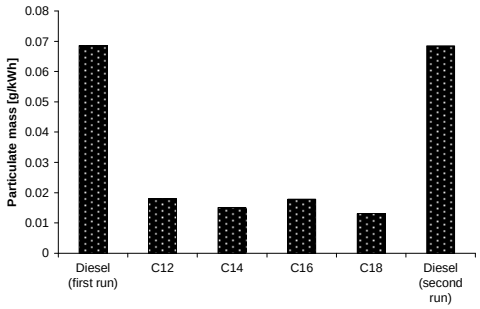

Figure C. 11 - Effect of chain length on total particulate matter emissions for constant ignition delay

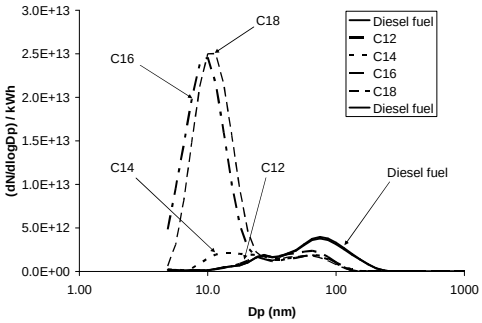

Figure C. 12- Particulate size distribution for constant ignition delay

Fatty acid alkyl ester molecules with varying degrees of saturation at constant injection timing

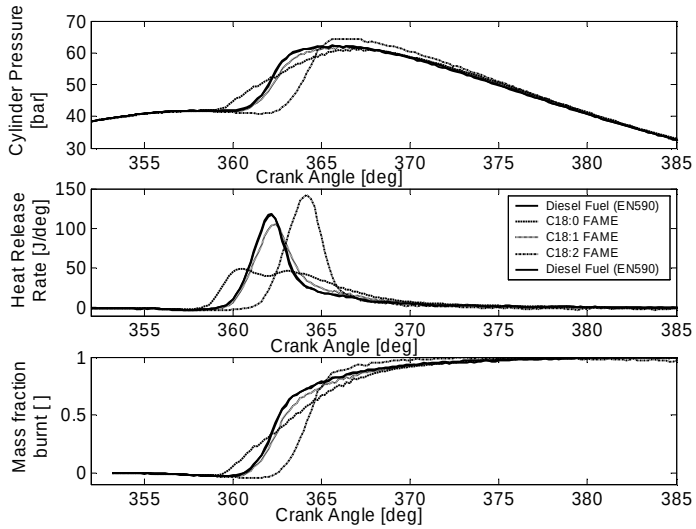

Figure C. 13 - Effect of fatty acid chain length on cylinder pressure, net heat release rate and mass fraction burnt at constant injection timing

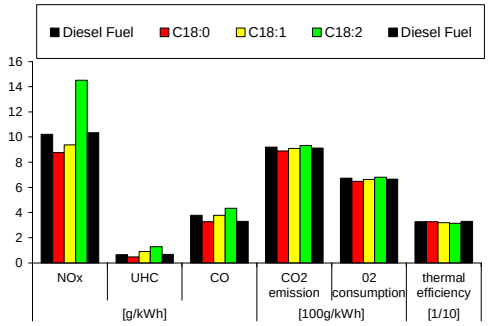

Figure C. 14-Effect of fatty acid chain length on gaseous exhaust emissions and indicated thermal efficiency at constant injection timing

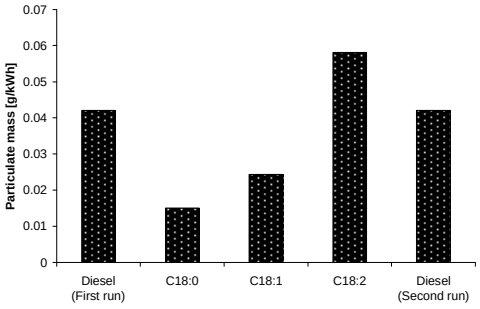

Figure C. 15- Effect of chain length on total particulate matter emissions for constant injection timing

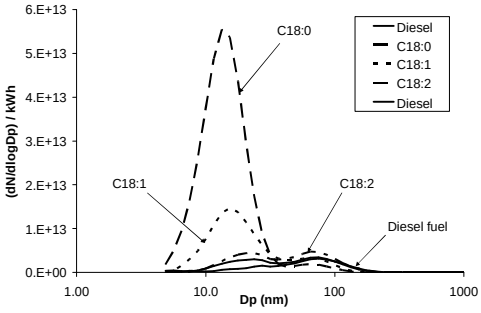

Figure C. 16- Particulate size distribution for constant injection timing

Fatty acid alkyl ester molecules with varying degrees of saturation at constant ignition timing

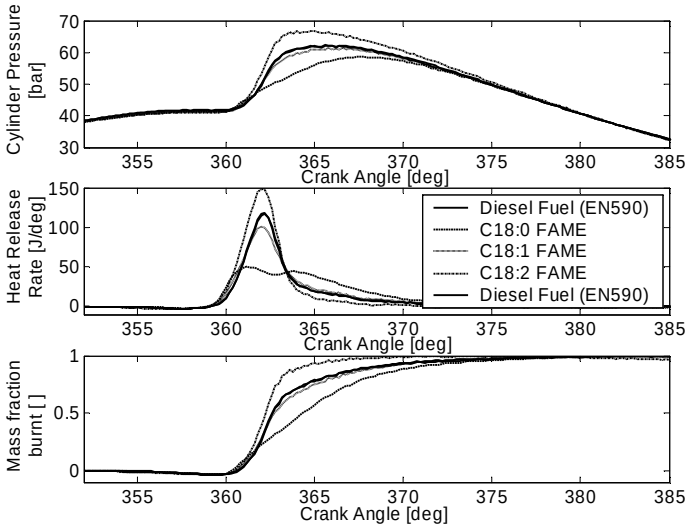

Figure C. 17- Effect of fatty acid chain length on cylinder pressure, net heat release rate and mass fraction burnt at constant ignition timing

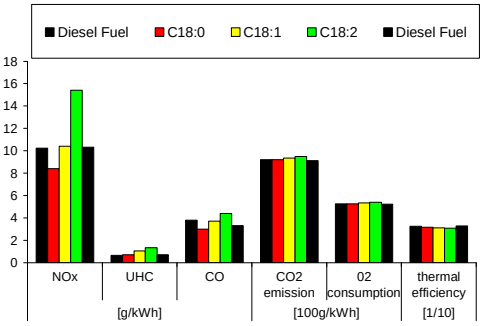

Figure C. 18-Effect of fatty acid chain length on gaseous exhaust emissions and indicated thermal efficiency at constant ignition timing

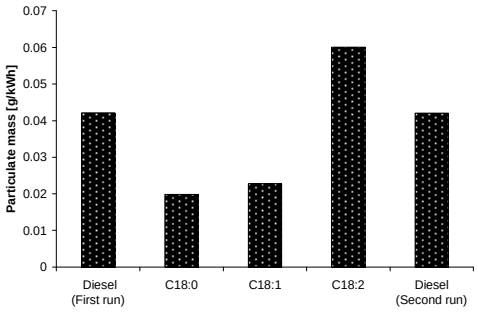

Figure C. 19 - Effect of chain length on total particulate matter emissions for constant ignition timing

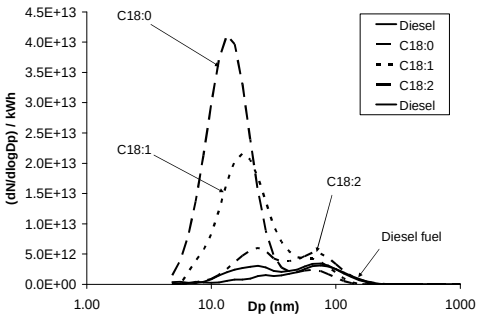

Figure C. 20 - Particulate size distribution for constant ignition timing

Fatty acid alkyl ester molecules with varying degrees of saturation at constant ignition delay

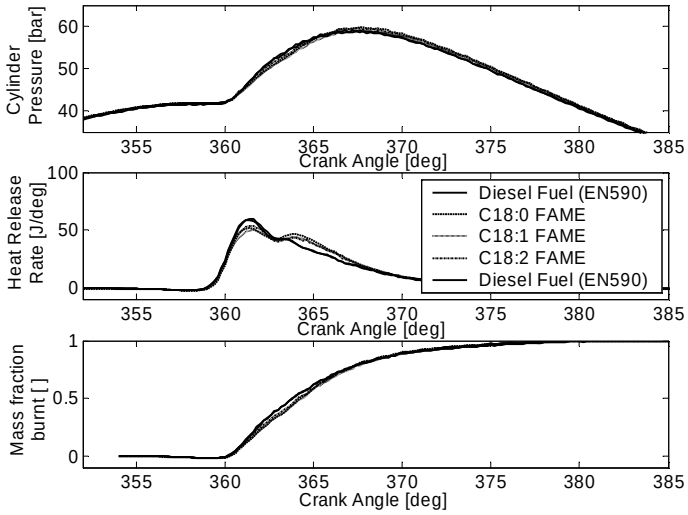

Figure C. 21 - Effect of fatty acid chain length on cylinder pressure, net heat release rate and mass fraction burnt at constant ignition delay

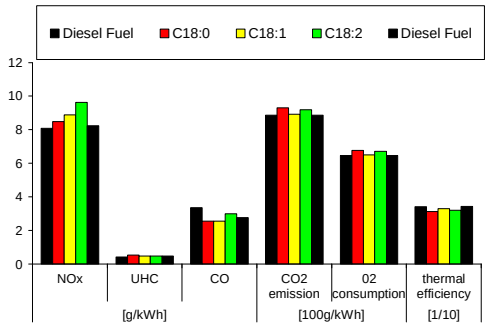

Figure C. 22 - Effect of fatty acid chain length on gaseous exhaust emissions and indicated thermal efficiency at constant ignition delay

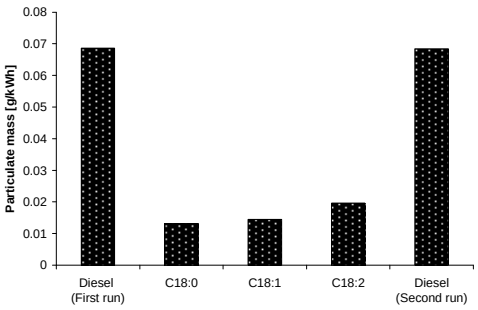

Figure C. 23 - Effect of chain length on total particulate matter emissions for constant ignition delay

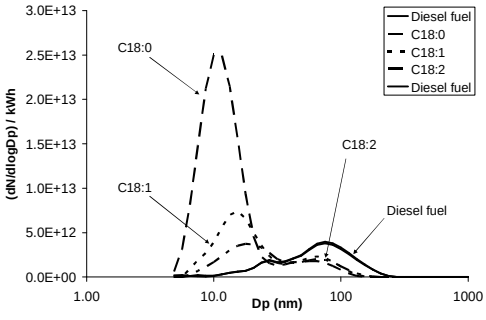

Figure C. 24 - Particulate size distribution for constant ignition delay

Fatty acid alkyl ester molecules with varying alcohol chain lengths at constant injection timing

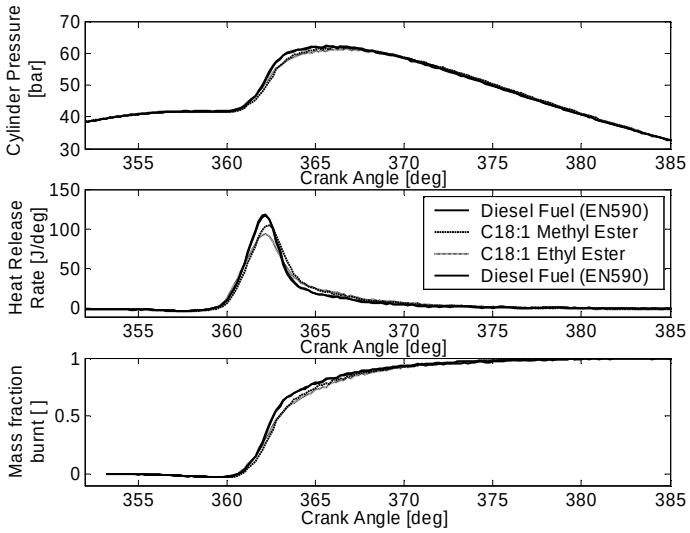

Figure C. 25 - Effect of fatty acid chain length on cylinder pressure, net heat release rate and mass fraction burnt at constant injection timing

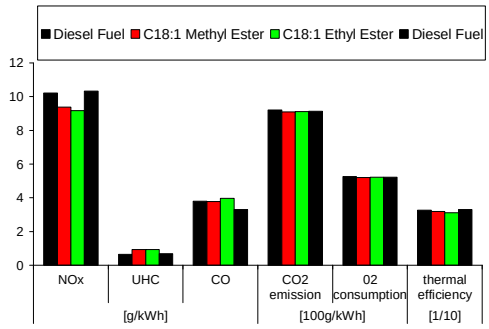

Figure C. 26 - Effect of fatty acid chain length on gaseous exhaust emissions and indicated thermal efficiency at constant injection timing

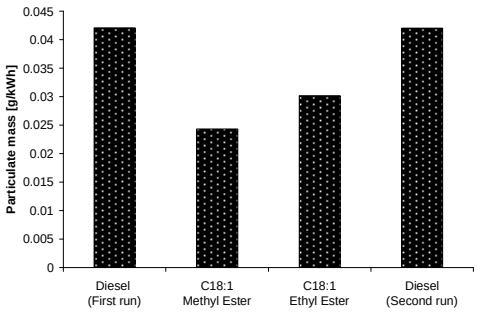

Figure C. 27 - Effect of chain length on total particulate matter emissions for constant injection timing

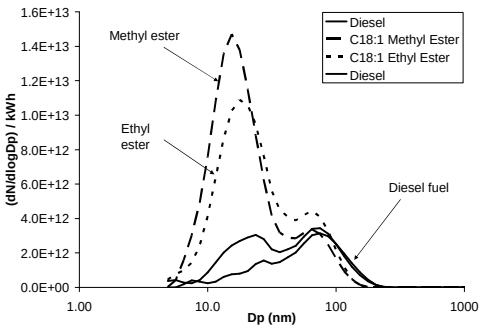

Figure C. 28 - Particulate size distribution for constant injection timing

Fatty acid alkyl ester molecules with varying alcohol chain lengths at constant ignition timing

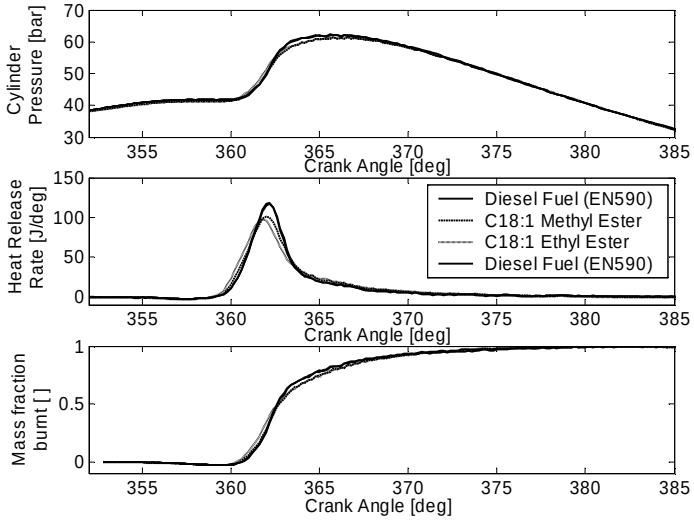

Figure C. 29- Effect of fatty acid chain length on cylinder pressure, net heat release rate and mass fraction burnt at constant ignition timing

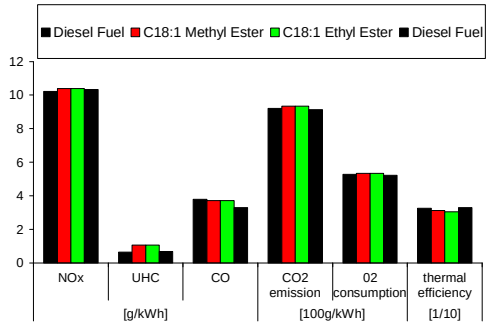

Figure C. 30-Effect of fatty acid chain length on gaseous exhaust emissions and indicated thermal efficiency at constant ignition timing

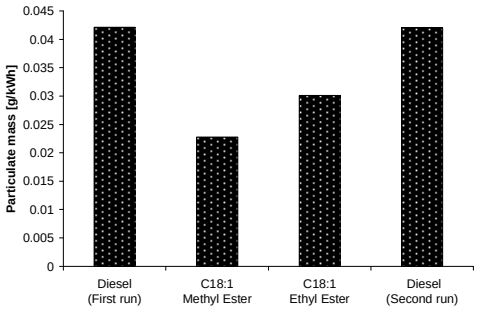

Figure C. 31 - Effect of chain length on total particulate matter emissions for constant ignition timing

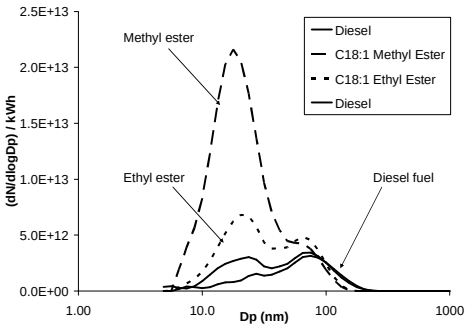

Figure C. 32 - Particulate size distribution for constant ignition timing

Fatty acid alkyl ester molecules with varying alcohol chain lengths at constant ignition delay

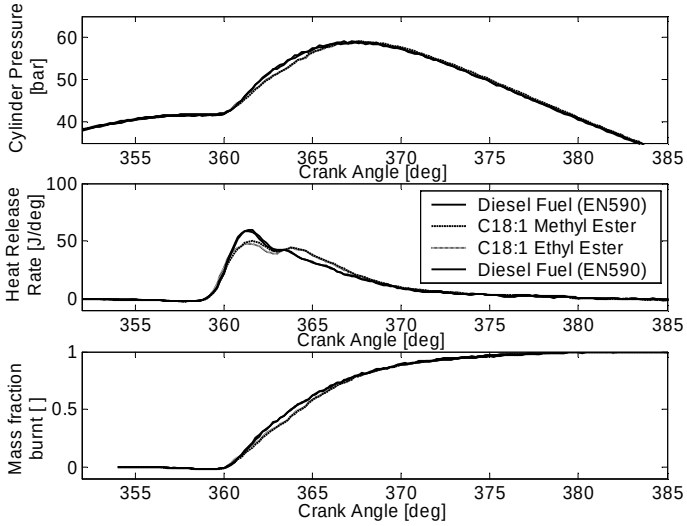

Figure C. 33 - Effect of fatty acid chain length on cylinder pressure, net heat release rate and mass fraction burnt at constant ignition delay

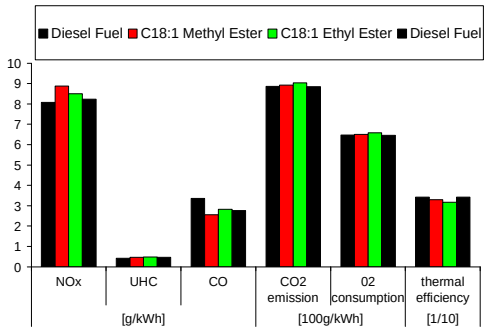

Figure C. 34 - Effect of fatty acid chain length on gaseous exhaust emissions and indicated thermal efficiency at constant ignition delay

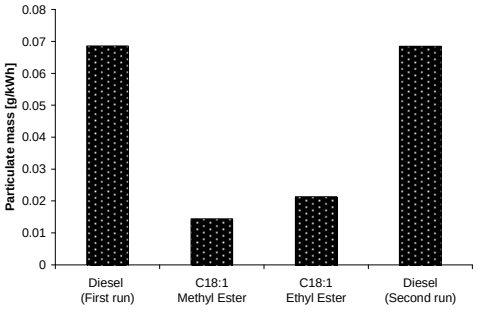

Figure C. 35 - Effect of chain length on total particulate matter emissions for constant ignition delay

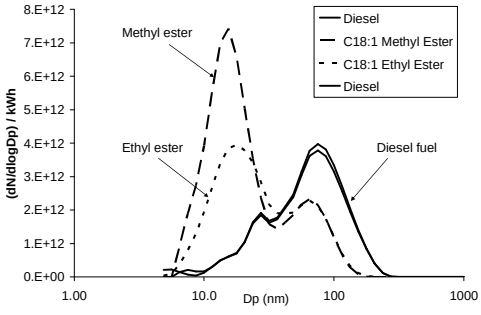

Figure C. 36 - Particulate size distribution for constant ignition delay

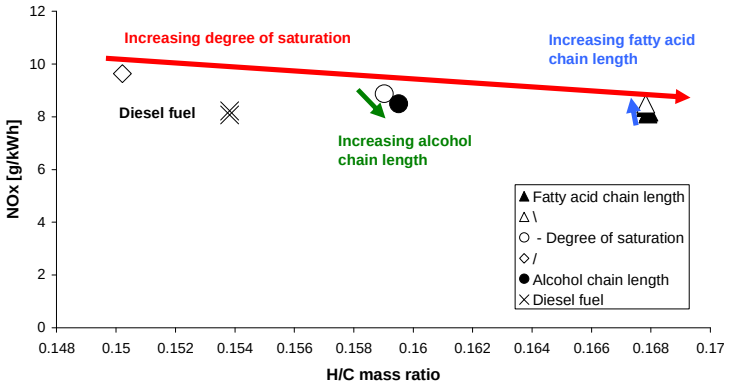

Figure C. 37 - Effect of hydrogen to carbon mass ratio of Biodiesel molecules on NO_x emissions

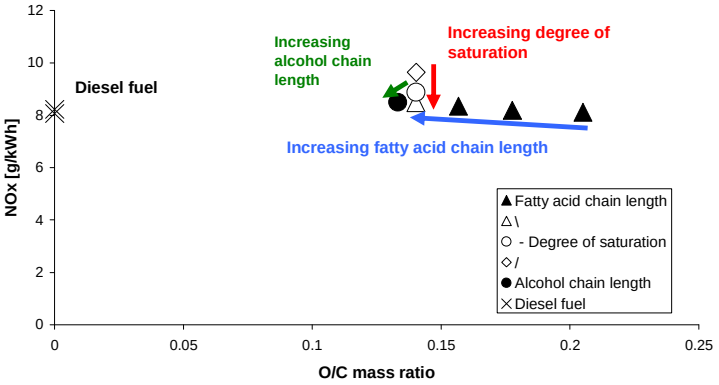

Figure C. 38 - Effect of oxygen to carbon mass ratio of Biodiesel molecules on NO_x emissions

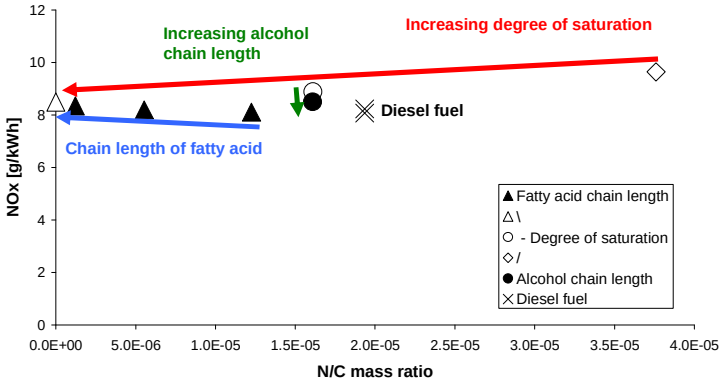

Figure C. 39 - Effect of nitrogen to carbon mass ratio of Biodiesel molecules on NO_x emissions

Additional experimental results for section 7.2.1

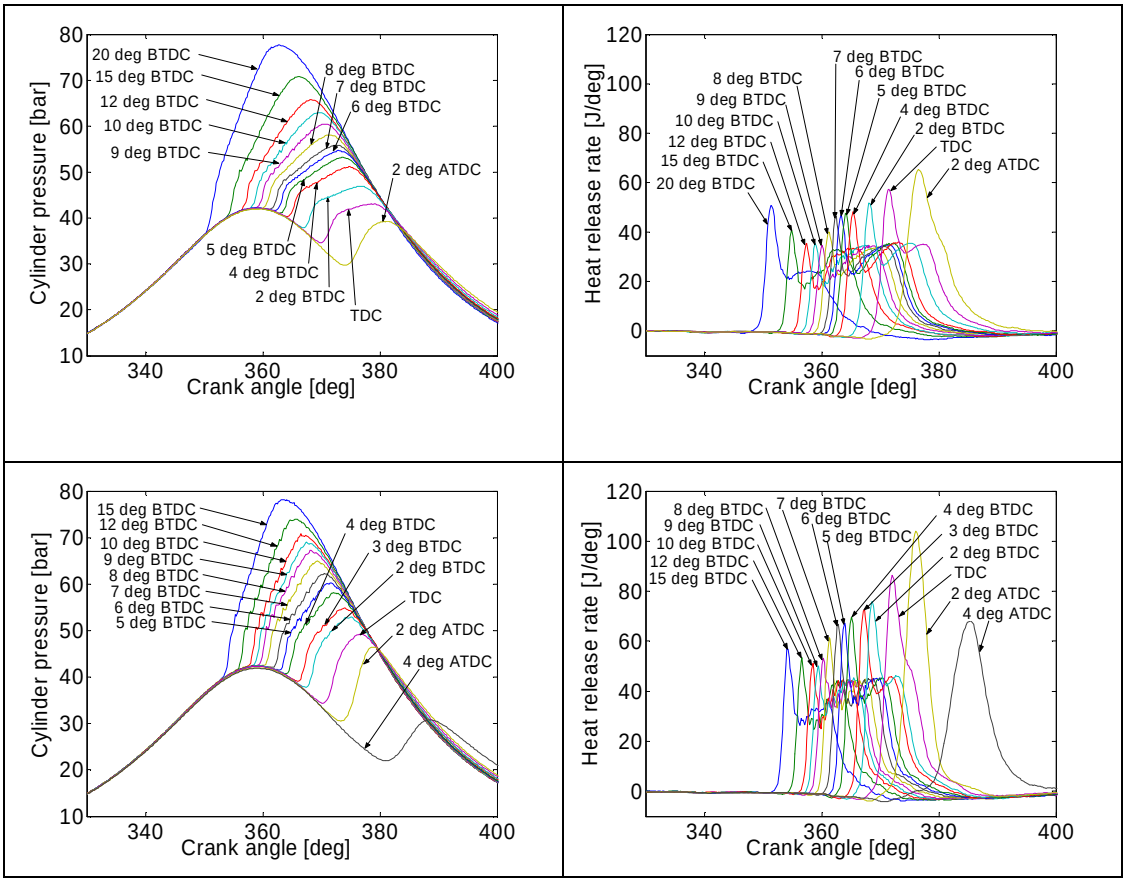

Figure C. 40 - Cylinder pressure (left) and heat release rates (right) for the combustion of DME at 250 bar (top) and 400 bar (bottom) injection pressures

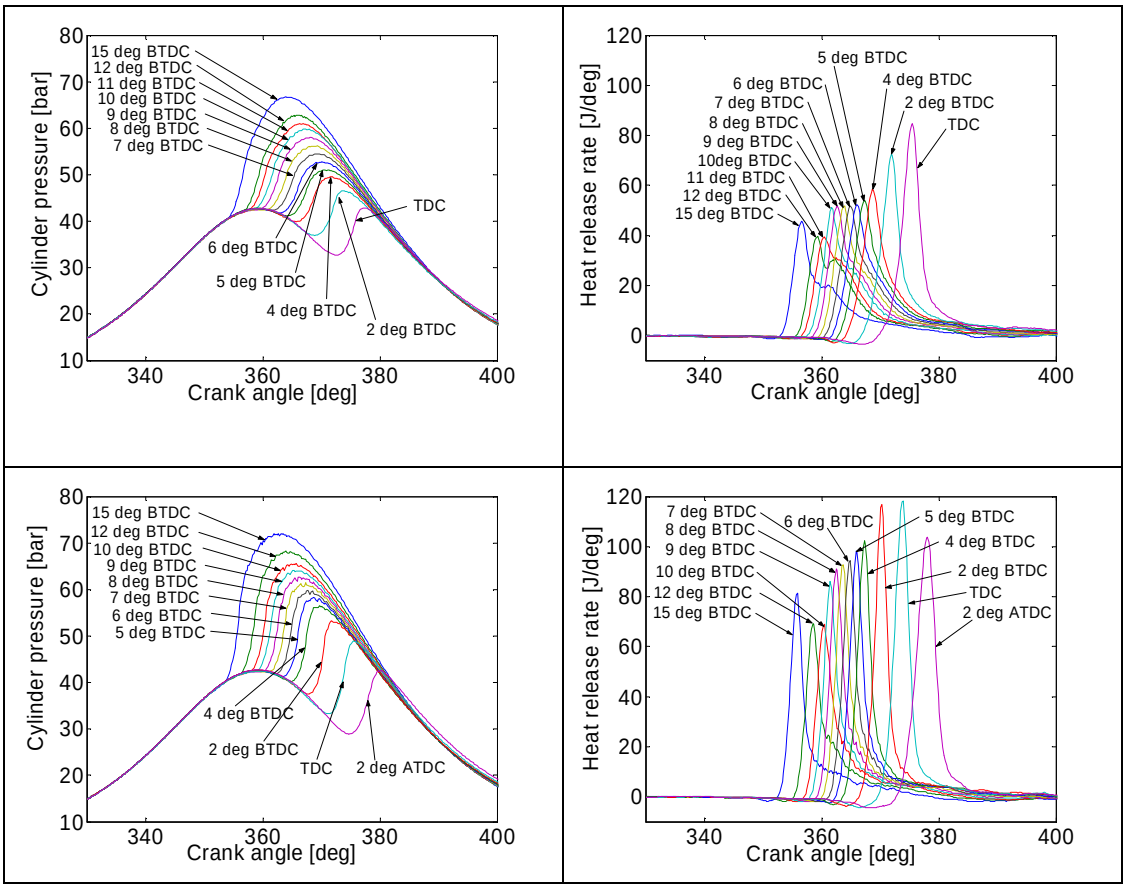

Figure C. 41 - Cylinder pressure (left) and heat release rates (right) for the combustion of fossil diesel fuel oil at 250 bar (top) and 400 bar (bottom) injection pressures

Appendix D. Details of experimental running conditions

Details of experimental conditions for Section 6.2

Constant injection timing: (ULVFS = Ultra low volume fuel system)

	I.M.E.P. [MPa]	Engine speed [rpm]	Injection timing [°CA BTDC]	Ignition timing [°CA BTDC]	Injection pressure [MPa]	Air temp. [° C]	Oil temp [° C]	Coolant [° C]	Exhaust [° C]	ULVFS [° C]	Injector pulse width [µs]
Fossil Diesel fuel oil	0.40	1200	7.1	TDC	45	27	82.5	83	241	77	697
Di-n-butyl ether	0.40	1200	7.1	1.68	45	27	83.5	85	229	78.5	776
1,1 Dibutoxybutane	0.40	1200	7.1	1.18	45	26.5	83.5	84.5	224.5	77.5	832
2,2 Dibutoxypropane	0.40	1200	7.1	0.88	45	27	83.5	84	229	77	782
2,2 Diethoxybutane	0.40	1200	7.1	-2.23	45	27	83.5	84.5	225	77.5	832
Di-n-butoxybutane	0.40	1200	7.1	0.68	45	27	83	85	221	77	805
Fossil Diesel fuel oil	0.40	1200	7.1	TDC	45	26.5	83.5	85	239	77.5	698

Constant ignition timing:

	I.M.E.P. [MPa]	Engine speed [rpm]	Injection timing [°CA BTDC]	Ignition timing [°CA BTDC]	Injection pressure [MPa]	Air temp. [° C]	Oil temp [° C]	Coolant [° C]	Exhaust [° C]	ULVFS [° C]	Injector pulse width [µs]
Fossil Diesel fuel oil	0.40	1200	7.1	TDC	45	27	83.5	84	242	79	698
Di-n-butyl ether	0.40	1200	5.4	TDC	45	27	83.5	84	234	79	768
1,1 Dibutoxybutane	0.40	1200	5.9	TDC	45	27	81	84.5	234	79.5	772
2,2 Dibutoxypropane	0.40	1200	6.1	TDC	45	27	82.5	84.5	231	77.5	792
2,2 Diethoxybutane	0.40	1200	9.3	TDC	45	27	83	84	223.5	78	849
Di-n-butoxybutane	0.40	1200	6.4	TDC	45	27	83	84.5	228.5	77.5	802
Fossil Diesel fuel oil	0.40	1200	7.1	TDC	45	27	83.5	84	240	77.5	696

Constant ignition delay:

	I.M.E.P. [MPa]	Engine speed [rpm]	Injection timing [°CA BTDC]	Ignition timing [°CA BTDC]	Injection pressure [MPa]	Air temp. [° C]	Oil temp [° C]	Coolant [° C]	Exhaust [° C]	ULVFS [° C]	Injector pulse width [µs]	2-EHN conc. [vol. %]
Fossil Diesel fuel oil	0.40	1200	5.40	TDC	45	29	81	83	244	25	705	4.0
Di-n-butyl ether	0.40	1200	5.40	TDC	45	26	84	85	234	29	775	0.0
1,1 Dibutoxybutane	0.40	1200	5.40	TDC	45	26	82	85	234	26	784	0.4
2,2 Dibutoxypropane	0.40	1200	5.40	TDC	45	27	83.5	85	232	28	790	0.8
2,2 Diethoxybutane	0.40	1200	5.40	TDC	45	26	81.5	85	227	30	838	16.0
Di-n-butoxybutane	0.40	1200	5.40	TDC	45	27	83	84	230	29	807	2.0
Fossil Diesel fuel oil	0.40	1200	5.40	TDC	45	26	82	85	243	25	714	4.0

Details of experimental conditions for Section6.3

Constant injection timing: (ULVFS = Ultra low volume fuel system)

	I.M.E.P.	Engine speed	Injection timing	Ignition timing	Injection pressure	Air temp.	Oil temp	Coolant	Exhaust	ULVFS	Injector pulse width
	[MPa]	[rpm]	[ºCA BTDC]	[ºCA BTDC]	[MPa]	[º C]	[º C]	[º C]	[º C]	[º C]	[µs]
Fossil Diesel fuel oil	0.4	1200	7.1	TDC	45	33	86	87.5	256.5	77.5	668
Di-n-butyl ether	0.4	1200	7.1	1.7	45	32	82	83	242	77	714
1,1 Dibutoxypropane	0.4	1200	7.1	0.98	45	32	81	83	242	77	728
2,2 Dibutoxypropane	0.4	1200	7.1	0.88	45	32	81	79	238	77	739
3-methyl-1-(3-methylbutoxymethoxy) butane	0.4	1200	7.1	-0.04	45	32	84	83	240	77.5	741
Fossil Diesel fuel oil	0.4	1200	7.1	TDC	45	32.5	82.5	82.5	251	77	665

Constant ignition timing: (ULVFS = Ultra low volume fuel system)

	I.M.E.P.	Engine speed	Injection timing	Ignition timing	Injection pressure	Air temp.	Oil temp	Coolant	Exhaust	ULVFS	Injector pulse width
	[MPa]	[rpm]	[ºCA BTDC]	[ºCA BTDC]	[MPa]	[º C]	[º C]	[º C]	[º C]	[º C]	[µs]
EN 590 Diesel	0.4	1200	7.1	TDC	45	33	84	79	249	77	710
Di-n-butyl ether	0.4	1200	5.4	TDC	45	33	84	83	241	78	752
1,1 Dibutoxypropane	0.4	1200	6.1	TDC	45	32	81	82	239	77	746
2,2 Dibutoxypropane	0.4	1200	6.2	TDC	45	34	80	83	239	77	740
3-methyl-1-(3-methylbutoxymethoxy) butane	0.4	1200	7.15	TDC	45	31	83	84	237	77	745
EN 590 Diesel	0.4	1200	7.1	TDC	45	33	80	80	245	77	667

Constant ignition delay:

	I.M.E.P.	Engine speed	Injection timing	Ignition timing	Injection pressure	Air temp.	Oil temp	Coolant	Exhaust	ULVFS	Injector pulse width	2-EHN conc.
	[MPa]	[rpm]	[ºCA BTDC]	[ºCA BTDC]	[MPa]	[º C]	[º C]	[º C]	[º C]	[º C]	[µs]	[vol. %]
EN 590 Diesel	0.4	1200	5.4	TDC	45	29	82	81	258	23.2	676	4
Di-n-butyl ether	0.4	1200	5.4	TDC	45	32	80	79	240.5	24.9	712	0
1,1 Dibutoxypropane	0.4	1200	5.4	TDC	45	31	81	84	240	22.2	734	0.4
2,2 Dibutoxypropane	0.4	1200	5.4	TDC	45	34	81	80	234	23	756	0.8
3-methyl-1-(3-methylbutoxymethoxy) butane	0.4	1200	5.4	TDC	45	34	74.5	81.5	238.5	23.5	754	16
EN 590 Diesel	0.4	1200	5.4	TDC	45	33	80.5	78.5	252.5	23	686	4

Appendix E. Engine air intake and exhaust system schematics

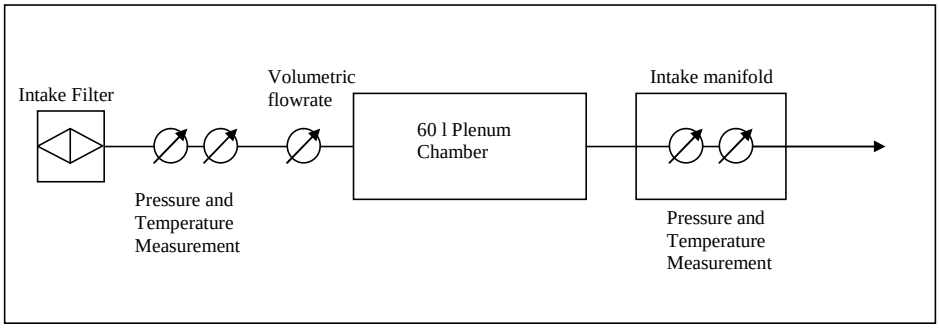

Figure E. 1 - Engine intake air schematic

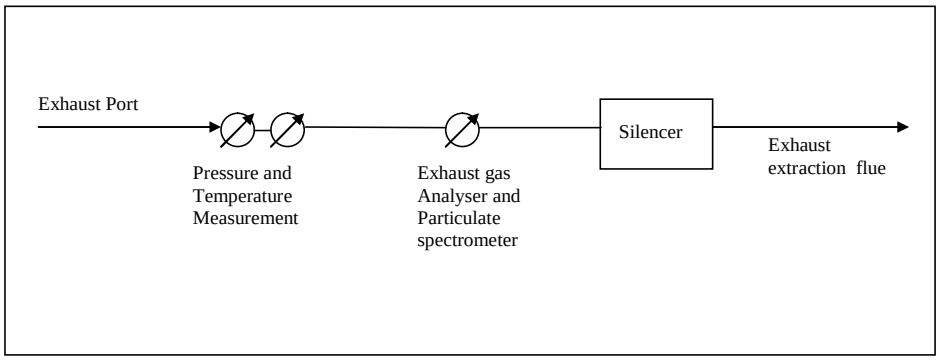

Figure E. 2 - Engine exhaust gas schematic

Appendix F. Photographs of fuels and experimental apparatus

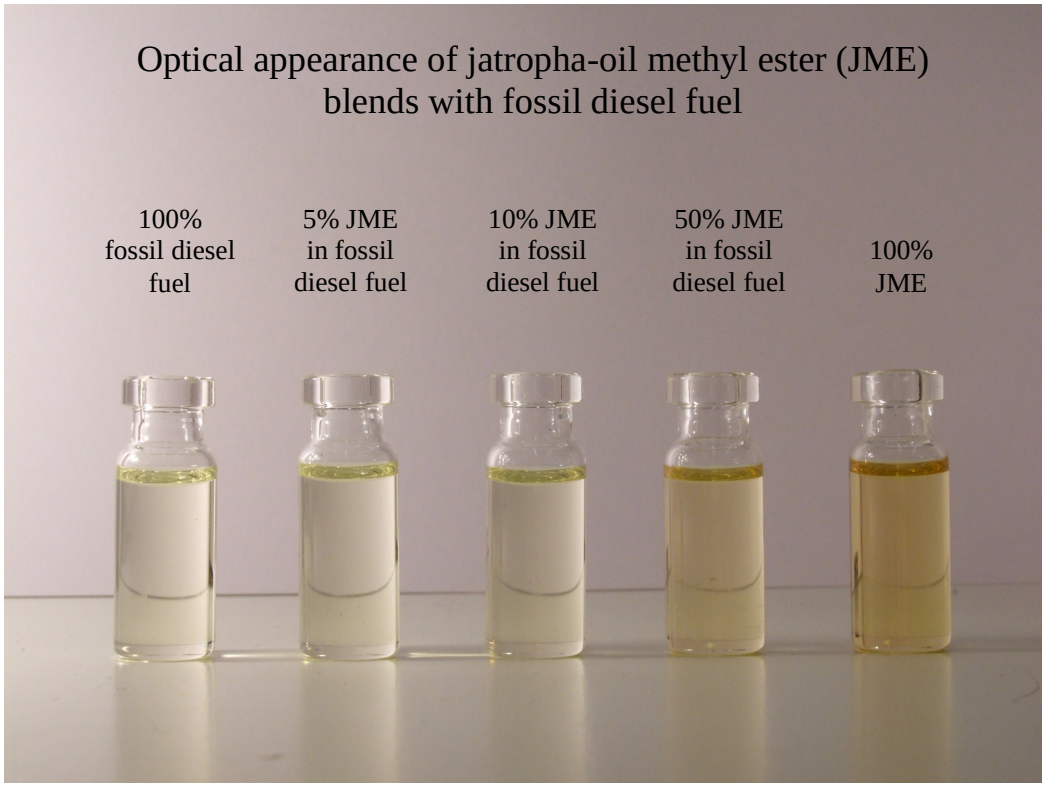

Figure F. 1- Optical appearance of jatropha methyl ester, fossil diesel fuel and their blends

Figure F. 2 - Optical appearance of pure diethyl ether, jatropha methyl ester and tallow methyl ester

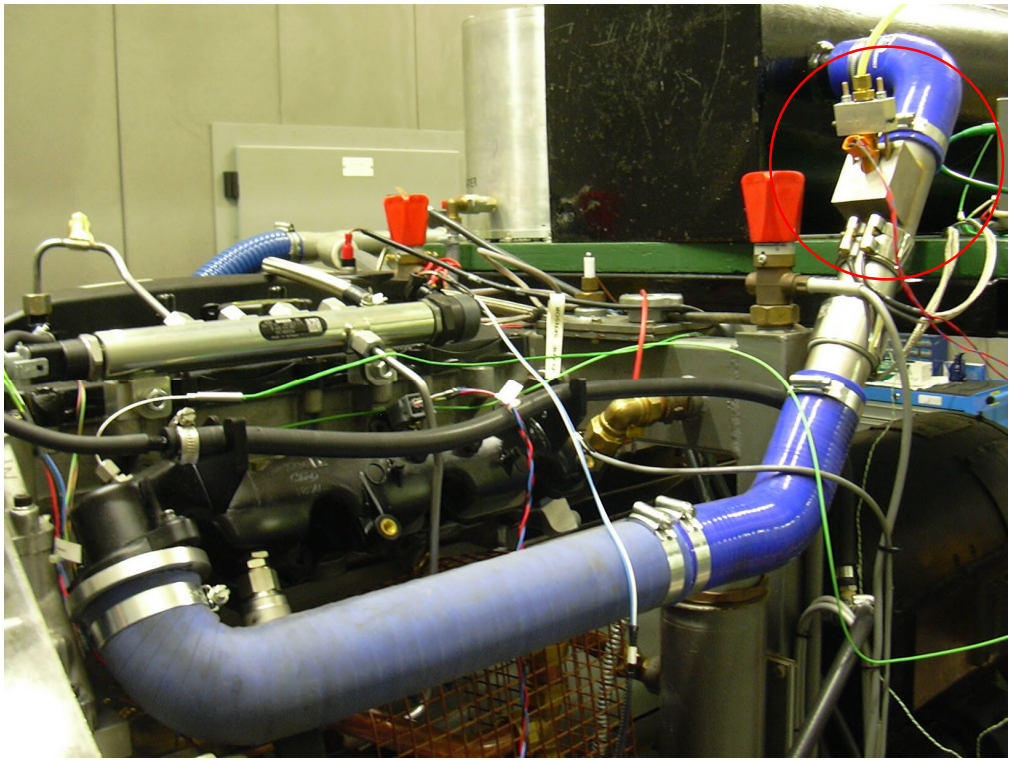

Figure F. 3 - Air intake port fuel-injector with heating system used to generate homogeneous premixed fuel-air mixtures (circled in red)

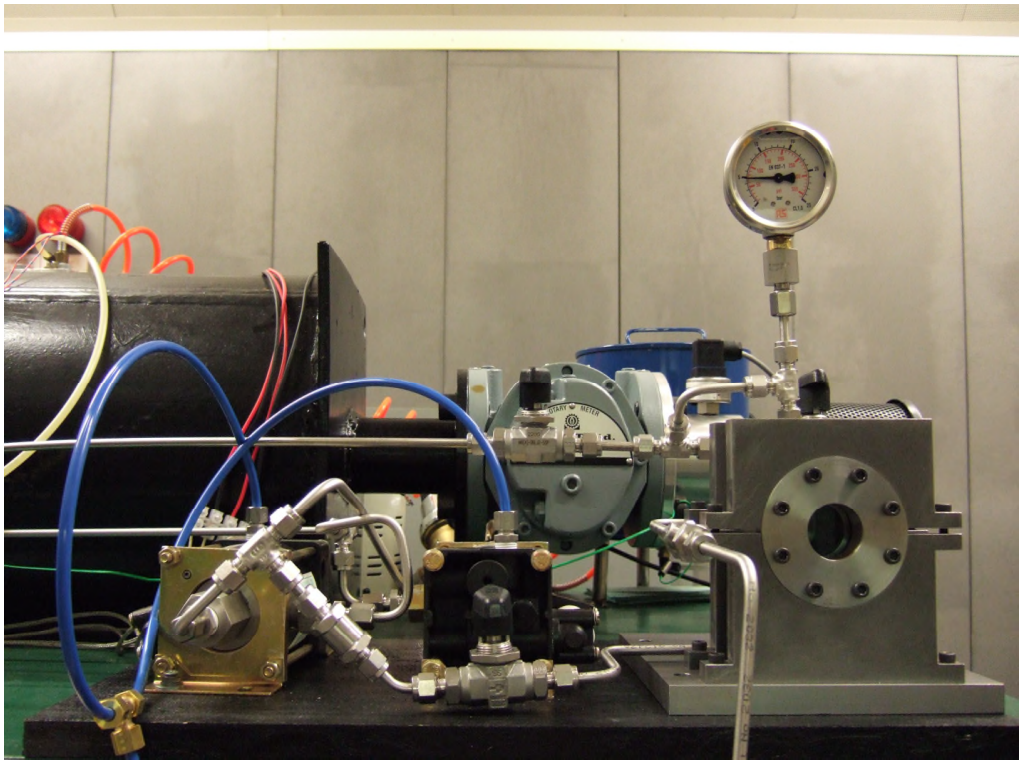

Figure F. 4 - Fuel system for gaseous fuels such as DME

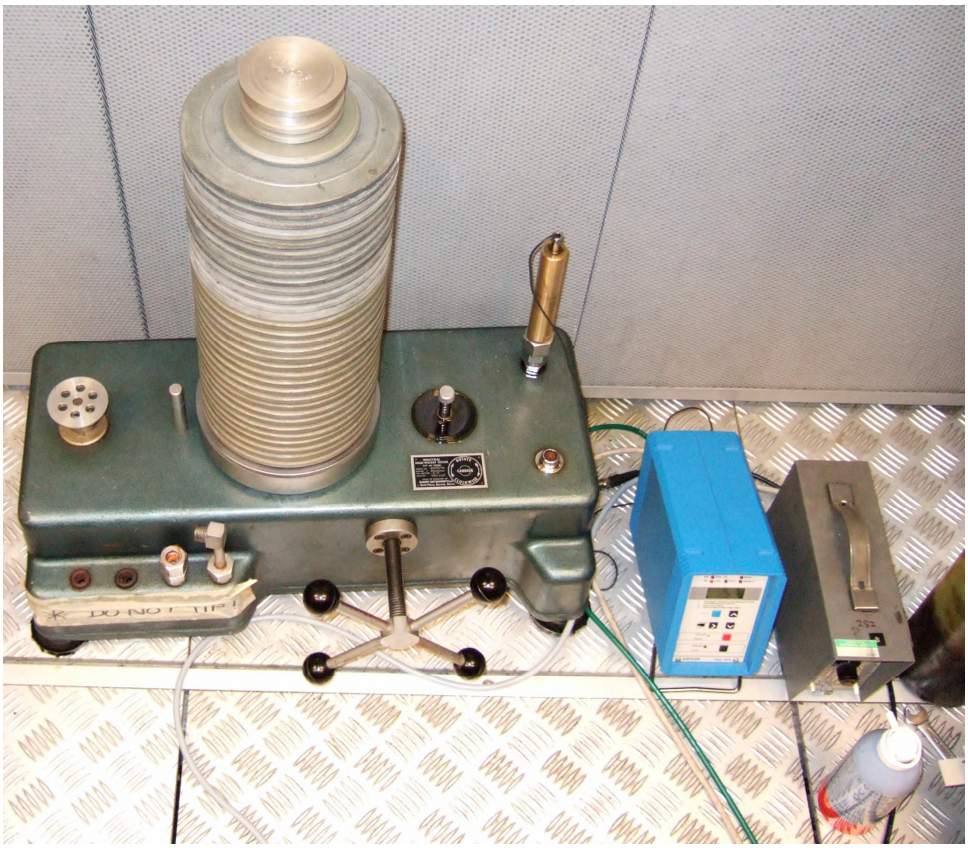

Figure F. 5 - Dead-weight calibrator used for the pressure sensor calibrations

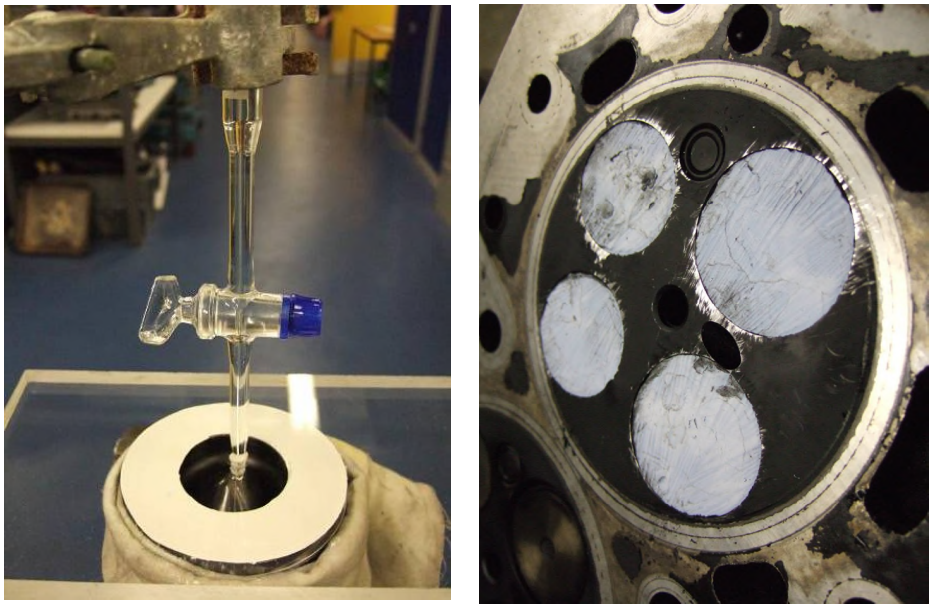

Figure F. 6 - Measurements of the combustion chamber clearance volume

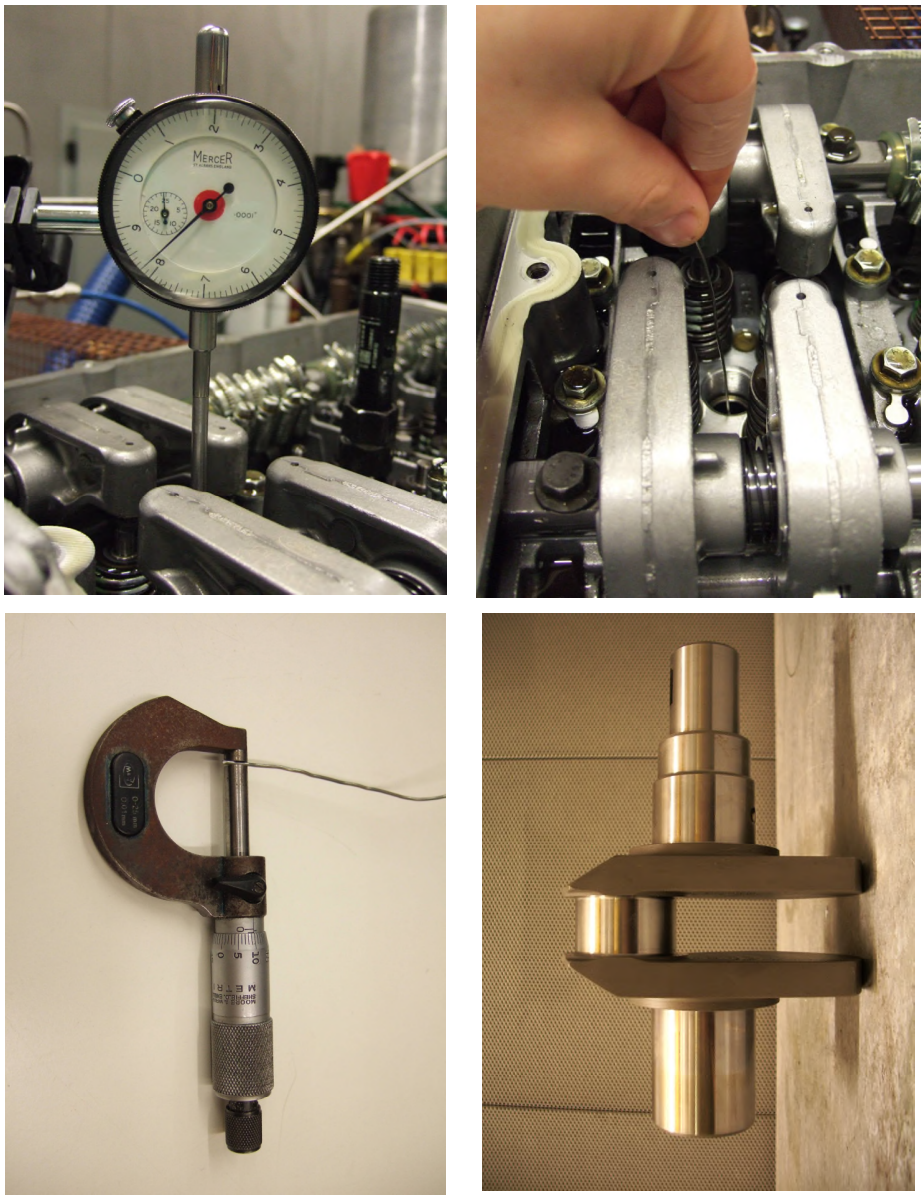

Figure F. 7 - Measurements of static TDC and engine geometry

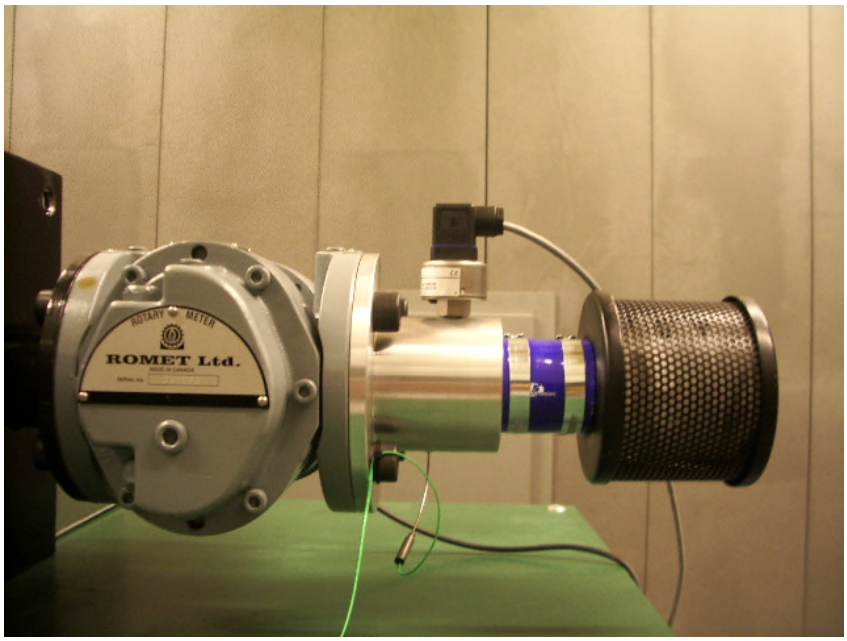

Figure F. 8 - Air flow measurements through the engine using thermocouple, pressure sensor and volumetric gas flow meter

Figure F. 9 - Ford duratorq donor engine before being dismantled for its parts that were used to build the single-cylinder research engine

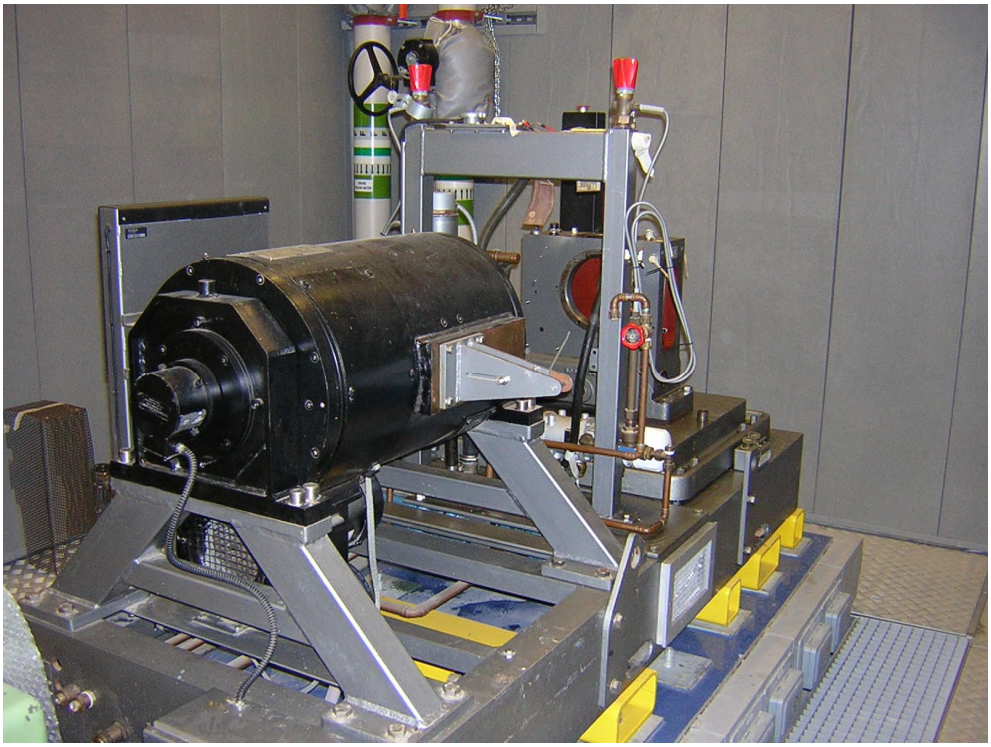

Figure F. 10 - Engine research facility at the beginning of its construction

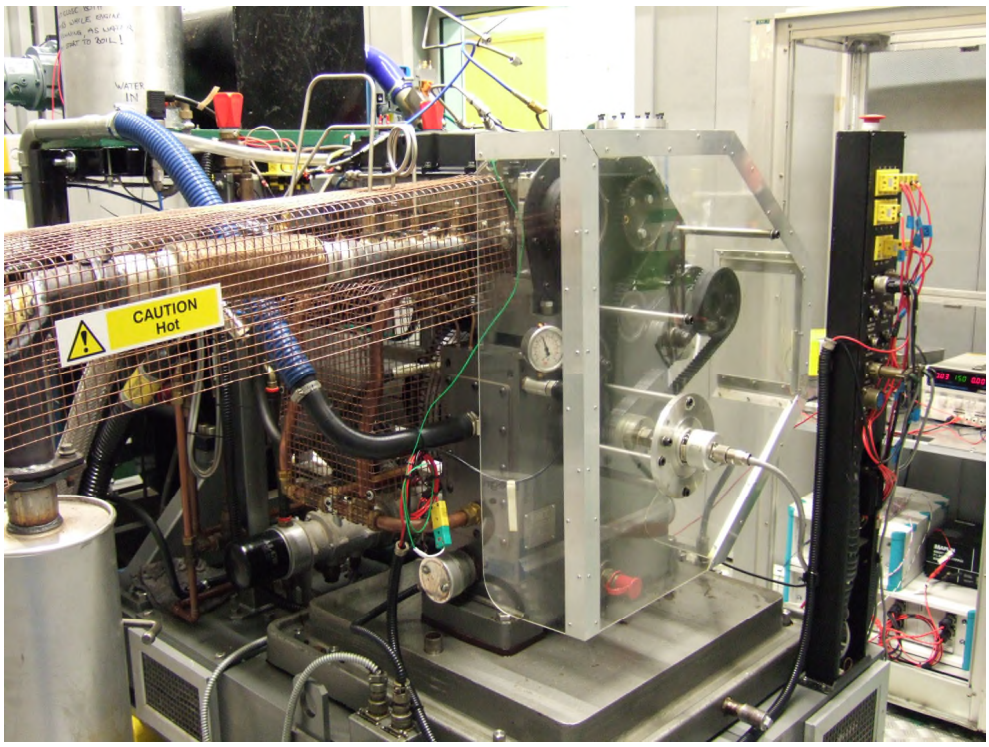

Figure F. 11 - Engine reasearch facility at the end of its construction and commissioning

Appendix G. Computational source codes

Computational source codes for the cylinder pressure and heat release analyses, as well as for the stoichiometric analysis of combustion reactants and products are included on a disc (CD-ROM) located in a pocket in the back sleeve of this thesis. The titles of these programs are:

Labview “Data acquisition code for an IC-engine with pressure and heat release analysis”

Labview “Data acquisition code for the dynamic calibration of TDC using entropy and temperature”

Matlab 6.1 “Cylinder pressure and heat release analysis code”

Matlab 6.1 “Simple stoichiometric analysis model”

Matlab 6.1 “Simple stoichiometric analysis model with EGR”

Matlab 6.1 “Detailed stoichiometric analysis model”

Matlab 6.1 “Detailed stoichiometric analysis model with EGR”